Analytical Chemistry Volume 2 (Harvey)

This text is disseminated via the Open Education Resource (OER) LibreTexts Project (https://LibreTexts.org) and like the hundreds of other texts available within this powerful platform, it is freely available for reading, printing and "consuming." Most, but not all, pages in the library have licenses that may allow individuals to make changes, save, and print this book. Carefully consult the applicable license(s) before pursuing such effects.

Instructors can adopt existing LibreTexts texts or Remix them to quickly build course-specific resources to meet the needs of their students. Unlike traditional textbooks, LibreTexts' web based origins allow powerful integration of advanced features and new technologies to support learning.

The LibreTexts mission is to unite students, faculty and scholars in a cooperative effort to develop an easy-to-use online platform for the construction, customization, and dissemination of OER content to reduce the burdens of unreasonable textbook costs to our students and society. The LibreTexts project is a multi-institutional collaborative venture to develop the next generation of open-access texts to improve postsecondary education at all levels of higher learning by developing an Open Access Resource environment. The project currently consists of 14 independently operating and interconnected libraries that are constantly being optimized by students, faculty, and outside experts to supplant conventional paper-based books. These free textbook alternatives are organized within a central environment that is both vertically (from advance to basic level) and horizontally (across different fields) integrated.

The LibreTexts libraries are Powered by NICE CXOne and are supported by the Department of Education Open Textbook Pilot Project, the UC Davis Office of the Provost, the UC Davis Library, the California State University Affordable Learning Solutions Program, and Merlot. This material is based upon work supported by the National Science Foundation under Grant No. 1246120, 1525057, and 1413739.

Any opinions, findings, and conclusions or recommendations expressed in this material are those of the author(s) and do not necessarily reflect the views of the National Science Foundation nor the US Department of Education.

Have questions or comments? For information about adoptions or adaptions contact info@LibreTexts.org. More information on our activities can be found via Facebook (https://facebook.com/Libretexts), Twitter (https://twitter.com/libretexts), or our blog (http://Blog.Libretexts.org).

This text was compiled on 03/09/2025

TABLE OF CONTENTS

5: Developing a Standard Method

6: Quality Assurance

7: Appendix

Detailed Licensing

Licensing

*A detailed breakdown of this resource's licensing can be found in **Back Matter/Detailed Licensing**.*

CHAPTER OVERVIEW

1: Spectroscopic Methods

An early example of a colorimetric analysis is Nessler's method for ammonia, which was introduced in 1856. Nessler found that adding an alkaline solution of HgI_2 and KI to a dilute solution of ammonia produced a yellow-to-reddish brown colloid, in which the colloid's color depended on the concentration of ammonia. By visually comparing the color of a sample to the colors of a series of standards, Nessler was able to determine the concentration of ammonia. Colorimetry, in which a sample absorbs visible light, is one example of a spectroscopic method of analysis. At the end of the nineteenth century, spectroscopy was limited to the absorption, emission, and scattering of visible, ultraviolet, and infrared electromagnetic radiation. Since then, spectroscopy has expanded to include other forms of electromagnetic radiation—such as X-rays, microwaves, and radio waves—and other energetic particles—such as electrons and ions.

1.1: Overview of Spectroscopy

The focus of this chapter is on the interaction of ultraviolet, visible, and infrared radiation with matter. Because these techniques use optical materials to disperse and focus the radiation, they often are identified as optical spectroscopies. For convenience we will use the simpler term spectroscopy in place of optical ***spectroscopy***; however, you should understand we will consider only a limited piece of what is a much broader area of analytical techniques.

Despite the difference in instrumentation, all spectroscopic techniques share several common features. Before we consider individual examples in greater detail, let's take a moment to consider some of these similarities. As you work through the chapter, this overview will help you focus on the similarities between different spectroscopic methods of analysis. You will find it easier to understand a new analytical method when you can see its relationship to other similar methods.

What is Electromagnetic Radiation?

Electromagnetic radiation—light—is a form of energy whose behavior is described by the properties of both waves and particles. Some properties of electromagnetic radiation, such as its refraction when it passes from one medium to another (Figure 10.1.1), are explained best when we describe light as a wave. Other properties, such as absorption and emission, are better described by treating light as a particle. The exact nature of electromagnetic radiation remains unclear, as it has since the development of quantum mechanics in the first quarter of the 20th century [Home, D.; Gribbin, J. *New Scientist* 1991, 2 Nov. 30–33]. Nevertheless, this dual model of wave and particle behavior provide a useful description for electromagnetic radiation.

Figure 10.1.1 . The Golden Gate bridge as seen through rain drops. Refraction of light by the rain drops produces the distorted images. Source: Brocken Inaglory (commons. Wikipedia.org).

Wave Properties of Electromagnetic Radiation

Electromagnetic radiation consists of oscillating electric and magnetic fields that propagate through space along a linear path and with a constant velocity. In a vacuum, electromagnetic radiation travels at the speed of light, c, which is 2.99792×10^8 m/s. When electromagnetic radiation moves through a medium other than a vacuum, its velocity, v, is less than the speed of light in a vacuum. The difference between v and c is sufficiently small (<0.1%) that the speed of light to three significant figures, 3.00×10^8 m/s, is accurate enough for most purposes.

The oscillations in the electric field and the magnetic field are perpendicular to each other and to the direction of the wave's propagation. Figure 10.1.2 shows an example of plane-polarized electromagnetic radiation, which consists of a single oscillating electric field and a single oscillating magnetic field.

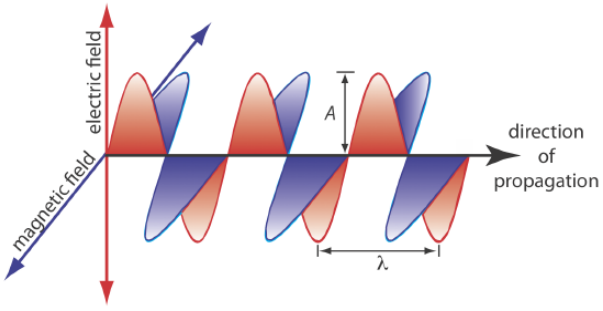

Figure 10.1.2 . Plane-polarized electromagnetic radiation showing the oscillating electric field in blue and the oscillating magnetic field in red. The radiation's amplitude, A, and its wavelength, λ, are shown. Normally, electromagnetic radiation is unpolarized, with oscillating electric and magnetic fields present in all possible planes perpendicular to the direction of propagation.

An electromagnetic wave is characterized by several fundamental properties, including its velocity, amplitude, frequency, phase angle, polarization, and direction of propagation [Ball, D. W. *Spectroscopy* **1994**, *9(5)*, 24–25]. For example, the amplitude of the oscillating electric field at any point along the propagating wave is

$$A_t = A_e \sin(2\pi\nu t + \Phi)$$

where A_t is the magnitude of the electric field at time t, A_e is the electric field's maximum ***amplitude***, ν is the wave's ***frequency***—the number of oscillations in the electric field per unit time—and Φ is a ***phase angle*** that accounts for the fact that A_t need not have a value of zero at t = 0. The identical equation for the magnetic field is

$$A_t = A_m \sin(2\pi\nu t + \Phi)$$

where A_m is the magnetic field's maximum amplitude.

Other properties also are useful for characterizing the wave behavior of electromagnetic radiation. The ***wavelength***, λ, is defined as the distance between successive maxima (see Figure 10.1.2). For ultraviolet and visible electromagnetic radiation the wavelength usually is expressed in nanometers (1 nm = 10^{-9} m), and for infrared radiation it is expressed in microns (1 mm = 10^{-6} m). The relationship between wavelength and frequency is

$$\lambda = \frac{c}{\nu}$$

Another unit useful unit is the ***wavenumber***, $\bar{\nu}$, which is the reciprocal of wavelength

$$\bar{\nu} = \frac{1}{\lambda}$$

Wavenumbers frequently are used to characterize infrared radiation, with the units given in cm^{-1}.

When electromagnetic radiation moves between different media—for example, when it moves from air into water—its frequency, ν, remains constant. Because its velocity depends upon the medium in which it is traveling, the electromagnetic radiation's wavelength, λ, changes. If we replace the speed of light in a vacuum, c, with its speed in the medium, v, then the wavelength is

$$\lambda = \frac{v}{\nu}$$

This change in wavelength as light passes between two media explains the refraction of electromagnetic radiation shown in Figure 10.1.1 .

Example 10.1.1

In 1817, Josef Fraunhofer studied the spectrum of solar radiation, observing a continuous spectrum with numerous dark lines. Fraunhofer labeled the most prominent of the dark lines with letters. In 1859, Gustav Kirchhoff showed that the D line in the sun's spectrum was due to the absorption of solar radiation by sodium atoms. The wavelength of the sodium D line is 589 nm. What are the frequency and the wavenumber for this line?

Solution

The frequency and wavenumber of the sodium D line are

$$\nu = \frac{c}{\lambda} = \frac{3.00 \times 10^8 \text{ m/s}}{589 \times 10^{-9} \text{ m}} = 5.09 \times 10^{14} \text{ s}^{-1}$$

$$\bar{\nu} = \frac{1}{\lambda} = \frac{1}{589 \times 10^{-9} \text{ m}} \times \frac{1 \text{ m}}{100 \text{ cm}} = 1.70 \times 10^4 \text{ cm}^{-1}$$

Exercise 10.1.1

Another historically important series of spectral lines is the Balmer series of emission lines from hydrogen. One of its lines has a wavelength of 656.3 nm. What are the frequency and the wavenumber for this line?

Answer

The frequency and wavenumber for the line are

$$\nu = \frac{c}{\lambda} = \frac{3.00 \times 10^8 \text{ m/s}}{656.3 \times 10^{-9} \text{ m}} = 4.57 \times 10^{14} \text{ s}^{-1}$$

$$\bar{\nu} = \frac{1}{\lambda} = \frac{1}{656.3 \times 10^{-9} \text{ m}} \times \frac{1 \text{ m}}{100 \text{ cm}} = 1.524 \times 10^4 \text{ cm}^{-1}$$

Particle Properties of Electromagnetic Radiation

When matter absorbs electromagnetic radiation it undergoes a change in energy. The interaction between matter and electromagnetic radiation is easiest to understand if we assume that radiation consists of a beam of energetic particles called photons. When a ***photon*** is absorbed by a sample it is "destroyed" and its energy acquired by the sample [Ball, D. W. *Spectroscopy* **1994**, *9(6)* 20–21]. The energy of a photon, in joules, is related to its frequency, wavelength, and wavenumber by the following equalities

$$E = h\nu = \frac{hc}{\lambda} = hc\bar{\nu}$$

where *h* is Planck's constant, which has a value of 6.626×10^{-34} Js.

Example 10.1.2

What is the energy of a photon from the sodium D line at 589 nm?

Solution

The photon's energy is

$$E = \frac{hc}{\lambda} = \frac{\left(6.626 \times 10^{-34} \text{ Js}\right)\left(3.00 \times 10^8 \text{ m/s}\right)}{589 \times 10^{-7} \text{ m}} = 3.37 \times 10^{-19} \text{ J}$$

Exercise 10.1.2

What is the energy of a photon for the Balmer line at a wavelength of 656.3 nm?

Answer

The photon's energy is

$$E = \frac{hc}{\lambda} = \frac{\left(6.626 \times 10^{-34} \text{ Js}\right)\left(3.00 \times 10^8 \text{ m/s}\right)}{656.3 \times 10^{-9} \text{ m}} = 3.03 \times 10^{-19} \text{ J}$$

The Electromagnetic Spectrum

The frequency and the wavelength of electromagnetic radiation vary over many orders of magnitude. For convenience, we divide electromagnetic radiation into different regions—the ***electromagnetic spectrum***—based on the type of atomic or molecular transitions that gives rise to the absorption or emission of photons (Figure 10.1.3). The boundaries between the regions of the electromagnetic spectrum are not rigid and overlap between spectral regions is possible.

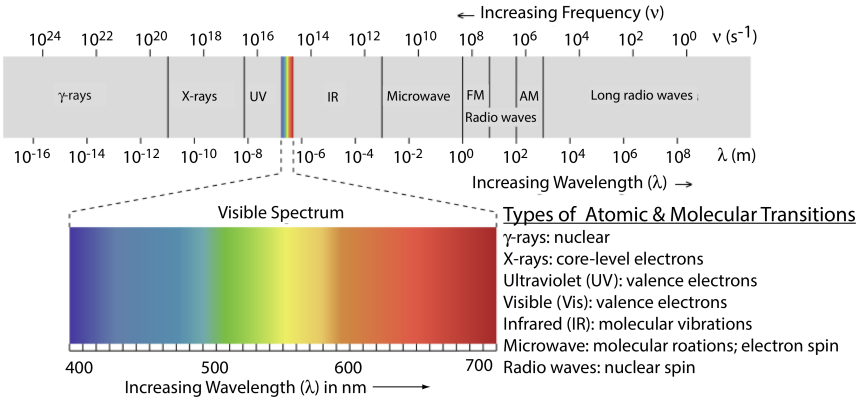

Figure 10.1.3 . The electromagnetic spectrum showing the boundaries between different regions and the type of atomic or molecular transitions responsible for the change in energy. The colored inset shows the visible spectrum. Source: modified from Zedh (www.commons.Wikipedia.org).

Photons as a Signal Source

In the previous section we defined several characteristic properties of electromagnetic radiation, including its energy, velocity, amplitude, frequency, phase angle, polarization, and direction of propagation. A spectroscopic measurement is possible only if the photon's interaction with the sample leads to a change in one or more of these characteristic properties.

We will divide spectroscopy into two broad classes of techniques. In one class of techniques there is a transfer of energy between the photon and the sample. Table 10.1.1 provides a list of several representative examples.

Table 10.1.1 . Examples of Spectroscopic Techniques That Involve an Exchange of Energy Between a Photon and the Sample

type of energy transfer	region of electromagnetic spectrum	spectroscopic technique
absorption	γ-ray	Mossbauer spectroscopy
	X-ray	X-ray absorption spectroscopy
	UV/Vis	*UV/Vis spectroscopy*
	IR	*infrared spectroscopy*
	microwave	raman spectroscopy
	radio wave	electron spin resonance nuclear magnetic resonance
emission (thermal excitation)	UV/Vis	*atomic emission spectroscopy*
photoluminescence	X-ray	X-ray fluorescence
	UV/Vis	*fluorescence spectroscopy* *phosphorescence spectroscopy* atomic fluorescence spectroscopy
chemiluminescence	UV/Vis	chemiluminescence spectroscopy
techniques discussed in this chapter are shown in *italics*		

In absorption spectroscopy a photon is absorbed by an atom or molecule, which undergoes a transition from a lower-energy state to a higher-energy, or excited state (Figure 10.1.4). The type of transition depends on the photon's energy. The electromagnetic spectrum in Figure 10.1.3 , for example, shows that absorbing a photon of visible light promotes one of the atom's or molecule's valence electrons to a higher-energy level. When an molecule absorbs infrared radiation, on the other hand, one of its chemical bonds experiences a change in vibrational energy.

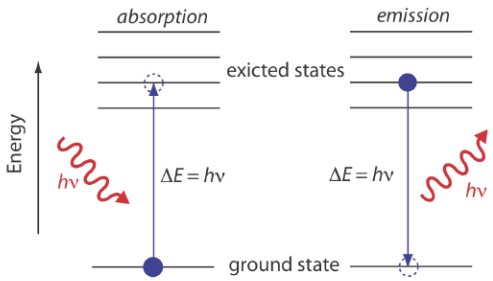

Figure 10.1.4 . A simplified energy diagram that shows the absorption and emission of a photon by an atom or a molecule. When a photon of energy $h\nu$ strikes the atom or molecule, absorption may occur if the difference in energy, ΔE, between the ground state and the excited state is equal to the photon's energy. An atom or molecule in an excited state may emit a photon and return to the ground state. The photon's energy, $h\nu$, equals the difference in energy, ΔE, between the two states.

When it absorbs electromagnetic radiation the number of photons passing through a sample decreases. The measurement of this decrease in photons, which we call ***absorbance***, is a useful analytical signal. Note that each energy level in Figure 10.1.4 has a well-defined value because each is quantized. Absorption occurs only when the photon's energy, $h\nu$, matches the difference in energy, ΔE, between two energy levels. A plot of absorbance as a function of the photon's energy is called an ***absorbance spectrum***. Figure 10.1.5 , for example, shows the absorbance spectrum of cranberry juice.

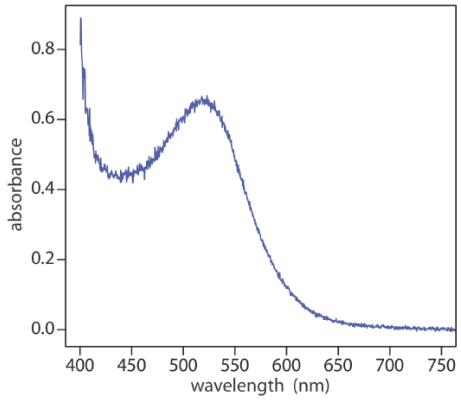

Figure 10.1.5 . Visible absorbance spectrum for cranberry juice. The anthocyanin dyes in cranberry juice absorb visible light with blue, green, and yellow wavelengths (see Figure 10.1.3). As a result, the juice appears red.

When an atom or molecule in an excited state returns to a lower energy state, the excess energy often is released as a photon, a process we call ***emission*** (Figure 10.1.4). There are several ways in which an atom or a molecule may end up in an excited state, including thermal energy, absorption of a photon, or as the result of a chemical reaction. Emission following the absorption of a photon is also called ***photoluminescence***, and that following a chemical reaction is called ***chemiluminescence***. A typical emission spectrum is shown in Figure 10.1.6 .

> Molecules also can release energy in the form of heat. We will return to this point later in the chapter.

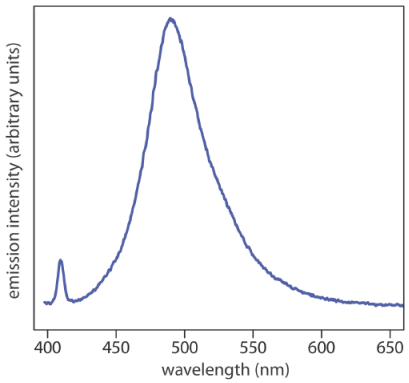

Figure 10.1.6 . Photoluminescence spectrum of the dye coumarin 343, which is incorporated in a reverse micelle suspended in cyclohexanol. The dye's absorbance spectrum (not shown) has a broad peak around 400 nm. The sharp peak at 409 nm is from the laser source used to excite coumarin 343. The broad band centered at approximately 500 nm is the dye's emission band. Because the dye absorbs blue light, a solution of coumarin 343 appears yellow in the absence of photoluminescence. Its photoluminescent emission is blue-green. Source: data from Bridget Gourley, Department of Chemistry & Biochemistry, DePauw University.

In the second broad class of spectroscopic techniques, the electromagnetic radiation undergoes a change in amplitude, phase angle, polarization, or direction of propagation as a result of its refraction, reflection, scattering, diffraction, or dispersion by the sample. Several representative spectroscopic techniques are listed in Table 10.1.2 .

Table 10.1.2 . Examples of Spectroscopic Techniques That Do Not Involve an Exchange of Energy Between a Photon and the Sample

region of electromagnetic spectrum	type of interaction	spectroscopic technique
X-ray	diffraction	X-ray diffraction
UV/Vis	refraction	refractrometry
	scattering	*nephelometry* *turbidimetry*
	dispersion	optical rotary dispersion
techniques discussed in this chapter are shown in *italics*		

Basic Components of Spectroscopic Instruments

The spectroscopic techniques in Table 10.1.1 and Table 10.1.2 use instruments that share several common basic components, including a source of energy, a means for isolating a narrow range of wavelengths, a detector for measuring the signal, and a signal processor that displays the signal in a form convenient for the analyst. In this section we introduce these basic components. Specific instrument designs are considered in later sections.

> You will find a more detailed treatment of these components in the additional resources for this chapter.

Sources of Energy

All forms of spectroscopy require a source of energy. In absorption and scattering spectroscopy this energy is supplied by photons. Emission and photoluminescence spectroscopy use thermal, radiant (photon), or chemical energy to promote the analyte to a suitable excited state.

Sources of Electromagnetic Radiation. A source of electromagnetic radiation must provide an output that is both intense and stable. Sources of electromagnetic radiation are classified as either continuum or line sources. A ***continuum source*** emits radiation over a broad range of wavelengths, with a relatively smooth variation in intensity (Figure 10.1.7). A ***line source***, on the other hand, emits radiation at selected wavelengths (Figure 10.1.8). Table 10.1.3 provides a list of the most common sources of electromagnetic radiation.

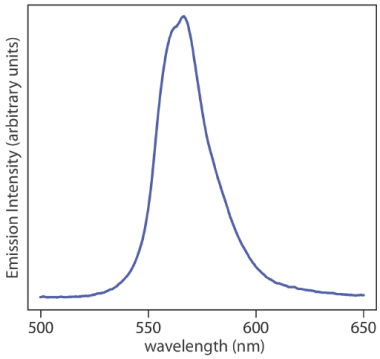

Figure 10.1.7 . Spectrum showing the emission from a green LED, which provides continuous emission over a wavelength range of approximately 530–640 nm.

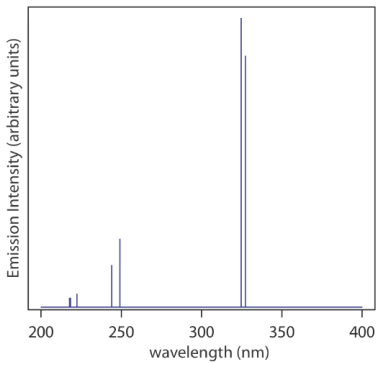

Figure 10.1.8 . Emission spectrum from a Cu hollow cathode lamp. This spectrum consists of seven distinct emission lines (the first two differ by only 0.4 nm and are not resolved at the scale shown in this spectrum). Each emission line has a width of approximately 0.01 nm at 1⁄2 of its maximum intensity.

Table 10.1.3 . Common Source of Electromagnetic Radiation

source	wavelength region	useful for...
H_2 and D_2 lamp	continuum source from 160–380 nm	molecular absorption
tungsten lamp	continuum source from 320–2400 nm	molecular absorption
Xe arc lamp	continuum source from 200–1000 nm	molecular fluorescence
nernst glower	continuum source from 0.4–20 µm	molecular absorption
globar	continuum source from 1–40 µm	molecular absorption
nichrome wire	continuum source from 0.75–20 µm	molecular absorption
hollow cathode lamp	line source in UV/Vis	atomic absorption
Hg vapor lamp	line source in UV/Vis	molecular fluorescence
laser	line source in UV/Vis/Ir	atomic and molecular absorption, fluorescence, and scattering

Sources of Thermal Radiation. The most common sources of thermal energy are flames and plasmas. A flame source uses a combustion of a fuel and an oxidant to achieve temperatures of 2000–3400 K. Plasmas, which are hot, ionized gases, provide temperatures of 6000–10000 K.

Chemical Sources of Energy. Exothermic reactions also may serve as a source of energy. In chemiluminescence the analyte is raised to a higher-energy state by means of a chemical reaction, emitting characteristic radiation when it returns to a lower-energy state. When the chemical reaction results from a biological or enzymatic reaction, the emission of radiation is called bioluminescence. Commercially available “light sticks” and the flash of light from a firefly are examples of chemiluminescence and bioluminescence.

Wavelength Selection

In Nessler's original colorimetric method for ammonia, which was described at the beginning of the chapter, the sample and several standard solutions of ammonia are placed in separate tall, flat-bottomed tubes. As shown in Figure 10.1.9 , after adding the reagents and allowing the color to develop, the analyst evaluates the color by passing ambient light through the bottom of the tubes and looking down through the solutions. By matching the sample's color to that of a standard, the analyst is able to determine the concentration of ammonia in the sample.

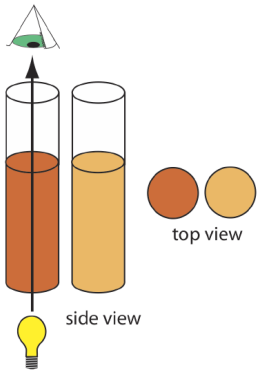

Figure 10.1.9 . Nessler's original method for comparing the color of two solutions. Natural light passes upwards through the samples and standards and the analyst views the solutions by looking down toward the light source. The top view, shown on the right, is what the analyst sees. To determine the analyte's concentration, the analyst exchanges standards until the two colors match.

In Figure 10.1.9 every wavelength of light from the source passes through the sample. This is not a problem if there is only one absorbing species in the sample. If the sample contains two components, then a quantitative analysis using Nessler's original method is impossible unless the standards contains the second component at the same concentration it has in the sample.

To overcome this problem, we want to select a wavelength that only the analyte absorbs. Unfortunately, we can not isolate a single wavelength of radiation from a continuum source, although we can narrow the range of wavelengths that reach the sample. As seen in Figure 10.1.10 , a wavelength selector always passes a narrow band of radiation characterized by a ***nominal wavelength***, an ***effective bandwidth***, and a maximum throughput of radiation. The effective bandwidth is defined as the width of the radiation at half of its maximum throughput.

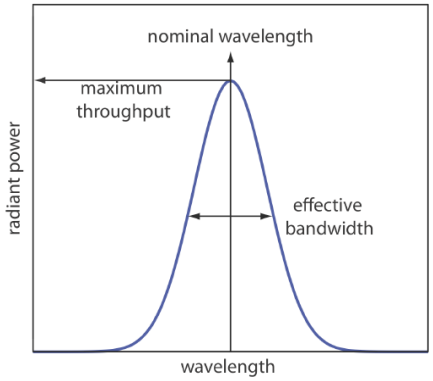

Figure 10.1.10 . Radiation exiting a wavelength selector showing the band's nominal wavelength and its effective bandwidth.

The ideal wavelength selector has a high throughput of radiation and a narrow effective bandwidth. A high throughput is desirable because the more photons that pass through the wavelength selector, the stronger the signal and the smaller the background noise. A narrow effective bandwidth provides a higher ***resolution***, with spectral features separated by more than twice the effective bandwidth being resolved. As shown in Figure 10.1.11 , these two features of a wavelength selector often are in opposition. A larger effective bandwidth favors a higher throughput of radiation, but provide less resolution. Decreasing the effective bandwidth improves resolution, but at the cost of a noisier signal [Jiang, S.; Parker, G. A. *Am. Lab.* **1981**, October, 38–43]. For a qualitative analysis, resolution usually is more important than noise and a smaller effective bandwidth is desirable; however, in a quantitative analysis less noise usually is desirable.

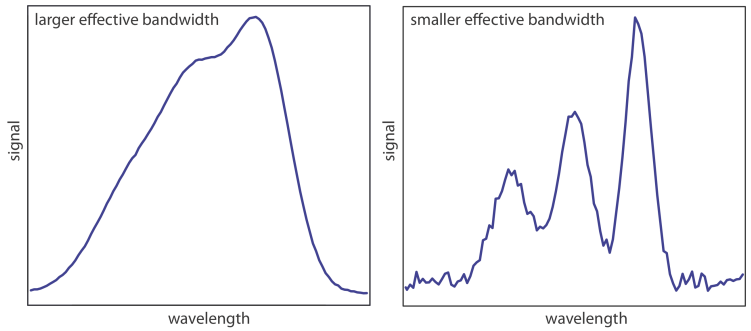

Figure 10.1.11 . Example showing the effect of the wavelength selector's effective bandwidth on resolution and noise. The spectrum with the smaller effective bandwidth (on the right) has a better resolution, allowing us to see the presence of three peaks, but at the expense of a noisier signal. The spectrum with the larger effective bandwidth (on the left) has less noise, but at the expense of less resolution between the three peaks.

Wavelength Selection Using Filters. The simplest method for isolating a narrow band of radiation is to use an absorption or interference ***filter***. Absorption filters work by selectively absorbing radiation from a narrow region of the electromagnetic spectrum. Interference filters use constructive and destructive interference to isolate a narrow range of wavelengths. A simple example of an absorption filter is a piece of colored glass. A purple filter, for example, removes the complementary color green from 500–560 nm.

Commercially available absorption filters provide effective bandwidths of 30–250 nm, although the throughput at the low end of this range often is only 10% of the source's emission intensity. Interference filters are more expensive than absorption filters, but have narrower effective bandwidths, typically 10–20 nm, with maximum throughputs of at least 40%.

Wavelength Selection Using Monochromators. A filter has one significant limitation—because a filter has a fixed nominal wavelength, if we need to make measurements at two different wavelengths, then we must use two different filters. A ***monochromator*** is an alternative method for selecting a narrow band of radiation that also allows us to continuously adjust the band's nominal wavelength.

The construction of a typical monochromator is shown in Figure 10.1.12 . Radiation from the source enters the monochromator through an entrance slit. The radiation is collected by a collimating mirror, which reflects a parallel beam of radiation to a diffraction grating. The diffraction grating is an optically reflecting surface with a large number of parallel grooves (see insert to Figure 10.1.12). The diffraction grating disperses the radiation and a second mirror focuses the radiation onto a planar surface that contains an exit slit. In some monochromators a prism is used in place of the diffraction grating.

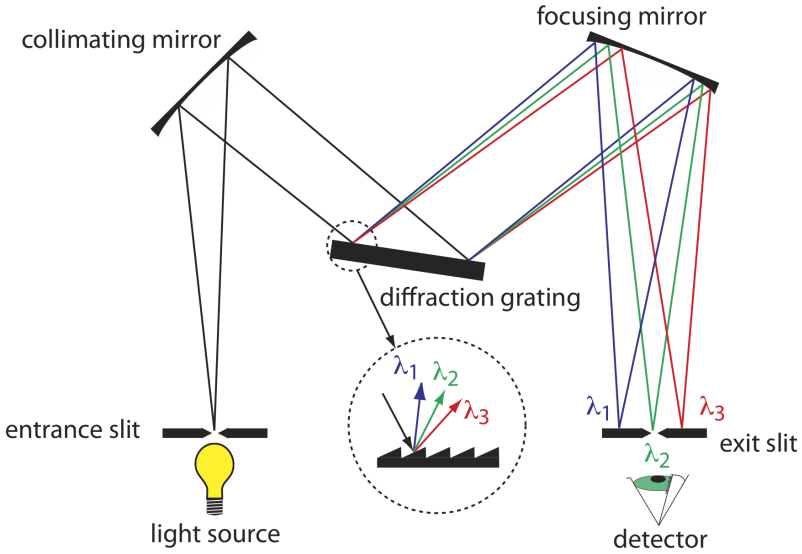

Figure 10.1.12 . Schematic diagram of a monochromator that uses a diffraction grating to disperse the radiation.

Radiation exits the monochromator and passes to the detector. As shown in Figure 10.1.12 , a monochromator converts a ***polychromatic*** source of radiation at the entrance slit to a ***monochromatic*** source of finite effective bandwidth at the exit slit. The choice of which wavelength exits the monochromator is determined by rotating the diffraction grating. A narrower exit slit provides a smaller effective bandwidth and better resolution than does a wider exit slit, but at the cost of a smaller throughput of radiation.

> Polychromatic means many colored. Polychromatic radiation contains many different wavelengths of light. Monochromatic means one color, or one wavelength. Although the light exiting a monochromator is not strictly of a single wavelength, its narrow effective bandwidth allows us to think of it as monochromatic.

Monochromators are classified as either fixed-wavelength or scanning. In a fixed-wavelength monochromator we manually select the wavelength by rotating the grating. Normally a fixed-wavelength monochromator is used for a quantitative analysis where measurements are made at one or two wavelengths. A scanning monochromator includes a drive mechanism that continuously rotates the grating, which allows successive wavelengths of light to exit from the monochromator. A scanning monochromator is used to acquire spectra, and, when operated in a fixed-wavelength mode, for a quantitative analysis.

Interferometers. An ***interferometer*** provides an alternative approach for wavelength selection. Instead of filtering or dispersing the electromagnetic radiation, an interferometer allows source radiation of all wavelengths to reach the detector simultaneously (Figure 10.1.13). Radiation from the source is focused on a beam splitter that reflects half of the radiation to a fixed mirror and transmits the other half to a moving mirror. The radiation recombines at the beam splitter, where constructive and destructive interference determines, for each wavelength, the intensity of light that reaches the detector. As the moving mirror changes position, the wavelength of light that experiences maximum constructive interference and maximum destructive interference also changes. The signal at the detector shows intensity as a function of the moving mirror's position, expressed in units of distance or time. The result is called an ***interferogram*** or a time domain spectrum. The time domain spectrum is converted mathematically, by a process called a Fourier transform, to a spectrum (a frequency domain spectrum) that shows intensity as a function of the radiation's energy.

> The mathematical details of the Fourier transform are beyond the level of this textbook. You can consult the chapter's additional resources for additional information.

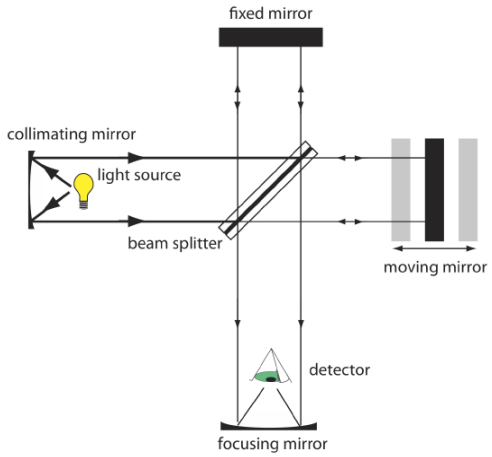

Figure 10.1.13 . Schematic diagram of an interferometers.

In comparison to a monochromator, an interferometer has two significant advantages. The first advantage, which is termed ***Jacquinot's advantage***, is the greater throughput of source radiation. Because an interferometer does not use slits and has fewer optical components from which radiation is scattered and lost, the throughput of radiation reaching the detector is $80-200\times$ greater than that for a monochromator. The result is less noise. The second advantage, which is called ***Fellgett's advantage***, is a savings in the time needed to obtain a spectrum. Because the detector monitors all frequencies simultaneously, a spectrum takes approximately one second to record, as compared to 10–15 minutes when using a scanning monochromator.

Detectors

In Nessler's original method for determining ammonia (Figure 10.1.9) the analyst's eye serves as the detector, matching the sample's color to that of a standard. The human eye, of course, has a poor range—it responds only to visible light—and it is not particularly sensitive or accurate. Modern detectors use a sensitive ***transducer*** to convert a signal consisting of photons into an easily measured electrical signal. Ideally the detector's signal, *S*, is a linear function of the electromagnetic radiation's power, *P*,

$$S = kP + D$$

where *k* is the detector's sensitivity, and *D* is the detector's ***dark current***, or the background current when we prevent the source's radiation from reaching the detector.

There are two broad classes of spectroscopic transducers: thermal transducers and photon transducers. Table 10.1.4 provides several representative examples of each class of transducers.

> Transducer is a general term that refers to any device that converts a chemical or a physical property into an easily measured electrical signal. The retina in your eye, for example, is a transducer that converts photons into an electrical nerve impulse; your eardrum is a transducer that converts sound waves into a different electrical nerve impulse.

Table 10.1.4 . Examples of Transducers for Spectroscopy

transducer	class	wavelength range	output signal
phototube	photon	200–1000 nm	current
photomultiplier	photon	110–1000 nm	current
Si photodiode	photon	250–1100 nm	current
photoconductor	photon	750–6000 nm	change in resistance
photovoltaic cell	photon	400–5000 nm	current or voltage
thermocouple	thermal	0.8–40 μm	voltage
thermistor	thermal	0.8–40 μm	change in resistance
pneumatic	thermal	0.8–1000 μm	membrane displacement
pyroelectric	thermal	0.3–1000 μm	current

Photon Transducers. Phototubes and photomultipliers use a photosensitive surface that absorbs radiation in the ultraviolet, visible, or near IR to produce an electrical current that is proportional to the number of photons reaching the transducer (Figure 10.1.14). Other photon detectors use a semiconductor as the photosensitive surface. When the semiconductor absorbs photons, valence electrons move to the semiconductor's conduction band, producing a measurable current. One advantage of the Si photodiode is that it is easy to miniaturize. Groups of photodiodes are gathered together in a linear array that contains 64–4096 individual photodiodes. With a width of 25 μm per diode, a linear array of 2048 photodiodes requires only 51.2 mm of linear space. By placing a ***photodiode array*** along the monochromator's focal plane, it is possible to monitor simultaneously an entire range of wavelengths.

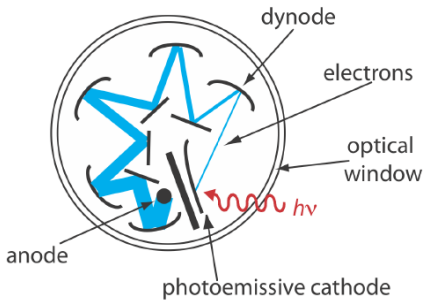

Figure 10.1.14 . Schematic of a photomultiplier. A photon strikes the photoemissive cathode producing electrons, which accelerate toward a positively charged dynode. Collision of these electrons with the dynode generates additional electrons, which accelerate toward the next dynode. A total of 10^6–10^7 electrons per photon eventually reach the anode, generating an electrical current.

Thermal Transducers. Infrared photons do not have enough energy to produce a measurable current with a photon transducer. A thermal transducer, therefore, is used for infrared spectroscopy. The absorption of infrared photons increases a thermal transducer's temperature, changing one or more of its characteristic properties. A pneumatic transducer, for example, is a small tube of xenon gas with an IR transparent window at one end and a flexible membrane at the other end. Photons enter the tube and are absorbed by a blackened surface, increasing the temperature of the gas. As the temperature inside the tube fluctuates, the gas expands and contracts and the flexible membrane moves in and out. Monitoring the membrane's displacement produces an electrical signal.

Signal Processors

A transducer's electrical signal is sent to a ***signal processor*** where it is displayed in a form that is more convenient for the analyst. Examples of signal processors include analog or digital meters, recorders, and computers equipped with digital acquisition boards. A signal processor also is used to calibrate the detector's response, to amplify the transducer's signal, to remove noise by filtering, or to mathematically transform the signal.

> If the retina in your eye and the eardrum in your ear are transducers, then your brain is the signal processor.

1.2: Spectroscopy Based on Absorption

In absorption spectroscopy a beam of electromagnetic radiation passes through a sample. Much of the radiation passes through the sample without a loss in intensity. At selected wavelengths, however, the radiation's intensity is attenuated. This process of attenuation is called absorption.

Absorption Spectra

There are two general requirements for an analyte's absorption of electromagnetic radiation. First, there must be a mechanism by which the radiation's electric field or magnetic field interacts with the analyte. For ultraviolet and visible radiation, absorption of a photon changes the energy of the analyte's valence electrons. A bond's vibrational energy is altered by the absorption of infrared radiation.

> Figure 10.1.3 provides a list of the types of atomic and molecular transitions associated with different types of electromagnetic radiation.

The second requirement is that the photon's energy, $h\nu$, must exactly equal the difference in energy, ΔE, between two of the analyte's quantized energy states. Figure 10.1.4 shows a simplified view of a photon's absorption, which is useful because it emphasizes that the photon's energy must match the difference in energy between a lower-energy state and a higher-energy state. What is missing, however, is information about what types of energy states are involved, which transitions between energy states are likely to occur, and the appearance of the resulting spectrum.

We can use the energy level diagram in Figure 10.2.1 to explain an absorbance spectrum. The lines labeled E_0 and E_1 represent the analyte's ground (lowest) electronic state and its first electronic excited state. Superimposed on each electronic energy level is a series of lines representing vibrational energy levels.

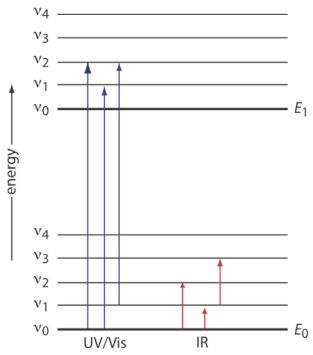

Figure 10.2.1 . Diagram showing two electronic energy levels (E_0 and E_1), each with five vibrational energy levels ν_{0-4}. Absorption of ultraviolet and visible radiation (shown by the blue arrows) leads to a change in the analyte's electronic energy levels and, possibly, a change in vibrational energy as well. A change in vibrational energy without a change in electronic energy levels occurs with the absorption of infrared radiation (shown by the red arrows).

Infrared Spectra for Molecules and Polyatomic Ions

The energy of infrared radiation produces a change in a molecule's or a polyatomic ion's vibrational energy, but is not sufficient to effect a change in its electronic energy. As shown in Figure 10.2.1 , vibrational energy levels are quantized; that is, a molecule or polyatomic ion has only certain, discrete vibrational energies. The energy for an allowed vibrational mode, E_ν, is

$$E_\nu = \nu + \frac{1}{2}h\nu_0$$

where ν is the vibrational quantum number, which has values of 0, 1, 2, ..., and ν_0 is the bond's fundamental vibrational frequency. The value of ν_0, which is determined by the bond's strength and by the mass at each end of the bond, is a characteristic property of a bond. For example, a carbon-carbon single bond (C–C) absorbs infrared radiation at a lower energy than a carbon-carbon double bond (C=C) because a single bond is weaker than a double bond.

At room temperature most molecules are in their ground vibrational state ($\nu = 0$) . A transition from the ground vibrational state to the first vibrational excited state ($\nu = 1$) requires absorption of a photon with an energy of $h\nu_0$. Transitions in which $\Delta\nu = \pm 1$ give rise to the fundamental absorption lines. Weaker absorption lines, called overtones, result from transitions in which $\Delta\nu$ is ±2 or ±3. The number of possible normal vibrational modes for a linear molecule is $3N - 5$, and for a non-linear molecule is $3N - 6$, where N is the number of atoms in the molecule. Not surprisingly, infrared spectra often show a considerable number of absorption bands. Even a relatively simple molecule, such as ethanol (C_2H_6O), for example, has $3 \times 9 - 6$, or 21 possible normal modes of vibration, although not all of these vibrational modes give rise to an absorption. The IR spectrum for ethanol is shown in Figure 10.2.2 .

Why does a non-linear molecule have $3N - 6$ vibrational modes? Consider a molecule of methane, CH_4. Each of methane's five atoms can move in one of three directions (x, y, and z) for a total of $5 \times 3 = 15$ different ways in which the molecule's atoms can move. A molecule can move in three ways: it can move from one place to another, which we call translational motion; it can rotate around an axis, which we call rotational motion; and its bonds can stretch and bend, which we call vibrational motion. Because the entire molecule can move in the x, y, and z directions, three of methane's 15 different motions are translational. In addition, the molecule can rotate about its x, y, and z axes, accounting for three additional forms of motion. This leaves 15 – 3 – 3 = 9 vibrational modes. A linear molecule, such as CO_2, has $3N - 5$ vibrational modes because it can rotate around only two axes.

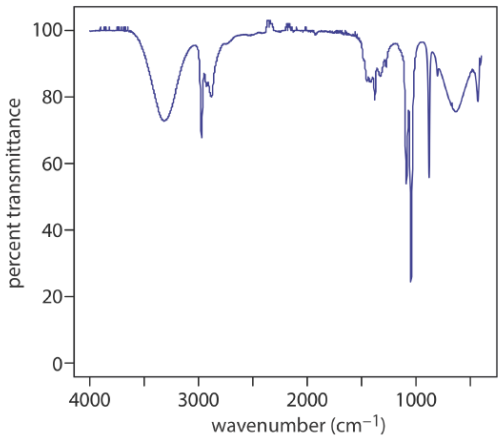

Figure 10.2.2 . Infrared spectrum of ethanol.

UV/Vis Spectra for Molecules and Ions

The valence electrons in organic molecules and polyatomic ions, such as CO_3^{2-}, occupy quantized sigma bonding (σ), pi bonding (π), and non-bonding (n) molecular orbitals (MOs). Unoccupied sigma antibonding (σ^*) and pi antibonding (π^*) molecular orbitals are slightly higher in energy. Because the difference in energy between the highest-energy occupied MOs and the lowest-energy unoccupied MOs corresponds to ultraviolet and visible radiation, absorption of a photon is possible.

Four types of transitions between quantized energy levels account for most molecular UV/Vis spectra. Table 10.2.1 lists the approximate wavelength ranges for these transitions, as well as a partial list of bonds, functional groups, or molecules responsible for these transitions. Of these transitions, the most important are $n \rightarrow \pi^*$ and $\pi \rightarrow \pi^*$ because they involve important functional groups that are characteristic of many analytes and because the wavelengths are easily accessible. The bonds and functional groups that give rise to the absorption of ultraviolet and visible radiation are called ***chromophores***.

Table 10.2.1 . Electronic Transitions Involving n, σ, and π Molecular Orbitals

transition	wavelength range	examples
$\sigma \rightarrow \sigma^*$	<200 nm	C—C, C—H
$n \rightarrow \sigma^*$	160–260 nm	H_2O, CH_3OH, CH_3Cl
$\pi \rightarrow \pi^*$	200–500 nm	C=C, C=O, C=N, C≡C

transition	wavelength range	examples
$n \rightarrow \pi^*$	250–600 nm	C=O, C=N, N=N, N=O

Many transition metal ions, such as Cu^{2+} and Co^{2+}, form colorful solutions because the metal ion absorbs visible light. The transitions that give rise to this absorption are valence electrons in the metal ion's *d*-orbitals. For a free metal ion, the five *d*-orbitals are of equal energy. In the presence of a complexing ligand or solvent molecule, however, the *d*-orbitals split into two or more groups that differ in energy. For example, in an octahedral complex of $Cu(H_2O)_6^{2+}$ the six water molecules perturb the *d*-orbitals into the two groups shown in Figure 10.2.3 . The resulting $d \rightarrow d$ transitions for transition metal ions are relatively weak.

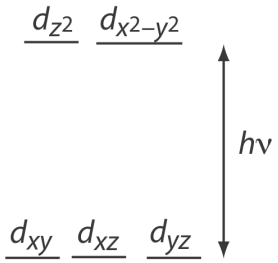

Figure 10.2.3 . Splitting of the *d*-orbitals in an octahedral field.

A more important source of UV/Vis absorption for inorganic metal–ligand complexes is charge transfer, in which absorption of a photon produces an excited state in which there is transfer of an electron from the metal, *M*, to the ligand, *L*.

$$M - L + h\nu \rightarrow \left(M^+ - L^-\right)^*$$

Charge-transfer absorption is important because it produces very large absorbances. One important example of a charge-transfer complex is that of *o*-phenanthroline with Fe^{2+}, the UV/Vis spectrum for which is shown in Figure 10.2.4 . Charge-transfer absorption in which an electron moves from the ligand to the metal also is possible.

> Why is a larger absorbance desirable? An analytical method is more sensitive if a smaller concentration of analyte gives a larger signal.

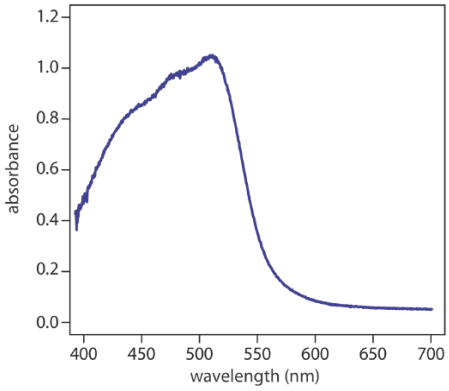

Figure 10.2.4 . UV/Vis spectrum for the metal–ligand complex $Fe(phen)_3^{2+}$, where phen is the ligand *o*-phenanthroline.

Comparing the IR spectrum in Figure 10.2.2 to the UV/Vis spectrum in Figure 10.2.4 shows us that UV/Vis absorption bands are often significantly broader than those for IR absorption. We can use Figure 10.2.1 to explain why this is true. When a species absorbs UV/Vis radiation, the transition between electronic energy levels may also include a transition between vibrational energy levels. The result is a number of closely spaced absorption bands that merge together to form a single broad absorption band.

UV/Vis Spectra for Atoms

The energy of ultraviolet and visible electromagnetic radiation is sufficient to cause a change in an atom's valence electron configuration. Sodium, for example, has a single valence electron in its 3*s* atomic orbital. As shown in Figure 10.2.5 , unoccupied,

higher energy atomic orbitals also exist.

> The valence shell energy level diagram in Figure 10.2.5 might strike you as odd because it shows that the 3*p* orbitals are split into two groups of slightly different energy. The reasons for this splitting are unimportant in the context of our treatment of atomic absorption. For further information about the reasons for this splitting, consult the chapter's additional resources.

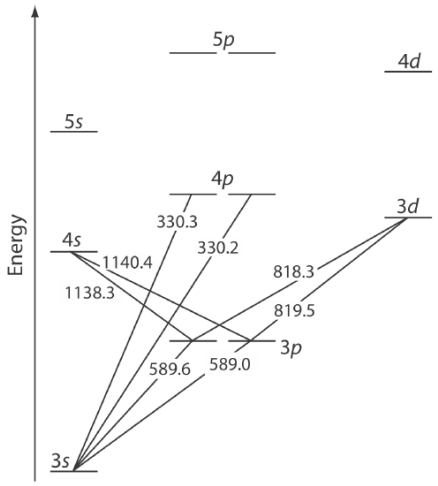

Figure 10.2.5 . Valence shell energy level diagram for sodium. The wavelengths (in wavenumbers) corresponding to several transitions are shown.

Absorption of a photon is accompanied by the excitation of an electron from a lower-energy atomic orbital to an atomic orbital of higher energy. Not all possible transitions between atomic orbitals are allowed. For sodium the only allowed transitions are those in which there is a change of ±1 in the orbital quantum number (*l*); thus transitions from $s \rightarrow p$ orbitals are allowed, but transitions from $s \rightarrow s$ and from $s \rightarrow d$ orbitals are forbidden.

The atomic absorption spectrum for Na is shown in Figure 10.2.6 , and is typical of that found for most atoms. The most obvious feature of this spectrum is that it consists of a small number of discrete absorption lines that correspond to transitions between the ground state (the 3*s* atomic orbital) and the 3*p* and the 4*p* atomic orbitals. Absorption from excited states, such as the $3p \rightarrow 4s$ and the $3p \rightarrow 3d$ transitions included in Figure 10.2.5 , are too weak to detect. Because an excited state's lifetime is short—an excited state atom typically returns to a lower energy state in 10^{-7} to 10^{-8} seconds—an atom in the exited state is likely to return to the ground state before it has an opportunity to absorb a photon.

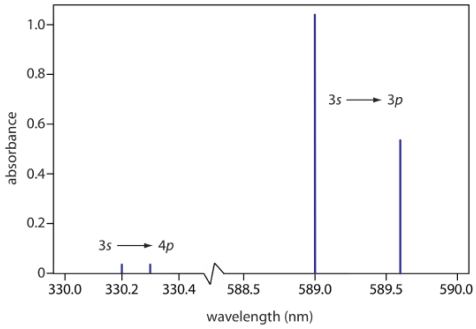

Figure 10.2.6 . Atomic absorption spectrum for sodium. Note that the scale on the *x*-axis includes a break.

Another feature of the atomic absorption spectrum in Figure 10.2.6 is the narrow width of the absorption lines, which is a consequence of the fixed difference in energy between the ground state and the excited state, and the lack of vibrational and rotational energy levels. Natural line widths for atomic absorption, which are governed by the uncertainty principle, are approximately 10^{-5} nm. Other contributions to broadening increase this line width to approximately 10^{-3} nm.

Transmittance and Absorbance

As light passes through a sample, its power decreases as some of it is absorbed. This attenuation of radiation is described quantitatively by two separate, but related terms: transmittance and absorbance. As shown in Figure 10.2.7 a, transmittance is the ratio of the source radiation's power as it exits the sample, P_T, to that incident on the sample, P_0.

$$T = \frac{P_T}{P_0} \tag{1.2.1}$$

Multiplying the transmittance by 100 gives the percent transmittance, $\%T$, which varies between 100% (no absorption) and 0% (complete absorption). All methods of detecting photons—including the human eye and modern photoelectric transducers—measure the transmittance of electromagnetic radiation.

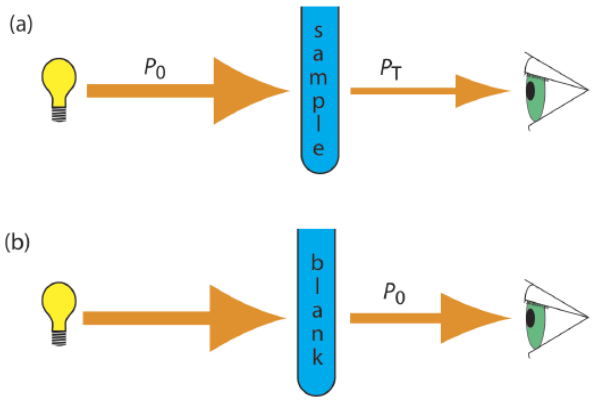

Figure 10.2.7 . (a) Schematic diagram showing the attenuation of radiation passing through a sample; P_0 is the source's radiant power and P_T is the radiant power transmitted by the sample. (b) Schematic diagram showing how we redefine P_0 as the radiant power transmitted by the blank. Redefining P_0 in this way corrects the transmittance in (a) for the loss of radiation due to scattering, reflection, absorption by the sample's container, and absorption by the sample's matrix.

Equation 1.2.1 does not distinguish between different mechanisms that prevent a photon emitted by the source from reaching the detector. In addition to absorption by the analyte, several additional phenomena contribute to the attenuation of radiation, including reflection and absorption by the sample's container, absorption by other components in the sample's matrix, and the scattering of radiation. To compensate for this loss of the radiation's power, we use a method blank. As shown in Figure 10.2.7 b, we redefine P_0 as the power exiting the method blank.

An alternative method for expressing the attenuation of electromagnetic radiation is absorbance, A, which we define as

$$A = -\log T = -\log \frac{P_T}{P_0} \tag{1.2.2}$$

Absorbance is the more common unit for expressing the attenuation of radiation because it is a linear function of the analyte's concentration.

> We will show that this is true in the next section when we introduce Beer's law.

Example 10.2.1

A sample has a percent transmittance of 50%. What is its absorbance?

Solution

A percent transmittance of 50.0% is the same as a transmittance of 0.500. Substituting into Equation 1.2.2 gives

$$A = -\log T = -\log(0.500) = 0.301$$

Exercise 10.2.1

What is the $\%T$ for a sample if its absorbance is 1.27?

Answer

To find the transmittance, T, we begin by noting that

$$A = 1.27 = -\log T$$

Solving for T

$$-1.27 = \log T$$
$$10^{-1.27} = T$$

gives a transmittance of 0.054, or a %T of 5.4%.

Equation 1.2.1 has an important consequence for atomic absorption. As we learned from Figure 10.2.6 , atomic absorption lines are very narrow. Even with a high quality monochromator, the effective bandwidth for a continuum source is $100 - 1000\times$ greater than the width of an atomic absorption line. As a result, little radiation from a continuum source is absorbed when it passes through a sample of atoms; because $P_0 \approx P_T$ the measured absorbance effectively is zero. For this reason, atomic absorption requires that we use a line source instead of a continuum source.

Absorbance and Concentration: Beer's Law

When monochromatic electromagnetic radiation passes through an infinitesimally thin layer of sample of thickness *dx*, it experiences a decrease in its power of *dP* (Figure 10.2.8).

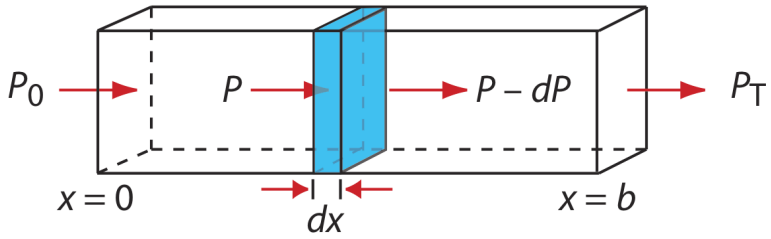

Figure 10.2.8 . Factors used to derive the Beer's law.

This fractional decrease in power is proportional to the sample's thickness and to the analyte's concentration, *C*; thus

$$-\frac{dP}{P} = \alpha C dx \tag{1.2.3}$$

where *P* is the power incident on the thin layer of sample and α is a proportionality constant. Integrating the left side of Equation 1.2.3 over the sample's full thickness

$$-\int_{P=P_0}^{P=P_t} \frac{dP}{P} = \alpha C \int_{x=0}^{x=b} dx$$
$$\ln \frac{P_0}{P_T} = \alpha b C$$

converting from ln to log, and substituting into Equation 1.2.2, gives

$$A = abC \tag{1.2.4}$$

where *a* is the analyte's ***absorptivity*** with units of cm^{-1} $conc^{-1}$. If we express the concentration using molarity, then we replace *a* with the ***molar absorptivity***, ε, which has units of cm^{-1} M^{-1}.

$$A = \varepsilon bC \tag{1.2.5}$$

The absorptivity and the molar absorptivity are proportional to the probability that the analyte absorbs a photon of a given energy. As a result, values for both *a* and ε depend on the wavelength of the absorbed photon.

✔ Example 10.2.2

A 5.00×10^{-4} M solution of analyte is placed in a sample cell that has a pathlength of 1.00 cm. At a wavelength of 490 nm, the solution's absorbance is 0.338. What is the analyte's molar absorptivity at this wavelength?

Solution

Solving Equation 1.2.5 for ϵ and making appropriate substitutions gives

$$\varepsilon = \frac{A}{bC} = \frac{0.338}{(1.00\text{ cm})\left(5.00 \times 10^{-4}\text{ M}\right)} = 676\text{ cm}^{-1}\text{ M}^{-1}$$

? Exercise 10.2.2

A solution of the analyte from Example 10.2.2 has an absorbance of 0.228 in a 1.00-cm sample cell. What is the analyte's concentration?

Answer

Making appropriate substitutions into Beer's law

$$A = 0.228 = \varepsilon bC = \left(676\text{ M}^{-1}\text{ cm}^{-1}\right)(1\text{ cm})C$$

and solving for *C* gives a concentration of 3.37×10^{-4} M.

Equation 1.2.4 and Equation 1.2.5, which establish the linear relationship between absorbance and concentration, are known as Beer's law. Calibration curves based on Beer's law are common in quantitative analyses.

As is often the case, the formulation of a law is more complicated than its name suggests. This is the case, for example, with Beer's law, which also is known as the Beer-Lambert law or the Beer-Lambert-Bouguer law. Pierre Bouguer, in 1729, and Johann Lambert, in 1760, noted that the transmittance of light decreases exponentially with an increase in the sample's thickness.

$$T \propto e^{-b}$$

Later, in 1852, August Beer noted that the transmittance of light decreases exponentially as the concentration of the absorbing species increases.

$$T \propto e^{-C}$$

Together, and when written in terms of absorbance instead of transmittance, these two relationships make up what we know as Beer's law.

Beer's Law and Multicomponent Samples

We can extend Beer's law to a sample that contains several absorbing components. If there are no interactions between the components, then the individual absorbances, A_i, are additive. For a two-component mixture of analyte's *X* and *Y*, the total absorbance, A_{tot}, is

$$A_{tot} = A_X + A_Y = \varepsilon_X bC_X + \varepsilon_Y bC_Y$$

Generalizing, the absorbance for a mixture of *n* components, A_{mix}, is

$$A_{mix} = \sum_{i=1}^{n} A_i = \sum_{i=1}^{n} \varepsilon_i bC_i \tag{1.2.6}$$

Limitations to Beer's Law

Beer's law suggests that a plot of absorbance vs. concentration—we will call this a Beer's law plot—is a straight line with a *y*-intercept of zero and a slope of *ab* or εb. In some cases a Beer's law plot deviates from this ideal behavior (see Figure 10.2.9), and such deviations from linearity are divided into three categories: fundamental, chemical, and instrumental.

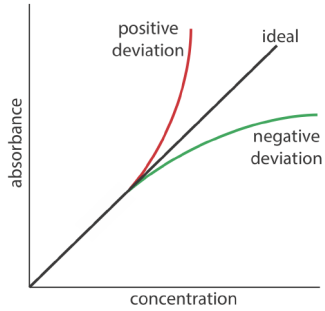

Figure 10.2.9 . Plots of absorbance vs. concentration showing positive and negative deviations from the ideal Beer's law relationship, which is a straight line.

Fundamental Limitations to Beer's Law

Beer's law is a limiting law that is valid only for low concentrations of analyte. There are two contributions to this fundamental limitation to Beer's law. At higher concentrations the individual particles of analyte no longer are independent of each other. The resulting interaction between particles of analyte may change the analyte's absorptivity. A second contribution is that an analyte's absorptivity depends on the solution's refractive index. Because a solution's refractive index varies with the analyte's concentration, values of a and ε may change. For sufficiently low concentrations of analyte, the refractive index essentially is constant and a Beer's law plot is linear.

Chemical Limitations to Beer's Law

A chemical deviation from Beer's law may occur if the analyte is involved in an equilibrium reaction. Consider, for example, the weak acid, HA. To construct a Beer's law plot we prepare a series of standard solutions—each of which contains a known total concentration of HA—and then measure each solution's absorbance at the same wavelength. Because HA is a weak acid, it is in equilibrium with its conjugate weak base, A^-.

> In the equations that follow, the conjugate weak base A^- is written as A as it is easy to mistake the symbol for anionic charge as a minus sign.

$$HA(aq) + H_2O(l) \rightleftharpoons H_3O^+(aq) + A^-(aq)$$

If both HA and A^- absorb at the selected wavelength, then Beer's law is

$$A = \varepsilon_{HA} b C_{HA} + \varepsilon_A b C_A \tag{1.2.7}$$

Because the weak acid's total concentration, C_{total}, is

$$C_{total} = C_{HA} + C_A$$

we can write the concentrations of HA and A^- as

$$C_{HA} = \alpha_{HA} C_{total} \tag{1.2.8}$$

$$C_A = (1 - \alpha_{HA}) C_{total} \tag{1.2.9}$$

where α_{HA} is the fraction of weak acid present as HA. Substituting Equation 1.2.8 and Equation 1.2.9 into Equation 1.2.7 and rearranging, gives

$$A = (\varepsilon_{HA}\alpha_{HA} + \varepsilon_A - \varepsilon_A\alpha_A)\, b C_{total} \tag{1.2.10}$$

To obtain a linear Beer's law plot, we must satisfy one of two conditions. If ε_{HA} and ε_A have the same value at the selected wavelength, then Equation 1.2.10 simplifies to

$$A = \varepsilon_A b C_{total} = \varepsilon_{HA} b C_{total}$$

Alternatively, if α_{HA} has the same value for all standard solutions, then each term within the parentheses of Equation 1.2.10 is constant—which we replace with k—and a linear calibration curve is obtained at any wavelength.

$$A = kbC_{\text{total}}$$

Because HA is a weak acid, the value of α_{HA} varies with pH. To hold α_{HA} constant we buffer each standard solution to the same pH. Depending on the relative values of α_{HA} and α_{A}, the calibration curve has a positive or a negative deviation from Beer's law if we do not buffer the standards to the same pH.

Instrumental Limitations to Beer's Law

There are two principal instrumental limitations to Beer's law. The first limitation is that Beer's law assumes that radiation reaching the sample is of a single wavelength—that is, it assumes a purely monochromatic source of radiation. As shown in Figure 10.1.10, even the best wavelength selector passes radiation with a small, but finite effective bandwidth. Polychromatic radiation always gives a negative deviation from Beer's law, but the effect is smaller if the value of ε essentially is constant over the wavelength range passed by the wavelength selector. For this reason, as shown in Figure 10.2.10 , it is better to make absorbance measurements at the top of a broad absorption peak. In addition, the deviation from Beer's law is less serious if the source's effective bandwidth is less than one-tenth of the absorbing species' natural bandwidth [(a) Strong, F. C., III *Anal. Chem.* **1984**, *56*, 16A–34A; Gilbert, D. D. *J. Chem. Educ.* **1991**, *68*, A278–A281]. When measurements must be made on a slope, linearity is improved by using a narrower effective bandwidth.

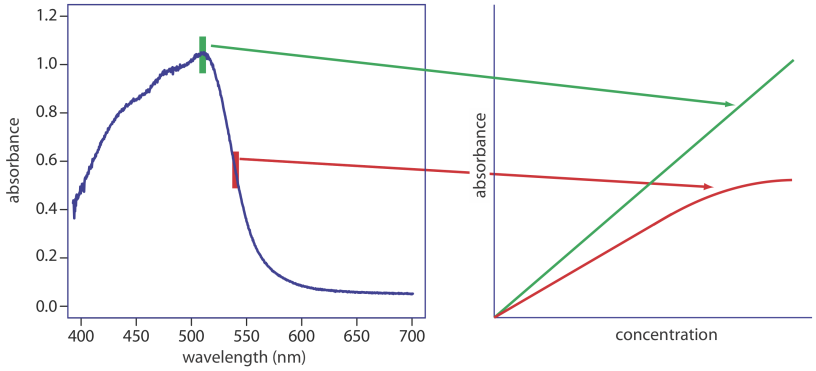

Figure 10.2.10 . Effect of wavelength selection on the linearity of a Beer's law plot. Another reason for measuring absorbance at the top of an absorbance peak is that it provides for a more sensitive analysis. Note that the green Beer's law plot has a steeper slope—and, therefore, a greater sensitivity—than the red Beer's law plot. A Beer's law plot, of course, is equivalent to a calibration curve.

Stray radiation is the second contribution to instrumental deviations from Beer's law. Stray radiation arises from imperfections in the wavelength selector that allow light to enter the instrument and to reach the detector without passing through the sample. Stray radiation adds an additional contribution, P_{stray}, to the radiant power that reaches the detector; thus

$$A = -\log \frac{P_{\text{T}} + P_{\text{stray}}}{P_0 + P_{\text{stray}}}$$

For a small concentration of analyte, P_{stray} is significantly smaller than P_0 and P_{T}, and the absorbance is unaffected by the stray radiation. For higher concentrations of analyte, less light passes through the sample and P_{T} and P_{stray} become similar in magnitude. This results is an absorbance that is smaller than expected, and a negative deviation from Beer's law.

1.3: UV/Vis and IR Spectroscopy

In Figure 10.1.9 we examined Nessler's original method for matching the color of a sample to the color of a standard. Matching colors is a labor intensive process for the analyst and, not surprisingly, spectroscopic methods of analysis were slow to find favor. The 1930s and 1940s saw the introduction of photoelectric transducers for ultraviolet and visible radiation, and thermocouples for infrared radiation. As a result, modern instrumentation for absorption spectroscopy routinely became available in the 1940s—further progress has been rapid ever since.

Instrumentation

Frequently an analyst must select from among several instruments of different design, the one instrument best suited for a particular analysis. In this section we examine several different instruments for molecular absorption spectroscopy, with an emphasis on their advantages and limitations. Methods of sample introduction also are covered in this section.

Instrument Designs for Molecular UV/Vis Absorption

Filter Photometer. The simplest instrument for molecular UV/Vis absorption is a ***filter photometer*** (Figure 10.3.1), which uses an absorption or interference filter to isolate a band of radiation. The filter is placed between the source and the sample to prevent the sample from decomposing when exposed to higher energy radiation. A filter photometer has a single optical path between the source and detector, and is called a ***single-beam*** instrument. The instrument is calibrated to 0% T while using a shutter to block the source radiation from the detector. After opening the shutter, the instrument is calibrated to 100% T using an appropriate blank. The blank is then replaced with the sample and its transmittance measured. Because the source's incident power and the sensitivity of the detector vary with wavelength, the photometer is recalibrated whenever the filter is changed. Photometers have the advantage of being relatively inexpensive, rugged, and easy to maintain. Another advantage of a photometer is its portability, making it easy to take into the field. Disadvantages of a photometer include the inability to record an absorption spectrum and the source's relatively large effective bandwidth, which limits the calibration curve's linearity.

> The percent transmittance varies between 0% and 100%. As we learned from Figure 10.2.7, we use a blank to determine P_0, which corresponds to 100%T. Even in the absence of light the detector records a signal. Closing the shutter allows us to assign 0%T to this signal. Together, setting 0% T and 100%T calibrates the instrument. The amount of light that passes through a sample produces a signal that is greater than or equal to 0%T and smaller than or equal to 100%T.

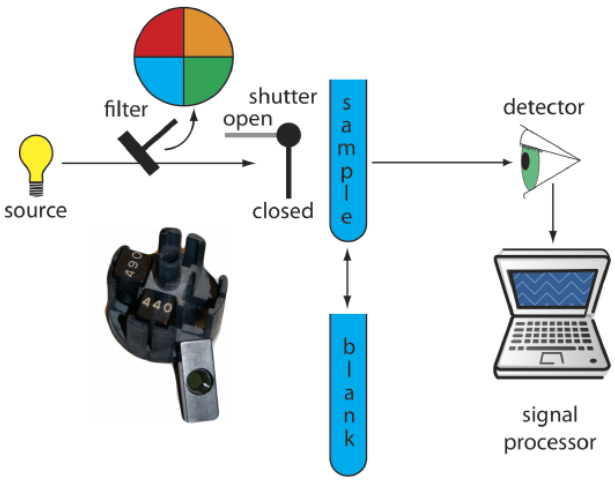

Figure 10.3.1 . Schematic diagram of a filter photometer. The analyst either inserts a removable filter or the filters are placed in a carousel, an example of which is shown in the photographic inset. The analyst selects a filter by rotating it into place.

Single-Beam Spectrophotometer. An instrument that uses a monochromator for wavelength selection is called a ***spectrophotometer***. The simplest spectrophotometer is a single-beam instrument equipped with a fixed-wavelength monochromator (Figure 10.3.2). Single-beam spectrophotometers are calibrated and used in the same manner as a photometer. One example of a

single-beam spectrophotometer is Thermo Scientific's Spectronic 20D+, which is shown in the photographic insert to Figure 10.3.2 . The Spectronic 20D+ has a wavelength range of 340–625 nm (950 nm when using a red-sensitive detector), and a fixed effective bandwidth of 20 nm. Battery-operated, hand-held single-beam spectrophotometers are available, which are easy to transport into the field. Other single-beam spectrophotometers also are available with effective bandwidths of 2–8 nm. Fixed wavelength single-beam spectrophotometers are not practical for recording spectra because manually adjusting the wavelength and recalibrating the spectrophotometer is awkward and time-consuming. The accuracy of a single-beam spectrophotometer is limited by the stability of its source and detector over time.

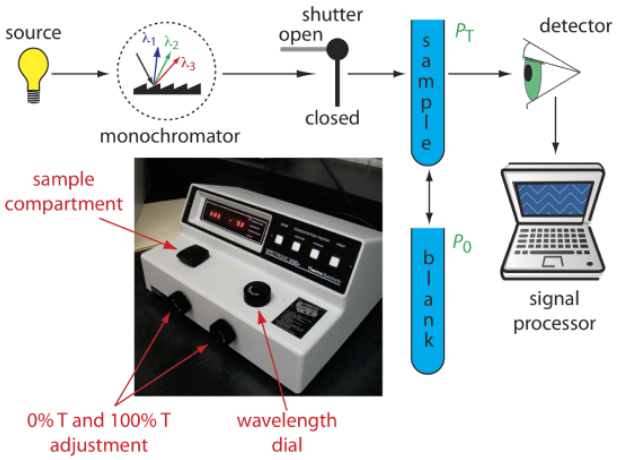

Figure 10.3.2 . Schematic diagram of a fixed-wavelength, single-beam spectrophotometer. The photographic inset shows a typical instrument. The shutter remains closed until the sample or blank is placed in the sample compartment. The analyst manually selects the wavelength by adjusting the wavelength dial. Inset photo modified from: Adi (www.commons.Wikipedia.org).

Double-Beam Spectrophotometer. The limitations of a fixed-wavelength, single-beam spectrophotometer is minimized by using a ***double-beam*** spectrophotometer (Figure 10.3.3). A chopper controls the radiation's path, alternating it between the sample, the blank, and a shutter. The signal processor uses the chopper's speed of rotation to resolve the signal that reaches the detector into the transmission of the blank, P_0, and the sample, P_T. By including an opaque surface as a shutter, it also is possible to continuously adjust 0%T. The effective bandwidth of a double-beam spectrophotometer is controlled by adjusting the monochromator's entrance and exit slits. Effective bandwidths of 0.2–3.0 nm are common. A scanning monochromator allows for the automated recording of spectra. Double-beam instruments are more versatile than single-beam instruments, being useful for both quantitative and qualitative analyses, but also are more expensive and not particularly portable.

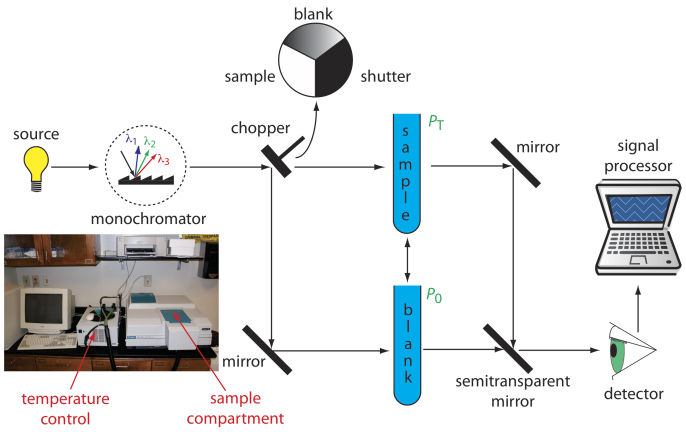

Figure 10.3.3 . Schematic diagram of a scanning, double-beam spectrophotometer. A chopper directs the source's radiation, using a transparent window to pass radiation to the sample and a mirror to reflect radiation to the blank. The chopper's opaque surface serves as a shutter, which allows for a constant adjustment of the spectrophotometer's 0%T. The photographic insert shows a typical instrument. The module in the middle of the photo is a temperature control unit that makes it possible to heat or cool the sample to a constant temperature.

Diode Array Spectrometer. An instrument with a single detector can monitor only one wavelength at a time. If we replace a single photomultiplier with an array of photodiodes, we can use the resulting detector to record a full spectrum in as little as 0.1 s. In a diode array spectrometer the source radiation passes through the sample and is dispersed by a grating (Figure 10.3.4). The

photodiode array detector is situated at the grating's focal plane, with each diode recording the radiant power over a narrow range of wavelengths. Because we replace a full monochromator with just a grating, a diode array spectrometer is small and compact.

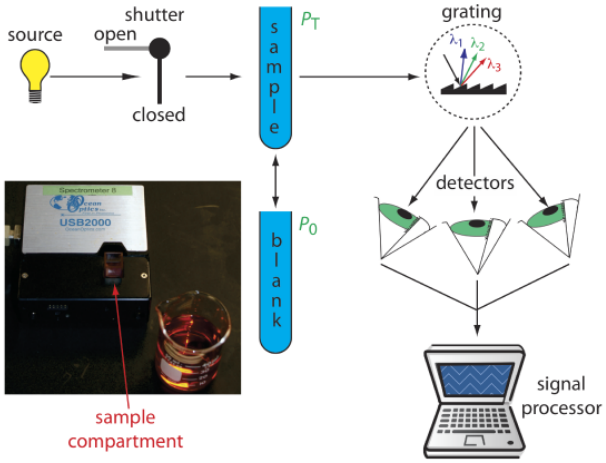

Figure 10.3.4 . Schematic diagram of a diode array spectrophotometer. The photographic insert shows a typical instrument. Note that the 50-mL beaker provides a sense of scale. Because the spectrometer is small and compact, it is easy to transport into the field.

One advantage of a diode array spectrometer is the speed of data acquisition, which allows us to collect multiple spectra for a single sample. Individual spectra are added and averaged to obtain the final spectrum. This ***signal averaging*** improves a spectrum's signal-to-noise ratio. If we add together n spectra, the sum of the signal at any point, x, increases as nS_x, where S_x is the signal. The noise at any point, N_x, is a random event, which increases as $\sqrt{n}N_x$ when we add together n spectra. The ***signal-to-noise ratio*** after n scans, $(S/N)_n$ is

$$\left(\frac{S}{N}\right)_n = \frac{nS_x}{\sqrt{n}N_x} = \sqrt{n}\frac{S_x}{N_x}$$

where S_x/N_x is the signal-to-noise ratio for a single scan. The impact of signal averaging is shown in Figure 10.3.5 . The first spectrum shows the signal after one scan, which consists of a single, noisy peak. Signal averaging using 4 scans and 16 scans decreases the noise and improves the signal-to-noise ratio. One disadvantage of a photodiode array is that the effective bandwidth per diode is roughly an order of magnitude larger than that for a high quality monochromator.

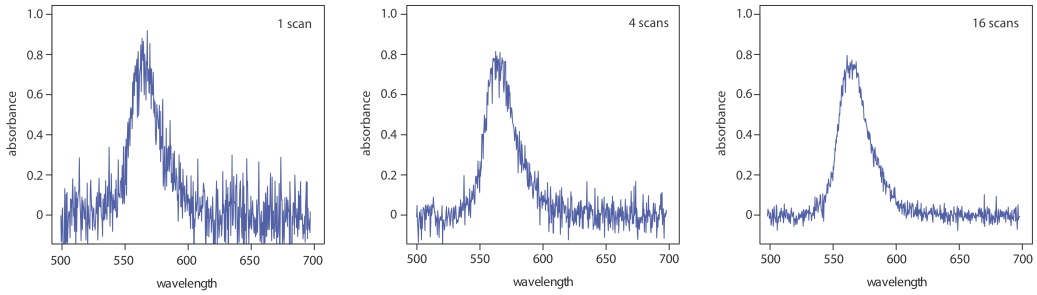

Figure 10.3.5 . Effect of signal averaging on a spectrum's signal-to-noise ratio. From top to bottom: spectrum for a single scan; average spectrum after four scans; and average spectrum after adding 16 scans.

For more details on signals and noise, see Introduction to Signals and Noise by Steven Petrovic, an on-line resource that is part of the Analytical Sciences Digital Library.

Sample Cells. The sample compartment provides a light-tight environment that limits stray radiation. Samples normally are in a liquid or solution state, and are placed in cells constructed with UV/Vis transparent materials, such as quartz, glass, and plastic (Figure 10.3.6). A quartz or fused-silica cell is required when working at a wavelength <300 nm where other materials show a significant absorption. The most common pathlength is 1 cm (10 mm), although cells with shorter (as little as 0.1 cm) and longer pathlengths (up to 10 cm) are available. Longer pathlength cells are useful when analyzing a very dilute solution or for gas

samples. The highest quality cells allow the radiation to strike a flat surface at a 90° angle, minimizing the loss of radiation to reflection. A test tube often is used as a sample cell with simple, single-beam instruments, although differences in the cell's pathlength and optical properties add an additional source of error to the analysis.

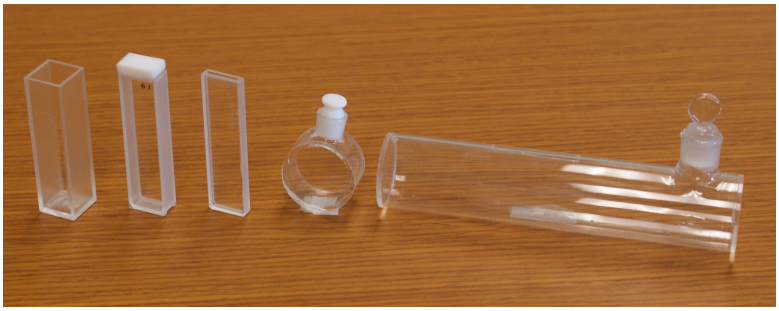

Figure 10.3.6 . Examples of sample cells for UV/Vis spectroscopy. From left to right (with path lengths in parentheses): rectangular plastic cuvette (10.0 mm), rectangular quartz cuvette (5.000 mm), rectangular quartz cuvette (1.000 mm), cylindrical quartz cuvette (10.00 mm), cylindrical glass cuvette with quartz windows (100.0 mm). Cells often are available as a matched pair, which is important when using a double-beam instrument.

If we need to monitor an analyte's concentration over time, it may not be possible to remove samples for analysis. This often is the case, for example, when monitoring an industrial production line or waste line, when monitoring a patient's blood, or when monitoring an environmental system, such as stream. With a ***fiber-optic probe*** we can analyze samples *in situ*. An example of a remote sensing fiber-optic probe is shown in Figure 10.3.7 . The probe consists of two bundles of fiber-optic cable. One bundle transmits radiation from the source to the probe's tip, which is designed to allow the sample to flow through the sample cell. Radiation from the source passes through the solution and is reflected back by a mirror. The second bundle of fiber-optic cable transmits the nonabsorbed radiation to the wavelength selector. Another design replaces the flow cell shown in Figure 10.3.7 with a membrane that contains a reagent that reacts with the analyte. When the analyte diffuses into the membrane it reacts with the reagent, producing a product that absorbs UV or visible radiation. The nonabsorbed radiation from the source is reflected or scattered back to the detector. Fiber optic probes that show chemical selectivity are called optrodes [(a) Seitz, W. R. *Anal. Chem.* **1984**, *56*, 16A–34A; (b) Angel, S. M. *Spectroscopy* **1987**, *2(2)*, 38–48].

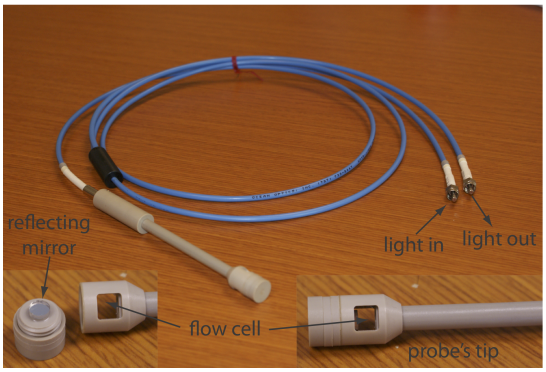

Figure 10.3.7 . Example of a fiber-optic probe. The inset photographs at the bottom of the figure provide close-up views of the probe's flow cell and the reflecting mirror.

Instrument Designs for Infrared Adsorption

Filter Photometer. The simplest instrument for IR absorption spectroscopy is a filter photometer similar to that shown in Figure 10.3.1 for UV/Vis absorption. These instruments have the advantage of portability and typically are used as dedicated analyzers for gases such as HCN and CO.

Double-beam spectrophotometer. Infrared instruments using a monochromator for wavelength selection use double-beam optics similar to that shown in Figure 10.3.3 . Double-beam optics are preferred over single-beam optics because the sources and detectors for infrared radiation are less stable than those for UV/Vis radiation. In addition, it is easier to correct for the absorption of infrared radiation by atmospheric CO_2 and H_2O vapor when using double-beam optics. Resolutions of 1–3 cm^{-1} are typical for most instruments.

Fourier transform spectrometer. In a Fourier transform infrared spectrometer, or FT–IR, the monochromator is replaced with an interferometer (Figure 10.1.13). Because an FT-IR includes only a single optical path, it is necessary to collect a separate spectrum

to compensate for the absorbance of atmospheric CO_2 and H_2O vapor. This is done by collecting a background spectrum without the sample and storing the result in the instrument's computer memory. The background spectrum is removed from the sample's spectrum by taking the ratio the two signals. In comparison to other instrument designs, an FT–IR provides for rapid data acquisition, which allows for an enhancement in signal-to-noise ratio through signal-averaging.

Sample Cells. Infrared spectroscopy routinely is used to analyze gas, liquid, and solid samples. Sample cells are made from materials, such as NaCl and KBr, that are transparent to infrared radiation. Gases are analyzed using a cell with a pathlength of approximately 10 cm. Longer pathlengths are obtained by using mirrors to pass the beam of radiation through the sample several times.

A liquid sample may be analyzed using a variety of different sample cells (Figure 10.3.8). For non-volatile liquids a suitable sample is prepared by placing a drop of the liquid between two NaCl plates, forming a thin film that typically is less than 0.01 mm thick. Volatile liquids are placed in a sealed cell to prevent their evaporation.

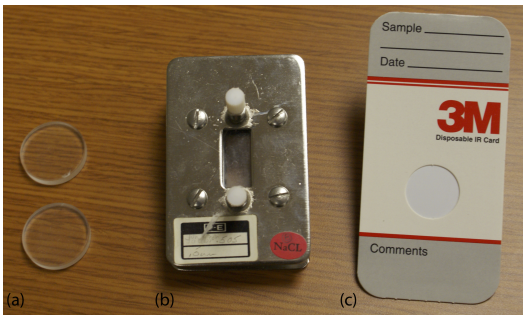

Figure 10.3.8 . Three examples of IR sample cells: (a) NaCl salts plates; (b) fixed pathlength (0.5 mm) sample cell with NaCl windows; (c) disposable card with a polyethylene window that is IR transparent with the exception of strong absorption bands at 2918 cm^{-1} and 2849 cm^{-1}.

The analysis of solution samples is limited by the solvent's IR absorbing properties, with CCl_4, CS_2, and $CHCl_3$ being the most common solvents. Solutions are placed in cells that contain two NaCl windows separated by a Teflon spacer. By changing the Teflon spacer, pathlengths from 0.015–1.0 mm are obtained.

Transparent solid samples are analyzed by placing them directly in the IR beam. Most solid samples, however, are opaque, and are first dispersed in a more transparent medium before recording the IR spectrum. If a suitable solvent is available, then the solid is analyzed by preparing a solution and analyzing as described above. When a suitable solvent is not available, solid samples are analyzed by preparing a mull of the finely powdered sample with a suitable oil. Alternatively, the powdered sample is mixed with KBr and pressed into an optically transparent pellet.

The analysis of an aqueous sample is complicated by the solubility of the NaCl cell window in water. One approach to obtaining an infrared spectrum of an aqueous solution is to use ***attenuated total reflectance*** instead of transmission. Figure 10.3.9 shows a diagram of a typical attenuated total reflectance (ATR) FT–IR instrument. The ATR cell consists of a high refractive index material, such as ZnSe or diamond, sandwiched between a low refractive index substrate and a lower refractive index sample. Radiation from the source enters the ATR crystal where it undergoes a series of internal reflections before exiting the crystal. During each reflection the radiation penetrates into the sample to a depth of a few microns, which results in a selective attenuation of the radiation at those wavelengths where the sample absorbs. ATR spectra are similar, but not identical, to those obtained by measuring the transmission of radiation.

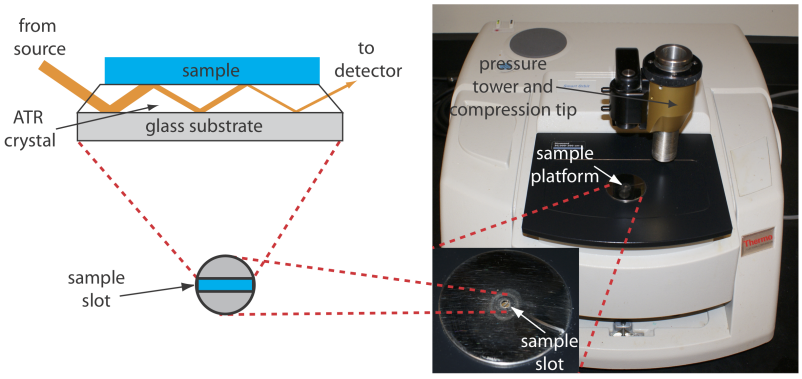

Figure 10.3.9 . FT-IR spectrometer equipped with a diamond ATR sample cell. The inserts show a close-up photo of the sample platform, a sketch of the ATR's sample slot, and a schematic showing how the source's radiation interacts with the sample. The pressure tower is used to ensure proper contact of a solid sample with the ATR crystal.

Solid samples also can be analyzed using an ATR sample cell. After placing the solid in the sample slot, a compression tip ensures that it is in contact with the ATR crystal. Examples of solids analyzed by ATR include polymers, fibers, fabrics, powders, and biological tissue samples. Another reflectance method is diffuse reflectance, in which radiation is reflected from a rough surface, such as a powder. Powdered samples are mixed with a non-absorbing material, such as powdered KBr, and the reflected light is collected and analyzed. As with ATR, the resulting spectrum is similar to that obtained by conventional transmission methods. Further details about these, and other methods for preparing solids for infrared analysis can be found in this chapter's additional resources.

Quantitative Applications

The determination of an analyte's concentration based on its absorption of ultraviolet or visible radiation is one of the most frequently encountered quantitative analytical methods. One reason for its popularity is that many organic and inorganic compounds have strong absorption bands in the UV/Vis region of the electromagnetic spectrum. In addition, if an analyte does not absorb UV/Vis radiation—or if its absorbance is too weak—we often can react it with another species that is strongly absorbing. For example, a dilute solution of Fe^{2+} does not absorb visible light. Reacting Fe^{2+} with *o*-phenanthroline, however, forms an orange–red complex of $Fe(phen)_3^{2+}$ that has a strong, broad absorbance band near 500 nm. An additional advantage to UV/Vis absorption is that in most cases it is relatively easy to adjust experimental and instrumental conditions so that Beer's law is obeyed.

A quantitative analysis based on the absorption of infrared radiation, although important, is encountered less frequently than with UV/Vis absorption. One reason is the greater tendency for instrumental deviations from Beer's law when using infrared radiation. Because an infrared absorption band is relatively narrow, any deviation due to the lack of monochromatic radiation is more pronounced. In addition, infrared sources are less intense than UV/Vis sources, which makes stray radiation more of a problem. Differences between the pathlengths for samples and for standards when using thin liquid films or KBr pellets are a problem, although an internal standard can correct for any difference in pathlength. Finally, establishing a 100%T ($A = 0$) baseline often is difficult because the optical properties of NaCl sample cells may change significantly with wavelength due to contamination and degradation. We can minimize this problem by measuring absorbance relative to a baseline established for the absorption band. Figure 10.3.10 shows how this is accomplished.

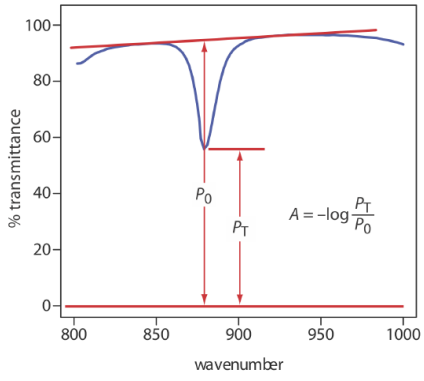

Figure 10.3.10 . Method for determining absorbance from an IR spectrum.

Another approach is to use a cell with a fixed pathlength, such as that shown in Figure 10.3.8 b.

Environmental Applications

The analysis of waters and wastewaters often relies on the absorption of ultraviolet and visible radiation. Many of these methods are outlined in Table 10.3.1 . Several of these methods are described here in more detail.

Table 10.3.1 . Examples of Molecular UV/Vis Analysis of Waters and Wastewaters

analyte	method	λ (nm)
trace metals		
aluminum	react with Eriochrome cyanide R dye at pH 6; forms red to pink complex	535
arsenic	reduce to AsH_3 using Zn and react with silver diethyldithiocarbamate; forms red complex	535
cadmium	extract into $CHCl_3$ containing dithizone from a sample made basic with NaOH; forms pink to red complex	518
chromium	oxidize to Cr(VI) and react with diphenylcarbazide; forms 540 red-violet product	540
copper	react with neocuprine in neutral to slightly acid solution and extract into $CHCl_3/CH_3OH$; forms yellow complex	457
iron	reduce to Fe^{2+} and react with *o*-phenanthroline; forms orange-red complex	510
lead	extract into $CHCl_3$ containing dithizone from sample made basic with NH_3/ NH_4^+ buffer; forms cherry red complex	510
manganese	oxidize to MnO_4^- with persulfate; forms purple solution	525
mercury	extract into $CHCl_3$ containing dithizone from acidic sample; forms orange complex	492
zinc	react with zincon at pH 9; forms blue complex	620
inorganic nonmetals		
ammonia	reaction with hypochlorite and phenol using a manganous 630 salt catalyst; forms blue indophenol as product	630
cyanide	react with chloroamine-T to form CNCl and then with a pyridine-barbituric acid; forms a red-blue dye	578
fluoride	react with red Zr-SPADNS lake; formation of ZrF_6^{2-} decreases color of the red lake	570

analyte	method	λ (nm)
chlorine (residual)	react with leuco crystal violet; forms blue product	592
nitrate	react with Cd to form NO_2^- and then react with sulfanilamide and *N*-(1-napthyl)-ethylenediamine; forms red azo 543 dye	543
phosphate	react with ammonium molybdate and then reduce with $SnCl_2$; forms molybdenum blue	690
organics		
phenol	react with 4-aminoantipyrine and $K_3Fe(CN)_6$; forms yellow antipyrine dye	460
anionic surfactants	react with cationic methylene blue dye and extract into $CHCl_3$; forms blue ion pair	652

Although the quantitative analysis of metals in waters and wastewaters is accomplished primarily by atomic absorption or atomic emission spectroscopy, many metals also can be analyzed following the formation of a colored metal–ligand complex. One advantage to these spectroscopic methods is that they easily are adapted to the analysis of samples in the field using a filter photometer. One ligand used for the analysis of several metals is diphenylthiocarbazone, also known as dithizone. Dithizone is not soluble in water, but when a solution of dithizone in $CHCl_3$ is shaken with an aqueous solution that contains an appropriate metal ion, a colored metal–dithizonate complex forms that is soluble in $CHCl_3$. The selectivity of dithizone is controlled by adjusting the sample's pH. For example, Cd^{2+} is extracted from solutions made strongly basic with NaOH, Pb^{2+} from solutions made basic with an NH_3/ NH_4^+ buffer, and Hg^{2+} from solutions that are slightly acidic.

The structure of dithizone is shown below. See Chapter 7 for a discussion of extracting metal ions using dithizone.

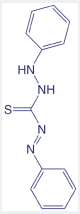

When chlorine is added to water the portion available for disinfection is called the chlorine residual. There are two forms of chlorine residual. The free chlorine residual includes Cl_2, HOCl, and OCl^-. The combined chlorine residual, which forms from the reaction of NH_3 with HOCl, consists of monochloramine, NH_2Cl, dichloramine, $NHCl_2$, and trichloramine, NCl_3. Because the free chlorine residual is more efficient as a disinfectant, there is an interest in methods that can distinguish between the total chlorine residual's different forms. One such method is the leuco crystal violet method. The free residual chlorine is determined by adding leuco crystal violet to the sample, which instantaneously oxidizes to give a blue-colored compound that is monitored at 592 nm. Completing the analysis in less than five minutes prevents a possible interference from the combined chlorine residual. The total chlorine residual (free + combined) is determined by reacting a separate sample with iodide, which reacts with both chlorine residuals to form HOI. When the reaction is complete, leuco crystal violet is added and oxidized by HOI, giving the same blue-colored product. The combined chlorine residual is determined by difference.

In Chapter 9 we explored how the total chlorine residual can be determined by a redox titration; see Representative Method 9.4.1 for further details. The method described here allows us to divide the total chlorine residual into its component parts.

The concentration of fluoride in drinking water is determined indirectly by its ability to form a complex with zirconium. In the presence of the dye SPADNS, a solution of zirconium forms a red colored compound, called a lake, that absorbs at 570 nm. When fluoride is added, the formation of the stable ZrF_6^{2-} complex causes a portion of the lake to dissociate, decreasing the absorbance. A plot of absorbance versus the concentration of fluoride, therefore, has a negative slope.

SPADNS, the structure of which is shown below, is an abbreviation for the sodium salt of 2-(4-sulfophenylazo)-1,8-dihydroxy-3,6-napthalenedisulfonic acid, which is a mouthful to say.

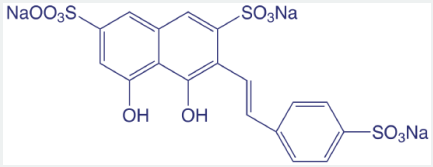

Spectroscopic methods also are used to determine organic constituents in water. For example, the combined concentrations of phenol and ortho- and meta-substituted phenols are determined by using steam distillation to separate the phenols from nonvolatile impurities. The distillate reacts with 4-aminoantipyrine at pH 7.9 ± 0.1 in the presence of $K_3Fe(CN)_6$ to a yellow colored antipyrine dye. After extracting the dye into $CHCl_3$, its absorbance is monitored at 460 nm. A calibration curve is prepared using only the unsubstituted phenol, C_6H_5OH. Because the molar absorptivity of substituted phenols generally are less than that for phenol, the reported concentration represents the minimum concentration of phenolic compounds.

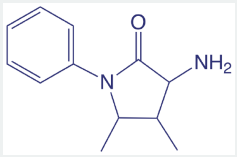

4-aminoantipyrene

Molecular absorption also is used for the analysis of environmentally significant airborne pollutants. In many cases the analysis is carried out by collecting the sample in water, converting the analyte to an aqueous form that can be analyzed by methods such as those described in Table 10.3.1 . For example, the concentration of NO_2 is determined by oxidizing NO_2 to NO_3^-. The concentration of NO_3^- is then determined by first reducing it to NO_2^- with Cd, and then reacting NO_2^- with sulfanilamide and *N*-(1-naphthyl)-ethylenediamine to form a red azo dye. Another important application is the analysis for SO_2, which is determined by collecting the sample in an aqueous solution of $HgCl_4^{2-}$ where it reacts to form $Hg(SO_3)_2^{2-}$. Addition of *p*-rosaniline and formaldehyde produces a purple complex that is monitored at 569 nm. Infrared absorption is useful for the analysis of organic vapors, including HCN, SO_2, nitrobenzene, methyl mercaptan, and vinyl chloride. Frequently, these analyses are accomplished using portable, dedicated infrared photometers.

Clinical Applications

The analysis of clinical samples often is complicated by the complexity of the sample's matrix, which may contribute a significant background absorption at the desired wavelength. The determination of serum barbiturates provides one example of how this problem is overcome. The barbiturates are first extracted from a sample of serum with $CHCl_3$ and then extracted from the $CHCl_3$ into 0.45 M NaOH (pH ≈ 13). The absorbance of the aqueous extract is measured at 260 nm, and includes contributions from the barbiturates as well as other components extracted from the serum sample. The pH of the sample is then lowered to approximately 10 by adding NH_4Cl and the absorbance remeasured. Because the barbiturates do not absorb at this pH, we can use the absorbance at pH 10, $A_{\text{pH 10}}$, to correct the absor-ance at pH 13, $A_{\text{pH 13}}$

$$A_{\text{barb}} = A_{\text{pH 13}} - \frac{V_{\text{samp}} + V_{\text{NH}_4\text{Cl}}}{V_{\text{samp}}} \times A_{\text{pH 10}}$$

where A_{barb} is the absorbance due to the serum barbiturates and V_{samp} and $V_{\text{NH}_4\text{Cl}}$ are the volumes of sample and NH_4Cl, respectively. Table 10.3.2 provides a summary of several other methods for analyzing clinical samples.

Table 10.3.2 . Examples of the Molecular UV/Vis Analysis of Clinical Samples

analyte	method	λ (nm)
total serum protein	react with NaOH and Cu^{2+}; forms blue-violet complex	540
serum cholesterol	react with Fe^{3+} in presence of isopropanol, acetic acid, and H_2SO_4; forms blue-violet complex	540
uric acid	react with phosphotungstic acid; forms tungsten blue	710
serum barbituates	extract into $CHCl_3$ to isolate from interferents and then extract into 0.45 M NaOH	260
glucose	react with *o*-toludine at 100°C; forms blue-green complex	630
protein-bound iodine	decompose protein to release iodide, which catalyzes redox reaction between Ce^{3+} and As^{3+}; forms yellow colored Ce^{4+}	420

Industrial Applications

UV/Vis molecular absorption is used for the analysis of a diverse array of industrial samples including pharmaceuticals, food, paint, glass, and metals. In many cases the methods are similar to those described in Table 10.3.1 and in Table 10.3.2 . For example, the amount of iron in food is determined by bringing the iron into solution and analyzing using the *o*-phenanthroline method listed in Table 10.3.1 .

Many pharmaceutical compounds contain chromophores that make them suitable for analysis by UV/Vis absorption. Products analyzed in this fashion include antibiotics, hormones, vitamins, and analgesics. One example of the use of UV absorption is in determining the purity of aspirin tablets, for which the active ingredient is acetylsalicylic acid. Salicylic acid, which is produced by the hydrolysis of acetylsalicylic acid, is an undesirable impurity in aspirin tablets, and should not be present at more than 0.01% w/w. Samples are screened for unacceptable levels of salicylic acid by monitoring the absorbance at a wavelength of 312 nm. Acetylsalicylic acid absorbs at 280 nm, but absorbs poorly at 312 nm. Conditions for preparing the sample are chosen such that an absorbance of greater than 0.02 signifies an unacceptable level of salicylic acid.

Forensic Applications

UV/Vis molecular absorption routinely is used for the analysis of narcotics and for drug testing. One interesting forensic application is the determination of blood alcohol using the Breathalyzer test. In this test a 52.5-mL breath sample is bubbled through an acidified solution of $K_2Cr_2O_7$, which oxidizes ethanol to acetic acid. The concentration of ethanol in the breath sample is determined by a decrease in the absorbance at 440 nm where the dichromate ion absorbs. A blood alcohol content of 0.10%, which is above the legal limit, corresponds to 0.025 mg of ethanol in the breath sample.

Developing a Quantitative Method for a Single Component

To develop a quantitative analytical method, the conditions under which Beer's law is obeyed must be established. First, the most appropriate wavelength for the analysis is determined from an absorption spectrum. In most cases the best wavelength corresponds to an absorption maximum because it provides greater sensitivity and is less susceptible to instrumental limitations. Second, if the instrument has adjustable slits, then an appropriate slit width is chosen. The absorption spectrum also aids in selecting a slit width by choosing a width that is narrow enough to avoid instrumental limita- tions to Beer's law, but wide enough to increase the throughput of source radiation. Finally, a calibration curve is constructed to determine the range of concentrations for which Beer's law is valid. Additional considerations that are important in any quantitative method are the effect of potential interferents and establishing an appropriate blank.

Representative Method 10.3.1: Determination of Iron in Water and Wastewater

The best way to appreciate the theoretical and the practical details discussed in this section is to carefully examine a typical analytical method. Although each method is unique, the following description of the determination of iron in water and wastewater provides an instructive example of a typical procedure. The description here is based on Method 3500-Fe B as published in *Standard Methods for the Examination of Water and Wastewater*, 20th Ed., American Public Health Association: Washington, D. C., 1998.

Description of Method

Iron in the +2 oxidation state reacts with *o*-phenanthroline to form the orange-red $\mathrm{Fe(phen)_3^{2+}}$ complex. The intensity of the complex's color is independent of the solution's acidity between a pH of 3 and 9. Because the complex forms more rapidly at lower pH levels, the reaction usually is carried out within a pH range of 3.0–3.5. Any iron present in the +3 oxidation state is reduced with hydroxylamine before adding *o*-phenanthroline. The most important interferents are strong oxidizing agents, polyphosphates, and metal ions such as Cu^{2+}, Zn^{2+}, Ni^{2+}, and Cd^{2+}. An interference from oxidizing agents is minimized by adding an excess of hydroxylamine, and an interference from polyphosphate is minimized by boiling the sample in the presence of acid. The absorbance of samples and standards are measured at a wavelength of 510 nm using a 1-cm cell (longer pathlength cells also may be used). Beer's law is obeyed for concentrations of within the range of 0.2–4.0 mg Fe/L.

Procedure

For a sample that contains less than 2 mg Fe/L, directly transfer a 50-mL portion to a 125-mL Erlenmeyer flask. Samples that contain more than 2 mg Fe/L are diluted before acquiring the 50-mL portion. Add 2 mL of concentrated HCl and 1 mL of hydroxylamine to the sample. Bring the solution to a boil and continue boiling until the solution's volume is reduced to between 15 and 20 mL. After cooling to room temperature, transfer the solution to a 50-mL volumetric flask, add 10 mL of an ammonium acetate buffer, 2 mL of a 1000 ppm solution of *o*-phenanthroline, and dilute to volume. Allow 10–15 minutes for color development before measuring the absorbance, using distilled water to set 100% T. Calibration standards, including a blank, are prepared by the same procedure using a stock solution that contains a known concentration of Fe^{2+}.

Questions

1. Explain why strong oxidizing agents are interferents and why an excess of hydroxylamine prevents the interference.

   A strong oxidizing agent will oxidize some Fe^{2+} to Fe^{3+}. Because $\mathrm{Fe(phen)_3^{3+}}$ does not absorb as strongly as $\mathrm{Fe(phen)_3^{2+}}$, the absorbance is smaller than expected, which produces a negative determinate error. The excess hydroxylamine reacts with the oxidizing agents, removing them from the solution.

2. The color of the complex is stable between pH levels of 3 and 9. What are some possible complications at more acidic or at more basic pH's?

   Because *o*-phenanthroline is a weak base, its conditional formation constant for $\mathrm{Fe(phen)_3^{2+}}$ becomes smaller at more acidic pH levels, where *o*-phenanthroline is present in its protonated form. The result is a decrease in absorbance and a less sensitive analytical method. When the pH is greater than 9, competition between OH^- and *o*-phenanthroline for Fe^{2+} also decreases the absorbance. In addition, if the pH is sufficiently basic there is a risk that the iron will precipitate as $Fe(OH)_2$.

3. Cadmium is an interferent because it forms a precipitate with *o*-phenanthroline. What effect does the formation of precipitate have on the determination of iron?

   Because *o*-phenanthroline is present in large excess (2000 µg of *o*-phenanthroline for 100 µg of $Fe2^+$), it is not likely that the interference is due to an insufficient amount of *o*-phenanthroline being available to react with the Fe^{2+}. The presence of a precipitate in the sample cell results in the scattering of radiation, which causes an apparent increase in absorbance. Because the measured absorbance increases, the reported concentration is too high. Although scattering is a problem here, it can serve as the basis of a useful analytical method. See Chapter 10.8 for further details.

4. Even high quality ammonium acetate contains a significant amount of iron. Why is this source of iron not a problem?

   Because all samples and standards are prepared using the same volume of ammonium acetate buffer, the contribution of this source of iron is accounted for by the calibration curve's reagent blank.

Quantitative Analysis for a Single Sample

To determine the concentration of an analyte we measure its absorbance and apply Beer's law using any of the standardization methods described in Chapter 5. The most common methods are a normal calibration curve using external standards and the method of standard additions. A single point standardization also is possible, although we must first verify that Beer's law holds for the concentration of analyte in the samples and the standard.

Example 10.3.1

The determination of iron in an industrial waste stream is carried out by the *o*-phenanthroline described in Representative Method 10.3.1. Using the data in the following table, determine the mg Fe/L in the waste stream.

mg Fe/L	absorbance
0.00	0.000
1.00	0.183
2.00	0.364
3.00	0.546
4.00	0.727
sample	0.269

Solution

Linear regression of absorbance versus the concentration of Fe in the standards gives the calibration curve and calibration equation shown here

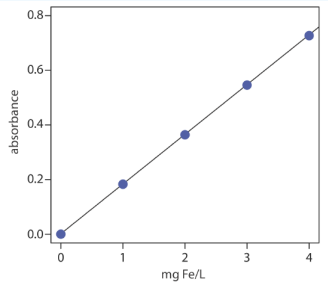

$$A = 0.0006 + \left(0.1817\ \text{mg}^{-1}\text{L}\right) \times (\text{mgFe/L})$$

Substituting the sample's absorbance into the calibration equation gives the concentration of Fe in the waste stream as 1.48 mg Fe/L

Exercise 10.3.1

The concentration of Cu^{2+} in a sample is determined by reacting it with the ligand cuprizone and measuring its absorbance at 606 nm in a 1.00-cm cell. When a 5.00-mL sample is treated with cuprizone and diluted to 10.00 mL, the resulting solution has an absorbance of 0.118. A second 5.00-mL sample is mixed with 1.00 mL of a 20.00 mg/L standard of Cu^{2+}, treated with cuprizone and diluted to 10.00 mL, giving an absorbance of 0.162. Report the mg Cu^{2+}/L in the sample.

Answer

For this standard addition we write equations that relate absorbance to the concentration of Cu^{2+} in the sample before the standard addition

$$0.118 = \varepsilon b \left[C_{\text{Cu}} \times \frac{5.00\ \text{mL}}{10.00\ \text{mL}} \right]$$

and after the standard addition

$$0.162 = \varepsilon b \left(C_{\text{Cu}} \times \frac{5.00\ \text{mL}}{10.00\ \text{mL}} + \frac{20.00\ \text{mg Cu}}{\text{L}} \times \frac{1.00\ \text{mL}}{10.00\ \text{mL}} \right)$$

in each case accounting for the dilution of the original sample and for the standard. The value of εb is the same in both equation. Solving each equation for εb and equating

$$\frac{0.162}{C_{\text{Cu}} \times \frac{5.00\ \text{mL}}{10.00\ \text{mL}} + \frac{20.00\ \text{mg Cu}}{\text{L}} \times \frac{1.00\ \text{mL}}{10.00\ \text{mL}}} = \frac{0.118}{C_{\text{Cu}} \times \frac{5.00\ \text{mL}}{10.00\ \text{mL}}}$$

leaves us with an equation in which C_{Cu} is the only variable. Solving for C_{Cu} gives its value as

$$\frac{0.162}{0.500 \times C_{\text{Cu}} + 2.00\ \text{mg Cu/L}} = \frac{0.118}{0.500 \times C_{\text{Cu}}}$$

$$0.0810 \times C_{\text{Cu}} = 0.0590 \times C_{\text{Ca}} + 0.236\ \text{mg Cu/L}$$

$$0.0220 \times C_{\text{Cu}} = 0.236\ \text{mg Cu/L}$$

$$C_{\text{Cu}} = 10.7\ \text{mg Cu/L}$$

Quantitative Analysis of Mixtures

Suppose we need to determine the concentration of two analytes, *X* and *Y*, in a sample. If each analyte has a wavelength where the other analyte does not absorb, then we can proceed using the approach in Example 10.3.5 . Unfortunately, UV/Vis absorption bands are so broad that frequently it is not possible to find suitable wavelengths. Because Beer's law is additive the mixture's absorbance, A_{mix}, is

$$(A_{mix})_{\lambda_1} = (\varepsilon_x)_{\lambda_1} bC_X + (\varepsilon_Y)_{\lambda_1} bC_Y \tag{1.3.1}$$

where λ_1 is the wavelength at which we measure the absorbance. Because Equation 1.3.1 includes terms for the concentration of both *X* and *Y*, the absorbance at one wavelength does not provide enough information to determine either C_X or C_Y. If we measure the absorbance at a second wavelength

$$(A_{mix})_{\lambda_2} = (\varepsilon_x)_{\lambda_2} bC_X + (\varepsilon_Y)_{\lambda_2} bC_Y \tag{1.3.2}$$

then we can determine C_X and C_Y by solving simultaneously Equation 1.3.1 and Equation 1.3.2. Of course, we also must determine the value for ε_X and ε_Y at each wavelength. For a mixture of *n* components, we must measure the absorbance at *n* different wavelengths.

Example 10.3.2

The concentrations of Fe^{3+} and Cu^{2+} in a mixture are determined following their reaction with hexacyanoruthenate (II), $Ru(CN)_6^{4-}$, which forms a purple-blue complex with Fe^{3+} (λ_{max} = 550 nm) and a pale-green complex with Cu^{2+} (λ_{max} = 396 nm) [DiTusa, M. R.; Schlit, A. A. *J. Chem. Educ.* **1985**, *62*, 541–542]. The molar absorptivities (M^{-1} cm^{-1}) for the metal complexes at the two wavelengths are summarized in the following table.

analyte	ε_{550}	ε_{396}
Fe^{3+}	9970	84
Cu^{2+}	34	856

When a sample that contains Fe^{3+} and Cu^{2+} is analyzed in a cell with a pathlength of 1.00 cm, the absorbance at 550 nm is 0.183 and the absorbance at 396 nm is 0.109. What are the molar concentrations of Fe^{3+} and Cu^{2+} in the sample?

Solution

Substituting known values into Equation 1.3.1 and Equation 1.3.2 gives

$$A_{550} = 0.183 = 9970C_{Fe} + 34C_{Cu}$$
$$A_{396} = 0.109 = 84C_{Fe} + 856C_{Cu}$$

To determine C_{Fe} and C_{Cu} we solve the first equation for C_{Cu}

$$C_{Cu} = \frac{0.183 - 9970C_{Fe}}{34}$$

and substitute the result into the second equation.

$$\begin{aligned} 0.109 &= 84C_{Fe} + 856 \times \frac{0.183 - 9970C_{Fe}}{34} \\ &= 4.607 - \left(2.51 \times 10^5\right) C_{Fe} \end{aligned}$$

Solving for C_{Fe} gives the concentration of Fe^{3+} as 1.8×10^{-5} M. Substituting this concentration back into the equation for the mixture's absorbance at 396 nm gives the concentration of Cu^{2+} as 1.3×10^{-4} M.

Another approach to solving Example 10.3.2 is to multiply the first equation by 856/34 giving

$$4.607 = 251009C_{Fe} + 856C_{Cu}$$

Subtracting the second equation from this equation

$$\begin{aligned} 4.607 &= 251009C_{Fe} + 856C_{Cu} \\ -0.109 &= 84C_{Fe} + 856C_{Cu} \end{aligned}$$

gives

$$4.498 = 250925C_{Fe}$$

and we find that C_{Fe} is 1.8×10^{-5}. Having determined C_{Fe} we can substitute back into one of the other equations to solve for C_{Cu}, which is 1.3×10^{-5}.

? Exercise 10.3.2

The absorbance spectra for Cr^{3+} and Co^{2+} overlap significantly. To determine the concentration of these analytes in a mixture, its absorbance is measured at 400 nm and at 505 nm, yielding values of 0.336 and 0.187, respectively. The individual molar absorptivities (M^{-1} cm^{-1}) for $Cr3^{+}$ are 15.2 at 400 nm and 0.533 at 505 nm; the values for Co^{2+} are 5.60 at 400 nm and 5.07 at 505 nm.

Answer

Substituting into Equation 1.3.1and Equation 1.3.2gives

$$A_{400} = 0.336 = 15.2C_{Cr} + 5.60C_{Co}$$

$$A_{400} = 0187 = 0.533C_{Cr} + 5.07C_{Co}$$

To determine C_{Cr} and C_{Co} we solve the first equation for C_{Co}

$$C_{Co} = \frac{0.336 - 15.2\mathrm{C}_{Co}}{5.60}$$

and substitute the result into the second equation.

$$0.187 = 0.533C_{Cr} + 5.07 \times \frac{0.336 - 15.2C_{Co}}{5.60}$$

$$0.187 = 0.3042 - 13.23C_{Cr}$$

Solving for C_{Cr} gives the concentration of Cr^{3+} as 8.86×10^{-3} M. Substituting this concentration back into the equation for the mixture's absorbance at 400 nm gives the concentration of Co^{2+} as 3.60×10^{-2} M.

To obtain results with good accuracy and precision the two wavelengths should be selected so that $\varepsilon_X > \varepsilon_Y$ at one wavelength and $\varepsilon_X < \varepsilon_Y$ at the other wavelength. It is easy to appreciate why this is true. Because the absorbance at each wavelength is dominated by one analyte, any uncertainty in the concentration of the other analyte has less of an impact. Figure 10.3.11 shows that the choice of wavelengths for Practice Exercise 10.3.2 are reasonable. When the choice of wavelengths is not obvious, one method for locating the optimum wavelengths is to plot $\varepsilon_X/\varepsilon_y$ as function of wavelength, and determine the wavelengths where $\varepsilon_X/\varepsilon_y$ reaches maximum and minimum values [Mehra, M. C.; Rioux, J. *J. Chem. Educ.* **1982**, *59*, 688–689].

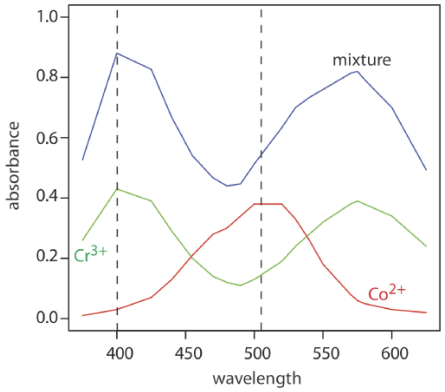

Figure 10.3.11 . Visible absorption spectra for 0.0250 M Cr^{3+}, 0.0750 M Co^{2+}, and for a mixture of Cr^{3+} and Co^{2+}. The two wavelengths used to analyze the mixture of Cr^{3+} and Co^{2+} are shown by the dashed lines. The data for the two standards are from Brewer, S. *Solving Problems in Analytical Chemistry*, John Wiley & Sons: New York, 1980.

When the analyte's spectra overlap severely, such that $\varepsilon_X \approx \varepsilon_Y$ at all wavelengths, other computational methods may provide better accuracy and precision. In a multiwavelength linear regression analysis, for example, a mixture's absorbance is compared to that for a set of standard solutions at several wavelengths [Blanco, M.; Iturriaga, H.; Maspoch, S.; Tarin, P. *J. Chem. Educ.* **1989**, *66*, 178–180]. If A_{SX} and A_{SY} are the absorbance values for standard solutions of components *X* and *Y* at any wavelength, then

$$A_{SX} = \varepsilon_X b C_{SX} \tag{1.3.3}$$

$$A_{SY} = \varepsilon_Y b C_{SY} \tag{1.3.4}$$

where C_{SX} and C_{SY} are the known concentrations of *X* and *Y* in the standard solutions. Solving Equation 1.3.3 and Equation 1.3.4 for ε_X and for ε_Y, substituting into Equation 1.3.1, and rearranging, gives

$$\frac{A_{\text{mix}}}{A_{SX}} = \frac{C_X}{C_{SX}} + \frac{C_Y}{C_{SY}} \times \frac{A_{SY}}{A_{SX}}$$

To determine C_X and C_Y the mixture's absorbance and the absorbances of the standard solutions are measured at several wavelengths. Graphing A_{mix}/A_{SX} versus A_{SY}/A_{SX} gives a straight line with a slope of C_Y/C_{SY} and a *y*-intercept of C_X/C_{SX}. This approach is particularly helpful when it is not possible to find wavelengths where $\varepsilon_X > \varepsilon_Y$ and $\varepsilon_X < \varepsilon_Y$.

The approach outlined here for a multiwavelength linear regression uses a single standard solution for each analyte. A more rigorous approach uses multiple standards for each analyte. The math behind the analysis of such data—which we call a multiple linear regression—is beyond the level of this text. For more details about multiple linear regression see Brereton, R. G. *Chemometrics: Data Analysis for the Laboratory and Chemical Plant*, Wiley: Chichester, England, 2003.

Example 10.3.3

Figure $PageIndex{10.11}$ shows visible absorbance spectra for a standard solution of 0.0250 M Cr^{3+}, a standard solution of 0.0750 M Co^{2+}, and a mixture that contains unknown concentrations of each ion. The data for these spectra are shown here.

λ (nm)	A_{Cr}	A_{Cu}	A_{mix}	λ (nm)	A_{Cr}	A_{Cu}	A_{mix}
375	0.26	0.01	0.53	520	0.19	0.38	0.63
400	0.43	0.03	0.88	530	0.24	0.33	0.70

425	0.39	0.07	0.83	540	0.28	0.26	0.73
440	0.29	0.13	0.67	550	0.32	0.18	0.76
455	0.20	0.21	0.54	570	0.38	0.08	0.81
470	0.14	0.28	0.47	575	0.39	0.06	0.82
480	0.12	0.30	0.44	580	0.38	0.05	0.79
490	0.11	0.34	0.45	600	0.34	0.03	0.70
500	0.13	0.38	0.51	625	0.24	0.02	0.49

Use a multiwavelength regression analysis to determine the composition of the unknown.

Solution

First we need to calculate values for A_{mix}/A_{SX} and for A_{SY}/A_{SX}. Let's define X as Co^{2+} and Y as Cr^{3+}. For example, at a wavelength of 375 nm A_{mix}/A_{SX} is 0.53/0.01, or 53 and A_{SY}/A_{SX} is 0.26/0.01, or 26. Completing the calculation for all wavelengths and graphing A_{mix}/A_{SX} versus A_{SY}/A_{SX} gives the calibration curve shown in Figure 10.3.12 . Fitting a straight-line to the data gives a regression model of

$$\frac{A_{\text{mix}}}{A_{SX}} = 0.636 + 2.01 \times \frac{A_{SY}}{A_{SX}}$$

Using the *y*-intercept, the concentration of Co^{2+} is

$$\frac{C_X}{C_{SX}} = \frac{[\text{Co}^{2+}]}{0.0750\text{M}} = 0.636$$

or $[Co^{2+}]$ = 0.048 M; using the slope the concentration of Cr^{3+} is

$$\frac{C_Y}{C_{SY}} = \frac{[\text{Cr}^{3+}]}{0.0250\text{M}} = 2.01$$

or $[Cr^{3+}]$ = 0.050 M.

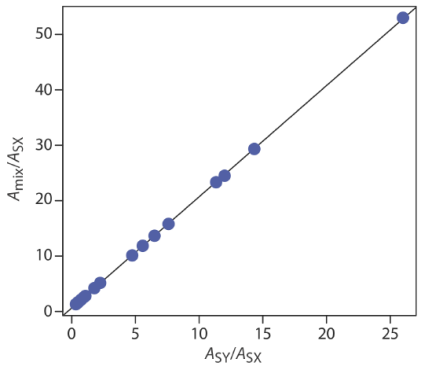

Figure 10.3.12 . Multiwavelength linear regression analysis for the data in Example 10.3.3 .

Exercise 10.3.3

A mixture of MnO_4^- and $Cr_2O_7^{2-}$, and standards of 0.10 mM $KMnO_4$ and of 0.10 mM $K_2Cr_2O_7$ give the results shown in the following table. Determine the composition of the mixture. The data for this problem is from Blanco, M. C.; Iturriaga, H.; Maspoch, S.; Tarin, P. *J. Chem. Educ.* **1989**, *66*, 178–180.

λ (nm)	A_{Mn}	A_{Cr}	A_{mix}
266	0.042	0.410	0.766

λ (nm)	A_{Mn}	A_{Cr}	A_{mix}
288	0.082	0.283	0.571
320	0.168	0.158	0.422
350	0.125	0.318	0.672
360	0.036	0.181	0.366

Answer

Letting *X* represent MnO_4^- and letting *Y* represent $Cr_2O_7^{2-}$, we plot the equation

$$\frac{A_{\text{mix}}}{A_{SX}} = \frac{C_X}{C_{SX}} + \frac{C_Y}{C_{SY}} \times \frac{A_{SY}}{A_{SX}}$$

placing A_{mix}/A_{SX} on the *y*-axis and A_{SY}/A_{SX} on the *x*-axis. For example, at a wavelength of 266 nm the value A_{mix}/A_{SX} of is 0.766/0.042, or 18.2, and the value of A_{SY}/A_{SX} is 0.410/0.042, or 9.76. Completing the calculations for all wavelengths and plotting the data gives the result shown here

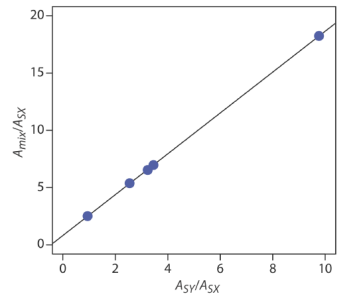

Fitting a straight-line to the data gives a regression model of

$$\frac{A_{\text{mix}}}{A_{\text{SX}}} = 0.8147 + 1.7839 \times \frac{A_{SY}}{A_{SX}}$$

Using the *y*-intercept, the concentration of MnO_4^- is

$$\frac{C_X}{C_{SX}} = 0.8147 = \frac{\left[MnO_4^-\right]}{1.0 \times 10^{-4}\ \text{M}\ MnO_4^-}$$

or 8.15×10^{-5} M MnO_4^-, and using the slope, the concentration of $Cr_2O_7^{2-}$ is

$$\frac{C_Y}{C_{SY}} = 1.7839 = \frac{\left[Cr_2O_7^{2-}\right]}{1.00 \times 10^{-4}\ \text{M}\ Cr_2O_7^{2-}}$$

or 1.78×10^{-4} M $Cr_2O_7^{2-}$.

Qualitative Applications

As discussed in Chapter 10.2, ultraviolet, visible, and infrared absorption bands result from the absorption of electromagnetic radiation by specific valence electrons or bonds. The energy at which the absorption occurs, and the intensity of that absorption, is determined by the chemical environment of the absorbing moiety. For example, benzene has several ultraviolet absorption bands due to $\pi \rightarrow \pi^*$ transitions. The position and intensity of two of these bands, 203.5 nm (ε = 7400 M^{-1} cm^{-1}) and 254 nm (ε = 204 M^{-1} cm^{-1}), are sensitive to substitution. For benzoic acid, in which a carboxylic acid group replaces one of the aromatic hydrogens, the two bands shift to 230 nm (ε = 11600 M^{-1} cm^{-1}) and 273 nm (ε = 970 M^{-1} cm^{-1}). A variety of rules have been developed to aid in correlating UV/Vis absorption bands to chemical structure. Similar correlations are available for infrared absorption bands. For example a carbonyl's C=O stretch is sensitive to adjacent functional groups, appearing at 1650 cm^{-1} for acids, 1700 cm^{-1} for

ketones, and 1800 cm^{-1} for acid chlorides. The interpretation of UV/ Vis and IR spectra receives adequate coverage elsewhere in the chemistry curriculum, notably in organic chemistry, and is not considered further in this text.

With the availability of computerized data acquisition and storage it is possible to build digital libraries of standard reference spectra. The identity of an a unknown compound often can be determined by comparing its spectrum against a library of reference spectra, a process known as ***spectral searching***. Comparisons are made using an algorithm that calculates the cumulative difference between the sample's spectrum and a reference spectrum. For example, one simple algorithm uses the following equation

$$D = \sum_{i=1}^{n} |(A_{sample})_i - (A_{reference})_i|$$

where D is the cumulative difference, A_{sample} is the sample's absorbance at wavelength or wavenumber i, $A_{reference}$ is the absorbance of the reference compound at the same wavelength or wavenumber, and n is the number of digitized points in the spectra. The cumulative difference is calculated for each reference spectrum. The reference compound with the smallest value of D is the closest match to the unknown compound. The accuracy of spectral searching is limited by the number and type of compounds included in the library, and by the effect of the sample's matrix on the spectrum.

Another advantage of computerized data acquisition is the ability to subtract one spectrum from another. When coupled with spectral searching it is possible to determine the identity of several components in a sample without the need of a prior separation step by repeatedly searching and sub- tracting reference spectra. An example is shown in Figure 10.3.13 in which the composition of a two-component mixture is determined by successive searching and subtraction. Figure 10.3.13 a shows the spectrum of the mixture. A search of the spectral library selects cocaine•HCl (Figure 10.3.13 b) as a likely component of the mixture. Subtracting the reference spectrum for cocaine•HCl from the mixture's spectrum leaves a result (Figure 10.3.13 c) that closely matches mannitol's reference spectrum (Figure 10.3.13 d). Subtracting the reference spectrum for mannitol leaves a small residual signal (Figure 10.3.13 e).

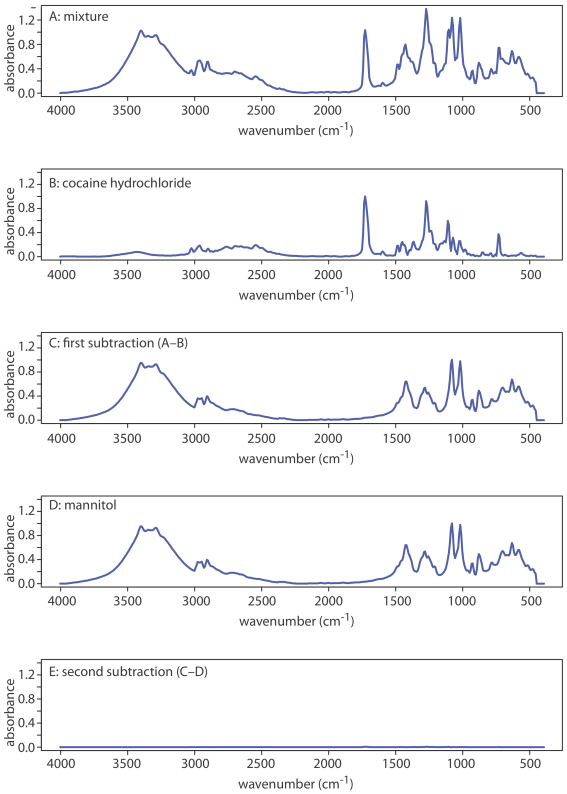

Figure 10.3.13 . Identifying the components of a mixture by spectral searching and subtracting. (a) IR spectrum of the mixture; (b) Reference IR spectrum of cocaine•HCl; (c) Result of subtracting the spectrum of cocaine•HCl from the mixture's spectrum; (d) Reference IR spectrum of mannitol; and (e) The residual spectrum after removing mannitol's contribution to the mixture's spectrum. IR spectra traditionally are displayed using percent transmittance, %T, along the *y*-axis (for example, see Figure 10.2.2). Because absorbance—not percent transmittance—is a linear function of concentration, spectral searching and spectral subtraction, is easier to do when displaying absorbance on the *y*-axis.

Characterization Applications

Molecular absorption, particularly in the UV/Vis range, has been used for a variety of different characterization studies, including determining the stoichiometry of metal–ligand complexes and determining equilibrium constants. Both of these examples are examined in this section.

Stoichiometry of a Metal-Ligand Complex

We can determine the stoichiometry of the metal–ligand complexation reaction

$$\mathrm{M} + y\mathrm{L} \rightleftharpoons \mathrm{ML}_y$$

using one of three methods: the method of continuous variations, the mole-ratio method, and the slope-ratio method. Of these approaches, the ***method of continuous variations***, also called Job's method, is the most popular. In this method a series of solutions is prepared such that the total moles of metal and of ligand, n_{total}, in each solution is the same. If $(n_{\mathrm{M}})_i$ and $(n_{\mathrm{L}})_i$ are, respectively, the moles of metal and ligand in solution i, then

$$n_{\text{total}} = (n_{\mathrm{M}})_i + (n_{\mathrm{L}})_i$$

The relative amount of ligand and metal in each solution is expressed as the mole fraction of ligand, $(X_{\mathrm{L}})i$, and the mole fraction of metal, $(X_{\mathrm{M}})_i$,

$$(X_{\mathrm{L}})_i = \frac{(n_{\mathrm{L}})_i}{n_{\text{total}}}$$

$$(X_M)_i = 1 - \frac{(n_{\mathrm{L}})_i}{n_{\text{total}}} = \frac{(n_{\mathrm{M}})_i}{n_{\text{total}}}$$

The concentration of the metal–ligand complex in any solution is determined by the limiting reagent, with the greatest concentration occurring when the metal and the ligand are mixed stoichiometrically. If we monitor the complexation reaction at a wavelength where only the metal–ligand complex absorbs, a graph of absorbance versus the mole fraction of ligand has two linear branches—one when the ligand is the limiting reagent and a second when the metal is the limiting reagent. The intersection of the two branches represents a stoichiometric mixing of the metal and the ligand. We use the mole fraction of ligand at the intersection to determine the value of y for the metal–ligand complex ML_y.

$$y = \frac{n_{\mathrm{L}}}{n_{\mathrm{M}}} = \frac{X_{\mathrm{L}}}{X_{\mathrm{M}}} = \frac{X_{\mathrm{L}}}{1 - X_{\mathrm{L}}}$$

> You also can plot the data as absorbance versus the mole fraction of metal. In this case, y is equal to $(1 - X_{\mathrm{M}})/X_{\mathrm{M}}$.

Example 10.3.4

To determine the formula for the complex between Fe^{2+} and *o*-phenanthroline, a series of solutions is prepared in which the total concentration of metal and ligand is held constant at 3.15×10^{-4} M. The absorbance of each solution is measured at a wavelength of 510 nm. Using the following data, determine the formula for the complex.

X_{L}	absorbance	X_{L}	absorbance
0.000	0.000	0.600	0.693
0.100	0.116	0.700	0.809
0.200	0.231	0.800	0.693
0.300	0.347	0.900	0.347
0.400	0.462	1.000	0.000
0.500	0.578		

Solution

A plot of absorbance versus the mole fraction of ligand is shown in Figure 10.3.14 . To find the maximum absorbance, we extrapolate the two linear portions of the plot. The two lines intersect at a mole fraction of ligand of 0.75. Solving for *y* gives

$$y = \frac{X_L}{1 - X_L} = \frac{0.75}{1 - 0.75} = 3$$

The formula for the metal–ligand complex is $\mathrm{Fe(phen)_3^{2+}}$.

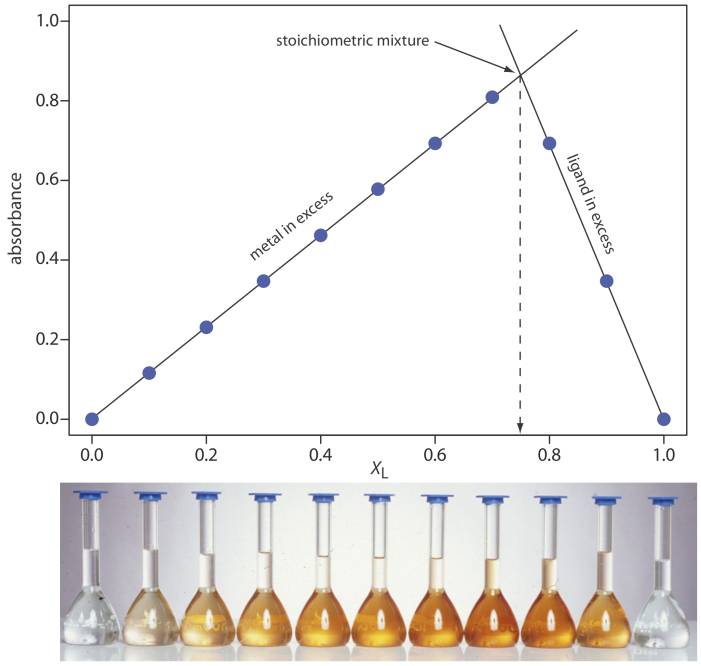

Figure 10.3.14 . Continuous variations plot for Example 10.3.4 . The photo shows the solutions used to gather the data. Each solution is displayed directly below its coresponding point on the continuous variations plot. To prepare these solutions I first prepared a solution of 3.15×10^{-4} M Fe^{2+} and a solution of 3.15×10^{-4} M *o*-phenanthroline. Because the two stock solutions have the same concentration, diluting a portion of one solution with the other solution gives a mixture in which the combined concentration of *o*-phenanthroline and Fe^{2+} is 3.15×10^{-4} M. Because each solution has the same volume, each solution also contains the same total moles of metal and ligand.

? Exercise 10.3.4

Use the continuous variations data in the following table to determine the formula for the complex between Fe^{2+} and SCN^-. The data for this problem is adapted from Meloun, M.; Havel, J.; Högfeldt, E. *Computation of Solution Equilibria*, Ellis Horwood: Chichester, England, 1988, p. 236.

X_L	absorbance	X_L	absorbance	X_L	absorbance	X_L	absorbance
0.0200	0.068	0.2951	0.670	0.5811	0.790	0.8923	0.324
0.0870	0.262	0.3887	0.767	0.6860	0.701	0.9787	0.071
0.1792	0.471	0.4964	0.807	0.7885	0.540		

Answer

The figure below shows a continuous variations plot for the data in this exercise. Although the individual data points show substantial curvature—enough curvature that there is little point in trying to draw linear branches for excess metal and excess ligand—the maximum absorbance clearly occurs at $X_L \approx 0.5$. The complex's stoichiometry, therefore, is $Fe(SCN)^{2+}$.

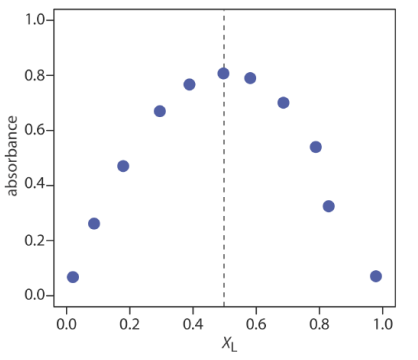

Several precautions are necessary when using the method of continuous variations. First, the metal and the ligand must form only one metal–ligand complex. To determine if this condition is true, plots of absorbance versus X_L are constructed at several different wavelengths and for several different values of n_{total}. If the maximum absorbance does not occur at the same value of X_L for each set of conditions, then more than one metal–ligand complex is present. A second precaution is that the metal–ligand complex's absorbance must obey Beer's law. Third, if the metal–ligand complex's formation constant is relatively small, a plot of absorbance versus X_L may show significant curvature. In this case it often is difficult to determine the stoichiometry by extrapolation. Finally, because the stability of a metal–ligand complex may be influenced by solution conditions, it is necessary to control carefully the composition of the solutions. When the ligand is a weak base, for example, each solutions must be buffered to the same pH.

In the ***mole-ratio method*** the moles of one reactant, usually the metal, is held constant, while the moles of the other reactant is varied. The absorbance is monitored at a wavelength where the metal–ligand complex absorbs. A plot of absorbance as a function of the ligand-to-metal mole ratio, n_L/n_M, has two linear branches that intersect at a mole–ratio corresponding to the complex's formula. Figure 10.3.15 a shows a mole-ratio plot for the formation of a 1:1 complex in which the absorbance is monitored at a wavelength where only the complex absorbs. Figure 10.3.15 b shows a mole-ratio plot for a 1:2 complex in which all three species —the metal, the ligand, and the complex—absorb at the selected wavelength. Unlike the method of continuous variations, the mole-ratio method can be used for complexation reactions that occur in a stepwise fashion if there is a difference in the molar absorptivities of the metal–ligand complexes, and if the formation constants are sufficiently different. A typical mole-ratio plot for the step-wise formation of ML and ML_2 is shown in Figure 10.3.15 c.

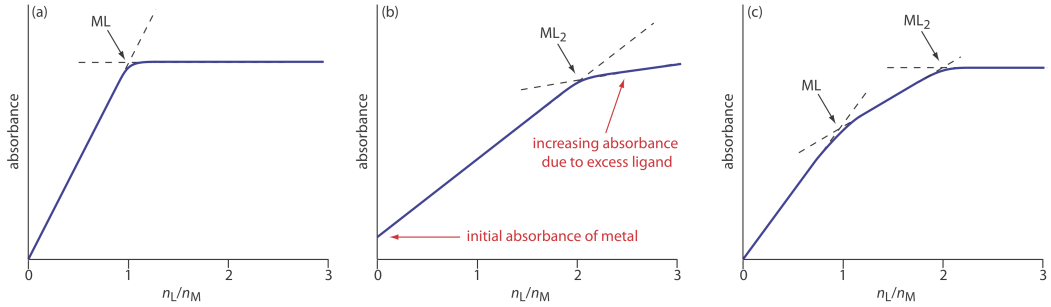

Figure 10.3.15 . Mole-ratio plots for: (a) a 1:1 metal–ligand complex in which only the complex absorbs; (b) a 1:2 metal–ligand complex in which the metal, the ligand, and the complex absorb; and (c) the stepwise formation of a 1:1 and a 1:2 metal–ligand complex.

For both the method of continuous variations and the mole-ratio method, we determine the complex's stoichiometry by extrapolating absorbance data from conditions in which there is a linear relationship between absorbance and the relative amounts of metal and ligand. If a metal–ligand complex is very weak, a plot of absorbance versus X_L or n_L/n_M becomes so curved that it is impossible to determine the stoichiometry by extrapolation. In this case the slope-ratio is used.

In the ***slope-ratio method*** two sets of solutions are prepared. The first set of solutions contains a constant amount of metal and a variable amount of ligand, chosen such that the total concentration of metal, C_M, is much larger than the total concentration of ligand, C_L. Under these conditions we may assume that essentially all the ligand reacts to form the metal–ligand complex. The concentration of the complex, which has the general form M_xL_y, is

$$[M_xL_y] = \frac{C_L}{y}$$

If we monitor the absorbance at a wavelength where only M_xL_y absorbs, then

$$A = \varepsilon b \left[M_xL_y\right] = \frac{\varepsilon b C_L}{y}$$

and a plot of absorbance versus C_L is linear with a slope, s_L, of

$$s_L = \frac{\varepsilon b}{y}$$

A second set of solutions is prepared with a fixed concentration of ligand that is much greater than a variable concentration of metal; thus

$$\left[M_xL_y\right] = \frac{C_M}{x}$$

$$A = \varepsilon b \left[M_xL_y\right] = \frac{\varepsilon b C_M}{x}$$

$$s_M = \frac{\varepsilon b}{x}$$

A ratio of the slopes provides the relative values of *x* and *y*.

$$\frac{s_M}{s_L} = \frac{\varepsilon b / x}{\varepsilon b / y} = \frac{y}{x}$$

An important assumption in the slope-ratio method is that the complexation reaction continues to completion in the presence of a sufficiently large excess of metal or ligand. The slope-ratio method also is limited to systems in which only a single complex forms and for which Beer's law is obeyed.

Determination of Equilibrium Constants

Another important application of molecular absorption spectroscopy is the determination of equilibrium constants. Let's consider, as a simple example, an acid–base reaction of the general form

$$HIn(aq) + H_2O(l) \rightleftharpoons H_3O^+(aq) + In^-(aq)$$

where HIn and In^- are the conjugate weak acid and weak base forms of an acid–base indicator. The equilibrium constant for this reaction is

$$K_a = \frac{\left[H_3O^+\right]\left[A^-\right]}{\left[HA\right]}$$

To determine the equilibrium constant's value, we prepare a solution in which the reaction is in a state of equilibrium and determine the equilibrium concentration for H_3O^+, HIn, and In^-. The concentration of H_3O^+ is easy to determine by measuring the solution's pH. To determine the concentration of HIn and In^- we can measure the solution's absorbance.

If both HIn and In^- absorb at the selected wavelength, then, from Beer's law, we know that

$$A = \varepsilon_{Hln} b [HIn] + \varepsilon_{ln} b [In^-] \tag{1.3.5}$$

where ε_{HIn} and ε_{In} are the molar absorptivities for HIn and In^-. The indicator's total concentration, *C*, is given by a mass balance equation

$$C = [HIn] + [In^-] \tag{1.3.6}$$

Solving Equation 1.3.6 for [HIn] and substituting into Equation 1.3.5 gives

$$A = \varepsilon_{Hln} b \left(C - \left[In^-\right]\right) + \varepsilon_{ln} b \left[In^-\right]$$

which we simplify to

$$A = \varepsilon_{Hln} bC - \varepsilon_{Hln} b \left[In^-\right] + \varepsilon_{ln} b \left[In^-\right]$$

$$A = A_{HIn} + b \left[In^-\right] \left(\varepsilon_{ln} - \varepsilon_{HIn}\right) \tag{1.3.7}$$

where A_{HIn}, which is equal to $\varepsilon_{\text{HIn}} bC$, is the absorbance when the pH is acidic enough that essentially all the indicator is present as HIn. Solving Equation 1.3.7 for the concentration of In^- gives

$$\left[\text{In}^-\right] = \frac{A - A_{\text{HIn}}}{b\left(\varepsilon_{\text{In}} - \varepsilon_{\text{HIn}}\right)} \tag{1.3.8}$$

Proceeding in the same fashion, we derive a similar equation for the concentration of HIn

$$[\text{HIn}] = \frac{A_{\text{In}} - A}{b\left(\varepsilon_{\text{In}} - \varepsilon_{\text{HIn}}\right)} \tag{1.3.9}$$

where A_{In}, which is equal to $\varepsilon_{\text{In}} bC$, is the absorbance when the pH is basic enough that only In^- contributes to the absorbance. Substituting Equation 1.3.8 and Equation 1.3.9 into the equilibrium constant expression for HIn gives

$$K_a = \frac{[\text{H}_3\text{O}^+][\text{In}^-]}{[\text{HIn}]} = [\text{H}_3\text{O}^+] \times \frac{A - A_{\text{HIn}}}{A_{\text{In}} - A} \tag{1.3.10}$$

We can use Equation 1.3.10 to determine K_a in one of two ways. The simplest approach is to prepare three solutions, each of which contains the same amount, C, of indicator. The pH of one solution is made sufficiently acidic such that [HIn] >> [In^-]. The absorbance of this solution gives A_{HIn}. The value of A_{In} is determined by adjusting the pH of the second solution such that [In^-] >> [HIn]. Finally, the pH of the third solution is adjusted to an intermediate value, and the pH and absorbance, A, recorded. The value of K_a is calculated using Equation 1.3.10.

Example 10.3.5

The acidity constant for an acid–base indicator is determined by preparing three solutions, each of which has a total concentration of indicator equal to 5.00×10^{-5} M. The first solution is made strongly acidic with HCl and has an absorbance of 0.250. The second solution is made strongly basic and has an absorbance of 1.40. The pH of the third solution is 2.91 and has an absorbance of 0.662. What is the value of K_a for the indicator?

Solution

The value of K_a is determined by making appropriate substitutions into 10.20 where [H_3O^+] is 1.23×10^{-3}; thus

$$K_a = \left(1.23 \times 10^{-3}\right) \times \frac{0.662 - 0.250}{1.40 - 0.662} = 6.87 \times 10^{-4}$$

Exercise 10.3.5

To determine the K_a of a merocyanine dye, the absorbance of a solution of 3.5×10^{-4} M dye was measured at a pH of 2.00, a pH of 6.00, and a pH of 12.00, yielding absorbances of 0.000, 0.225, and 0.680, respectively. What is the value of K_a for this dye? The data for this problem is adapted from Lu, H.; Rutan, S. C. *Anal. Chem.*, **1996**, *68*, 1381–1386.

Answer

The value of K_a is

$$K_a = \left(1.00 \times 10^{-6}\right) \times \frac{0.225 - 0.000}{0.680 - 0.225} = 4.95 \times 10^{-7}$$

A second approach for determining K_a is to prepare a series of solutions, each of which contains the same amount of indicator. Two solutions are used to determine values for A_{HIn} and A_{In}. Taking the log of both sides of Equation 1.3.10 and rearranging leave us with the following equation.

$$\log \frac{A - A_{\text{Hin}}}{A_{\text{In}^-} - A} = \text{pH} - \text{p}K_a \tag{1.3.11}$$

A plot of $\log[(A - A_{\text{HIn}})/(A_{\text{In}} - A)]$ versus pH is a straight-line with a slope of +1 and a y-intercept of $-\text{p}K_a$.

Exercise 10.3.6

To determine the K_a for the indicator bromothymol blue, the absorbance of each a series of solutions that contain the same concentration of bromothymol blue is measured at pH levels of 3.35, 3.65, 3.94, 4.30, and 4.64, yielding absorbance values of 0.170, 0.287, 0.411, 0.562, and 0.670, respectively. Acidifying the first solution to a pH of 2 changes its absorbance to 0.006, and adjusting the pH of the last solution to 12 changes its absorbance to 0.818. What is the value of K_a for bromothymol blue? The data for this problem is from Patterson, G. S. *J. Chem. Educ.*, **1999**, *76*, 395–398.

Answer

To determine K_a we use Equation 1.3.11, plotting $\log[(A - A_{HIn})/(A_{In} - A)]$ versus pH, as shown below.

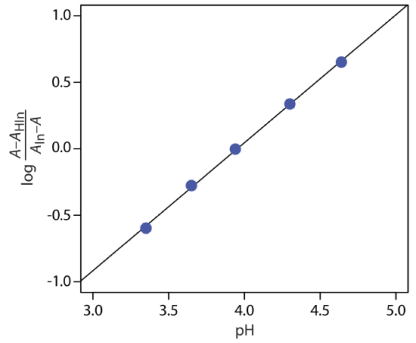

Fitting a straight-line to the data gives a regression model of

$$\log \frac{A - A_{HIn}}{A_{In} - A} = -3.80 + 0.962\text{pH}$$

The *y*-intercept is $-pK_a$; thus, the pK_a is 3.80 and the K_a is 1.58×10^{-4}.

In developing these approaches for determining K_a we considered a relatively simple system in which the absorbance of HIn and In^- are easy to measure and for which it is easy to determine the concentration of H_3O^+. In addition to acid–base reactions, we can adapt these approaches to any reaction of the general form

$$X(aq) + Y(aq) \rightleftharpoons Z(aq)$$

including metal–ligand complexation reactions and redox reactions, provided we can determine spectrophotometrically the concentration of the product, *Z*, and one of the reactants, either *X* or *Y*, and that we can determine the concentration of the other reactant by some other method. With appropriate modifications, a more complicated system in which we cannot determine the concentration of one or more of the reactants or products also is possible [Ramette, R. W. *Chemical Equilibrium and Analysis*, Addison-Wesley: Reading, MA, 1981, Chapter 13].

Evaluation of UV/Vis and IR Spectroscopy

Scale of Operations

Molecular UV/Vis absorption routinely is used for the analysis of trace analytes in macro and meso samples. Major and minor analytes are determined by diluting the sample before analysis, and concentrating a sample may allow for the analysis of ultratrace analytes. The scale of operations for infrared absorption is generally poorer than that for UV/Vis absorption.

Accuracy

Under normal conditions a relative error of 1–5% is easy to obtained with UV/Vis absorption. Accuracy usually is limited by the quality of the blank. Examples of the type of problems that are encountered include the pres- ence of particulates in the sample that scatter radiation, and the presence of interferents that react with analytical reagents. In the latter case the interferent may react to form an absorbing species, which leads to a positive determinate error. Interferents also may prevent the analyte from reacting, which leads to a negative determinate error. With care, it is possible to improve the accuracy of an analysis by as much as an order of magnitude.

Precision

In absorption spectroscopy, precision is limited by indeterminate errors—primarily instrumental noise—which are introduced when we measure absorbance. Precision generally is worse for low absorbances where $P_0 \approx P_T$, and for high absorbances where P_T approaches 0. We might expect, therefore, that precision will vary with transmittance.

We can derive an expression between precision and transmittance by applying the propagation of uncertainty as described in Chapter 4. To do so we rewrite Beer's law as

$$C = -\frac{1}{\varepsilon b}\log T \tag{1.3.12}$$

Table 4.3.1 in Chapter 4 helps us complete the propagation of uncertainty for Equation 1.3.12; thus, the absolute uncertainty in the concentration, s_C, is

$$s_c = -\frac{0.4343}{\varepsilon b} \times \frac{s_T}{T} \tag{1.3.13}$$

where s_T is the absolute uncertainty in the transmittance. Dividing Equation 1.3.13 by Equation 1.3.12 gives the relative uncertainty in concentration, s_C/C, as

$$\frac{s_c}{C} = \frac{0.4343 s_T}{T \log T}$$

If we know the transmittance's absolute uncertainty, then we can determine the relative uncertainty in concentration for any measured transmittance.

Determining the relative uncertainty in concentration is complicated because s_T is a function of the transmittance. As shown in Table 10.3.3 , three categories of indeterminate instrumental error are observed [Rothman, L. D.; Crouch, S. R.; Ingle, J. D. Jr. *Anal. Chem.* **1975**, *47*, 1226–1233]. A constant s_T is observed for the uncertainty associated with reading %T on a meter's analog or digital scale. Typical values are ±0.2–0.3% (a k_1 of ±0.002–0.003) for an analog scale and ±0.001% a (k_1 of ±0.00001) for a digital scale.

Table 10.3.3 . Effect of Indeterminate Errors on Relative Uncertainty in Concentration

category	sources of indeterminate error	relative uncertainty in concentration
$s_T = k_1$	%T readout resolution noise in thermal detectors	$\frac{s_C}{C} = \frac{0.4343 k_1}{T \log T}$
$s_T = k_2\sqrt{T^2 + T}$	noise in photon detectors	$\frac{s_C}{C} = \frac{0.4343 k_2}{\log T}\sqrt{1 + \frac{1}{T}}$
$s_T = k_3 T$	positioning of sample cell fluctuations in source intensity	$\frac{s_C}{C} = \frac{0.4343 k_3}{\log T}$

A constant s_T also is observed for the thermal transducers used in infrared spectrophotometers. The effect of a constant s_T on the relative uncertainty in concentration is shown by curve A in Figure 10.3.16 . Note that the relative uncertainty is very large for both high absorbances and low absorbances, reaching a minimum when the absorbance is 0.4343. This source of indeterminate error is important for infrared spectrophotometers and for inexpensive UV/Vis spectrophotometers. To obtain a relative uncertainty in concentration of ±1–2%, the absorbance is kept within the range 0.1–1.

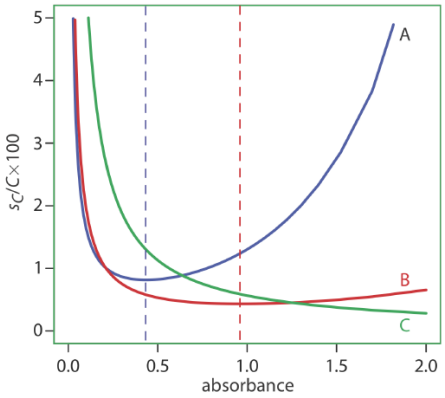

Figure 10.3.16 . Percent relative uncertainty in concentration as a function of absorbance for the categories of indeterminate errors in Table 1.3.10.3. A: k_1 = ±0.0030; B: k_2 = ±0.0030; and C: k_3= ±0.0130. The dashed lines correspond to the minimum uncertainty for curve A (absorbance of 0.4343) and for curve B (absorbance of 0.963).

Values of s_T are a complex function of transmittance when indeterminate errors are dominated by the noise associated with photon detectors. Curve B in Figure 10.3.16 shows that the relative uncertainty in concentration is very large for low absorbances, but is smaller at higher absorbances. Although the relative uncertainty reaches a minimum when the absorbance is 0.963, there is little change in the relative uncertainty for absorbances between 0.5 and 2. This source of indeterminate error generally limits the precision of high quality UV/Vis spectrophotometers for mid-to-high absorbances.

Finally, the value of s_T is directly proportional to transmittance for indeterminate errors that result from fluctuations in the source's intensity and from uncertainty in positioning the sample within the spectrometer. The latter is particularly important because the optical properties of a sample cell are not uniform. As a result, repositioning the sample cell may lead to a change in the intensity of transmitted radiation. As shown by curve C in Figure 10.3.16 , the effect is important only at low absorbances. This source of indeterminate errors usually is the limiting factor for high quality UV/Vis spectrophotometers when the absorbance is relatively small.

When the relative uncertainty in concentration is limited by the %T readout resolution, it is possible to improve the precision of the analysis by redefining 100% T and 0% T. Normally 100% T is established using a blank and 0% T is established while preventing the source's radiation from reaching the detector. If the absorbance is too high, precision is improved by resetting 100% T using a standard solution of analyte whose concentration is less than that of the sample (Figure 10.3.17 a). For a sample whose absorbance is too low, precision is improved by redefining 0% T using a standard solution of the analyte whose concentration is greater than that of the analyte (Figure 10.3.17 b). In this case a calibration curve is required because a linear relationship between absorbance and concentration no longer exists. Precision is further increased by combining these two methods (Figure 10.3.17 c). Again, a calibration curve is necessary since the relation- ship between absorbance and concentration is no longer linear.

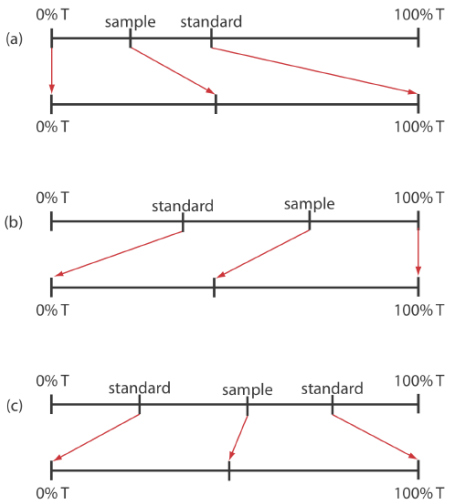

Figure 10.3.17 . Methods for improving the precision of absorption methods: (a) high-absorbance method; (b) low-absorbance method; (c) maximum precision method.

Sensitivity

The sensitivity of a molecular absorption method, which is the slope of a Beer's law calibration curve, is the product of the analyte's absorptivity and the pathlength of the sample cell (εb). You can improve a method's sensitivity by selecting a wavelength where absorbance is at a maximum or by increasing pathlength.

> See Figure 10.2.10 for an example of how the choice of wavelength affects a calibration curve's sensitivity.

Selectivity

Selectivity rarely is a problem in molecular absorption spectrophotometry. In many cases it is possible to find a wavelength where only the analyte absorbs. When two or more species do contribute to the measured absorbance, a multicomponent analysis is still possible, as shown in Example 10.3.2 and Example 10.3.3 .

Time, Cost, and Equipment

The analysis of a sample by molecular absorption spectroscopy is relatively rapid, although additional time is required if we need to convert a nonabsorbing analyte into an absorbing form. The cost of UV/Vis instrumentation ranges from several hundred dollars for a simple filter photometer, to more than $50,000 for a computer-controlled, high-resolution double-beam instrument equipped with variable slit widths, and operating over an extended range of wavelengths. Fourier transform infrared spectrometers can be obtained for as little as $15,000–$20,000, although more expensive models are available.

1.4: Atomic Absorption Spectroscopy

Guystav Kirchoff and Robert Bunsen first used atomic absorption—along with atomic emission—in 1859 and 1860 as a means for identify atoms in flames and hot gases. Although atomic emission continued to develop as an analytical technique, progress in atomic absorption languished for almost a century. Modern atomic absorption spectroscopy has its beginnings in 1955 as a result of the independent work of A. C. Walsh and C. T. J. Alkemade [(a) Walsh, A. *Anal. Chem.* **1991**, *63*, 933A–941A; (b) Koirtyohann, S. R. *Anal. Chem.* **1991**, *63*, 1024A–1031A; (c) Slavin, W. *Anal. Chem.* **1991**, *63*, 1033A–1038A]. Commercial instruments were in place by the early 1960s, and the importance of atomic absorption as an analytical technique soon was evident.

Instrumentation

Atomic absorption spectrophotometers use the same single-beam or double-beam optics described earlier for molecular absorption spectrophotometers (see Figure 10.3.2 and Figure 10.3.3). There is, however, an important additional need in atomic absorption spectroscopy: we first must covert the analyte into free atoms. In most cases the analyte is in solution form. If the sample is a solid, then we must bring the analyte into solution before the analysis. When analyzing a lake sediment for Cu, Zn, and Fe, for example, we bring the analytes into solution as Cu^{2+}, Zn^{2+}, and Fe^{3+} by extracting them with a suitable reagent. For this reason, only the introduction of solution samples is considered in this chapter.

> What reagent we choose to use to bring an analyte into solution depends on our research goals. If we need to know the total amount of metal in the sediment, then we might try a microwave digestion using a mixture of concentrated acids, such as HNO_3, HCl, and HF. This destroys the sediment's matrix and brings everything into solution. On the other hand, if our interest is biologically available metals, we might extract the sample under milder conditions using, for example, a dilute solution of HCl or CH_3COOH at room temperature.

Atomization

The process of converting an analyte to a free gaseous atom is called ***atomization***. Converting an aqueous analyte into a free atom requires that we strip away the solvent, volatilize the analyte, and, if necessary, dissociate the analyte into free atoms. Desolvating an aqueous solution of $CuCl_2$, for example, leaves us with solid particulates of $CuCl_2$. Converting the particulate $CuCl_2$ to gas phases atoms of Cu and Cl requires thermal energy.

$$\mathrm{CuCl_2}(aq) \rightarrow \mathrm{CuCl_2}(s) \rightarrow \mathrm{Cu}(g) + 2\mathrm{Cl}(g)$$

There are two common atomization methods: flame atomization and electrothermal atomization, although a few elements are atomized using other methods.

Flame Atomizer

Figure 10.4.1 shows a typical flame atomization assembly with close-up views of several key components. In the unit shown here, the aqueous sample is drawn into the assembly by passing a high-pressure stream of compressed air past the end of a capillary tube immersed in the sample. When the sample exits the nebulizer it strikes a glass impact bead, which converts it into a fine aerosol mist within the spray chamber. The aerosol mist is swept through the spray chamber by the combustion gases—compressed air and acetylene in this case—to the burner head where the flame's thermal energy desolvates the aerosol mist to a dry aerosol of small, solid particulates. The flame's thermal energy then volatilizes the particles, producing a vapor that consists of molecular species, ionic species, and free atoms.

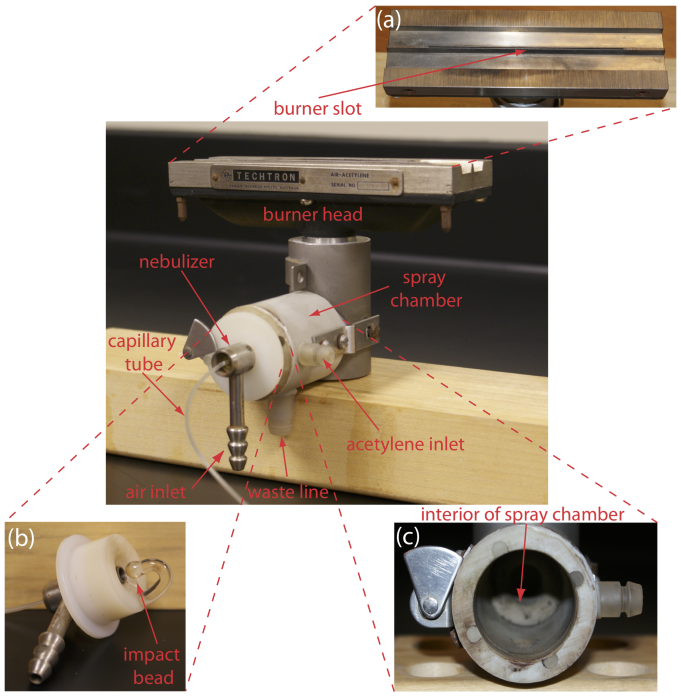

Figure 10.4.1 . Flame atomization assembly with expanded views of (a) the burner head showing the burner slot where the flame is located; (b) the nebulizer's impact bead; and (c) the interior of the spray chamber. Although the unit shown here is from an instrument dating to the 1970s, the basic components of a modern flame AA spectrometer are the same.

Burner. The slot burner in Figure 10.4.1 a provides a long optical pathlength and a stable flame. Because absorbance is directly proportional to pathlength, a long pathlength provides greater sensitivity. A stable flame minimizes uncertainty due to fluctuations in the flame.

The burner is mounted on an adjustable stage that allows the entire assembly to move horizontally and vertically. Horizontal adjustments ensure the flame is aligned with the instrument's optical path. Vertical adjustments change the height within the flame from which absorbance is monitored. This is important because two competing processes affect the concentration of free atoms in the flame. The more time an analyte spends in the flame the greater the atomization efficiency; thus, the production of free atoms increases with height. On the other hand, a longer residence time allows more opportunity for the free atoms to combine with oxygen to form a molecular oxide. As seen in Figure 10.4.2 , for a metal this is easy to oxidize, such as Cr, the concentration of free atoms is greatest just above the burner head. For a metal, such as Ag, which is difficult to oxidize, the concentration of free atoms increases steadily with height.

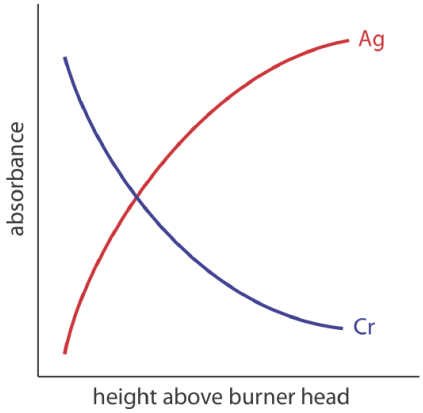

Figure 10.4.2 . Absorbance versus height profiles for Ag and Cr in flame atomic absorption spectroscopy.

Flame. The flame's temperature, which affects the efficiency of atomization, depends on the fuel–oxidant mixture, several examples of which are listed in Table 10.4.1 . Of these, the air–acetylene and the nitrous oxide–acetylene flames are the most

popular. Normally the fuel and oxidant are mixed in an approximately stoichiometric ratio; however, a fuel-rich mixture may be necessary for easily oxidized analytes.

Table 10.4.1 . Fuels and Oxidants Used for Flame Combustion

fuel	oxidant	temperature range (^{o}C)
natural gas	air	1700–1900
hydrogen	air	2000–2100
acetylene	air	2100–2400
acetylene	nitrous oxide	2600–2800
acetylene	oxygen	3050–3150

Figure 10.4.3 shows a cross-section through the flame, looking down the source radiation's optical path. The primary combustion zone usually is rich in gas combustion products that emit radiation, limiting is useful- ness for atomic absorption. The interzonal region generally is rich in free atoms and provides the best location for measuring atomic absorption. The hottest part of the flame typically is 2–3 cm above the primary combustion zone. As atoms approach the flame's secondary combustion zone, the decrease in temperature allows for formation of stable molecular species.

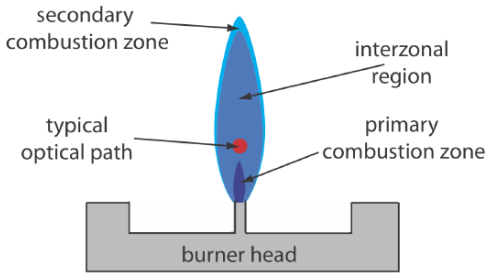

Figure 10.4.3 . Profile of typical flame using a slot burner. The relative size of each zone depends on many factors, including the choice of fuel and oxidant, and their relative proportions.

Sample Introduction. The most common means for introducing a sample into a flame atomizer is a continuous aspiration in which the sample flows through the burner while we monitor absorbance. Continuous aspiration is sample intensive, typically requiring from 2–5 mL of sample.

Flame microsampling allows us to introduce a discrete sample of fixed volume, and is useful if we have a limited amount of sample or when the sample's matrix is incompatible with the flame atomizer. For example, continuously aspirating a sample that has a high concentration of dissolved solids—sea water, for example, comes to mind—may build-up a solid de- posit on the burner head that obstructs the flame and that lowers the absorbance. Flame microsampling is accomplished using a micropipet to place 50–250 µL of sample in a Teflon funnel connected to the nebulizer, or by dipping the nebulizer tubing into the sample for a short time. Dip sampling usually is accomplished with an automatic sampler. The signal for flame microsampling is a transitory peak whose height or area is proportional to the amount of analyte that is injected.

Advantages and Disadvantages of Flame Atomization. The principal advantage of flame atomization is the reproducibility with which the sample is introduced into the spectrophotometer; a significant disadvantage is that the efficiency of atomization is quite poor. There are two reasons for poor atomization efficiency. First, the majority of the aerosol droplets produced during nebulization are too large to be carried to the flame by the combustion gases. Consequently, as much as 95% of the sample never reaches the flame, which is the reason for the waste line shown at the bottom of the spray chamber in Figure 10.4.1 . A second reason for poor atomization efficiency is that the large volume of combustion gases significantly dilutes the sample. Together, these contributions to the efficiency of atomization reduce sensitivity because the analyte's concentration in the flame may be a factor of 2.5×10^{-6} less than that in solution [Ingle, J. D.; Crouch, S. R. *Spectrochemical Analysis*, Prentice-Hall: Englewood Cliffs, NJ, 1988; p. 275].

Electrothermal Atomizers

A significant improvement in sensitivity is achieved by using the resistive heating of a graphite tube in place of a flame. A typical electrothermal atomizer, also known as a ***graphite furnace***, consists of a cylindrical graphite tube approximately 1–3 cm in length

and 3–8 mm in diameter. As shown in Figure 10.4.4 , the graphite tube is housed in an sealed assembly that has an optically transparent window at each end. A continuous stream of inert gas is passed through the furnace, which protects the graphite tube from oxidation and removes the gaseous products produced during atomization. A power supply is used to pass a current through the graphite tube, resulting in resistive heating.

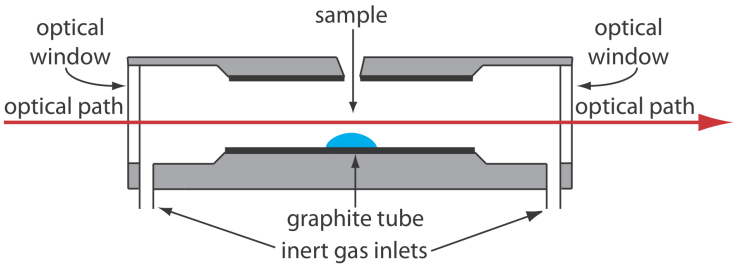

Figure 10.4.4 . Diagram showing a cross-section of an electrothermal analyzer.

Samples of between 5–50 μL are injected into the graphite tube through a small hole at the top of the tube. Atomization is achieved in three stages. In the first stage the sample is dried to a solid residue using a current that raises the temperature of the graphite tube to about 110°C. In the second stage, which is called ashing, the temperature is increased to between 350–1200°C. At these temperatures organic material in the sample is converted to CO_2 and H_2O, and volatile inorganic materials are vaporized. These gases are removed by the inert gas flow. In the final stage the sample is atomized by rapidly increasing the temperature to between 2000–3000°C. The result is a transient absorbance peak whose height or area is proportional to the absolute amount of analyte injected into the graphite tube. Together, the three stages take approximately 45–90 s, with most of this time used for drying and ashing the sample.

Electrothermal atomization provides a significant improvement in sensitivity by trapping the gaseous analyte in the small volume within the graphite tube. The analyte's concentration in the resulting vapor phase is as much as 1000× greater than in a flame atomization [Parsons, M. L.; Major, S.; Forster, A. R. *Appl. Spectrosc.* **1983**, *37*, 411–418]. This improvement in sensitivity—and the resulting improvement in detection limits—is offset by a significant decrease in precision. Atomization efficiency is influenced strongly by the sample's contact with the graphite tube, which is difficult to control reproducibly.

Miscellaneous Atomization Methods

A few elements are atomized by using a chemical reaction to produce a volatile product. Elements such as As, Se, Sb, Bi, Ge, Sn, Te, and Pb, for example, form volatile hydrides when they react with $NaBH_4$ in the presence of acid. An inert gas carries the volatile hydride to either a flame or to a heated quartz observation tube situated in the optical path. Mercury is determined by the cold-vapor method in which it is reduced to elemental mercury with $SnCl_2$. The volatile Hg is carried by an inert gas to an unheated observation tube situated in the instrument's optical path.

Quantitative Applications

Atomic absorption is used widely for the analysis of trace metals in a variety of sample matrices. Using Zn as an example, there are standard atomic absorption methods for its determination in samples as diverse as water and wastewater, air, blood, urine, muscle tissue, hair, milk, breakfast cereals, shampoos, alloys, industrial plating baths, gasoline, oil, sediments, and rocks.

Developing a quantitative atomic absorption method requires several considerations, including choosing a method of atomization, selecting the wavelength and slit width, preparing the sample for analysis, minimizing spectral and chemical interferences, and selecting a method of standardization. Each of these topics is considered in this section.

Developing a Quantitative Method

Flame or Electrothermal Atomization? The most important factor in choosing a method of atomization is the analyte's concentration. Because of its greater sensitivity, it takes less analyte to achieve a given absorbance when using electrothermal atomization. Table 10.4.2 , which compares the amount of analyte needed to achieve an absorbance of 0.20 when using flame atomization and electrothermal atomization, is useful when selecting an atomization method. For example, flame atomization is the method of choice if our samples contain 1–10 mg Zn^{2+}/L, but electrothermal atomization is the best choice for samples that contain 1–10 μg Zn^{2+}/L.

Table 10.4.2 . Concentration of Analyte (in mg/L) That Yields an Absorbance of 0.20

element	flame atomization	electrothermal atomization
Ag	1.5	0.0035
Al	40	0.015
As	40	0.050
Ca	0.8	0.003
Cd	0.6	0.001
Co	2.5	0.021
Cr	2.5	0.0075
Cu	1.5	0.012
Fe	2.5	0.006
Hg	70	0.52
Mg	0.15	0.00075
Mn	1	0.003
Na	0.3	0.00023
Ni	2	0.024
Pb	5	0.080
Pt	70	0.29
Sn	50	0.023
Zn	0.3	0.00071

Source: Varian Cookbook, SpectraAA Software Version 4.00 Pro.
As: 10 mg/L by hydride vaporization; Hg: 11.5 mg/L by cold-vapor; and Sn:18 mg/L by hydride vaporization

Selecting the Wavelength and Slit Width. The source for atomic absorption is a hollow cathode lamp that consists of a cathode and anode enclosed within a glass tube filled with a low pressure of an inert gas, such as Ne or Ar (Figure 10.4.5). Applying a potential across the electrodes ionizes the filler gas. The positively charged gas ions collide with the negatively charged cathode, sputtering atoms from the cathode's surface. Some of the sputtered atoms are in the excited state and emit radiation characteristic of the metal(s) from which the cathode is manufactured. By fashioning the cathode from the metallic analyte, a hollow cathode lamp provides emission lines that correspond to the analyte's absorption spectrum.

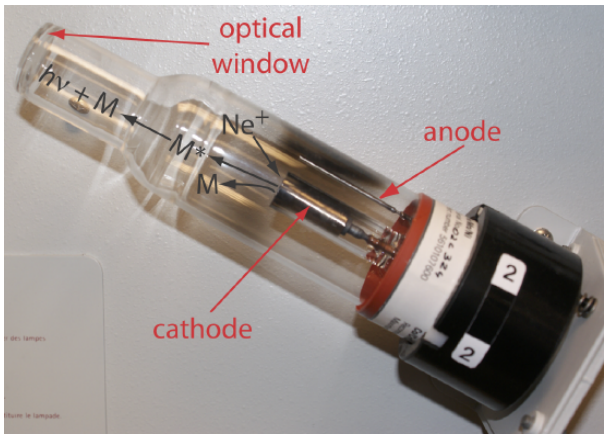

Figure 10.4.5 . Photo of a typical multielemental hollow cathode lamp. The cathode in this lamp is fashioned from an alloy of Co, Cr, Cu, Fe, Mn, and Ni, and is surrounded by a glass shield that isolates it from the anode. The lamp is filled with Ne gas. Also shown is the process that leads to atomic emission. Note the black deposit of sputtered metal on the outer wall of the hollow cathode lamp. See the text for additional details.

Because atomic absorption lines are narrow, we need to use a line source instead of a continuum source (compare, for example, Figure 10.2.4 with Figure 10.2.6). The effective bandwidth when using a continuum source is roughly 1000× larger than an atomic absorption line; thus, $P_T \approx P_0$, $\%T \approx 100$, and $A \approx 0$. Because a hollow cathode lamp is a line source, P_T and P_0 have different values giving a $\%T < 100$ and $A > 0$.

Each element in a hollow cathode lamp provides several atomic emission lines that we can use for atomic absorption. Usually the wavelength that provides the best sensitivity is the one we choose to use, although a less sensitive wavelength may be more appropriate for a sample that has higher concentration of analyte. For the Cr hollow cathode lamp in Table 10.4.3 , the best sensitivity is obtained using a wavelength of 357.9 nm.

Table 10.4.3 . Atomic Emission Lines for a Cr Hollow Cathode Lamp

wavelength (nm)	slit width (nm)	mg Cr/L giving $A = 0.20$	P_0 (relative)
357.9	0.2	2.5	40
425.4	0.2	12	85
429.0	0.5	20	100
520.5	0.2	1500	15
520.8	0.2	500	20

Another consideration is the emission line's intensity. If several emission lines meet our requirements for sensitivity, we may wish to use the emission line with the largest relative P_0 because there is less uncertainty in measuring P_0 and P_T. When analyzing a sample that is ≈10 mg Cr/L, for example, the first three wavelengths in Table 10.4.3 provide an appropriate sensitivity; the wavelengths of 425.4 nm and 429.0 nm, however, have a greater P_0 and will provide less uncertainty in the measured absorbance.

The emission spectrum for a hollow cathode lamp includes, in addition to the analyte's emission lines, additional emission lines from impurities present in the metallic cathode and from the filler gas. These additional lines are a potential source of stray radiation that could result in an instrumental deviation from Beer’s law. The monochromator’s slit width is set as wide as possible to improve the throughput of radiation and narrow enough to eliminate these sources of stray radiation.

Preparing the Sample. Flame and electrothermal atomization require that the analyte is in solution. Solid samples are brought into solution by dissolving in an appropriate solvent. If the sample is not soluble it is digested, either on a hot-plate or by microwave, using HNO_3, H_2SO_4, or $HClO_4$. Alternatively, we can extract the analyte using a Soxhlet extractor. Liquid samples are analyzed directly or the analytes extracted if the matrix is in- compatible with the method of atomization. A serum sample, for instance, is difficult to aspirate when using flame atomization and may produce an unacceptably high background absorbance when using electrothermal atomization. A liquid–liquid extraction using an organic solvent and a chelating agent frequently is used to

concentrate analytes. Dilute solutions of Cd^{2+}, Co^{2+}, Cu^{2+}, Fe^{3+}, Pb^{2+}, Ni^{2+}, and Zn^{2+}, for example, are concentrated by extracting with a solution of ammonium pyrrolidine dithiocarbamate in methyl isobutyl ketone.

Minimizing Spectral Interference. A spectral interference occurs when an analyte's absorption line overlaps with an interferent's absorption line or band. Because they are so narrow, the overlap of two atomic absorption lines seldom is a problem. On the other hand, a molecule's broad absorption band or the scattering of source radiation is a potentially serious spectral interference.

An important consideration when using a flame as an atomization source is its effect on the measured absorbance. Among the products of combustion are molecular species that exhibit broad absorption bands and particulates that scatter radiation from the source. If we fail to compensate for these spectral interferences, then the intensity of transmitted radiation is smaller than expected. The result is an apparent increase in the sample's absorbance. Fortunately, absorption and scattering of radiation by the flame are corrected by analyzing a blank.

Spectral interferences also occur when components of the sample's matrix other than the analyte react to form molecular species, such as oxides and hydroxides. The resulting absorption and scattering constitutes the sample's background and may present a significant problem, particularly at wavelengths below 300 nm where the scattering of radiation becomes more important. If we know the composition of the sample's matrix, then we can prepare our samples using an identical matrix. In this case the background absorption is the same for both the samples and the standards. Alternatively, if the background is due to a known matrix component, then we can add that component in excess to all samples and standards so that the contribution of the naturally occurring interferent is insignificant. Finally, many interferences due to the sample's matrix are eliminated by increasing the atomization temperature. For example, switching to a higher temperature flame helps prevents the formation of interfering oxides and hydroxides.

If the identity of the matrix interference is unknown, or if it is not possible to adjust the flame or furnace conditions to eliminate the interference, then we must find another method to compensate for the background interference. Several methods have been developed to compensate for matrix interferences, and most atomic absorption spectrophotometers include one or more of these methods.

One of the most common methods for ***background correction*** is to use a continuum source, such as a D_2 lamp. Because a D_2 lamp is a continuum source, absorbance of its radiation by the analyte's narrow absorption line is negligible. Only the background, therefore, absorbs radiation from the D_2 lamp. Both the analyte and the background, on the other hand, absorb the hollow cathode's radiation. Subtracting the absorbance for the D_2 lamp from that for the hollow cathode lamp gives a corrected absorbance that compensates for the background interference. Although this method of background correction is effective, it does assume that the background absorbance is constant over the range of wavelengths passed by the monochromator. If this is not true, then subtracting the two absorbances underestimates or overestimates the background.

> Other methods of background correction have been developed, including Zeeman effect background correction and Smith–Hieftje background correction, both of which are included in some commercially available atomic absorption spectrophotometers. Consult the chapter's additional resources for additional information.

Minimizing Chemical Interferences. The quantitative analysis of some elements is complicated by chemical interferences that occur during atomization. The most common chemical interferences are the formation of nonvolatile compounds that contain the analyte and ionization of the analyte.

One example of the formation of a nonvolatile compound is the effect of PO_4^{3-} or Al^{3+} on the flame atomic absorption analysis of Ca^{2+}. In one study, for example, adding 100 ppm Al^{3+} to a solution of 5 ppm Ca^{2+} decreased calcium ion's absorbance from 0.50 to 0.14, while adding 500 ppm PO_4^{3-} to a similar solution of Ca^{2+} decreased the absorbance from 0.50 to 0.38. These interferences are attributed to the formation of nonvolatile particles of $Ca_3(PO_4)_2$ and an Al–Ca–O oxide [Hosking, J. W.; Snell, N. B.; Sturman, B. T. *J. Chem. Educ.* **1977**, *54*, 128–130].

When using flame atomization, we can minimize the formation of non-volatile compounds by increasing the flame's temperature by changing the fuel-to-oxidant ratio or by switching to a different combination of fuel and oxidant. Another approach is to add a releasing agent or a protecting agent to the sample. A ***releasing agent*** is a species that reacts preferentially with the interferent, releasing the analyte during atomization. For example, Sr^{2+} and La^{3+} serve as releasing agents for the analysis of Ca^{2+} in the presence of PO_4^{3-} or Al^{3+}. Adding 2000 ppm $SrCl_2$ to the Ca^{2+}/ PO_4^{3-} and to the Ca^{2+}/Al^{3+} mixtures described in the previous

paragraph increased the absorbance to 0.48. A ***protecting agent*** reacts with the analyte to form a stable volatile complex. Adding 1% w/w EDTA to the Ca^{2+}/ PO_4^{3-} solution described in the previous paragraph increased the absorbance to 0.52.

An ionization interference occurs when thermal energy from the flame or the electrothermal atomizer is sufficient to ionize the analyte

$$M(s) \rightleftharpoons M^+(aq) + e^- \tag{1.4.1}$$

where M is the analyte. Because the absorption spectra for M and M^+ are different, the position of the equilibrium in reaction 1.4.1 affects the absorbance at wavelengths where M absorbs. To limit ionization we add a high concentration of an ***ionization suppressor***, which is a species that ionizes more easily than the analyte. If the ionization suppressor's concentration is sufficient, then the increased concentration of electrons in the flame pushes reaction 1.4.1 to the left, preventing the analyte's ionization. Potassium and cesium frequently are used as an ionization suppressor because of their low ionization energy.

Standardizing the Method. Because Beer's law also applies to atomic absorption, we might expect atomic absorption calibration curves to be linear. In practice, however, most atomic absorption calibration curves are nonlinear or linear over a limited range of concentrations. Nonlinearity in atomic absorption is a consequence of instrumental limitations, including stray radiation from the hollow cathode lamp and the variation in molar absorptivity across the absorption line. Accurate quantitative work, therefore, requires a suitable means for computing the calibration curve from a set of standards.

When possible, a quantitative analysis is best conducted using external standards. Unfortunately, matrix interferences are a frequent problem, particularly when using electrothermal atomization. For this reason the method of standard additions often is used. One limitation to this method of standardization, however, is the requirement of a linear relationship between absorbance and concentration.

> Most instruments include several different algorithms for computing the calibration curve. The instrument in my lab, for example, includes five algorithms. Three of the algorithms fit absorbance data using linear, quadratic, or cubic polynomial functions of the analyte's concentration. It also includes two algorithms that fit the concentrations of the standards to quadratic functions of the absorbance.

Representative Method 10.4.1: Determination of Cu and Zn in Tissue Samples

The best way to appreciate the theoretical and the practical details discussed in this section is to carefully examine a typical analytical method. Although each method is unique, the following description of the determination of Cu and Zn in biological tissues provides an instructive example of a typical procedure. The description here is based on Bhattacharya, S. K.; Goodwin, T. G.; Crawford, A. J. *Anal. Lett.* **1984**, *17*, 1567–1593, and Crawford, A. J.; Bhattacharya, S. K. Varian Instruments at Work, Number AA–46, April 1985.

Description of Method.

Copper and zinc are isolated from tissue samples by digesting the sample with HNO_3 after first removing any fatty tissue. The concentration of copper and zinc in the supernatant are determined by atomic absorption using an air-acetylene flame.

Procedure.

Tissue samples are obtained by a muscle needle biopsy and dried for 24–30 h at 105°C to remove all traces of moisture. The fatty tissue in a dried sample is removed by extracting overnight with anhydrous ether. After removing the ether, the sample is dried to obtain the fat-free dry tissue weight (FFDT). The sample is digested at 68°C for 20–24 h using 3 mL of 0.75 M HNO_3. After centrifuging at 2500 rpm for 10 minutes, the supernatant is transferred to a 5-mL volumetric flask. The digestion is repeated two more times, for 2–4 hours each, using 0.9-mL aliquots of 0.75 M HNO_3. These supernatants are added to the 5-mL volumetric flask, which is diluted to volume with 0.75 M HNO_3. The concentrations of Cu and Zn in the diluted supernatant are determined by flame atomic absorption spectroscopy using an air-acetylene flame and external standards. Copper is analyzed at a wavelength of 324.8 nm with a slit width of 0.5 nm, and zinc is analyzed at 213.9 nm with a slit width of 1.0 nm. Background correction using a D_2 lamp is necessary for zinc. Results are reported as μg of Cu or Zn per gram of FFDT.

Questions.

1. Describe the appropriate matrix for the external standards and for the blank?

The matrix for the standards and the blank should match the matrix of the samples; thus, an appropriate matrix is 0.75 M HNO_3. Any interferences from other components of the sample matrix are minimized by background correction.

2. Why is a background correction necessary for the analysis of Zn, but not for the analysis of Cu?

Background correction compensates for background absorption and scattering due to interferents in the sample. Such interferences are most severe when using a wavelength less than 300 nm. This is the case for Zn, but not for Cu.

3. A Cu hollow cathode lamp has several emission lines, the properties of which are shown in the following table. Explain why this method uses the line at 324.8 nm.

wavelength (nm)	slit width (nm)	mg Cu/L for A = 0.20	P_0 (relative)
217.9	0.2	15	3
218.2	0.2	15	3
222.6	0.2	60	5
244.2	0.2	400	15
249.2	0.5	200	24
324.8	0.5	1.5	100
327.4	0.5	3	87

With 1.5 mg Cu/L giving an absorbance of 0.20, the emission line at 324.8 nm has the best sensitivity. In addition, it is the most intense emission line, which decreases the uncertainty in the measured absorbance.

Example 10.4.1

To evaluate the method described in Representative Method 10.4.1, a series of external standard is prepared and analyzed, providing the results shown here [Crawford, A. J.; Bhattacharya, S. K. “Microanalysis of Copper and Zinc in Biopsy-Sized Tissue Specimens by Atomic Absorption Spectroscopy Using a Stoichiometric Air-Acetylene Flame,” Varian Instruments at Work, Number AA–46, April 1985].

µg Cu/mL	absorbance	µg Cu/mL	absorbance
0.000	0.000	0.500	0.033
0.100	0.006	0.600	0.039
0.200	0.013	0.700	0.046
0.300	0.020	1.00	0.066
0.400	0.026		

A bovine liver standard reference material is used to evaluate the method’s accuracy. After drying and extracting the sample, a 11.23-mg FFDT tissue sample gives an absorbance of 0.023. Report the amount of copper in the sample as µg Cu/g FFDT.

Solution

Linear regression of absorbance versus the concentration of Cu in the standards gives the calibration curve shown below and the following calibration equation.

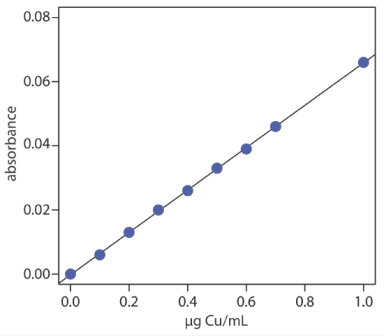

$$A = -0.0002 + 0.0661 \times \frac{\mu g\ Cu}{mL}$$

Substituting the sample's absorbance into the calibration equation gives the concentration of copper as 0.351 µg/mL. The concentration of copper in the tissue sample, therefore, is

$$\frac{\frac{0.351 \mu g\ Cu}{mL} \times 5.000\ mL}{0.01123\ g\ sample} = 156\ \mu g\ Cu/g\ FDT$$

Evaluation of Atomic Absorption Spectroscopy

Scale of Operation

Atomic absorption spectroscopy is ideally suited for the analysis of trace and ultratrace analytes, particularly when using electrothermal atomization. For minor and major analytes, sample are diluted before the analysis. Most analyses use a macro or a meso sample. The small volume requirement for electrothermal atomization or for flame microsampling, however, makes practical the analysis of micro and ultramicro samples.

Accuracy

If spectral and chemical interferences are minimized, an accuracy of 0.5–5% is routinely attainable. When the calibration curve is nonlinear, accuracy is improved by using a pair of standards whose absorbances closely bracket the sample's absorbance and assuming that the change in absorbance is linear over this limited concentration range. Determinate errors for electrothermal atomization often are greater than those obtained with flame atomization due to more serious matrix interferences.

Precision

For an absorbance greater than 0.1–0.2, the relative standard deviation for atomic absorption is 0.3–1% for flame atomization and 1–5% for electrothermal atomization. The principle limitation is the uncertainty in the concentration of free analyte atoms that result from variations in the rate of aspiration, nebulization, and atomization for a flame atomizer, and the consistency of injecting samples for electrothermal atomization.

Sensitivity

The sensitivity of a flame atomic absorption analysis is influenced by the flame's composition and by the position in the flame from which we monitor the absorbance. Normally the sensitivity of an analysis is optimized by aspirating a standard solution of analyte and adjusting the fuel-to-oxidant ratio, the nebulizer flow rate, and the height of the burner, to give the greatest absorbance. With electrothermal atomization, sensitivity is influenced by the drying and ashing stages that precede atomization. The temperature and time at each stage is optimized for each type of sample.

Sensitivity also is influenced by the sample's matrix. We already noted, for example, that sensitivity is decreased by a chemical interference. An increase in sensitivity may be realized by adding a low molecular weight alcohol, ester, or ketone to the solution, or by using an organic solvent.

Selectivity

Due to the narrow width of absorption lines, atomic absorption provides excellent selectivity. Atomic absorption is used for the analysis of over 60 elements at concentrations at or below the level of µg/L.

Time, Cost, and Equipment

The analysis time when using flame atomization is short, with sample throughputs of 250–350 determinations per hour when using a fully automated system. Electrothermal atomization requires substantially more time per analysis, with maximum sample throughputs of 20–30 determinations per hour. The cost of a new instrument ranges from between $10,000– $50,000 for flame atomization, and from $18,000–$70,000 for electrothermal atomization. The more expensive instruments in each price range include double-beam optics, automatic samplers, and can be programmed for multielemental analysis by allowing the wavelength and hollow cathode lamp to be changed automatically.

1.5: Emission Spectroscopy

An analyte in an excited state possesses an energy, E_2, that is greater than its energy when it is in a lower energy state, E_1. When the analyte returns to its lower energy state—a process we call relaxation—the excess energy, ΔE

$$\Delta E = E_2 - E_1$$

is released. Figure 10.1.4 shows a simplified picture of this process.

The amount of time an analyte, *A*, spends in its excited state—what we call the excited state's ***lifetime***—is short, typically 10^{-5}–10^{-9} s for an electronic excited state and 10–15 s for a vibrational excited state. Relaxation of the analyte's excited state, *A**, occurs through several mechanisms, including collisions with other species in the sample, photochemical reactions, and the emission of photons. In the first process, which we call vibrational relaxation or nonradiative relaxation, the excess energy is released as heat.

$$A^* \longrightarrow A + \text{heat}$$

Relaxation by a photochemical reaction may involve simple decomposition

$$A^* \longrightarrow X + Y$$

or a reaction between *A** and another species

$$A^* + Z \longrightarrow X + Y$$

In both cases the excess energy is used up in the chemical reaction or released as heat.

In the third mechanism, the excess energy is released as a photon of electromagnetic radiation.

$$A^* \longrightarrow A + h\nu$$

The release of a photon following thermal excitation is called emission and that following the absorption of a photon is called photoluminescence. In chemiluminescence and bioluminescence, excitation results from a chemical or a biochemical reaction, respectively. Spectroscopic methods based on photoluminescence are the subject of the next section and atomic emission is covered in Chapter 10.7.

1.6: Photoluminescent Spectroscopy

Photoluminescence is divided into two categories: fluorescence and phosphorescence. A pair of electrons that occupy the same electronic ground state have opposite spins and are in a singlet spin state (Figure 10.6.1 a).

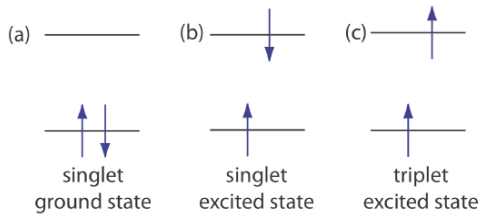

Figure 10.6.1 . Electron configurations for (a) a singlet ground state; (b) a singlet excited state; and (c) a triplet excited state.

When an analyte absorbs an ultraviolet or a visible photon, one of its valence electrons moves from the ground state to an excited state with a conservation of the electron's spin (Figure 10.6.1 b). Emission of a photon from a ***singlet excited state*** to the singlet ground state—or between any two energy levels with the same spin—is called ***fluorescence***. The probability of fluorescence is very high and the average lifetime of an electron in the excited state is only 10^{-5}–10^{-8} s. Fluorescence, therefore, rapidly decays once the source of excitation is removed.

In some cases an electron in a singlet excited state is transformed to a ***triplet excited state*** (Figure 10.6.1 c) in which its spin no is longer paired with the ground state. Emission between a triplet excited state and a singlet ground state—or between any two energy levels that differ in their respective spin states–is called ***phosphorescence***. Because the average lifetime for phosphorescence ranges from 10^{-4}–10^{4} s, phosphorescence may continue for some time after we remove the excitation source.

The use of molecular fluorescence for qualitative analysis and for semi-quantitative analysis dates to the early to mid 1800s, with more accurate quantitative methods appearing in the 1920s. Instrumentation for fluorescence spectroscopy using a filter or a monochromator for wavelength selection appeared in, respectively, the 1930s and 1950s. Although the discovery of phosphorescence preceded that of fluorescence by almost 200 years, qualitative and quantitative applications of molecular phosphorescence did not receive much attention until after the development of fluorescence instrumentation.

> As you might expect, the persistence of long-lived phosphorescence made it more noticeable.

Fluorescence and Phosphorescence Spectra

To appreciate the origin of fluorescence and phosphorescence we must consider what happens to a molecule following the absorption of a photon. Let's assume the molecule initially occupies the lowest vibrational energy level of its electronic ground state, which is the singlet state labeled S_0 in Figure 10.6.2 . Absorption of a photon excites the molecule to one of several vibrational energy levels in the first excited electronic state, S_1, or the second electronic excited state, S_2, both of which are singlet states. Relaxation to the ground state occurs by a number of mechanisms, some of which result in the emission of a photon and others that occur without the emission of a photon. These relaxation mechanisms are shown in Figure 10.6.2 . The most likely relaxation pathway from any excited state is the one with the shortest lifetime.

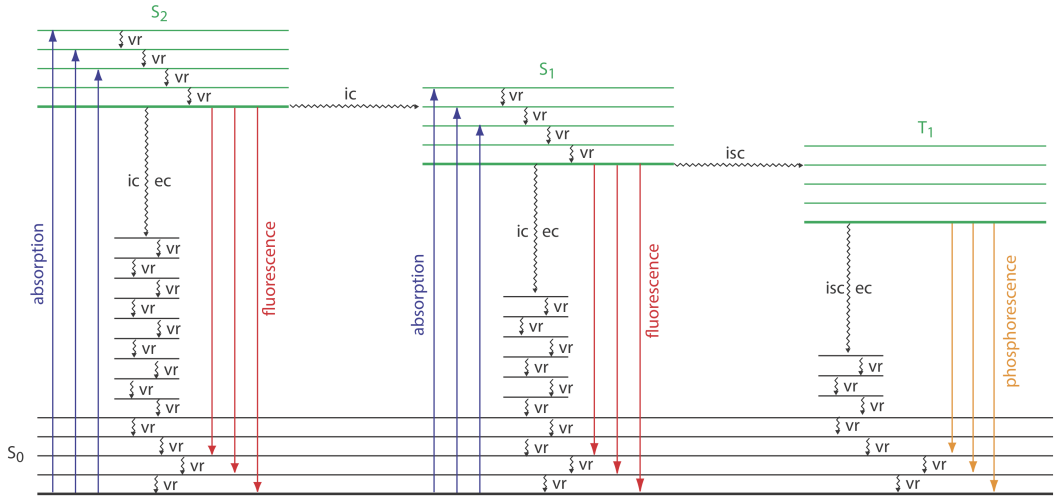

Figure 10.6.2 . Energy level diagram for a molecule that shows pathways for the deactivation of an excited state: ***vr*** is vibrational relaxation; ***ic*** is internal conversion; ***ec*** is external conversion; and ***isc*** is an intersystem crossing. The lowest vibrational energy for each electronic state is indicated by the thicker line. The electronic ground state is shown in black and the three electronic excited states are shown in green. The absorption, fluorescence, and phosphorescence of photons also are shown.

Radiationless Deactivation

When a molecule relaxes without emitting a photon we call the process ***radiationless deactivation***. One example of radiationless deactivation is ***vibrational relaxation***, in which a molecule in an excited vibrational energy level loses energy by moving to a lower vibrational energy level in the same electronic state. Vibrational relaxation is very rapid, with an average lifetime of $<10^{-12}$ s. Because vibrational relaxation is so efficient, a molecule in one of its excited state's higher vibrational energy levels quickly returns to the excited state's lowest vibrational energy level.

Another form of radiationless deactivation is an ***internal conversion*** in which a molecule in the ground vibrational level of an excited state passes directly into a higher vibrational energy level of a lower energy electronic state of the same spin state. By a combination of internal conversions and vibrational relaxations, a molecule in an excited electronic state may return to the ground electronic state without emitting a photon. A related form of radiationless deactivation is an ***external conversion*** in which excess energy is transferred to the solvent or to another component of the sample's matrix.

> Let's use Figure 10.6.2 to illustrate how a molecule can relax back to its ground state without emitting a photon. Suppose our molecule is in the highest vibrational energy level of the second electronic excited state. After a series of vibrational relaxations brings the molecule to the lowest vibrational energy level of S_2, it undergoes an internal conversion into a higher vibrational energy level of the first excited electronic state. Vibrational relaxations bring the molecule to the lowest vibrational energy level of S_1. Following an internal conversion into a higher vibrational energy level of the ground state, the molecule continues to undergo vibrational relaxation until it reaches the lowest vibrational energy level of S_0.

A final form of radiationless deactivation is an ***intersystem crossing*** in which a molecule in the ground vibrational energy level of an excited electronic state passes into one of the higher vibrational energy levels of a lower energy electronic state with a different spin state. For example, an intersystem crossing is shown in Figure 10.6.2 between the singlet excited state S_1 and the triplet excited state T_1.

Relaxation by Fluorescence

Fluorescence occurs when a molecule in an excited state's lowest vibrational energy level returns to a lower energy electronic state by emitting a photon. Because molecules return to their ground state by the fastest mechanism, fluorescence is observed only if it is a more efficient means of relaxation than a combination of internal conversions and vibrational relaxations.

A quantitative expression of fluorescence efficiency is the fluorescent ***quantum yield***, Φ_f, which is the fraction of excited state molecules that return to the ground state by fluorescence. The fluorescent quantum yields range from 1 when every molecule in an excited state undergoes fluorescence, to 0 when fluorescence does not occur.

The intensity of fluorescence, I_f, is proportional to the amount of radiation absorbed by the sample, $P_0 - P_T$, and the fluorescent quantum yield

$$I_f = k\Phi_f (P_0 - P_T) \tag{1.6.1}$$

where k is a constant that accounts for the efficiency of collecting and detecting the fluorescent emission. From Beer's law we know that

$$\frac{P_T}{P_0} = 10^{-\varepsilon bC} \tag{1.6.2}$$

where C is the concentration of the fluorescing species. Solving Equation 1.6.2 for P_T and substituting into Equation 1.6.1 gives, after simplifying

$$I_f = k\Phi_f P_0 \left(1 - 10^{-\varepsilon bC}\right) \tag{1.6.3}$$

When $\varepsilon bC < 0.01$, which often is the case when the analyte's concentration is small, Equation 1.6.3 simplifies to

$$I_f = 2.303 k\Phi_f \varepsilon bC P_0 = k' P_0 \tag{1.6.4}$$

where k' is a collection of constants. The intensity of fluorescence, therefore, increases with an increase in the quantum efficiency, the source's incident power, and the molar absorptivity and the concentration of the fluorescing species.

Fluorescence generally is observed when the molecule's lowest energy absorption is a $\pi \rightarrow \pi^*$ transition, although some $n \rightarrow \pi^*$ transitions show weak fluorescence. Many unsubstituted, nonheterocyclic aromatic compounds have a favorable fluorescence quantum yield, although substitutions on the aromatic ring can effect Φ_f significantly. For example, the presence of an electron-withdrawing group, such as $-NO_2$, decreases Φ_f, while adding an electron-donating group, such as –OH, increases Φ_f. Fluorrescence also increases for aromatic ring systems and for aromatic molecules with rigid planar structures. Figure 10.6.3 shows the fluorescence of quinine under a UV lamp.

Figure 10.6.3 . Tonic water, which contains quinine, is fluorescent when placed under a UV lamp. Source: Splarka (commons.Wikipedia.org).

A molecule's fluorescent quantum yield also is influenced by external variables, such as temperature and solvent. Increasing the temperature generally decreases Φ_f because more frequent collisions between the molecule and the solvent increases external conversion. A decrease in the solvent's viscosity decreases Φ_f for similar reasons. For an analyte with acidic or basic functional groups, a change in pH may change the analyte's structure and its fluorescent properties.

As shown in Figure 10.6.2 , fluorescence may return the molecule to any of several vibrational energy levels in the ground electronic state. Fluorescence, therefore, occurs over a range of wavelengths. Because the change in energy for fluorescent emission generally is less than that for absorption, a molecule's fluorescence spectrum is shifted to higher wavelengths than its absorption spectrum.

Relaxation by Phosphorescence

A molecule in a triplet electronic excited state's lowest vibrational energy level normally relaxes to the ground state by an intersystem crossing to a singlet state or by an external conversion. Phosphorescence occurs when the molecule relaxes by emitting a photon. As shown in Figure 10.6.2 , phosphorescence occurs over a range of wavelengths, all of which are at lower energies than the molecule's absorption band. The intensity of phosphorescence, I_p, is given by an equation similar to Equation 1.6.4 for fluorescence

$$I_P = 2.303k\Phi_P\varepsilon bCP_0 \tag{1.6.5}$$

$$= k'P_0 \tag{1.6.6}$$

where Φ_p is the ***phosphorescent quantum yield***.

Phosphorescence is most favorable for molecules with $n \rightarrow \pi^*$ transitions, which have a higher probability for an intersystem crossing than $\pi \rightarrow \pi^*$ transitions. For example, phosphorescence is observed with aromatic molecules that contain carbonyl groups or heteroatoms. Aromatic compounds that contain halide atoms also have a higher efficiency for phosphorescence. In general, an increase in phosphorescence corresponds to a decrease in fluorescence.

Because the average lifetime for phosphorescence can be quite long, ranging from 10^{-4}–10^4 s, the phosphorescent quantum yield usually is quite small. An improvement in Φ_p is realized by decreasing the efficiency of external conversion. This is accomplished in several ways, including lowering the temperature, using a more viscous solvent, depositing the sample on a solid substrate, or trapping the molecule in solution. Figure 10.6.4 shows an example of phosphorescence.

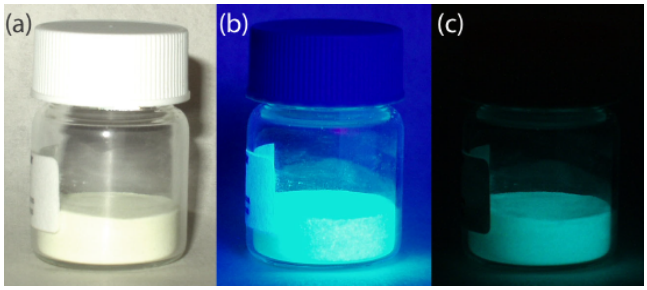

Figure 10.6.4 . An europium doped strontium silicate-aluminum oxide powder under (a) natural light, (b) a long-wave UV lamp, and (c) in total darkness. The photo taken in total darkness shows the phosphorescent emission. Source: modified from Splarka (commons.Wikipedia.org).

Excitation Versus Emission Spectra

Photoluminescence spectra are recorded by measuring the intensity of emitted radiation as a function of either the excitation wavelength or the emission wavelength. An ***excitation spectrum*** is obtained by monitoring emission at a fixed wavelength while varying the excitation wavelength. When corrected for variations in the source's intensity and the detector's response, a sample's excitation spectrum is nearly identical to its absorbance spectrum. The excitation spectrum provides a convenient means for selecting the best excitation wavelength for a quantitative or qualitative analysis.

In an ***emission spectrum*** a fixed wavelength is used to excite the sample and the intensity of emitted radiation is monitored as function of wavelength. Although a molecule has a single excitation spectrum, it has two emission spectra, one for fluorescence and one for phosphorescence. Figure 10.6.5 shows the UV absorption spectrum and the UV fluorescence emission spectrum for quinine.

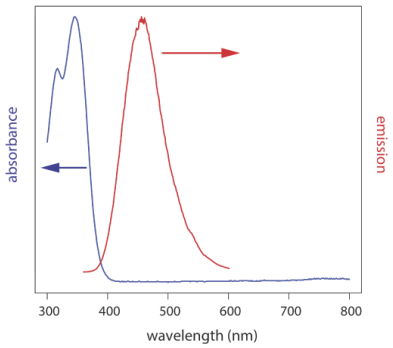

Figure 10.6.5 . Absorbance spectrum and fluorescence emission spectrum for quinine in 0.05 M H_2SO_4. The emission spectrum uses an excitation wavelength of 350 nm with a bandwidth of 20 nm. Both spectra are normalized so that the maximum absorbance is 1.00 and the maximum emission is 1.00. The actual maximum absorbance is 0.444 and the actual maximum emission is 126747. Source: data from Daniel Scott, Department of Chemistry & Biochemistry, DePauw University.

Instrumentation

The basic instrumentation for monitoring fluorescence and phosphorescence—a source of radiation, a means of selecting a narrow band of radiation, and a detector—are the same as those for absorption spectroscopy. The unique demands of fluorescence and phosphorescence, however, require some modifications to the instrument designs seen earlier in Figure 10.3.1 (filter photometer), Figure 10.3.2 (single-beam spectrophotometer), Figure 10.3.3 (double-beam spectrophotometer), and Figure 10.3.4 (diode array spectrometer). The most important difference is that the detector cannot be placed directly across from the source. Figure 10.6.6 shows why this is the case. If we place the detector along the source's axis it receives both the transmitted source radiation, P_T, and the fluorescent, I_f, or phosphorescent, I_p, radiation. Instead, we rotate the director and place it at 90^o to the source.

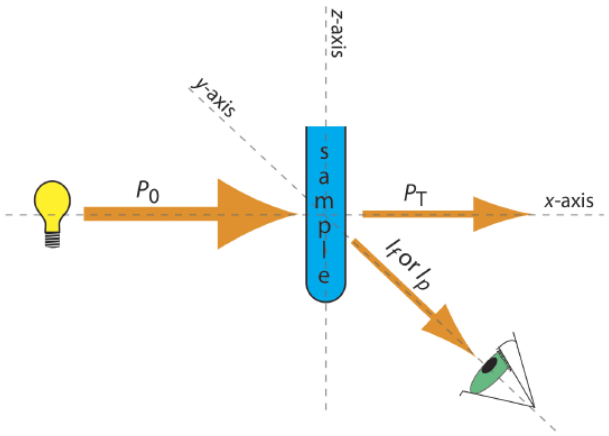

Figure 10.6.6 . Schematic diagram showing the orientation of the source and the detector when measuring fluorescence and phosphorescence. Contrast this to Figure 10.2.7, which shows the orientation for absorption spectroscopy.

Instruments for Measuring Fluorescence

Figure 10.6.7 shows the basic design of an instrument for measuring fluorescence, which includes two wavelength selectors, one for selecting the source's excitation wavelength and one for selecting the analyte's emission wavelength. In a ***fluorimeter*** the excitation and emission wavelengths are selected using absorption or interference filters. The excitation source for a fluorimeter usually is a low-pressure Hg vapor lamp that provides intense emission lines distributed throughout the ultraviolet and visible region. When a monochromator is used to select the excitation and the emission wavelengths, the instrument is called a ***spectrofluorometer***. With a monochromator the excitation source usually is a high-pressure Xe arc lamp, which has a continuous emission spectrum. Either instrumental design is appropriate for quantitative work, although only a spectrofluorometer can record an excitation or emission spectrum.

> A Hg vapor lamp has emission lines at 254, 312, 365, 405, 436, 546, 577, 691, and 773 nm.

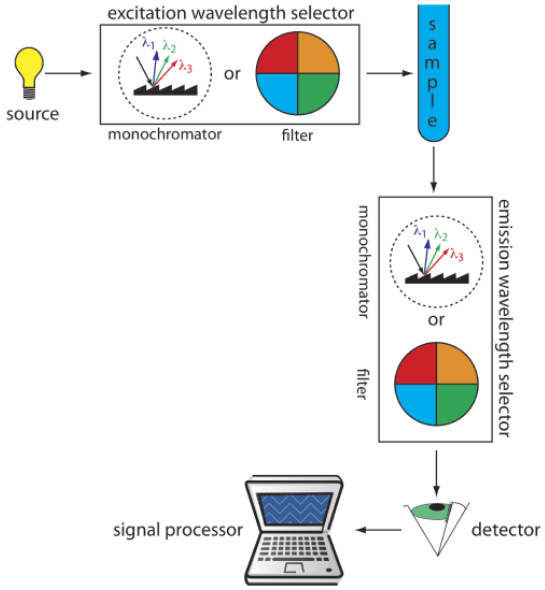

Figure 10.6.7 . Schematic diagram for measuring fluorescence showing the placement of the wavelength selectors for excitation and emission. When a filter is used the instrument is called a fluorimeter and when a monochromator is used the instrument is called a spectrofluorimeter.

The sample cells for molecular fluorescence are similar to those for molecular absorption (see Figure 10.3.6). Remote sensing using a fiber optic probe (see Figure 10.3.7) is possible using with either a fluorimeter or spectrofluorometer. An analyte that is fluorescent is monitored directly. For an analyte that is not fluorescent, a suitable fluorescent probe molecule is incorporated into the tip of the fiber optic probe. The analyte's reaction with the probe molecule leads to an increase or decrease in fluorescence.

Instruments for Measuring Phosphorescence

An instrument for molecular phosphorescence must discriminate between phosphorescence and fluorescence. Because the lifetime for fluorescence is shorter than that for phosphorescence, discrimination is achieved by incorporating a delay between exciting the sample and measuring the phosphorescent emission. Figure 10.6.8 shows how two out-of-phase choppers allow us to block fluorescent emission from reaching the detector when the sample is being excited and to prevent the source radiation from causing fluorescence when we are measuring the phosphorescent emission.

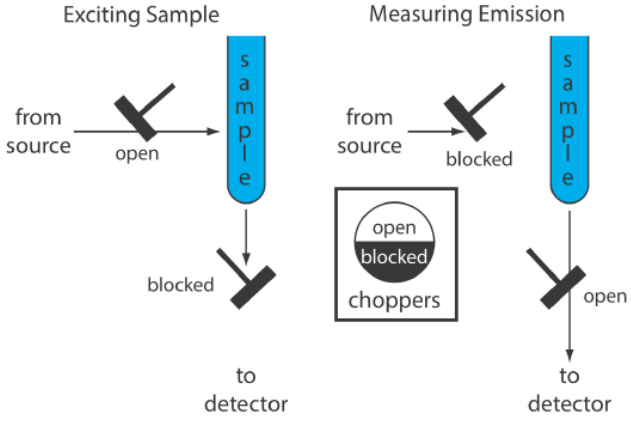

Figure 10.6.8 . Schematic diagram showing how choppers are used to prevent fluorescent emission from interfering with the measurement of phosphorescent emission.

Because phosphorescence is such a slow process, we must prevent the excited state from relaxing by external conversion. One way this is accomplished is by dissolving the sample in a suitable organic solvent, usually a mixture of ethanol, isopentane, and diethylether. The resulting solution is frozen at liquid-N_2 temperatures to form an optically clear solid. The solid matrix minimizes external conversion due to collisions between the analyte and the solvent. External conversion also is minimized by immobilizing the sample on a solid substrate, making possible room temperature measurements. One approach is to place a drop of a solution that contains the analyte on a small disc of filter paper. After drying the sample under a heat lamp, the sample is placed in the

spectrofluorometer for analysis. Other solid substrates include silica gel, alumina, sodium acetate, and sucrose. This approach is particularly useful for the analysis of thin layer chromatography plates.

Quantitative Applications

Molecular fluorescence and, to a lesser extent, phosphorescence are used for the direct or indirect quantitative analysis of analytes in a variety of matrices. A direct quantitative analysis is possible when the analyte's fluorescent or phosphorescent quantum yield is favorable. If the analyte is not fluorescent or phosphorescent, or if the quantum yield is unfavorable, then an indirect analysis may be feasible. One approach is to react the analyte with a reagent to form a product that is fluorescent or phosphorescent. Another approach is to measure a decrease in fluorescence or phosphores- cence when the analyte is added to a solution that contains a fluorescent or phosphorescent probe molecule. A decrease in emission is observed when the reaction between the analyte and the probe molecule enhances radiationless deactivation or results in a nonemitting product. The application of fluorescence and phosphorescence to inorganic and organic analytes are considered in this section.

Inorganic Analytes

Except for a few metal ions, most notably UO_2^+, most inorganic ions are not sufficiently fluorescent for a direct analysis. Many metal ions are determined indirectly by reacting with an organic ligand to form a fluorescent or, less commonly, a phosphorescent metal–ligand complex. One example is the reaction of Al^{3+} with the sodium salt of 2, 4, 3′-trihydroxyazobenzene-5′-sulfonic acid —also known as alizarin garnet R—which forms a fluorescent metal–ligand complex (Figure 10.6.9). The analysis is carried out using an excitation wavelength of 470 nm, with fluorescence monitored at 500 nm. Table 10.6.1 provides additional examples of chelating reagents that form fluorescent metal–ligand complexes with metal ions. A few inorganic nonmetals are determined by their ability to decrease, or quench, the fluorescence of another species. One example is the analysis for F^- based on its ability to quench the fluorescence of the Al^{3+}–alizarin garnet R complex.

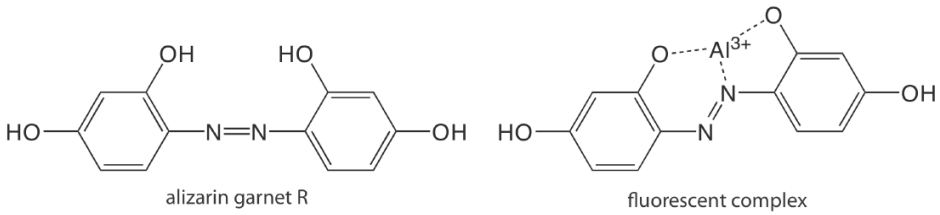

Figure 10.6.9 . Structure of alizarin garnet R and its metal–ligand complex with Al^{3+}.

Table 10.6.1 . Chelating Agents for the Fluorescent Analysis of Metal Ions

chelating agent	metal ions
8-hydroxyquinoline	Al^{3+}, Be^{2+}, Zn^{2+}, Li^+, Mg^{2+} (and others)
flavonal	Zr^{2+}, Sn^{4+}
benzoin	$B_4O_6^{2-}$, Zn^{2+}
$2', 3', 4', 5, 7-$ pentahydroxylflavone	Be^{2+}
2-(*o*-hydroxyphenyl) benzoxazole	Cd^{2+}

Organic Analytes

As noted earlier, organic compounds that contain aromatic rings generally are fluorescent and aromatic heterocycles often are phosphorescent. Table 10.6.2 provides examples of several important biochemical, pharmaceutical, and environmental compounds that are analyzed quantitatively by fluorimetry or phosphorimetry. If an organic analyte is not naturally fluorescent or phosphorescent, it may be possible to incorporate it into a chemical reaction that produces a fluorescent or phosphorescent product. For example, the enzyme creatine phosphokinase is determined by using it to catalyze the formation of creatine from phosphocreatine. Reacting the creatine with ninhydrin produces a fluorescent product of unknown structure.

Table 10.6.2 . Examples of Naturally Photoluminescent Organic Analytes

class	compounds (F = fluorescence, P = phosphorescence)

class	compounds (F = fluorescence, P = phosphorescence)
aromatic amino acids	phenylalanine (F) tyrosine (F) tryptophan (F, P)
vitamins	vitamin A (F) vitamin B2 (F) vitamin B6 (F) vitamin B12 (F) vitamin E (F) folic acid (F)
catecholamines	dopamine (F) norepinephrine (F)
pharmaceuticals and drugs	quinine (F) salicylic acid (F, P) morphine (F) barbiturates (F) LSD (F) codeine (P) caffeine (P) sulfanilamide (P)
environmental pollutants	pyrene (F) benzo[a]pyrene (F) organothiophosphorous pesticides (F) carbamate insecticides (F) DDT (P)

Standardizing the Method

From Equation 1.6.4 and Equation 1.6.6 we know that the intensity of fluorescence or phosphorescence is a linear function of the analyte's concentration provided that the sample's absorbance of source radiation ($A = \varepsilon bC$) is less than approximately 0.01. Calibration curves often are linear over four to six orders of magnitude for fluorescence and over two to four orders of magnitude for phosphorescence. For higher concentrations of analyte the calibration curve becomes nonlinear because the assumptions that led to Equation 1.6.4 and Equation 1.6.6 no longer apply. Nonlinearity may be observed for smaller concentrations of analyte fluorescent or phosphorescent contaminants are present. As discussed earlier, quantum efficiency is sensitive to temperature and sample matrix, both of which must be con- trolled when using external standards. In addition, emission intensity depends on the molar absorptivity of the photoluminescent species, which is sensitive to the sample matrix.

Representative Method 10.6.1: Determination of Quinine in Urine

The best way to appreciate the theoretical and the practical details discussed in this section is to carefully examine a typical analytical method. Although each method is unique, the following description of the determination of quinine in urine provides an instructive example of a typical procedure. The description here is based on Mule, S. J.; Hushin, P. L. *Anal. Chem.* **1971**, *43*, 708–711, and O'Reilly, J. E.; *J. Chem. Educ.* **1975**, *52*, 610–612. Figure 10.6.3 shows the fluorescence of the quinine in tonic water.

Description of the Method

Quinine is an alkaloid used to treat malaria. It is a strongly fluorescent compound in dilute solutions of H_2SO_4 ($\Phi_f = 0.55$). Quinine's excitation spectrum has absorption bands at 250 nm and 350 nm and its emission spectrum has a single emission band at 450 nm. Quinine is excreted rapidly from the body in urine and is determined by measuring its fluorescence following its extraction from the urine sample.

Procedure

Transfer a 2.00-mL sample of urine to a 15-mL test tube and use 3.7 M NaOH to adjust its pH to between 9 and 10. Add 4 mL of a 3:1 (v/v) mixture of chloroform and isopropanol and shake the contents of the test tube for one minute. Allow the organic and the aqueous (urine) layers to separate and transfer the organic phase to a clean test tube. Add 2.00 mL of 0.05 M H_2SO_4 to the organic phase and shake the contents for one minute. Allow the organic and the aqueous layers to separate and transfer the aqueous phase to the sample cell. Measure the fluorescent emission at 450 nm using an excitation wavelength of 350 nm. Determine the concentration of quinine in the urine sample using a set of external standards in 0.05 M H_2SO_4, prepared from a 100.0 ppm solution of quinine in 0.05 M H_2SO_4. Use distilled water as a blank.

Questions

1. Chloride ion quenches the intensity of quinine's fluorescent emission. For example, in the presence of 100 ppm NaCl (61 ppm Cl^-) quinine's emission intensity is only 83% of its emission intensity in the absence of chloride. The presence of 1000 ppm NaCl (610 ppm Cl^-) further reduces quinine's fluorescent emission to less than 30% of its emission intensity in the absence of chloride. The concentration of chloride in urine typically ranges from 4600–6700 ppm Cl^-. Explain how this procedure prevents an interference from chloride.

> The procedure uses two extractions. In the first of these extractions, quinine is separated from urine by extracting it into a mixture of chloroform and isopropanol, leaving the chloride ion behind in the original sample.

2. Samples of urine may contain small amounts of other fluorescent compounds, which will interfere with the analysis if they are carried through the two extractions. Explain how you can modify the procedure to take this into account?

> One approach is to prepare a blank that uses a sample of urine known to be free of quinine. Subtracting the blank's fluorescent signal from the measured fluorescence from urine samples corrects for the interfering compounds.

The fluorescent emission for quinine at 450 nm can be induced using an excitation frequency of either 250 nm or 350 nm. The fluorescent quantum efficiency is the same for either excitation wavelength. Quinine's absorption spectrum shows that ε_{250} is greater than ε_{350}. Given that quinine has a stronger absorbance at 250 nm, explain why its fluorescent emission intensity is greater when using 350 nm as the excitation wavelength.

> From Equation 1.6.4 we know that I_f is a function of the following terms: k, Φ_f, P_0, ε, b, and C. We know that Φ_f, b, and C are the same for both excitation wavelengths and that ε is larger for a wavelength of 250 nm; we can, therefore, ignore these terms. The greater emission intensity when using an excitation wavelength of 350 nm must be due to a larger value for P_0 or k. In fact, P_0 at 350 nm for a high-pressure Xe arc lamp is about 170% of that at 250 nm. In addition, the sensitivity of a typical photomultiplier detector (which contributes to the value of k) at 350 nm is about 140% of that at 250 nm.

Example 10.6.1

To evaluate the method described in Representative Method 10.6.1, a series of external standard are prepared and analyzed, providing the results shown in the following table. All fluorescent intensities are corrected using a blank prepared from a quinine-free sample of urine. The fluorescent intensities are normalized by setting I_f for the highest concentration standard to 100.

[quinine] (μg/mL)	I_f
1.00	10.11
3.00	30.20
5.00	49.84
7.00	69.89
10.00	100.0

After ingesting 10.0 mg of quinine, a volunteer provides a urine sample 24-h later. Analysis of the urine sample gives a relative emission intensity of 28.16. Report the concentration of quinine in the sample in mg/L and the percent recovery for the ingested quinine.

Solution

Linear regression of the relative emission intensity versus the concentration of quinine in the standards gives the calibration curve shown below and the following calibration equation.

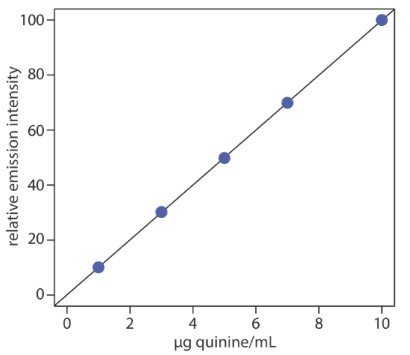

$$I_f = 0.122 + 9.978 \times \frac{\text{g quinine}}{\text{mL}}$$

Substituting the sample's relative emission intensity into the calibration equation gives the concentration of quinine as 2.81 µg/mL. Because the volume of urine taken, 2.00 mL, is the same as the volume of 0.05 M H_2SO_4 used to extract the quinine, the concentration of quinine in the urine also is 2.81 µg/mL. The recovery of the ingested quinine is

$$\frac{\frac{2.81\ \mu\text{g quinine}}{\text{mL urine}} \times 2.00\ \text{mL urine} \times \frac{1\text{mg}}{1000\ \mu\text{g}}}{10.0\ \text{mg quinine ingested}} \times 100 = 0.0562\%$$

It can take 10–11 days for the body to completely excrete quinine so it is not surprising that such a small amount of quinine is recovered from this sample of urine.

Evaluation of Photoluminescence Spectroscopy

Scale of Operation

Photoluminescence spectroscopy is used for the routine analysis of trace and ultratrace analytes in macro and meso samples. Detection limits for fluorescence spectroscopy are influenced by the analyte's quantum yield. For an analyte with $\Phi_f > 0.5$, a picomolar detection limit is possible when using a high quality spectrofluorometer. For example, the detection limit for quinine sulfate, for which Φ is 0.55, generally is between 1 part per billion and 1 part per trillion. Detection limits for phosphorescence are somewhat higher, with typical values in the nanomolar range for low-temperature phosphorimetry and in the micromolar range for room-temperature phosphorimetry using a solid substrate.

Accuracy

The accuracy of a fluorescence method generally is between 1–5% when spectral and chemical interferences are insignificant. Accuracy is limited by the same types of problems that affect other optical spectroscopic methods. In addition, accuracy is affected by interferences that affect the fluorescent quantum yield. The accuracy of phosphorescence is somewhat greater than that for fluorescence.

Precision

The relative standard deviation for fluorescence usually is between 0.5–2% when the analyte's concentration is well above its detection limit. Precision usually is limited by the stability of the excitation source. The precision for phosphorescence often is limited by reproducibility in preparing samples for analysis, with relative standard deviations of 5–10% being common.

Sensitivity

From Equation 1.6.4 and Equation 1.6.6 we know that the sensitivity of a fluorescent or a phosphorescent method is affected by a number of parameters. We already have considered the importance of quantum yield and the effect of temperature and solution composition on Φ_f and Φ_p. Besides quantum yield, sensitivity is improved by using an excitation source that has a greater emission intensity, P_0, at the desired wavelength, and by selecting an excitation wavelength for which the analyte has a greater molar absorptivity, ε. Another approach for improving sensitivity is to increase the volume from which emission is monitored.

Figure 10.6.10 shows how rotating a monochromator's slits from their usual vertical orientation to a horizontal orientation increases the sampling volume. The result can in- crease the emission from the sample by $5 - 30\times$.

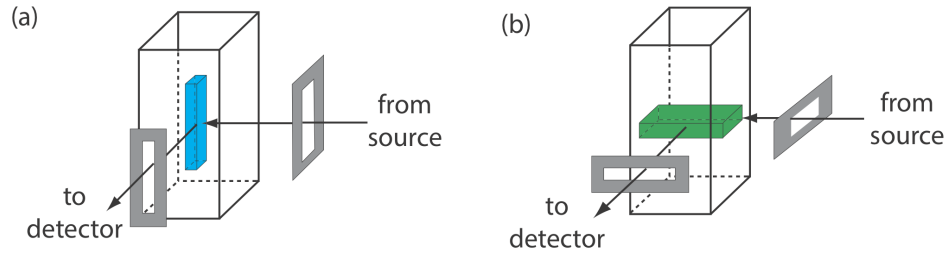

Figure 10.6.10 . Use of slit orientation to change the volume from which fluorescence is measured: (a) vertical slit orientation; (b) horizontal slit orientation. Suppose the slit's dimensions are 0.1 mm × 3 mm. In (a) the dimensions of the sampling volume are 0.1 mm × 0.1 mm × 3 mm, or 0.03 mm^3. For (b) the dimensions of the sampling volume are 0.1 mm × 3 mm × 3 mm, or 0.9 mm^3, a 30-fold increase in the sampling volume.

Selectivity

The selectivity of fluorescence and phosphorescence is superior to that of absorption spectrophotometry for two reasons: first, not every compound that absorbs radiation is fluorescent or phosphorescent; and, second, selectivity between an analyte and an interferent is possible if there is a difference in either their excitation or their emission spectra. The total emission intensity is a linear sum of that from each fluorescent or phosphorescent species. The analysis of a sample that contains *n* analytes, therefore, is accomplished by measuring the total emission intensity at *n* wavelengths.

Time, Cost, and Equipment

As with other optical spectroscopic methods, fluorescent and phosphorescent methods provide a rapid means for analyzing samples and are capable of automation. Fluorimeters are relatively inexpensive, ranging from several hundred to several thousand dollars, and often are satisfactory for quantitative work. Spectrofluorometers are more expensive, with models often exceeding $50,000.

1.7: Atomic Emission Spectroscopy

The focus of this section is on the emission of ultraviolet and visible radiation following the thermal excitation of atoms. Atomic emission spectroscopy has a long history. Qualitative applications based on the color of flames were used in the smelting of ores as early as 1550 and were more fully developed around 1830 with the observation of atomic spectra generated by flame emission and spark emission [Dawson, J. B. *J. Anal. At. Spectrosc.* **1991**, *6*, 93–98]. Quantitative applications based on the atomic emission from electric sparks were developed by Lockyer in the early 1870 and quantitative applications based on flame emission were pioneered by Lundegardh in 1930. Atomic emission based on emission from a plasma was introduced in 1964.

> For an on-line introduction to much of the material in this section, see Atomic Emission Spectroscopy (AES) by Tomas Spudich and Alexander Scheeline, a resource that is part of the Analytical Sciences Digital Library.

Atomic Emission Spectra

Atomic emission occurs when a valence electron in a higher energy atomic orbital returns to a lower energy atomic orbital. Figure 10.7.1 shows a portion of the energy level diagram for sodium, which consists of a series of discrete lines at wavelengths that correspond to the difference in energy between two atomic orbitals.

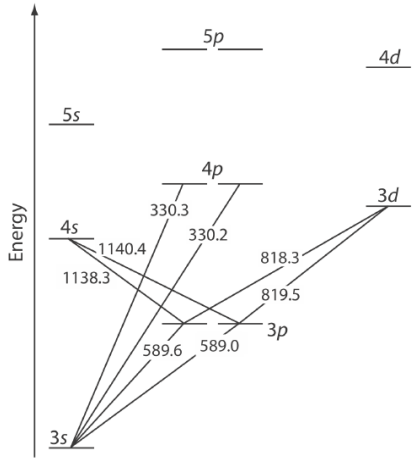

Figure 10.7.1 . Valence shell energy level diagram for sodium. The wavelengths corresponding to several transitions are shown. Note that this is the same energy level diagram as Figure 10.2.5.

The intensity of an atomic emission line, I_e, is proportional to the number of atoms, N^*, that populate the excited state,

$$I_e = kN^* \tag{1.7.1}$$

where k is a constant that accounts for the efficiency of the transition. If a system of atoms is in thermal equilibrium, the population of excited state i is related to the total concentration of atoms, N, by the Boltzmann distribution. For many elements at temperatures of less than 5000 K the Boltzmann distribution is approximated as

$$N^* = N\left(\frac{g_i}{g_0}\right)e^{-E_i/kT} \tag{1.7.2}$$

where g_i and g_0 are statistical factors that account for the number of equivalent energy levels for the excited state and the ground state, E_i is the energy of the excited state relative to a ground state energy, E_0, k is Boltzmann's constant (1.3807×10^{-23} J/K), and T is the temperature in Kelvin. From Equation 1.7.2 we expect that excited states with lower energies have larger populations and more intense emission lines. We also expect emission intensity to increase with temperature.

Equipment

An atomic emission spectrometer is similar in design to the instrumentation for atomic absorption. In fact, it is easy to adapt most flame atomic absorption spectrometers for atomic emission by turning off the hollow cathode lamp and monitoring the difference between the emission intensity when aspirating the sample and when aspirating a blank. Many atomic emission spectrometers,

however, are dedicated instruments designed to take advantage of features unique to atomic emission, including the use of plasmas, arcs, sparks, and lasers as atomization and excitation sources, and an enhanced capability for multielemental analysis.

Atomization and Excitation

Atomic emission requires a means for converting into a free gaseous atom an analyte that is present in a solid, liquid, or solution sample. The same source of thermal energy used for atomization usually serves as the excitation source. The most common methods are flames and plasmas, both of which are useful for liquid or solution samples. Solid samples are analyzed by dissolving in a solvent and using a flame or plasma atomizer.

Flame Sources

Atomization and excitation in flame atomic emission is accomplished with the same nebulization and spray chamber assembly used in atomic absorption (Figure 10.4.1). The burner head consists of a single or multiple slots, or a Meker-style burner. Older atomic emission instruments often used a total consumption burner in which the sample is drawn through a capillary tube and injected directly into the flame.

> A Meker burner is similar to the more common Bunsen burner found in most laboratories; it is designed to allow for higher temperatures and for a larger diameter flame.

Plasma Sources

A ***plasma*** is a hot, partially ionized gas that contains an abundant concentration of cations and electrons. The plasma used in atomic emission is formed by ionizing a flowing stream of argon gas, producing argon ions and electrons. A plasma's high temperature results from resistive heating as the electrons and argon ions move through the gas. Because a plasma operates at a much higher temperature than a flame, it provides for a better atomization efficiency and a higher population of excited states.

A schematic diagram of the inductively coupled plasma source (ICP) is shown in Figure 10.7.2 . The ICP torch consists of three concentric quartz tubes, surrounded at the top by a radio-frequency induction coil. The sample is mixed with a stream of Ar using a nebulizer, and is carried to the plasma through the torch's central capillary tube. Plasma formation is initiated by a spark from a Tesla coil. An alternating radio-frequency current in the induction coil creates a fluctuating magnetic field that induces the argon ions and the electrons to move in a circular path. The resulting collisions with the abundant unionized gas give rise to resistive heating, providing temperatures as high as 10000 K at the base of the plasma, and between 6000 and 8000 K at a height of 15–20 mm above the coil, where emission usually is measured. At these high temperatures the outer quartz tube must be thermally isolated from the plasma. This is accomplished by the tangential flow of argon shown in the schematic diagram.

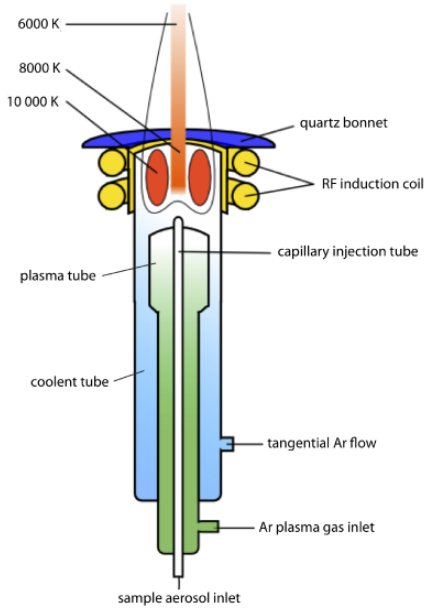

Figure 10.7.2 . Schematic diagram of an inductively coupled plasma torch.

Multielemental Analysis

Atomic emission spectroscopy is ideally suited for a multielemental analysis because all analytes in a sample are excited simultaneously. If the instrument includes a scanning monochromator, we can program it to move rapidly to an analyte's desired wavelength, pause to record its emission intensity, and then move to the next analyte's wavelength. This sequential analysis allows for a sampling rate of 3–4 analytes per minute.

Another approach to a multielemental analysis is to use a multichannel instrument that allows us to monitor simultaneously many analytes. A simple design for a multichannel spectrometer, shown in Figure 10.7.3 , couples a monochromator with multiple detectors that are positioned in a semicircular array around the monochromator at positions that correspond to the wavelengths for the analytes.

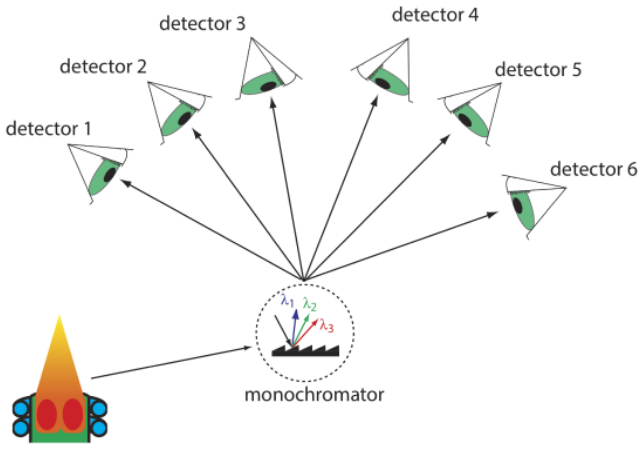

Figure 10.7.3 . Schematic diagram of a multichannel atomic emission spectrometer for the simultaneous analysis of several elements. Instruments may contain as many as 48–60 detectors.

Quantitative Applications

Atomic emission is used widely for the analysis of trace metals in a variety of sample matrices. The development of a quantitative atomic emission method requires several considerations, including choosing a source for atomization and excitation, selecting a wavelength and slit width, preparing the sample for analysis, minimizing spectral and chemical interferences, and selecting a method of standardization.

Choice of Atomization and Excitation Source

Except for the alkali metals, detection limits when using an ICP are significantly better than those obtained with flame emission (Table 10.7.1). Plasmas also are subject to fewer spectral and chemical interferences. For these reasons a plasma emission source is usually the better choice.

Table \(\PageIndex{1}). Detection Limits for Atomic Emission

element	detection limit (µg/mL): flame emission	detection limit (µg/mL): ICP
Ag	2	0.2
Al	3	0.2
As	2000	2
Ca	0.1	0.0001
Cd	300	0.07
Co	5	0.1
Cr	1	0.08
Fe	10	0.09
Hg	150	1

element	detection limit (µg/mL): flame emission	detection limit (µg/mL): ICP
K	0.01	30
Li	0.001	0.02
Mg	1	0.02
Mn	1	0.01
Na	0.01	0.1
Ni	10	0.2
Pb	0.2	1
Pt	2000	0.9
Sn	100	3
Zn	1000	0.1

Source: Parsons, M. L.; Major, S.; Forster, A. R.; App. Spectrosc. 1983, 37, 411–418.

Selecting the Wavelength and Slit Width

The choice of wavelength is dictated by the need for sensitivity and the need to avoid interferences from the emission lines of other constituents in the sample. Because an analyte's atomic emission spectrum has an abundance of emission lines—particularly when using a high temperature plasma source—it is inevitable that there will be some overlap between emission lines. For example, an analysis for Ni using the atomic emission line at 349.30 nm is complicated by the atomic emission line for Fe at 349.06 nm.

A narrower slit width provides better resolution, but at the cost of less radiation reaching the detector. The easiest approach to selecting a wavelength is to record the sample's emission spectrum and look for an emission line that provides an intense signal and is resolved from other emission lines.

Preparing the Sample

Flame and plasma sources are best suited for samples in solution and in liquid form. Although a solid sample can be analyzed by directly inserting it into the flame or plasma, they usually are first brought into solution by digestion or extraction.

Minimizing Spectral Interferences

The most important spectral interference is broad, background emission from the flame or plasma and emission bands from molecular species. This background emission is particularly severe for flames because the temperature is insufficient to break down refractory compounds, such as oxides and hydroxides. Background corrections for flame emission are made by scanning over the emission line and drawing a baseline (Figure 10.7.4). Because a plasma's temperature is much higher, a background interference due to molecular emission is less of a problem. Although emission from the plasma's core is strong, it is insignificant at a height of 10–30 mm above the core where measurements normally are made.

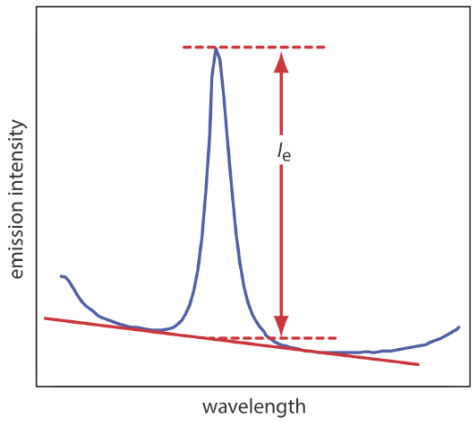

Figure 10.7.4 . Method for correcting an analyte's emission for the flame's background emission.

Minimizing Chemical Interferences

Flame emission is subject to the same types of chemical interferences as atomic absorption; they are minimized using the same methods: by adjusting the flame's composition and by adding protecting agents, releasing agents, or ionization suppressors. An additional chemical interference results from ***self-absorption***. Because the flame's temperature is greatest at its center, the concentration of analyte atoms in an excited state is greater at the flame's center than at its outer edges. If an excited state atom in the flame's center emits a photon, then a ground state atom in the cooler, outer regions of the flame may absorb the photon, which decreases the emission intensity. For higher concentrations of analyte self-absorption may invert the center of the emission band (Figure 10.7.5).

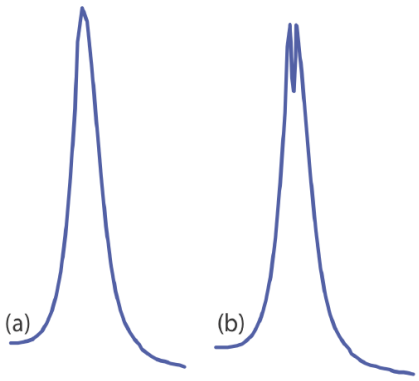

Figure 10.7.5 . Atomic emission lines for (a) a low concentration of analyte, and (b) a high concentration of analyte showing the effect of self-absorption.

Chemical interferences when using a plasma source generally are not significant because the plasma's higher temperature limits the formation of nonvolatile species. For example, PO_4^{3-} is a significant interferent when analyzing samples for Ca^{2+} by flame emission, but has a negligible effect when using a plasma source. In addition, the high concentration of electrons from the ionization of argon minimizes ionization interferences.

Standardizing the Method

From Equation 1.7.1 we know that emission intensity is proportional to the population of the analyte's excited state, N^*. If the flame or plasma is in thermal equilibrium, then the excited state population is proportional to the analyte's total population, N, through the Boltzmann distribution (Equation 1.7.2).

A calibration curve for flame emission usually is linear over two to three orders of magnitude, with ionization limiting linearity when the analyte's concentrations is small and self-absorption limiting linearity at higher concentrations of analyte. When using a plasma, which suffers from fewer chemical interferences, the calibration curve often is linear over four to five orders of magnitude and is not affected significantly by changes in the matrix of the standards.

Emission intensity is affected significantly by many parameters, including the temperature of the excitation source and the efficiency of atomization. An increase in temperature of 10 K, for example, produces a 4% increase in the fraction of Na atoms in

the 3*p* excited state, an uncertainty in the signal that may limit the use of external standards. The method of internal standards is used when the variations in source parameters are difficult to control. To compensate for changes in the temperature of the excitation source, the internal standard is selected so that its emission line is close to the analyte's emission line. In addition, the internal standard should be subject to the same chemical interferences to compensate for changes in atomization efficiency. To accurately correct for these errors the analyte and internal standard emission lines are monitored simultaneously.

Representative Method 10.7.1: Determination of Sodium in a Salt Substitute

The best way to appreciate the theoretical and the practical details discussed in this section is to carefully examine a typical analytical method. Although each method is unique, the following description of the determination of sodium in salt substitutes provides an instructive example of a typical procedure. The description here is based on Goodney, D. E. *J. Chem. Educ.* **1982**, *59*, 875–876.

Description of Method

Salt substitutes, which are used in place of table salt for individuals on low-sodium diets, replaces NaCl with KCl. Depending on the brand, fumaric acid, calcium hydrogen phosphate, or potassium tartrate also are present. Although intended to be sodium-free, salt substitutes contain small amounts of NaCl as an impurity. Typically, the concentration of sodium in a salt substitute is about 100 μg/g The exact concentration of sodium is determined by flame atomic emission. Because it is difficult to match the matrix of the standards to that of the sample, the analysis is accomplished by the method of standard additions.

Procedure

A sample is prepared by placing an approximately 10-g portion of the salt substitute in 10 mL of 3 M HCl and 100 mL of distilled water. After the sample has dissolved, it is transferred to a 250-mL volumetric flask and diluted to volume with distilled water. A series of standard additions is prepared by placing 25-mL portions of the diluted sample into separate 50-mL volumetric flasks, spiking each with a known amount of an approximately 10 mg/L standard solution of Na^+, and diluting to volume. After zeroing the instrument with an appropriate blank, the instrument is optimized at a wavelength of 589.0 nm while aspirating a standard solution of Na^+. The emission intensity is measured for each of the standard addition samples and the concentration of sodium in the salt substitute is reported in μg/g.

Questions

1. Potassium ionizes more easily than sodium. What problem might this present if you use external standards prepared from a stock solution of 10 mg Na/L instead of using a set of standard additions?

> Because potassium is present at a much higher concentration than is sodium, its ionization suppresses the ionization of sodium. Normally suppressing ionization is a good thing because it increases emission intensity. In this case, however, the difference between the standard's matrix and the sample's matrix means that the sodium in a standard experiences more ionization than an equivalent amount of sodium in a sample. The result is a determinate error.

2. One way to avoid a determinate error when using external standards is to match the matrix of the standards to that of the sample. We could, for example, prepare external standards using reagent grade KCl to match the matrix to that of the sample. Why is this not a good idea for this analysis?

> Sodium is a common contaminant in many chemicals. Reagent grade KCl, for example, may contain 40–50 μg Na/g. This is a significant source of sodium, given that the salt substitute contains approximately 100 μg Na/g.

3. Suppose you decide to use an external standardization. Given the previous questions, is the result of your analysis likely to underestimate or to overestimate the amount of sodium in the salt substitute?

> The solid black line in Figure 10.7.6 shows the ideal calibration curve, assuming we match the standard's matrix to the sample's matrix, and that we do so without adding any additional sodium. If we prepare the external standards without adding KCl, the emission for each standard decreases due to increased ionization. This is shown by the lower of the two dashed red lines. Preparing the standards by adding reagent grade KCl increases the concentration of sodium due to its contamination. Because we underestimate the actual concentration of sodium in the standards, the resulting calibration curve is shown by the other dashed red line. In both cases, the sample's emission results in our overestimating the concentration of sodium in the sample.

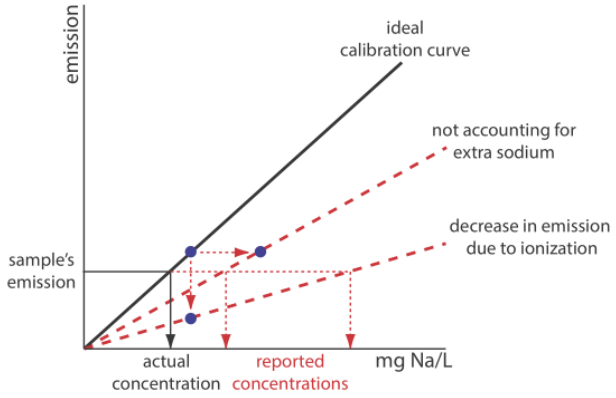

Figure 10.7.6 . External standards calibration curves for the flame atomic emission analysis of Na in a salt substitute. The solid black line shows the ideal calibration curve assuming we match the matrix of the samples and the standards using pure KCl. The lower of the two dashed red lines shows the effect of failing to add KCl to the external standards, which decreases emission. The other dashed red line shows the effect of using KCl that is contaminated with NaCl, which causes us to underestimate the concentration of Na in the standards. In both cases, the result is a positive determinate error in the analysis of samples.

4. One problem with analyzing salt samples is their tendency to clog the aspirator and burner assembly. What effect does this have on the analysis?

Clogging the aspirator and burner assembly decreases the rate of aspiration, which decreases the analyte's concentration in the flame. The result is a decrease in the emission intensity and a negative determinate error.

Example 10.7.1

To evaluate the method described in Representative Method 10.7.1, a series of standard additions is prepared using a 10.0077-g sample of a salt substitute. The results of a flame atomic emission analysis of the standards is shown here [Goodney, D. E. *J. Chem. Educ.* **1982**, *59*, 875–876].

added Na (µg/mL)	I_e (arb. units)
0.000	1.79
0.420	2.63
1.051	3.54
2.102	4.94
3.153	6.18

What is the concentration of sodium, in µg/g, in the salt substitute.

Solution

Linear regression of emission intensity versus the concentration of added Na gives the standard additions calibration curve shown below, which has the following calibration equation.

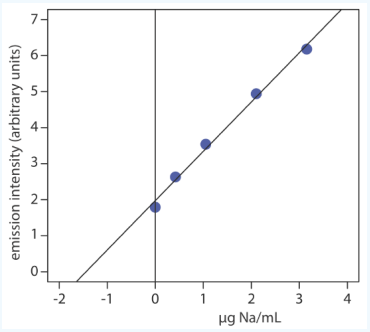

$$I_e = 1.97 + 1.37 \times \frac{\mu\text{g Na}}{\text{mL}}$$

The concentration of sodium in the sample is the absolute value of the calibration curve's *x*-intercept. Substituting zero for the emission intensity and solving for sodium's concentration gives a result of 1.44 μgNa/mL. The concentration of sodium in the salt substitute is

$$\frac{\frac{1.44\ \mu\text{g Na}}{\text{mL}} \times \frac{50.00\ \text{mL}}{25.00\ \text{mL}} \times 250.0\ \text{mL}}{10.0077\ \text{g sample}} = 71.9\ \mu\text{g Na/g}$$

Evaluation of Atomic Emission Spectroscopy

Scale of Operation

The scale of operations for atomic emission is ideal for the direct analysis of trace and ultratrace analytes in macro and meso samples. With appropriate dilutions, atomic emission can be applied to major and minor analytes.

Accuracy

When spectral and chemical interferences are insignificant, atomic emission can achieve quantitative results with accuracies of 1–5%. For flame emission, accuracy frequently is limited by chemical interferences. Because the higher temperature of a plasma source gives rise to more emission lines, accuracy when using plasma emission often is limited by stray radiation from overlapping emission lines.

Precision

For samples and standards in which the analyte's concentration exceeds the detection limit by at least a factor of 50, the relative standard deviation for both flame and plasma emission is about 1–5%. Perhaps the most important factor that affect precision is the stability of the flame's or the plasma's temperature. For example, in a 2500 K flame a temperature fluctuation of ± 2.5 K gives a relative standard deviation of 1% in emission intensity. Significant improvements in precision are realized when using internal standards.

Sensitivity

Sensitivity is influenced by the temperature of the excitation source and the composition of the sample matrix. Sensitivity is optimized by aspirating a standard solution of analyte and maximizing the emission by adjusting the flame's composition and the height from which we monitor the emission. Chemical interferences, when present, decrease the sensitivity of the analysis. Because the sensitivity of plasma emission is less affected by the sample matrix, a calibration curve prepared using standards in a matrix of distilled water is possible even for samples that have more complex matrices.

Selectivity

The selectivity of atomic emission is similar to that of atomic absorption. Atomic emission has the further advantage of rapid sequential or simultaneous analysis of multiple analytes.

Time, Cost, and Equipment

Sample throughput with atomic emission is rapid when using an automated system that can analyze multiple analytes. For example, sampling rates of 3000 determinations per hour are possible using a multichannel ICP, and sampling rates of 300 determinations per hour when using a sequential ICP. Flame emission often is accomplished using an atomic absorption spectrometer, which typically costs between $10,000–$50,000. Sequential ICP's range in price from $55,000–$150,000, while an ICP capable of simultaneous multielemental analysis costs between $80,000–$200,000. Combination ICP's that are capable of both sequential and simultaneous analysis range in price from $150,000–$300,000. The cost of Ar, which is consumed in significant quantities, can not be overlooked when considering the expense of operating an ICP.

1.8: Spectroscopy Based on Scattering

The blue color of the sky during the day and the red color of the sun at sunset are the result of light scattered by small particles of dust, molecules of water, and other gases in the atmosphere. The efficiency of a photon's scattering depends on its wavelength. We see the sky as blue during the day because violet and blue light scatter to a greater extent than other, longer wavelengths of light. For the same reason, the sun appears red at sunset because red light is less efficiently scattered and is more likely to pass through the atmosphere than other wavelengths of light. The scattering of radiation has been studied since the late 1800s, with applications beginning soon thereafter. The earliest quantitative applications of scattering, which date from the early 1900s, used the elastic scattering of light by colloidal suspensions to determine the concentration of colloidal particles.

Origin of Scattering

If we send a focused, monochromatic beam of radiation with a wavelength λ through a medium of particles with dimensions $< 1.5\lambda$, the radiation scatters in all directions. For example, visible radiation of 500 nm is scattered by particles as large as 750 nm in the longest dimension. Two general categories of scattering are recognized. In elastic scattering, radiation is first absorbed by the particles and then emitted without undergoing a change in the radiation's energy. When the radiation emerges with a change in energy, the scattering is inelastic. Only elastic scattering is considered in this text.

Elastic scattering is divided into two types: Rayleigh, or small-particle scattering, and large-particle scattering. Rayleigh scattering occurs when the scattering particle's largest dimension is less than 5% of the radiation's wavelength. The intensity of the scattered radiation is proportional to its frequency to the fourth power, ν^4—which accounts for the greater scattering of blue light than red light—and is distributed symmetrically (Figure 10.8.1 a). For larger particles, scattering increases in the forward direction and decreases in the backward direction as the result of constructive and destructive interferences (Figure 10.8.1 b).

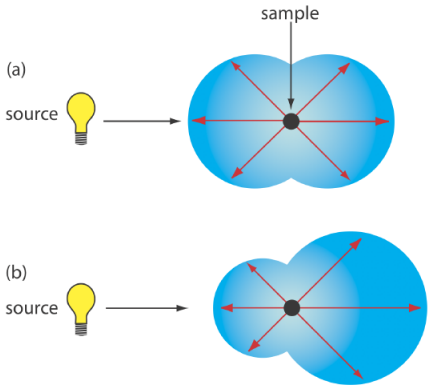

Figure 10.8.1 . Distribution of radiation for (a) Rayleigh, or small-particle scattering, and (b) large-particle scattering.

Turbidimetry and Nephelometry

Turbidimetry and nephelometry are two techniques that rely on the elastic scattering of radiation by a suspension of colloidal particles. In ***turbidimetry*** the detector is placed in line with the source and the decrease in the radiation's transmitted power is measured. In ***nephelometry*** the scattered radiation is measured at an angle of 90^o to the source. The similarity of turbidimetry to absorbance spectroscopy and of nephelometry to fluorescence spectroscopy is evident in the instrumental designs shown in Figure 10.8.2 . In fact, we can use a UV/Vis spectrophotometer for turbidimetry and we can use a spectrofluorometer for nephelometry.

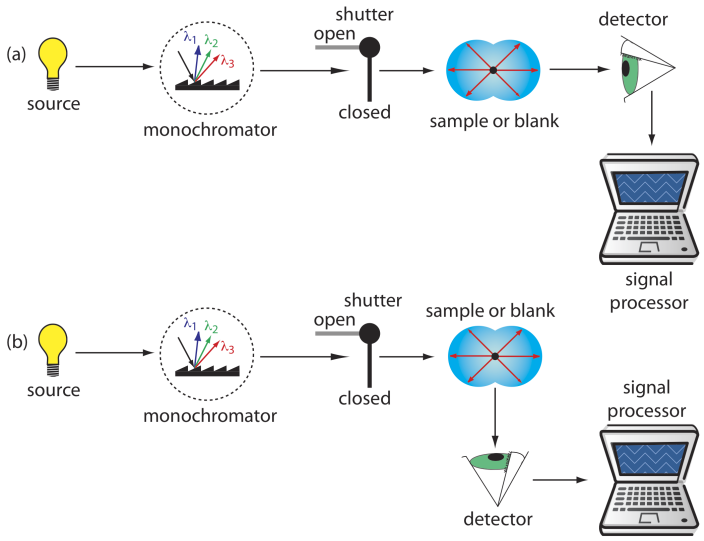

Figure 10.8.2 . Schematic diagrams for (a) a turbimeter, and (b) a nephelometer.

Turbidimetry or Nephelometry?

When developing a scattering method the choice between using turbidimetry or using nephelometry is determined by two factors. The most important consideration is the intensity of the scattered radiation relative to the intensity of the source's radiation. If the solution contains a small concentration of scattering particles, then the intensity of the transmitted radiation, I_T, is approximately the same as the intensity of the source's radiation, I_0. As we learned earlier in the section on molecular absorption, there is substantial uncertainty in determining a small difference between two intense signals. For this reason, nephelometry is a more appropriate choice for a sample that contains few scattering particles. Turbidimetry is a better choice when the sample contains a high concentration of scattering particles.

A second consideration in choosing between turbidimetry and nephelometry is the size of the scattering particles. For nephelometry, the intensity of scattered radiation at 90º increases when the particles are small and Rayleigh scattering is in effect. For larger particles, as shown in Figure 10.8.1 , the intensity of scattering decreases at 90º. When using an ultraviolet or a visible source of radiation, the optimum particle size is 0.1–1 μm. The size of the scattering particles is less important for turbidimetry where the signal is the relative decrease in transmitted radiation. In fact, turbidimetric measurements are feasible even when the size of the scattering particles results in an increase in reflection and refraction, although a linear relationship between the signal and the concentration of scattering particles may no longer hold.

Determining Concentration by Turbidimetry

For turbidimetry the measured transmittance, T, is the ratio of the intensity of source radiation transmitted by the sample, I_T, to the intensity of source radiation transmitted by a blank, I_0.

$$T = \frac{I_T}{I_0}$$

The relationship between transmittance and the concentration of the scattering particles is similar to that given by Beer's law

$$-\log T = kbC \tag{1.8.1}$$

where C is the concentration of the scattering particles in mass per unit volume (w/v), b is the pathlength, and k is a constant that depends on several factors, including the size and shape of the scattering particles and the wavelength of the source radiation. The exact relationship is established by a calibration curve prepared using a series of standards that contain known concentrations of analyte. As with Beer's law, Equation 1.8.1 may show appreciable deviations from linearity.

Determining Concentration by Nephelometry

For nephelometry the relationship between the intensity of scattered radiation, I_S, and the concentration of scattering particles is

$$I_s = kI_0C \tag{1.8.2}$$

where k is an empirical constant for the system and I_0 is the intensity of the source radiation. The value of k is determined from a calibration curve prepared using a series of standards that contain known concentrations of analyte.

Selecting a Wavelength for the Incident Radiation

The choice of wavelength is based primarily on the need to minimize potential interferences. For turbidimetry, where the incident radiation is transmitted through the sample, a monochromator or filter allow us to avoid wavelengths that are absorbed instead of scattered by the sample. For nephelometry, the absorption of incident radiation is not a problem unless it induces fluorescence from the sample. With a nonfluorescent sample there is no need for wavelength selection and a source of white light may be used as the incident radiation. For both techniques, other considerations in choosing a wavelength including the intensity of scattering, the trans- ducer's sensitivity (many common photon transducers are more sensitive to radiation at 400 nm than at 600 nm), and the source's intensity.

Preparing the Sample for Analysis

Although Equation 1.8.1 and Equation 1.8.2 relate scattering to the concentration of the scattering particles, the intensity of scattered radiation also is influenced by the size and the shape of the scattering particles. Samples that contain the same number of scattering particles may show significantly different values for $-\log T$ or I_S depending on the average diameter of the particles. For a quantitative analysis, therefore, it is necessary to maintain a uniform distribution of particle sizes throughout the sample and between samples and standards.

Most turbidimetric and nephelometric methods rely on precipitation reaction to form the scattering particles. As we learned in Chapter 8, a precipitate's properties, including particle size, are determined by the conditions under which it forms. To maintain a reproducible distribution of particle sizes between samples and standards, it is necessary to control parameters such as the concentration of reagents, the order of adding reagents, the pH and temperature, the agitation or stirring rate, the ionic strength, and the time between the precipitate's initial formation and the measurement of transmittance or scattering. In many cases a surface-active agent—such as glycerol, gelatin, or dextrin—is added to stabilize the precipitate in a colloidal state and to prevent the coagulation of the particles.

Applications

Turbidimetry and nephelometry are used to determine the clarity of water. The primary standard for measuring clarity is formazin, an easily prepared, stable polymer suspension (Figure 10.8.3) [Hach, C. C.; Bryant, M. "Turbidity Standards," Technical Information Series, Booklet No. 12, Hach Company: Loveland, CO, 1995]. A stock standard of formazin is prepared by combining a 1g/100mL solution of hydrazine sulfate, $N_2H_4{\bullet}H_2SO_4$, with a 10 g/100 mL solution of hexamethylenetetramine to produce a suspension of particles that is defined as 4000 nephelometric turbidity units (NTU). A set of external standards with NTUs between 0 and 40 is prepared by diluting the stock standard. This method is readily adapted to the analysis of the clarity of orange juice, beer, and maple syrup.

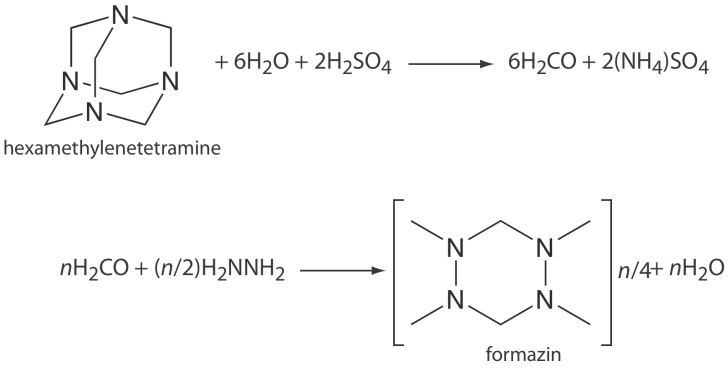

Figure 10.8.3 . Scheme for preparing formazin for use as a turbidity standard.

A number of inorganic cations and anions are determined by precipitating them under well-defined conditions. The transmittance or scattering of light, as defined by Equation 1.8.1 or Equation 1.8.2, is proportional to the concentration of the scattering particles, which, in turn, is related by the stoichiometry of the precipitation reaction to the analyte's concentration. Several examples of analytes determined in this way are listed in Table 10.8.1 .

Table 10.8.1 . Examples of Analytes Determined by Turbidimetry or Nephelometry

analyte	precipitant	precipitate
Ag^+	NaCl	AgCl
Ca^{2+}	$Na_2C_2O_4$	CaC_2O_4
Cl^-	$AgNO_3$	AgCl
CN^-	$AgNO_3$	AgCN
CO_3^{2-}	$BaCl_2$	$BaCO_3$
F^-	$CaCl_2$	CaF_2
SO_4^{2-}	$BaCl_2$	$BaSO_4$

Representative Method 10.8.1: Turbidimetric Determination of Sulfate in Water

The best way to appreciate the theoretical and the practical details discussed in this section is to carefully examine a typical analytical method. Although each method is unique, the following description of the determination of sulfate in water provides an instructive example of a typical procedure. The description here is based on Method 4500–SO42—C in *Standard Methods for the Analysis of Water and Wastewater*, American Public Health Association: Washington, D. C. 20th Ed., 1998.

Description of Method

Adding $BaCl_2$ to an acidified sample precipitates SO_4^{2-} as $BaSO_4$. The concentration of SO_4^{2-} is determined either by turbidimetry or by nephelometry using an incident source of radiation of 420 nm. External standards that contain know concentrations of SO_4^{2-} are used to standardize the method.

Procedure

Transfer a 100-mL sample to a 250-mL Erlenmeyer flask along with 20.00 mL of an appropriate buffer. For a sample that contains more than 10 mg SO_4^{2-}/L, the buffer's composition is 30 g of $MgCl_2$•$6H_2O$, 5 g of CH_3COONa•$3H_2O$, 1.0 g of KNO_3, and 20 mL of glacial CH_3COOH per liter. The buffer for a sample that contain less than 10 mg SO_4^{2-}/L is the same except for the addition of 0.111 g of Na_2SO_4 per L.

Place the sample and the buffer on a magnetic stirrer operated at the same speed for all samples and standards. Add a spoonful of 20–30 mesh $BaCl_2$, using a measuring spoon with a capacity of 0.2–0.3 mL, to precipitate the SO_4^{2-} as BaSO4. Begin timing when the $BaCl_2$ is added and stir the suspension for 60 ± 2 s. When the stirring is complete, allow the solution to sit without stirring for 5.0± 0.5 min before measuring its transmittance or its scattering.

Prepare a calibration curve over the range 0–40 mg SO_4^{2-}/L by diluting a stock standard that is 100-mg SO_4^{2-}/L. Treat each standard using the procedure described above for the sample. Prepare a calibration curve and use it to determine the amount of sulfate in the sample.

Questions

1. What is the purpose of the buffer?

    If the precipitate's particles are too small, I_T is too small to measure reliably. Because rapid precipitation favors the formation of micro-crystalline particles of $BaSO_4$, we use conditions that favor the precipitate's growth over the nucleation of new particles. The buffer's high ionic strength and its acidity favor the precipitate's growth and prevent the formation of microcrystalline $BaSO_4$.

2. Why is it important to use the same stirring rate and time for the samples and standards?

    How fast and how long we stir the sample after we add $BaCl_2$ influences the size of the precipitate's particles.

3. Many natural waters have a slight color due to the presence of humic and fulvic acids, and may contain suspended matter (Figure 10.8.4). Explain why these might interfere with the analysis for sulfate. For each interferent, suggest a way to minimize its effect on the analysis.

Figure 10.8.4 . Waterfall on the River Swale in Richmond, England. The river, which flows out of the moors in the Yorkshire Dales, is brown in color as the result of organic matter that leaches from the peat found in the moors.

Suspended matter in a sample contributes to scattering and, therefore, results in a positive determinate error. We can eliminate this interference by filtering the sample prior to its analysis. A sample that is colored may absorb some of the source's radiation, leading to a positive determinate error. We can compensate for this interference by taking a sample through the analysis without adding $BaCl_2$. Because no precipitate forms, we use the transmittance of this sample blank to correct for the interference.

4. Why is Na_2SO_4 added to the buffer for samples that contain less than 10 mg SO_4^{2-}/L?

The uncertainty in a calibration curve is smallest near its center. If a sample has a high concentration of SO_4^{2-}, we can dilute it so that its concentration falls near the middle of the calibration curve. For a sample with a small concentration of SO_4^{2-}, the buffer increases the concentration of sulfate by

$$\frac{0.111\text{ g }Na_2SO_4}{\text{L}} \times \frac{96.06\text{ g }SO_4^{2-}}{142.04\text{ g }Na_2SO_4} \times \frac{1000\text{ mg}}{\text{g}} \times \frac{20.00\text{ mL}}{250.0\text{ mL}} = 6.00\text{ mg }SO_4^{2-}/\text{L}$$

After using the calibration curve to determine the amount of sulfate in the sample as analyzed, we subtract 6.00 mg SO_4^{2-}/L to determine the amount of sulfate in the original sample.

Example 10.8.1

To evaluate the method described in Representative Method 10.8.1, a series of external standard was prepared and analyzed, providing the results shown in the following table.

mg SO_4^{2-}/L	transmittance
0.00	1.00
10.00	0.646
20.00	0.417
30.00	0.269
40.00	0.174

Analysis of a 100.0-mL sample of a surface water gives a transmittance of 0.538. What is the concentration of sulfate in the sample?

Solution

Linear regression of –log*T* versus concentration of SO_4^{2-} gives the calibration curve shown below, which has the following calibration equation.

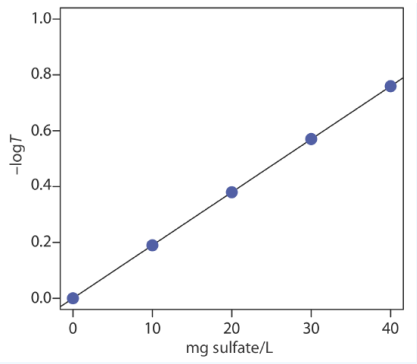

$$-\log T = -1.04 \times 10^{-5} + 0.0190 \times \frac{\text{mg } SO_4^{2-}}{\text{L}}$$

Substituting the sample's transmittance into the calibration curve's equation gives the concentration of sulfate in sample as 14.2 mg SO_4^{2-}/L.

1.9: Problems

1. Provide the missing information in the following table.

wavelength (m)	frequency (s^{-1})	wavenumber (cm^{-1})	energy (J)
4.50×10^{-9}			
	1.33×10^{15}		
		3215	
			7.20×10^{-19}

2. Provide the missing information in the following table.

[analyte] (M)	absorbance	%T	molar absorptivity (M^{-1} cm^{-1})	pathlength (cm)
1.40×10^{-4}			1120	1.00
	0.563		750	1.00
2.56×10^{-4}	0.225		456540	
1.55×10^{-3}	0.167		1550	5.00
		33.3		1.00
4.35×10^{-3}		21.2		
1.20×10^{-4}		81.3		10.00

3. A solution's transmittance is 35.0%. What is the transmittance if you dilute 25.0 mL of the solution to 50.0 mL?

4. A solution's transmittance is 85.0% when measured in a cell with a pathlength of 1.00 cm. What is the %T if you increase the pathlength to 10.00 cm?

5. The accuracy of a spectrophotometer is evaluated by preparing a solution of 60.06 ppm $K_2Cr_2O_7$ in 0.0050 M H_2SO_4, and measuring its absorbance at a wavelength of 350 nm in a cell with a pathlength of 1.00 cm. The expected absorbance is 0.640. What is the expected molar absorptivity of $K_2Cr_2O_7$ at this wavelength?

6. A chemical deviation to Beer's law may occur if the concentration of an absorbing species is affected by the position of an equilibrium reaction. Consider a weak acid, HA, for which K_a is 2×10^{-5}. Construct Beer's law calibration curves of absorbance versus the total concentration of weak acid (C_{total} = [HA] + [A^-]), using values for C_{total} of 1.0×10^{-5}, 3.0×10^{-5}, 5.0×10^{-5}, 7.0×10^{-5}, 9.0×10^{-5}, 11×10^{-5}, and 13×10^{-5} M for the following sets of conditions and comment on your results:

(a) $\varepsilon_{HA} = \varepsilon_{A^-} = 2000$ M^{-1} cm^{-1}; unbuffered solution.

(b) $\varepsilon_{HA} = 2000$ M^{-1} cm^{-1}; $\varepsilon_{A^-} = 500$ M^{-1} cm^{-1}; unbuffered solution.

(c) $\epsilon_{HA} = 2000$ M^{-1} cm^{-1}; $\epsilon_{A^-} = 500$ M^{-1} cm^{-1}; solution buffered to a pH of 4.5.

Assume a constant pathlength of 1.00 cm for all samples.

7. One instrumental limitation to Beer's law is the effect of polychromatic radiation. Consider a line source that emits radiation at two wavelengths, λ' and λ''. When treated separately, the absorbances at these wavelengths, A' and A'', are

$$A' = -\log \frac{P'_T}{P'_0} = \varepsilon' bC \qquad A'' = -\log \frac{P''_T}{P''_0} = \varepsilon'' bC$$

If both wavelengths are measured simultaneously the absorbance is

$$A = -\log \frac{\left(P'_T + P''_T\right)}{\left(P'_0 + P''_0\right)}$$

(a) Show that if the molar absorptivities at λ' and λ'' are the same ($\varepsilon' = \varepsilon'' = \varepsilon$), then the absorbance is equivalent to

$$A = \varepsilon b C$$

(b) Construct Beer's law calibration curves over the concentration range of zero to 1×10^{-4} M using $\varepsilon' = 1000$ M^{-1} cm^{-1} and $\varepsilon'' = 1000$ M^{-1} cm^{-1}, and $\varepsilon' = 1000$ M^{-1} cm^{-1} and $\varepsilon'' = 100$ M^{-1} cm^{-1}. Assume a value of 1.00 cm for the pathlength and that $P'_0 = P''_0 = 1$. Explain the difference between the two curves.

8. A second instrumental limitation to Beer's law is stray radiation. The following data were obtained using a cell with a pathlength of 1.00 cm when stray light is insignificant (P_{stray} = 0).

[analyte] (mM)	absorbance
0.00	0.00
2.00	0.40
4.00	0.80
6.00	1.20
8.00	1.60
10.00	3.00

Calculate the absorbance of each solution when P_{stray} is 5% of P_0, and plot Beer's law calibration curves for both sets of data. Explain any differences between the two curves. (*Hint*: Assume P_0 is 100).

9. In the process of performing a spectrophotometric determination of iron, an analyst prepares a calibration curve using a single-beam spectrophotometer similar to that shown in Figure 10.3.2. After preparing the calibration curve, the analyst drops and breaks the cuvette. The analyst acquires a new cuvette, measures the absorbance of the sample, and determines the %w/w Fe in the sample. Does the change in cuvette lead to a determinate error in the analysis? Explain.

10. The spectrophotometric methods for determining Mn in steel and for determining glucose use a chemical reaction to produce a colored spe- cies whose absorbance we can monitor. In the analysis of Mn in steel, colorless Mn^{2+} is oxidized to give the purple MnO_4^- ion. To analyze for glucose, which is also colorless, we react it with a yellow colored solution of the $Fe(CN)_6^{3-}$, forming the colorless $Fe(CN)_6^{4-}$ ion. The directions for the analysis of Mn do not specify precise reaction conditions, and samples and standards are treated separately. The conditions for the analysis of glucose, however, require that the samples and standards are treated simultaneously at exactly the same temperature and for exactly the same length of time. Explain why these two experimental procedures are so different.

11. One method for the analysis of Fe^{3+}, which is used with a variety of sample matrices, is to form the highly colored Fe^{3+}–thioglycolic acid complex. The complex absorbs strongly at 535 nm. Standardizing the method is accomplished using external standards. A 10.00-ppm Fe^{3+} working standard is prepared by transferring a 10-mL aliquot of a 100.0 ppm stock solution of Fe^{3+} to a 100-mL volumetric flask and diluting to volume. Calibration standards of 1.00, 2.00, 3.00, 4.00, and 5.00 ppm are prepared by transferring appropriate amounts of the 10.0 ppm working solution into separate 50-mL volumetric flasks, each of which contains 5 mL of thioglycolic acid, 2 mL of 20% w/v ammonium citrate, and 5 mL of 0.22 M NH_3. After diluting to volume and mixing, the absorbances of the external standards are measured against an appropriate blank. Samples are prepared for analysis by taking a portion known to contain approximately 0.1 g of Fe^{3+}, dissolving it in a minimum amount of HNO_3, and diluting to volume in a 1-L volumetric flask. A 1.00-mL aliquot of this solution is transferred to a 50-mL volumetric flask, along with 5 mL of thioglycolic acid, 2 mL of 20% w/v ammonium citrate, and 5 mL of 0.22 M NH_3 and diluted to volume. The absorbance of this solution is used to determine the concentration of $Fe3^+$ in the sample.

(a) What is an appropriate blank for this procedure?

(b) Ammonium citrate is added to prevent the precipitation of Al^{3+}. What is the effect on the reported concentration of iron in the sample if there is a trace impurity of Fe^{3+} in the ammonium citrate?

(c) Why does the procedure specify that the sample contain approximately 0.1 g of Fe^{3+}?

(d) Unbeknownst to the analyst, the 100-mL volumetric flask used to prepare the 10.00 ppm working standard of Fe^{3+} has a volume that is significantly smaller than 100.0 mL. What effect will this have on the reported concentration of iron in the sample?

12. A spectrophotometric method for the analysis of iron has a linear calibration curve for standards of 0.00, 5.00, 10.00, 15.00, and 20.00 mg Fe/L. An iron ore sample that is 40–60% w/w is analyzed by this method. An approximately 0.5-g sample is taken, dissolved in a minimum of concentrated HCl, and diluted to 1 L in a volumetric flask using distilled water. A 5.00 mL aliquot is removed with a pipet. To what volume—10, 25, 50, 100, 250, 500, or 1000 mL—should it be diluted to minimize the uncertainty in the analysis? Explain.

13. Lozano-Calero and colleagues developed a method for the quantitative analysis of phosphorous in cola beverages based on the formation of the blue-colored phosphomolybdate complex, $(NH_4)_3[PO_4(MoO_3)_{12}]$ [Lozano-Calero, D.; Martín-Palomeque, P.; Madueño-Loriguillo, S. *J. Chem. Educ.* **1996**, *73*, 1173–1174]. The complex is formed by adding $(NH_4)_6Mo_7O_{24}$ to the sample in the presence of a reducing agent, such as ascorbic acid. The concentration of the complex is determined spectrophotometrically at a wavelength of 830 nm, using an external standards calibration curve.

In a typical analysis, a set of standard solutions that contain known amounts of phosphorous is prepared by placing appropriate volumes of a 4.00 ppm solution of P_2O_5 in a 5-mL volumetric flask, adding 2 mL of an ascorbic acid reducing solution, and diluting to volume with distilled water. Cola beverages are prepared for analysis by pouring a sample into a beaker and allowing it to stand for 24 h to expel the dissolved CO_2. A 2.50-mL sample of the degassed sample is transferred to a 50-mL volumetric flask and diluted to volume. A 250-µL aliquot of the diluted sample is then transferred to a 5-mL volumetric flask, treated with 2 mL of the ascorbic acid reducing solution, and diluted to volume with distilled water.

(a) The authors note that this method can be applied only to noncol- ored cola beverages. Explain why this is true.

(b) How might you modify this method so that you can apply it to any cola beverage?

(c) Why is it necessary to remove the dissolved gases?

(d) Suggest an appropriate blank for this method?

(e) The author's report a calibration curve of

$$A = -0.02 + \left(0.72\ \text{ppm}^{-1}\right) \times C_{P_2O_5}$$

A sample of Crystal Pepsi, analyzed as described above, yields an absorbance of 0.565. What is the concentration of phosphorous, reported as ppm P, in the original sample of Crystal Pepsi?

> Crystal Pepsi was a colorless, caffeine-free soda produced by PepsiCo. It was available in the United States from 1992 to 1993.

14. EDTA forms colored complexes with a variety of metal ions that may serve as the basis for a quantitative spectrophotometric method of analysis. The molar absorptivities of the EDTA complexes of Cu^{2+}, Co^{2+}, and Ni^{2+} at three wavelengths are summarized in the following table (all values of ε are in M^{-1} cm^{-1}).

metal ion	$\varepsilon_{462.9}$	$\varepsilon_{732.0}$	$\varepsilon_{378.7}$
Co^{2+}	15.8	2.11	3.11
Cu^{2+}	2.32	95.2	7.73
Ni^{2+}	1.79	3.03	13.5

Using this information determine the following, assuming a pathlength, *b*, of 1.00 cm for all measurements:

(a) The concentration of Cu^{2+} in a solution that has an absorbance of 0.338 at a wavelength of 732.0 nm.

(b) The concentrations of Cu^{2+} and Co^{2+} in a solution that has an absorbance of 0.453 at a wavelength of 732.0 nm and 0.107 at a wavelength of 462.9 nm.

(c) The concentrations of Cu^{2+}, Co^{2+}, and Ni^{2+} in a sample that has an absorbance of 0.423 at a wavelength of 732.0 nm, 0.184 at a wavelength of 462.9 nm, and 0.291 at a wavelength of 378.7 nm.

15. The concentration of phenol in a water sample is determined by using steam distillation to separate the phenol from non-volatile impurities, followed by reacting the phenol in the distillate with 4-aminoantipyrine and $K_3Fe(CN)_6$ at pH 7.9 to form a colored antipyrine dye. A phenol standard with a concentration of 4.00 ppm has an absorbance of 0.424 at a wavelength of 460 nm using a 1.00 cm cell. A water sample is steam distilled and a 50.00-mL aliquot of the distillate is placed in a 100-mL volumetric flask and diluted to volume with distilled water. The absorbance of this solution is 0.394. What is the concentration of phenol (in parts per million) in the water sample?

16. Saito describes a quantitative spectrophotometric procedure for iron based on a solid-phase extraction using bathophenanthroline in a poly(vinyl chloride) membrane [Saito, T. *Anal. Chim. Acta* **1992**, *268*, 351–355]. In the absence of Fe^{2+} the membrane is colorless, but when immersed in a solution of Fe^{2+} and I^-, the membrane develops a red color as a result of the formation of an Fe^{2+}–bathophenanthroline complex. A calibration curve determined using a set of external standards with known concentrations of Fe^{2+} gave a standardization relationship of

$$A = \left(8.60 \times 10^3\ \mathrm{M}^{-1}\right) \times \left[\mathrm{Fe}^{2+}\right]$$

What is the concentration of iron, in mg Fe/L, for a sample with an absorbance of 0.100?

17. In the DPD colorimetric method for the free chlorine residual, which is reported as mg Cl_2/L, the oxidizing power of free chlorine converts the colorless amine N,N-diethyl-*p*-phenylenediamine to a colored dye that absorbs strongly over the wavelength range of 440–580 nm. Analysis of a set of calibration standards gave the following results.

mg Cl_2/L	absorbance
0.00	0.000
0.50	0.270
1.00	0.543
1.50	0.813
2.00	1.084

A sample from a public water supply is analyzed to determine the free chlorine residual, giving an absorbance of 0.113. What is the free chlorine residual for the sample in mg Cl_2/L?

18. Lin and Brown described a quantitative method for methanol based on its effect on the visible spectrum of methylene blue [Lin, J.; Brown, C. W. *Spectroscopy* **1995**, *10(5)*, 48–51]. In the absence of methanol, methylene blue has two prominent absorption bands at 610 nm and 663 nm, which correspond to the monomer and the dimer, respectively. In the presence of methanol, the intensity of the dimer's absorption band decreases, while that for the monomer increases. For concentrations of methanol between 0 and 30% v/v, the ratio of the two absorbance, A_{663}/A_{610}, is a linear function of the amount of methanol. Use the following standardization data to determine the %v/v methanol in a sample if A_{610} is 0.75 and A_{663} is 1.07.

%v/v methanol	A_{663}/A_{610}	%v/v methanol	A_{663}/A_{610}
0.0	1.21	20.0	1.62
5.0	1.29	25.0	1.74
10.0	1.42	30.0	1.84
15.0	1.52		

19. The concentration of the barbiturate barbital in a blood sample is determined by extracting 3.00 mL of blood with 15 mL of $CHCl_3$. The chloroform, which now contains the barbital, is extracted with 10.0 mL of 0.45 M NaOH (pH ≈ 13). A 3.00-mL sample of the aqueous extract is placed in a 1.00-cm cell and an absorbance of 0.115 is measured. The pH of the sample in the absorption cell is then adjusted to approximately 10 by adding 0.50 mL of 16% w/v NH_4Cl, giving an absorbance of 0.023. When

3.00 mL of a standard barbital solution with a concentration of 3 mg/100 mL is taken through the same procedure, the absorbance at pH 13 is 0.295 and the absorbance at a pH of 10 is 0.002. Report the mg barbital/100 mL in the sample.

20. Jones and Thatcher developed a spectrophotometric method for analyzing analgesic tablets that contain aspirin, phenacetin, and caffeine [Jones, M.; Thatcher, R. L. *Anal. Chem.* **1951**, *23*, 957–960]. The sample is dissolved in $CHCl_3$ and extracted with an aqueous solution of $NaHCO_3$ to remove the aspirin. After the extraction is complete, the chloroform is transferred to a 250-mL volumetric flask and diluted to volume with $CHCl_3$. A 2.00-mL portion of this solution is then diluted to volume in a 200-mL volumetric flask with $CHCl_3$. The absorbance of the final solution is measured at wavelengths of 250 nm and 275 nm, at which the absorptivities, in $ppm^{-1}\ cm^{-1}$, for caffeine and phenacetin are

analyte	ε_{250}	ε_{275}
caffeine	0.0131	0.0485
phenacetin	0.0702	0.0159

Aspirin is determined by neutralizing the $NaHCO_3$ in the aqueous solution and extracting the aspirin into $CHCl_3$. The combined extracts are diluted to 500 mL in a volumetric flask. A 20.00-mL portion of the solution is placed in a 100-mL volumetric flask and diluted to volume with $CHCl_3$. The absorbance of this solution is measured at 277 nm, where the absorptivity of aspirin is 0.00682 $ppm^{-1}\ cm^{-1}$. An analgesic tablet treated by this procedure is found to have absorbances of 0.466 at 250 nm, 0.164 at 275 nm, and 0.600 at 277 nm when using a cell with a 1.00 cm pathlength. Report the milligrams of aspirin, caffeine, and phenacetin in the analgesic tablet.

21. The concentration of SO_2 in a sample of air is determined by the *p*-rosaniline method. The SO_2 is collected in a 10.00-mL solution of $HgCl_4^{2-}$, where it reacts to form $Hg(SO_3)_2$, by pulling air through the solution for 75 min at a rate of 1.6 L/min. After adding *p*-rosaniline and formaldehyde, the colored solution is diluted to 25 mL in a volumetric flask. The absorbance is measured at 569 nm in a 1-cm cell, yielding a value of 0.485. A standard sample is prepared by substituting a 1.00-mL sample of a standard solution that contains the equivalent of 15.00 ppm SO_2 for the air sample. The absorbance of the standard is found to be 0.181. Report the concentration of SO_2 in the air in mg SO_2/L. The density of air is 1.18 g/liter.

22. Seaholtz and colleagues described a method for the quantitative analysis of CO in automobile exhaust based on the measurement of infrared radiation at 2170 cm^{-1} [Seaholtz, M. B.; Pence, L. E.; Moe, O. A. Jr. *J. Chem. Educ.* **1988**, *65*, 820–823]. A calibration curve is prepared by filling a 10-cm IR gas cell with a known pressure of CO and measuring the absorbance using an FT-IR, giving a calibration equation of

$$A = -1.1 \times 10^{-4} + \left(9.9 \times 10^{-4}\right) \times P_{CO}$$

Samples are prepared by using a vacuum manifold to fill the gas cell. After measuring the total pressure, the absorbance at 2170 cm^{-1} is measured. Results are reported as %CO (P_{CO}/P_{total}). The analysis of five exhaust samples from a 1973 coupe gives the following results.

P_{total} (torr)	absorbance
595	0.1146
354	0.0642
332	0.0591
233	0.0412
143	0.0254

Determine the %CO for each sample, and report the mean and the 95% confidence interval.

23. Figure 10.3.8 shows an example of a disposable IR sample card made using a thin sheet of polyethylene. To prepare an analyte for analysis, it is dissolved in a suitable solvent and a portion of the sample placed on the IR card. After the solvent evaporates, leaving the analyte behind as a thin film, the sample's IR spectrum is obtained. Because the thickness of the polyethylene film is not uniform, the primary application of IR cards is for a qualitative analysis. Zhao and Malinowski reported how an internal standardization with KSCN can be used for a quantitative IR analysis of polystyrene [Zhao, Z.; Malinowski, E. R. *Spectroscopy*

1996, *11(7)*, 44–49]. Polystyrene is monitored at 1494 cm^{-1} and KSCN at 2064 cm^{-1}. Standard solutions are prepared by placing weighed portions of polystyrene in a 10-mL volumetric flask and diluting to volume with a solution of 10 g/L KSCN in methyl isobutyl ketone. A typical set of results is shown here.

g polystyrene	0.1609	0.3290	0.4842	0.6402	0.8006
A_{1494}	0.0452	0.1138	0.1820	0.3275	0.3195
A_{2064}	0.1948	0.2274	0.2525	0.3580	0.2703

When a 0.8006-g sample of a poly(styrene/maleic anhydride) copolymer is analyzed, the following results are obtained.

replicate	A_{1494}	A_{2064}
1	0.2729	0.3582
2	0.2074	0.2820
3	0.2785	0.3642

What is the %w/w polystyrene in the copolymer? Given that the reported %w/w polystyrene is 67%, is there any evidence for a determinate error at $\alpha = 0.05$?

24. The following table lists molar absorptivities for the Arsenazo complexes of copper and barium [Grossman, O.; Turanov, A. N. *Anal. Chim. Acta* **1992**, *257*, 195–202]. Suggest appropriate wavelengths for analyzing mixtures of copper and barium using their Arsenzao complexes.

wavelength (nm)	ε_{Cu} (M^{-1} cm^{-1})	ε_{Ba} (M^{-1} cm^{-1})
595	11900	7100
600	15500	7200
607	18300	7400
611	19300	6900
614	19300	7000
620	17800	7100
626	16300	8400
635	10900	9900
641	7500	10500
645	5300	10000
650	3500	8600
655	2200	6600
658	1900	6500
665	1500	3900
670	1500	2800
680	1800	1500

25. Blanco and colleagues report several applications of multiwavelength linear regression analysis for the simultaneous determination of two-component mixtures [Blanco, M.; Iturriaga, H.; Maspoch, S.; Tarin, P. *J. Chem. Educ.* **1989**, *66*, 178–180]. For each of the following, determine the molar concentration of each analyte in the mixture.

(a) Titanium and vanadium are determined by forming complexes with H_2O_2. Results for a mixture of Ti(IV) and V(V) and for stan-dards of 63.1 ppm Ti(IV) and 96.4 ppm V(V) are listed in the following table.

wavelength (nm)	$A_{Ti(V)\ Std}$	$A_{V(V)\ Std}$	A_{mix}
390	0.895	0.326	0.651
430	0.884	0.497	0.743
450	0.694	0.528	0.665
470	0.481	0.512	0.547
510	0.173	0.374	0.314

(b) Copper and zinc are determined by forming colored complexes with 2-pyridyl-azo-resorcinol (PAR). The absorbances for PAR, a mixture of Cu^{2+} and Zn^{2+}, and standards of 1.00 ppm Cu^{2+} and 1.00 ppm Zn^{2+} are listed in the following table. Note that you must correct the absorbances for the each metal for the contribution from PAR.

wavelength (nm)	A_{PAR}	$A_{Cu\ Std}$	$A_{Zn\ Std}$	A_{mix}
480	0.211	0.698	0.971	0.656
496	0.137	0.732	1.018	0.668
510	0.100	0.732	0.891	0.627
526	0.072	0.602	0.672	0.498
540	0.056	0.387	0.306	0.290

26. The stoichiometry of a metal–ligand complex, ML_n, is determined by the method of continuous variations. A series of solutions is prepared in which the combined concentrations of M and L are held constant at 5.15×10^{-4} M. The absorbances of these solutions are measured at a wavelength where only the metal–ligand complex absorbs. Using the following data, determine the formula of the metal–ligand complex.

mole fraction of M	mole fraction of L	absorbance
1.0	0.0	0.001
0.9	0.1	0.126
0.8	0.2	0.260
0.7	0.3	0.389
0.6	0.4	0.515
0.5	0.5	0.642
0.4	0.6	0.775
0.3	0.7	0.771
0.2	0.8	0.513
0.1	0.9	0.253
0.0	1.0	0.000

27. The stoichiometry of a metal–ligand complex, ML_n, is determined by the mole-ratio method. A series of solutions are prepared in which the metal's concentration is held constant at 3.65×10^{-4} M and the ligand's concentration is varied from 1×10^{-4} M to 1×10^{-3} M. Using the following data, determine the stoichiometry of the metal-ligand complex.

[ligand] (M)	absorbance	[ligand] (M)	absorbance
1.0×10^{-4}	0.122	6.0×10^{-4}	0.752
2.0×10^{-4}	0.251	7.0×10^{-4}	0.873
3.0×10^{-4}	0.376	8.0×10^{-4}	0.937
4.0×10^{-4}	0.496	9.0×10^{-4}	0.962
5.0×10^{-4}	0.625	1.0×10^{-3}	1.002

28. The stoichiometry of a metal–ligand complex, ML_n, is determined by the slope-ratio method. Two sets of solutions are prepared. For the first set of solutions the metal's concentration is held constant at 0.010 M and the ligand's concentration is varied. The following data are obtained at a wavelength where only the metal–ligand complex absorbs.

[ligand] (M)	absorbance
1.0×10^{-5}	0.012
2.0×10^{-5}	0.029
3.0×10^{-5}	0.042
4.0×10^{-5}	0.055
5.0×10^{-5}	0.069

For the second set of solutions the concentration of the ligand is held constant at 0.010 M, and the concentration of the metal is varied, yielding the following absorbances.

[metal] (M)	absorbance
1.0×10^{-5}	0.040
2.0×10^{-5}	0.085
3.0×10^{-5}	0.125
4.0×10^{-5}	0.162
5.0×10^{-5}	0.206

Using this data, determine the stoichiometry of the metal-ligand complex.

29. Kawakami and Igarashi developed a spectrophotometric method for nitrite based on its reaction with 5, 10, 15, 20-tetrakis(4-aminophenyl) porphrine (TAPP). As part of their study they investigated the stoichiometry of the reaction between TAPP and NO_2^-. The following data are derived from a figure in their paper [Kawakami, T.; Igarashi, S. *Anal. Chim. Acta* **1996**, *333*, 175–180].

[TAPP] (M)	$[NO_2^-]$ (M)	absorbance
8.0×10^{-7}	0	0.227
8.0×10^{-7}	4.0×10^{-8}	0.223
8.0×10^{-7}	8.0×10^{-8}	0.211
8.0×10^{-7}	1.6×10^{-7}	0.191
8.0×10^{-7}	3.2×10^{-7}	0.152
8.0×10^{-7}	4.8×10^{-7}	0.127

8.0×10^{-7}	6.4×10^{-7}	0.107
8.0×10^{-7}	8.0×10^{-7}	0.092
8.0×10^{-7}	1.6×10^{-6}	0.058
8.0×10^{-7}	2.4×10^{-6}	0.045
8.0×10^{-7}	3.2×10^{-6}	0.037
8.0×10^{-7}	4.0×10^{-6}	0.034

What is the stoichiometry of the reaction?

30. The equilibrium constant for an acid–base indicator is determined by preparing three solutions, each of which has a total indicator concentration of 1.35×10^{-5} M. The pH of the first solution is adjusted until it is acidic enough to ensure that only the acid form of the indicator is present, yielding an absorbance of 0.673. The absorbance of the second solution, whose pH is adjusted to give only the base form of the indicator, is 0.118. The pH of the third solution is adjusted to 4.17 and has an absorbance of 0.439. What is the acidity constant for the acid–base indicator?

31. The acidity constant for an organic weak acid is determined by measuring its absorbance as a function of pH while maintaining a constant total concentration of the acid. Using the data in the following table, determine the acidity constant for the organic weak acid.

pH	absorbance	pH	absorbance
1.53	0.010	4.88	0.193
2.20	0.010	5.09	0.227
3.66	0.035	5.69	0.288
4.11	0.072	7.20	0.317
4.35	0.103	7.78	0.317
4.75	0.169		

32. Suppose you need to prepare a set of calibration standards for the spectrophotometric analysis of an analyte that has a molar absorptivity of 1138 M^{-1} cm^{-1} at a wavelength of 625 nm. To maintain an acceptable precision for the analysis, the %T for the standards should be between 15% and 85%.

(a) What is the concentration for the most concentrated and for the least concentrated standard you should prepare, assuming a 1.00-cm sample cell.

(b) Explain how you will analyze samples with concentrations that are 10 μM, 0.1 mM, and 1.0 mM in the analyte.

33. When using a spectrophotometer whose precision is limited by the uncertainty of reading %T, the analysis of highly absorbing solutions can lead to an unacceptable level of indeterminate errors. Consider the analysis of a sample for which the molar absorptivity is 1.0×10^4 M^{-1} cm^{-1} and for which the pathlength is 1.00 cm.

(a) What is the relative uncertainty in concentration for an analyte whose concentration is 2.0×10^{-4} M if s_T is ±0.002?

(b) What is the relative uncertainty in the concentration if the spectrophotometer is calibrated using a blank that consists of a 1.0×10^{-4} M solution of the analyte?

34. Hobbins reported the following calibration data for the flame atomic absorption analysis for phosphorous [Hobbins, W. B. “Direct Determination of Phosphorous in Aqueous Matricies by Atomic Absorption,” Varian Instruments at Work, Number AA-19, February 1982].

mg P/L	absorbance
2130	0.048

mg P/L	absorbance
4260	0.110
6400	0.173
8530	0.230

To determine the purity of a sample of Na_2HPO_4, a 2.469-g sample is dissolved and diluted to volume in a 100-mL volumetric flask. Analysis of the resulting solution gives an absorbance of 0.135. What is the purity of the Na_2HPO_4?

35. Bonert and Pohl reported results for the atomic absorption analysis of several metals in the caustic suspensions produced during the manufacture of soda by the ammonia-soda process [Bonert, K.; Pohl, B. "The Determination of Cd, Cr, Cu, Ni, and Pb in Concentrated $CaCl_2$/NaCl solutions by AAS," AA Instruments at Work (Varian) Number 98, November, 1990].

(a) The concentration of Cu is determined by acidifying a 200.0-mL sample of the caustic solution with 20 mL of concentrated HNO_3, adding 1 mL of 27% w/v H_2O_2, and boiling for 30 min. The resulting solution is diluted to 500 mL in a volumetric flask, filtered, and analyzed by flame atomic absorption using matrix matched standards. The results for a typical analysis are shown in the following table.

solution	mg Cu/L	absorbance
blank	0.000	0.007
standard 1	0.200	0.014
standard 2	0.500	0.036
standard 3	1.000	0.072
standard 4	2.000	0.146
sample		0.027

Determine the concentration of Cu in the caustic suspension.

(b) The determination of Cr is accomplished by acidifying a 200.0-mL sample of the caustic solution with 20 mL of concentrated HNO_3, adding 0.2 g of Na_2SO_3 and boiling for 30 min. The Cr is isolated from the sample by adding 20 mL of NH_3, producing a precipitate that includes the chromium as well as other oxides. The precipitate is isolated by filtration, washed, and transferred to a beaker. After acidifying with 10 mL of HNO_3, the solution is evaporated to dryness. The residue is redissolved in a combination of HNO_3 and HCl and evaporated to dryness. Finally, the residue is dissolved in 5 mL of HCl, filtered, diluted to volume in a 50-mL volumetric flask, and analyzed by atomic absorption using the method of standard additions. The atomic absorption results are summarized in the following table.

sample	mg Cr_{added}/L	absorbance
blank		0.001
sample		0.045
standard addition 1	0.200	0.083
standard addition 2	0.500	0.118
standard addition 3	1.000	0.192

Report the concentration of Cr in the caustic suspension.

36. Quigley and Vernon report results for the determination of trace metals in seawater using a graphite furnace atomic absorption spectrophotometer and the method of standard additions [Quigley, M. N.; Vernon, F. *J. Chem. Educ.* **1996**, *73*, 671–673]. The trace metals are first separated from their complex, high-salt matrix by coprecipitating with Fe^{3+}. In a typical analysis a 5.00-mL portion of 2000 ppm Fe^{3+} is added to 1.00 L of seawater. The pH is adjusted to 9 using NH_4OH, and the precipitate of $Fe(OH)_3$ allowed to

stand overnight. After isolating and rinsing the precipitate, the $Fe(OH)_3$ and coprecipitated metals are dissolved in 2 mL of concentrated HNO_3 and diluted to volume in a 50-mL volumetric flask. To analyze for Mn^{2+}, a 1.00-mL sample of this solution is diluted to 100 mL in a volumetric flask. The following samples are injected into the graphite furnace and analyzed.

sample	absorbance
2.5-µL sample + 2.5 µL of 0 ppb Mn^{2+}	0.223
2.5-µL sample + 2.5 µL of 2.5 ppb Mn^{2+}	0.294
2.5-µL sample + 2.5 µL of 5.0 ppb Mn^{2+}	0.361

Report the ppb Mn^{2+} in the sample of seawater.

37. The concentration of Na in plant materials are determined by flame atomic emission. The material to be analyzed is prepared by grinding, homogenizing, and drying at 103°C. A sample of approximately 4 g is transferred to a quartz crucible and heated on a hot plate to char the organic material. The sample is heated in a muffle furnace at 550°C for several hours. After cooling to room temperature the residue is dissolved by adding 2 mL of 1:1 HNO_3 and evaporated to dryness. The residue is redissolved in 10 mL of 1:9 HNO_3, filtered and diluted to 50 mL in a volumetric flask. The following data are obtained during a typical analysis for the concentration of Na in a 4.0264-g sample of oat bran.

sample	mg Na/L	emission (arbitrary units)
blank	0.00	0.0
standard 1	2.00	90.3
standard 2	4.00	181
standard 3	6.00	272
standard 4	8.00	363
standard 5	10.00	448
sample		238

Report the concentration of µg Na/g sample.

38. Yan and colleagues developed a method for the analysis of iron based its formation of a fluorescent metal–ligand complex with the ligand 5-(4-methylphenylazo)-8-aminoquinoline [Yan, G.; Shi, G.; Liu, Y. *Anal. Chim. Acta* **1992**, *264*, 121–124]. In the presence of the surfactant cetyltrimethyl ammonium bromide the analysis is carried out using an excitation wavelength of 316 nm with emission monitored at 528 nm. Standardization with external standards gives the following calibration curve.

$$I_f = -0.03 + \left(1.594\ \text{mg}^{-1}\ \text{L}\right) \times \frac{\text{mg Fe}^{3+}}{\text{L}}$$

A 0.5113-g sample of dry dog food is ashed to remove organic materials, and the residue dissolved in a small amount of HCl and diluted to volume in a 50-mL volumetric flask. Analysis of the resulting solution gives a fluorescent emission intensity of 5.72. Determine the mg Fe/L in the sample of dog food.

39. A solution of 5.00×10^{-5} M 1,3-dihydroxynaphthelene in 2 M NaOH has a fluorescence intensity of 4.85 at a wavelength of 459 nm. What is the concentration of 1,3-dihydroxynaphthelene in a solution that has a fluorescence intensity of 3.74 under identical conditions?

40. The following data is recorded for the phosphorescent intensity of several standard solutions of benzo[a]pyrene.

[benzo[a]pyrene] (M)	emission intensity
0	0.00
1.00×10^{-5}	0.98

3.00×10^{-5}	3.22
6.00×10^{-5}	6.25
1.00×10^{-4}	10.21

What is the concentration of benzo[a]pyrene in a sample that yields a phosphorescent emission intensity of 4.97?

41. The concentration of acetylsalicylic acid, $C_9H_8O_4$, in aspirin tablets is determined by hydrolyzing it to the salicylate ion, $C_7H_5O_2^-$, and determining its concentration spectrofluorometrically. A stock standard solution is prepared by weighing 0.0774 g of salicylic acid, $C_7H_6O_2$, into a 1-L volumetric flask and diluting to volume. A set of calibration standards is prepared by pipeting 0, 2.00, 4.00, 6.00, 8.00, and 10.00 mL of the stock solution into separate 100-mL volumetric flasks that contain 2.00 mL of 4 M NaOH and diluting to volume. Fluorescence is measured at an emission wavelength of 400 nm using an excitation wavelength of 310 nm with results shown in the following table.

mL of stock solution	emission intensity
0.00	0.00
2.00	3.02
4.00	5.98
6.00	9.18
8.00	12.13
10.00	14.96

Several aspirin tablets are ground to a fine powder in a mortar and pestle. A 0.1013-g portion of the powder is placed in a 1-L volumetric flask and diluted to volume with distilled water. A portion of this solution is filtered to remove insoluble binders and a 10.00-mL aliquot transferred to a 100-mL volumetric flask that contains 2.00 mL of 4 M NaOH. After diluting to volume the fluorescence of the resulting solution is 8.69. What is the %w/w acetylsalicylic acid in the aspirin tablets?

42. Selenium (IV) in natural waters is determined by complexing with ammonium pyrrolidine dithiocarbamate and extracting into $CHCl_3$. This step serves to concentrate the Se(IV) and to separate it from Se(VI). The Se(IV) is then extracted back into an aqueous matrix using HNO_3. After complexing with 2,3-diaminonaphthalene, the complex is extracted into cyclohexane. Fluorescence is measured at 520 nm following its excitation at 380 nm. Calibration is achieved by adding known amounts of Se(IV) to the water sample before beginning the analysis. Given the following results what is the concentration of Se(IV) in the sample.

[Se(IV)] added (nM)	emission intensity
0.00	323
2.00	597
4.00	862
6.00	1123

43. Fibrinogen is a protein that is produced by the liver and found in human plasma. Its concentration in plasma is clinically important. Many of the analytical methods used to determine the concentration of fibrinogen in plasma are based on light scattering following its precipitation. For example, da Silva and colleagues describe a method in which fibrino- gen precipitates in the presence of ammonium sulfate in a guanidine hydrochloride buffer [da Silva, M. P.; Fernandez-Romero, J. M.; Luque de Castro, M. D. *Anal. Chim. Acta* **1996**, *327*, 101–106]. Light scattering is measured nephelometrically at a wavelength of 340 nm. Analysis of a set of external calibration standards gives the following calibration equation

$$I_s = -4.66 + 9907.63C$$

where I_s is the intensity of scattered light and C is the concentration of fibrinogen in g/L. A 9.00-mL sample of plasma is collected from a patient and mixed with 1.00 mL of an anticoagulating agent. A 1.00-mL aliquot of this solution is diluted to 250 mL in a

volumetric flask and is found to have a scattering intensity of 44.70. What is the concentration of fibrinogen, in gram per liter, in the plasma sample?

1.10: Additional Resources

The following set of experiments introduce students to the applications of spectroscopy. Experiments are grouped into five categories: UV/Vis spectroscopy, IR spectroscopy, atomic absorption and atomic emission, fluorescence and phosphorescence, and signal averaging.

UV/Vis Spectroscopy

- Abney, J. R.; Scalettar, B. A. "Saving Your Students' Skin. Undergraduate Experiments That Probe UV Protection by Sunscreens and Sunglasses," *J. Chem. Educ.* **1998**, *75*, 757–760.
- Ainscough, E. W.; Brodie, A. M. "The Determination of Vanillin in Vanilla Extract," *J. Chem. Educ.* **1990**, *67*, 1070–1071.
- Allen, H. C.; Brauers, T.; Finlayson-Pitts, B. J. "Illustrating Deviations in the Beer-Lambert Law in an Instrumental Analysis Laboratory: Measuring Atmospheric Pollutants by Differential Optical Absorption Spectrometry," *J. Chem. Educ.* **1997**, *74*, 1459–1462.
- Blanco, M.; Iturriaga, H.; Maspoch, S.; Tarîn, P. "A Simple Method for Spectrophotometric Determination of Two-Components with Overlapped Spectra," *J. Chem. Educ.* **1989**, *66*, 178–180.
- Bonicamp, J. M.; Martin, K. L.; McBride, G. R.; Clark, R. W. "Beer's Law is Not a Straight Line: Amplification of Errors by Transformation," *Chem. Educator* **1999**, *4*, 81–88.
- Bruneau, E.; Lavabre, D.; Levy, G.; Micheau, J. C. "Quantitative Analysis of Continuous-Variation Plots with a Comparison of Several Methods," *J. Chem. Educ.* **1992**, *69*, 833–837.
- Cappas, C.; Hoffman, N.; Jones, J.; Young, S. "Determination of Concentrations of Species Whose Absorption Bands Overlap Extensively," *J. Chem. Educ.* **1991**, *68*, 300–303.
- Crisp, P. T.; Eckert, J. M.; Gibson, N. A. "The Determination of Anionic Surfactants in Natural and Waste Waters," *J. Chem. Educ.* **1983**, *60*, 236–238.
- Dilbeck, C. W.; Ganske, J. A. "Detection of NOx in Automobile Exhaust: An Applied Experiment in Atmospheric/Environmental Chemistry for the General Chemistry Laboratory," *Chem. Educator* **2008**, *13*, 1–5.
- Domínguez, A., Fernández, A.; González, N.; Iglesias, E.; Montenegro, L. "Determination of Critical Micelle Concentration of Some Surfactants by Three Techniques," *J. Chem. Educ.* **1997**, *74*, 1227– 1231.
- Gilbert, D. D. "Determining Optimum Spectral Bandwidth," *J. Chem. Educ.* **1991**, *68*, A278– A281.
- Han, J.; Story, T.; Han, G. "A Spectrophotometric Method for Quantitative Determination of Bromine Using Tris(2-carboxyethyl)phophine," *J. Chem. Educ.* **1999**, *76*, 976–977.
- Higginbotham, C.; Pike, C. F.; Rice, J, K. "Spectroscopy in Sol-Gel Matricies," *J. Chem. Educ.* **1998**, *75*, 461–464.
- Hill, Z. D.; MacCarthy, P. "Novel Approach to Job's Method," *J. Chem. Educ.* **1986**, *63*, 162–167.
- Ibañez, G. A.; Olivieri, A. C.; Escandar, G. M. "Determination of Equilibrium Constants of Metal Complexes from Spectrophotometric Measurements," *J. Chem. Educ.* **1999**, *76*, 1277–1281.
- Long, J. R.; Drago, R. S. "The Rigorous Evaluation of Spectrophotometric Data to Obtain an Equilibrium Constant," *J. Chem. Educ.* **1982**, *59*, 1037–1039.
- Lozano-Calero; D.; Martin-Palomeque, P. "Determination of Phosphorous in Cola Drinks," *J. Chem. Educ.* **1996**, *73*, 1173–1174.
- Maloney, K. M.; Quiazon, E. M.; Indralingam, R. "Measurement of Iron in Egg Yolk: An Instrumental Analysis Measurement Using Biochemical Principles," *J. Chem. Educ.* **2008**, *85*, 399–400.
- Mascotti, D. P.; Waner, M. J. "Complementary Spectroscopic Assays for Investigation Protein-Ligand Binding Activity: A Project for the Advanced Chemistry Laboratory," *J. Chem. Educ.* **2010**, *87*, 735– 738.
- McClain, R. L. "Construction of a Photometer as an Instructional Tool for Electronics and Instrumentation," *J. Chem. Educ.* **2014**, *91*, 747–750.
- McDevitt, V. L.; Rodriquez, A.; Williams, K. R. "Analysis of Soft Drinks: UV Spectrophotometry, Liquid Chromatography, and Capillary Electrophoresis," *J. Chem. Educ.* **1998**, *75*, 625–629.
- Mehra, M. C.; Rioux, J. "An Analytical Chemistry Experiment in Simultaneous Spectrophotometric Determination of Fe(III) and Cu(II) with Hexacyanoruthenate(II) Reagent," *J. Chem. Educ.* **1982**, *59*, 688–689.
- Mitchell-Koch, J. T.; Reid, K. R.; Meyerhoff, M. E. "Salicylate Detection by Complexation with Iron(III) and Optical Absorbance Spectroscopy," *J. Chem. Educ.* **2008**, *85*, 1658–1659.
- Msimanga, H. Z.; Wiese, J. "Determination of Acetaminophen in Analgesics by the Standard Addition Method: A Quantitative Analytical Chemistry Laboratory," *Chem. Educator* **2005**, *10*, 1–7.

- Örstan, A.; Wojcik, J. F. "Spectroscopic Determination of Protein-Ligand Binding Constants," *J. Chem. Educ.* **1987**, *64*, 814–816.
- Pandey, S.; Powell, J. R.; McHale, M. E. R.; Acree Jr., W. E. "Quantitative Determination of Cr(III) and Co(II) Using a Spectroscopic H-Point Standard Addition," *J. Chem. Educ.* **1997**, *74*, 848–850.
- Parody-Morreale, A.; Cámara-Artigas, A.; Sánchez-Ruiz, J. M. "Spectrophotometric Determination of the Binding Constants of Succinate and Chloride to Glutamic Oxalacetic Transaminase," *J. Chem. Educ.* **1990**, *67*, 988–990.
- Ravelo-Perez, L. M.; Hernández-Borges, J.; Rodríguez-Delgado, M. A.; Borges-Miquel, T. "Spectrophotometric Analysis of Lycopene in Tomatoes and Watermelons: A Practical Class," *Chem. Educator* **2008**, *13*, 1–3.
- Russell, D. D.; Potts, J.; Russell, R. M.; Olson, C.; Schimpf, M. "Spectroscopic and Potentiometric Investigation of a Diprotic Acid: An Experimental Approach to Understanding Alpha Functions," *Chem. Educator* **1999**, *4*, 68–72.
- Smith, E. T.; Matachek, J. R. "A Colorful Investigation of a Diprotic Acid: A General Chemistry Laboratory Exercise," *Chem. Educator* **2002**, *7*, 359–363
- Tello-Solis, S. R. "Thermal Unfolding of Lysozyme Studied by UV Difference Spectroscopy," *Chem. Educator* **2008**, *13*, 16–18.
- Tucker, S.; Robinson, R.; Keane, C.; Boff, M.; Zenko, M.; Batish, S.; Street, Jr., K. W. "Colorimetric Determination of pH," *J. Chem. Educ.* **1989**, *66*, 769–771.
- Vitt, J. E. "Troubleshooting 101: An Instrumental Analysis Experiment," *J. Chem. Educ.* **2008**, *85*, 1660–1662.
- Williams, K. R.; Cole, S. R.; Boyette, S. E.; Schulman, S. G. "The Use of Dristan Nasal Spray as the Unknown for Simultaneous Spectrophotometric Analysis of a Mixture," *J. Chem. Educ.* **1990**, *67*, 535.
- Walmsley, F. "Aggregation in Dyes: A Spectrophotometric Study," *J. Chem. Educ.* **1992**, *69*, 583. Wells, T. A. "Construction of a Simple Myoglobin-Based Optical Biosensor," *Chem. Educator* **2007**, *12*, 1–3.
  Yarnelle, M. K.; West, K. J. "Modification of an Ultraviolet Spectrophotometric Determination of the Active Ingredients in APC Tablets," *J. Chem. Educ.* **1989**, *66*, 601–602.

IR Spectroscopy

- Dragon, S.; Fitch, A. "Infrared Spectroscopy Determination of Lead Binding to Ethylenediaminetetraacetic Acid," *J. Chem. Educ.* **1998**, *75*, 1018–1021.
- Frohlich, H. "Using Infrared Spectroscopy Measurements to Study Intermolecular Hydrogen Bonding," *J. Chem. Educ.* **1993**, *70*, A3–A6.
- Garizi, N.; Macias, A.; Furch, T.; Fan, R.; Wagenknecht, P.; Singmaster, K. A. "Cigarette Smoke Analysis Using an Inexpensive Gas-Phase IR Cell," *J. Chem. Educ.* **2001**, *78*, 1665–1666.
- Indralingam, R.; Nepomuceno, A. I. "The Use of Disposable IR Cards for Quantitative Analysis Using an Internal Standard," *J. Chem. Educ.* **2001**, *78*, 958–960.
- Mathias, L. J.; Hankins, M. G.; Bertolucci, C. M.; Grubb, T. L.; Muthiah, J. "Quantitative Analysis by FTIR: Thin Films of Copolymers of Ethylene and Vinyl Acetate," *J. Chem. Educ.* **1992**, *69*, A217– A219.
- Schuttlefield, J. D.; Grassian, V. H. "ATR-FTIR Spectroscopy in the Undergraduate Chemistry Laboratory. Part I: Fundamentals and Examples," *J. Chem. Educ.* **2008**, *85*, 279–281.
- Schuttlefield, J. D.; Larsen, S. C.; Grassian, V. H. "ATR-FTIR Spectroscopy in the Undergraduate Chemistry Laboratory. Part II: A Physical Chemistry Laboratory Experiment on Surface Adsorption," *J. Chem. Educ.* **2008**, *85*, 282–284.
- Seasholtz, M. B.; Pence, L. E.; Moe Jr., O. A. "Determination of Carbon Monoxide in Automobile Exhaust by FTIR Spectroscopy," *J. Chem. Educ.* **1988**, *65*, 820–823.

Atomic Absorption and Atomic Emission Spectroscopy

- Amarasiriwardena, D. "Teaching analytical atomic spectroscopy advances in an environmental chemistry class using a project-based laboratory approach: investigation of lead and arsenic distributions in a lead arsenate contaminated apple orchard," *Anal. Bioanal. Chem.* **2007**, *388*, 307–314.
- Bazzi, A.; Bazzi, J.; Deng, Y.' Ayyash, M. "Flame Atomic Absorption Spectroscopic Determination of Iron in Breakfast Cereals: A Validated Experiment for the Analytical Chemistry Laboratory," *Chem. Educator* **2014**, *19*, 283–286.
- Buffen, B. P. "Removal of Heavy Metals from Water: An Environmentally Significant Atomic Absorption Spectrometry Experiment," *J. Chem. Educ.* **1999**, *76*, 1678–1679.
- Dockery, C. R.; Blew, M. J.; Goode, S. R. "Visualizing the Solute Vaporization Interference in Flame Atomic Absorption Spectroscopy," *J. Chem. Educ.* **2008**, *85*, 854–858.

- Donas, M. K.; Whissel, G.; Dumas, A.; Golden, K. “Analyzing Lead Content in Ancient Bronze Coins by Flame Atomic Absorption Spectroscopy,” *J. Chem. Educ.* **2009**, *86*, 343–346.
- Finch, L. E.; Hillyer, M. M.; Leopold, M. C. “Quantitative Analysis of Heavy Metals in Children’s Toys and Jewelry: A Multi-Instrument, Multitechnique Exercise in Analytical Chemistry and Public Health,” *J. Chem. Educ.* **2015**, *92*, 849–854.
- Garrison, N.; Cunningham, M.; Varys, D.; Schauer, D. J. “Discovering New Biosorbents with Atomic Absorption Spectroscopy: An Undergraduate Laboratory Experiment,” *J. Chem. Educ.* **2014**, *91*, 583–585.
- Gilles de Pelichy, L. D.; Adams, C.; Smith, E. T. “Analysis of the Essential Nutrient Strontium in Marine Aquariums by Atomic Absorption Spectroscopy,” *J. Chem. Educ.* **1997**, *74*, 1192–1194.
- Hoskins, L. C.; Reichardt, P. B.; Stolzberg, R. J. “Determination of the Extraction Constant for Zinc Pyrrolidinecarbodithioate,” *J. Chem. Educ.* **1981**, *58*, 580–581.
- Kooser, A. S.; Jenkins, J. L.; Welch, L. E. “Inductively Coupled Plasma-Atomic Emission Spectroscopy: Two Laboratory Activities for the Undergraduate Instrumental Analysis Course,” *J. Chem. Educ.* **2003**, *80*, 86–88.
- Kostecka, K. S. “Atomic Absorption Spectroscopy of Calcium in Foodstuffs in Non-Science-Major Courses,” *J. Chem. Educ.* **2000**, *77*, 1321–1323.
- Kristian, K. E.; Friedbauer, S.; Kabashi, D.; Ferencz, K. M.; Barajas, J. C.; O’Brien, K. “A Simplified Digestion Protocol for the Analysis of Hg in Fish by Cold Vapor Atomic Absorption Spectroscopy,” *J. Chem. Educ.* **2015**, *92*, 698–702.
- Lehman, T. A.; Everett, W. W. “Solubility of Lead Sulfate in Water and in Sodium Sulfate Solutions,” *J. Chem. Educ.* **1982**, *59*, 797.
- Markow, P. G. “Determining the Lead Content of Paint Chips,” *J. Chem. Educ.* **1996**, *73*, 178–179.
- Masina, M. R.; Nkosi, P. A.; Rasmussen, P. W.; Shelembe, J. S.; Tyobeka, T. E. “Determination of Metal Ions in Pineapple Juice and Effluent of a Fruit Canning Industry,” *J. Chem. Educ.* **1989**, *66*, 342–343.
- Quigley, M. N. “Determination of Calcium in Analgesic Tablets using Atomic Absorption Spectrophotometry,” *J. Chem. Educ.* **1994**, *71*, 800.
- Quigley, M. N.; Vernon, F. “Determination of Trace Metal Ion Concentrations in Seawater,” *J. Chem. Educ.* **1996**, *73*, 671–675.
- Quigley, M. N.; Vernon, F. “A Matrix Modification Experiment for Use in Electrothermal Atomic Absorption Spectrophotometry,” *J. Chem. Educ.* **1996**, *73*, 980–981.
- Palkendo, J. A.; Kovach, J.; Betts, T. A. “Determination of Wear Metals in Used Motor Oil by Flame Atomic Absorption Spectroscopy,” *J. Chem. Educ.* **2014**, *91*, 579–582.
- Rheingold, A. L.; Hues, S.; Cohen, M. N. “Strontium and Zinc Content in Bones as an Indication of Diet,” *J. Chem. Educ*. **1983**, *60*, 233–234.
- Rocha, F. R. P.; Nóbrega, J. A. “Effects of Solution Physical Properties on Copper and Chromium Signals in Flame Atomic Absorption Spectrometry,” *J. Chem. Educ.* **1996**, *73*, 982–984.

Fluorescence and Phosphorescence Spectroscopy

- Bigger, S. W.; Bigger, A. S.; Ghiggino, K. P. “*FluSpec*: A Simulated Experiment in Fluorescence Spectroscopy,” *J. Chem. Educ.* **2014**, *91*, 1081–1083.
- Buccigross, J. M.; Bedell, C. M.; Suding-Moster, H. L. “Fluorescent Measurement of TNS Binding to Calmodulin,” *J. Chem. Educ.* **1996**, *73*, 275–278.
- Henderleiter, J. A.; Hyslopo, R. M. “The Analysis of Riboflavin in Urine by Fluorescence,” *J. Chem. Educ.* **1996**, *73*, 563–564.
- Koenig, M. H.; Yi, E. P.; Sandridge, M. J.; Mathew, A. S.; Demas, J. N. “Open-Box Approach to Measuring Fluorescence Quenching Using an iPad Screen and Digital SLR Camera,” *J. Chem. Educ.* **2015**, *92*, 310–316.
- Lagoria, M. G.; Román, E. S. “How Does Light Scattering Affect Luminescence? Fluorescence Spectra and Quantum Yields in the Solid Form,” *J. Chem. Educ.* **2002**, *79*, 1362–1367.
- Richardson, D. P.; Chang, R. “Lecture Demonstrations of Fluorescence and Phosphorescence,” *Chem. Educator* **2007**, *12*, 272–274.
- Seixas de Melo, J. S.; Cabral, C.; Burrows, H. D. “Photochemistry and Photophysics in the Laboratory. Showing the Role of Radiationless and Radiative Decay of Excited States,” *Chem. Educator* **2007**, *12*, 1–6.
- Sheffield, M. C.; Nahir, T. M. “Analysis of Selenium in Brazil Nuts by Microwave Digestion and Fluorescence Detection,” *J. Chem. Educ.* **2002**, *79*, 1345–1347.

Signal Averaging

- Blitz, J. P.; Klarup, D. G. “Signal-to-Noise Ratio, Signal Processing, and Spectral Information in the Instrumental Analysis Laboratory,” *J. Chem. Educ.* **2002**, *79*, 1358–1360.
- Stolzberg, R. J. “Introduction to Signals and Noise in an Instrumental Method Course,” *J. Chem. Educ.* **1983**, *60*, 171–172.
- Tardy, D. C. “Signal Averaging. A Signal-to-Noise Enhancement Experiment for the Advanced Chemistry Laboratory,” *J. Chem. Educ.* **1986**, *63*, 648–650.

The following sources provide additional information on spectroscopy in the following areas: general spectroscopy, Beer’s law, instrumentation, Fourier transforms, IR spectroscopy, atomic asorption and emission, luminescence, and applications.

General Spectroscopy

- Ball, D. W. “Units! Units! Units!” *Spectroscopy* **1995**, *10(8)*, 44–47.
- *A History of Analytical Chemistry*, *Laitinen, H. A.; Ewing, G. W, Eds. The Division of Analytical Chemistry of the American Chemical Society: Washington, D. C., 1977, p103–243.*
- Ingle, J. D.; Crouch, S. R. *Spectrochemical Analysis*, Prentice Hall, Englewood Cliffs, N. J.; 1988.
- Macomber, R. S. “A Unifying Approach to Absorption Spectroscopy at the Undergraduate Level,” *J. Chem. Educ.* **1997**, *74*, 65–67.
- Orchin, M.; Jaffe, H. H. *Symmetry, Orbitals and Spectra*, Wiley-Interscience: New York, 1971.
- Thomas, N. C. “The Early History of Spectroscopy,” *J. Chem. Educ.* **1991**, *68*, 631–633.

Beer’s Law

- Lykos, P. “The Beer-Lambert Law Revisited: A Development without Calculus,” *J. Chem. Educ.* **1992**, *69*, 730–732.
- Ricci, R. W.; Ditzler, M. A.; Nestor, L. P. “Discovering the Beer-Lambert Law,” *J. Chem. Educ.* **1994**, *71*, 983–985.

Instrumentation

• Altermose, I. R. “Evolution of Instrumentation for UV-Visible Spectrophotometry: Part I,” *J. Chem. Educ.* **1986**, *63*, A216–A223.

- Altermose, I. R. “Evolution of Instrumentation for UV-Visible Spectrophotometry: Part II,” *J. Chem. Educ.* **1986**, *63*, A262–A266.
- Grossman, W. E. L. “The Optical Characteristics and Production of Diffraction Gratings,” *J. Chem. Educ.* **1993**, *70*, 741–748.
- Jones, D. G. “Photodiode Array Detectors in UV-Vis Spectroscopy: Part I,” *Anal. Chem.* **1985**, *57*,1057A–1073A.
- Jones, D. G. “Photodiode Array Detectors in UV-Vis Spectroscopy: Part II,” *Anal. Chem.* **1985**, 11, 1207A–1214A.
- Palmer, C. “Diffraction Gratings,” *Spectroscopy*, **1995**, *10(2)*, 14–15.

Fourier Transforms

- Bracewell, R. N. “The Fourier Transform,” *Sci. American* **1989**, *260(6)*, 85–95.
- Glasser, L. “Fourier Transforms for Chemists: Part I. Introduction to the Fourier Transform,” *J. Chem. Educ.* **1987**, *64*, A228–A233.
- Glasser, L. “Fourier Transforms for Chemists: Part II. Fourier Transforms in Chemistry and Spectroscopy,” *J. Chem. Educ.* **1987**, *64*, A260–A266.
- Glasser, L. “Fourier Transforms for Chemists: Part III. Fourier Transforms in Data Treatment,” *J. Chem. Educ.* **1987**, *64*, A306–A313.
- Graff, D. K. “Fourier and Hadamard: Transforms in Spectroscopy,” *J. Chem. Educ.* **1995**, *72*, 304–309.
- Griffiths, P. R. *Chemical Fourier Transform Spectroscopy*, Wiley-Interscience: New York, 1975.
- *Transform Techniques in Chemistry*, *Griffiths, P. R. Ed., Plenum Press: New York, 1978.*
- Perkins, W. E. “Fourier Transform Infrared Spectroscopy: Part I. Instrumentation,” *J. Chem. Educ.* **1986**, *63*, A5–A10.
- Perkins, W. E. “Fourier Transform Infrared Spectroscopy: Part II. Advantages of FT-IR,” *J. Chem. Educ.* **1987**, *64*, A269–A271.
- Perkins, W. E. “Fourier Transform Infrared Spectroscopy: Part III. Applications,” *J. Chem. Educ.* **1987**, *64*, A296–A305.
- Strong III, F. C. “How the Fourier Transform Infrared Spectrophotometer Works,” *J. Chem. Educ.* **1979**, *56*, 681–684.

IR Spectroscopy.

- *Optical Spectroscopy: Sampling Techniques Manual*, *Harrick Scientific Corporation: Ossining, N. Y., 1987.*
- Leyden, D. E.; Shreedhara Murthy, R. S. “Surface-Selective Sampling Techniques in Fourier Transform Infrared Spectroscopy,” *Spectroscopy* **1987**, *2(2)*, 28–36.

- Porro, T. J.; Pattacini, S. C. “Sample Handling for Mid-Infrared Spectroscopy, Part I: Solid and Liquid Sampling,” *Spectroscopy* **1993**, *8(7)*, 40–47.
- Porro, T. J.; Pattacini, S. C. “Sample Handling for Mid-Infrared Spectroscopy, Part II: Specialized Techniques,” *Spectroscopy* **1993**, *8(8)*, 39–44.

Atomic Absorption and Emission

- Blades, M. W.; Weir, D. G. “Fundamental Studies of the Inductively Coupled Plasma,” *Spectroscopy* **1994**, *9*, 14–21.
- Greenfield, S. “Invention of the Annular Inductively Coupled Plasma as a Spectroscopic Source,” *J. Chem. Educ.* **2000**, *77*, 584–591.
- Hieftje, G. M. “Atomic Absorption Spectrometry - Has it Gone or Where is it Going?” *J. Anal. At. Spectrom.* **1989**, *4*, 117–122.
- Jarrell, R. F. “A Brief History of Atomic Emission Spectrochemical Analysis, 1666–1950,” *J. Chem. Educ.* **2000**, *77*, 573–576
- Koirtyohann, S. R. “A History of Atomic Absorption Spectrometry From an Academic Perspective,”*Anal. Chem.* **1991**, *63*, 1024A–1031A.
- L’Vov, B. V. “Graphite Furnace Atomic Absorption Spectrometry,” *Anal. Chem.* **1991**, *63*, 924A–931A.
- Slavin, W. “A Comparison of Atomic Spectroscopic Analytical Techniques,” *Spectroscopy*, **1991**, *6*, 16–21.
- Van Loon, J. C. *Analytical Atomic Absorption Spectroscopy*, Academic Press: New York, 1980.
- Walsh, A. “The Development of Atomic Absorption Methods of Elemental Analysis 1952–1962,” *Anal. Chem.* **1991**, *63*, 933A–941A.
- Welz, B. *Atomic Absorption Spectroscopy*, VCH: Deerfield Beach, FL, 1985.

Luminescence Spectroscopy

- Guilbault, G. G. *Practical Fluorescence*, Decker: New York, 1990.
- Schenk, G. “Historical Overview of Fluorescence Analysis to 1980,” *Spectroscopy* **1997**, *12*, 47–56.
- Vo-Dinh, T. *Room-Temperature Phosphorimetry for Chemical Analysis*, Wiley-Interscience: New York, 1984.
- Winefordner, J. D.; Schulman, S. G.; O’Haver, T. C. *Luminescence Spectroscopy in Analytical Chemistry*, Wiley-Interscience: New York, 1969.

Applications

- *Trace Analysis and Spectroscopic Methods for Molecules, Christian, G. D.; Callis, J. B. Eds., Wiley-Interscience: New York, 1986.*
- Vandecasteele, C.; Block, C. B. *Modern Methods for Trace Element Determination*, Wiley: Chichester, England, 1994.
- Skoog, D. A.; Holler, F. J.; Nieman, T. A. *Principles of Instrumental Analysis*, Saunders: Philadelphia, 1998.
- Van Loon, J. C. *Selected Methods of Trace Metal Analysis: Biological and Environmental Samples*, Wiley- Interscience: New York, 1985.

Gathered here are resources and experiments for analyzing multicomponent samples using mathematical techniques not covered in this textbook.

- Aberasturi, F.; Jimenez, A. I.; Jimenez, F.; Arias, J. J. “UV-Visible First-Derivative Spectrophotometry Applied to an Analysis of a Vitamin Mixture,” *J. Chem. Educ.* **2001**, *78*, 793–795.
- Afkhami, A.; Abbasi-Tarighat, M.; Bahram, M.; Abdollahi, H. “A new strategy for solving matrix effect in multivariate calibration standard addition data using combination of H-point curve isolation and H-point standard addition methods,” *Anal. Chim. Acta* **2008**, *613*, 144–151.
- Brown, C. W.; Obremski, R. J. “Multicomponent Quantitative Analysis,” *Appl. Spectrosc. Rev.* **1984**, *20*, 373–418.
- Charles, M. J.; Martin, N. W.; Msimanga, H. Z. “Simultaneous Determination of Aspirin, Salicylamide, and Caffeine in Pain Relievers by Target Factor Analysis,” *J. Chem. Educ.* **1997**, *74*, 1114–1117.
- Dado, G.; Rosenthal, J. “Simultaneous Determination of Cobalt, Copper, and Nickel by Multivariate Linear Regression,” *J. Chem. Educ.* **1990**, *67*, 797–800.
- DiTusa, M. R.; Schilt, A. A. “Selection of Wavelengths for Optimum Precision in Simultaneous Spectrophotometric Determinations,” *J. Chem. Educ.* **1985**, *62*, 541–542.
- Gómez, D. G.; de la Peña, A. M.; Mansilla, A. E.; Olivieri, A. C. “Spectrophotometric Analysis of Mixtures by Classical Least-Squares Calibration: An Advanced Experiment Introducing MATLAB,” *Chem. Educator* **2003**, *8*, 187–191.
- Harvey, D. T.; Bowman, A. “Factor Analysis of Multicomponent Samples,” *J. Chem. Educ.* **1990**, *67*, 470–472.

- Lucio-Gutierrez, J. R.; Salazar-Cavazos, M. L.; de Torres, N. W. “Chemometrics in the Teaching Lab. Quantification of a Ternary Mixture of Common Pharmaceuticals by First- and Second-Derivative IR Spectroscopy,” *Chem. Educator* **2004**, *9*, 234–238.
- Padney, S.; McHale, M. E. R.; Coym, K. S.; Acree Jr., W. E. “Bilinear Regression Analysis as a Means to Reduce Matrix Effects in Simultaneous Spectrophotometric Determination of Cr(III) and Co(II),” *J. Chem. Educ.* **1998**, *75*, 878–880.
- Raymond, M.; Jochum, C.; Kowalski, B. R. “Optimal Multicomponent Analysis Using the Generalized Standard Addition Method,” *J. Chem. Educ.* **1983**, *60*, 1072–1073.
- Ribone, M. E.; Pagani, A. P.; Olivieri, A. C.; Goicoechea, H. C. “Determination of the Active Principle in a Spectrophotometry and Principal Component Regression Analysis,” *J. Chem. Educ.* **2000**, *77*, 1330–1333.
- Rojas, F. S.; Ojeda, C. B. “Recent developments in derivative ultraviolet/visible absorption spectrophotometry: 2004–2008,” *Anal. Chim. Acta* **2009**, *635*, 22–44.

1.11: Chapter Summary and Key Terms

Chapter Summary

The spectrophotometric methods of analysis covered in this chapter include those based on the absorption, emission, or scattering of electromagnetic radiation. When a molecule absorbs UV/Vis radiation it undergoes a change in its valence shell electron configuration. A change in vibrational energy results from the absorption of IR radiation. Experimentally we measure the fraction of radiation transmitted, *T*, by the sample. Instrumentation for measuring absorption requires a source of electromagnetic radiation, a means for selecting a wavelength, and a detector for measuring transmittance. Beer's law relates absorbance to both transmittance and to the concentration of the absorbing species ($A = -\log T = \varepsilon b C$).

In atomic absorption we measure the absorption of radiation by gas phase atoms. Samples are atomized using thermal energy from either a flame or a graphite furnace. Because the width of an atom's absorption band is so narrow, the continuum sources common for molecular absorption are not used. Instead, a hollow cathode lamp provides the necessary line source of radiation. Atomic absorption suffers from a number of spectral and chemical interferences. The absorption or scattering of radiation from the sample's matrix are important spectral interferences that are minimized by background correction. Chemical interferences include the formation of nonvolatile forms of the analyte and ionization of the analyte. The former interference is minimized by using a releasing agent or a protecting agent, and an ionization suppressor helps minimize the latter interference.

When a molecule absorbs radiation it moves from a lower energy state to a higher energy state. In returning to the lower energy state the molecule may emit radiation. This process is called photoluminescence. One form of photoluminescence is fluorescence in which the analyte emits a photon without undergoing a change in its spin state. In phosphorescence, emission occurs with a change in the analyte's spin state. For low concentrations of analyte, both fluorescent and phosphorescent emission intensities are a linear function of the analyte's concentration. Thermally excited atoms also emit radiation, forming the basis for atomic emission spectroscopy. Thermal excitation is achieved using either a flame or a plasma.

Spectroscopic measurements also include the scattering of light by a particulate form of the analyte. In turbidimetry, the decrease in the radiation's transmission through the sample is measured and related to the ana- lyte's concentration through an equation similar to Beer's law. In nephelometry we measure the intensity of scattered radiation, which varies linearly with the analyte's concentration.

Key Terms

absorbance	absorbance spectrum	absorptivity
amplitude	attenuated total reflectance	atomization
background correction	Beer’s law	chemiluminescence
chromophore	continuum source	dark current
double-beam	effective bandwidth	electromagnetic radiation
electromagnetic spectrum	emission	emission spectrum
excitation spectrum	external conversion	Fellgett’s advantage
fiber-optic probe	filter	filter photometer
fluorescence	fluorescent quantum yield	fluorimeter
frequency	graphite furnace	interferogram
interferometer	internal conversion	intersystem crossing
ionization suppressor	Jacquinot’s advantage	lifetime
line source	method of continuous variations	molar absorptivity
mole-ratio method	monochromatic	monochromator
nephelometry	nominal wavelength	phase angle
phosphorescence	phosphorescent quantum yield	photodiode array
photoluminescence	photon	plasma
polychromatic	protecting agent	radiationless deactivation
relaxation	releasing agent	resolution
self-absorption	signal averaging	signal processor
signal-to-noise ratio	single-beam	singlet excited state
slope-ratio method	spectral searching	spectrofluorometer
spectrophotometer	spectroscopy	stray radiation
transducer	transmittance	triplet excited state
turbidimetry	vibrational relaxation	wavelength
wavenumber		

CHAPTER OVERVIEW

2: Electrochemical Methods

In Chapter 10 we examined several spectroscopic techniques that take advantage of the interaction between electromagnetic radiation and matter. In this chapter we turn our attention to electrochemical techniques in which the potential, current, or charge in an electrochemical cell serves as the analytical signal.

Although there are only three fundamental electrochemical signals, there are many possible experimental designs—too many, in fact, to cover adequately in an introductory textbook. The simplest division of electrochemical techniques is between bulk techniques, in which we measure a property of the solution in the electrochemical cell, and interfacial techniques, in which the potential, current, or charge depends on the species present at the interface between an electrode and the solution in which it sits. The measurement of a solution's conductivity, which is proportional to the total concentration of dissolved ions, is one example of a bulk electrochemical technique. A determination of pH using a pH electrode is an example of an interfacial electrochemical technique. Only interfacial electrochemical methods receive further consideration in this chapter.

2.1: Overview of Electrochemistry

The focus of this chapter is on analytical techniques that use a measurement of potential, current, or charge to determine an analyte's concentration or to characterize an analyte's chemical reactivity. Collectively we call this area of analytical chemistry ***electrochemistry*** because its originated from the study of the movement of electrons in an oxidation–reduction reaction.

Despite the difference in instrumentation, all electrochemical techniques share several common features. Before we consider individual examples in greater detail, let's take a moment to consider some of these similarities. As you work through the chapter, this overview will help you focus on similarities between different electrochemical methods of analysis. You will find it easier to understand a new analytical method when you can see its relationship to other similar methods.

Five Important Concepts

To understand electrochemistry we need to appreciate five important and interrelated concepts: (1) the electrode's potential determines the analyte's form at the electrode's surface; (2) the concentration of analyte at the electrode's surface may not be the same as its concentration in bulk solution; (3) in addition to an oxidation–reduction reaction, the analyte may participate in other chemical reactions; (4) current is a measure of the rate of the analyte's oxidation or reduction; and (5) we cannot control simultaneously current and potential.

> The material in this section—particularly the five important concepts—draws upon a vision for understanding electrochemistry outlined by Larry Faulkner in the article "Understanding Electrochemistry: Some Distinctive Concepts," *J. Chem. Educ.* **1983**, *60*, 262–264. See also, Kissinger, P. T.; Bott, A. W. "Electrochemistry for the Non-Electrochemist," *Current Separations*, **2002**, *20:2*, 51–53.

The Electrode's Potential Determines the Analyte's Form

In Chapter 6 we introduced the ladder diagram as a tool for predicting how a change in solution conditions affects the position of an equilibrium reaction. Figure 11.1.1 , for example, shows a ladder diagram for the Fe^{3+}/Fe^{2+} and the Sn^{4+}/Sn^{2+} equilibria. If we place an electrode in a solution of Fe^{3+} and Sn^{4+} and adjust its potential to +0.500 V, Fe^{3+} is reduced to Fe^{2+} but Sn^{4+} is not reduced to Sn^{2+}.

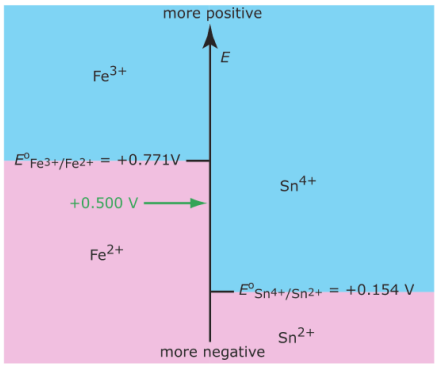

Figure 11.1.1 . Redox ladder diagram for Fe^{3+}/Fe^{2+} and for Sn^{4+}/Sn^{2+} redox couples. The areas in blue show the potential range where the oxidized forms are the predominate species; the reduced forms are the predominate species in the areas shown in pink. Note that a more positive potential favors the oxidized forms. At a potential of +0.500 V (green arrow) Fe^{3+} reduces to Fe^{2+}, but Sn^{4+} remains unchanged. You may wish to review the earlier treatment of oxidation–reduction reactions in Chapter 6.4 and the development of ladder diagrams for oxidation–reduction reactions in Chapter 6.6.

Interfacial Concentrations May Not Equal Bulk Concentrations

In Chapter 6 we introduced the Nernst equation, which provides a mathematical relationship between the electrode's potential and the concentrations of an analyte's oxidized and reduced forms in solution. For example, the Nernst equation for Fe^{3+} and Fe^{2+} is

$$E = E_{Fe^{3+}/Fe^{2+}} - \frac{RT}{nF}\ln\frac{[Fe^{2+}]}{[Fe^{3+}]} = \frac{0.05916}{1}\log\frac{[Fe^{2+}]}{[Fe^{3+}]} \quad (2.1.1)$$

where E is the electrode's potential and $E^{\circ}_{Fe^{3+}/Fe^{2+}}$ is the standard-state reduction potential for the reaction $Fe^{3+}(aq) \rightleftharpoons Fe^{2+}(aq) + e^-$. Because it is the potential of the electrode that determines the analyte's form at the electrode's surface, the concentration terms in Equation 2.1.1 are those of Fe^{2+} and Fe^{3+} at the electrode's surface, not their concentrations in bulk solution.

This distinction between a species' surface concentration and its bulk concentration is important. Suppose we place an electrode in a solution of Fe^{3+} and fix its potential at 1.00 V. From the ladder diagram in Figure 11.1.1 , we know that Fe^{3+} is stable at this potential and, as shown in Figure 11.1.2 a, the concentration of Fe^{3+} is the same at all distances from the electrode's surface. If we change the electrode's potential to +0.500 V, the concentration of Fe^{3+} at the electrode's surface decreases to approximately zero. As shown in Figure 11.1.2 b, the concentration of Fe^{3+} increases as we move away from the electrode's surface until it equals the concentration of Fe^{3+} in bulk solution. The resulting concentration gradient causes additional Fe^{3+} from the bulk solution to diffuse to the electrode's surface.

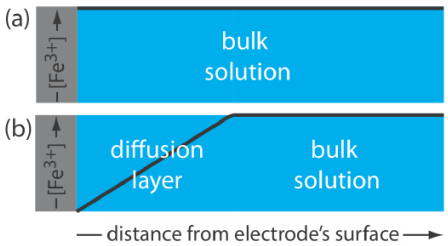

Figure 11.1.2 . Concentration of Fe^{3+} as a function of distance from the electrode's surface at (a) E = +1.00 V and (b) E = +0.500 V. The electrode is shown in gray and the solution in blue.

> We call the region of solution that contains this concentration gradient in Fe^{3+} the diffusion layer. We will have more to say about this in Chapter 11.4.

The Analyte May Participate in Other Reactions

Figure 11.1.1 and Figure 11.1.2 shows how the electrode's potential affects the concentration of Fe^{3+} and how the concentration of Fe^{3+} varies as a function of distance from the electrode's surface. The reduction of Fe^{3+} to Fe^{2+}, which is governed by Equation 2.1.1, may not be the only reaction that affects the concentration of Fe^{3+} in bulk solution or at the electrode's surface. The adsorption of Fe^{3+} at the electrode's surface or the formation of a metal–ligand complex in bulk solution, such as $Fe(OH)^{2+}$, also affects the concentration of Fe^{3+}.

Current is a Measure of Rate

The reduction of Fe^{3+} to Fe^{2+} consumes an electron, which is drawn from the electrode. The oxidation of another species, perhaps the solvent, at a second electrode is the source of this electron. Because the reduction of Fe^{3+} to Fe^{2+} consumes one electron, the flow of electrons between the electrodes—in other words, the current—is a measure of the rate at which Fe^{3+} is reduced. One important consequence of this observation is that the current is zero when the reaction $Fe^{3+}(aq) \rightleftharpoons Fe^{2+}(aq) + e^-$ is at equilibrium.

> The rate of the reaction $Fe^{3+}(aq) \rightleftharpoons Fe^{2+}(aq) + e^-$ is the change in the concentration of Fe^{3+} as a function of time.

We Cannot Control Simultaneously Both the Current and the Potential

If a solution of Fe^{3+} and Fe^{2+} is at equilibrium, the current is zero and the potential is given by Equation 2.1.1. If we change the potential away from its equilibrium position, current flows as the system moves toward its new equilibrium position. Although the initial current is quite large, it decreases over time, reaching zero when the reaction reaches equilibrium. The current, therefore, changes in response to the applied potential. Alternatively, we can pass a fixed current through the electrochemical cell, forcing the reduction of Fe^{3+} to Fe^{2+}. Because the concentrations of Fe^{3+} decreases and the concentration of Fe^{2+} increases, the potential, as given by Equation 2.1.1, also changes over time. In short, if we choose to control the potential, then we must accept the resulting current, and we must accept the resulting potential if we choose to control the current.

Controlling and Measuring Current and Potential

Electrochemical measurements are made in an electrochemical cell that consists of two or more electrodes and the electronic circuitry needed to control and measure the current and the potential. In this section we introduce the basic components of electrochemical instrumentation.

The simplest electrochemical cell uses two electrodes. The potential of one electrode is sensitive to the analyte's concentration, and is called the ***working electrode*** or the ***indicator electrode***. The second electrode, which we call the ***counter electrode***, completes the electrical circuit and provides a reference potential against which we measure the working electrode's potential. Ideally the counter electrode's potential remains constant so that we can assign to the working electrode any change in the overall cell potential. If the counter electrode's potential is not constant, then we replace it with two electrodes: a ***reference electrode*** whose potential remains constant and an ***auxiliary electrode*** that completes the electrical circuit.

Because we cannot control simultaneously the current and the potential, there are only three basic experimental designs: (1) we can measure the potential when the current is zero, (2) we can measure the potential while we control the current, and (3) we can measure the current while we control the potential. Each of these experimental designs relies on ***Ohm's law***, which states that the current, *i*, passing through an electrical circuit of resistance, *R*, generates a potential, *E*.

$$E = iR$$

Each of these experimental designs uses a different type of instrument. To help us understand how we can control and measure current and potential, *we will describe these instruments as if the analyst is operating them manually*. To do so the analyst observes a change in the current or the potential and manually adjusts the instrument's settings to maintain the desired experimental conditions. It is important to understand that modern electrochemical instruments provide an automated, electronic means for controlling and measuring current and potential, and that they do so by using very different electronic circuitry than that described here.

> This point bears repeating: It is important to understand that the experimental designs in Figure 11.1.3 , Figure 11.1.4 , and Figure 11.1.5 do not represent the electrochemical instruments you will find in today's analytical labs. For further information about modern electrochemical instrumentation, see this chapter's additional resources.

Potentiometers

To measure the potential of an electrochemical cell under a condition of zero current we use a ***potentiometer***. Figure 11.1.3 shows a schematic diagram for a manual potentiometer that consists of a power supply, an electrochemical cell with a working electrode and a counter electrode, an ammeter to measure the current that passes through the electrochemical cell, an adjustable, slide-wire resistor, and a tap key for closing the circuit through the electrochemical cell. Using Ohm's law, the current in the upper half of the circuit is

$$i_{\text{upper}} = \frac{E_{\text{PS}}}{R_{ab}}$$

where E_{PS} is the power supply's potential, and R_{ab} is the resistance between points *a* and *b* of the slide-wire resistor. In a similar manner, the current in the lower half of the circuit is

$$i_{\text{lower}} = \frac{E_{\text{cell}}}{R_{cb}}$$

where E_{cell} is the potential difference between the working electrode and the counter electrode, and R_{cb} is the resistance between the points *c* and *b* of the slide-wire resistor. When $i_{\text{upper}} = i_{\text{lower}} = 0$, no current flows through the ammeter and the potential of the electrochemical cell is

$$E_{\text{coll}} = \frac{R_{cb}}{R_{ab}} \times E_{\text{PS}} \tag{2.1.2}$$

To determine E_{cell} we briefly press the tap key and observe the current at the ammeter. If the current is not zero, then we adjust the slide wire resistor and remeasure the current, continuing this process until the current is zero. When the current is zero, we use Equation 2.1.2 to calculate E_{cell}.

Using the tap key to briefly close the circuit through the electrochemical cell minimizes the current that passes through the cell and limits the change in the electrochemical cell's composition. For example, passing a current of 10^{-9} A through the electrochemical cell for 1 s changes the concentrations of species in the cell by approximately 10^{-14} moles. Modern potentiometers use operational amplifiers to create a high-impedance voltmeter that measures the potential while drawing a current of less than 10^{-9} A.

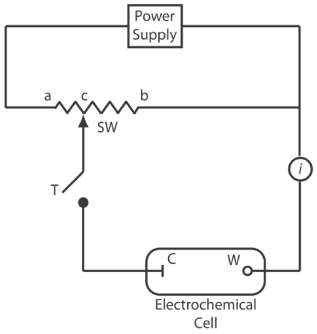

Figure 11.1.3 . Schematic diagram of a manual potentiometer: C is the counter electrode; W is the working electrode; SW is a slide-wire resistor; T is a tap key and *i* is an ammeter for measuring current.

Galvanostats

A ***galvanostat***, a schematic diagram of which is shown in Figure 11.1.4 , allows us to control the current that flows through an electrochemical cell. The current from the power supply through the working electrode is

$$i = \frac{E_{\text{PS}}}{R + R_{\text{cell}}}$$

where E_{PS} is the potential of the power supply, R is the resistance of the resistor, and R_{cell} is the resistance of the electrochemical cell. If $R >> R_{\text{cell}}$, then the current between the auxiliary and working electrodes

$$i = \frac{E_{\text{PS}}}{R} \approx \text{constant}$$

maintains a constant value. To monitor the working electrode's potential, which changes as the composition of the electrochemical cell changes, we can include an optional reference electrode and a high-impedance potentiometer.

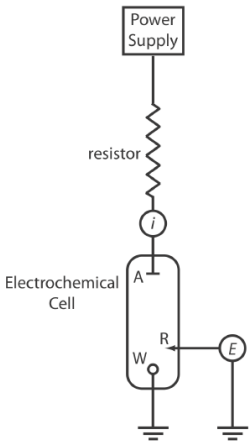

Figure 11.1.4 . Schematic diagram of a galvanostat: A is the auxiliary electrode; W is the working electrode; R is an optional reference electrode, *E* is a high-impedance potentiometer, and *i* is an ammeter. The working electrode and the optional reference electrode are connected to a ground.

Potentiostats

A ***potentiostat***, a schematic diagram of which is shown in Figure 11.1.5 , allows us to control the working electrode's potential. The potential of the working electrode is measured relative to a constant-potential reference electrode that is connected to the working electrode through a high-impedance potentiometer. To set the working electrode's potential we adjust the slide wire resistor that is connected to the auxiliary electrode. If the working electrode's potential begins to drift, we adjust the slide wire resistor to return the potential to its initial value. The current flowing between the auxiliary electrode and the working electrode is measured with an

ammeter. Modern potentiostats include waveform generators that allow us to apply a time-dependent potential profile, such as a series of potential pulses, to the working electrode.

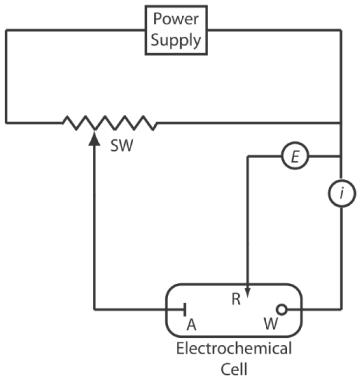

Figure 11.1.5 . Schematic diagram for a manual potentiostat: W is the working electrode; A is the auxiliary electrode; R is the reference electrode; SW is a slide-wire resistor, *E* is a high-impendance potentiometer; and *i* is an ammeter.

Interfacial Electrochemical Techniques

Because interfacial electrochemistry is such a broad field, let's use Figure 11.1.6 to organize techniques by the experimental conditions we choose to use (Do we control the potential or the current? How do we change the applied potential or applied current? Do we stir the solution?) and the analytical signal we decide to measure (Current? Potential?).

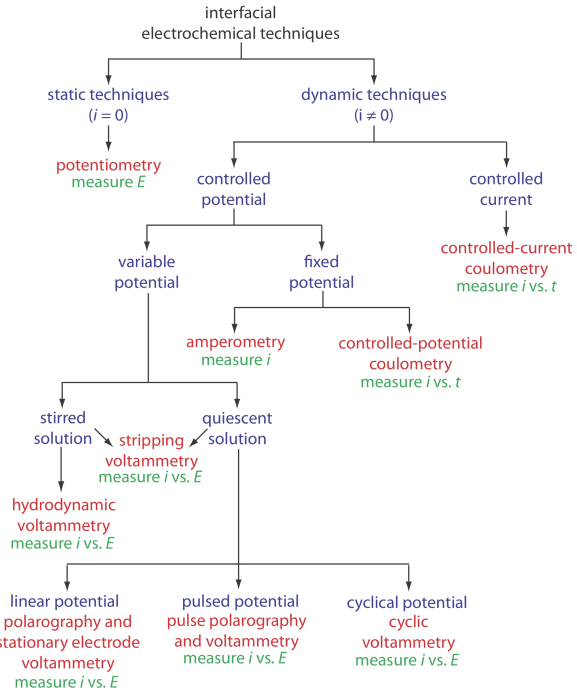

Figure 11.1.6 . Family tree that highlights the similarities and differences between a number of interfacial electrochemical techniques. The specific techniques are shown in red, the experimental conditions are shown in blue, and the analytical signals are shown in green.

At the first level, we divide interfacial electrochemical techniques into static techniques and dynamic techniques. In a static technique we do not allow current to pass through the electrochemical cell and, as a result, the concentrations of all species remain constant. Potentiometry, in which we measure the potential of an electrochemical cell under static conditions, is one of the most important quantitative electrochemical methods and is discussed in detail in Chapter 11.2.

Dynamic techniques, in which we allow current to flow and force a change in the concentration of species in the electrochemical cell, comprise the largest group of interfacial electrochemical techniques. Coulometry, in which we measure current as a function of time, is covered in Chapter 11.3. Amperometry and voltammetry, in which we measure current as a function of a fixed or variable potential, is the subject of Chapter 11.4.

2.2: Potentiometric Methods

In potentiometry we measure the potential of an electrochemical cell under static conditions. Because no current—or only a negligible current—flows through the electrochemical cell, its composition remains unchanged. For this reason, potentiometry is a useful quantitative method of analysis. The first quantitative potentiometric applications appeared soon after the formulation, in 1889, of the Nernst equation, which relates an electrochemical cell's potential to the concentration of electroactive species in the cell [Stork, J. T. *Anal. Chem.* **1993**, *65*, 344A–351A].

> For an on-line introduction to much of the material in this section, see Analytical Electrochemistry: Potentiometry by Erin Gross, Richard S. Kelly, and Donald M. Cannon, Jr., a resource that is part of the Analytical Sciences Digital Library.

Potentiometry initially was restricted to redox equilibria at metallic electrodes, which limited its application to a few ions. In 1906, Cremer discovered that the potential difference across a thin glass membrane is a function of pH when opposite sides of the membrane are in contact with solutions that have different concentrations of H_3O^+. This discovery led to the development of the glass pH electrode in 1909. Other types of membranes also yield useful potentials. For example, in 1937 Kolthoff and Sanders showed that a pellet of AgCl can be used to determine the concentration of Ag^+. Electrodes based on membrane potentials are called ion-selective electrodes, and their continued development extends potentiometry to a diverse array of analytes.

Potentiometric Measurements

As shown in Figure 11.1.3, we use a potentiometer to determine the difference between the potential of two electrodes. The potential of one electrode—the working or indicator electrode—responds to the analyte's activity and the other electrode—the counter or reference electrode—has a known, fixed potential. In this section we introduce the conventions for describing potentiometric electrochemical cells, and the relationship between the measured potential and the analyte's activity.

> In Chapter 6 we noted that a chemical reaction's equilibrium position is a function of the activities of the reactants and products, not their concentrations. To be correct, we should write the Nernst equation in terms of activities. So why didn't we use activities in Chapter 9 when we calculated redox titration curves? There are two reasons for that choice. First, concentrations are always easier to calculate than activities. Second, in a redox titration we determine the analyte's concentration from the titration's end point, not from the potential at the end point. The only reasons for calculating a titration curve is to evaluate its feasibility and to help us select a useful indicator. In most cases, the error we introduce by assuming that concentration and activity are identical is too small to be a significant concern.
>
> In potentiometry we cannot ignore the difference between activity and concentration. Later in this section we will consider how we can design a potentiometric method so that we can ignore the difference between activity and concentration. See Chapter 6.9 to review our earlier discussion of activity and concentration.

Potentiometric Electrochemical Cells

A schematic diagram of a typical potentiometric electrochemical cell is shown in Figure 11.2.1 . The electrochemical cell consists of two half-cells, each of which contains an electrode immersed in a solution of ions whose activities determine the electrode's potential. A ***salt bridge*** that contains an inert electrolyte, such as KCl, connects the two half-cells. The ends of the salt bridge are fixed with porous frits, which allow the electrolyte's ions to move freely between the half-cells and the salt bridge. This movement of ions in the salt bridge completes the electrical circuit.

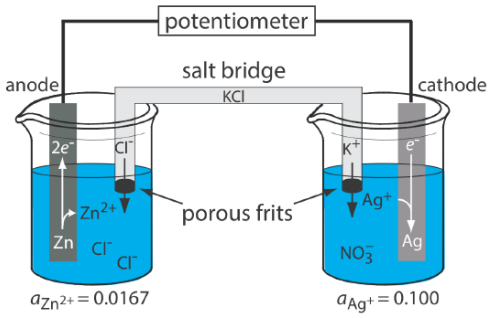

Figure 11.2.1 . Example of a potentiometric electrochemical cell. The activities of Zn^{2+} and Ag^{+} are shown below the two half-cells.

By convention, we identify the electrode on the left as the ***anode*** and assign to it the oxidation reaction; thus

$$\mathrm{Zn}(s) \rightleftharpoons \mathrm{Zn}^{2+}(aq) + 2e^{-}$$

The electrode on the right is the ***cathode***, where the reduction reaction occurs.

$$\mathrm{Ag}^{+}(aq) + e^{-} \rightleftharpoons \mathrm{Ag}(s)$$

The potential of the electrochemical cell in Figure 11.2.1 is for the reaction

$$\mathrm{Zn}(s) + 2\mathrm{Ag}^{+}(aq) \rightleftharpoons 2\mathrm{Ag}(s) + \mathrm{Zn}^{2+}(\mathrm{aq})$$

We also define potentiometric electrochemical cells such that the cathode is the indicator electrode and the anode is the reference electrode.

> The reason for separating the electrodes is to prevent the oxidation reaction and the reduction reaction from occurring at one of the electrodes. For example, if we place a strip of Zn metal in a solution of $AgNO_3$, the reduction of Ag^{+} to Ag occurs on the surface of the Zn at the same time as a potion of the Zn metal oxidizes to Zn^{2+}. Because the transfer of electrons from Zn to Ag^{+} occurs at the electrode's surface, we can not pass them through the potentiometer.

Shorthand Notation for Electrochemical Cells

Although Figure 11.2.1 provides a useful picture of an electrochemical cell, it is not a convenient way to represent it (Imagine having to draw a picture of each electrochemical cell you are using!). A more useful way to describe an electrochemical cell is a shorthand notation that uses symbols to identify different phases and that lists the composition of each phase. We use a vertical slash (|) to identify a boundary between two phases where a potential develops, and a comma (,) to separate species in the same phase or to identify a boundary between two phases where no potential develops. Shorthand cell notations begin with the anode and continue to the cathode. For example, we describe the electrochemical cell in Figure 11.2.1 using the following shorthand notation.

$$\mathrm{Zn}(s)|\mathrm{ZnCl_2}(aq, a_{\mathrm{Zn^{2+}}} = 0.0167)||\mathrm{AgNO_3}(aq, a_{\mathrm{Ag^{+}}} = 0.100)|\mathrm{Ag}(s)$$

The double vertical slash (||) represents the salt bridge, the contents of which we usually do not list. Note that a double vertical slash implies that there is a potential difference between the salt bridge and each half-cell.

✔ Example 11.2.1

What are the anodic, the cathodic, and the overall reactions responsible for the potential of the electrochemical cell in Figure 11.2.2 ? Write the shorthand notation for the electrochemical cell.

Solution

The oxidation of Ag to Ag^{+} occurs at the anode, which is the left half-cell. Because the solution contains a source of Cl^{-}, the anodic reaction is

$$\mathrm{Ag}(s) + \mathrm{Cl}^{-}(aq) \rightleftharpoons \mathrm{AgCl}(s) + e^{-}$$

The cathodic reaction, which is the right half-cell, is the reduction of Fe^{3+} to Fe^{2+}.

$$Fe^{3+}(aq) + e^- \rightleftharpoons Fe^{2+}(aq)$$

The overall cell reaction, therefore, is

$$Ag(s) + Fe^{3+}(aq) + Cl^-(aq) \rightleftharpoons AgCl(s) + Fe^{2+}(aq)$$

The electrochemical cell's shorthand notation is

$$Ag(s)|HCl(aq, a_{Cl^-} = 0.100), AgCl(sat'd)||FeCl_2(aq, a_{Fe^{2+}} = 0.0100),\ Fe^{3+}(aq, a_{Fe^{3+}} = 0.0500)|Pt(s)$$

Note that the Pt cathode is an inert electrode that carries electrons to the reduction half-reaction. The electrode itself does not undergo reduction.

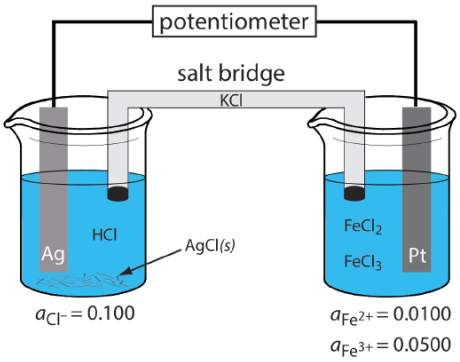

Figure 11.2.2 . Potentiometric electrochemical cell for Example 11.2.1 .

Exercise 11.2.1

Write the reactions occurring at the anode and the cathode for the potentiometric electrochemical cell with the following shorthand notation.

$$Pt(s) \mid H_2(g), H^+(aq) \parallel Cu^{2+}(aq) \mid Cu(s)$$

Answer

The oxidation of H_2 to H^+ occurs at the anode

$$H_2(g) \rightleftharpoons 2H^+(aq) + 2e^-$$

and the reduction of Cu^{2+} to Cu occurs at the cathode.

$$Cu^{2+}(aq) + 2e^- \rightleftharpoons Cu(s)$$

The overall cell reaction, therefore, is

$$Cu^{2+}(aq) + H_2(g) \rightleftharpoons 2H^+(aq) + Cu(s)$$

Potential and Activity—The Nernst Equation

The potential of a potentiometric electrochemical cell is

$$E_{cell} = E_{cathode} - E_{anode} \tag{2.2.1}$$

where $E_{cathode}$ and E_{anode} are reduction potentials for the redox reactions at the cathode and the anode, respectively. Each reduction potential is given by the Nernst equation

$$E = E^\circ - \frac{RT}{nF} \ln Q$$

where E^o is the standard-state reduction potential, R is the gas constant, T is the temperature in Kelvins, n is the number of electrons in the redox reaction, F is Faraday's constant, and Q is the reaction quotient. At a temperature of 298 K (25°C) the Nernst equation is

$$E = E^\circ - \frac{0.05916}{n} \log Q \tag{2.2.2}$$

where E is in volts.

Using Equation 2.2.2, the potential of the anode and cathode in Figure 11.2.1 are

$$E_{\text{anode}} = E^\circ_{\text{Zn}^{2+}/\text{Zn}} - \frac{0.05916}{2} \log \frac{1}{a_{\text{Zn}^{2+}}}$$

$$E_{\text{anode}} = E^\circ_{\text{Ag}^{+}/\text{Ag}} - \frac{0.05916}{1} \log \frac{1}{a_{\text{Ag}^{+}}}$$

Even though an oxidation reaction is taking place at the anode, we define the anode's potential in terms of the corresponding reduction reaction and the standard-state reduction potential. See Chapter 6.4 for a review of using the Nernst equation in calculations.

Substituting E_{cathode} and E_{anode} into Equation 2.2.1, along with the activities of Zn^{2+} and Ag^{+} and the standard-state reduction potentials, gives E_{cell} as

$$E_{\text{cell}} = \left(E^\circ_{\text{Ag}^{+}/\text{Ag}} - \frac{0.05916}{1} \log \frac{1}{a_{\text{Ag}^{+}}} \right) - \left(E^\circ_{\text{Zn}^{2+}/\text{Zn}} - \frac{0.05916}{2} \log \frac{1}{a_{\text{Zn}^{2+}}} \right)$$

$$E_{\text{cell}} = \left(0.7996 - \frac{0.05916}{1} \log \frac{1}{0.100} \right) - \left(-0.7618 - \frac{0.05916}{2} \log \frac{1}{0.0167} \right) = 1.555 \text{ V}$$

You will find values for the standard-state reduction potentials in Appendix 13.

Example 11.2.2

What is the potential of the electrochemical cell shown in Example 11.2.1 ?

Solution

Substituting E_{cathode} and E_{anode} into Equation 2.2.1, along with the concentrations of Fe^{3+}, Fe^{2+}, and Cl^{-} and the standard-state reduction potentials gives

$$E_{\text{cell}} = \left(E^\circ_{\text{Fe}^{3+}/\text{Fe}^{2+}} - \frac{0.05916}{1} \log \frac{a_{\text{Fe}^{2+}}}{a_{\text{Fe}^{3+}}} \right) - \left(E^\circ_{\text{AgCl}/\text{Ag}} - \frac{0.05916}{1} \log a_{\text{Cl}^{-}} \right)$$

$$E_{\text{cell}} = \left(0.771 - \frac{0.05916}{1} \log \frac{0.0100}{0.0500} \right) - \left(0.2223 - \frac{0.05916}{1} \log (0.100) \right) = 0.531 \text{ V}$$

Exercise 11.2.2

What is the potential for the electrochemical cell in Exercise 11.2.1 if the activity of H^{+} in the anodic half-cell is 0.100, the fugacity of H_2 in the anodic half-cell is 0.500, and the activity of Cu^{2+} in the cathodic half-cell is 0.0500? Fugacity, f, is the equivalent term for the activity of a gas.

Answer

Making appropriate substitutions into Equation 2.2.1and solving for E_{cell} gives its value as

$$E_{\text{cell}} = \left(E^\circ_{\text{Cu}^{2+}/\text{Cu}} - \frac{0.05916}{2} \log \frac{1}{a_{\text{Cu}^{2+}}} \right) - \left(E^\circ_{\text{H}^{+}/\text{H}_2} - \frac{0.05916}{2} \log \frac{f_{\text{H}_2}}{a^2_{\text{H}^{+}}} \right)$$

$$E_{\text{cell}} = \left(0.3419 - \frac{0.05916}{2} \log \frac{1}{0.0500} \right) - \left(0.0000 - \frac{0.05916}{2} \log \frac{0.500}{(0.100)^2} \right) = 0.3537 \text{ V}$$

In potentiometry, we assign the reference electrode to the anodic half-cell and assign the indicator electrode to the cathodic half-cell. Thus, if the potential of the cell in Figure 11.2.1 is +1.50 V and the activity of Zn^{2+} is 0.0167, then we can solve the following equation for a_{Ag^+}

$$1.50 \text{ V} = \left(0.7996 - \frac{0.05916}{1}\log\frac{1}{a_{Ag^+}}\right) - \left(-0.7618 - \frac{0.05916}{2}\log\frac{1}{0.0167}\right)$$

obtaining an activity of 0.0118.

Example 11.2.3

What is the activity of Fe^{3+} in an electrochemical cell similar to that in Example 11.2.1 if the activity of Cl^- in the left-hand cell is 1.0, the activity of Fe^{2+} in the right-hand cell is 0.015, and E_{cell} is +0.546 V?

Solution

Making appropriate substitutions into Equation 2.2.1

$$0.546 = \left(0.771 - \frac{0.05916}{1}\log\frac{0.0100}{a_{Fe^{3+}}}\right) - \left(0.2223 - \frac{0.05916}{1}\log(1.0)\right)$$

and solving for $a_{Fe^{3+}}$ gives its activity as 0.0135.

Exercise 11.2.3

What is the activity of Cu^{2+} in the electrochemical cell in Exercise 11.2.1 if the activity of H^+ in the anodic half-cell is 1.00 with a fugacity of 1.00 for H_2, and an E_{cell} of +0.257 V?

Answer

Making appropriate substitutions into Equation 2.2.1

$$0.257 \text{ V} = \left(0.3419 - \frac{0.05916}{2}\log\frac{1}{a_{Cu^{2+}}}\right) - \left(0.0000 - \frac{0.05916}{2}\log\frac{1.00}{(1.00)^2}\right)$$

and solving for $a_{Cu^{2+}}$ gives its activity as 1.35×10^{-3}.

Despite the apparent ease of determining an analyte's activity using the Nernst equation, there are several problems with this approach. One problem is that standard-state potentials are temperature-dependent and the values in reference tables usually are for a temperature of 25°C. We can overcome this problem by maintaining the electrochemical cell at 25°C or by measuring the standard-state potential at the desired temperature.

Another problem is that a standard-sate reduction potential may have a significant matrix effect. For example, the standard-state reduction potential for the Fe^{3+}/Fe^{2+} redox couple is +0.735 V in 1 M $HClO_4$, +0.70 V in 1 M HCl, and +0.53 V in 10 M HCl. The difference in potential for equimolar solutions of HCl and $HClO_4$ is the result of a difference in the activity coefficients for Fe^{3+} and Fe^{2+} in these two media. The shift toward a more negative potential with an increase in the concentration of HCl is the result of chloride's ability to form a stronger complex with Fe^{3+} than with Fe^{2+}. We can minimize this problem by replacing the standard-state potential with a matrix-dependent formal potential. Most tables of standard-state potentials, including those in Appendix 13, include selected formal potentials.

Finally, a more serious problem is the presence of additional potentials in the electrochemical cell not included in Equation 2.2.1. In writing the shorthand notation for an electrochemical cell we use a double slash (||) to indicate the salt bridge, suggesting a potential exists at the interface between each end of the salt bridge and the solution in which it is immersed. The origin of this potential is discussed in the following section.

Junction Potentials

A ***junction potential*** develops at the interface between two ionic solution if there is a difference in the concentration and mobility of the ions. Consider, for example, a porous membrane that separations a solution of 0.1 M HCl from a solution of 0.01 M HCl (Figure 11.2.3 a). Because the concentration of HCl on the membrane's left side is greater than that on the right side of the membrane, H^+ and Cl^- will diffuse in the direction of the arrows. The mobility of H^+, however, is greater than that for Cl^-, as shown by the difference in the lengths of their respective arrows. Because of this difference in mobility, the solution on the right side of the membrane develops an excess concentration of H^+ and a positive charge (Figure 11.2.3 b). Simultaneously, the solution on the membrane's left side develops a negative charge because there is an excess concentration of Cl^-. We call this difference in potential across the membrane a junction potential and represent it as E_j.

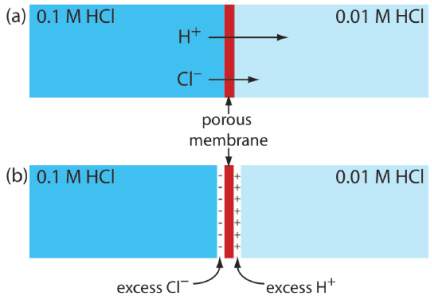

Figure 11.2.3 . Origin of the junction potential between a solution of 0.1 M HCl and a solution of 0.01 M HCl.

The magnitude of the junction potential depends upon the difference in the concentration of ions on the two sides of the interface, and may be as large as 30–40 mV. For example, a junction potential of 33.09 mV has been measured at the interface between solutions of 0.1 M HCl and 0.1 M NaCl [Sawyer, D. T.; Roberts, J. L., Jr. *Experimental Electrochemistry for Chemists*, Wiley-Interscience: New York, 1974, p. 22]. A salt bridge's junction potential is minimized by using a salt, such as KCl, for which the mobilities of the cation and anion are approximately equal. We also can minimize the junction potential by incorporating a high concentration of the salt in the salt bridge. For this reason salt bridges frequently are constructed using solutions that are saturated with KCl. Nevertheless, a small junction potential, generally of unknown magnitude, is always present.

When we measure the potential of an electrochemical cell, the junction potential also contributes to E_{cell}; thus, we rewrite Equation 2.2.1 as

$$E_{\text{cell}} = E_{\text{cathode}} - E_{\text{anode}} + E_j$$

to include its contribution. If we do not know the junction potential's actual value—which is the usual situation—then we cannot directly calculate the analyte's concentration using the Nernst equation. Quantitative analytical work is possible, however, if we use one of the standardization methods—external standards, the method of standard additions, or internal standards—discussed in Chapter 5.3.

Reference Electrodes

In a potentiometric electrochemical cell one of the two half-cells provides a fixed reference potential and the potential of the other half-cell responds the analyte's concentration. By convention, the reference electrode is the anode; thus, the short hand notation for a potentiometric electrochemical cell is

$$\text{reference electrode} \,||\, \text{indicator electrode}$$

and the cell potential is

$$E_{\text{cell}} = E_{\text{ind}} - E_{\text{ref}} + E_j$$

The ideal reference electrode provides a stable, known potential so that we can attribute any change in E_{cell} to the analyte's effect on the indicator electrode's potential. In addition, it should be easy to make and to use the reference electrode. Three common reference electrodes are discussed in this section.

Standard Hydrogen Electrode

Although we rarely use the ***standard hydrogen electrode*** (SHE) for routine analytical work, it is the reference electrode used to establish standard-state potentials for other half-reactions. The SHE consists of a Pt electrode immersed in a solution in which the

activity of hydrogen ion is 1.00 and in which the fugacity of $H_2(g)$ is 1.00 (Figure 11.2.4). A conventional salt bridge connects the SHE to the indicator half-cell. The short hand notation for the standard hydrogen electrode is

$$\mathrm{Pt}(s),\ \mathrm{H_2}\ (g, f_{\mathrm{H_2}} = 1.00)\ |\ \mathrm{H^+}\ (aq, a_{\mathrm{H^+}} = 1.00)\ ||$$

and the standard-state potential for the reaction

$$\mathrm{H^+}(aq) + e^- = \frac{1}{2}\mathrm{H_2}(g)$$

is, by definition, 0.00 V at all temperatures. Despite its importance as the fundamental reference electrode against which we measure all other potentials, the SHE is rarely used because it is difficult to prepare and inconvenient to use.

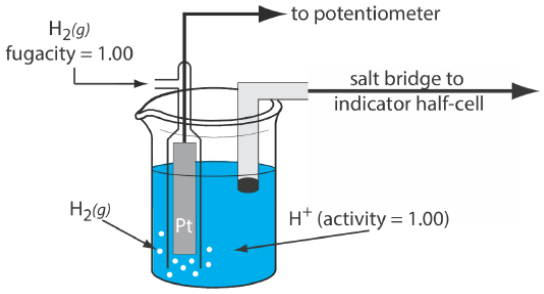

Figure 11.2.4 . Schematic diagram showing the standard hydrogen electrode.

Calomel Electrodes

A calomel reference electrode is based on the following redox couple between Hg_2Cl_2 and Hg (calomel is the common name for Hg_2Cl_2)

$$\mathrm{Hg_2Cl_2}(s) + 2e^- \rightleftharpoons 2\mathrm{Hg}(l) + 2\mathrm{Cl^-}(aq)$$

for which the potential is

$$E = E^{\circ}_{\mathrm{Hg_2Cl_2/Hg}} - \frac{0.05916}{2}\log\left(a_{\mathrm{Cl^-}}\right)^2 = +0.2682\mathrm{V} - \frac{0.05916}{2}\log\left(a_{\mathrm{Cl^-}}\right)^2$$

The potential of a calomel electrode, therefore, depends on the activity of Cl^- in equilibrium with Hg and Hg_2Cl_2.

As shown in Figure 11.2.5 , in a ***saturated calomel electrode*** (SCE) the concentration of Cl^- is determined by the solubility of KCl. The electrode consists of an inner tube packed with a paste of Hg, Hg_2Cl_2, and KCl, situated within a second tube that contains a saturated solution of KCl. A small hole connects the two tubes and a porous wick serves as a salt bridge to the solution in which the SCE is immersed. A stopper in the outer tube provides an opening for adding addition saturated KCl. The short hand notation for this cell is

$$\mathrm{Hg}(l)|\mathrm{Hg_2Cl_2}(s), \mathrm{KCl}(aq,\ \mathrm{sat'd}\ )||$$

Because the concentration of Cl^- is fixed by the solubility of KCl, the potential of an SCE remains constant even if we lose some of the inner solution to evaporation. A significant disadvantage of the SCE is that the solubility of KCl is sensitive to a change in temperature. At higher temperatures the solubility of KCl increases and the electrode's potential decreases. For example, the potential of the SCE is +0.2444 V at 25ºC and +0.2376 V at 35ºC. The potential of a calomel electrode that contains an unsaturated solution of KCl is less dependent on the temperature, but its potential changes if the concentration, and thus the activity of Cl^-, increases due to evaporation.

> For example, the potential of a calomel electrode is +0.280 V when the concentration of KCl is 1.00 M and +0.336 V when the concentration of KCl is 0.100 M. If the activity of Cl^- is 1.00, the potential is +0.2682 V.

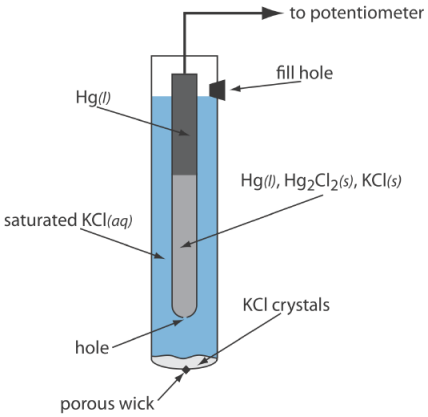

Figure 11.2.5 . Schematic diagram showing the saturated calomel electrode.

Silver/Silver Chloride Electrodes

Another common reference electrode is the ***silver/silver chloride electrode***, which is based on the reduction of AgCl to Ag.

$$\mathrm{AgCl}(s) + e^- \rightleftharpoons \mathrm{Ag}(s) + \mathrm{Cl}^-(aq)$$

As is the case for the calomel electrode, the activity of $Cl^–$ determines the potential of the Ag/AgCl electrode; thus

$$E = E^\circ_{\mathrm{AgCl/Ag}} - 0.05916 \log a_{\mathrm{Cl}^-} = 0.2223 \text{ V} - 0.05916 \log a_{\mathrm{Cl}^-}$$

When prepared using a saturated solution of KCl, the electrode's potential is +0.197 V at 25°C. Another common Ag/AgCl electrode uses a solution of 3.5 M KCl and has a potential of +0.205 V at 25°C. As you might expect, the potential of a Ag/AgCl electrode using a saturated solution of KCl is more sensitive to a change in temperature than an electrode that uses an unsaturated solution of KCl.

A typical Ag/AgCl electrode is shown in Figure 11.2.6 and consists of a silver wire, the end of which is coated with a thin film of AgCl, immersed in a solution that contains the desired concentration of KCl. A porous plug serves as the salt bridge. The electrode's short hand notation is

$$\mathrm{Ag}(s) | \mathrm{Ag\,Cl}(s), \mathrm{KCl}\,(aq, a_{\mathrm{Cl}^-} = x) \,||$$

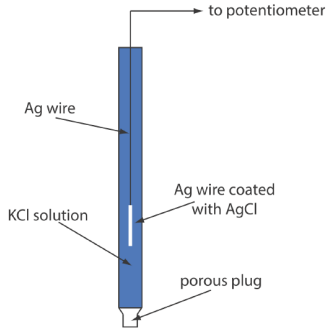

Figure 11.2.6 . Schematic diagram showing a Ag/AgCl electrode. Because the electrode does not contain solid KCl, this is an example of an unsaturated Ag/AgCl electrode.

Converting Potentials Between Reference Electrodes

The standard state reduction potentials in most tables are reported relative to the standard hydrogen electrode's potential of +0.00 V. Because we rarely use the SHE as a reference electrode, we need to convert an indicator electrode's potential to its equivalent value when using a different reference electrode. As shown in the following example, this is easy to do.

Example 11.2.4

The potential for an Fe^{3+}/Fe^{2+} half-cell is +0.750 V relative to the standard hydrogen electrode. What is its potential if we use a saturated calomel electrode or a saturated silver/silver chloride electrode?

Solution

When we use a standard hydrogen electrode the potential of the electrochemical cell is

$$E_{\text{cell}} = E_{\text{Fe}^{3+}/\text{Fe}^{2+}} - E_{\text{SHE}} = 0.750\ \text{V} - 0.000\ \text{V} = 0.750\ \text{V}$$

We can use the same equation to calculate the potential if we use a saturated calomel electrode

$$E_{\text{cell}} = E_{\text{Fe}^{3+}/\text{Fe}^{2+}} - E_{\text{SHE}} = 0.750\ \text{V} - 0.2444\ \text{V} = 0.506\ \text{V}$$

or a saturated silver/silver chloride electrode

$$E_{\text{cell}} = E_{\text{Fe}^{3+}/\text{Fe}^{2+}} - E_{\text{SHE}} = 0.750\ \text{V} - 0.197\ \text{V} = 0.553\ \text{V}$$

Figure 11.2.7 provides a pictorial representation of the relationship between these different potentials.

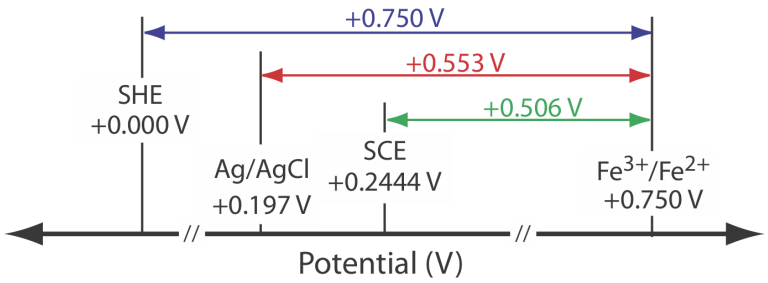

Figure 11.2.7 . Relationship between the potential of an Fe^{3+}/Fe^{2+} half-cell relative to the reference electrodes in Example 11.2.4 . The potential relative to a standard hydrogen electrode is shown in blue, the potential relative to a saturated silver/silver chloride electrode is shown in red, and the potential relative to a saturated calomel electrode is shown in green.

Exercise 11.2.4

The potential of a UO_2^+/U^{4+} half-cell is –0.0190 V relative to a saturated calomel electrode. What is its potential when using a saturated silver/silver chloride electrode or a standard hydrogen electrode?

Answer

When using a saturated calomel electrode, the potential of the electro- chemical cell is

$$E_{\text{cell}} = E_{UO_2^+/U^{4+}} - E_{\text{SCE}}$$

Substituting in known values

$$-0.0190\ \text{V} = E_{UO_2^+/U^{4+}} - 0.2444\ \text{V}$$

and solving for $E_{UO_2^+/U^{4+}}$ gives its value as +0.2254 V. The potential relative to the Ag/AgCl electrode is

$$E_{\text{cell}} = E_{UO_2^+/U^{4+}} - E_{\text{Ag/AgCl}} = 0.2254\ \text{V} - 0.197\ \text{V} = 0.028\ \text{V}$$

and the potential relative to the standard hydrogen electrode is

$$E_{\text{cell}} = E_{UO_2^+/U^{4+}} - E_{\text{SHE}} = 0.2254\ \text{V} - 0.000\ \text{V} = 0.2254\ \text{V}$$

Metallic Indicator Electrodes

In potentiometry, the potential of the indicator electrode is proportional to the analyte's activity. Two classes of indicator electrodes are used to make potentiometric measurements: metallic electrodes, which are the subject of this section, and ion-selective electrodes, which are covered in the next section.

Electrodes of the First Kind

If we place a copper electrode in a solution that contains Cu^{2+}, the electrode's potential due to the reaction

$$Cu^{2+}(aq) + 2e^- \rightleftharpoons Cu(s)$$

is determined by the activity of Cu^{2+}.

$$E = E^\circ_{Cu^{2+}/Cu} - \frac{0.05916}{2}\log\frac{1}{a_{Cu^{2+}}} = +0.3419V - \frac{0.05916}{2}\log\frac{1}{a_{Cu^{2+}}}$$

If copper is the indicator electrode in a potentiometric electrochemical cell that also includes a saturated calomel reference electrode

$$SCE \| Cu^{2+}\,(aq, a_{Cu^{2+}} = x)\,|Cu(s)$$

then we can use the cell potential to determine an unknown activity of Cu^{2+} in the indicator electrode's half-cell

$$E_{cell} = E_{ind} - E_{SCE} + E_j = +0.3419V - \frac{0.05916}{2}\log\frac{1}{a_{Cu^{2+}}} - 0.2224V + E_j$$

An indicator electrode in which the metal is in contact with a solution containing its ion is called an ***electrode of the first kind***. In general, if a metal, *M*, is in a solution of M^{n+}, the cell potential is

$$E_{call} = K - \frac{0.05916}{n}\log\frac{1}{a_{M^{n+}}} = K + \frac{0.05916}{n}\log a_{M^{n+}}$$

where *K* is a constant that includes the standard-state potential for the M^{n+}/M redox couple, the potential of the reference electrode, and the junction potential.

> Note that including E_j in the constant *K* means we do not need to know the junction potential's actual value; however, the junction potential must remain constant if *K* is to maintain a constant value.

For a variety of reasons—including the slow kinetics of electron transfer at the metal–solution interface, the formation of metal oxides on the electrode's surface, and interfering reactions—electrodes of the first kind are limited to the following metals: Ag, Bi, Cd, Cu, Hg, Pb, Sn, Tl, and Zn.

> Many of these electrodes, such as Zn, cannot be used in acidic solutions because they are easily oxidized by H^+.
>
> $$Zn(s) + 2H^+(aq) \rightleftharpoons H_2(g) + Zn^{2+}(aq)$$

Electrodes of the Second Kind

The potential of an electrode of the first kind responds to the activity of M^{n+}. We also can use this electrode to determine the activity of another species if it is in equilibrium with M^{n+}. For example, the potential of a Ag electrode in a solution of Ag^+ is

$$E = 0.7996V + 0.05916\log a_{Ag^+} \tag{2.2.3}$$

If we saturate the indicator electrode's half-cell with AgI, the solubility reaction

$$AgI(s) \rightleftharpoons Ag^+(aq) + I^-(aq)$$

determines the concentration of Ag^+; thus

$$a_{Ag^+} = \frac{K_{sp,AgI}}{a_{I^-}} \tag{2.2.4}$$

where $K_{sp,AgI}$ is the solubility product for AgI. Substituting Equation 2.2.4 into Equation 2.2.3

$$E = 0.7996\ V + 0.05916\log\frac{K_{sp,\ AgI}}{a_{I^-}}$$

shows that the potential of the silver electrode is a function of the activity of I^-. If we incorporate this electrode into a potentiometric electrochemical cell with a saturated calomel electrode

$$\text{SCE}||\text{AgI}(s),\ \text{I}^-\ (aq, a_{\text{I}^-} = x)\,|\text{Ag(s)}$$

then the cell potential is

$$E_{\text{cell}} = K - 0.05916 \log a_{\text{I}^-}$$

where K is a constant that includes the standard-state potential for the Ag^+/Ag redox couple, the solubility product for AgI, the reference electrode's potential, and the junction potential.

If an electrode of the first kind responds to the activity of an ion in equilibrium with M^{n+}, we call it an ***electrode of the second kind***. Two common electrodes of the second kind are the calomel and the silver/silver chloride reference electrodes.

> In an electrode of the second kind we link together a redox reaction and another reaction, such as a solubility reaction. You might wonder if we can link together more than two reactions. The short answer is yes. An electrode of the third kind, for example, links together a redox reaction and two other reactions. Such electrodes are less common and we will not consider them in this text.

Redox Electrodes

An electrode of the first kind or second kind develops a potential as the result of a redox reaction that involves the metallic electrode. An electrode also can serve as a source of electrons or as a sink for electrons in an unrelated redox reaction, in which case we call it a ***redox electrode.*** The Pt cathode in Figure 11.2.2 and Example 11.2.1 is a redox electrode because its potential is determined by the activity of Fe^{2+} and Fe^{3+} in the indicator half-cell. Note that a redox electrode's potential often responds to the activity of more than one ion, which limits its usefulness for direct potentiometry.

Membrane Electrodes

If metals were the only useful materials for constructing indicator electrodes, then there would be few useful applications of potentiometry. In 1906, Cremer discovered that the potential difference across a thin glass membrane is a function of pH when opposite sides of the membrane are in contact with solutions that have different concentrations of H_3O^+. The existence of this ***membrane potential*** led to the development of a whole new class of indicator electrodes, which we call ***ion-selective electrodes*** (ISEs). In addition to the glass pH electrode, ion-selective electrodes are available for a wide range of ions. It also is possible to construct a membrane electrode for a neutral analyte by using a chemical reaction to generate an ion that is monitored with an ion-selective electrode. The development of new membrane electrodes continues to be an active area of research.

Membrane Potentials

Figure 11.2.8 shows a typical potentiometric electrochemical cell equipped with an ion-selective electrode. The short hand notation for this cell is

$$\text{ref (sample)}\ \ ||[\text{A}]_{\text{samp}}\ (aq, a_{\text{A}} = x)\,|[\text{A}]_{\text{int}}\ (aq, a_{\text{A}} = y)||\ \ \text{ref (internal)}$$

where the ion-selective membrane is represented by the vertical slash that separates the two solutions that contain analyte: the sample solution and the ion-selective electrode's internal solution. The potential of this electrochemical cell includes the potential of each reference electrode, a junction potential, and the membrane's potential

$$E_{\text{cell}} = E_{\text{ref(int)}} - E_{\text{ref(samp)}} + E_{\text{mem}} + E_j \tag{2.2.5}$$

where E_{mem} is the potential across the membrane and The notations ref(sample) and ref(internal) represent a reference electrode immersed in the sample and a reference electrode immersed in the ISE's internal solution. Because the junction potential and the potential of the two reference electrodes are constant, any change in E_{cell} reflects a change in the membrane's potential.

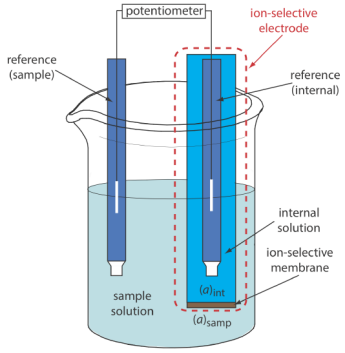

Figure 11.2.8 . Schematic diagram that shows a typical potentiometric cell with an ion-selective electrode. The ion-selective electrode's membrane separates the sample, which contains the analyte at an activity of $(a_A)_{samp}$, from an internal solution that contains the analyte with an activity of $(a_A)_{int}$.

The analyte's interaction with the membrane generates a membrane potential if there is a difference in its activity on the membrane's two sides. Current is carried through the membrane by the movement of either the analyte or an ion already present in the membrane's matrix. The membrane potential is given by the following Nernst-like equation

$$E_{mem} = E_{asym} - \frac{RT}{zF} \ln \frac{(a_A)_{int}}{(a_A)_{samp}} \tag{2.2.6}$$

where $(a_A)_{samp}$ is the analyte's activity in the sample, $(a_A)_{int}$ is the analyte's activity in the ion-selective electrode's internal solution, and z is the analyte's charge. Ideally, E_{mem} is zero when $(a_A)_{int} = (a_A)_{samp}$. The term E_{asym}, which is an ***asymmetry potential***, accounts for the fact that E_{mem} usually is not zero under these conditions.

> For now we simply note that a difference in the analyte's activity results in a membrane potential. As we consider different types of ion-selective electrodes, we will explore more specifically the source of the membrane potential.

Substituting Equation 2.2.6 into Equation 2.2.5, assuming a temperature of 25°C, and rearranging gives

$$E_{cell} = K + \frac{0.05916}{z} \log (a_A)_{samp} \tag{2.2.7}$$

where K is a constant that includes the potentials of the two reference electrodes, the junction potentials, the asymmetry potential, and the analyte's activity in the internal solution. Equation 2.2.7 is a general equation and applies to all types of ion-selective electrodes.

Selectivity of Membranes

A membrane potential results from a chemical interaction between the analyte and active sites on the membrane's surface. Because the signal depends on a chemical process, most membranes are not selective toward a single analyte. Instead, the membrane potential is proportional to the concentration of each ion that interacts with the membrane's active sites. We can rewrite Equation 2.2.7 to include the contribution to the potential of an interferent, I

$$E_{cell} = K + \frac{0.05916}{z_A} \log \left\{ a_A + K_{A,I} (a_I)^{z_A/z_I} \right\}$$

where z_A and z_I are the charges of the analyte and the interferent, and $K_{A,I}$ is a selectivity coefficient that accounts for the relative response of the interferent. The selectivity coefficient is defined as

$$K_{A,I} = \frac{(a_A)_e}{(a_I)_e^{z_A/z_I}} \tag{2.2.8}$$

where $(a_A)_e$ and $(a_I)_e$ are the activities of analyte and the interferent that yield identical cell potentials. When the selectivity coefficient is 1.00, the membrane responds equally to the analyte and the interferent. A membrane shows good selectivity for the analyte when $K_{A,I}$ is significantly less than 1.00.

Selectivity coefficients for most commercially available ion-selective electrodes are provided by the manufacturer. If the selectivity coefficient is not known, it is easy to determine its value experimentally by preparing a series of solutions, each of which contains the same activity of interferent, $(a_I)_{add}$, but a different activity of analyte. As shown in Figure 11.2.9 , a plot of cell potential versus the log of the analyte's activity has two distinct linear regions. When the analyte's activity is significantly larger than $K_{A,I} \times (a_I)_{add}$, the potential is a linear function of log(a_A), as given by Equation 2.2.7. If $K_{A,I} \times (a_I)_{add}$ is significantly larger than the analyte's activity, however, the cell's potential remains constant. The activity of analyte and interferent at the intersection of these two linear regions is used to calculate $K_{A,I}$.

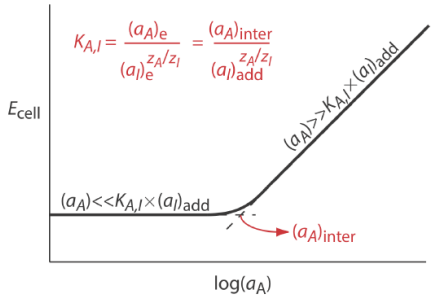

Figure 11.2.9 . Diagram showing the experimental determination of an ion-selective electrode's selectivity for an analyte. The activity of analyte that corresponds to the intersection of the two linear portions of the curve, $(a_A)_{inter}$, produces a cell potential identical to that of the interferent. The equation for the selectivity coefficient, $K_{A,I}$, is shown in red.

Example 11.2.5

Sokalski and co-workers described a method for preparing ion-selective electrodes with significantly improved selectivities [Sokalski, T.; Ceresa, A.; Zwicki, T.; Pretsch, E. *J. Am. Chem. Soc.* **1997**, *119*, 11347–11348]. For example, a conventional Pb^{2+} ISE has a log $K_{Pb^{2+}/Mg^{2+}}$ of –3.6. If the potential for a solution in which the activity of Pb^{2+} is 4.1×10^{-12} is identical to that for a solution in which the activity of Mg^{2+} is 0.01025, what is the value of log $K_{Pb^{2+}/Mg^{2+}}$ for their ISE?

Solution

Making appropriate substitutions into Equation 2.2.8, we find that

$$K_{Pb^{2+}/Mg^{2+}} = \frac{(a_{Pb^{2+}})_e}{(a_{Mg^{2+}})_e^{z_{Pb^{2+}}/z_{Mg^{2+}}}} = \frac{4.1 \times 10^{-12}}{(0.01025)^{+2/+2}} = 4.0 \times 10^{-10}$$

The value of log $K_{Pb^{2+}/Mg^{2+}}$, therefore, is –9.40.

Exercise 11.2.5

A ion-selective electrode for NO_2^- has log$K_{A,I}$ values of –3.1 for F^-, –4.1 for SO_4^{2-}, –1.2 for I^-, and –3.3 for NO_3^-. Which ion is the most serious interferent and for what activity of this interferent is the potential equivalent to a solution in which the activity of NO_2^- is 2.75×10^{-4}?

Answer

The larger the value of $K_{A,I}$ the more serious the interference. Larger values for $K_{A,I}$ correspond to more positive (less negative) values for log$K_{A,I}$; thus, I^-, with a $K_{A,I}$ of 6.3×10^{-2}, is the most serious of these interferents. To find the activity of I^- that gives a potential equivalent to a NO_2^- activity of 2.75×10^{-4}, we note that

$$a_{NO_2^-} = K_{A,I} \times a_{I^-}$$

Making appropriate substitutions

$$2.75 \times 10^{-4} = \left(6.3 \times 10^{-2}\right) \times a_{I^-}$$

and solving for a_{I^-} gives its activity as 4.4×10^{-3}.

Glass Ion-Selective Electrodes

The first commercial ***glass electrodes*** were manufactured using Corning 015, a glass with a composition that is approximately 22% Na_2O, 6% CaO, and 72% SiO_2. When immersed in an aqueous solution for several hours, the outer approximately 10 nm of the membrane's surface becomes hydrated, resulting in the formation of negatively charged sites, —SiO^-. Sodium ions, Na^+, serve as counter ions. Because H^+ binds more strongly to —SiO^- than does Na^+, they displace the sodium ions

$$H^+ + -SiO^-Na^+ \rightleftharpoons -SiO^-H^+ + Na^+$$

explaining the membrane's selectivity for H^+. The transport of charge across the membrane is carried by the Na^+ ions. The potential of a glass electrode using Corning 015 obeys the equation

$$E_{cell} = K + 0.05916 \log a_{H^+} \tag{2.2.9}$$

over a pH range of approximately 0.5 to 9. At more basic pH values the glass membrane is more responsive to other cations, such as Na^+ and K^+.

Example 11.2.6

For a Corning 015 glass membrane, the selectivity coefficient K_{H^+/Na^+} is $\approx 10^{-11}$. What is the expected error if we measure the pH of a solution in which the activity of H^+ is 2×10^{-13} and the activity of Na^+ is 0.05?

Solution

A solution in which the actual activity of H^+, $(a_{H^+})_{act}$, is 2×10^{-13} has a pH of 12.7. Because the electrode responds to both H^+ and Na^+, the apparent activity of H^+, $(a_{H^+})_{app}$, is

$$(a_{H^+})_{app} = (a_{H^+})_{act} + (K_{H^+/Na^+} \times a_{Na^+}) = 2 \times 10^{-13} + (10^{-11} \times 0.05) = 7 \times 10^{-13}$$

The apparent activity of H^+ is equivalent to a pH of 12.2, an error of –0.5 pH units.

Replacing Na_2O and CaO with Li_2O and BaO extends the useful pH range of glass membrane electrodes to pH levels greater than 12.

Glass membrane pH electrodes often are available in a combination form that includes both the indicator electrode and the reference electrode. The use of a single electrode greatly simplifies the measurement of pH. An example of a typical combination electrode is shown in Figure 11.2.10 .

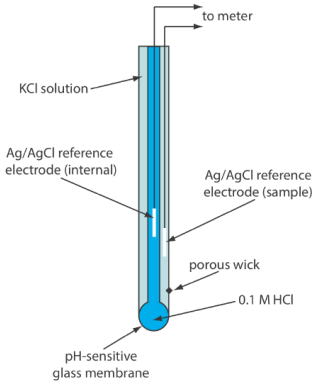

Figure 11.2.10 . Schematic diagram showing a combination glass electrode for measuring pH. The indicator electrode consists of a pH-sensitive glass membrane and an internal Ag/AgCl reference electrode in a solution of 0.1 M HCl. The sample's reference electrode is a Ag/AgCl electrode in a solution of KCl (which may be saturated with KCl or contain a fixed concentration of KCl). A porous wick serves as a salt bridge between the sample and its reference electrode.

The observation that the Corning 015 glass membrane responds to ions other than H^+ (see Example 11.2.6) led to the development of glass membranes with a greater selectivity for other cations. For example, a glass membrane with a composition of 11% Na_2O, 18% Al_2O_3, and 71% SiO_2 is used as an ion-selective electrode for Na^+. Other glass ion-selective electrodes have been developed for the analysis of Li^+, K^+, Rb^+, Cs^+, NH_4^+, Ag^+, and Tl^+. Table 11.2.1 provides several examples.

Table 11.2.1 . Representative Examples of Glass Membrane Ion-Selective Electrodes for Analytes Other Than H^+

analyte	membrane composition	selectivity coefficients
Na^+	11% Na_2O, 18% Al_2O_3, 71% SiO_2	$K_{Na^+/H^+} = 1000$ $K_{Na^+/K^+} = 0.001$ $K_{Na^+/Li^+} = 0.001$
Li^+	15% Li_2O, 25% Al_2O_3, 60% SiO_2	$K_{Li^+/Na^+} = 0.3$ $K_{Li^+/K^+} = 0.001$
K^+	27% Na_2O, 5% Al_2O_3, 68% SiO_2	$K_{K^+/Na^+} = 0.05$

Selectivity coefficients are approximate; values found experimentally may vary substantially from the listed values. See Cammann, K. *Working With Ion-Selective Electrodes*, Springer-Verlag: Berlin, 1977.

Because an ion-selective electrode's glass membrane is very thin—it is only about 50 μm thick—they must be handled with care to avoid cracks or breakage. Glass electrodes usually are stored in a storage buffer recommended by the manufacturer, which ensures that the membrane's outer surface remains hydrated. If a glass electrode dries out, it is reconditioned by soaking for several hours in a solution that contains the analyte. The composition of a glass membrane will change over time, which affects the electrode's performance. The average lifetime for a typical glass electrode is several years.

Solid-State Ion-Selective Electrodes

A s***olid-state ion-selective electrode*** has a membrane that consists of either a polycrystalline inorganic salt or a single crystal of an inorganic salt. We can fashion a polycrystalline solid-state ion-selective electrode by sealing a 1–2 mm thick pellet of AgS—or a mixture of AgS and a second silver salt or another metal sulfide—into the end of a nonconducting plastic cylinder, filling the cylinder with an internal solution that contains the analyte, and placing a reference electrode into the internal solution. Figure 11.2.11 shows a typical design.

> The NaCl in a salt shaker is an example of polycrystalline material because it consists of many small crystals of sodium chloride. The NaCl salt plates used in IR spectroscopy (see Chapter 10), on the other hand, are an example of a single crystal of sodium chloride.

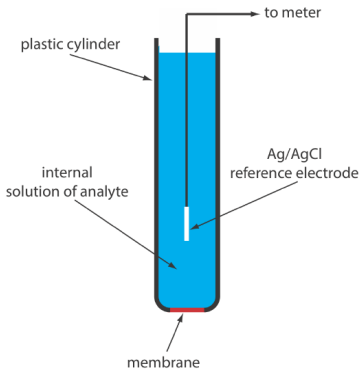

Figure 11.2.11 . Schematic diagram of a solid-state electrode. The internal solution contains a solution of analyte of fixed activity.

The membrane potential for a Ag_2S pellet develops as the result of a difference in the extent of the solubility reaction

$$Ag_2S(s) \rightleftharpoons 2Ag^+(aq) + S^{2-}(aq)$$

on the membrane's two sides, with charge carried across the membrane by Ag^+ ions. When we use the electrode to monitor the activity of Ag^+, the cell potential is

$$E_{cell} = K + 0.05916 \log a_{Ag^+}$$

The membrane also responds to the activity of S^{2-}, with a cell potential of

$$E_{cell} = K - \frac{0.05916}{2} \log a_{S^{2-}}$$

If we combine an insoluble silver salt, such as AgCl, with the Ag_2S, then the membrane potential also responds to the concentration of Cl^-, with a cell potential of

$$E_{cell} = K - 0.05916 \log a_{Cl^-}$$

By mixing Ag_2S with CdS, CuS, or PbS, we can make an ion-selective electrode that responds to the activity of Cd^{2+}, Cu^{2+}, or Pb^{2+}. In this case the cell potential is

$$E_{cell} = K + \frac{0.05916}{2} \ln a_{M^{2+}}$$

where $a_{M^{2+}}$ is the activity of the metal ion.

Table 11.2.2 provides examples of polycrystalline, Ag_2S-based solid-state ion-selective electrodes. The selectivity of these ion-selective electrodes depends on the relative solubility of the compounds. A Cl^- ISE using a Ag_2S/AgCl membrane is more selective for Br^- ($K_{Cl^-/Br^-} = 10^2$) and for I^- ($K_{Cl^-/I^-} = 10^6$) because AgBr and AgI are less soluble than AgCl. If the activity of Br^- is sufficiently high, AgCl at the membrane/solution interface is replaced by AgBr and the electrode's response to Cl^- decreases substantially. Most of the polycrystalline ion-selective electrodes listed in Table 11.2.2 operate over an extended range of pH levels. The equilibrium between S^{2-} and HS^- limits the analysis for S^{2-} to a pH range of 13–14.

11.2.2 . Representative Examples of Polycrystalline Solid-State Ion-Selective Electrodes

analyte	membrane composition	selectivity coefficients
Ag^+	Ag_2S	$K_{Ag^+/Cu^{2+}} = 10^{-6}$ $K_{Ag^+/Pb^{2+}} = 10^{-10}$ Hg^{2+} interferes
Cd^{2+}	CdS/Ag_2S	$K_{Cd^{2+}/Fe^{2+}} = 200$ $K_{Cd^{2+}/Pb^{2+}} = 6$ Ag^+, Hg^{2+}, and Cu^{2+} must be absent
Cu^{2+}	CuS/Ag_2S	$K_{Cu^{2+}/Fe^{3+}} = 10$ $K_{Cu^{2+}/Cu^+} = 10^{-6}$ Ag^+ and Hg^{2+} must be absent
Pb^{2+}	PbS/Ag_2S	$K_{Pb^{2+}/Fe^{3+}} = 1$ $K_{Pb^{2+}/Cd^{2+}} = 1$ Ag^+, Hg^{2+}, and Cu^{2+} must be absent
Br^-	$AgBr/Ag_2S$	$K_{Br^-/I^-} = 5000$ $K_{Br^-/Cl^-} = 0.005$ $K_{Br^-/OH^-} = 10^{-5}$ S^{2-} must be absent
Cl^-	$AgCl/Ag_2S$	$K_{Cl^-/I^-} = 10^6$ $K_{Cl^-/Br^-} = 100$ $K_{Cl^-/OH^-} = 0.01$ S^{2-} must be absent
I^-	AgI/Ag_2S	$K_{I^-/S^{2-}} = 30$ $K_{I^-/Br^-} = 10^{-4}$ $K_{I^-/Cl^-} = 10^{-6}$ $K_{I^-/OH^-} = 10^{-7}$
SCN^-	$AgSCN/Ag_2S$	$K_{SCN^-/I^-} = 10^3$ $K_{SCN^-/Br^-} = 100$ $K_{SCN^-/Cl^-} = 0.1 K_{SCN^-/OH^-} = 0.01$ S^{2-} must be absent

analyte	membrane composition	selectivity coefficients
S^{2-}	Ag_2S	Hg^{2+} must be absent

Selectivity coefficients are approximate; values found experimentally may vary substantially from the listed values. See Cammann, K. *Working With Ion-Selective Electrodes*, Springer-Verlag: Berlin, 1977.

The membrane of a F^- ion-selective electrode is fashioned from a single crystal of LaF_3, which usually is doped with a small amount of EuF_2 to enhance the membrane's conductivity. Because EuF_2 provides only two F^- ions—compared to the three F^- ions in LaF_3—each EuF_2 produces a vacancy in the crystal's lattice. Fluoride ions pass through the membrane by moving into adjacent vacancies. As shown in Figure 11.2.11 , the LaF_3 membrane is sealed into the end of a non-conducting plastic cylinder, which contains a standard solution of F^-, typically 0.1 M NaF, and a Ag/AgCl reference electrode.

The membrane potential for a F^- ISE results from a difference in the solubility of LaF_3 on opposite sides of the membrane, with the potential given by

$$E_{\text{cell}} = K - 0.05916 \log a_{F^-}$$

One advantage of the F^- ion-selective electrode is its freedom from interference. The only significant exception is OH^- (K_{F^-/OH^-} = 0.1), which imposes a maximum pH limit for a successful analysis. Below a pH of 4 the predominate form of fluoride in solution is HF, which does not contribute to the membrane potential. For this reason, an analysis for fluoride is carried out at a pH greater than 4.

Example 11.2.7

What is the maximum pH that we can tolerate if we need to analyze a solution in which the activity of F^- is 1×10^{-5} with an error of less than 1%?

Solution

In the presence of OH^- the cell potential is

$$E_{\text{cell}} = K - 0.05916 \left\{ a_{F^-} + K_{F^-/OH^-} \times a_{OH^-} \right\}$$

To achieve an error of less than 1%, the term $K_{F^-/OH^-} \times a_{OH^-}$ must be less than 1% of a_{F^-}; thus

$$K_{F^-/OH^-} \times a_{OH^-} \leq 0.01 \times a_{F^-}$$

$$0.10 \times a_{OH^-} \leq 0.01 \times \left(1.0 \times 10^{-5}\right)$$

Solving for a_{OH^-} gives the maximum allowable activity for OH^- as 1×10^{-6} , which corresponds to a pH of less than 8.

Exercise 11.2.6

Suppose you wish to use the nitrite-selective electrode in Exercise 11.2.5 to measure the activity of NO_2^-. If the activity of NO_2^- is 2.2×10^{-4}, what is the maximum pH you can tolerate if the error due to OH^- must be less than 10%? The selectivity coefficient for OH^-, $K_{NO_2^-/OH^-}$, is 630. Do you expect the electrode to have a lower pH limit? Clearly explain your answer.

Answer

In the presence of OH^- the cell potential is

$$E_{\text{cell}} = K - 0.05916 \log \left\{ a_{NO_2^-} + K_{NO_2^-/OH^-} \times a_{OH^-} \right\}$$

To achieve an error of less than 10%, the term $K_{NO_2^-/OH^-} \times a_{OH^-}$ must be less than 1% of $a_{NO_2^-}$; thus

$$K_{NO_2^-/OH^-} \times a_{OH^-} \leq 0.10 \times a_{NO_2^-}$$

$$630 \times a_{OH^-} \leq 0.10 \times \left(2.2 \times 10^{-4}\right)$$

Solving for a_{OH^-} gives its maximum allowable activity as 3.5×10^{-8}, which corresponds to a pH of less than 6.54.

The electrode does have a lower pH limit. Nitrite is the conjugate weak base of HNO_2, a species to which the ISE does not respond. As shown by the ladder diagram below, at a pH of 4.15 approximately 10% of nitrite is present as HNO_2. A minimum pH of 4.5 is the usual recommendation when using a nitrite ISE. This corresponds to a NO_2^-/HNO_2 ratio of

$$pH = pK_a + \log \frac{[NO_2^-]}{[HNO_2]}$$

$$4.5 = 3.15 + \log \frac{[NO_2^-]}{[HNO_2]}$$

$$\frac{[NO_2^-]}{[HNO_2]} \approx 22$$

Thus, at a pH of 4.5 approximately 96% of nitrite is present as NO_2^-.

Unlike a glass membrane ion-selective electrode, a solid-state ISE does not need to be conditioned before it is used, and it may be stored dry. The surface of the electrode is subject to poisoning, as described above for a Cl^- ISE in contact with an excessive concentration of Br^-. If an electrode is poisoned, it can be returned to its original condition by sanding and polishing the crystalline membrane.

Poisoning simply means that the surface has been chemically modified, such as AgBr forming on the surface of a AgCl membrane.

Liquid-Based Ion-Selective Electrodes

Another class of ion-selective electrodes uses a hydrophobic membrane that contains a liquid organic complexing agent that reacts selectively with the analyte. Three types of organic complexing agents have been used: cation exchangers, anion exchangers, and neutral ionophores. A membrane potential exists if the analyte's activity is different on the two sides of the membrane. Current is carried through the membrane by the analyte.

An ***ionophore*** is a ligand whose exterior is hydrophobic and whose interior is hydrophilic. The crown ether shown here is one example of a neutral ionophore.

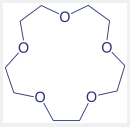

One example of a ***liquid-based ion-selective electrode*** is that for Ca^{2+}, which uses a porous plastic membrane saturated with the cation exchanger di-(*n*-decyl) phosphate. As shown in Figure 11.2.12 , the membrane is placed at the end of a non-conducting cylindrical tube and is in contact with two reservoirs. The outer reservoir contains di-(*n*-decyl) phosphate in di-*n*-octylphenylphosphonate, which soaks into the porous membrane. The inner reservoir contains a standard aqueous solution of Ca^{2+} and a Ag/AgCl reference electrode. Calcium ion-selective electrodes also are available in which the di-(*n*-decyl) phosphate is immobilized in a polyvinyl chloride (PVC) membrane that eliminates the need for the outer reservoir.

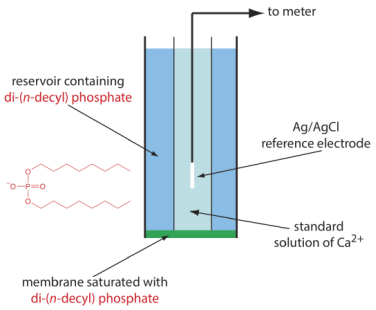

Figure 11.2.12 . Schematic diagram showing a liquid-based ion-selective electrode for Ca^{2+}. The structure of the cation exchanger, di-(*n*-decyl) phosphate, is shown in red.

The membrane potential for the Ca^{2+} ISE develops as the result of a difference in the extent of the complexation reaction

$$Ca^{2+}(aq) + 2(C_{10}H_{21}O)_2PO_2^-(mem) \rightleftharpoons Ca[(C_{10}H_{21}O)_2PO_2]_2(mem)$$

on the two sides of the membrane, where (*mem*) indicates a species that is present in the membrane. The cell potential for the Ca^{2+} ion-selective electrode is

$$E_{cell} = K + \frac{0.05916}{2}\log a_{ca^{2+}}$$

The selectivity of this electrode for Ca^{2+} is very good, with only Zn^{2+} showing greater selectivity.

Table 11.2.3 lists the properties of several liquid-based ion-selective electrodes. An electrode using a liquid reservoir can be stored in a dilute solution of analyte and needs no additional conditioning before use. The lifetime of an electrode with a PVC membrane, however, is proportional to its exposure to aqueous solutions. For this reason these electrodes are best stored by covering the membrane with a cap along with a small amount of wetted gauze to maintain a humid environment. Before using the electrode it is conditioned in a solution of analyte for 30–60 minutes.

Table 11.2.3 . Representative Examples of Liquid-Based Ion-Selective Electrodes

analyte	membrane composition	selectivity coefficients
Ca^{2+}	di-(*n*-decyl) phosphate in PVC	$K_{Ca^{2+}/Zn^{2+}} = 1-5$ $K_{Ca^{2+}/Al^{3+}} = 0.90$ $K_{Ca^{2+}/Mn^{2+}} = 0.38$ $K_{Ca^{2+}/Cu^{2+}} = 0.070$ $K_{Ca^{2+}/Mg^{2+}} = 0.032$
K^+	valinomycin in PVC	$K_{K^+/Rb^+} = 1.9$ $K_{K^+/Cs^+} = 0.38$ $K_{K^+/Li^+} = 10^{-4}$
Li^+	ETH 149 in PVC	$K_{Li^+/H^+} = 1$ $K_{Li^+/Na^+} = 0.03$ $K_{Li^+/K^+} = 0.007$
NH_4^+	nonactin and monactin in PVC	$K_{NH_4^+/K^+} = 0.12$ $K_{NH_4^+/H^+} = 0.016$ $K_{NH_4^+/Li^+} = 0.0042$ $K_{NH_4^+/Na^+} = 0.002$
ClO_3^-	$Fe(o\text{-phen})_3^{3+}$ in *p*-nitrocymene with porous membrane	$K_{ClO_4^-/OH^-} = 1$ $K_{ClO_4^-/I^-} = 0.012$ $K_{ClO_4^-/NO_3^-} = 0.0015$ $K_{ClO_4^-/Br^-} = 5.6 \times 10^{-4}$ $K_{ClO_4^-/Cl^-} = 2.2 \times 10^{-4}$

analyte	membrane composition	selectivity coefficients
NO_3^-	tetradodecyl ammonium nitrate in pVC	$K_{NO_3^-/Cl^-} = 0.006$ $K_{NO_3^-/F^-} = 9 \times 10^{-4}$
Selectivity coefficients are approximate; values found experimentally may vary substantially from the listed values. See Cammann, K. *Working With Ion-Selective Electrodes*, Springer-Verlag: Berlin, 1977.		

Gas-Sensing Electrodes

A number of membrane electrodes respond to the concentration of a dissolved gas. The basic design of a ***gas-sensing electrode***, as shown in Figure 11.2.13 , consists of a thin membrane that separates the sample from an inner solution that contains an ion-selective electrode. The membrane is permeable to the gaseous analyte, but impermeable to nonvolatile components in the sample's matrix. The gaseous analyte passes through the membrane where it reacts with the inner solution, producing a species whose concentration is monitored by the ion-selective electrode. For example, in a CO_2 electrode, CO_2 diffuses across the membrane where it reacts in the inner solution to produce H_3O^+.

$$CO_2(aq) + 2H_2O(l) \rightleftharpoons HCO_3^-(aq) + H_3O^+(aq) \tag{2.2.10}$$

The change in the activity of H_3O^+ in the inner solution is monitored with a pH electrode, for which the cell potential is given by Equation 2.2.9. To find the relationship between the activity of H_3O^+ in the inner solution and the activity of CO_2 in the inner solution we rearrange the equilibrium constant expression for reaction 2.2.10; thus

$$a_{H_3O^+} = K_a \times \frac{a_{CO_2}}{a_{HCO_3^-}} \tag{2.2.11}$$

where K_a is the equilibrium constant. If the activity of HCO_3^- in the internal solution is sufficiently large, then its activity is not affected by the small amount of CO_2 that passes through the membrane. Substituting Equation 2.2.11 into Equation 2.2.9 gives

$$E_{cell} = K' + 0.05916 \log a_{co_2}$$

where K′ is a constant that includes the constant for the pH electrode, the equilibrium constant for reaction 2.2.10 and the activity of HCO_3^- in the inner solution.

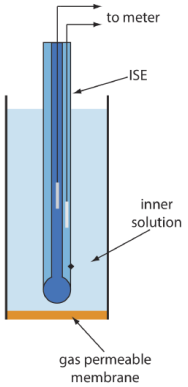

Figure 11.2.13 . Schematic diagram of a gas-sensing membrane electrode.

Table 11.2.4 lists the properties of several gas-sensing electrodes. The composition of the inner solution changes with use, and both the inner solution and the membrane must be replaced periodically. Gas-sensing electrodes are stored in a solution similar to the internal solution to minimize their exposure to atmospheric gases.

Table 11.2.4 . Representative Examples of Gas-Sensing Electrodes

analyte	inner solution	reaction in inner solution	ion-selective electrode
CO_2	10 mM $NaHCO_3$ 10 mM NaCl	$CO_2(aq) + 2H_2O(l) \rightleftharpoons$ $HCO_3^-(aq) + H_3O^+(aq)$	glass pH ISE

analyte	inner solution	reaction in inner solution	ion-selective electrode
HCN	10 mM $KAg(CN)_2$	$HCN(aq) + H_2O(l) \rightleftharpoons CN^-(aq) + H_3O^+(aq)$	Ag_2S solid-state ISE
HF	1 M H_3O^+	$HF(aq) + H_2O(l) \rightleftharpoons F^-(aq) + H_3O^+(aq)$	F^- solid-state ISE
H_2S	pH 5 citrate buffer	$H_2S(aq) + H_2O(l) \rightleftharpoons HS^-(aq) + H_3O^+(aq)$	Ag_2S solid state ISE
NH_3	10 mM NH_4Cl 0.1 M KNO_3	$NH_3(aq) + H_2O(l) \rightleftharpoons NH_4^+(aq) + OH^-(aq)$	glass pH ISE
NO_2	20 mM $NaNO_2$ 0.1 M KNO_3	$2NO_2(aq) + 3H_2O(l) \rightleftharpoons NO_3^-(aq) + NO_2^-(aq) + 2H_3O^+(aq)$	glass pH ISE
SO_2	1 mM $NaHSO_3$ pH 5	$SO_2(aq) + 2H_2O(l) \rightleftharpoons HSO_3^-(aq) + H_3O^+(aq)$	glass pH ISE

Source: Cammann, K. *Working With Ion-Selective Electrodes*, Springer-Verlag: Berlin, 1977.

Potentiometric Biosensors

The approach for developing gas-sensing electrodes can be modified to create potentiometric electrodes that respond to a biochemically important species. The most common class of potentiometric biosensors are ***enzyme electrodes***, in which we trap or immobilize an enzyme at the surface of a potentiometric electrode. The analyte's reaction with the enzyme produces a product whose concentration is monitored by the potentiometric electrode. Potentiometric biosensors also have been designed around other biologically active species, including antibodies, bacterial particles, tissues, and hormone receptors.

One example of an enzyme electrode is the urea electrode, which is based on the catalytic hydrolysis of urea by urease

$$CO(NH_2)_2(aq) + 2H_2O(l) \rightleftharpoons 2NH_4^+(aq) + CO_3^-(aq)$$

Figure 11.2.14 shows one version of the urea electrode, which modifies a gas-sensing NH_3 electrode by adding a dialysis membrane that traps a pH 7.0 buffered solution of urease between the dialysis membrane and the gas permeable membrane [(a) Papastathopoulos, D. S.; Rechnitz, G. A. *Anal. Chim. Acta* **1975**, *79*, 17–26; (b) Riechel, T. L. *J. Chem. Educ*. **1984**, *61*, 640–642]. An NH_3 electrode, as shown in Table 11.2.4 , uses a gas-permeable membrane and a glass pH electrode. The NH_3 diffuses across the membrane where it changes the pH of the internal solution.

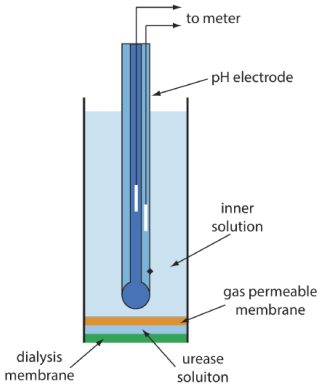

Figure 11.2.14 . Schematic diagram showing an enzyme-based potentiometric biosensor for urea. A solution of the enzyme urease is trapped between a dialysis membrane and a gas permeable membrane. Urea diffuses across the dialysis membrane and reacts with urease, producing NH_3 that diffuses across the gas permeable membrane. The resulting change in the internal solution's pH is measured with the pH electrode.

When immersed in the sample, urea diffuses through the dialysis membrane where it reacts with the enzyme urease to form the ammonium ion, NH_4^+, which is in equilibrium with NH_3.

$$NH_4^+(aq) + H_2O(l) \rightleftharpoons H_3O^+(aq) + NH_3(aq)$$

The NH_3, in turn, diffuses through the gas permeable membrane where a pH electrode measures the resulting change in pH. The electrode's response to the concentration of urea is

$$E_{cell} = K - 0.05916 \log a_{urea} \tag{2.2.12}$$

Another version of the urea electrode (Figure 11.2.15) immobilizes the enzyme urease in a polymer membrane formed directly on the tip of a glass pH electrode [Tor, R.; Freeman, A. *Anal. Chem.* **1986**, *58*, 1042–1046]. In this case the response of the electrode is

$$pH = Ka_{urea} \tag{2.2.13}$$

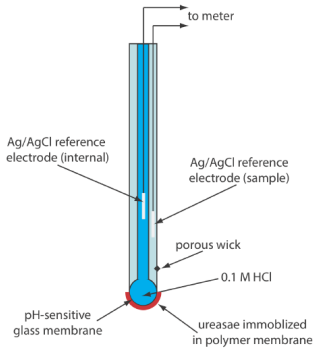

Figure 11.2.15 . Schematic diagram of an enzyme-based potentiometric biosensor for urea in which urease is immobilized in a polymer membrane coated onto the pH-sensitive glass membrane of a pH electrode.

Few potentiometric biosensors are available commercially. As shown in Figure 11.2.14 and Figure 11.2.15 , however, it is possible to convert an ion-selective electrode or a gas-sensing electrode into a biosensor. Several representative examples are described in Table 11.2.5 , and additional examples can be found in this chapter's additional resources.

Table 11.2.5 . Representative Examples of Potentiometric Biosensors

analyte	biologically active phase	substance determined
5′-AMP	AMP-deaminase (E)	NH_3
L-arginine	arginine and urease (E)	NH_3
asparagine	asparaginase (E)	NH_4^+
L-cysteine	*Proteus morganii* (B)	H_2S
L-glutamate	yellow squash (T)	CO_2
L-glutamine	*Sarcina flava* (B)	NH_3
oxalate	oxalate decarboxylase (E)	CO_2
penicillin	penicllinase (E)	H_3O^+
L-phenylalanine	L-amino acid oxidase/horseradish peroxidase (E)	I^-
sugars	bacteria from dental plaque (B)	H_3O^+
urea	urease (E)	NH_3 or H_3O^+

Source: Complied from Cammann, K. *Working With Ion-Selective Electrodes*, Springer-Verlag: Berlin, 1977 and Lunte, C. E.; Heineman, W. R. "Electrochemical techniques in Bioanalysis," in Steckham, E. ed. *Topics in Current Chemistry*, Vol. 143, Springer-Verlag: Berlin, 1988, p.8.
Abbreviations for biologically active phase: E = enzyme; B = bacterial particle; T = tissue.

Quantitative Applications

The potentiometric determination of an analyte's concentration is one of the most common quantitative analytical techniques. Perhaps the most frequent analytical measurement is the determination of a solution's pH, a measurement we will consider in more detail later in this section. Other areas where potentiometry is important are clinical chemistry, environmental chemistry, and potentiometric titrations. Before we consider representative applications, however, we need to examine more closely the relationship between cell potential and the analyte's concentration and methods for standardizing potentiometric measurements.

Activity and Concentration

The Nernst equation relates the cell potential to the analyte's activity. For example, the Nernst equation for a metallic electrode of the first kind is

$$E_{\text{cll}} = K + \frac{0.05916}{n} \log a_{M^{n+}} \tag{2.2.14}$$

where $a_{M^{n+}}$ is the metal ion's activity. When we use a potentiometric electrode, however, our goal is to determine the analyte's concentration. As we learned in Chapter 6, an ion's activity is the product of its concentration, $[M^{n+}]$, and a matrix-dependent activity coefficient, $\gamma_{Mn^{n+}}$.

$$a_{M^{n+}} = \left[M^{n+}\right] \gamma_{M^{n+}} \tag{2.2.15}$$

Substituting Equation 2.2.15 into Equation 2.2.14 and rearranging, gives

$$E_{\text{cell}} = K + \frac{0.05916}{n} \log \gamma_{M^{n+}} + \frac{0.05916}{n} \log \left[M^{n+}\right] \tag{2.2.16}$$

We can solve Equation 2.2.16 for the metal ion's concentration if we know the value for its activity coefficient. Unfortunately, if we do not know the exact ionic composition of the sample's matrix—which is the usual situation—then we cannot calculate the value of $\gamma_{Mn^{n+}}$. There is a solution to this dilemma. If we design our system so that the standards and the samples have an identical matrix, then the value of $\gamma_{Mn^{n+}}$ remains constant and Equation 2.2.16 simplifies to

$$E_{\text{cell}} = K' + \frac{0.05916}{n} \log \left[M^{n+}\right]$$

where K' includes the activity coefficient.

Quantitative Analysis Using External Standards

Before we can determine the concentration of analyte in a sample, we must standardize the electrode. If the electrode's response obeys the Nernst equation, then we can determine the constant K using a single external standard. Because a small deviation from the ideal slope of $\pm RT/nF$ or $\pm RT/zF$ is not unexpected, we usually use two or more external standards.

> To review the use of external standards, see Chapter 5.3.

In the absence of interferents, a calibration curve of E_{cell} versus $\log a_A$, where A is the analyte, is a straight-line. A plot of E_{cell} versus $\log[A]$, however, may show curvature at higher concentrations of analyte as a result of a matrix-dependent change in the analyte's activity coefficient. To maintain a consistent matrix we add a high concentration of an inert electrolyte to all samples and standards. If the concentration of added electrolyte is sufficient, then the difference between the sample's matrix and the matrix of the standards will not affect the ionic strength and the activity coefficient essentially remains constant. The inert electrolyte added to the sample and the standards is called a ***total ionic strength adjustment buffer*** (TISAB).

✔ Example 11.2.8

The concentration of Ca^{2+} in a water sample is determined using the method of external standards. The ionic strength of the samples and the standards is maintained at a nearly constant level by making each solution 0.5 M in KNO_3. The measured cell potentials for the external standards are shown in the following table.

$[Ca^{2+}]$ (M)	E_{cell} (V)

$[Ca^{2+}]$ (M)	E_{cell} (V)
1.00×10^{-5}	–0.125
5.00×10^{-5}	–0.103
1.00×10^{-4}	–0.093
5.00×10^{-4}	–0.072
1.00×10^{-3}	–0.063
5.00×10^{-3}	–0.043
1.00×10^{-2}	–0.033

What is the concentration of Ca^{2+} in a water sample if its cell potential is found to be –0.084 V?

Solution

Linear regression gives the calibration curve in Figure 11.2.16 , with an equation of

$$E_{cell} = 0.027 + 0.0303 \log\left[Ca^{2+}\right]$$

Substituting the sample's cell potential gives the concentration of Ca^{2+} as 2.17×10^{-4} M. Note that the slope of the calibration curve, which is 0.0303, is slightly larger than its ideal value of 0.05916/2 = 0.02958; this is not unusual and is one reason for using multiple standards.

One reason that it is not unusual to find that the experimental slope deviates from its ideal value of 0.05916/*n* is that this ideal value assumes that the temperature is 25°C.

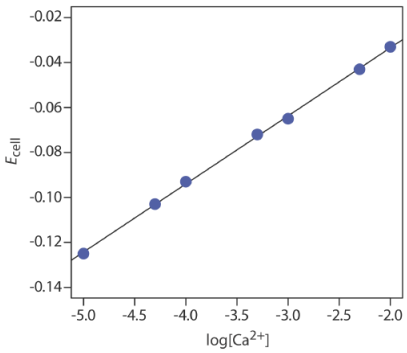

Figure 11.2.16 . Calibration curve for the data in Example 11.2.8 .

Quantitative Analysis Using the Method of Standard Additions

Another approach to calibrating a potentiometric electrode is the method of standard additions. First, we transfer a sample with a volume of V_{samp} and an analyte concentration of C_{samp} into a beaker and measure the potential, $(E_{cell})_{samp}$. Next, we make a standard addition by adding to the sample a small volume, V_{std}, of a standard that contains a known concentration of analyte, C_{std}, and measure the potential, (E_{cell})std. If V_{std} is significantly smaller than V_{samp}, then we can safely ignore the change in the sample's matrix and assume that the analyte's activity coefficient is constant. Example 11.2.9 demonstrates how we can use a one-point standard addition to determine the concentration of analyte in a sample.

To review the method of standard additions, see Chapter 5.3.

Example 11.2.9

The concentration of Ca^{2+} in a sample of sea water is determined using a Ca ion-selective electrode and a one-point standard addition. A 10.00-mL sample is transferred to a 100-mL volumetric flask and diluted to volume. A 50.00-mL aliquot of the sample is placed in a beaker with the Ca ISE and a reference electrode, and the potential is measured as –0.05290 V. After adding a 1.00-mL aliquot of a 5.00×10^{-2} M standard solution of Ca^{2+} the potential is –0.04417 V. What is the concentration of Ca^{2+} in the sample of sea water?

Solution

To begin, we write the Nernst equation before and after adding the standard addition. The cell potential for the sample is

$$(E_{\text{cell}})_{\text{samp}} = K + \frac{0.05916}{2}\log C_{\text{samp}}$$

and that following the standard addition is

$$(E_{\text{cell}})_{\text{std}} = K + \frac{0.05916}{2}\log\left\{\frac{V_{\text{samp}}}{V_{\text{tot}}}C_{\text{samp}} + \frac{V_{\text{std}}}{V_{\text{tot}}}C_{\text{std}}\right\}$$

where V_{tot} is the total volume (V_{samp} + V_{std}) after the standard addition. Subtracting the first equation from the second equation gives

$$\Delta E = (E_{\text{cell}})_{\text{std}} - (E_{\text{cell}})_{\text{samp}} = \frac{0.05916}{2}\log\left\{\frac{V_{\text{samp}}}{V_{\text{tot}}}C_{\text{samp}} + \frac{V_{\text{std}}}{V_{\text{tot}}}C_{\text{std}}\right\} - \frac{0.05916}{2}\log C_{\text{samp}}$$

Rearranging this equation leaves us with

$$\frac{2\Delta E_{cell}}{0.05916} = \log\left\{\frac{V_{\text{samp}}}{V_{\text{tot}}} + \frac{V_{\text{std}}C_{\text{std}}}{V_{\text{tot}}C_{\text{samp}}}\right\}$$

Substituting known values for ΔE, V_{samp}, V_{std}, V_{tot} and C_{std},

$$\frac{2\times\{-0.04417-(-0.05290)\}}{0.05916} =$$
$$\log\left\{\frac{50.00\text{ mL}}{51.00\text{ mL}} + \frac{(1.00\text{ mL})(5.00\times10^{-2}\text{M})}{(51.00\text{ mL})C_{\text{samp}}}\right\}$$
$$0.2951 = \log\left\{0.9804 + \frac{9.804\times10^{-4}}{C_{\text{samp}}}\right\}$$

and taking the inverse log of both sides gives

$$1.973 = 0.9804 + \frac{9.804 \times 10^{-4}}{C_{\text{samp}}}$$

Finally, solving for C_{samp} gives the concentration of Ca^{2+} as 9.88×10^{-4} M. Because we diluted the original sample of seawater by a factor of 10, the concentration of Ca^{2+} in the seawater sample is 9.88×10^{-3} M.

Free Ions Versus Complexed Ions

Most potentiometric electrodes are selective toward the free, uncomplexed form of the analyte, and do not respond to any of the analyte's complexed forms. This selectivity provides potentiometric electrodes with a significant advantage over other quantitative methods of analysis if we need to determine the concentration of free ions. For example, calcium is present in urine both as free Ca^{2+} ions and as protein-bound Ca^{2+} ions. If we analyze a urine sample using atomic absorption spectroscopy, the signal is proportional to the total concentration of Ca^{2+} because both free and bound calcium are atomized. Analyzing urine with a Ca^{2+} ISE, however, gives a signal that is a function of only free Ca^{2+} ions because the protein-bound Ca^{2+} can not interact with the electrode's membrane.

The best way to appreciate the theoretical and the practical details discussed in this section is to carefully examine a typical analytical method. Although each method is unique, the following description of the determination of F^- in toothpaste provides an instructive example of a typical procedure. The description here is based on Kennedy, J. H. *Analytical Chemistry — Practice*, Harcourt Brace Jaovanovich: San Diego, 1984, p. 117–118.

Representative Method 11.2.1: Determination of Fluoride in Toothpaste

Description of the Method

The concentration of fluoride in toothpastes that contains soluble F^- is determined with a F^- ion-selective electrode using a calibration curve prepared with external standards. Although the F^- ISE is very selective (only OH^- with a K_{F^-/OH^-} of 0.1 is a significant interferent), Fe^{3+} and Al^{3+} interfere with the analysis because they form soluble fluoride complexes that do not interact with the ion-selective electrode's membrane. This interference is minimized by reacting any Fe^{3+} and Al^{3+} with a suitable complexing agent.

Procedure

Prepare 1 L of a standard solution of 1.00% w/v SnF_2 and transfer it to a plastic bottle for storage. Using this solution, prepare 100 mL each of standards that contain 0.32%, 0.36%, 0.40%, 0.44% and 0.48% w/v SnF_2, adding 400 mg of malic acid to each solution as a stabilizer. Transfer the standards to plastic bottles for storage. Prepare a total ionic strength adjustment buffer (TISAB) by mixing 500 mL of water, 57 mL of glacial acetic acid, 58 g of NaCl, and 4 g of disodium DCTA (*trans*-1,2-cyclohexanetetraacetic acid) in a 1-L beaker, stirring until dissolved. Cool the beaker in a water bath and add 5 M NaOH until the pH is between 5–5.5. Transfer the contents of the beaker to a 1-L volumetric flask and dilute to volume. Prepare each external standard by placing approximately 1 g of a fluoride-free toothpaste, 30 mL of distilled water, and 1.00 mL of standard into a 50-mL plastic beaker and mix vigorously for two min with a stir bar. Quantitatively transfer the resulting suspension to a 100-mL volumetric flask along with 50 mL of TISAB and dilute to volume with distilled water. Store the entire external standard in a 250-mL plastic beaker until you are ready to measure the potential. Prepare toothpaste samples by obtaining an approximately 1-g portion and treating in the same manner as the standards. Measure the cell potential for the external standards and the samples using a F^- ion-selective electrode and an appropriate reference electrode. When measuring the potential, stir the solution and allow two to three minutes to reach a stable potential. Report the concentration of F^- in the toothpaste %w/w SnF_2.

Questions

1. The total ionic strength adjustment buffer serves several purposes in this procedure. Identify these purposes.

   The composition of the TISAB has three purposes:

   (a) The high concentration of NaCl (the final solutions are approximately 1 M NaCl) ensures that the ionic strength of each external standard and each sample is essentially identical. Because the activity coefficient for fluoride is the same in all solutions, we can write the Nernst equation in terms of fluoride's concentration instead of its activity.

   (b) The combination of glacial acetic acid and NaOH creates an acetic acid/acetate buffer of pH 5–5.5. As shown in Figure 11.2.17 , the pH of this buffer is high enough to ensure that the predominate form of fluoride is F^- instead of HF. This pH also is sufficiently acidic that it avoids an interference from OH^- (see Example 2.2.8).

   (c) DCTA is added as a complexing agent for Fe^{3+} or Al^{3+}, preventing the formation of FeF_6^{3-} or AlF_6^{3-}.

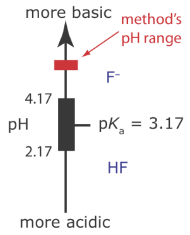

Figure 11.2.17 . Ladder diagram for HF/F^-. Maintaining a pH greater than 4.2 ensures that the only significant form of fluoride is F^-.

2. Why is a fluoride-free toothpaste added to the standard solutions?

   Adding a fluoride-free toothpaste protects against any unaccounted for matrix effects that might influence the ion-selective electrode's response. This assumes, of course, that the matrices of the two toothpastes are otherwise similar.

3. The procedure specifies that the standards and the sample should be stored in plastic containers. Why is it a bad idea to store the solutions in glass containers?

   The fluoride ion is capable of reacting with glass to form SiF_4.

4. Suppose your calibration curve has a slope of –57.98 mV for each 10-fold change in the concentration of F^-. The ideal slope from the Nernst equation is –59.16 mV per 10-fold change in concentration. What effect does this have on the quantitative analysis for fluoride in toothpaste?

No effect at all! This is why we prepare a calibration curve using multiple standards.

Measurement of pH

With the availability of inexpensive glass pH electrodes and pH meters, the determination of pH is one of the most common quantitative analytical measurements. The potentiometric determination of pH, however, is not without complications, several of which we discuss in this section.

One complication is confusion over the meaning of pH [Kristensen, H. B.; Saloman, A.; Kokholm, G. *Anal. Chem.* **1991**, *63*, 885A–891A]. The conventional definition of pH in most general chemistry textbooks is

$$\mathrm{pH} = -\log\left[\mathrm{H}^+\right] \tag{2.2.17}$$

As we now know, pH actually is a measure of the activity of H^+.

$$\mathrm{pH} = -\log a_{\mathrm{H}^+} \tag{2.2.18}$$

> Try this experiment—find several general chemistry textbooks and look up *pH* in each textbook's index. Turn to the appropriate pages and see how it is defined. Next, look up *activity* or *activity coefficient* in each textbook's index and see if these terms are indexed.

Equation 2.2.17 only approximates the true pH. If we calculate the pH of 0.1 M HCl using Equation 2.2.17, we obtain a value of 1.00; the solution's actual pH, as defined by Equation 2.2.18, is 1.1 [Hawkes, S. J. *J. Chem. Educ.* **1994**, *71*, 747–749]. The activity and the concentration of H^+ are not the same in 0.1 M HCl because the activity coefficient for H^+ is not 1.00 in this matrix. Figure 11.2.18 shows a more colorful demonstration of the difference between activity and concentration.

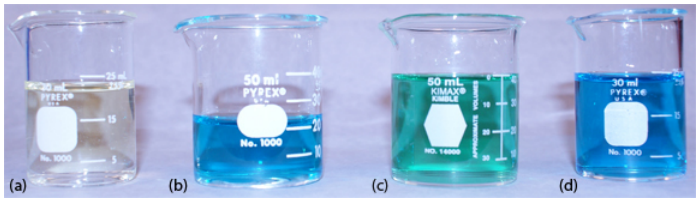

Figure 11.2.18 . A demonstration of the difference between activity and concentration using the indicator methyl green. The indicator is pale yellow in its acid form (beaker a: 1.0 M HCl) and is blue in its base form (beaker d: H_2O). In 10 mM HCl the indicator is in its base form (beaker b: 20 mL of 10 mM HCl with 3 drops of methyl green). Adding 20 mL of 5 M LiCl to this solution shifts the indicator's color to green (beaker c); although the concentration of HCl is cut in half to 5 mM, the activity of H^+ has increased as evidenced by the green color that is intermediate between the indicator's pale yellow, acid form and its blue, base form. The demonstration shown here is adapted from McCarty, C. G.; Vitz, E. "pH Paradoxes: Demonstrating That It Is Not True That pH ≡ –log[H^+]," *J. Chem. Educ.* **2006**, *83*, 752–757. This paper provides several additional demonstrations that illustrate the difference between concentration and activity.

A second complication in measuring pH is the uncertainty in the relationship between potential and activity. For a glass membrane electrode, the cell potential, (E_{cell})samp, for a sample of unknown pH is

$$(E_{\text{cell}})_{\text{samp}} = K - \frac{RT}{F}\ln\frac{1}{a_{\mathrm{H}^+}} = K - \frac{2.303RT}{F}\mathrm{pH}_{\text{samp}} \tag{2.2.19}$$

where K includes the potential of the reference electrode, the asymmetry potential of the glass membrane, and any junction potentials in the electrochemical cell. All the contributions to K are subject to uncertainty, and may change from day-to-day, as well as from electrode-to-electrode. For this reason, before using a pH electrode we calibrate it using a standard buffer of known pH. The cell potential for the standard, $(E_{\text{cell}})_{\text{std}}$, is

$$(E_{\text{ccll}})_{\text{std}} = K - \frac{2.303RT}{F}\mathrm{pH}_{\text{std}} \tag{2.2.20}$$

where pH_{std} is the standard's pH. Subtracting Equation 2.2.20 from Equation 2.2.19 and solving for $\mathrm{pH}_{\text{samp}}$ gives

$$\mathrm{pH}_{\mathrm{samp}} = \mathrm{pH}_{\mathrm{std}} - \frac{\left\{(E_{\mathrm{cell}})_{\mathrm{samp}} - (E_{\mathrm{cell}})_{\mathrm{std}}\right\} F}{2.303RT} \tag{2.2.21}$$

which is the operational definition of pH adopted by the International Union of Pure and Applied Chemistry [Covington, A. K.; Bates, R. B.; Durst, R. A. *Pure & Appl. Chem.* **1985**, *57*, 531–542].

Calibrating a pH electrode presents a third complication because we need a standard with an accurately known activity for H^+. Table 11.2.6 provides pH values for several primary standard buffer solutions accepted by the National Institute of Standards and Technology.

Table 11.2.6 . pH Values for Selected NIST Primary Standard Buffers

temp (°C)	saturated (at 25°C) KHC_4H4O_7 (tartrate)	0.05 m $KH_2C_6H_5O_7$ (citrate)	0.05 m $KHC_8H_4O_4$ (phthlate)	0.025 m KH_2PO_4, 0.025 m $NaHPO_4$	0.008695 m KH_2PO_4, 0.03043 m Na_2HPO_4	0.01 m $Na_4B_4O_7$	0.025 m $NaHCO_3$, 0.025 m Na_2CO_3
0	—	3.863	4.003	6.984	7.534	9.464	10.317
5	—	3.840	3.999	6.951	7.500	9.395	10.245
10	—	3.820	3.998	6.923	7.472	9.332	10.179
15	—	3.802	3.999	6.900	7.448	9.276	10.118
20	—	3.788	4.002	6.881	7.429	9.225	10.062
25	3.557	3.776	4.008	6.865	7.413	9.180	10.012
30	3.552	3.766	4.015	6.854	7.400	9.139	9.966
35	3.549	3.759	4.024	6.844	7.389	9.012	9.925
40	3.547	3.753	4.035	6.838	7.380	9.068	9.889
45	3.547	3.750	4.047	6.834	7.373	9.038	9.856
50	3.549	3.749	4.060	6.833	7.367	9.011	9.828

Source: Values taken from Bates, R. G. *Determination of pH: Theory and Practice*, 2nd ed. Wiley: New York, 1973. See also Buck, R. P., et. al."Measurement of pH. Definition, Standards, and Procedures," *Pure. Appl. Chem.* **2002**, *74*, 2169–2200. All concentrations are molal (m).

To standardize a pH electrode using two buffers, choose one near a pH of 7 and one that is more acidic or basic depending on your sample's expected pH. Rinse your pH electrode in deionized water, blot it dry with a laboratory wipe, and place it in the buffer with the pH closest to 7. Swirl the pH electrode and allow it to equilibrate until you obtain a stable reading. Adjust the "Standardize" or "Calibrate" knob until the meter displays the correct pH. Rinse and dry the electrode, and place it in the second buffer. After the electrode equilibrates, adjust the "Slope" or "Temperature" knob until the meter displays the correct pH.

Some pH meters can compensate for a change in temperature. To use this feature, place a temperature probe in the sample and connect it to the pH meter. Adjust the "Temperature" knob to the solution's temperature and calibrate the pH meter using the "Calibrate" and "Slope" controls. As you are using the pH electrode, the pH meter compensates for any change in the sample's temperature by adjusting the slope of the calibration curve using a Nernstian response of $2.303RT/F$.

Clinical Applications

Because of their selectivity for analytes in complex matricies, ion-selective electrodes are important sensors for clinical samples. The most common analytes are electrolytes, such as Na^+, K^+, Ca^{2+}, H^+, and Cl^-, and dissolved gases such as CO_2. For extracellular fluids, such as blood and urine, the analysis can be made *in vitro*. An *in situ* analysis, however, requires a much smaller electrode that we can insert directly into a cell. Liquid-based membrane microelectrodes with tip diameters smaller than 1 μm are constructed by heating and drawing out a hard-glass capillary tube with an initial diameter of approximately 1–2 mm (Figure 11.2.19). The microelectrode's tip is made hydrophobic by dipping into a solution of dichlorodimethyl silane, and an inner solution appropriate

for the analyte and a Ag/AgCl wire reference electrode are placed within the microelectrode. The microelectrode is dipped into a solution of the liquid complexing agent, which through capillary action draws a small volume of the liquid complexing agent into the tip. Potentiometric microelectrodes have been developed for a number of clinically important analytes, including H^+, K^+, Na^+, Ca^{2+}, Cl^-, and I^- [Bakker, E.; Pretsch, E. *Trends Anal. Chem.* **2008**, *27*, 612–618].

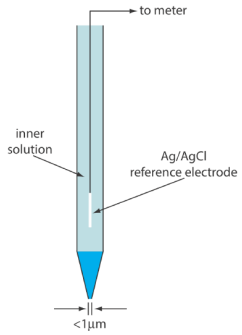

Figure 11.2.19 . Schematic diagram of a liquid-based ion-selective microelectrode.

Environmental Applications

Although ion-selective electrodes are used in environmental analysis, their application is not as widespread as in clinical analysis. Although standard potentiometric methods are available for the analysis of CN^-, F^-, NH_3, and NO_3^- in water and wastewater, other analytical methods generally provide better detection limits. One potential advantage of an ion-selective electrode is the ability to incorporate it into a flow cell for the continuous monitoring of wastewater streams.

Potentiometric Titrations

One method for determining the equivalence point of an acid–base titration is to use a pH electrode to monitor the change in pH during the titration. A potentiometric determination of the equivalence point is possible for acid–base, complexation, redox, and precipitation titrations, as well as for titrations in aqueous and nonaqueous solvents. Acid–base, complexation, and precipitation potentiometric titrations usually are monitored with an ion-selective electrode that responds the analyte, although an electrode that responds to the titrant or a reaction product also can be used. A redox electrode, such as a Pt wire, and a reference electrode are used for potentiometric redox titrations. More details about potentiometric titrations are found in Chapter 9.

Evaluation

Scale of Operation

The working range for most ion-selective electrodes is from a maximum concentration of 0.1–1 M to a minimum concentration of $10^{-5} - 10^{-11}$ M [(a) Bakker, E.; Pretsch, E. *Anal. Chem.* **2002**, *74*, 420A–426A; (b) Bakker, E.; Pretsch, E. *Trends Anal. Chem.* **2005**, *24*, 199–207]. This broad working range extends from major analytes to ultratrace analytes, and is significantly greater than many other analytical techniques. To use a conventional ion-selective electrode we need a minimum sample volume of several mL (a macro sample). Microelectrodes, such as the one shown in Figure 11.2.19 , are used with an ultramicro sample, although care is needed to ensure that the sample is representative of the original sample.

Accuracy

The accuracy of a potentiometric analysis is limited by the error in measuring E_{cell}. Several factors contribute to this measurement error, including the contribution to the potential from interfering ions, the finite current that passes through the cell while we measure the potential, differences between the analyte's activity coefficient in the samples and the standard solutions, and junction potentials. We can limit the effect of an interfering ion by including a separation step before the potentiometric analysis. Modern high impedance potentiometers minimize the amount of current that passes through the electrochemical cell. Finally, we can minimize the errors due to activity coefficients and junction potentials by matching the matrix of the standards to that of the sample. Even in the best circumstances, however, a difference of approximately ±1 mV for samples with equal concentrations of analyte is not unusual.

We can evaluate the effect of uncertainty on the accuracy of a potentiometric measurement by using a propagation of uncertainty. For a membrane ion-selective electrode the general expression for potential is

$$E_{\text{cell}} = K + \frac{RT}{zF}\ln[A]$$

where *z* is the analyte's, *A*, charge. From Table 4.3.1 in Chapter 4, the uncertainty in the cell potential, ΔE_{cell} is

$$\triangle E_{\text{cell}} = \frac{RT}{zF} \times \frac{\Delta[A]}{[A]}$$

Rearranging and multiplying through by 100 gives the percent relative error in concentration as

$$\%\text{ relative error } = \frac{\Delta[A]}{[A]} \times 100 = \frac{\triangle E_{\text{cell}}}{RT/zF} \times 100 \tag{2.2.22}$$

The relative error in concentration, therefore, is a function of the measurement error for the electrode's potential, ΔE_{cell}, and the analyte's charge. Table 11.2.7 provides representative values for ions with charges of ±1 and ±2 at a temperature of 25°C. Accuracies of 1–5% for monovalent ions and 2–10% for divalent ions are typical. Although Equation 2.2.22 applies to membrane electrodes, we can use if for a metallic electrode by replacing *z* with *n*.

Table 11.2.7 . Relationship Between the Uncertainty in Measuring E_{cell} and the Relative Error in the Analyte's Concentration

$\Delta E_{\text{cell}}\,(\pm\text{ mV})$	% relative error when $z = \pm 1$	% relative error when $z = \pm 2$
0.1	±0.4	±0.8
0.5	±1.9	±3.9
1.0	±3.0	±7.8
1.5	±5.8	±11.1
2.0	±7.8	±15.6

Precision

Precision in potentiometry is limited by variations in temperature and the sensitivity of the potentiometer. Under most conditions—and when using a simple, general-purpose potentiometer—we can measure the potential with a repeatability of ±0.1 mV. Using Table 11.2.7 , this corresponds to an uncertainty of ±0.4% for monovalent analytes and ±0.8% for divalent analytes. The reproducibility of potentiometric measurements is about a factor of ten poorer.

Sensitivity

The sensitivity of a potentiometric analysis is determined by the term *RT*/*nF* or *RT*/*zF* in the Nernst equation. Sensitivity is best for smaller values of *n* or *z*.

Selectivity

As described earlier, most ion-selective electrodes respond to more than one analyte; the selectivity for the analyte, however, often is significantly greater than the sensitivity for the interfering ions. The manufacturer of an ion-selective usually provides an ISE's selectivity coefficients, which allows us to determine whether a potentiometric analysis is feasible for a given sample.

Time, Cost, and Equipment

In comparison to other techniques, potentiometry provides a rapid, relatively low-cost means for analyzing samples. The limiting factor when analyzing a large number of samples is the need to rinse the electrode between samples. The use of inexpensive, disposable ion-selective electrodes can increase a lab's sample throughput. Figure 11.2.20 shows one example of a disposable ISE for Ag^+ [Tymecki, L.; Zwierkowska, E.; Głąb, S.; Koncki, R. *Sens. Actuators B* **2003**, *96*, 482–488]. Commercial instruments for measuring pH or potential are available in a variety of price ranges, and includes portable models for use in the field.

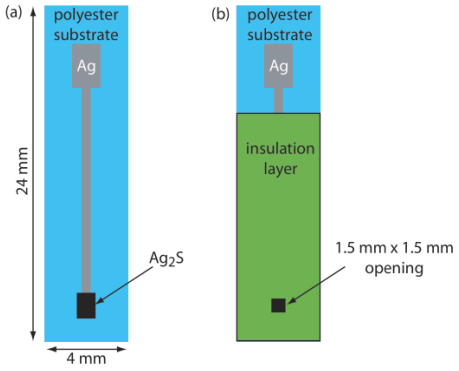

Figure 11.2.20 . Schematic diagram of a disposable ion-selective electrode created by screen-printing. In (a) a thin film of conducting silver is printed on a polyester substrate and a film of Ag_2S overlaid near the bottom. In (b) an insulation layer with a small opening is layered on top exposes a portion of the Ag_2S membrane that is immersed in the sample. The top of the polyester substrate remains uncoated, which allows us to connect the electrode to a potentiometer through the Ag film. The small inset shows the electrode's actual size.

2.3: Coulometric Methods

In a potentiometric method of analysis we determine an analyte's concentration by measuring the potential of an electrochemical cell under static conditions in which no current flows and the concentrations of species in the electrochemical cell remain fixed. Dynamic techniques, in which current passes through the electrochemical cell and concentrations change, also are important electrochemical methods of analysis. In this section we consider coulometry. Voltammetry and amperometry are covered in Chapter 11.4.

Coulometry is based on an exhaustive electrolysis of the analyte. By exhaustive we mean that the analyte is oxidized or reduced completely at the working electrode, or that it reacts completely with a reagent generated at the working electrode. There are two forms of coulometry: ***controlled-potential coulometry***, in which we apply a constant potential to the electrochemical cell, and ***controlled-current coulometry***, in which we pass a constant current through the electrochemical cell.

During an electrolysis, the total charge, Q, in coulombs, that passes through the electrochemical cell is proportional to the absolute amount of analyte by ***Faraday's law***

$$Q = nFN_A \tag{2.3.1}$$

where n is the number of electrons per mole of analyte, F is Faraday's constant (96 487 C mol^{-1}), and N_A is the moles of analyte. A coulomb is equivalent to an A•sec; thus, for a constant current, i, the total charge is

$$Q = it_e \tag{2.3.2}$$

where t_e is the electrolysis time. If the current varies with time, as it does in controlled-potential coulometry, then the total charge is

$$Q = \int_0^{t_e} i(t)dt \tag{2.3.3}$$

In coulometry, we monitor current as a function of time and use either Equation 2.3.2 or Equation 2.3.3 to calculate Q. Knowing the total charge, we then use Equation 2.3.1 to determine the moles of analyte. To obtain an accurate value for N_A, all the current must oxidize or reduce the analyte; that is, coulometry requires 100% ***current efficiency*** or an accurate measurement of the current efficiency using a standard.

> Current efficiency is the percentage of current that actually leads to the analyte's oxidation or reduction.

Controlled-Potential Coulometry

The easiest way to ensure 100% current efficiency is to hold the working electrode at a constant potential where the analyte is oxidized or reduced completely and where no potential interfering species are oxidized or reduced. As electrolysis progresses, the analyte's concentration and the current decrease. The resulting current-versus-time profile for controlled-potential coulometry is shown in Figure 11.3.1 . Integrating the area under the curve (Equation 2.3.3) from t = 0 to $t = t_e$ gives the total charge. In this section we consider the experimental parameters and instrumentation needed to develop a controlled-potential coulometric method of analysis.

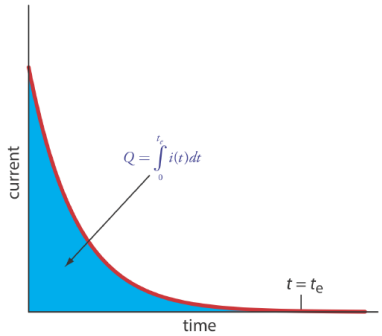

Figure 11.3.1 . Current versus time for a controlled-potential coulometric analysis. The measured current is shown by the red curve. The integrated area under the curve, shown in blue, is the total charge.

Selecting a Constant Potential

To understand how an appropriate potential for the working electrode is selected, let's develop a constant-potential coulometric method for Cu^{2+} based on its reduction to copper metal at a Pt working electrode.

$$Cu^{2+}(aq) + 2e^- \rightleftharpoons Cu(s) \tag{2.3.4}$$

Figure 11.3.2 shows a ladder diagram for an aqueous solution of Cu^{2+}. From the ladder diagram we know that reaction 2.3.4 is favored when the working electrode's potential is more negative than +0.342 V versus the standard hydrogen electrode. To ensure a 100% current efficiency,

however, the potential must be sufficiently more positive than +0.000 V so that the reduction of H_3O^+ to H_2 does not contribute significantly to the total current flowing through the electrochemical cell.

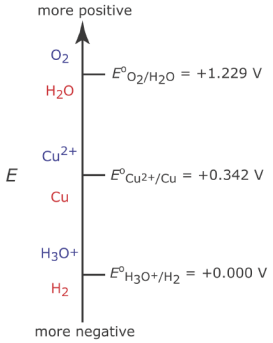

Figure 11.3.2 . Ladder diagram for an aqueous solution of Cu^{2+} showing steps for the reductions of O_2 to H_2O, of Cu^{2+} to Cu, and of H_3O^+ to H_2. For each step, the oxidized species is in blue and the reduced species is in red

We can use the Nernst equation for reaction 2.3.4 to estimate the minimum potential for quantitatively reducing Cu^{2+}.

$$E = E^{o}_{Cu^{2+}/Cu} - \frac{0.05916}{2}\log\frac{1}{[Cu^{2+}]} \tag{2.3.5}$$

So why are we using the concentration of Cu^{2+} in Equation 2.3.5 instead of its activity? In potentiometry we use activity because we use E_{cell} to determine the analyte's concentration. Here we use the Nernst equation to help us select an appropriate potential. Once we identify a potential, we can adjust its value as needed to ensure a quantitative reduction of Cu^{2+}. In addition, in coulometry the analyte's concentration is given by the total charge, not the applied potential.

If we define a quantitative electrolysis as one in which we reduce 99.99% of $^{Cu2+}$ to Cu, then the concentration of Cu^{2+} at t_e is

$$[Cu^{2+}]_{t_e} = 0.0001 \times [Cu^{2+}]_0 \tag{2.3.6}$$

where $[Cu^{2+}]_0$ is the initial concentration of Cu^{2+} in the sample. Substituting Equation 2.3.6 into Equation 2.3.5 allows us to calculate the desired potential.

$$E = E^{\circ}_{Cu^{2+}/Cu} - \frac{0.05916}{2}\log\frac{1}{0.0001 \times [Cu^{2+}]}$$

If the initial concentration of Cu^{2+} is 1.00×10^{-4} M, for example, then the working electrode's potential must be more negative than +0.105 V to quantitatively reduce Cu^{2+} to Cu. Note that at this potential H_3O^+ is not reduced to H_2, maintaining 100% current efficiency.

Many controlled-potential coulometric methods for Cu^{2+} use a potential that is negative relative to the standard hydrogen electrode—see, for example, Rechnitz, G. A. *Controlled-Potential Analysis*, Macmillan: New York, 1963, p.49. Based on the ladder diagram in Figure 11.3.2 you might expect that applying a potential <0.000 V will partially reduce H_3O^+ to H_2, resulting in a current efficiency that is less than 100%. The reason we can use such a negative potential is that the reaction rate for the reduction of H_3O^+ to H_2 is very slow at a Pt electrode. This results in a significant ***overpotential***—the need to apply a potential more positive or a more negative than that predicted by thermodynamics—which shifts E^o for the H_3O^+/H_2 redox couple to a more negative value.

Minimizing Electrolysis Time

In controlled-potential coulometry, as shown in Figure 11.3.1 , the current decreases over time. As a result, the rate of electrolysis—recall from Chapter 11.1 that current is a measure of rate—becomes slower and an exhaustive electrolysis of the analyte may require a long time. Because time is an important consideration when designing an analytical method, we need to consider the factors that affect the analysis time.

We can approximate the current's change as a function of time in Figure 11.3.1 as an exponential decay; thus, the current at time t is

$$i_t = i_0 e^{-kt} \tag{2.3.7}$$

where i_0 is the current at $t = 0$ and k is a rate constant that is directly proportional to the area of the working electrode and the rate of stirring, and that is inversely proportional to the volume of solution. For an exhaustive electrolysis in which we oxidize or reduce 99.99% of the analyte, the current at the end of the analysis, t_e, is

$$i_{t_e} \leq 0.0001 \times i_0 \tag{2.3.8}$$

Substituting Equation 2.3.8 into Equation 2.3.7 and solving for t_e gives the minimum time for an exhaustive electrolysis as

$$t_e = -\frac{1}{k} \times \ln(0.0001) = \frac{9.21}{k}$$

From this equation we see that a larger value for *k* reduces the analysis time. For this reason we usually carry out a controlled-potential coulometric analysis in a small volume electrochemical cell, using an electrode with a large surface area, and with a high stirring rate. A quantitative electrolysis typically requires approximately 30–60 min, although shorter or longer times are possible.

Instrumentation

A three-electrode potentiostat is used to set the potential in controlled-potential coulometry (see Figure 11.1.5). The working electrodes is usually one of two types: a cylindrical Pt electrode manufactured from platinum-gauze (Figure 11.3.3), or a Hg pool electrode. The large overpotential for the reduction of H_3O^+ at Hg makes it the electrode of choice for an analyte that requires a negative potential. For example, a potential more negative than –1 V versus the SHE is feasible at a Hg electrode—but not at a Pt electrode—even in a very acidic solution. Because mercury is easy to oxidize, it is less useful if we need to maintain a potential that is positive with respect to the SHE. Platinum is the working electrode of choice when we need to apply a positive potential.

Figure 11.3.3 . Example of a cylindrical Pt-gauze electrode used in controlled-potential coulometry. The electrode shown here has a diameter of 13 mm and a height of 48 mm, and was fashioned from Pt wire with a diameter of approximately 0.15 mm. The electrode's surface has 360 openings/cm^2 and a total surface area of approximately 40 cm^2.

The auxiliary electrode, which often is a Pt wire, is separated by a salt bridge from the analytical solution. This is necessary to prevent the electrolysis products generated at the auxiliary electrode from reacting with the analyte and interfering in the analysis. A saturated calomel or Ag/AgCl electrode serves as the reference electrode.

The other essential need for controlled-potential coulometry is a means for determining the total charge. One method is to monitor the current as a function of time and determine the area under the curve, as shown in Figure 11.3.1 . Modern instruments use electronic integration to monitor charge as a function of time. The total charge at the end of the electrolysis is read directly from a digital readout.

Electrogravimetry

If the product of controlled-potential coulometry forms a deposit on the working electrode, then we can use the change in the electrode's mass as the analytical signal. For example, if we apply a potential that reduces Cu^{2+} to Cu at a Pt working electrode, the difference in the electrode's mass before and after electrolysis is a direct measurement of the amount of copper in the sample. As we learned in Chapter 8, we call an analytical technique that uses mass as a signal a gravimetric technique; thus, we call this ***electrogravimetry***.

Controlled-Current Coulometry

A second approach to coulometry is to use a constant current in place of a constant potential, which results in the current-versus-time profile shown in Figure 11.3.4 . Controlled-current coulometry has two advantages over controlled-potential coulometry. First, the analysis time is shorter because the current does not decrease over time. A typical analysis time for controlled-current coulometry is less than 10 min, compared to approximately 30–60 min for controlled-potential coulometry. Second, because the total charge simply is the product of current and time (Equation 2.3.2), there is no need to integrate the current-time curve in Figure 11.3.4 .

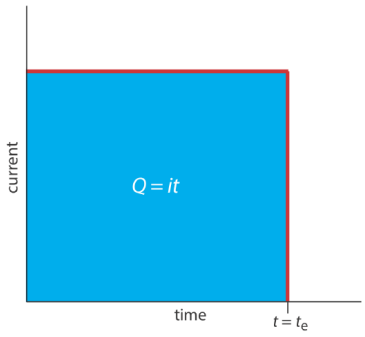

Figure 11.3.4 . Current versus time for a controlled-current coulometric analysis. The measured current is shown by the red curve. The integrated area under the curve, shown in blue, is the total charge.

Using a constant current presents us with two important experimental problems. First, during electrolysis the analyte's concentration—and, therefore, the current that results from its oxidation or reduction—decreases continuously. To maintain a constant current we must allow the potential to change until another oxidation reaction or reduction reaction occurs at the working electrode. Unless we design the system carefully, this secondary reaction results in a current efficiency that is less than 100%. The second problem is that we need a method to determine when the analyte's electrolysis is complete. As shown in Figure 11.3.1 , in a controlled-potential coulometric analysis we know that electrolysis is complete when the current reaches zero, or when it reaches a constant background or residual current. In a controlled-current coulometric analysis, however, current continues to flow even when the analyte's electrolysis is complete. A suitable method for determining the reaction's endpoint, t_e, is needed.

Maintaining Current Efficiency

To illustrate why a change in the working electrode's potential may result in a current efficiency of less than 100%, let's consider the coulometric analysis for Fe^{2+} based on its oxidation to Fe^{3+} at a Pt working electrode in 1 M H_2SO_4.

$$Fe^{2+}(aq) \rightleftharpoons Fe^{3+}(aq) + e^-$$

Figure 11.3.5 shows the ladder diagram for this system. At the beginning of the analysis, the potential of the working electrode remains nearly constant at a level near its initial value.

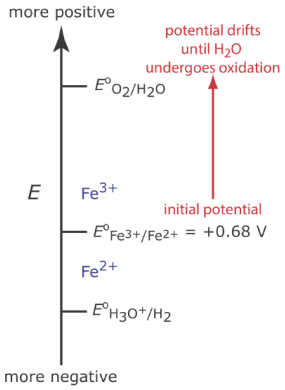

Figure 11.3.5 . Ladder diagram for the constant-current coulometric analysis of Fe^{2+}. The red arrow and text shows how the potential drifts to more positive values, decreasing the current efficiency.

As the concentration of Fe^{2+} decreases and the concentration of Fe^{3+} increases, the working electrode's potential shifts toward more positive values until the oxidation of H_2O begins.

$$2H_2O(l) \rightleftharpoons O_2(g) + 4H^+(aq) + 4e^-$$

Because a portion of the total current comes from the oxidation of H_2O, the current efficiency for the analysis is less than 100% and we cannot use Equation 2.3.1 to determine the amount of Fe^{2+} in the sample.

Although we cannot prevent the potential from drifting until another species undergoes oxidation, we can maintain a 100% current efficiency if the product of that secondary oxidation reaction both rapidly and quantitatively reacts with the remaining Fe^{2+}. To accomplish this we add an excess of Ce^{3+} to the analytical solution. As shown in Figure 11.3.6 , when the potential of the working electrode shifts to a more positive potential, Ce^{3+} begins to oxidize to Ce^{4+}

$$Ce^{3+}(aq) \rightleftharpoons Ce^{4+}(aq) + e^- \tag{2.3.9}$$

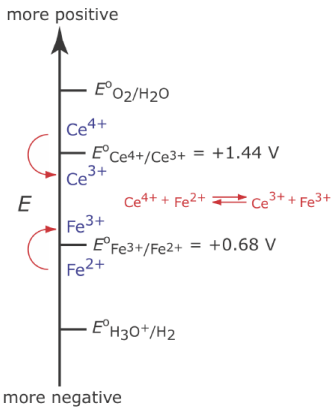

Figure 11.3.6 . Ladder diagram for the constant-current coulometric analysis of Fe^{2+} in the presence of a Ce^{3+} mediator. As the potential drifts to more positive values, we eventually reach a potential where Ce^{3+} undergoes oxidation. Because Ce^{4+}, the product of the oxidation of Ce^{3+}, reacts with Fe^{2+}, we maintain current efficiency.

The Ce^{4+} that forms at the working electrode rapidly mixes with the solution where it reacts with any available Fe^{2+}.

$$Ce^{4+}(aq) + Fe^{2+}(aq) \rightleftharpoons Ce^{3+}(aq) + Fe^{3+}(aq) \tag{2.3.10}$$

Combining reaction 2.3.9 and reaction 2.3.10 shows that the net reaction is the oxidation of Fe^{2+} to Fe^{3+}

$$Fe^{2+}(aq) \rightleftharpoons Fe^{3+}(aq) + e^-$$

which maintains a current efficiency of 100%. A species used to maintain 100% current efficiency is called a ***mediator***.

Endpoint Determination

Adding a mediator solves the problem of maintaining 100% current efficiency, but it does not solve the problem of determining when the analyte's electrolysis is complete. Using the analysis for Fe^{2+} in Figure 11.3.6 , when the oxidation of Fe^{2+} is complete current continues to flow from the oxidation of Ce^{3+}, and, eventually, the oxidation of H_2O. What we need is a signal that tells us when no more Fe^{2+} is present in the solution.

For our purposes, it is convenient to treat a controlled-current coulometric analysis as a reaction between the analyte, Fe^{2+}, and the mediator, Ce^{3+}, as shown by reaction 2.3.10. This reaction is identical to a redox titration; thus, we can use the end points for a redox titration—visual indicators and potentiometric or conductometric measurements—to signal the end of a controlled-current coulometric analysis. For example, ferroin provides a useful visual endpoint for the Ce^{3+} mediated coulometric analysis for Fe^{2+}, changing color from red to blue when the electrolysis of Fe^{2+} is complete.

> Reaction 2.3.10 is the same reaction we used in Chapter 9 to develop our understanding of redox titrimetry.

Instrumentation

Controlled-current coulometry normally is carried out using a two-electrode galvanostat, which consists of a working electrode and a counter electrode. The working electrode—often a simple Pt electrode—also is called the generator electrode since it is where the mediator reacts to generate the species that reacts with the analyte. If necessary, the counter electrode is isolated from the analytical solution by a salt bridge or a porous frit to prevent its electrolysis products from reacting with the analyte. Alternatively, we can generate the oxidizing agent or the reducing agent externally, and allow it to flow into the analytical solution. Figure 11.3.7 shows one simple method for accomplishing this. A solution that contains the mediator flows into a small-volume electrochemical cell with the products exiting through separate tubes. Depending upon the analyte, the oxidizing agent or the reducing reagent is delivered to the analytical solution. For example, we can generate Ce^{4+} using an aqueous solution of Ce^{3+}, directing the Ce^{4+} that forms at the anode to our sample.

> Figure 11.1.4 shows an example of a manual galvanostat. Although a modern galvanostat uses very different circuitry, you can use Figure 11.1.4 and the accompanying discussion to understand how we can use the working electrode and the counter electrode to control the current. Figure 11.1.4 includes an optional reference electrode, but its presence or absence is not important if we are not interested in monitoring the working electrode's potential.

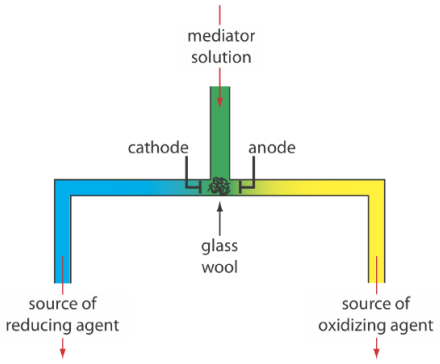

Figure 11.3.7 . One example of a device for the external generation of oxidizing agents and reducing agents for controlled-current coulometry. A solution containing the mediator flows into a small-volume electrochemical cell. The resulting oxidation products, which form at the anode, flow to the right and serve as an oxidizing agent. Reduction at the cathode generates a reducing agent.

There are two other crucial needs for controlled-current coulometry: an accurate clock for measuring the electrolysis time, t_e, and a switch for starting and stopping the electrolysis. An analog clock can record time to the nearest ±0.01 s, but the need to stop and start the electrolysis as we approach the endpoint may result in an overall uncertainty of ±0.1 s. A digital clock allows for a more accurate measurement of time, with an overall uncertainty of ±1 ms. The switch must control both the current and the clock so that we can make an accurate determination of the electrolysis time.

Coulometric Titrations

A controlled-current coulometric method sometimes is called a coulometric titration because of its similarity to a conventional titration. For example, in the controlled-current coulometric analysis for Fe^{2+} using a Ce^{3+} mediator, the oxidation of Fe^{2+} by Ce^{4+} (reaction 2.3.10) is identical to the reaction in a redox titration.

There are other similarities between controlled-current coulometry and titrimetry. If we combine Equation 2.3.1 and Equation 2.3.2 and solve for the moles of analyte, N_A, we obtain the following equation.

$$N_A = \frac{i}{nF} \times t_e \tag{2.3.11}$$

Compare Equation 2.3.11 to the relationship between the moles of analyte, N_A, and the moles of titrant, N_T, in a titration

$$N_A = N_T = M_T \times V_T$$

where M_T and V_T are the titrant's molarity and the volume of titrant at the end point. In constant-current coulometry, the current source is equivalent to the titrant and the value of that current is analogous to the titrant's molarity. Electrolysis time is analogous to the volume of titrant, and t_e is equivalent to the a titration's end point. Finally, the switch for starting and stopping the electrolysis serves the same function as a buret's stopcock.

> For simplicity, we assumed above that the stoichiometry between the analyte and titrant is 1:1. The assumption, however, is not important and does not effect our observation of the similarity between controlled-current coulometry and a titration.

Quantitative Applications

Coulometry is used for the quantitative analysis of both inorganic and organic analytes. Examples of controlled-potential and controlled-current coulometric methods are discussed in the following two sections.

Controlled-Potential Coulometry

The majority of controlled-potential coulometric analyses involve the determination of inorganic cations and anions, including trace metals and halides ions. Table 11.3.1 summarizes several of these methods.

Table 11.3.1 . Representative Controlled-Potential Coulometric Analyses for Inorganic Ions

analyte	electrolytic reaction	electrode
antimony	$\mathrm{Sb(III) + 3e^- \rightleftharpoons Sb}$	Pt
arsenic	$\mathrm{As(III) \rightleftharpoons As(V) + 2e^-}$	Pt
cadmium	$\mathrm{Cd(II) + 2e^- \rightleftharpoons Cd}$	Pt or Hg
cobalt	$\mathrm{Co(II) + 2e^- \rightleftharpoons Co}$	Pt or Hg

analyte	electrolytic reaction	electrode
copper	$\mathrm{Cu(II)} + 2e^- \rightleftharpoons \mathrm{Cu}$	Pt or Hg
halides (X^-)	$\mathrm{Ag} + \mathrm{X}^- \rightleftharpoons \mathrm{AgX} + e^-$	Ag
iron	$\mathrm{Fe(II)} \rightleftharpoons \mathrm{Fe(III)} + e^-$	Pt
lead	$\mathrm{Pb(II)} + 2e^- \rightleftharpoons \mathrm{Pb}$	Pt or Hg
nickel	$\mathrm{Ni(II)} + 2e^- \rightleftharpoons \mathrm{Ni}$	Pt or Hg
plutonium	$\mathrm{Pu(III)} \rightleftharpoons \mathrm{Pu(IV)} + e^-$	Pt
silver	$\mathrm{Ag(I)} + 1e^- \rightleftharpoons \mathrm{Ag}$	Pt
tin	$\mathrm{Sn(II)} + 2e^- \rightleftharpoons \mathrm{Sn}$	Pt
uranium	$\mathrm{U(VI)} + 2e^- \rightleftharpoons \mathrm{U(IV)}$	Pt or Hg
zinc	$\mathrm{Zn(II)} + 2e^- \rightleftharpoons \mathrm{Zn}$	Pt or Hg

Source: Rechnitz, G. A. *Controlled-Potential Analysis*, Macmillan: New York, 1963.
Electrolytic reactions are written in terms of the change in the analyte's oxidation state. The actual species in solution depends on the analyte.

The ability to control selectivity by adjusting the working electrode's potential makes controlled-potential coulometry particularly useful for the analysis of alloys. For example, we can determine the composition of an alloy that contains Ag, Bi, Cd, and Sb by dissolving the sample and placing it in a matrix of 0.2 M H_2SO_4 along with a Pt working electrode and a Pt counter electrode. If we apply a constant potential of +0.40 V versus the SCE, Ag(I) deposits on the electrode as Ag and the other metal ions remain in solution. When electrolysis is complete, we use the total charge to determine the amount of silver in the alloy. Next, we shift the working electrode's potential to –0.08 V versus the SCE, depositing Bi on the working electrode. When the coulometric analysis for bismuth is complete, we determine antimony by shifting the working electrode's potential to –0.33 V versus the SCE, depositing Sb. Finally, we determine cadmium following its electrodeposition on the working electrode at a potential of –0.80 V versus the SCE.

We also can use controlled-potential coulometry for the quantitative analysis of organic compounds, although the number of applications is significantly less than that for inorganic analytes. One example is the six-electron reduction of a nitro group, $–NO_2$, to a primary amine, $–NH_2$, at a mercury electrode. Solutions of picric acid—also known as 2,4,6-trinitrophenol, or TNP, a close relative of TNT—is analyzed by reducing it to triaminophenol.

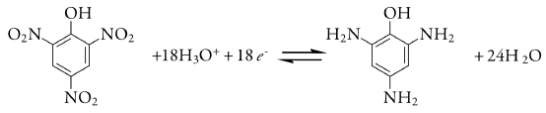

Another example is the successive reduction of trichloroacetate to dichloroacetate, and of dichloroacetate to monochloroacetate

$$\mathrm{Cl_3CCOO^-}(aq) + \mathrm{H_3O^+}(aq) + 2e^- \rightleftharpoons \mathrm{Cl_2HCCOO^-}(aq) + \mathrm{Cl^-}(aq) + \mathrm{H_2O}(l)$$

$$\mathrm{Cl_2HCCOO^-}(aq) + \mathrm{H_3O^+}(aq) + 2e^- \rightleftharpoons \mathrm{ClH_2CCOO^-}(aq) + \mathrm{Cl^-}(aq) + \mathrm{H_2O}(l)$$

We can analyze a mixture of trichloroacetate and dichloroacetate by selecting an initial potential where only the more easily reduced trichloroacetate reacts. When its electrolysis is complete, we can reduce dichloroacetate by adjusting the potential to a more negative potential. The total charge for the first electrolysis gives the amount of trichloroacetate, and the difference in total charge between the first electrolysis and the second electrolysis gives the amount of dichloroacetate.

Controlled-Current Coulometry (Coulometric Titrations)

The use of a mediator makes a coulometric titration a more versatile analytical technique than controlled-potential coulometry. For example, the direct oxidation or reduction of a protein at a working electrode is difficult if the protein's active redox site lies deep within its structure. A coulometric titration of the protein is possible, however, if we use the oxidation or reduction of a mediator to produce a solution species that reacts with the protein. Table 11.3.2 summarizes several controlled-current coulometric methods based on a redox reaction using a mediator.

Table 11.3.2 . Representative Examples of Coulometric Redox Titrations

mediator	electrochemically generated reagent and reaction	representative application
Ag^+	$\mathrm{Ag^+} \rightleftharpoons \mathbf{Ag^{2+}} + e^-$	$\mathbf{H_2C_2O_4}(aq) + 2\mathrm{Ag^{2+}}(aq) + 2\mathrm{H_2O}(l) \rightleftharpoons 2\mathrm{CO_2}(g) + 2\mathrm{Ag^+}(aq) + 2\mathrm{H_3O^+}(aq)$

mediator	electrochemically generated reagent and reaction	representative application
Br^-	$2Br^- \rightleftharpoons \mathbf{Br_2} + 2e^-$	$\mathbf{H_2S}(aq) + Br_2(aq) + 2H_2O(l) \rightleftharpoons S(s) + 2Br^-(aq) + 2H_3O^+(aq)$
Ce^{3+}	$Ce^{3+} \rightleftharpoons \mathbf{Ce^{4+}} + e^-$	$\mathbf{Fe(CN)_6^{4-}}(aq) + Ce^{4+}(aq) \rightleftharpoons Fe(CN)_6^{3-}(aq) + Ce^{3+}(aq)$
Cl^-	$2Cl^- \rightleftharpoons \mathbf{Cl_2} + 2e^-$	$\mathbf{Ti(I)}(aq) + Cl_2(aq) \rightleftharpoons Ti(III)(aq) + 2Cl^-(aq$
Fe^{3+}	$Fe^{3+} + e^- \rightleftharpoons \mathbf{Fe^{2+}}$	$\mathbf{Cr_2O_7^{2-}}(aq) + 6Fe^{2+}(aq) + 14H_3O^+(aq) \rightleftharpoons 2Cr^{3+}(aq) + 6Fe^{3+}(aq) + 21H_2O(l)$
I^-	$3I^- \rightleftharpoons \mathbf{I_3^-} + 2e^-$	$\mathbf{2S_2O_3^{2-}}(aq) + I_3^-(aq) \rightleftharpoons S_4O_6^{2-}(aq) + 3I^-(aq)$
Mn^{2+}	$Mn^{2+} \rightleftharpoons \mathbf{Mn^{3+}} + e^-$	$\mathbf{As(III)}(aq) + 2Mn^{3+}(aq) \rightleftharpoons As(V)(aq) + 2Mn$

Note: The electrochemically generated reagent and the analyte are shown in **bold**.

For an analyte that is not easy to oxidize or reduce, we can complete a coulometric titration by coupling a mediator's oxidation or reduction to an acid–base, precipitation, or complexation reaction that involves the analyte. For example, if we use H_2O as a mediator, we can generate H_3O^+at the anode

$$6H_2O(l) \rightleftharpoons 4H_3O^+(aq) + O_2(g) + 4e^-$$

and generate OH^- at the cathode.

$$2H_2O(l) + 2e^- \rightleftharpoons 2OH^-(aq) + H_2(g)$$

If we carry out the oxidation or reduction of H_2O using the generator cell in Figure 11.3.7 , then we can selectively dispense H_3O^+ or OH^- into a solution that contains the analyte. The resulting reaction is identical to that in an acid–base titration. Coulometric acid–base titrations have been used for the analysis of strong and weak acids and bases, in both aqueous and non-aqueous matrices. Table 11.3.3 summarizes several examples of coulometric titrations that involve acid–base, complexation, and precipitation reactions.

Table 11.3.3 . Representative Coulometric Titrations Using Acid–Base, Complexation, and Precipitation Reactions

type of reaction	mediator	electrochemically generated reagent and reaction	representative application
acid-base	H_2O	$6H_2O \rightleftharpoons 4\mathbf{H_3O^+} + O_2 + e^-$	$\mathbf{OH^-}(aq) + H_3O^+(aq) \rightleftharpoons 2H_2O(l)$
acid-base	H_2O	$2H_2O + 2e^- \rightleftharpoons 2\mathbf{OH^-} + H_2$	$\mathbf{H_3O^+}(aq) + OH^-(aq) \rightleftharpoons 2H_2O(l)$
complexation	$HgNH_3Y^{2-}$ (Y = EDTA)	$HgNH_3Y^{2-} + NH_4^+ + 2e^- \rightleftharpoons \mathbf{HY^{3-}} + Hg + 2NH_3$	$\mathbf{Ca^{2+}}(aq) + HY^{3-}(aq) + H_2O(l) \rightleftharpoons CaY^{2-}(aq) + H_3O^+(aq)$
complexation	Ag	$Ag \rightleftharpoons \mathbf{Ag^+} + e^-$	$\mathbf{I^-}(aq) + Ag^+(aq) \rightleftharpoons AgI(s)$
precipitation	Hg	$2Hg \rightleftharpoons \mathbf{Hg_2^{2+}} + 2e^-$	$\mathbf{2Cl^-}(aq) + Hg_2^{2+}(aq) \rightleftharpoons Hg_2Cl_2(s$
precipitation	$Fe(CN)_6^{3-}$	$Fe(CN)_6^{3-} + e^- \rightleftharpoons \mathbf{Fe(CN)_6^{4-}}$	$\mathbf{3Zn^{2+}}(aq) + K^+(aq) + 2Fe(CN)_6^{4-} \rightleftharpoons K_2Zn_3[Fe(CN)_6]_2(s)$

Note: The electrochemically generated reagent and the analyte are shown in **bold**.

In comparison to a conventional titration, a coulometric titration has two important advantages. The first advantage is that electrochemically generating a titrant allows us to use a reagent that is unstable. Although we cannot prepare and store a solution of a highly reactive reagent, such as Ag^{2+} or Mn^{3+}, we can generate them electrochemically and use them in a coulometric titration. Second, because it is relatively easy to measure a small quantity of charge, we can use a coulometric titration to determine an analyte whose concentration is too small for a conventional titration.

Quantitative Calculations

The absolute amount of analyte in a coulometric analysis is determined using Faraday's law (Equation 2.3.1) and the total charge given by Equation 2.3.2 or by Equation 2.3.3. The following example shows the calculations for a typical coulometric analysis.

✔ Example 11.3.1

To determine the purity of a sample of $Na_2S_2O_3$, a sample is titrated coulometrically using I^- as a mediator and I_3^- as the titrant. A sample weighing 0.1342 g is transferred to a 100-mL volumetric flask and diluted to volume with distilled water. A 10.00-mL portion is transferred to an electrochemical cell along with 25 mL of 1 M KI, 75 mL of a pH 7.0 phosphate buffer, and several drops of a starch indicator solution. Electrolysis at a constant current of 36.45 mA requires 221.8 s to reach the starch indicator endpoint. Determine the sample's purity.

Solution

As shown in Table 11.3.2 , the coulometric titration of $S_2O_3^{2-}$ with I_3^- is

$$2S_2O_3^{2-}(aq) + I_3^-(aq) \rightleftharpoons S_4O_6^{2-}(aq) + 3I^-(aq)$$

The oxidation of $S_2O_3^{2-}$ to $S_4O_6^{2-}$ requires one electron per $S_2O_3^{2-}$ (n = 1). Combining Equation 2.3.1 and Equation 2.3.2, and solving for the moles and grams of $Na_2S_2O_3$ gives

$$N_A = \frac{it_e}{nF} = \frac{(0.03645\text{ A})(221.8\text{ s})}{\left(\frac{1\text{ mol } e^-}{\text{mol } Na_2S_2O_3}\right)\left(\frac{96487\text{ C}}{\text{mol } e^-}\right)} = 8.379 \times 10^{-5}\text{ mol } Na_2S_2O_3$$

This is the amount of $Na_2S_2O_3$ in a 10.00-mL portion of a 100-mL sample; thus, there are 0.1325 grams of $Na_2S_2O_3$ in the original sample. The sample's purity, therefore, is

$$\frac{0.1325\text{ g } Na_2S_2O_3}{0.1342\text{ g sample}} \times 100 = 98.73\%\text{ w/w } Na_2S_2O_3$$

Note that for Equation 2.3.1 and Equation 2.3.2 it does not matter whether $S_2O_3^{2-}$ is oxidized at the working electrode or is oxidized by I_3^-.

? Exercise 11.3.1

To analyze a brass alloy, a 0.442-g sample is dissolved in acid and diluted to volume in a 500-mL volumetric flask. Electrolysis of a 10.00-mL sample at –0.3 V versus a SCE reduces Cu^{2+} to Cu, requiring a total charge of 16.11 C. Adjusting the potential to –0.6 V versus a SCE and completing the electrolysis requires 0.442 C to reduce Pb^{2+} to Pb. Report the %w/w Cu and Pb in the alloy.

Answer

The reduction of Cu^{2+} to Cu requires two electrons per mole of Cu (n = 2). Using Equation 2.3.1, we calculate the moles and the grams of Cu in the portion of sample being analyzed.

$$N_{Cu} = \frac{Q}{nF} = \frac{16.11\text{ C}}{\frac{2\text{ mol } e^-}{\text{mol Cu}} \times \frac{96487\text{ C}}{\text{mol } e^-}} = 8.348 \times 10^{-5}\text{ mol Cu}$$

$$8.348 \times 10^{-5}\text{ mol Cu} \times \frac{63.55\text{ g Cu}}{\text{mol Cu}} = 5.301 \times 10^{-3}\text{ g Cu}$$

This is the Cu from a 10.00 mL portion of a 500.0 mL sample; thus, the %/w/w copper in the original sample of brass is

$$\frac{5.301 \times 10^{-3}\text{ g Cu} \times \frac{500.0\text{ mL}}{10.00\text{ mL}}}{0.442\text{ g sample}} \times 100 = 60.0\%\text{ w/w Cu}$$

For lead, we follow the same process; thus

$$N_{Pb} = \frac{Q}{nF} = \frac{0.422\text{ C}}{\frac{2\text{ mol } e^-}{\text{mol Pb}} \times \frac{96487\text{ C}}{\text{mol } e^-}} = 2.19 \times 10^{-6}\text{ mol Pb}$$

$$2.19 \times 10^{-6}\text{ mol Pb} \times \frac{207.2\text{ g Pb}}{\text{mol Cu}} = 4.53 \times 10^{-4}\text{ g Pb}$$

$$\frac{4.53 \times 10^{-4}\text{ g Pb} \times \frac{500.0\text{ mL}}{10.00\text{ mL}}}{0.442\text{ g sample}} \times 100 = 5.12\%\text{ w/w Pb}$$

Representative Method 11.3.1: Determination of Dichromate by a Coulometric Redox Titration

The best way to appreciate the theoretical and the practical details discussed in this section is to carefully examine a typical analytical method. Although each method is unique, the following description of the determination of $Cr_2O_7^{2-}$ provides an instructive example of a typical procedure. The description here is based on Bassett, J.; Denney, R. C.; Jeffery, G. H.; Mendham, J. *Vogel's Textbook of Quantitative Inorganic Analysis*, Longman: London, 1978, p. 559–560.

Description of the Method

Thee concentration of $Cr_2O_7^{2-}$ in a sample is determined by a coulometric redox titration using Fe^{3+} as a mediator and electrogenerated Fe^{3+} as the titrant. The endpoint of the titration is determined potentiometrically.

Procedure

The electrochemical cell consists of a Pt working electrode and a Pt counter electrode placed in separate cells connected by a porous glass disk. Fill the counter electrode's cell with 0.2 M Na_2SO_4, keeping the level above that of the solution in the working electrode's cell. Connect a platinum electrode and a tungsten electrode to a potentiometer so that you can measure the working electrode's potential during the analysis. Prepare a mediator solution of approximately 0.3 M $NH_4Fe(SO_4)_2$. Add 5.00 mL of sample, 2 mL of 9 M H_2SO_4, and 10–25 mL of the mediator solution to the working electrode's cell, and add distilled water as needed to cover the electrodes. Bubble pure N_2 through the solution for 15 min to remove any O_2 that is present. Maintain the flow of N_2 during the electrolysis, turning if off momentarily when measuring the potential. Stir the solution using a magnetic stir bar. Adjust the current to 15–50 mA and begin the titration. Periodically stop the titration and measure the potential. Construct a titration curve of potential versus time and determine the time needed to reach the equivalence point.

Questions

1. Is the platinum working electrode the cathode or the anode?

    Reduction of Fe^{3+} to Fe^{2+} occurs at the working electrode, making it the cathode in this electrochemical cell.

2. Why is it necessary to remove dissolved oxygen by bubbling N_2 through the solution?

    Any dissolved O_2 will oxidize Fe^{2+} back to Fe^{3+}, as shown by the following reaction.

$$4Fe^{2+}(aq) + O_2 + 4H_3O^+(aq) \rightleftharpoons 4Fe^{3+}(aq) + 6H_2O(l)$$

    To maintain current efficiency, all the Fe^{2+} must react with $Cr_2O_7^{2-}$. The reaction of Fe^{2+} with O_2 means that more of the Fe^{3+} mediator is needed, increasing the time to reach the titration's endpoint. As a result, we report the presence of too much $Cr_2O_7^{2-}$.

3. What is the effect on the analysis if the $NH_4Fe(SO_4)_2$ is contaminated with trace amounts of Fe^{2+}? How can you compensate for this source of Fe^{2+}?

    There are two sources of Fe^{2+}: that generated from the mediator and that present as an impurity. Because the total amount of Fe^{2+} that reacts with $Cr_2O_7^{2-}$ remains unchanged, less Fe^{2+} is needed from the mediator. This decreases the time needed to reach the titration's end point. Because the apparent current efficiency is greater than 100%, the reported concentration of $Cr_2O_7^{2-}$ is too small. We can remove trace amount of Fe^{2+} from the mediator's solution by adding H_2O_2 and heating at 50–70°C until the evolution of O_2 ceases, converting the Fe^{2+} to Fe^{3+}. Alternatively, we can complete a blank titration to correct for any impurities of Fe^{2+} in the mediator.

4. Why is the level of solution in the counter electrode's cell maintained above the solution level in the working electrode's cell?

    This prevents the solution that contains the analyte from entering the counter electrode's cell. The oxidation of H_2O at the counter electrode produces O_2, which can react with the Fe^{2+} generated at the working electrode or the Cr^{3+} resulting from the reaction of Fe^{2+} and $Cr_2O_7^{2-}$. In either case, the result is a positive determinate error.

Characterization Applications

One useful application of coulometry is determining the number of electrons involved in a redox reaction. To make the determination, we complete a controlled-potential coulometric analysis using a known amount of a pure compound. The total charge at the end of the electrolysis is used to determine the value of *n* using Faraday's law (Equation 2.3.1).

Example 11.3.2

A 0.3619-g sample of tetrachloropicolinic acid, $C_6HNO_2Cl_4$, is dissolved in distilled water, transferred to a 1000-mL volumetric flask, and diluted to volume. An exhaustive controlled-potential electrolysis of a 10.00-mL portion of this solution at a spongy silver cathode requires 5.374 C of charge. What is the value of *n* for this reduction reaction?

Solution

The 10.00-mL portion of sample contains 3.619 mg, or 1.39×10^{-5} mol of tetrachloropicolinic acid. Solving Equation 2.3.1 for *n* and making appropriate substitutions gives

$$n = \frac{Q}{FN_A} = \frac{5.374\ \text{C}}{(96478\ \text{C/mol}\ e^-)\left(1.39 \times 10^{-5}\ \text{mol}\ C_6HNO_2Cl_4\right)} = 4.01\ \text{mol}\ e^-/\text{mol}\ C_6HNO_2Cl_4$$

Thus, reducing a molecule of tetrachloropicolinic acid requires four electrons. The overall reaction, which results in the selective formation of 3,6-dichloropicolinic acid, is

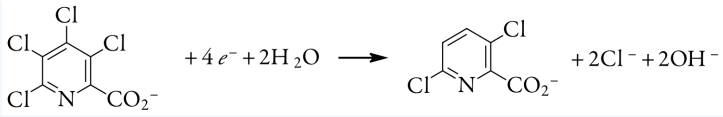

Evaluation

Scale of Operation

A coulometric method of analysis can analyze a small absolute amount of an analyte. In controlled-current coulometry, for example, the moles of analyte consumed during an exhaustive electrolysis is given by Equation 2.3.11. An electrolysis using a constant current of 100 μA for 100 s, for example, consumes only 1×10^{-7} mol of analyte if $n = 1$. For an analyte with a molecular weight of 100 g/mol, 1×10^{-7} mol of analyte corresponds to only 10 μg. The concentration of analyte in the electrochemical cell, however, must be sufficient to allow an accurate determination of the endpoint. When using a visual end point, the smallest concentration of analyte that can be determined by a coulometric titration is approximately 10^{-4} M. As is the case for a conventional titration, a coulometric titration using a visual end point is limited to major and minor analytes. A coulometric titration to a preset potentiometric endpoint is feasible even if the analyte's concentration is as small as 10^{-7} M, extending the analysis to trace analytes [Curran, D. J. "Constant-Current Coulometry," in Kissinger, P. T.; Heineman, W. R., eds., *Laboratory Techniques in Electroanalytical Chemistry*, Marcel Dekker Inc.: New York, 1984, pp. 539–568].

Accuracy

In controlled-current coulometry, accuracy is determined by the accuracy with which we can measure current and time, and by the accuracy with which we can identify the end point. The maximum measurement errors for current and time are about ±0.01% and ±0.1%, respectively. The maximum end point error for a coulometric titration is at least as good as that for a conventional titration, and is often better when using small quantities of reagents. Together, these measurement errors suggest that an accuracy of 0.1%–0.3% is feasible. The limiting factor in many analyses, therefore, is current efficiency. A current efficiency of more than 99.5% is fairly routine, and it often exceeds 99.9%.

In controlled-potential coulometry, accuracy is determined by current efficiency and by the determination of charge. If the sample is free of interferents that are easier to oxidize or reduce than the analyte, a current efficiency of greater than 99.9% is routine. When an interferent is present, it can often be eliminated by applying a potential where the exhaustive electrolysis of the interferents is possible without the simultaneous electrolysis of the analyte. Once the interferent is removed the potential is switched to a level where electrolysis of the analyte is feasible. The limiting factor in the accuracy of many controlled-potential coulometric methods of analysis is the determination of charge. With electronic integrators the total charge is determined with an accuracy of better than 0.5%.

If we cannot obtain an acceptable current efficiency, an electrogravimetric analysis is possible if the analyte—and only the analyte—forms a solid deposit on the working electrode. In this case the working electrode is weighed before beginning the electrolysis and reweighed when the electrolysis is complete. The difference in the electrode's weight gives the analyte's mass.

Precision

Precision is determined by the uncertainties in measuring current, time, and the endpoint in controlled-current coulometry or the charge in controlled-potential coulometry. Precisions of ±0.1–0.3% are obtained routinely in coulometric titrations, and precisions of ±0.5% are typical for controlled-potential coulometry.

Sensitivity

For a coulometric method of analysis, the calibration sensitivity is equivalent to nF in Equation 2.3.1. In general, a coulometric method is more sensitive if the analyte's oxidation or reduction involves a larger value of n.

Selectivity

Selectivity in controlled-potential and controlled-current coulometry is improved by adjusting solution conditions and by selecting the electrolysis potential. In controlled-potential coulometry, the potential is fixed by the potentiostat, and in controlled-current coulometry the potential is determined by the redox reaction with the mediator. In either case, the ability to control the electrolysis potential affords some measure of selectivity. By adjusting pH or by adding a complexing agent, it is possible to shift the potential at which an analyte or interferent undergoes oxidation or reduction. For example, the standard-state reduction potential for Zn^{2+} is –0.762 V versus the SHE. If we add a solution of NH_3, forming $Zn(NH_3)_4^{2+}$, the standard state potential shifts to –1.04 V. This provides an additional means for controlling selectivity when an analyte and an interferent undergo electrolysis at similar potentials.

Time, Cost, and Equipment

Controlled-potential coulometry is a relatively time consuming analysis, with a typical analysis requiring 30–60 min. Coulometric titrations, on the other hand, require only a few minutes, and are easy to adapt to an automated analysis. Commercial instrumentation for both controlled-potential and controlled-current coulometry is available, and is relatively inexpensive. Low cost potentiostats and constant-current sources are available for approximately $1000.

2.4: Voltammetric and Amperometric Methods

In ***voltammetry*** we apply a time-dependent potential to an electrochemical cell and measure the resulting current as a function of that potential. We call the resulting plot of current versus applied potential a ***voltammogram***, and it is the electrochemical equivalent of a spectrum in spectroscopy, providing quantitative and qualitative information about the species involved in the oxidation or reduction reaction [Maloy, J. T. *J. Chem. Educ.* **1983**, *60*, 285–289]. The earliest voltammetric technique is polarography, developed by Jaroslav Heyrovsky in the early 1920s—an achievement for which he was awarded the Nobel Prize in Chemistry in 1959. Since then, many different forms of voltammetry have been developed, a few of which are highlighted in Figure 11.1.6. Before examining these techniques and their applications in more detail, we must first consider the basic experimental design for voltammetry and the factors influencing the shape of the resulting voltammogram.

For an on-line introduction to much of the material in this section, see Analytical Electrochemistry: The Basic Concepts by Richard S. Kelly, a resource that is part of the Analytical Sciences Digital Library.

Voltammetric Measurements

Although early voltammetric methods used only two electrodes, a modern voltammeter makes use of a three-electrode potentiostat, such as that shown in Figure 11.1.5. In voltammetry we apply a time-dependent potential excitation signal to the working electrode —changing its potential relative to the fixed potential of the reference electrode—and measure the current that flows between the working electrode and the auxiliary electrode. The auxiliary electrode generally is a platinum wire and the reference electrode usually is a SCE or a Ag/AgCl electrode.

Figure 11.1.5 shows an example of a manual three-electrode potentiostat. Although a modern potentiostat uses very different circuitry, you can use Figure 11.1.5 and the accompanying discussion to understand how we can control the potential of working electrode and measure the resulting current.

For the working electrode we can choose among several different materials, including mercury, platinum, gold, silver, and carbon. The earliest voltammetric techniques used a mercury working electrode. Because mercury is a liquid, the working electrode usual is a drop suspended from the end of a capillary tube. In the ***hanging mercury drop electrode***, or HMDE, we extrude the drop of Hg by rotating a micrometer screw that pushes the mercury from a reservoir through a narrow capillary tube (Figure 11.4.1 a).

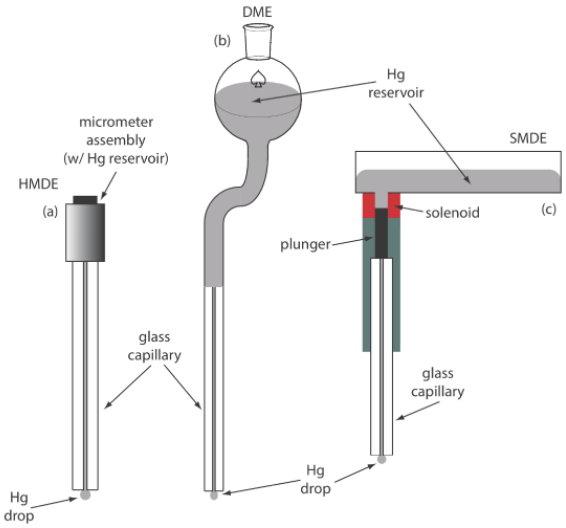

Figure 11.4.1 . Three examples of mercury electrodes: (a) hanging mercury drop electrode, or HMDE; (b) dropping mercury electrode, or DME; and (c) static mercury drop electrode, or SMDE.

In the ***dropping mercury electrode***, or DME, mercury drops form at the end of the capillary tube as a result of gravity (Figure 11.4.1 b). Unlike the HMDE, the mercury drop of a DME grows continuously—as mercury flows from the reservoir under the influence of gravity—and has a finite lifetime of several seconds. At the end of its lifetime the mercury drop is dislodged, either

manually or on its own, and is replaced by a new drop. The ***static mercury drop electrode***, or SMDE, uses a solenoid driven plunger to control the flow of mercury (Figure 11.4.1 c). Activation of the solenoid momentarily lifts the plunger, allowing mercury to flow through the capillary, forming a single, hanging Hg drop. Repeated activation of the solenoid produces a series of Hg drops. In this way the SMDE may be used as either a HMDE or a DME. There is one additional type of mercury electrode: the ***mercury film electrode***. A solid electrode—typically carbon, platinum, or gold—is placed in a solution of Hg^{2+} and held at a potential where the reduction of Hg^{2+} to Hg is favorable, depositing a thin film of mercury on the solid electrode's surface.

Mercury has several advantages as a working electrode. Perhaps its most important advantage is its high overpotential for the reduction of H_3O^+ to H_2, which makes accessible potentials as negative as –1 V versus the SCE in acidic solutions and –2 V versus the SCE in basic solutions (Figure 11.4.2). A species such as Zn^{2+}, which is difficult to reduce at other electrodes without simultaneously reducing H_3O^+, is easy to reduce at a mercury working electrode. Other advantages include the ability of metals to dissolve in mercury—which results in the formation of an ***amalgam***—and the ability to renew the surface of the electrode by extruding a new drop. One limitation to mercury as a working electrode is the ease with which it is oxidized. Depending on the solvent, a mercury electrode can not be used at potentials more positive than approximately –0.3 V to +0.4 V versus the SCE.

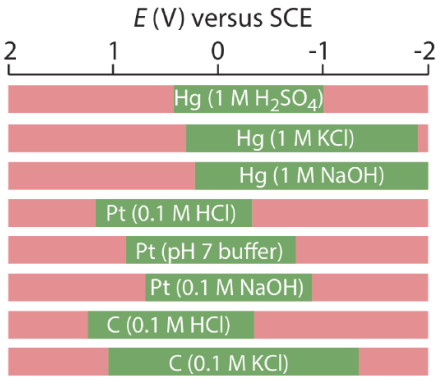

Figure 11.4.2 . Approximate potential windows for mercury, platinum, and carbon (graphite) electrodes in acidic, neutral, and basic aqueous solvents. The useful potential windows are shown in green; potentials in red result in the oxidation or the reduction of the solvent or the electrode. Complied from Adams, R. N. *Electrochemistry at Solid Electrodes*, Marcel Dekker, Inc.: New York, 1969 and Bard, A. J.; Faulkner, L. R. *Electro- chemical Methods*, John Wiley & Sons: New York, 1980.

Solid electrodes constructed using platinum, gold, silver, or carbon may be used over a range of potentials, including potentials that are negative and positive with respect to the SCE (Figure 11.4.2). For example, the potential window for a Pt electrode extends from approximately +1.2 V to –0.2 V versus the SCE in acidic solutions, and from +0.7 V to –1 V versus the SCE in basic solutions. A solid electrode can replace a mercury electrode for many voltammetric analyses that require negative potentials, and is the electrode of choice at more positive potentials. Except for the carbon paste electrode, a solid electrode is fashioned into a disk and sealed into the end of an inert support with an electrical lead (Figure 11.4.3). The carbon paste electrode is made by filling the cavity at the end of the inert support with a paste that consists of carbon particles and a viscous oil. Solid electrodes are not without problems, the most important of which is the ease with which the electrode's surface is altered by the adsorption of a solution species or by the formation of an oxide layer. For this reason a solid electrode needs frequent reconditioning, either by applying an appropriate potential or by polishing.

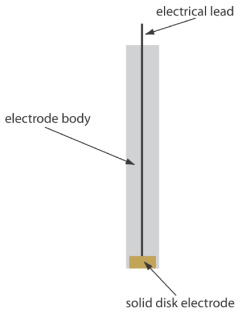

Figure 11.4.3 . Schematic showing a solid electrode. The electrode is fashioned into a disk and sealed in the end of an inert polymer support along with an electrical lead.

A typical arrangement for a voltammetric electrochemical cell is shown in Figure 11.4.4 . In addition to the working electrode, the reference electrode, and the auxiliary electrode, the cell also includes a N_2-purge line for removing dissolved O_2, and an optional

stir bar. Electrochemical cells are available in a variety of sizes, allowing the analysis of solution volumes ranging from more than 100 mL to as small as 50 μL.

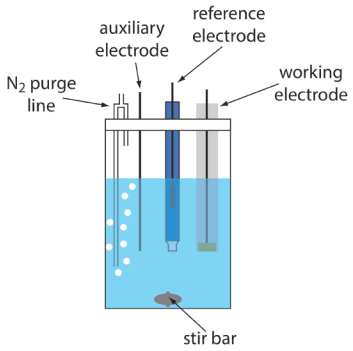

Figure 11.4.4 . Typical electrochemical cell for voltammetry.

Current In Voltammetry

When we oxidize an analyte at the working electrode, the resulting electrons pass through the potentiostat to the auxiliary electrode, reducing the solvent or some other component of the solution matrix. If we reduce the analyte at the working electrode, the current flows from the auxiliary electrode to the cathode. In either case, the current from the redox reactions at the working electrode and the auxiliary electrodes is called a ***faradaic current***. In this section we consider the factors affecting the magnitude of the faradaic current, as well as the sources of any non-faradaic currents.

Sign Conventions

Because the reaction of interest occurs at the working electrode, we describe the faradaic current using this reaction. A faradaic current due to the analyte's reduction is a ***cathodic current***, and its sign is positive. An ***anodic current*** results from the analyte's oxidation at the working electrode, and its sign is negative.

Influence of Applied Potential on the Faradaic Current

As an example, let's consider the faradaic current when we reduce $\mathrm{Fe(CN)_6^{3-}}$ to $\mathrm{Fe(CN)_6^{4-}}$ at the working electrode. The relationship between the concentrations of $\mathrm{Fe(CN)_6^{3-}}$, the concentration of $\mathrm{Fe(CN)_6^{4-}}$, and the potential is given by the Nernst equation

$$E = +0.356\ \mathrm{V} - 0.05916 \log \frac{\left[\mathrm{Fe(CN)_6^{4-}}\right]_{x=0}}{\left[\mathrm{Fe(CN)_6^{3-}}\right]_{x=0}}$$

where +0.356V is the standard-statepotential for the $\mathrm{Fe(CN)_6^{3-}/Fe(CN)_6^{4-}}$ redox couple, and x = 0 indicates that the concentrations of $\mathrm{Fe(CN)_6^{3-}}$- and $\mathrm{Fe(CN)_6^{4-}}$ are those at the surface of the working electrode. We use surface concentrations instead of bulk concentrations because the equilibrium position for the redox reaction

$$\mathrm{Fe(CN)_6^{3-}}(aq) + e^- \rightleftharpoons \mathrm{Fe(CN)_6^{4-}}(aq)$$

is established at the electrode's surface.

Let's assume we have a solution for which the initial concentration of $\mathrm{Fe(CN)_6^{3-}}$ is 1.0 mM and that $\mathrm{Fe(CN)_6^{4-}}$ is absent. Figure 11.4.5 shows the ladder diagram for this solution.

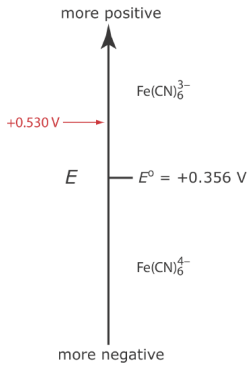

Figure 11.4.5 . Ladder diagram for the $Fe(CN)_6^{3-}/Fe(CN)_6^{4-}$ redox half-reaction.

If we apply a potential of +0.530 V to the working electrode, the concentrations of $Fe(CN)_6^{3-}$ and $Fe(CN)_6^{4-}$ at the surface of the electrode are unaffected, and no faradaic current is observed. If we switch the potential to +0.356 V some of the $Fe(CN)_6^{3-}$ at the electrode's surface is reduced to $Fe(CN)_6^{4-}$until we reach a condition where

$$\left[Fe(CN)_6^{3-}\right]_{x=0} = \left[Fe(CN)_6^{4-}\right]_{x=0} = 0.50 \text{ mM}$$

> This is the first of the five important principles of electrochemistry outlined in Chapter 11.1: the electrode's potential determines the analyte's form at the electrode's surface.

If this is all that happens after we apply the potential, then there would be a brief surge of faradaic current that quickly returns to zero, which is not the most interesting of results. Although the concentrations of $Fe(CN)_6^{3-}$ and $Fe(CN)_6^{4-}$ at the electrode surface are 0.50 mM, their concentrations in bulk solution remains unchanged.

> This is the second of the five important principles of electrochemistry outlined in Chapter 11.1: the analyte's concentration at the electrode may not be the same as its concentration in bulk solution.

Because of this difference in concentration, there is a concentration gradient between the solution at the electrode's surface and the bulk solution. This concentration gradient creates a driving force that transports $Fe(CN)_6^{4-}$ away from the electrode and that transports $Fe(CN)_6^{3-}$ to the electrode (Figure 11.4.6). As the $Fe(CN)_6^{3-}$ arrives at the electrode it, too, is reduced to $Fe(CN)_6^{4-}$. A faradaic current continues to flow until there is no difference between the concentrations of $Fe(CN)_6^{3-}$ and $Fe(CN)_6^{4-}$ at the electrode and their concentrations in bulk solution.

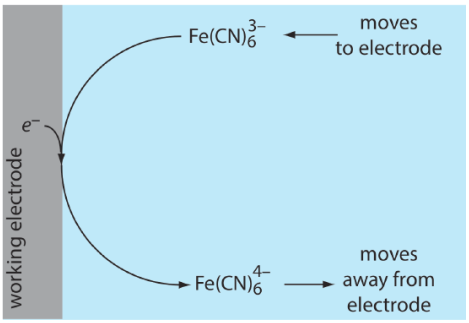

Figure 11.4.6 . Schematic diagram showing the transport of $Fe(CN)_6^{4-}$ away from the electrode's surface and the transport of $Fe(CN)_6^{3-}$ toward the electrode's surface following the reduction of $Fe(CN)_6^{3-}$ to $Fe(CN)_6^{4-}$.

Although the potential at the working electrode determines if a faradaic current flows, the magnitude of the current is determined by the rate of the resulting oxidation or reduction reaction. Two factors contribute to the rate of the electrochemical reaction: the rate at which the reactants and products are transported to and from the electrode—what we call ***mass transport***—and the rate at which electrons pass between the electrode and the reactants and products in solution.

This is the fourth of the five important principles of electrochemistry outlined in Chapter 11.1: current is a measure of rate.

Influence of Mass Transport on the Faradaic Current

There are three modes of mass transport that affect the rate at which reactants and products move toward or away from the electrode surface: diffusion, migration, and convection. ***Diffusion*** occurs whenever the concentration of an ion or a molecule at the surface of the electrode is different from that in bulk solution. If we apply a potential sufficient to completely reduce $\mathrm{Fe(CN)_6^{3-}}$ at the electrode surface, the result is a concentration gradient similar to that shown in Figure 11.4.7 . The region of solution over which diffusion occurs is the ***diffusion layer***. In the absence of other modes of mass transport, the width of the diffusion layer, δ, increases with time as the $\mathrm{Fe(CN)_6^{3-}}$ must diffuse from an increasingly greater distance.

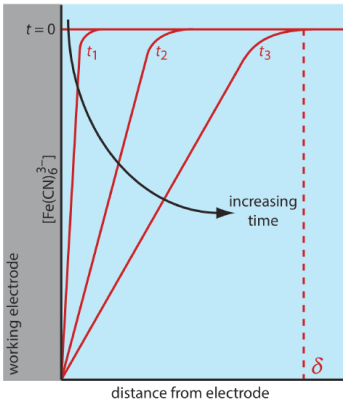

Figure 11.4.7 . Concentration gradients (in red) for $\mathrm{Fe(CN)_6^{3-}}$ following the application of a potential that completely reduces it to $\mathrm{Fe(CN)_6^{4-}}$. Before we apply the potential (t = 0) the concentration of $\mathrm{Fe(CN)_6^{3-}}$ is the same at all distances from the electrode's surface. After we apply the potential, its concentration at the electrode's surface decreases to zero and $\mathrm{Fe(CN)_6^{3-}}$ diffuses to the electrode from bulk solution. The longer we apply the potential, the greater the distance over which diffusion occurs. The dashed red line shows the extent of the diffusion layer at time t_3. These profiles assume that convection and migration do not contribute significantly to the mass transport of $\mathrm{Fe(CN)_6^{3-}}$.

Convection occurs when we mix the solution, which carries reactants toward the electrode and removes products from the electrode. The most common form of convection is stirring the solution with a stir bar; other methods include rotating the electrode and incorporating the electrode into a flow-cell.

The final mode of mass transport is ***migration***, which occurs when a charged particle in solution is attracted to or repelled from an electrode that carries a surface charge. If the electrode carries a positive charge, for example, an anion will move toward the electrode and a cation will move toward the bulk solution. Unlike diffusion and convection, migration affects only the mass transport of charged particles.

The movement of material to and from the electrode surface is a complex function of all three modes of mass transport. In the limit where diffusion is the only significant form of mass transport, the current in a voltammetric cell is equal to

$$i = \frac{nFAD\left(C_{\text{bulk}} - C_{x=0}\right)}{\delta} \tag{2.4.1}$$

where n the number of electrons in the redox reaction, F is Faraday's constant, A is the area of the electrode, D is the diffusion coefficient for the species reacting at the electrode, C_{bulk} and $C_{x\,=\,0}$ are its concentrations in bulk solution and at the electrode surface, and δ is the thickness of the diffusion layer.

For Equation 2.4.1 to be valid, convection and migration must not interfere with the formation of a diffusion layer. We can eliminate migration by adding a high concentration of an inert supporting electrolyte. Because ions of similar charge equally are attracted to or repelled from the surface of the electrode, each has an equal probability of undergoing migration. A large excess of an inert electrolyte ensures that few reactants or products experience migration. Although it is easy to eliminate convection by not stirring the solution, there are experimental designs where we cannot avoid convection, either because we must stir the solution or because we are using an electrochemical flow cell. Fortunately, as shown in Figure 11.4.8 , the dynamics of a fluid moving past an electrode results in a small diffusion layer—typically 1–10 μm in thickness—in which the rate of mass transport by convection drops to zero.

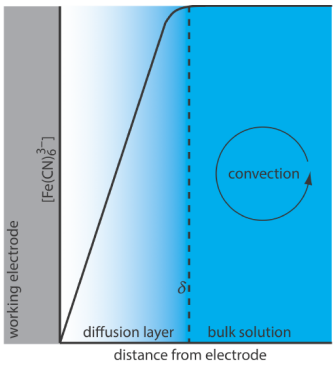

Figure 11.4.8 . Concentration gradient for $\mathrm{Fe(CN)_6^{3-}}$ when stirring the solution. Diffusion is the only significant form of mass transport close to the electrode's surface. At distances greater than δ, convection is the only significant form of mass transport, maintaining a homogeneous solution in which the concentration of $\mathrm{Fe(CN)_6^{3-}}$ at δ is the same as its concentration in bulk solution.

Effect of Electron Transfer Kinetics on the Faradaic Current

The rate of mass transport is one factor that influences the current in voltammetry. The ease with which electrons move between the electrode and the species that reacts at the electrode also affects the current. When electron transfer kinetics are fast, the redox reaction is at equilibrium. Under these conditions the redox reaction is ***electrochemically reversible*** and the Nernst equation applies. If the electron transfer kinetics are sufficiently slow, the concentration of reactants and products at the electrode surface—and thus the magnitude of the faradaic current—are not what is predicted by the Nernst equation. In this case the system is ***electrochemically irreversible***.

Charging Currents

In addition to the faradaic current from a redox reaction, the current in an electrochemical cell includes other, nonfaradaic sources. Suppose the charge on an electrode is zero and we suddenly change its potential so that the electrode's surface acquires a positive charge. Cations near the electrode's surface will respond to this positive charge by migrating away from the electrode; anions, on the other hand, will migrate toward the electrode. This migration of ions occurs until the electrode's positive surface charge and the negative charge of the solution near the electrode are equal. Because the movement of ions and the movement of electrons are indistinguishable, the result is a small, short-lived ***nonfaradaic current*** that we call the ***charging current***. Every time we change the electrode's potential, a transient charging current flows.

> The migration of ions in response to the electrode's surface charge leads to the formation of a structured electrode-solution interface that we call the ***electrical double layer***, or EDL. When we change an electrode's potential, the charging current is the result of a restructuring of the EDL. The exact structure of the electrical double layer is not important in the context of this text, but you can consult this chapter's additional resources for additional information.

Residual Current

Even in the absence of analyte, a small, measurable current flows through an electrochemical cell. This ***residual current*** has two components: a faradaic current due to the oxidation or reduction of trace impurities and a nonfaradaic charging current. Methods for discriminating between the analyte's faradaic current and the residual current are discussed later in this chapter.

Shape of Voltammograms

The shape of a voltammogram is determined by several experimental factors, the most important of which are how we measure the current and whether convection is included as a means of mass transport. As shown in Figure 11.4.9 , despite an abundance of different voltammetric techniques, several of which are discussed in this chapter, there are only three common shapes for voltammograms.

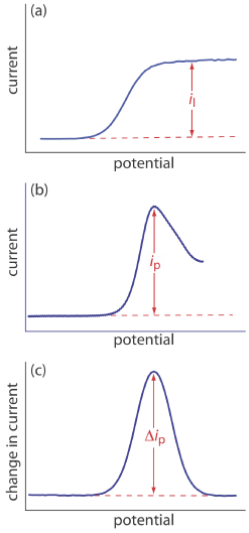

Figure 11.4.9 . The three common shapes for voltammograms. The dashed red line shows the residual current.

For the voltammogram in Figure 11.4.9 a, the current increases from a background residual current to a ***limiting current***, i_l. Because the faradaic current is inversely proportional to δ (Equation 2.4.1), a limiting current occurs only if the thickness of the diffusion layer remains constant because we are stirring the solution (see Figure 11.4.8). In the absence of convection the diffusion layer increases with time (see Figure 11.4.7). As shown in Figure 11.4.9 b, the resulting voltammogram has a ***peak current*** instead of a limiting current.

For the voltammograms in Figure 11.4.9 a and Figure 11.4.9 b, we measure the current as a function of the applied potential. We also can monitor the change in current, Δi, following a change in potential. The resulting voltammogram, shown in Figure 11.4.9 c, also has a peak current.

Quantitative and Qualitative Aspects of Voltammetry

Earlier we described a voltammogram as the electrochemical equivalent of a spectrum in spectroscopy. In this section we consider how we can extract quantitative and qualitative information from a voltammogram. For simplicity we will limit our treatment to voltammograms similar to Figure 11.4.9 a.

Determining Concentration

Let's assume that the redox reaction at the working electrode is

$$O + ne^- \rightleftharpoons R \tag{2.4.2}$$

where *O* is the analyte's oxidized form and *R* is its reduced form. Let's also assume that only *O* initially is present in bulk solution and that we are stirring the solution. When we apply a potential that results in the reduction of *O* to *R*, the current depends on the rate at which *O* diffuses through the fixed diffusion layer shown in Figure 11.4.7 . Using Equation 2.4.1, the current, *i*, is

$$i = K_O \left([O]_{\text{bulk}} - [O]_{x=0} \right) \tag{2.4.3}$$

where K_O is a constant equal to $nFAD_O/\delta$. When we reach the limiting current, i_l, the concentration of *O* at the electrode surface is zero and Equation 2.4.3 simplifies to

$$i_l = K_O [O]_{\text{bulk}} \tag{2.4.4}$$

Equation 2.4.4 shows us that the limiting current is a linear function of the concentration of *O* in bulk solution. To determine the value of K_O we can use any of the standardization methods covered in Chapter 5. Equations similar to Equation 2.4.4 can be developed for the other two types of voltammograms shown in Figure 11.4.9 .

Determining the Standard-State Potential

To extract the standard-state potential from a voltammogram, we need to rewrite the Nernst equation for reaction 2.4.2

$$E = E^{\circ}_{O/R} - \frac{0.05916}{n} \log \frac{[R]_{x=0}}{[O]_{x=0}} \tag{2.4.5}$$

in terms of current instead of the concentrations of *O* and *R*. We will do this in several steps. First, we substitute Equation 2.4.4 into Equation 2.4.3 and rearrange to give

$$[O]_{x=0} = \frac{i_l - i}{K_O} \tag{2.4.6}$$

Next, we derive a similar equation for $[R]_{x=0}$, by noting that

$$i = K_R \left([R]_{x=0} - [R]_{\text{bulk}} \right)$$

Because the concentration of $[R]_{\text{bulk}}$ is zero—remember our assumption that the initial solution contains only *O*—we can simplify this equation

$$i = K_R [R]_{x=0}$$

and solve for $[R]_{x=0}$.

$$[R]_{x=0} = \frac{i}{K_R} \tag{2.4.7}$$

Now we are ready to finish our derivation. Substituting Equation 2.4.7 and Equation 2.4.6 into Equation 2.4.5 and rearranging leaves us with

$$E = E^{\circ}_{O/R} - \frac{0.05916}{n} \log \frac{K_O}{K_R} - \frac{0.05916}{n} \log \frac{i}{i_l - i} \tag{2.4.8}$$

When the current, *i*, is half of the limiting current, i_l,

$$i = 0.5 \times i_l$$

we can simplify Equation 2.4.8 to

$$E_{1/2} = E^{\circ}_{O/R} - \frac{0.05916}{n} \log \frac{K_O}{K_R} \tag{2.4.9}$$

where $E_{1/2}$ is the half-wave potential (Figure 11.4.10). If K_O is approximately equal to K_R, which often is the case, then the half-wave potential is equal to the standard-state potential. Note that Equation 2.4.9 is valid only if the redox reaction is electrochemically reversible.

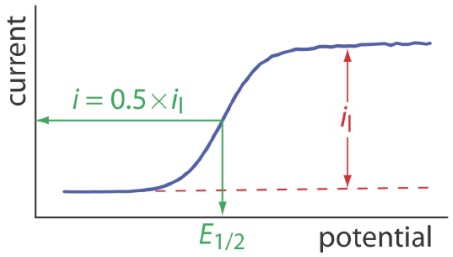

Figure 11.4.10 . Determination of the limiting current, i_l, and the half-wave potential, $E_{1/2}$, for the voltammogram in Figure 11.4.9 a.

Voltammetric Techniques

In voltammetry there are three important experimental parameters under our control: how we change the potential applied to the working electrode, when we choose to measure the current, and whether we choose to stir the solution. Not surprisingly, there are many different voltammetric techniques. In this section we consider several important examples.

Polarography

The first important voltammetric technique to be developed—***polarography***—uses the dropping mercury electrode shown in Figure 11.4.1 b as the working electrode. As shown in Figure 11.4.11 , the current is measured while applying a linear potential ramp.

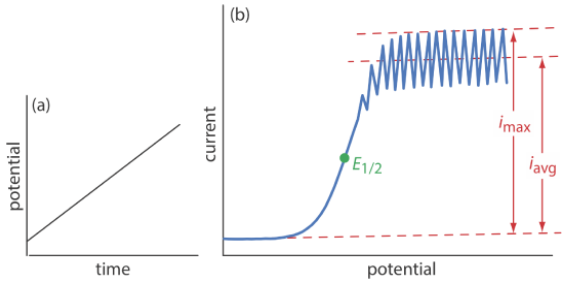

Figure 11.4.11 . Details of normal polarography: (a) the linear potential-excitation signal, and (b) the resulting voltammogram.

Although polarography takes place in an unstirred solution, we obtain a limiting current instead of a peak current. When a Hg drop separates from the glass capillary and falls to the bottom of the electrochemical cell, it mixes the solution. Each new Hg drop, therefore, grows into a solution whose composition is identical to the bulk solution. The oscillations in the current are a result of the Hg drop's growth, which leads to a time-dependent change in the area of the working electrode. The limiting current—which also is called the diffusion current—is measured using either the maximum current, i_{max}, or from the average current, i_{avg}. The relationship between the analyte's concentration, C_A, and the limiting current is given by the Ilkovic equations

$$i_{\text{max}} = 706nD^{1/2}m^{2/3}t^{1/6}C_A = K_{\text{max}}C_A$$

$$i_{avg} = 607nD^{1/2}m^{2/3}t^{1/6}C_A = K_{\text{avg}}C_A$$

where n is the number of electrons in the redox reaction, D is the analyte's diffusion coefficient, m is the flow rate of Hg, t is the drop's lifetime and K_{max} and K_{avg} are constants. The half-wave potential, $E_{1/2}$, provides qualitative information about the redox reaction.

Normal polarography has been replaced by various forms of ***pulse polarography***, several examples of which are shown in Figure 11.4.12 [Osteryoung, J. *J. Chem. Educ.* **1983**, *60*, 296–298]. Normal pulse polarography (Figure 11.4.12 a), for example, uses a series of potential pulses characterized by a cycle of time τ, a pulse-time of t_{p}, a pulse potential of ΔE_{p}, and a scan rate of $\Delta E/\Delta t$. Typical experimental conditions for normal pulse polarography are $\tau \approx 1\ \text{s}$, $t_{\text{p}} \approx 50$ ms, and $\Delta E/\Delta t \approx 2\ \text{mV/s}$. The initial value of $\Delta E_{\text{p}} \approx 2\ \text{mV}$, and it increases by ≈ 2 mV with each pulse. The current is sampled at the end of each potential pulse for approximately 17 ms before returning the potential to its initial value. The shape of the resulting voltammogram is similar to Figure 11.4.11 , but without the current oscillations. Because we apply the potential for only a small portion of the drop's lifetime, there is less time for the analyte to undergo oxidation or reduction and a smaller diffusion layer. As a result, the faradaic current in normal pulse polarography is greater than in the polarography, resulting in better sensitivity and smaller detection limits.

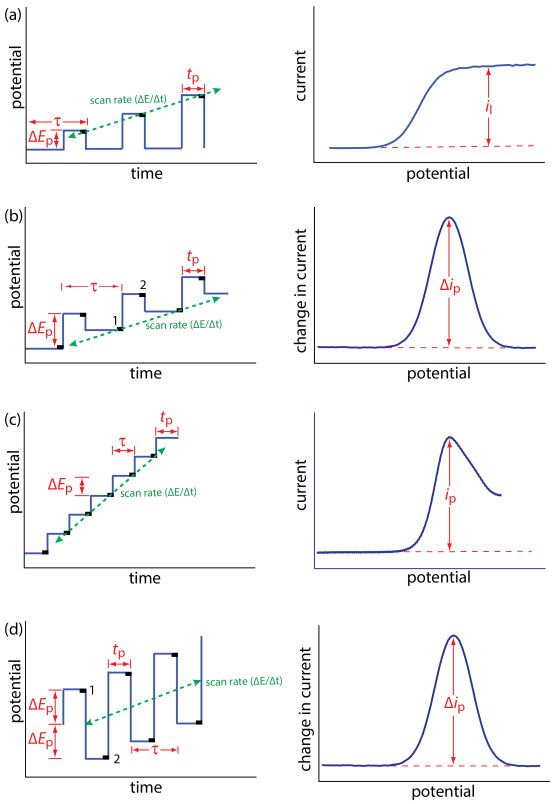

Figure 11.4.12 . Potential-excitation signals and voltammograms for (a) normal pulse polarography, (b) differential pulse polarography, (c) staircase polarography, and (d) square-wave polarography. The current is sampled at the time intervals shown by the black rectangles. When measuring a change in current, Δi, the current at point 1 is subtracted from the current at point 2. The symbols in the diagrams are as follows: τ is the cycle time; ΔE_{p} is a fixed or variable pulse potential relative to the beginning of the cycle; and t_{p} is the pulse time. The scan rate (change in potential per unit time) is shown by the dashed arrow.

In differential pulse polarography (Figure 11.4.12 b) the current is measured twice per cycle: for approximately 17 ms before applying the pulse and for approximately 17 ms at the end of the cycle. The difference in the two currents gives rise to the peak-shaped voltammogram. Typical experimental conditions for differential pulse polarography are $\tau \approx 1$ s, $t_{\text{p}} \approx 50$ ms, $\Delta E_{\text{p}} \approx 50$ mV, and $\Delta E/\Delta t \approx 2$ mV/s.

> The voltammogram for differential pulse polarography is approximately the first derivative of the voltammogram for normal pulse polarography. To see why this is the case, note that the change in current over a fixed change in potential, $\Delta i/\Delta E$, approximates the slope of the voltammogram for normal pulse polarography. You may recall that the first derivative of a function returns the slope of the function at each point. The first derivative of a sigmoidal function is a peak-shaped function.

Other forms of pulse polarography include staircase polarography (Figure 11.4.12 c) and square-wave polarography (Figure 11.4.12 d). One advantage of square-wave polarography is that we can make τ very small—perhaps as small as 5 ms, compared to 1 s for other forms of pulse polarography—which significantly decreases analysis time. For example, suppose we need to scan a potential range of 400 mV. If we use normal pulse polarography with a $\Delta E/\Delta t$ of 2 mV/cycle and a τ of 1 s/cycle, then we need 200 s to complete the scan. If we use square-wave polarography with a $\Delta E/\Delta t$ of 2 mV/cycle and a τ of 5 ms/cycle, we can complete the scan in 1 s. At this rate, we can acquire a complete voltammogram using a single drop of Hg!

Polarography is used extensively for the analysis of metal ions and inorganic anions, such as IO_3^- and NO_3^-. We also can use polarography to study organic compounds with easily reducible or oxidizable functional groups, such as carbonyls, carboxylic acids, and carbon-carbon double bonds.

Hydrodynamic Voltammetry

In polarography we obtain a limiting current because each drop of mercury mixes the solution as it falls to the bottom of the electrochemical cell. If we replace the DME with a solid electrode (see Figure 11.4.3), we can still obtain a limiting current if we mechanically stir the solution during the analysis, using either a stir bar or by rotating the electrode. We call this approach ***hydrodynamic voltammetry***.

Hydrodynamic voltammetry uses the same potential profiles as in polarography, such as a linear scan (Figure 11.4.11) or a differential pulse (Figure 11.4.12 b). The resulting voltammograms are identical to those for polarography, except for the lack of current oscillations from the growth of the mercury drops. Because hydrodynamic voltammetry is not limited to Hg electrodes, it is useful for analytes that undergo oxidation or reduction at more positive potentials.

Stripping Voltammetry

Another important voltammetric technique is ***stripping voltammetry***, which consists of three related techniques: anodic stripping voltammetry, cathodic stripping voltammetry, and adsorptive stripping voltammetry. Because anodic stripping voltammetry is the more widely used of these techniques, we will consider it in greatest detail.

Anodic stripping voltammetry consists of two steps (Figure 11.4.13). The first step is a controlled potential electrolysis in which we hold the working electrode—usually a hanging mercury drop or a mercury film electrode—at a cathodic potential sufficient to deposit the metal ion on the electrode. For example, when analyzing Cu^{2+} the deposition reaction is

$$Cu^{2+} + 2e^- \rightleftharpoons Cu(Hg)$$

where Cu(Hg) indicates that the copper is amalgamated with the mercury. This step serves as a means of concentrating the analyte by transferring it from the larger volume of the solution to the smaller volume of the electrode. During most of the electrolysis we stir the solution to increase the rate of deposition. Near the end of the deposition time we stop the stirring—eliminating convection as a mode of mass transport—and allow the solution to become quiescent. Typical deposition times of 1–30 min are common, with analytes at lower concentrations requiring longer times.

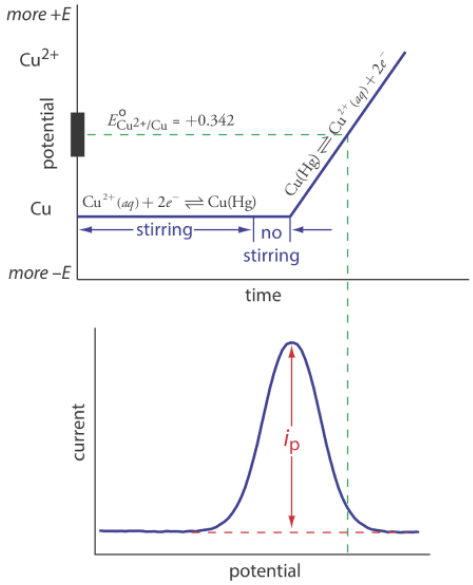

Figure 11.4.13 . Potential-excitation signal and voltammogram for anodic stripping voltammetry at a hanging mercury drop electrode or a mercury film electrode. Note the ladder diagram for copper in the upper figure.

In the second step, we scan the potential anodically—that is, toward a more positive potential. When the working electrode's potential is sufficiently positive, the analyte is stripped from the electrode, returning to solution in its oxidized form.

$$Cu(Hg) \rightleftharpoons Cu^{2+} + 2e^-$$

Monitoring the current during the stripping step gives a peak-shaped voltammogram, as shown in Figure 11.4.13 . The peak current is proportional to the analyte's concentration in the solution. Because we are concentrating the analyte in the electrode, detection limits are much smaller than other electrochemical techniques. An improvement of three orders of magnitude—the equivalent of parts per billion instead of parts per million—is routine.

Anodic stripping voltammetry is very sensitive to experimental conditions, which we must carefully control to obtain results that are accurate and precise. Key variables include the area of the mercury film or the size of the hanging Hg drop, the deposition time, the rest time, the rate of stirring, and the scan rate during the stripping step. Anodic stripping voltammetry is particularly useful for metals that form amalgams with mercury, several examples of which are listed in Table 11.4.1 .

Table 11.4.1 . Representative Examples of Analytes Determined by Stripping Voltammetry

anodic stripping voltammetry	cathodic stripping voltammetry	adsorptive stripping voltammetry
Bi^{3+}	Br^-	bilirubin
Cd^{2+}	Cl^-	codeine
Cu^{2+}	I^-	cocaine
Ga^{3+}	mercaptans (RSH)	digitoxin
In^{3+}	S^{2-}	dopamine
Pb^{2+}	SCN^-	heme
Tl^+		monesin
Sn^{2+}		testosterone
Zn^{2+}		

Source: Compiled from Peterson, W. M.; Wong, R. V. *Am. Lab.* November 1981, 116–128; Wang, J. *Am. Lab.* May 1985, 41–50.

The experimental design for cathodic stripping voltammetry is similar to anodic stripping voltammetry with two exceptions. First, the deposition step involves the oxidation of the Hg electrode to Hg_2^{2+}, which then reacts with the analyte to form an insoluble film at the surface of the electrode. For example, when Cl^- is the analyte the deposition step is

$$2Hg(l) + 2Cl^-(aq) \rightleftharpoons Hg_2Cl_2(s) + 2e^-$$

Second, stripping is accomplished by scanning cathodically toward a more negative potential, reducing Hg_2^{2+} back to Hg and returning the analyte to solution.

$$Hg_2Cl_2(s) + 2e^- \rightleftharpoons 2Hg(l) + 2Cl^-(aq)$$

Table 11.4.1 lists several analytes analyzed successfully by cathodic stripping voltammetry.

In adsorptive stripping voltammetry, the deposition step occurs without electrolysis. Instead, the analyte adsorbs to the electrode's surface. During deposition we maintain the electrode at a potential that enhances adsorption. For example, we can adsorb a neutral molecule on a Hg drop if we apply a potential of –0.4 V versus the SCE, a potential where the surface charge of mercury is approximately zero. When deposition is complete, we scan the potential in an anodic or a cathodic direction, depending on whether we are oxidizing or reducing the analyte. Examples of compounds that have been analyzed by absorptive stripping voltammetry also are listed in Table 11.4.1 .

Cyclic Voltammetry

In the voltammetric techniques consider to this point we scan the potential in one direction, either to more positive potentials or to more negative potentials. In ***cyclic voltammetry*** we complete a scan in both directions. Figure 11.4.14 a shows a typical potential-excitation signal. In this example, we first scan the potential to more positive values, resulting in the following oxidation reaction for the species *R*.

$$R \rightleftharpoons O + ne^-$$

When the potential reaches a predetermined switching potential, we reverse the direction of the scan toward more negative potentials. Because we generated the species *O* on the forward scan, during the reverse scan it reduces back to *R*.

$$O + ne^- \rightleftharpoons R$$

Cyclic voltammetry is carried out in an unstirred solution, which, as shown in Figure 11.4.14 b, results in peak currents instead of limiting currents. The voltammogram has separate peaks for the oxidation reaction and for the reduction reaction, each characterized by a peak potential and a peak current.

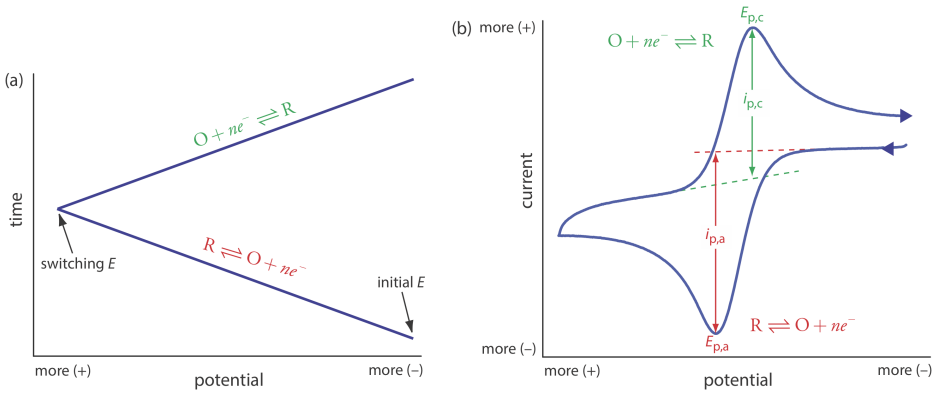

Figure 11.4.14 . Details for cyclic voltammetry. (a) One cycle of the triangular potential-excitation signal showing the initial potential and the switching potential. A cyclic voltammetry experiment can consist of one cycle or many cycles. Although the initial potential in this example is the negative switching potential, the cycle can begin with an intermediate initial potential and cycle between two limits. (b) The resulting cyclic voltammogram showing the measurement of the peak currents and peak potentials.

The peak current in cyclic voltammetry is given by the Randles-Sevcik equation

$$i_p = \left(2.69 \times 10^5\right) n^{3/2} A D^{1/2} \nu^{1/2} C_A$$

where n is the number of electrons in the redox reaction, A is the area of the working electrode, D is the diffusion coefficient for the electroactive species, ν is the scan rate, and C_A is the concentration of the electroactive species at the electrode. For a well-behaved system, the anodic and the cathodic peak currents are equal, and the ratio $i_{p,a}/i_{p,c}$ is 1.00. The half-wave potential, $E_{1/2}$, is midway between the anodic and cathodic peak potentials.

$$E_{1/2} = \frac{E_{p,a} + E_{p,c}}{2}$$

Scanning the potential in both directions provides an opportunity to explore the electrochemical behavior of species generated at the electrode. This is a distinct advantage of cyclic voltammetry over other voltammetric techniques. Figure 11.4.15 shows the cyclic voltammogram for the same redox couple at both a faster and a slower scan rate. At the faster scan rate, 11.4.15 a, we see two peaks. At the slower scan rate in Figure 11.4.15 b, however, the peak on the reverse scan disappears. One explanation for this is that the products from the reduction of R on the forward scan have sufficient time to participate in a chemical reaction whose products are not electroactive.

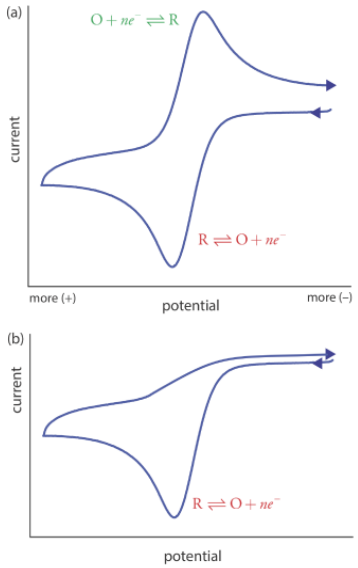

Figure 11.4.15 . Cyclic voltammograms for *R* obtained at (a) a faster scan rate and at (b) a slower scan rate. One of the principal uses of cyclic voltammetry is to study the chemical and electrochemical behavior of compounds. See this chapter's additional resources for further information.

Amperometry

The final voltammetric technique we will consider is ***amperometry***, in which we apply a constant potential to the working electrode and measure current as a function of time. Because we do not vary the potential, amperometry does not result in a voltammogram.

One important application of amperometry is in the construction of chemical sensors. One of the first amperometric sensors was developed in 1956 by L. C. Clark to measure dissolved O_2 in blood. Figure 11.4.16 shows the sensor's design, which is similar to a potentiometric membrane electrode. A thin, gas-permeable membrane is stretched across the end of the sensor and is separated from the working electrode and the counter electrode by a thin solution of KCl. The working electrode is a Pt disk cathode, and a Ag ring anode serves as the counter electrode. Although several gases can diffuse across the membrane, including O_2, N_2, and CO_2, only oxygen undergoes reduction at the cathode

$$O_2(g) + 4H_3O^+(aq) + 4e^- \rightleftharpoons 6H_2O(l)$$

with its concentration at the electrode's surface quickly reaching zero. The concentration of O_2 at the membrane's inner surface is fixed by its diffusion through the membrane, which creates a diffusion profile similar to that in Figure 11.4.8 . The result is a steady-state current that is proportional to the concentration of dissolved oxygen. Because the electrode consumes oxygen,the sample is stirred to prevent the depletion of O_2 at the membrane's outer surface.

> The oxidation of the Ag anode is the other half-reaction.
>
> $$Ag(s) + Cl^-(aq) \rightleftharpoons AgCl(s) + e^-$$

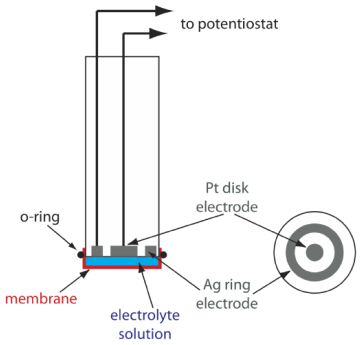

Figure 11.4.16 . Clark amperometric sensor for determining dissolved O_2. The diagram on the right is a cross-section through the electrode, which shows the Ag ring electrode and the Pt disk electrode.

Another example of an amperometric sensor is a glucose sensor. In this sensor the single membrane in Figure 11.4.16 is replaced with three membranes. The outermost membrane of polycarbonate is permeable to glucose and O_2. The second membrane contains an immobilized preparation of glucose oxidase that catalyzes the oxidation of glucose to gluconolactone and hydrogen peroxide.

$$\beta-\mathrm{D}-\text{glucose}\,(aq)+\ \mathrm{O_2}(aq)+\mathrm{H_2O}(l)\rightleftharpoons\text{gluconolactone}\,(aq)+\ \mathrm{H_2O_2}(aq)$$

The hydrogen peroxide diffuses through the innermost membrane of cellulose acetate where it undergoes oxidation at a Pt anode.

$$\mathrm{H_2O_2}(aq)+2\mathrm{OH^-}(aq)\rightleftharpoons\ \mathrm{O_2}(aq)+2\mathrm{H_2O}(l)+2e^-$$

Figure 11.4.17 summarizes the reactions that take place in this amperometric sensor. FAD is the oxidized form of flavin adenine nucleotide—the active site of the enzyme glucose oxidase—and $FADH_2$ is the active site's reduced form. Note that O_2 serves a mediator, carrying electrons to the electrode.

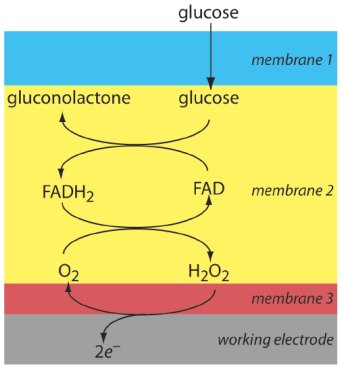

Figure 11.4.17 . Schematic showing the reactions by which an amperometric biosensor responds to glucose.

By changing the enzyme and mediator, it is easy to extend to the amperometric sensor in Figure 11.4.17 to the analysis of other analytes. For example, a CO_2 sensor has been developed using an amperometric O_2 sensor with a two-layer membrane, one of which contains an immobilized preparation of autotrophic bacteria [Karube, I.; Nomura, Y.; Arikawa, Y. *Trends in Anal. Chem.* **1995**, *14*, 295–299]. As CO_2 diffuses through the membranes it is converted to O_2 by the bacteria, increasing the concentration of O_2 at the Pt cathode.

Quantitative Applications

Voltammetry has been used for the quantitative analysis of a wide variety of samples, including environmental samples, clinical samples, pharmaceutical formulations, steels, gasoline, and oil.

Selecting the Voltammetric Technique

The choice of which voltammetric technique to use depends on the sample's characteristics, including the analyte's expected concentration and the sample's location. For example, amperometry is ideally suited for detecting analytes in flow systems, including the *in vivo* analysis of a patient's blood or as a selective sensor for the rapid analysis of a single analyte. The portability of amperometric sensors, which are similar to potentiometric sensors, also make them ideal for field studies. Although cyclic

voltammetry is used to determine an analyte's concentration, other methods described in this chapter are better suited for quantitative work.

Pulse polarography and stripping voltammetry frequently are interchangeable. The choice of which technique to use often depends on the analyte's concentration and the desired accuracy and precision. Detection limits for normal pulse polarography generally are on the order of 10^{-6} M to 10^{-7} M, and those for differential pulse polarography, staircase, and square wave polarography are between 10^{-7} M and 10^{-9} M. Because we concentrate the analyte in stripping voltammetry, the detection limit for many analytes is as little as 10^{-10} M to 10^{-12} M. On the other hand, the current in stripping voltammetry is much more sensitive than pulse polarography to changes in experimental conditions, which may lead to poorer precision and accuracy. We also can use pulse polarography to analyze a wider range of inorganic and organic analytes because there is no need to first deposit the analyte at the electrode surface.

Stripping voltammetry also suffers from occasional interferences when two metals, such as Cu and Zn, combine to form an intermetallic compound in the mercury amalgam. The deposition potential for Zn . is sufficiently negative that any Cu^{2+} in the sample also deposits into the mercury drop or film, leading to the formation of intermetallic compounds such as CuZn and $CuZn_2$. During the stripping step, zinc in the intermetallic compounds strips at potentials near that of copper, decreasing the current for zinc at its usual potential and increasing the apparent current for copper. It is possible to overcome this problem by adding an element that forms a stronger intermetallic compound with the interfering metal. Thus, adding Ga^{3+} minimizes the interference of Cu when analyzing for Zn by forming an intermetallic compound of Cu and Ga.

Correcting the Residual Current

In any quantitative analysis we must correct the analyte's signal for signals that arise from other sources. The total current, i_{tot}, in voltammetry consists of two parts: the current from the analyte's oxidation or reduction, i_A, and a background or residual current, i_r.

$$i_{tot} = i_A + i_r$$

The residual current, in turn, has two sources. One source is a faradaic current from the oxidation or reduction of trace interferents in the sample, i_{int}. The other source is the charging current, i_{ch}, that accompanies a change in the working electrode's potential.

$$i_r = i_{\text{int}} + i_{ch}$$

We can minimize the faradaic current due to impurities by carefully preparing the sample. For example, one important impurity is dissolved O_2, which undergoes a two-step reduction: first to H_2O_2 at a potential of –0.1 V versus the SCE, and then to H_2O at a potential of –0.9 V versus the SCE. Removing dissolved O_2 by bubbling an inert gas such as N_2 through the sample eliminates this interference. After removing the dissolved O_2, maintaining a blanket of N_2 over the top of the solution prevents O_2 from reentering the solution.

> The cell in Figure 11.4.4 shows a typical N_2 purge line.

There are two methods to compensate for the residual current. One method is to measure the total current at potentials where the analyte's faradaic current is zero and extrapolate it to other potentials. This is the method shown in Figure 11.4.9 . One advantage of extrapolating is that we do not need to acquire additional data. An important disadvantage is that an extrapolation assumes that any change in the residual current with potential is predictable, which may not be the case. A second, and more rigorous approach, is to obtain a voltammogram for an appropriate blank. The blank's residual current is then subtracted from the sample's total current.

Analysis for Single Components

The analysis of a sample with a single analyte is straightforward using any of the standardization methods discussed in Chapter 5.

Example 11.4.1

The concentration of As(III) in water is determined by differential pulse polarography in 1 M HCl. The initial potential is set to –0.1 V versus the SCE and is scanned toward more negative potentials at a rate of 5 mV/s. Reduction of As(III) to As(0) occurs at a potential of approximately –0.44 V versus the SCE. The peak currents for a set of standard solutions, corrected for the residual current, are shown in the following table.

[As(III)] (μM)	i_p (μM)
1.00	0.298
3.00	0.947
6.00	1.83
9.00	2.72

What is the concentration of As(III) in a sample of water if its peak current is 1.37 μA?

Solution

Linear regression gives the calibration curve shown in Figure 11.4.18 , with an equation of

$$i_p = 0.0176 + 3.01 \times [\text{As(III)}]$$

Substituting the sample's peak current into the regression equation gives the concentration of As(III) as 4.49 μM.

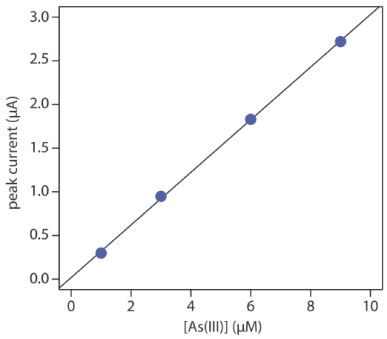

Figure 11.4.18 . Calibration curve for the data in Example 11.4.1 .

? Exercise 11.4.1

The concentration of copper in a sample of sea water is determined by anodic stripping voltammetry using the method of standard additions. The analysis of a 50.0-mL sample gives a peak current of 0.886 μA. After adding a 5.00-μL spike of 10.0 mg/L Cu^{2+}, the peak current increases to 2.52 μA. Calculate the μg/L copper in the sample of sea water.

Answer

For anodic stripping voltammetry, the peak current, i_p, is a linear function of the analyte's concentration

$$i_p = K \times C_{\text{Cu}}$$

where K is a constant that accounts for experimental parameters such as the electrode's area, the diffusion coefficient for Cu^{2+}, the deposition time, and the rate of stirring. For the analysis of the sample before the standard addition we know that the current is

$$i_p = 0.886\ \mu\text{A} = K \times C_{\text{Cu}}$$

and after the standard addition the current is

$$i_p = 2.52\ \mu\text{A} = K \left\{ C_{\text{Cu}} \times \frac{50.00\ \text{mL}}{50.005\ \text{mL}} + \frac{10.00\text{mgCu}}{\text{L}} \times \frac{0.005\ \text{mL}}{50.005\ \text{mL}} \right\}$$

where 50.005 mL is the total volume after we add the 5.00 μL spike. Solving each equation for K and combining leaves us with the following equation.

$$\frac{0.886\ \mu\text{A}}{C_{\text{Cu}}} = K = \frac{2.52\ \mu\text{A}}{C_{\text{Cu}} \times \frac{50.00\ \text{mL}}{50.005\ \text{mL}} + \frac{10.00\ \text{mg Cu}}{\text{L}} \times \frac{0.005\ \text{mL}}{50.005\ \text{mL}}}$$

Solving this equation for C_{Cu} gives its value as 5.42×10^{-4} mg Cu^{2+}/L, or 0.542 μg Cu^{2+}/L.

Multicomponent Analysis

Voltammetry is a particularly attractive technique for the analysis of samples that contain two or more analytes. Provided that the analytes behave independently, the voltammogram of a multicomponent mixture is a summation of each analyte's individual voltammograms. As shown in Figure 11.4.19 , if the separation between the half-wave potentials or between the peak potentials is sufficient, we can determine the presence of each analyte as if it is the only analyte in the sample. The minimum separation between the half-wave potentials or peak potentials for two analytes depends on several factors, including the type of electrode and the potential-excitation signal. For normal polarography the separation is at least ±0.2–0.3 V, and differential pulse voltammetry requires a minimum separation of ±0.04–0.05 V.

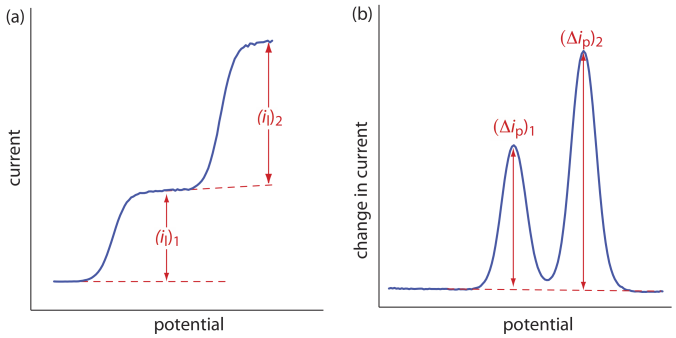

Figure 11.4.19 . Voltammograms for a sample that contains two analytes showing the measurement of (a) limiting currents, and (b) peak currents.

If the voltammograms for two analytes are not sufficiently separated, a simultaneous analysis may be possible. An example of this approach is outlined the following example.

Example 11.4.2

The differential pulse polarographic analysis of a mixture of indium and cadmium in 0.1 M HCl is complicated by the overlap of their respective voltammograms [Lanza P. *J. Chem. Educ.* **1990**, *67*, 704–705]. The peak potential for indium is at –0.557 V and that for cadmium is at –0.597 V. When a 0.800-ppm indium standard is analyzed, Δi_p (in arbitrary units) is 200.5 at –0.557 V and 87.5 at –0.597 V relative to a saturated Ag/AgCl reference electorde. A standard solution of 0.793 ppm cadmium has a Δi_p of 58.5 at –0.557 V and 128.5 at –0.597 V. What is the concentration of indium and cadmium in a sample if Δi_p is 167.0 at a potential of –0.557 V and 99.5 at a potential of –0.597V.

Solution

The change in current, Δi_p, in differential pulse polarography is a linear function of the analyte's concentration

$$\Delta i_p = k_A C_A$$

where k_A is a constant that depends on the analyte and the applied potential, and C_A is the analyte's concentration. To determine the concentrations of indium and cadmium in the sample we must first find the value of k_A for each analyte at each potential. For simplicity we will identify the potential of –0.557 V as E_1, and that for –0.597 V as E_2. The values of k_A are

$$k_{\text{In},E_1} = \frac{200.5}{0.800 \text{ ppm}} = 250.6 \text{ ppm}^{-1}$$

$$k_{\text{In},E_2} = \frac{87.5}{0.800 \text{ ppm}} = 109.4 \text{ ppm}^{-1}$$

$$k_{\text{Cd}E_1} = \frac{58.5}{0.793 \text{ ppm}} = 73.8 \text{ ppm}^{-1}$$

$$k_{\text{Cd}E_2} = \frac{128.5}{0.793 \text{ ppm}} = 162.0 \text{ ppm}^{-1}$$

Next, we write simultaneous equations for the current at the two potentials.

$$\Delta i_{E_1} = 167.0 = 250.6 \text{ ppm}^{-1} \times C_{\text{In}} + 73.8 \text{ ppm}^{-1} \times C_{\text{Cd}}$$
$$\triangle i_{E_2} = 99.5 = 109.4 \text{ ppm}^{-1} \times C_{\text{In}} + 162.0 \text{ ppm}^{-1} \times C_{\text{Cd}}$$

Solving the simultaneous equations, which is left as an exercise, gives the concentration of indium as 0.606 ppm and the concentration of cadmium as 0.205 ppm.

Environmental Samples

Voltammetry is one of several important analytical techniques for the analysis of trace metals in environmental samples, including groundwater, lakes, rivers and streams, seawater, rain, and snow. Detection limits at the parts-per-billion level are routine for many trace metals using differential pulse polarography, with anodic stripping voltammetry providing parts-per-trillion detection limits for some trace metals.

One interesting environmental application of anodic stripping voltammetry is the determination of a trace metal's chemical form within a water sample. Speciation is important because a trace metal's bioavailability, toxicity, and ease of transport through the environment often depends on its chemical form. For example, a trace metal that is strongly bound to colloidal particles generally is not toxic because it is not available to aquatic lifeforms. Unfortunately, anodic stripping voltammetry can not distinguish a trace metal's exact chemical form because closely related species, such as Pb^{2+} and $PbCl^{+}$, produce a single stripping peak. Instead, trace metals are divided into "operationally defined" categories that have environmental significance.

Operationally defined means that an analyte is divided into categories by the specific methods used to isolate it from the sample. There are many examples of operational definitions in the environmental literature. The distribution of trace metals in soils and sediments, for example, often is defined in terms of the reagents used to extract them; thus, you might find an operational definition for Zn^{2+} in a lake sediment as that extracted using 1.0 M sodium acetate, or that extracted using 1.0 M HCl.

Although there are many speciation schemes in the environmental literature, we will consider one proposed by Batley and Florence [see (a) Batley, G. E.; Florence, T. M. *Anal. Lett.* **1976**, *9*, 379–388; (b) Batley, G. E.; Florence, T. M. *Talanta* **1977**, *24*, 151–158; (c) Batley, G. E.; Florence, T. M. *Anal. Chem.* **1980**, *52*, 1962–1963; (d) Florence, T. M., Batley, G. E.; *CRC Crit. Rev. Anal. Chem.* **1980**, *9*, 219–296]. This scheme, which is outlined in Table 11.4.2 , combines anodic stripping voltammetry with ion-exchange and UV irradiation, dividing soluble trace metals into seven groups. In the first step, anodic stripping voltammetry in a pH 4.8 acetic acid buffer differentiates between labile metals and nonlabile metals. Only labile metals—those present as hydrated ions, weakly bound complexes, or weakly adsorbed on colloidal surfaces—deposit at the electrode and give rise to a signal. Total metal concentration are determined by ASV after digesting the sample in 2 M HNO_3 for 5 min, which converts all metals into an ASV-labile form.

Table 11.4.2 . Operational Speciation of Soluble Trace Metals

method	speciation of soluble metals						
ASV	labile metals			nonlabile or bound metals			
Ion-Exchange	removed	not removed		removed		not removed	
UV Irradiation		released	not released	released	not released	released	not released
Groups	I	II	III	IV	V	VI	VII
Group I: free metal ions; weaker labile organic complexes and inorganic complexes							
Group II: stronger labile organic complexes; labile metals absorbed on organic solids							
Group III: stronger labile inorganic complexes; labile metals absorbed on inorganic solids							
Group IV: weaker nonlabile organic complexes							
Group V: weaker nonlabile inorganic complexes							
Group VI: stronger nonlabile organic complexes; nonlabile metals absorbed on organic solids							
Group VII: stronger nonlabile inorganic complexes; nonlabile metals absorbed on inorganic solids							

method	speciation of soluble metals

Operational definitions of speciation from (a)Batley,G.E.;Florence,T.M.*Anal.Lett.***1976**,*9*,379–388; (b)Batley,G.E.;Florence,T.M.*Talanta***1977**,*24*,151–158; (c) Batley, G. E.; Florence, T. M. *Anal. Chem.* **1980**, *52*, 1962–1963; (d) Florence, T. M., Batley, G. E.; *CRC Crit. Rev. Anal. Chem.* **1980**, *9*, 219–296.

A Chelex-100 ion-exchange resin further differentiates between strongly bound metals—usually metals bound to inorganic and organic solids, but also those tightly bound to chelating ligands—and more loosely bound metals. Finally, UV radiation differentiates between metals bound to organic phases and inorganic phases. The analysis of seawater samples, for example, suggests that cadmium, copper, and lead are present primarily as labile organic complexes or as labile adsorbates on organic colloids (Group II in Table 11.4.2).

Differential pulse polarography and stripping voltammetry are used to determine trace metals in airborne particulates, incinerator fly ash, rocks, minerals, and sediments. The trace metals, of course, are first brought into solution using a digestion or an extraction.

Amperometric sensors also are used to analyze environmental samples. For example, the dissolved O_2 sensor described earlier is used to determine the level of dissolved oxygen and the biochemical oxygen demand, or BOD, of waters and wastewaters. The latter test—which is a measure of the amount of oxygen required by aquatic bacteria as they decompose organic matter—is important when evaluating the efficiency of a wastewater treatment plant and for monitoring organic pollution in natural waters. A high BOD suggests that the water has a high concentration of organic matter. Decomposition of this organic matter may seriously deplete the level of dissolved oxygen in the water, adversely affecting aquatic life. Other amperometric sensors are available to monitor anionic surfactants in water, and CO_2, H_2SO_4, and NH_3 in atmospheric gases.

Clinical Samples

Differential pulse polarography and stripping voltammetry are used to determine the concentration of trace metals in a variety of clinical samples, including blood, urine, and tissue. The determination of lead in blood is of considerable interest due to concerns about lead poisoning. Because the concentration of lead in blood is so small, anodic stripping voltammetry frequently is the more appropriate technique. The analysis is complicated, however, by the presence of proteins that may adsorb to the mercury electrode, inhibiting either the deposition or stripping of lead. In addition, proteins may prevent the electrodeposition of lead through the formation of stable, nonlabile complexes. Digesting and ashing the blood sample mini- mizes this problem. Differential pulse polarography is useful for the routine quantitative analysis of drugs in biological fluids, at concentrations of less than 10^{-6} M [Brooks, M. A. “Application of Electrochemistry to Pharmaceutical Analysis,” Chapter 21 in Kissinger, P. T.; Heinemann, W. R., eds. *Laboratory Techniques in Electroanalytical Chemistry*, Marcel Dekker, Inc.: New York, 1984, pp 539–568.]. Amperometric sensors using enzyme catalysts also have many clinical uses, several examples of which are shown in Table 11.4.3 .

Table 11.4.3 . Representative Amperometric Biosensors

analyte	enzyme	species detected
choline	choline oxidase	H_2O_2
ethanol	alcohol oxidase	H_2O_2
formaldehyde	formaldehyde dehydrogenase	NADH
glucose	glucose oxidase	H_2O_2
glutamine	glutaminase, glutamine oxidase	H_2O_2
glycerol	glycerol dehydrogenase	NADH, O_2
lactate	lactate oxidase	H_2O_2
phenol	polyphenol oxidase	quinone
inorganic phosphorous	nucleoside phosphoylase	O_2

Source: Cammann, K.; Lemke, U.; Rohen, A.; Sander, J.; Wilken, H.; Winter, B. *Angew. Chem. Int. Ed. Engl.* **1991**, *30*, 516–539.

Miscellaneous Samples

In addition to environmental samples and clinical samples, differential pulse polarography and stripping voltammetry are used for the analysis of trace metals in other sample, including food, steels and other alloys, gasoline, gunpowder residues, and pharmaceuticals. Voltammetry is an important technique for the quantitative analysis of organics, particularly in the pharmaceutical industry where it is used to determine the concentration of drugs and vitamins in formulations. For example, voltammetric methods are available for the quantitative analysis of vitamin A, niacinamide, and riboflavin. When the compound of interest is not electroactive, it often can be derivatized to an electroactive form. One example is the differential pulse polarographic determination of sulfanilamide, which is converted into an electroactive azo dye by coupling with sulfamic acid and 1-napthol.

Representative Method 11.4.1: Determination of Chloropromazine in a Pharmaceutical Product

The best way to appreciate the theoretical and the practical details discussed in this section is to carefully examine a typical analytical method. Although each method is unique, the following description of the determination of chloropromazine in a pharmaceutical product provides an instructive example of a typical procedure. The description here is based on a method from Pungor, E. *A Practical Guide to Instrumental Analysis*, CRC Press: Boca Raton, FL, 1995, pp. 34–37.

Description of Method

Chlorpromazine, also is known by its trade name Thorazine, is an antipsychotic drug used in the treatment of schizophrenia. The amount of chlorpromazine in a pharmaceutical product is determined voltammetrically at a graphite working electrode in a unstirred solution, with calibration by the method of standard additions.

Procedure

Add 10.00 mL of an electrolyte solution consisting of 0.01 M HCl and 0.1 M KCl to the electrochemical cell. Place a graphite working electrode, a Pt auxiliary electrode, and a SCE reference electrode in the cell, and record the voltammogram from 0.2 V to 2.0 V at a scan rate of 50 mV/s. Weigh out an appropriate amount of the pharmaceutical product and dissolve it in a small amount of the electrolyte. Transfer the solution to a 100-mL volumetric flask and dilute to volume with the electrolyte. Filter a small amount of the diluted solution and transfer 1.00 mL of the filtrate to the voltammetric cell. Mix the contents of the voltammetric cell and allow the solution to sit for 10 s before recording the voltammogram. Return the potential to 0.2 V, add 1.00 mL of a chlorpromazine standard and record the voltammogram. Report the %w/w chlorpromazine in the formulation.

Questions

1. Is chlorpromazine undergoing oxidation or reduction at the graphite working electrode?

    Because we are scanning toward more positive potentials, we are oxidizing chlorpromazine.

2. Why does this procedure use a graphite electrode instead of a Hg electrode?

    As shown in Figure 11.4.2 , the potential window for a Hg electrode extends from approximately –0.3 V to between –1V and –2 V, de- pending on the pH. Because we are scanning the potential from 0.2 V to 2.0 V, we cannot use a Hg electrode.

3. Many voltammetric procedures require that we first remove dissolved O_2 by bubbling N_2 through the solution. Why is this not necessary for this analysis?

    Dissolved O_2 is a problem when we scan toward more negative potentials, because its reduction may produce a significant cathodic current. In this procedure we are scanning toward more positive potentials and generating anodic currents; thus, dissolved O_2 is not an interferent and does not need to be removed.

4. What is the purpose of recording a voltammogram in the absence of chlorpromazine?

    This voltammogram serves as a blank, which provides a measurement of the residual current due to the electrolyte. Because the potential window for a graphite working electrode (see Figure 11.4.2) does not extend to 2.0 V, there is a measurable anodic residual current due to the solvent's oxidation. Having measured this residual current, we can subtract it from the total current in the presence of chlorpromazine.

5. Based on the description of this procedure, what is the shape of the resulting voltammogram. You may wish to review the three common shapes shown in Figure 11.4.9 .

    Because the solution is unstirred, the voltammogram will have a peak current similar to that shown in Figure 11.4.9 b.

Characterization Applications

In the previous section we learned how to use voltammetry to determine an analyte's concentration in a variety of different samples. We also can use voltammetry to characterize an analyte's properties, including verifying its electrochemical reversibility, determining the number of electrons transferred during its oxidation or reduction, and determining its equilibrium constant in a coupled chemical reaction.

Electrochemical Reversibility and Determination of *n*

Earlier in this chapter we derived a relationship between $E_{1/2}$ and the standard-state potential for a redox couple (Equation 2.4.9), noting that a redox reaction must be electrochemically reversible. How can we tell if a redox reaction is reversible by looking at its voltammogram? For a reversible redox reaction Equation 2.4.8, which we repeat here, describes the relationship between potential and current for a voltammetric experiment with a limiting current.

$$E = E^{\circ}_{O/R} - \frac{0.05916}{n}\log\frac{K_O}{K_R} - \frac{0.05916}{n}\log\frac{i}{i_l - i}$$

If a reaction is electrochemically reversible, a plot of E versus $\log(i/i_l - i)$ is a straight line with a slope of –0.05916/n. In addition, the slope should yield an integer value for n.

Example 11.4.3

The following data were obtained from a linear scan hydrodynamic voltammogram of a reversible reduction reaction.

E (V vs. SCE)	current (μA)
–0.358	0.37
–0.372	0.95
–0.382	1.71
–0.400	3.48
–0.410	4.20
–0.435	4.97

The limiting current is 5.15 μA. Show that the reduction reaction is reversible, and determine values for n and for $E_{1/2}$.

Solution

Figure 11.4.20 shows a plot of E versus $\log(i/i_l - i)$. Because the result is a straight-line, we know the reaction is electrochemically reversible under the conditions of the experiment. A linear regression analysis gives the equation for the straight line as

$$E = -0.391\text{V} - 0.0300\log\frac{i}{i_l - i}$$

From Equation 2.4.8, the slope is equivalent to –0.05916/n; solving for n gives a value of 1.97, or 2 electrons. From Equation 2.4.8 and Equation 2.4.9, we know that $E_{1/2}$ is the y-intercept for a plot of E versus $\log(i/i_l - i)$; thus, $E_{1/2}$ for the data in this example is –0.391 V versus the SCE.

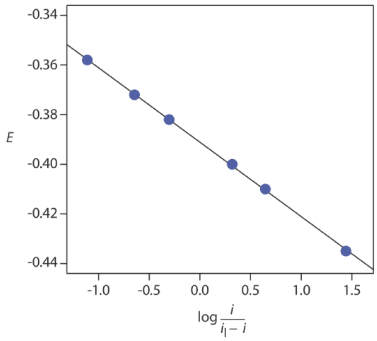

Figure 11.4.20 . Determination of electrochemical reversibility for the data in Example 11.4.3 .

We also can use cyclic voltammetry to evaluate electrochemical reversibility by looking at the difference between the peak potentials for the anodic and the cathodic scans. For an electrochemically reversible reaction, the following equation holds true.

$$\Delta E_p = E_{p,a} - E_{p,c} = \frac{0.05916 \text{ V}}{n}$$

As an example, for a two-electron reduction we expect a ΔE_p of approximately 29.6 mV. For an electrochemically irreversible reaction the value of ΔE_p is larger than expected.

Determining Equilibrium Constants for Coupled Chemical Reactions

Another important application of voltammetry is determining the equilibrium constant for a solution reaction that is coupled to a redox reaction. The presence of the solution reaction affects the ease of electron transfer in the redox reaction, shifting $E_{1/2}$ to a more negative or to a more positive potential. Consider, for example, the reduction of *O* to R

$$O + ne^- \rightleftharpoons R$$

the voltammogram for which is shown in Figure 11.4.21 . If we introduce a ligand, *L*, that forms a strong complex with *O*, then we also must consider the reaction

$$O + pL \rightleftharpoons OL_p$$

In the presence of the ligand, the overall redox reaction is

$$OL_p + ne^- \rightleftharpoons R + pL$$

Because of its stability, the reduction of the OL_p complex is less favorable than the reduction of *O*. As shown in Figure 11.4.21 , the resulting voltammogram shifts to a potential that is more negative than that for *O*. Furthermore, the shift in the voltammogram increases as we increase the ligand's concentration.

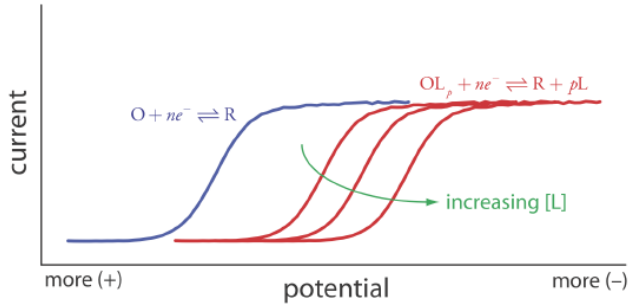

Figure 11.4.21 . Effect of a metal-ligand complexation reaction on a voltammogram. The voltammogram in blue is for the reduction of *O* in the absence of ligand. Adding the ligand shifts the potentials to more negative potentials, as shown by the voltammograms in red.

We can use this shift in the value of $E_{1/2}$ to determine both the stoichiometry and the formation constant for a metal-ligand complex. To derive a relationship between the relevant variables we begin with two equations: the Nernst equation for the reduction of *O*

$$E = E^{\circ}_{O/R} - \frac{0.05916}{n} \log \frac{[R]_{x=0}}{[O]_{x=0}} \tag{2.4.10}$$

and the stability constant, β_p for the metal-ligand complex at the electrode surface.

$$\beta_p = \frac{[OL_p]_{x=0}}{[O]_{x=0}[L]^p_{x=0}} \tag{2.4.11}$$

In the absence of ligand the half-wave potential occurs when $[R]_{x = 0}$ and $[O]_{x = 0}$ are equal; thus, from the Nernst equation we have

$$\left(E_{1/2}\right)_{nc} = E^{\circ}_{O/R} \tag{2.4.12}$$

where the subscript "*nc*" signifies that the complex is not present.

When ligand is present we must account for its effect on the concentration of *O*. Solving Equation 2.4.1 for $[O]_{x = 0}$ and substituting into the Equation 2.4.10 gives

$$E = E^{\circ}_{O/R} - \frac{0.05916}{n} \log \frac{[R]_{x=0}[L]^p_{x=0}\beta_p}{[OL_p]_{x=0}} \tag{2.4.13}$$

If the formation constant is sufficiently large, such that essentially all *O* is present as the complex OL_p, then $[R]_{x = 0}$ and $[OL_p]_{x = 0}$ are equal at the half-wave potential, and Equation 2.4.13 simplifies to

$$\left(E_{1/2}\right)_{c} = E^{\circ}_{O/R} - \frac{0.05916}{n} \log [L]^p_{x=0}\beta_p \tag{2.4.14}$$

where the subscript "*c*" indicates that the complex is present. Defining $\Delta E_{1/2}$ as

$$\triangle E_{1/2} = \left(E_{1/2}\right)_{c} - \left(E_{1/2}\right)_{nc} \tag{2.4.15}$$

and substituting Equation 2.4.12 and Equation 2.4.14 and expanding the log term leaves us with the following equation.

$$\Delta E_{1/2} = -\frac{0.05916}{n} \log \beta_p - \frac{0.05916p}{n} \log [L] \tag{2.4.16}$$

A plot of $\Delta E_{1/2}$ versus log[L] is a straight-line, with a slope that is a function of the metal-ligand complex's stoichiometric coefficient, *p*, and a *y*-intercept that is a function of its formation constant β_p.

Example 11.4.4

A voltammogram for the two-electron reduction (n = 2) of a metal, *M*, has a half-wave potential of –0.226 V versus the SCE. In the presence of an excess of ligand, *L*, the following half-wave potentials are recorded.

[L] (M)	$(E_{1/2})_c$ (V vs. SCE)
0.020	–0.494
0.040	–0.512
0.060	–0.523
0.080	–0.530
0.100	–0.536

Determine the stoichiometry of the metal-ligand complex and its formation constant.

Solution

We begin by calculating values of $\Delta E_{1/2}$ using Equation 2.4.15, obtaining the values in the following table.

[L] (M)	$\Delta E_{1/2}$ (V vs. SCE)
0.020	–0.268

[L] (M)	$\Delta E_{1/2}$ (V vs. SCE)
0.040	–0.286
0.020	–0.268
0.080	–0.304
0.040	–0.286
0.100	–0.310
0.060	–0.297
0.080	–0.304
0.100	–0.310

Figure 11.4.22 shows the resulting plot of $\Delta E_{1/2}$ as a function of log[L]. A linear regression analysis gives the equation for the straight line as

$$\triangle E_{1/2} = -0.370\text{V} - 0.0601 \log [L]$$

From Equation 2.4.16 we know that the slope is equal to –0.05916p/n. Using the slope and n = 2, we solve for p obtaining a value of 2.03 ≈ 2. The complex's stoichiometry, therefore, is ML_2. We also know, from Equation 2.4.16, that the y-intercept is equivalent to –(0.05916/n)logβ_p. Solving for β_2 gives a formation constant of 3.2×10^{12}.

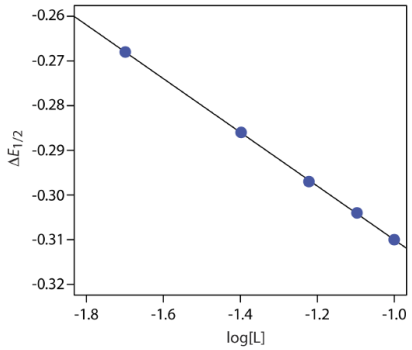

Figure 11.4.22 . Determination of the stoichiometry and formation constant for a metal-ligand complex using the data in Example 11.4.4 .

Exercise 11.4.2

The voltammogram for 0.50 mM Cd^{2+} has an $E_{1/2}$ of –0.565 V versus an SCE. After making the solution 0.115 M in ethylenediamine, $E_{1/2}$ is –0.845 V, and $E_{1/2}$ is –0.873 V when the solution is 0.231 M in ethylenediamine. Determine the stoichiometry of the Cd^{2+}–ethylenediamine complex and its formation constant. The data in this problem comes from Morinaga, K. "Polarographic Studies of Metal Complexes. V. Ethylenediamine Complexes of Cadmium, Nickel, and Zinc," *Bull. Chem. Soc. Japan* **1956**, *29*, 793–799.

Answer

For simplicity, we will use *en* as a shorthand notation for ethylenediamine. From the three half-wave potentials we have a $\Delta E_{1/2}$ of –0.280 V for 0.115 M en and a $\Delta E_{1/2}$ of –0.308 V for 0.231 M en. Using Equation 2.4.16 we write the following two equations.

$$-0.280 = -\frac{0.05916}{2}\log \beta_p - \frac{0.05916p}{2}\log(0.115)$$
$$-0.308 = -\frac{0.05916}{2}\log \beta_p - \frac{0.05916p}{2}\log(0.231)$$

To solve for the value of p, we first subtract the second equation from the first equation

$$0.028 = -\frac{0.05916p}{2}\log(0.115) - \left\{-\frac{0.05916p}{2}\log(0.231)\right\}$$

which eliminates the term with β_p. Next we solve this equation for p

$$0.028 = \left(2.778 \times 10^{-2}\right) \times p - \left(1.882 \times 10^{-2}\right) \times p = \left(8.96 \times 10^{-3}\right) \times p$$

obtaining a value of 3.1, or $p \approx 3$. Thus, the complex is $Cd(en)_3$. To find the formation complex, β_3, we return to Equation 2.4.16, using our value for p. Using the data for an en concentration of 0.115 M

$$-0.280 = -\frac{0.05916}{2}\log\beta_3 - \frac{0.05916 \times 3}{2}\log(0.115)$$

$$-0.363 = -\frac{0.05916}{2}\log\beta_3$$

gives a value for β_3 of 1.92×10^{12}. Using the data for an en concentration of 0.231 M gives a value of 2.10×10^{12}.

As suggested by Figure 11.4.15 , cyclic voltammetry is one of the most powerful electrochemical techniques for exploring the mechanism of coupled electrochemical and chemical reactions. The treatment of this aspect of cyclic voltammetry is beyond the level of this text, although you can consult this chapter's additional resources for additional information.

Evaluation

Scale of Operation

Detection levels at the parts-per-million level are routine. For some analytes and for some voltammetric techniques, lower detection limits are possible. Detection limits at the parts-per-billion and the part-per-trillion level are possible with stripping voltammetry. Although most analyses are carried out in conventional electrochemical cells using macro samples, the availability of microelectrodes with diameters as small as 2 μm, allows for the analysis of samples with volumes under 50 μL. For example, the concentration of glucose in 200-μm pond snail neurons was monitored successfully using an amperometric glucose electrode with a 2 mm tip [Abe, T.; Lauw, L. L.; Ewing, A. G. *J. Am. Chem. Soc.* **1991**, *113*, 7421–7423].

Accuracy

The accuracy of a voltammetric analysis usually is limited by our ability to correct for residual currents, particularly those due to charging. For an analyte at the parts-per-million level, an accuracy of ±1–3% is routine. Accuracy decreases for samples with significantly smaller concentrations of analyte.

Precision

Precision generally is limited by the uncertainty in measuring the limiting current or the peak current. Under most conditions, a precision of ±1–3% is reasonable. One exception is the analysis of ultratrace analytes in complex matrices by stripping voltammetry, in which the precision may be as poor as ±25%.

Sensitivity

In many voltammetric experiments, we can improve the sensitivity by adjusting the experimental conditions. For example, in stripping voltammetry we can improve sensitivity by increasing the deposition time, by increasing the rate of the linear potential scan, or by using a differential-pulse technique. One reason that potential pulse techniques are popular is that they provide an improvement in current relative to a linear potential scan.

Selectivity

Selectivity in voltammetry is determined by the difference between half-wave potentials or peak potentials, with a minimum difference of ±0.2–0.3 V for a linear potential scan and ±0.04–0.05 V for differential pulse voltammetry. We often can improve selectivity by adjusting solution conditions. The addition of a complexing ligand, for example, can substantially shift the potential where a species is oxidized or reduced to a potential where it no longer interferes with the determination of an analyte. Other solution parameters, such as pH, also can be used to improve selectivity.

Time, Cost, and Equipment

Commercial instrumentation for voltammetry ranges from <$1000 for simple instruments to >$20,000 for a more sophisticated instrument. In general, less expensive instrumentation is limited to linear potential scans. More expensive instruments provide for more complex potential-excitation signals using potential pulses. Except for stripping voltammetry, which needs a long deposition time, voltammetric analyses are relatively rapid.

2.5: Problems

1. Identify the anode and the cathode for the following electrochemical cells, and identify the oxidation or the reduction reaction at each electrode.

(a) Pt| $FeCl_2$ (*aq*, 0.015), $FeCl_3$ (*aq*, 0.045) || $AgNO_3$ (*aq*, 0.1) | Ag

(b) Ag | AgBr(*s*), NaBr (*aq*, 1.0) || $CdCl_2$ (*aq*, 0.05) | Cd

(c) Pb | $PbSO_4$ (*s*), H_2SO_4 (*aq*, 1.5) || H_2SO_4 (*aq*, 2.0), $PbSO_4$ (*s*) | PbO_2

2. Calculate the potential for each electrochemical cell in problem 1. The values in parentheses are the activities of the associated species.

3. Calculate the activity of KI, *x*, in the following electrochemical cell if the potential is +0.294 V.

$$\text{Ag | AgCl (}s\text{), NaCl (}aq\text{, 0.1) || KI (aq, }x\text{), I}_2\text{ (}s\text{) | Pt}$$

4. What reaction prevents us from using Zn as an electrode of the first kind in an acidic solution? Which other metals do you expect to behave in the same manner as Zn when immersed in an acidic solution?

5. Creager and colleagues designed a salicylate ion-selective electrode using a PVC membrane impregnated with tetraalkylammonium salicylate [Creager, S. E.; Lawrence, K. D.; Tibbets, C. R. *J. Chem. Educ.* **1995**, *72*, 274–276]. To determine the ion-selective electrode's selectivity coefficient for benzoate, they prepared a set of salicylate calibration standards in which the concentration of benzoate was held constant at 0.10 M. Using the following data, determine the value of the selectivity coefficient.

[salicylate] (M)	potential (mV)
1.0	20.2
1.0×10^{-1}	73.5
1.0×10^{-2}	126
1.0×10^{-3}	168
1.0×10^{-4}	182
1.0×10^{-5}	182
1.0×10^{-6}	177

What is the maximum acceptable concentration of benzoate if you plan to use this ion-selective electrode to analyze a sample that contains as little as 10^{-5} M salicylate with an accuracy of better than 1%?

6. Watanabe and co-workers described a new membrane electrode for the determination of cocaine, a weak base alkaloid with a pK_a of 8.64 [Watanabe, K.; Okada, K.; Oda, H.; Furuno, K.; Gomita, Y.; Katsu, T. *Anal. Chim. Acta* **1995**, *316*, 371–375]. The electrode's response for a fixed concentration of cocaine is independent of pH in the range of 1–8, but decreases sharply above a pH of 8. Offer an explanation for this pH dependency.

7. Figure 11.2.14 shows a schematic diagram for an enzyme electrode that responds to urea by using a gas-sensing NH_3 electrode to measure the amount of ammonia released following the enzyme's reaction with urea. In turn, the NH_3 electrode uses a pH electrode to monitor the change in pH due to the ammonia. The response of the urea electrode is given by equation 11.2.12. Beginning with equation 11.2.19, which gives the potential of a pH electrode, show that equation 11.2.12 for the urea electrode is correct.

8. Explain why the response of an NH_3-based urea electrode (Figure 11.2.14 and equation 11.2.12) is different from the response of a urea electrode in which the enzyme is coated on the glass membrane of a pH electrode (Figure 11.2.15 and equation 11.2.13).

9. A potentiometric electrode for HCN uses a gas-permeable membrane, a buffered internal solution of 0.01 M $KAg(CN)_2$, and a Ag_2S ISE electrode that is immersed in the internal solution. Consider the equilibrium reactions that take place within the internal solution and derive an equation that relates the electrode's potential to the concentration of HCN in the sample. To check your work, search on-line for US Patent 3859191 and consult Figure 2.

10. Mifflin and associates described a membrane electrode for the quantitative analysis of penicillin in which the enzyme penicillinase is immobilized in a polyacrylamide gel coated on the glass membrane of a pH electrode [Mifflin, T. E.; Andriano, K. M.; Robbins, W. B. *J. Chem. Educ.* **1984**, *61*, 638–639]. The following data were collected using a set of penicillin standards.

[penicillin] (M)	potential (mV)
1.0×10^{-2}	220
2.0×10^{-3}	204
1.0×10^{-3}	190
2.0×10^{-4}	153
1.0×10^{-4}	135
1.0×10^{-5}	96
1.0×10^{-6}	80

(a) Over what range of concentrations is there a linear response?

(b) What is the calibration curve's equation for this concentration range?

(c) What is the concentration of penicillin in a sample that yields a potential of 142 mV?

11. An ion-selective electrode can be placed in a flow cell into which we inject samples or standards. As the analyte passes through the cell, a potential spike is recorded instead of a steady-state potential. The concentration of K^+ in serum has been determined in this fashion using standards prepared in a matrix of 0.014 M NaCl [Meyerhoff, M. E.; Kovach, P. M. *J. Chem. Educ.* **1983**, *9*, 766–768].

$[K^+]$ (mM)	*E* (arb. units)	$[K^+]$ (mM)	*E* (arb. units)
0.10	25.5	0.60	58.7
0.20	37.2	0.80	64.0
0.40	50.8	1.00	66.8

A 1.00-mL sample of serum is diluted to volume in a 10-mL volumetric flask and analyzed, giving a potential of 51.1 (arbitrary units). Report the concentration of K^+ in the sample of serum.

12. Wang and Taha described an interesting application of potentiometry, which they call batch injection [Wang, J.; Taha, Z. *Anal. Chim. Acta* **1991**, *252*, 215–221]. As shown in the figure below, an ion-selective electrode is placed in an inverted position in a large volume tank, and a fixed volume of a sample or a standard solution is injected toward the electrode's surface using a micropipet. The response of the electrode is a spike in potential that is proportional to the analyte's concentration. The following data were collected using a pH electrode and a set of pH standards.

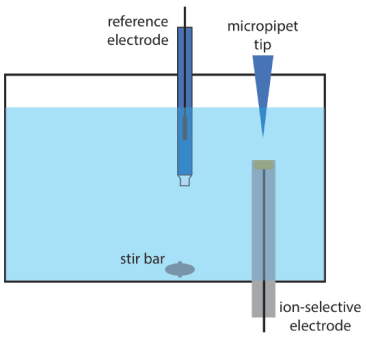

pH	potential (mV)

pH	potential (mV)
2.0	+300
3.0	+240
4.0	+168
5.0	+81
6.0	+35
8.0	–92
9.0	–168
10.0	–235
11.0	–279

Determine the pH of the following samples given the recorded peak potentials: tomato juice, 167 mV; tap water, –27 mV; coffee, 122 mV.

13. The concentration of NO_3^- in a water sample is determined by a one-point standard addition using a NO_3^- ion-selective electrode. A 25.00-mL sample is placed in a beaker and a potential of 0.102 V is measured. A 1.00-mL aliquot of a 200.0-mg/L standard solution of NO_3^- is added, after which the potential is 0.089 V. Report the mg NO_3^-/L in the water sample.

14. In 1977, when I was an undergraduate student at Knox College, my lab partner and I completed an experiment to determine the concentration of fluoride in tap water and the amount of fluoride in toothpaste. The data in this problem are from my lab notebook.

(a) To analyze tap water, we took three 25.0-mL samples and added 25.0 mL of TISAB to each. We measured the potential of each solution using a F^- ISE and an SCE reference electrode. Next, we made five 1.00-mL additions of a standard solution of 100.0 ppm F^- to each sample, and measured the potential after each addition, recording the potential three times.

mL of standard added	potential (mV), replicate 1	potential (mV), replicate 2	potential (mV), replicate 3
0.00	–79	–82	–83
1.00	–119	–119	–118
2.00	–133	–133	–133
3.00	–142	–142	–142
4.00	–149	–148	–148
5.00	–154	–153	–153

Report the parts-per-million of F^- in the tap water.

(b) To analyze the toothpaste, we measured 0.3619 g into a 100-mL volumetric flask, added 50.0 mL of TISAB, and diluted to volume with distilled water. After we ensured that the sample was thoroughly mixed, we transferred three 20.0-mL portions into separate beakers and measured the potential of each using a F^- ISE and an SCE reference electrode. Next, we made five 1.00-mL additions of a standard solution of 100.0 ppm F^- to each sample, and measured the potential after each addition, recording the potential three times.

mL of standard added	potential (mV), replicate 1	potential (mV), replicate 2	potential (mV), replicate 3
0.00	–55	–54	–55
1.00	–82	–82	–83
2.00	–94	–94	–94
3.00	–102	–103	–102

4.00	–108	–108	–109
5.00	–112	–112	–113

Report the parts-per-million F^- in the toothpaste.

15. You are responsible for determining the amount of KI in iodized salt and decide to use an I^- ion-selective electrode. Describe how you would perform this analysis using external standards and how you would per-form this analysis using the method of standard additions.

16. Explain why each of the following decreases the analysis time in controlled-potential coulometry: a larger surface area for the working electrode; a smaller volume of solution; and a faster stirring rate.

17. The purity of a sample of picric acid, $C_6H_3N_3O_7$, is determined by controlled-potential coulometry, converting picric acid to triaminophenol, $C_6H_9N_3O$.

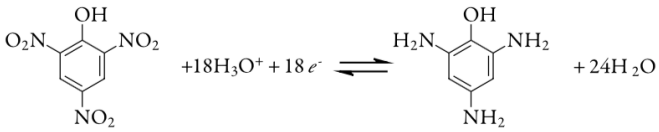

A 0.2917-g sample of picric acid is placed in a 1000-mL volumetric flask and diluted to volume. A 10.00-mL portion of this solution is transferred to a coulometric cell and sufficient water added so that the Pt cathode is immersed. An exhaustive electrolysis of the sample re-quires 21.67 C of charge. Report the purity of the picric acid.

18. The concentration of H_2S in the drainage from an abandoned mine is determined by a coulometric titration using KI as a mediator and I_3^- as the titrant.

$$H_2S(aq) + I_3^-(aq) + 2H_2O(l) \rightleftharpoons 2H_3O^+(aq) + 3I^-(aq) + S(s)$$

A 50.00-mL sample of water is placed in a coulometric cell, along with an excess of KI and a small amount of starch as an indicator. Electrolysis is carried out at a constant current of 84.6 mA, requiring 386 s to reach the starch end point. Report the concentration of H_2S in the sample in μg/mL.

19. One method for the determination of a given mass of H_3AsO_3 is a coulometric titration using I_3^- as a titrant. The relevant standard-state reactions and potentials are summarized here

$$H_3AsO_4(aq) + 2H^+(aq) + 2e^- \rightleftharpoons H_3AsO_3(aq) + H_2O(l)$$
$$I_3^-(aq) + 2e^- \rightleftharpoons 3I^-(aq)$$

with standard state reduction potentials of, respectively, +0.559 V and +0.536 V. Explain why the coulometric titration is carried out in a neutral solution (pH ≈ 7) instead of in a strongly acidic solution (pH < 0).

20. The production of adiponitrile, $NC(CH_2)_4CN$, from acrylonitrile, CH_2=CHCN, is an important industrial process. A 0.594-g sample of acrylonitrile is placed in a 1-L volumetric flask and diluted to volume. An exhaustive controlled-potential electrolysis of a 1.00-mL portion of the diluted acrylonitrile requires 1.080 C of charge. What is the value of *n* for the reduction of acrylonitrile to adiponitrile?

21. The linear-potential scan hydrodynamic voltammogram for a mixture of Fe^{2+} and Fe^{3+} is shown in the figure below where $i_{l,a}$ and $i_{l,c}$ are the anodic and cathodic limiting currents.

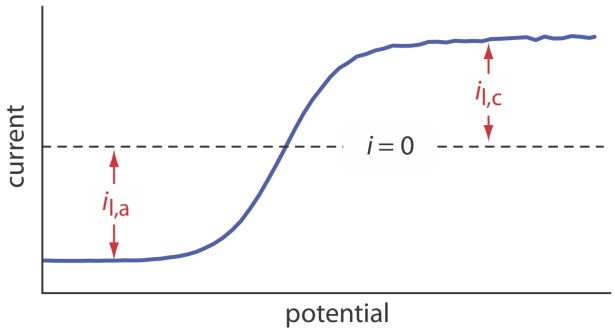

(a) Show that the potential is given by

$$E = E^{\circ}_{Fe^{3+}/Fe^{2+}} - 0.05916 \log \frac{K_{Fe^{3+}}}{K_{Fe^{2+}}} - 0.05916 \log \frac{i - i_{l,a}}{i_{l,c} - i}$$

(b) What is the potential when i = 0 for a solution that is 0.100 mM Fe^{3+} and 0.050 mM Fe^{2+}?

22. The amount of sulfur in aromatic monomers is determined by differential pulse polarography. Standard solutions are prepared for analysis by dissolving 1.000 mL of the purified monomer in 25.00 mL of an electrolytic solvent, adding a known amount of sulfur, deaerating, and measuring the peak current. The following results were obtained for a set of calibration standards.

µg S added	peak current (µA)
0	0.14
28	0.70
56	1.23
112	2.41
168	3.42

Analysis of a 1.000-mL sample, treated in the same manner as the standards, gives a peak current of 1.77 µA. Report the mg S/mL in the sample.

23. The purity of a sample of $K_3Fe(CN)_6$ is determined using linear-potential scan hydrodynamic voltammetry at a glassy carbon electrode. The following data were obtained for a set of external calibration standards.

$[K_3Fe(CN)_6]$ (mM)	limiting current (µA)
2.0	127
4.0	252
6.0	376
8.0	500
10.0	624

A sample of impure $K_3Fe(CN)_6$ is prepared for analysis by diluting a 0.246-g portion to volume in a 100-mL volumetric flask. The limiting current for the sample is 444 µA. Report the purity of this sample of $K_3Fe(CN)_6$.

24. One method for determining whether an individual recently fired a gun is to look for traces of antimony in residue collected from the individual's hands. Anodic stripping voltammetry at a mercury film electrode is ideally suited for this analysis. In a typical analysis a sample is collected from a suspect using a cotton-tipped swab wetted with 5% v/v HNO_3. After returning to the lab, the swab is placed in a vial that contains 5.0 mL of 4 M HCl that is 0.02 M in hydrazine sulfate. After soaking the swab, a 4.0-mL portion of the solution is transferred to an electrochemical cell along with 100 µL of 0.01 M $HgCl_2$. After depositing the thin film

of mercury and the antimony, the stripping step gives a peak current of 0.38 μA. After adding a standard addition of 100 μL of 5.00×10^2 ppb Sb, the peak current increases to 1.14 μA. How many nanograms of Sb were collected from the suspect's hand?

25. Zinc is used as an internal standard in an analysis of thallium by differential pulse polarography. A standard solution of 5.00×10^{-5} M Zn^{2+} and 2.50×10^{-5} M Tl^{+} has peak currents of 5.71 μA and 3.19 μA, respectively. An 8.713-g sample of a zinc-free alloy is dissolved in acid, transferred to a 500-mL volumetric flask, and diluted to volume. A 25.0-mL portion of this solution is mixed with 25.0 mL of 5.00×10^{-4} M Zn^{2+}. Analysis of this solution gives peak currents of 12.3 μA and of 20.2 μA for Zn^{2+} and Tl^{+}, respectively. Report the %w/w Tl in the alloy.

26. Differential pulse voltammetry at a carbon working electrode is used to determine the concentrations of ascorbic acid and caffeine in drug formulations [Lau, O.; Luk, S.; Cheung, Y. *Analyst* **1989**, *114*, 1047–1051]. In a typical analysis a 0.9183-g tablet is crushed and ground into a fine powder. A 0.5630-g sample of this powder is transferred to a 100-mL volumetric flask, brought into solution, and diluted to volume. A 0.500-mL portion of this solution is then transferred to a voltammetric cell that contains 20.00 mL of a suitable supporting electrolyte. The resulting voltammogram gives peak currents of 1.40 μA and 3.88 μA for ascorbic acid and for caffeine, respectively. A 0.500-mL aliquot of a standard solution that contains 250.0 ppm ascorbic acid and 200.0 ppm caffeine is then added. A voltammogram of this solution gives peak currents of 2.80 μA and 8.02 μA for ascorbic acid and caffeine, respectively. Report the milligrams of ascorbic acid and milligrams of caffeine in the tablet.

27. Ratana-ohpas and co-workers described a stripping analysis method for determining tin in canned fruit juices [Ratana-ohpas, R.; Kanatharana, P.; Ratana-ohpas, W.; Kongsawasdi, W. *Anal. Chim. Acta* **1996**, *333*, 115–118]. Standards of 50.0 ppb Sn^{4+}, 100.0 ppb Sn^{4+}, and 150.0 ppb Sn^{4+} were analyzed giving peak currents (arbitrary units) of 83.0, 171.6, and 260.2, respectively. A 2.00-mL sample of lychee juice is mixed with 20.00 mL of 1:1 HCl/HNO_3. A 0.500-mL portion of this mixture is added to 10 mL of 6 M HCl and the volume adjusted to 30.00 mL. Analysis of this diluted sample gave a signal of 128.2 (arbitrary units). Report the parts-per-million Sn^{4+} in the original sample of lychee juice.

28. Sittampalam and Wilson described the preparation and use of an amperometric sensor for glucose [Sittampalam, G.; Wilson, G. S. *J. Chem. Educ.* **1982**, *59*, 70–73]. The sensor is calibrated by measuring the steady-state current when it is immersed in standard solutions of glucose. A typical set of calibration data is shown here.

[glucose] (mg/100 mL)	current (arb. units)
2.0	17.2
4.0	32.9
6.0	52.1
8.0	68.0
10.0	85.8

A 2.00-mL sample is diluted to 10 mL in a volumetric flask and a steady-state current of 23.6 (arbitrary units) is measured. What is the concentration of glucose in the sample in mg/100 mL?

29. Differential pulse polarography is used to determine the concentrations of lead, thallium, and indium in a mixture. Because the peaks for lead and thallium, and for thallium and indium overlap, a simultaneous analysis is necessary. Peak currents (in arbitrary units) at –0.385 V, –0.455 V, and –0.557 V are measured for a single standard solution, and for a sample, giving the results shown in the following table. Report the mg/mL of Pb^{2+}, Tl^{+} and In^{3+} in the sample.

analyte	[standard] (μg/mL)	peak current at –0.385 V	peak current at –0.455 V	peak current at –0.557 V
Pb^{2+}	1.0	26.1	2.9	0
Tl^{+}	2.0	7.8	23.5	3.2
In^{3+}	0.4	0	0	22.9
sample		60.6	28.8	54.1

30. Abass and co-workers developed an amperometric biosensor for NH_4^+ that uses the enzyme glutamate dehydrogenase to catalyze the following reaction

$$2\text{ - oxyglutarate }(aq) + NH_4^+(aq) + NADH(aq) \rightleftharpoons \text{ glutamate }(aq) + NAD^+(aq) + H_2O(l)$$

where NADH is the reduced form of nicotinamide adenine dinucleotide [Abass, A. K.; Hart, J. P.; Cowell, D. C.; Chapell, A. *Anal. Chim. Acta* **1988**, *373*, 1–8]. The biosensor actually responds to the concentration of NADH, however, the rate of the reaction depends on the concentration of NH_4^+. If the initial concentrations of 2-oxyglutarate and NADH are the same for all samples and standards, then the signal is proportional to the concentration of NH_4^+. As shown in the following table, the sensitivity of the method is dependent on pH.

pH	sensitivity (nA S^{-1} M^{-1})
6.2	1.67×10^3
6.75	5.00×10^3
7.3	9.33×10^3
7.7	1.04×10^4
8.3	1.27×10^4
9.3	2.67×10^3

Two possible explanations for the effect of pH on the sensitivity of this analysis are the acid–base chemistry of NH_4^+ and the acid–base chemistry of the enzyme. Given that the pK_a for NH_4^+ is 9.244, explain the source of this pH-dependent sensitivity.

31. The speciation scheme for trace metals in Table 11.4.2 divides them into seven operationally defined groups by collecting and analyzing two samples following each of four treatments, requiring a total of eight samples and eight measurements. After removing insoluble particulates by filtration (treatment 1), the solution is analyzed for the concentration of ASV labile metals and for the total concentration of metals. A portion of the filtered solution is then passed through an ion-exchange column (treatment 2), and the concentrations of ASV metal and of total metal are determined. A second portion of the filtered solution is irradiated with UV light (treatment 3), and the concentrations of ASV metal and of total metal are measured. Finally, a third portion of the filtered solution is irradiated with UV light and passed through an ion-exchange column (treatment 4), and the concentrations of ASV labile metal and of total metal again are determined. The groups that are included in each measurement are summarized in the following table.

treatment	groups removed by treatement	groups contributing to ASV-labile metals	groups contributing to total metals
1	none	I, II, III	I, II, III, IV, V, VI, VII
2	I, IV, V	II, III	II, III, V1, VII
3	none	I, II, III, IV, VI	I, II, III, IV, V, VI, VII
4	I, II, IV, V, VI	III	III, VII

(a) Explain how you can use these eight measurements to determine the concentration of metals present in each of the seven groups identified in Table 11.4.2.

(b) Batley and Florence report the following results for the speciation of cadmium, lead, and copper in a sample of seawater [Batley, G. E.; Florence, T. M. *Anal. Lett.* **1976**, *9*, 379–388]. Determine the speciation of each metal in comment on your results.

measurement treatement: ASV-labile or total	ppb Cd^{2+}	ppb Pb^{2+}	ppb Cu^{2+}
1: ASV-labile	0.24	0.39	0.26
2: total	0.28	0.50	0.40

measurement treatement: ASV-labile or total	ppb Cd^{2+}	ppb Pb^{2+}	ppb Cu^{2+}
2: ASV-labile	0.21	0.33	0.17
2: total	0.26	0.43	0.24
3: ASV-labile	0.26	0.37	0.33
3: total	0.28	0.5	0.43
4: ASV-labile	0.00	0.00	0.00
4: total	0.02	0.12	0.10

32. The concentration of Cu^{2+} in seawater is determined by anodic stripping voltammetry at a hanging mercury drop electrode after first releasing any copper bound to organic matter. To a 20.00-mL sample of seawater is added 1 mL of 0.05 M HNO_3 and 1 mL of 0.1% H_2O_2. The sample is irradiated with UV light for 8 hr and then diluted to volume in a 25-mL volumetric flask. Deposition of Cu^{2+} takes place at –0.3 V versus an SCE for 10 min, producing a peak current of 26.1 (arbitrary units). A second 20.00-mL sample of the seawater is treated identically, except that 0.1 mL of a 5.00 μM solution of Cu^{2+} is added, producing a peak current of 38.4 (arbitrary units). Report the concentration of Cu^{2+} in the seawater in mg/L.

33. Thioamide drugs are determined by cathodic stripping analysis [Davidson, I. E.; Smyth, W. F. Anal. Chem. 1977, 49, 1195–1198]. Deposition occurs at +0.05 V versus an SCE. During the stripping step the potential is scanned cathodically and a stripping peak is observed at –0.52 V. In a typical application a 2.00-mL sample of urine is mixed with 2.00 mL of a pH 4.78 buffer. Following a 2.00 min deposition, a peak current of 0.562 μA is measured. A 0.10-mL addition of a 5.00 μM solution of the drug is added to the same solution. A peak current of 0.837 μA is recorded using the same deposition and stripping conditions. Report the drug's molar concentration in the urine sample.

34. The concentration of vanadium (V) in sea water is determined by adsorptive stripping voltammetry after forming a complex with catechol [van der Berg, C. M. G.; Huang, Z. Q. *Anal. Chem.* **1984**, *56*, 2383–2386]. The catechol-V(V) complex is deposited on a hanging mercury drop electrode at a potential of –0.1 V versus a Ag/AgCl reference electrode. A cathodic potential scan gives a stripping peak that is proportional to the concentration of V(V). The following standard additions are used to analyze a sample of seawater.

$[V(V)]_{added}$ (M)	peak current (μA)
2.0×10^{-8}	24
4.0×10^{-8}	33
8.0×10^{-8}	52
1.2×10^{-7}	69
1.8×10^{-7}	97
2.8×10^{-7}	140

Determine the molar concentration of V (V) in the sample of sea water, assuming that the standard additions result in a negligible change in the sample's volume.

35. The standard-state reduction potential for Cu^{2+} to Cu is +0.342 V versus the SHE. Given that Cu^{2+} forms a very stable complex with the ligand EDTA, do you expect that the standard-state reduction potential for $Cu(EDTA)^{2-}$ is greater than +0.342 V, less than +0.342 V, or equal to +0.342 V? Explain your reasoning.

36. The polarographic half-wave potentials (versus the SCE) for Pb^{2+} and for Tl^{+} in 1 M HCl are, respectively, –0.44 V and –0.45 V. In an electrolyte of 1 M NaOH, however, the half-wave potentials are –0.76 V for Pb^{2+} and –0.48 V for Tl^{+}. Why does the change in electrolyte have such a significant effect on the half-wave potential for Pb^{2+}, but not on the half-wave potential for Tl^{+}?

37. The following data for the reduction of Pb^{2+} were collected by normal-pulse polarography.

potential (V vs. SCE)	current (μA)
–0.345	0.16
–0.370	0.98
–0.383	2.05
–0.393	3.13
–0.409	4.62
–0.420	5.16

The limiting current was 5.67 μA. Verify that the reduction reaction is reversible and determine values for n and $E_{1/2}$. The half-wave potentials for the normal-pulse polarograms of Pb^{2+} in the presence of several different concentrations of OH^- are shown in the following table.

$[OH^-]$ (M)	$E_{1/2}$ (V vs. SCE)	$[OH^-]$ (M)	$E_{1/2}$ (V vs. SCE)
0.050	–0.646	0.150	–0.689
0.100	–0.673	0.300	–0.715

Determine the stoichiometry of the Pb-hydroxide complex and its formation constant.

38. In 1977, when I was an undergraduate student at Knox College, my lab partner and I completed an experiment to study the voltammetric behavior of Cd^{2+} (in 0.1 M KNO_3) and Ni^{2+} (in 0.2 M KNO_3) at a dropping mercury electrode. The data in this problem are from my lab notebook. All potentials are relative to an SCE reference electrode.

potential for Cd^{2+} (V)	current for Cd^{2+} (μA)	potential for Ni^{2+} (V)	current for Ni^{2+} (μA)
–0.60	4.5	–1.07	1.90
–0.58	3.4	–1.05	1.75
–0.56	2.1	–1.03	1.50
–0.54	0.6	–1.02	1.25
–0.52	0.2	–1.00	1.00

The limiting currents for Cd^{2+} was 4.8 μA and that for Ni^{2+} was 2.0 μA. Evaluate the electrochemical reversibility for each metal ion and comment on your results.

39. Baldwin and co-workers report the following data from a cyclic voltammetry study of the electrochemical behavior of *p*-phenylenediamine in a pH 7 buffer [Baldwin, R. P.; Ravichandran, K.; Johnson, R. K. *J. Chem. Educ.* **1984**, *61*, 820–823]. All potentials are measured relative to an SCE.

scan rate (mV/s)	$E_{p,a}$ (V)	$E_{p,c}$ (V)	$i_{p,a}$ (mA)	$i_{p,c}$ (mA)
2	0.148	0.104	0.34	0.30
5	0.149	0.098	0.56	0.53
10	0.152	0.095	1.00	0.04
20	0.161	0.095	1.44	1.44
50	0.167	0.082	2.12	1.81
100	0.180	0.063	2.50	2.19

The initial scan is toward more positive potentials, leading to the oxidation reaction shown here.

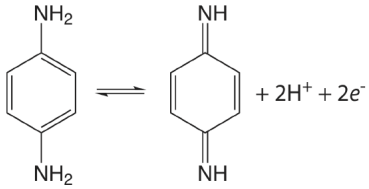

Use this data to show that the reaction is electrochemically irreversible. A reaction may show electrochemical irreversibility because of slow electron transfer kinetics or because the product of the oxidation reaction participates in a chemical reaction that produces an nonelectroactive species. Based on the data in this problem, what is the likely source of *p*-phenylenediamine's electrochemical irreversibility?

2.6: Additional Resources

The following set of experiments introduce students to the applications of electrochemistry. Experiments are grouped into four categories: general electrochemistry, preparation of electrodes, potentiometry, coulometry, and voltammetry and amperometry.

General Electrochemistry

- Chatmontree, A.; Chairam, S.; Supasorn, S.; Amatatongchai, M.; Jarujamrus, P; Tamuang, S.; Somsook E. "Student Fabriaction and Use of Simple, Low-Cost, Paper-Based Galvanic Cells to Investigate Electrochemistry," *J. Chem. Educ.* **2015**, *92*, 1044–1048.
- Mills, K. V.; Herrick, R. S.; Guilmette, L. W.; Nestor, L. P.; Shafer, H.; Ditzler, M. A. "Introducing Undergraduate Students to Electrochemistry: A Two-Week Discovery Chemistry Experiment," *J. Chem. Educ.* **2008**, *85*, 1116–119.

Preparation of Electrodes

- Christopoulos, T. K.; Diamandis, E. P. "Use of a Sintered Glass Crucible for Easy Construction of Liquid-Membrane Ion-Selective Electrodes," *J. Chem. Educ.* **1988**, *65*, 648.
- Fricke, G. H.; Kuntz, M. J. "Inexpensive Solid-State Ion-Selective Electrodes for Student Use," *J. Chem. Educ.* **1977**, *54*, 517–520.
- Inamdar, S. N.; Bhat, M. A.; Haram, S. K. "Construction of Ag/AgCl Reference Electrode form Used Felt-Tipped Pen Barrel for Undergraduate Laboratory," *J. Chem. Educ.* **2009**, *86*, 355–356.
- Lloyd, B. W.; O'Brien, F. L.; Wilson, W. D. "Student Preparation and Analysis of Chloride and Calcium Ion Selective Electrodes," *J. Chem. Educ.* **1976**, *53*, 328–330.
- Mifflin, T. E.; Andriano, K. M.; Robbins, W. B. "Determination of Penicillin Using an Immobilized Enzyme Electrode," *J. Chem. Educ.* **1984**, *61*, 638–639.
- Palanivel, A.; Riyazuddin, P. "Fabrication of an Inexpensive Ion-Selective Electrode," *J. Chem. Educ.* **1984**, *61*, 290.
- Ramaley, L; Wedge, P. J.; Crain, S. M. "Inexpensive Instrumental Analysis: Part 1. Ion-Selective Electrodes," *J. Chem. Educ.* **1994**, *71*, 164–167.
- Selig, W. S. "Potentiometric Titrations Using Pencil and Graphite Sensors," *J. Chem. Educ.* **1984**, *61*, 80–81.

Potentiometry

- Chan, W. H; Wong, M. S.; Yip, C. W. "Ion-Selective Electrode in Organic Analysis: A Salicylate Electrode," *J. Chem. Educ.* **1986**, *63*, 915–916.
- Harris, T. M. "Potentiometric Measurement in a Freshwater Aquarium," *J. Chem. Educ.* **1993**, *70*, 340–341.
- Kauffman, C. A.; Muza, A. L.; Porambo, M. W.; Marsh, A. L. "Use of a Commercial Silver-Silver Chloride Electrode for the Measurement of Cell Potentials to Determine Mean Ionic Activity Coefficients," *Chem. Educator* **2010**, *15*, 178–180.
- Martínez-Fàbregas, E.; Alegret, S. "A Practical Approach to Chemical Sensors through Potentiometric Transducers: Determination of Urea in Serum by Means of a Biosensor," *J. Chem. Educ.* **1994**, *71*, A67–A70.
- Moresco, H.; Sansón, P.; Seoane, G. "Simple Potentiometric Determination of Reducing Sugars," *J. Chem. Educ.* **2008**, *85*, 1091–1093.
- Radic, N.; Komijenovic, J. "Potentiometric Determination of an Overall Formation Constant Using an Ion-Selective Membrane Electrode," *J. Chem. Educ.* **1993**, *70*, 509–511.
- Riyazuddin, P.; Devika, D. "Potentiometric Acid–Base Titrations with Activated Graphite Electrodes,"*J. Chem. Educ.* **1997**, *74*, 1198–1199.

Coulometry

- Bertotti, M.; Vaz, J. M.; Telles, R. "Ascorbic Acid Determination in Natural Orange Juice," *J. Chem. Educ.* **1995**, *72*, 445–447.
- Kalbus, G. E.; Lieu, V. T. "Dietary Fat and Health: An Experiment on the Determination of Iodine Number of Fats and Oils by Coulometric Titration," *J. Chem. Educ.* **1991**, *68*, 64–65.
- Lötz, A. "A Variety of Electrochemical Methods in a Coulometric Titration Experiment," *J. Chem. Educ.* **1998**, *75*, 775–777.
- Swim, J.; Earps, E.; Reed, L. M.; Paul, D. "Constant-Current Coulometric Titration of Hydrochloric Acid," *J. Chem. Educ.* **1996**, *73*, 679–683.

Voltammetry and Amperometry

- Blanco-López, M. C.; Lobo-Castañón, M. J.; Miranda-Ordieres, A. J. “Homemade Bienzymatic-Amperometric Biosensor for Beverages Analysis,” *J. Chem. Educ.* **2007**, *84*, 677–680.
- García-Armada, P.; Losada, J.; de Vicente-Pérez, S. “Cation Analysis Scheme by Differential Pulse Polarography,” *J. Chem. Educ.* **1996**, *73*, 544–547.
- Herrera-Melián, J. A.; Doña-Rodríguez, J. M.; Hernández-Brito, J.; Pérez-Peña, J. “Voltammetric Determination of Ni and Co in Water Samples,” *J. Chem. Educ.* **1997**, *74*, 1444–1445.
- King, D.; Friend, J.; Kariuki, J. “Measuring Vitamin C Content of Commercial Orange Juice Using a Pencil Lead Electrode,” *J. Chem. Educ.* **2010**, *87*, 507–509.
- Marin, D.; Mendicuti, F. “Polarographic Determination of Composition and Thermodynamic Stability Constant of a Complex Metal Ion,” *J. Chem. Educ.* **1988**, *65*, 916–918.
- Messersmith, S. J. “Cyclic Voltammetry Simulations with DigiSim Software: An Upper-Level Undergraduate Experiment,” *J. Chem. Educ.* **2014**, *91*, 1498–1500.
- Sadik, O. A.; Brenda, S.; Joasil, P.; Lord, J. “Electropolymerized Conducting Polymers as Glucose Sensors,” *J. Chem. Educ.* **1999**, *76*, 967–970.
- Sittampalam, G.; Wilson, G. S. “Amperometric Determination of Glucose at Parts Per Million Levels with Immobilized Glucose Oxidase,” *J. Chem. Educ.* **1982**, *59*, 70–73.
- Town, J. L.; MacLaren, F.; Dewald, H. D. “Rotating Disk Voltammetry Experiment,” *J. Chem. Educ.* **1991**, *68*, 352–354.
- Wang, J. “Sensitive Electroanalysis Using Solid Electrodes,” *J. Chem. Educ.* **1982**, *59*, 691–692.
- Wang, J. “Anodic Stripping Voltammetry,” *J. Chem. Educ.* **1983**, *60*, 1074–1075.
- Wang, J.; Maccà, C. “Use of Blood-Glucose Test Strips for Introducing Enzyme Electrodes and Modern Biosensors,” *J. Chem. Educ.* **1996**, *73*, 797–800.
- Wang, Q.; Geiger, A.; Frias, R; Golden, T. D. “An Introduction to Electrochemistry for Undergraduates: Detection of Vitamin C (Ascorbic Acid) by Inexpensive Electrode Sensors,” *Chem. Educator* **2000**, *5*, 58–60.

The following general references providing a broad introduction to electrochemistry.

- Adams, R. N. *Electrochemistry at Solid Surfaces*, Marcel Dekker: New York, 1969.
- Bard, A. J.; Faulkner, L. R. *Electrochemical Methods*, Wiley: New York, 1980.
- Faulkner, L. R. “Electrochemical Characterization of Chemical Systems” in Kuwana, T. E., ed. *Physical Methods in Modern Chemical Analysis*, Vol. 3, Academic Press: New York, 1983, pp. 137–248.
- Kissinger, P. T.; Heineman, W. R. *Laboratory Techniques in Electroanalytical Chemistry*, Marcel Dekker: New York, 1984.
- Lingane, J. J. *Electroanalytical Chemistry*, 2nd Ed., Interscience: New York, 1958.
- Sawyer, D. T.; Roberts, J. L., Jr. *Experimental Electrochemistry for Chemists*, Wiley-Interscience: New York, 1974.
- Vassos, B. H.; Ewing, G. W. *Electroanalytical Chemistry*, Wiley-Interscience: New York, 1983.

These short articles provide a good introduction to important principles of electrochemistry.

- Faulkner, L. R. “Understanding Electrochemistry: Some Distinctive Concepts,” *J. Chem. Educ.* **1983**, *60*, 262–264.
- Huddle, P. A.; White, M. D.; Rogers, F. “Using a Teaching Model to Correct Known Misconceptions in Electrochemistry,” *J. Chem. Educ.* **2000**, *77*, 104–110.
- Maloy, J. T. “Factors Affecting the Shape of Current-Potential Curves,” *J. Chem. Educ.* **1983**, *60*, 285–289.
- Miles, D. T. “Run-D.M.C.: A Mnemonic Aid for Explaining Mass Transfer in Electrochemical Systems,” *J. Chem. Educ.* **2013**, *90*, 1649–1653.
- Thompson, R. Q.; Craig, N. C. “Unified Electroanalytical Chemistry: Application of the Concept of Equilibrium,” *J. Chem. Educ.* **2001**, *78*, 928–934.
- Zoski, C. G. “Charging Current Discrimination in Analytical Voltammetry,” *J. Chem. Educ.* **1986**, *63*, 910–914.

Additional information on potentiometry and ion-selective electrodes can be found in the following sources.

- Bakker, E.; Diamond, D.; Lewenstam, A.; Pretsch, E. “Ions Sensors: Current Limits and New Trends,” *Anal. Chim. Acta* **1999**, *393*, 11–18.
- Bates, R. G. *Determination of pH: Theory and Practice*, 2nd ed., Wiley: New York, 1973.
- Bobacka, J.; Ivaska, A.; Lewenstam, A. “Potentiometric Ion Sensors,” *Chem. Rev.* **2008**, *108*, 329–351.
- Buck, R. P. “Potentiometry: pH Measurements and Ion Selective Electrodes” in Weissberger, A., ed. *Physical Methods of Organic Chemistry*, Vol. 1, Part IIA, Wiley: New York, 1971, pp. 61–162.
- Cammann, K. *Working With Ion-Selective Electrodes*, Springer-Verlag: Berlin, 1977.

- Evans, A. P*otentiometry and Ion-Selective Electrodes*, Wiley: New York, 1987.
- Frant, M. S. “Where Did Ion Selective Electrodes Come From?” *J. Chem. Educ.* **1997**, *74*, 159–166.
- Light, T. S. “Industrial Use and Application of Ion-Selective Electrodes,” *J. Chem. Educ.* **1997**, *74*, 171–177.
- Rechnitz, G. A. “Ion and Bio-Selective Membrane Electrodes,” *J. Chem. Educ.* **1983**, *60*, 282–284.
- Ruzicka, J. “The Seventies—Golden Age for Ion-Selective Electrodes,” *J. Chem. Educ.* **1997**, *74*, 167– 170.
- Young, C. C. “Evolution of Blood Chemistry Analyzers Based on Ion Selective Electrodes,” *J. Chem. Educ.* **1997**, *74*, 177–182.

The following sources provide additional information on electrochemical biosensors.

- Alvarez-Icasa, M.; Bilitewski, U. “Mass Production of Biosensors,” *Anal. Chem.* **1993**, *65*, 525A– 533A.
- Meyerhoff, M. E.; Fu, B.; Bakker, E. Yun, J-H; Yang, V. C. “Polyion-Sensititve Membrane Electrodes for Biomedical Analysis,” *Anal. Chem.* **1996**, *68*, 168A–175A.
- Nicolini, C.; Adami, M; Antolini, F.; Beltram, F.; Sartore, M.; Vakula, S. “Biosensors: A Step to Bioelectronics,” *Phys. World*, May 1992, 30–34.
- Rogers, K. R.; Williams. L. R. “Biosensors for Environmental Monitoring: A Regulatory Perspective,” *Trends Anal. Chem.* **1995**, *14*, 289–294.
- Schultz, J. S. “Biosensors,” *Sci. Am.* August 1991, 64–69.
- Thompson, M.; Krull, U. “Biosensors and the Transduction of Molecular Recognition,” *Anal. Chem.* **1991**, *63*, 393A–405A.
- Vadgama, P. “Designing Biosensors,” *Chem. Brit.* **1992**, *28*, 249–252.

A good source covering the clinical application of electrochemistry is listed below.

- Wang, J. *Electroanalytical Techniques in Clinical Chemistry and Laboratory Medicine*, VCH: New York, 1998.

Coulometry is covered in the following texts.

- Rechnitz, G. A. *Controlled-Potential Analysis*, Macmillan: New York, 1963.
- Milner, G. W. C.; Philips, G. *Coulometry in Analytical Chemistry*, Pergamon: New York, 1967.

For a description of electrogravimetry, see the following resource.

- Tanaka, N. “Electrodeposition”, in Kolthoff, I. M.; Elving, P. J., eds. *Treatise on Analytical Chemistry, Part I: Theory and Practice*, Vol. 4, Interscience: New York, 1963.

The following sources provide additional information on polarography and pulse polarography.

- Flato, J. B. “The Renaissance in Polarographic and Voltammetric Analysis,” *Anal. Chem.* **1972**, *44(11)*, 75A–87A.
- Kolthoff, I. M.; Lingane, J. J. *Polarography*, Interscience: New York, 1952.
- Osteryoung, J. “Pulse Voltammetry,” *J. Chem. Educ.* **1983**, *60*, 296–298.

Additional Information on stripping voltammetry is available in the following text.

- Wang, J. *Stripping Analysis*, VCH Publishers: Deerfield Beach, FL, 1985.

The following papers discuss the numerical simulation of voltammetry.

- Bozzini, B. “A Simple Numerical Procedure for the Simulation of “Lifelike” Linear-Sweep Voltammo- grams,” *J. Chem. Educ.* **2000**, *77*, 100–103.
- Howard, E.; Cassidy, J. “Analysis with Microelectrodes Using Microsoft Excel Solver,” *J. Chem. Educ.* **2000**, *77*, 409–411.
- Kätelhön, E.; Compton, R. G. “Testing and Validating Electroanalytical Simulations,” *Analyst*, **2015**, *140*, 2592–2598.
- Messersmith, S. J. “Cyclic Voltammetry Simulations with DigiSim Software: An Upper-Level Undergraduate Experiment,” *J. Chem. Educ.* **2014**, *91*, 1498–1500.

Gathered together here are many useful resources for cyclic voltammetry, including experiments.

- Carriedo, G. A. “The Use of Cyclic Voltammetry in the Study of the Chemistry of Metal–Carbonyls,” *J. Chem. Educ.* **1988**, *65*, 1020–1022.
- García-Jareño, J. J.; Benito, D.; Navarro-Laboulais, J.; Vicente, F. “Electrochemical Behavior of Electrodeposited Prussian Blue Films on ITO Electrodes,” *J. Chem. Educ.* **1998**, *75*, 881–884.
- Gilles de Pelichy, L. D.; Smith, E. T. “A Study of the Oxidation Pathway of Adrenaline by Cyclic Voltammetry,” *Chem. Educator* **1997**, *2(2)*, 1–13.
- Gomez, M. E.; Kaifer, A. E. “Voltammetric Behavior of a Ferrocene Derivative,” *J. Chem. Educ.* **1992**, *69*, 502–505.

- Heffner, J. E.; Raber, J. C.; Moe, O. A.; Wigal, C. T. “Using Cyclic Voltammetry and Molecular Modeling to Determine Substituent Effects in the One-Electron Reduction of Benzoquinones,” *J. Chem. Educ.* **1998**, *75*, 365–367.
- Heinze, J. “Cyclic Voltammetry—Electrochemical Spectroscopy,” *Angew. Chem, Int. Ed. Eng.* **1984**, *23*, 831–918.
- Holder, G. N.; Farrar, D. G.; McClure, L. L. “Voltammetric Reductions of Ring-Substituted Acetophenones. 1. Determination of an Electron-Transfer Mechanism Using Cyclic Voltammetry and Computer Modeling: The Formation and Fate of a Radical Anion,” *Chem. Educator* **2001**, *6*, 343–349.
- Ibanez, J. G.; Gonzalez, I.; Cardenas, M. A. “The Effect of Complex Formation Upon the Redox Potentials of Metal Ions: Cyclic Voltammetry Experiments,” *J. Chem. Educ.* **1988**, *65*, 173–175.
- Ito, T.; Perara, D. M. N. T.; Nagasaka, S. “Gold Electrodes Modified with Self-Assembled Monolayers for Measuring l-Ascobric acid,” *J. Chem. Educ.* **2008**, *85*, 1112–1115.
- Kissinger, P. T.; Heineman, W. R. “Cyclic Voltammetry,” *J. Chem. Educ.* **1983**, *60*, 702–706.
- Mabbott, G. A. “An Introduction to Cyclic Voltammetry,” *J. Chem. Educ.* **1983**, *60*, 697–702.
- Petrovic, S. “Cyclic Voltammetry of Hexachloroiridate (IV): An Alternative to the Electrochemical Study of the Ferricyanide Ion,” *Chem. Educator* **2000**, *5*, 231–235.
- Toma, H. E.; Araki, K.; Dovidauskas, S. “A Cyclic Voltammetry Experiment Illustrating Redox Potentials, Equilibrium Constants and Substitution Reaction in Coordination Chemistry,” *J. Chem. Educ.* **2000**, *77*, 1351–1353.
- Walczak, M. W.; Dryer, D. A.; Jacobson, D. D,; Foss, M. G.; Flynn, N. T. “pH-Dependent Redox Couple: Illustrating the Nernst Equation Using Cyclic Voltammetry,” *J. Chem. Educ.* **1997**, *74*, 1195–1197.

2.7: Chapter Summary and Key Terms

Chapter Summary

In this chapter we introduced three electrochemical methods of analysis: potentiometry, coulometry, and voltammetry. In potentiometry we measure the potential at an indicator electrode without allowing any significant current to pass through the electrochemical cell, and use the Nernst equation to calculate the analyte's activity after accounting for junction potentials.

There are two broad classes of potentiometric electrodes: metallic electrodes and membrane electrodes. The potential of a metallic electrode is the result of a redox reaction at the electrode's surface. An electrode of the first kind responds to the concentration of its cation in solution; thus, the potential of a Ag wire is determined by the activity of Ag^+ in solution. If another species is in equilibrium with the metal ion, the electrode's potential also responds to the concentration of that species. For example, the potential of a Ag wire in a solution of Cl^- responds to the concentration of Cl^- because the relative concentrations of Ag^+ and Cl^- are fixed by the solubility product for AgCl. We call this an electrode of the second kind.

The potential of a membrane electrode is determined by a difference in the composition of the solution on each side of the membrane. Electrodes that use a glass membrane respond to ions that bind to negatively charged sites on the membrane's surface. A pH electrode is one example of a glass membrane electrode. Other kinds of membrane electrodes include those that use insoluble crystalline solids or liquid ion-exchangers incorporated into a hydrophobic membrane. The F^- ion-selective electrode, which uses a single crystal of LaF_3 as the ion-selective membrane, is an example of a solid-state electrode. The Ca^{2+} ion-selective electrode, in which the chelating ligand di-(*n*-decyl)phosphate is immobilized in a PVC membrane, is an example of a liquid-based ion-selective electrode.

Potentiometric electrodes are designed to respond to molecules by using a chemical reaction that produces an ion whose concentration is determined using a traditional ion-selective electrode. A gas-sensing electrode, for example, includes a gas permeable membrane that isolates the ion-selective electrode from the gas. When a gas-phase analyte diffuses across the membrane it alters the composition of the inner solution, which is monitored with an ion-selective electrode. An enzyme electrodes operate in the same way.

Coulometric methods are based on Faraday's law that the total charge or current passed during an electrolysis is proportional to the amount of reactants and products participating in the redox reaction. If the electrolysis is 100% efficient—which means that only the analyte is oxidized or reduced—then we can use the total charge or total current to determine the amount of analyte in a sample. In controlled-potential coulometry we apply a constant potential and measure the resulting current as a function of time. In controlled-current coulometry the current is held constant and we measure the time required to completely oxidize or reduce the analyte.

In voltammetry we measure the current in an electrochemical cell as a function of the applied potential. There are several different voltammetric methods that differ in terms of the choice of working electrode, how we apply the potential, and whether we include convection (stirring) as a means for transporting of material to the working electrode.

Polarography is a voltammetric technique that uses a mercury electrode and an unstirred solution. Normal polarography uses a dropping mercury electrode, or a static mercury drop electrode, and a linear potential scan. Other forms of polarography include normal pulse polarography, differential pulse polarography, staircase polarography, and square-wave polarography, all of which use a series of potential pulses.

In hydrodynamic voltammetry the solution is stirred using either a magnetic stir bar or by rotating the electrode. Because the solution is stirred a dropping mercury electrode is not used; instead we use a solid electrode. Both linear potential scans and potential pulses can be applied.

In stripping voltammetry the analyte is deposited on the electrode, usually as the result of an oxidation or reduction reaction. The potential is then scanned, either linearly or using potential pulses, in a direction that removes the analyte by a reduction or oxidation reaction.

Amperometry is a voltammetric method in which we apply a constant potential to the electrode and measure the resulting current. Amperometry is most often used in the construction of chemical sensors for the quantitative analysis of single analytes. One important example is the Clark O_2 electrode, which responds to the concentration of dissolved O_2 in solutions such as blood and water.

Key Terms

amalgam	amperometry	anode
anodic current	asymmetry potential	auxiliary electrode
cathode	cathodic current	charging current
controlled-current coulometry	controlled-potential coulometry	convection
coulometric titrations	coulometry	counter electrode
current efficiency	cyclic voltammetry	diffusion
diffusion layer	dropping mercury electrode	electrical double layer
electrochemically irreversible	electrochemically reversible	electrode of the first kind
electrode of the second kind	electrochemistry	electrogravimetry
enzyme electrodes	faradaic current	Faraday's law
galvanostat	gas-sensing electrode	glass electrode
hanging mercury drop electrode	hydrodynamic voltammetry	indicator electrode
ionophore	ion selective electrode	junction potential
limiting current	liquid-based ion-selective electrode	mass transport
mediator	membrane potential	mercury film electrode
migration	nonfaradaic current	Ohm's law
overpotential	peak current	polarography
potentiometer	potentiostat	pulse polarography
redox electrode	reference electrode	residual current
salt bridge	saturated calomel electrode	selectivity coefficient
silver/silver chloride electrode	solid-state ion-selective electrodes	standard hydrogen electrode
static mercury drop electrode	stripping voltammetry	total ionic strength adjustment buffer
voltammetry	voltammogram	working electrode

CHAPTER OVERVIEW

3: Chromatographic and Electrophoretic Methods

Drawing from an arsenal of analytical techniques—many of which were the subject of the preceding four chapters—analytical chemists design methods that detect increasingly smaller concentrations of analyte in increasingly more complex matrices. Despite the power of these analytical techniques, they often suffer from a lack of selectivity. For this reason, many analytical procedures include a step to separate the analyte from potential interferents. Although effective, each additional step in an analytical procedure increases the analysis time and the cost of the analysis, and introduces uncertainty. In this chapter we consider two analytical techniques that avoid these limitations by combining the separation and analysis: chromatography and electrophoresis.

3.1: Overview of Analytical Separations

In Chapter 7 we examined several methods for separating an analyte from potential interferents. For example, in a liquid–liquid extraction the analyte and interferent initially are present in a single liquid phase. We add a second, immiscible liquid phase and thoroughly mix them by shaking. During this process the analyte and interferents partition between the two phases to different extents, effecting their separation. After allowing the phases to separate, we draw off the phase enriched in analyte. Despite the power of liquid–liquid extractions, there are significant limitations.

Two Limitations of Liquid-Liquid Extractions

Suppose we have a sample that contains an analyte in a matrix that is incompatible with our analytical method. To determine the analyte's concentration we first separate it from the matrix using a simple liquid–liquid extraction. If we have several analytes, we may need to complete a separate extraction for each analyte. For a complex mixture of analytes this quickly becomes a tedious process. This is one limitation to a liquid–liquid extraction.

A more significant limitation is that the extent of a separation depends on the distribution ratio of each species in the sample. If the analyte's distribution ratio is similar to that of another species, then their separation becomes impossible. For example, let's assume that an analyte, *A*, and an interferent, *I*, have distribution ratios of, respectively, 5 and 0.5. If we use a liquid–liquid extraction with equal volumes of sample and extractant, then it is easy to show that a single extraction removes approximately 83% of the analyte and 33% of the interferent. Although we can remove 99% of the analyte with three extractions, we also remove 70% of the interferent. In fact, there is no practical combination of number of extractions or volumes of sample and extractant that produce an acceptable separation.

From Chapter 7 we know that the distribution ratio, *D*, for a solute, *S*, is

$$D = \frac{[S]_{\text{ext}}}{[S]_{\text{samp}}}$$

where $[S]_{\text{ext}}$ is its equilibrium concentration in the extracting phase and $[S]_{\text{samp}}$ is its equilibrium concentration in the sample. We can use the distribution ratio to calculate the fraction of *S* that remains in the sample, q_{samp}, after an extraction

$$q_{\text{samp}} = \frac{V_{\text{samp}}}{DV_{\text{ext}} + V_{\text{samp}}}$$

where V_{samp} is the volume of sample and V_{ext} is the volume of the extracting phase. For example, if $D = 10$, $V_{\text{samp}} = 20$, and $V_{\text{ext}} = 5$, the fraction of *S* remaining in the sample after the extraction is

$$q_{\text{sanp}} = \frac{20}{10 \times 5 + 20} = 0.29$$

or 29%. The remaining 71% of the analyte is in the extracting phase.

A Better Way to Separate Mixtures

The problem with a liquid–liquid extraction is that the separation occurs in one direction only: from the sample to the extracting phase. Let's take a closer look at the liquid–liquid extraction of an analyte and an interferent with distribution ratios of, respectively, 5 and 0.5. Figure 12.1.1 shows that a single extraction using equal volumes of sample and extractant transfers 83% of the analyte and 33% of the interferent to the extracting phase. If the original concentrations of *A* and *I* are identical, then their concentration ratio in the extracting phase after one extraction is

$$\frac{[A]}{[I]} = \frac{0.83}{0.33} = 2.5$$

A single extraction, therefore, enriches the analyte by a factor of $2.5\times$. After completing a second extraction (Figure 12.1.1) and combining the two extracting phases, the separation of the analyte and the interferent, surprisingly, is less efficient.

$$\frac{[A]}{[I]} = \frac{0.97}{0.55} = 1.8$$

Figure 12.1.1 makes it clear why the second extraction results in a poorer overall separation: the second extraction actually favors the interferent!

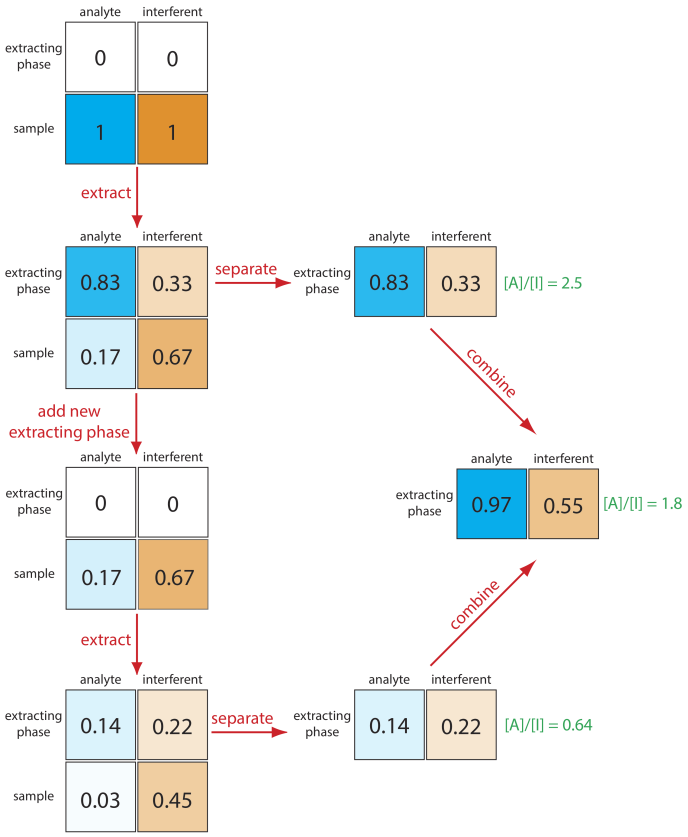

Figure 12.1.1 . Progress of a traditional liquid–liquid extraction using two identical extractions of a single sample using fresh portions of the extractant. The numbers give the fraction of analyte and interferent in each phase assuming equal volumes of sample and extractant and distribution ratios of 5 and 0.5 for the analyte and the interferent, respectively. The opacity of the colors equals the fraction of analyte and interferent present.

We can improve the separation by first extracting the solutes from the sample into the extracting phase and then extracting them back into a fresh portion of solvent that matches the sample's matrix (Figure 12.1.2). Because the analyte has the larger distribution ratio, more of it moves into the extractant during the first extraction and less of it moves back to the sample phase during the second extraction. In this case the concentration ratio in the extracting phase after two extractions is significantly greater.

$$\frac{[A]}{[I]} = \frac{0.69}{0.11} = 6.3$$

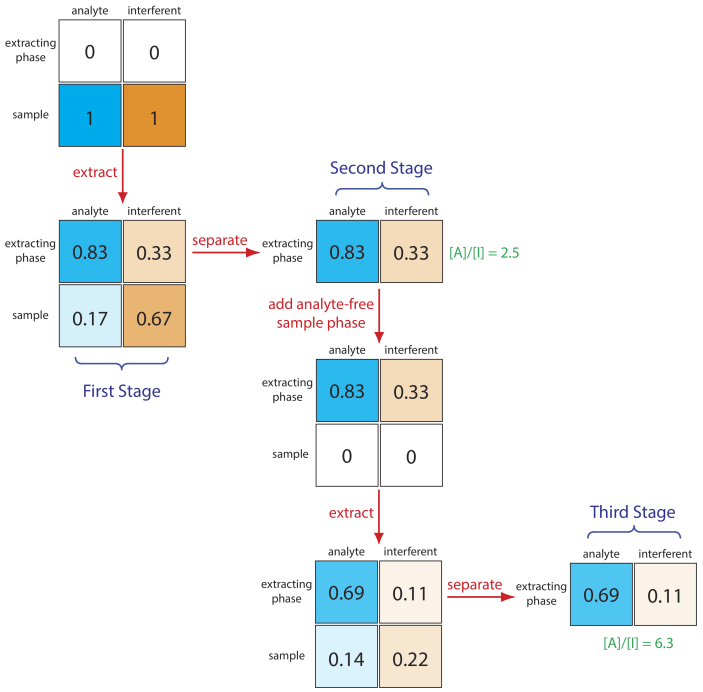

Figure 12.1.2 . Progress of a liquid–liquid extraction in which we first extract the solutes into the extracting phase and then extract them back into an analyte-free portion of the sample's phase. The numbers give the fraction of analyte and interferent in each phase assuming equal volumes of sample and extractant and distribution ratios of 5 and 0.5 for the analyte and the interferent, respectively. The opacity of the colors equals the fraction of analyte and interferent present.

Not shown in Figure 12.2 is that we can add a fresh portion of the extracting phase to the sample that remains after the first extraction (the bottom row of the first stage in Figure 12.2, beginning the process anew. As we increase the number of extractions, the analyte and the interferent each spread out in space over a series of stages. Because the interferent's distribution ratio is smaller than the analyte's, the interferent lags behind the analyte. With a sufficient number of extractions—that is, a sufficient number of stages—a complete separation of the analyte and interferent is possible. This process of extracting the solutes back and forth between fresh portions of the two phases, which we call a ***countercurrent extraction***, was developed by Craig in the 1940s [Craig, L. C. *J. Biol. Chem.* **1944**, *155*, 519–534]. The same phenomenon forms the basis of modern chromatography.

> See Appendix 16 for a more detailed consideration of the mathematics behind a countercurrent extraction.

Chromatographic Separations

In ***chromatography*** we pass a sample-free phase, which we call the ***mobile phase***, over a second sample-free ***stationary phase*** that remains fixed in space (Figure 12.1.3). We inject or place the sample into the mobile phase. As the sample moves with the mobile phase, its components partition between the mobile phase and the stationary phase. A component whose distribution ratio favors the stationary phase requires more time to pass through the system. Given sufficient time and sufficient stationary and mobile phase, we can separate solutes even if they have similar distribution ratios.

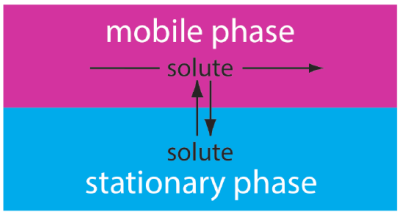

Figure 12.1.3 . In chromatography we pass a mobile phase over a stationary phase. When we inject a sample into the mobile phase, the sample's components both move with the mobile phase and partition into the stationary phase. The solute that spends the most time in the stationary phase takes the longest time to move through the system.

There are many ways in which we can identify a chromatographic separation: by describing the physical state of the mobile phase and the stationary phase; by describing how we bring the stationary phase and the mobile phase into contact with each other; or by describing the chemical or physical interactions between the solute and the stationary phase. Let's briefly consider how we might use each of these classifications.

> We can trace the history of chromatography to the turn of the century when the Russian botanist Mikhail Tswett used a column packed with calcium carbonate and a mobile phase of petroleum ether to separate colored pigments from plant extracts. As the sample moved through the column, the plant's pigments separated into individual colored bands. After effecting the separation, the calcium carbonate was removed from the column, sectioned, and the pigments recovered. Tswett named the technique chromatography, combining the Greek words for "color" and "to write." There was little interest in Tswett's technique until Martin and Synge's pioneering development of a theory of chromatography (see Martin, A. J. P.; Synge, R. L. M. "A New Form of Chromatogram Employing Two Liquid Phases," *Biochem. J.* **1941**, *35*, 1358–1366). Martin and Synge were awarded the 1952 Nobel Prize in Chemistry for this work.

Types of Mobile Phases and Stationary Phases

The mobile phase is a liquid or a gas, and the stationary phase is a solid or a liquid film coated on a solid substrate. We often name chromatographic techniques by listing the type of mobile phase followed by the type of stationary phase. In gas–liquid chromatography, for example, the mobile phase is a gas and the stationary phase is a liquid film coated on a solid substrate. If a technique's name includes only one phase, as in gas chromatography, it is the mobile phase.

Contact Between the Mobile Phase and the Stationary Phase

There are two common methods for bringing the mobile phase and the stationary phase into contact. In ***column chromatography*** we pack the stationary phase into a narrow column and pass the mobile phase through the column using gravity or by applying pressure. The stationary phase is a solid particle or a thin liquid film coated on either a solid particulate packing material or on the column's walls.

In ***planar chromatography*** the stationary phase is coated on a flat surface—typically, a glass, metal, or plastic plate. One end of the plate is placed in a reservoir that contains the mobile phase, which moves through the stationary phase by capillary action. In paper chromatography, for example, paper is the stationary phase.

Interaction Between the Solute and the Stationary Phase

The interaction between the solute and the stationary phase provides a third method for describing a separation (Figure 12.1.4). In ***adsorption chromatography***, solutes separate based on their ability to adsorb to a solid stationary phase. In ***partition chromatography***, the stationary phase is a thin liquid film on a solid support. Separation occurs because there is a difference in the equilibrium partitioning of solutes between the stationary phase and the mobile phase. A stationary phase that consists of a solid support with covalently attached anionic (e.g., $-\mathrm{SO}_3^-$) or cationic (e.g., $-\mathrm{N}(\mathrm{CH}_3)_3^+$) functional groups is the basis for ion-exchange chromatography in which ionic solutes are attracted to the stationary phase by electrostatic forces. In size-exclusion chromatography the stationary phase is a porous particle or gel, with separation based on the size of the solutes. Larger solutes are unable to penetrate as deeply into the porous stationary phase and pass more quickly through the column.

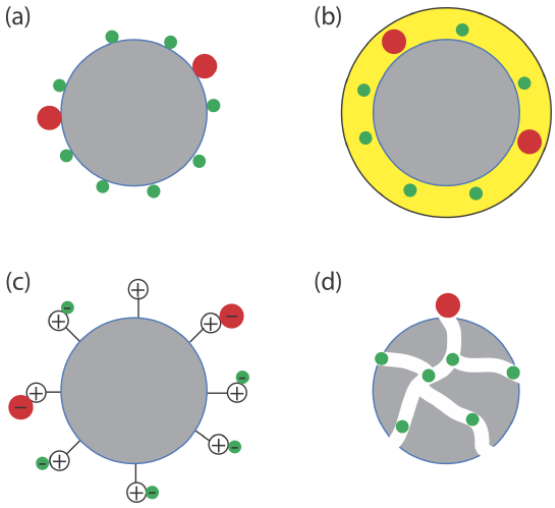

Figure 12.1.4 . Four examples of interactions between a solute and the stationary phase: (a) adsorption on a solid surface, (b) partitioning into a liquid phase, (c) ion-exchange, and (d) size exclusion. For each example, the smaller, green solute is more strongly retained than the larger, red solute.

There are other interactions that can serve as the basis of a separation. In affinity chromatography the interaction between an antigen and an antibody, between an enzyme and a substrate, or between a receptor and a ligand forms the basis of a separation. See this chapter's additional resources for some suggested readings.

Electrophoretic Separations

In chromatography, a separation occurs because there is a difference in the equilibrium partitioning of solutes between the mobile phase and the stationary phase. Equilibrium partitioning, however, is not the only basis for effecting a separation. In an electrophoretic separation, for example, charged solutes migrate under the influence of an applied potential. A separation occurs because of differences in the charges and the sizes of the solutes (Figure 12.1.5).

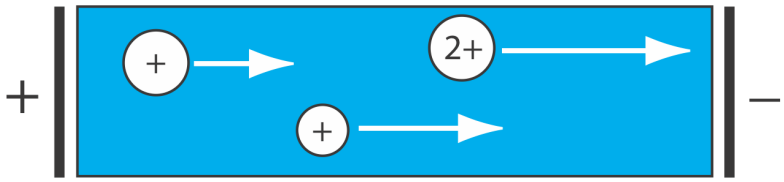

Figure 12.1.5 . Movement of charged solutes under the influence of an applied potential. The lengths of the arrows indicate the relative speed of the solutes. In general, a larger solute moves more slowly than a smaller solute of equal charge, and a solute with a larger charge move more quickly than a solute with a smaller charge.

3.2: General Theory of Column Chromatography

Of the two methods for bringing the stationary phase and the mobile phases into contact, the most important is column chromatography. In this section we develop a general theory that we may apply to any form of column chromatography.

Figure 12.2.1 provides a simple view of a liquid–solid column chromatography experiment. The sample is introduced as a narrow band at the top of the column. Ideally, the solute's initial concentration profile is rectangular (Figure 12.2.2 a). As the sample moves down the column, the solutes begin to separate (Figure 12.2.1 b,c) and the individual solute bands begin to broaden and develop a Gaussian profile (Figure 12.2.2 b,c). If the strength of each solute's interaction with the stationary phase is sufficiently different, then the solutes separate into individual bands (Figure 12.2.1 d and Figure 12.2.2 d).

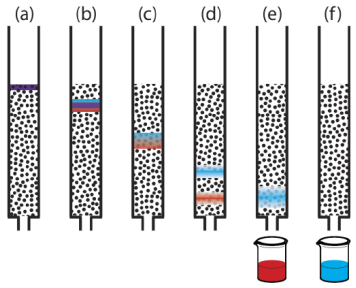

Figure 12.2.1 . Progress of a column chromatographic separation of a two-component mixture. In (a) the sample is layered on top of the stationary phase. As mobile phase passes through the column, the sample separates into two solute bands (b–d). In (e) and (f), we collect each solute as it elutes from the column.

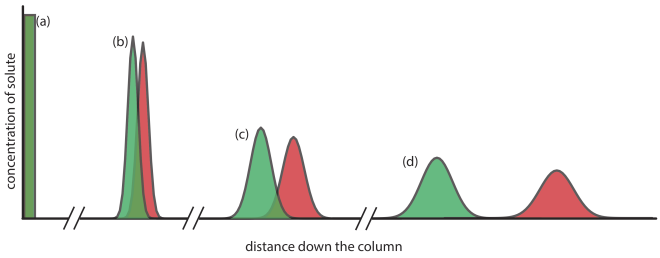

Figure 12.2.2 . An alternative view of the separation in Figure 12.2.1 showing the concentration of each solute as a function of distance down the column.

We can follow the progress of the separation by collecting fractions as they elute from the column (Figure 12.2.1 e,f), or by placing a suitable detector at the end of the column. A plot of the detector's response as a function of elution time, or as a function of the volume of mobile phase, is known as a ***chromatogram*** (Figure 12.2.3), and consists of a peak for each solute.

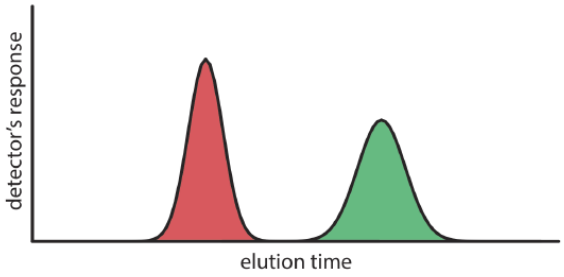

Figure 12.2.3 . Chromatogram for the separation shown in Figure 12.2.1 and Figure 12.2.2 , showing the detector's response as a function of the elution time.

> There are many possible detectors that we can use to monitor the separation. Later sections of this chapter describe some of the most popular.

We can characterize a chromatographic peak's properties in several ways, two of which are shown in Figure 12.2.4 . ***Retention time***, t_r, is the time between the sample's injection and the maximum response for the solute's peak. A chromatographic peak's ***baseline width***, w, as shown in Figure 12.2.4 , is determined by extending tangent lines from the inflection points on either side of the peak through the baseline. Although usually we report t_r and w using units of time, we can report them using units of volume by multiplying each by the mobile phase's velocity, or report them in linear units by measuring distances with a ruler.

> For example, a solute's retention volume,V_r, is $t_r \times u$ where u is the mobile phase's velocity through the column.

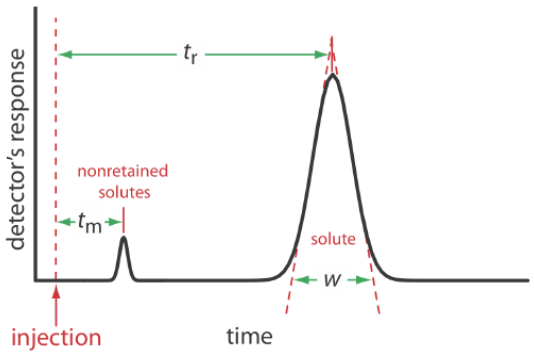

Figure 12.2.4 . Chromatogram showing a solute's retention time, t_r, and baseline width, w, and the column's void time, t_m, for nonretained solutes.

In addition to the solute's peak, Figure 12.2.4 also shows a small peak that elutes shortly after the sample is injected into the mobile phase. This peak contains all ***nonretained solutes***, which move through the column at the same rate as the mobile phase. The time required to elute the nonretained solutes is called the column's ***void time***, t_m.

Chromatographic Resolution

The goal of chromatography is to separate a mixture into a series of chromatographic peaks, each of which constitutes a single component of the mixture. The ***resolution*** between two chromatographic peaks, R_{AB}, is a quantitative measure of their separation, and is defined as

$$R_{AB} = \frac{t_{t,B} - t_{t,A}}{0.5\,(w_B + w_A)} = \frac{2\Delta t_r}{w_B + w_A} \tag{3.2.1}$$

where B is the later eluting of the two solutes. As shown in Figure 12.2.5 , the separation of two chromatographic peaks improves with an increase in R_{AB}. If the areas under the two peaks are identical—as is the case in Figure 12.2.5 —then a resolution of 1.50 corresponds to an overlap of only 0.13% for the two elution profiles. Because resolution is a quantitative measure of a separation's success, it is a useful way to determine if a change in experimental conditions leads to a better separation.

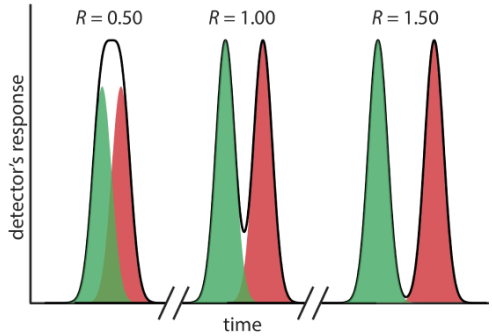

Figure 12.2.5 . Three examples that show the relationship between resolution and the separation of a two component mixture. The green peak and the red peak are the elution profiles for the two components. The chromatographic peak— which is the sum of the two elution profiles—is shown by the solid black line.

Example 12.2.1

In a chromatographic analysis of lemon oil a peak for limonene has a retention time of 8.36 min with a baseline width of 0.96 min. γ-Terpinene elutes at 9.54 min with a baseline width of 0.64 min. What is the resolution between the two peaks?

Solution

Using Equation 3.2.1 we find that the resolution is

$$R_{AB} = \frac{2\Delta t_r}{w_B + w_A} = \frac{2(9.54\text{ min} - 8.36\text{ min})}{0.64\text{ min} + 0.96\text{ min}} = 1.48$$

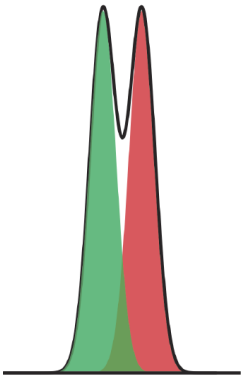

Figure 12.2.6 . Chromatogram for Exercise 12.2.1 .

? Exercise 12.2.1

Figure 12.2.6 shows the separation of a two-component mixture. What is the resolution between the two components? Use a ruler to measure Δt_r, w_A, and w_B in millimeters.

Answer

Because the relationship between elution time and distance is proportional, we can measure Δt_r, w_A, and w_B using a ruler. My measurements are 8.5 mm for Δt_r, and 12.0 mm each for w_A and w_B. Using these values, the resolution is

$$R_{AB} = \frac{2\Delta t_t}{w_A + w_B} = \frac{2(8.5\text{ mm})}{12.0\text{ mm} + 12.0\text{ mm}} = 0.70$$

Your measurements for Δt_r, w_A, and w_B will depend on the relative size of your monitor or printout; however, your value for the resolution should be similar to the answer above.

Equation 3.2.1 suggests that we can improve resolution by increasing Δt_r, or by decreasing w_A and w_B (Figure 12.2.7). To increase Δt_r we can use one of two strategies. One approach is to adjust the separation conditions so that both solutes spend less time in the mobile phase—that is, we increase each *solute's retention factor*—which provides more time to effect a separation. A second approach is to increase *selectivity* by adjusting conditions so that only one solute experiences a significant change in its retention time. The baseline width of a solute's peak depends on the solutes movement within and between the mobile phase and the stationary phase, and is governed by several factors that collectively we call *column efficiency*. We will consider each of these approaches for improving resolution in more detail, but first we must define some terms.

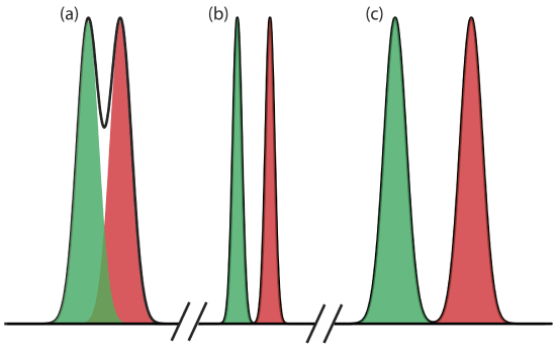

Figure 12.2.7 . Two method for improving chromatographic resolution: (a) original chromatogram; (b) chromatogram after decreasing w_A and w_B by $4\times$; and (c) chromatogram after increasing Δt_r by $2\times$.

Solute Retention Factor

Let's assume we can describe a solute's distribution between the mobile phase and stationary phase using the following equilibrium reaction

$$S_m \rightleftharpoons S_s$$

where S_m is the solute in the mobile phase and S_s is the solute in the stationary phase. Following the same approach we used in Chapter 7.7 for liquid–liquid extractions, the equilibrium constant for this reaction is an equilibrium partition coefficient, K_D.

$$K_D = \frac{[S_s]}{[S_m]}$$

This is not a trivial assumption. In this section we are, in effect, treating the solute's equilibrium between the mobile phase and the stationary phase as if it is identical to the equilibrium in a liquid–liquid extraction. You might question whether this is a reasonable assumption. There is an important difference between the two experiments that we need to consider. In a liquid–liquid extraction, which takes place in a separatory funnel, the two phases remain in contact with each other at all times, allowing for a true equilibrium. In chromatography, however, the mobile phase is in constant motion. A solute that moves into the stationary phase from the mobile phase will equilibrate back into a different portion of the mobile phase; this does not describe a true equilibrium.

So, we ask again: Can we treat a solute's distribution between the mobile phase and the stationary phase as an equilibrium process? The answer is yes, if the mobile phase velocity is slow relative to the kinetics of the solute's movement back and forth between the two phase. In general, this is a reasonable assumption.

In the absence of any additional equilibrium reactions in the mobile phase or the stationary phase, K_D is equivalent to the distribution ratio, D,

$$D = \frac{[S_0]}{[S_m]} = \frac{(\text{mol S})_s / V_s}{(\text{mol S})_m / V_m} = K_D \tag{3.2.2}$$

where V_s and V_m are the volumes of the stationary phase and the mobile phase, respectively.

A conservation of mass requires that the total moles of solute remain constant throughout the separation; thus, we know that the following equation is true.

$$(\text{mol S})_{tot} = (\text{mol S})_m + (\text{mol S})_s \tag{3.2.3}$$

Solving Equation 3.2.3 for the moles of solute in the stationary phase and substituting into Equation 3.2.2 leaves us with

$$D = \frac{\{(\text{mol S})_{tot} - (\text{mol S})_m\} / V_s}{(\text{mol S})_m / V_m}$$

Rearranging this equation and solving for the fraction of solute in the mobile phase, f_m, gives

$$f_m = \frac{(\text{mol S})_m}{(\text{mol S})_{tot}} = \frac{V_m}{DV_s + V_m} \tag{3.2.4}$$

which is identical to the result for a liquid-liquid extraction (see Chapter 7). Because we may not know the exact volumes of the stationary phase and the mobile phase, we simplify Equation 3.2.4 by dividing both the numerator and the denominator by V_m; thus

$$f_m = \frac{V_m / V_m}{DV_s / V_m + V_m / V_m} = \frac{1}{DV_s / V_m + 1} = \frac{1}{1 + k} \tag{3.2.5}$$

where k

$$k = D \times \frac{V_s}{V_m} \tag{3.2.6}$$

is the solute's ***retention factor***. Note that the larger the retention factor, the more the distribution ratio favors the stationary phase, leading to a more strongly retained solute and a longer retention time.

Other (older) names for the retention factor are capacity factor, capacity ratio, and partition ratio, and it sometimes is given the symbol k'. Keep this in mind if you are using other resources. Retention factor is the approved name from the IUPAC Gold Book.

We can determine a solute's retention factor from a chromatogram by measuring the column's void time, t_m, and the solute's retention time, t_r (see Figure 12.2.4). Solving Equation 3.2.5 for k, we find that

$$k = \frac{1 - f_m}{f_m} \tag{3.2.7}$$

Earlier we defined f_m as the fraction of solute in the mobile phase. Assuming a constant mobile phase velocity, we also can define f_m as

$$f_m = \frac{\text{time spent in the mobile phase}}{\text{time spent in the stationary phase}} = \frac{t_m}{t_r}$$

Substituting back into Equation 3.2.7 and rearranging leaves us with

$$k = \frac{1 - \frac{t_m}{t_t}}{\frac{t_m}{t_r}} = \frac{t_t - t_m}{t_m} = \frac{t'_r}{t_m} \tag{3.2.8}$$

where t'_r is the ***adjusted retention time***.

Example 12.2.2

In a chromatographic analysis of low molecular weight acids, butyric acid elutes with a retention time of 7.63 min. The column's void time is 0.31 min. Calculate the retention factor for butyric acid.

Solution

$$k_{but} = \frac{t_r - t_m}{t_m} = \frac{7.63 \text{ min} - 0.31 \text{ min}}{0.31 \text{ min}} = 23.6$$

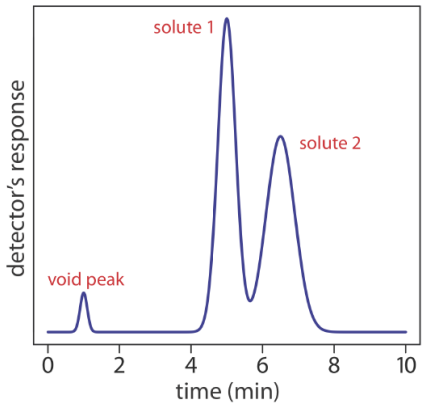

Figure 12.2.8 . Chromatogram for Exercise 12.2.2 .

Exercise 12.2.2

Figure 12.2.8 is the chromatogram for a two-component mixture. Determine the retention factor for each solute assuming the sample was injected at time t = 0.

Answer

Because the relationship between elution time and distance is proportional, we can measure t_m, $t_{r,1}$, and $t_{r,2}$ using a ruler. My measurements are 7.8 mm, 40.2 mm, and 51.5 mm, respectively. Using these values, the retention factors for solute A and solute B are

$$k_1 = \frac{t_{r1} - t_m}{t_m} = \frac{40.2 \text{ mm} - 7.8 \text{ mm}}{7.8 \text{ mm}} = 4.15$$

$$k_2 = \frac{t_{r2} - t_m}{t_m} = \frac{51.5 \text{ mm} - 7.8 \text{ mm}}{7.8 \text{ mm}} = 5.60$$

Your measurements for t_m, $t_{r,1}$, and $t_{r,2}$ will depend on the relative size of your monitor or printout; however, your value for the resolution should be similar to the answer above.

Selectivity

Selectivity is a relative measure of the retention of two solutes, which we define using a selectivity factor, α

$$\alpha = \frac{k_B}{k_A} = \frac{t_{r,B} - t_{\text{m}}}{t_{r,A} - t_{\text{m}}} \tag{3.2.9}$$

where solute A has the smaller retention time. When two solutes elute with identical retention time, $\alpha = 1.00$; for all other conditions $\alpha > 1.00$.

Example 12.2.3

In the chromatographic analysis for low molecular weight acids described in Example 12.2.2 , the retention time for isobutyric acid is 5.98 min. What is the selectivity factor for isobutyric acid and butyric acid?

Solution

First we must calculate the retention factor for isobutyric acid. Using the void time from Example 12.2.2 we have

$$k_{\text{iso}} = \frac{t_{\text{r}} - t_{\text{m}}}{t_{\text{m}}} = \frac{5.98 \text{ min} - 0.31 \text{ min}}{0.31 \text{ min}} = 18.3$$

The selectivity factor, therefore, is

$$\alpha = \frac{k_{\text{but}}}{k_{\text{iso}}} = \frac{23.6}{18.3} = 1.29$$

Exercise 12.2.3

Determine the selectivity factor for the chromatogram in Exercise 12.2.2 .

Answer

Using the results from Exercise 12.2.2 , the selectivity factor is

$$\alpha = \frac{k_2}{k_1} = \frac{5.60}{4.15} = 1.35$$

Your answer may differ slightly due to differences in your values for the two retention factors.

Column Efficiency

Suppose we inject a sample that has a single component. At the moment we inject the sample it is a narrow band of finite width. As the sample passes through the column, the width of this band continually increases in a process we call ***band broadening***. Column efficiency is a quantitative measure of the extent of band broadening.

See Figure 12.2.1 and Figure 12.2.2 . When we inject the sample it has a uniform, or rectangular concentration profile with respect to distance down the column. As it passes through the column, the band broadens and takes on a Gaussian concentration profile.

In their original theoretical model of chromatography, Martin and Synge divided the chromatographic column into discrete sections, which they called theoretical plates. Within each theoretical plate there is an equilibrium between the solute present in the stationary phase and the solute present in the mobile phase [Martin, A. J. P.; Synge, R. L. M. *Biochem. J.* **1941**, *35*, 1358–1366]. They described column efficiency in terms of the number of ***theoretical plates***, N,

$$N = \frac{L}{H} \tag{3.2.10}$$

where L is the column's length and H is the height of a theoretical plate. For any given column, the column efficiency improves—and chromatographic peaks become narrower—when there are more theoretical plates.

If we assume that a chromatographic peak has a Gaussian profile, then the extent of band broadening is given by the peak's variance or standard deviation. The height of a theoretical plate is the peak's variance per unit length of the column

$$H = \frac{\sigma^2}{L} \tag{3.2.11}$$

where the standard deviation, σ, has units of distance. Because retention times and peak widths usually are measured in seconds or minutes, it is more convenient to express the standard deviation in units of time, τ, by dividing σ by the solute's average linear velocity, $\overline{u}$, which is equivalent to dividing the distance it travels, L, by its retention time, t_r.

$$\tau = \frac{\sigma}{\overline{u}} = \frac{\sigma t_r}{L} \tag{3.2.12}$$

For a Gaussian peak shape, the width at the baseline, w, is four times its standard deviation, τ.

$$w = 4\tau \tag{3.2.13}$$

Combining Equation 3.2.11, Equation 3.2.12, and Equation 3.2.13 defines the height of a theoretical plate in terms of the easily measured chromatographic parameters t_r and w.

$$H = \frac{Lw^2}{16t_r^2} \tag{3.2.14}$$

Combing Equation 3.2.14 and Equation 3.2.10 gives the number of theoretical plates.

$$N = 16\frac{t_r^2}{w^2} = 16\left(\frac{t_r}{w}\right)^2 \tag{3.2.15}$$

Example 12.2.4

A chromatographic analysis for the chlorinated pesticide Dieldrin gives a peak with a retention time of 8.68 min and a baseline width of 0.29 min. Calculate the number of theoretical plates? Given that the column is 2.0 m long, what is the height of a theoretical plate in mm?

Solution

Using Equation 3.2.15, the number of theoretical plates is

$$N = 16\frac{t_r^2}{w^2} = 16 \times \frac{(8.68\text{ min})^2}{(0.29\text{ min})^2} = 14300\text{ plates}$$

Solving Equation 3.2.10 for H gives the average height of a theoretical plate as

$$H = \frac{L}{N} = \frac{2.00\text{ m}}{14300\text{ plates}} \times \frac{1000\text{ mm}}{\text{m}} = 0.14\text{ mm/plate}$$

Exercise 12.2.4

For each solute in the chromatogram for Exercise 12.2.2 , calculate the number of theoretical plates and the average height of a theoretical plate. The column is 0.5 m long.

Answer

Because the relationship between elution time and distance is proportional, we can measure $t_{r,1}$, $t_{r,2}$, w_1, and w_2 using a ruler. My measurements are 40.2 mm, 51.5 mm, 8.0 mm, and 13.5 mm, respectively. Using these values, the number of theoretical plates for each solute is

$$N_1 = 16\frac{t_{r,1}^2}{w_1^2} = 16 \times \frac{(40.2\text{ mm})^2}{(8.0\text{ mm})^2} = 400\text{ theoretical plates}$$

$$N_2 = 16\frac{t_{r,2}^2}{w_2^2} = 16 \times \frac{(51.5\text{ mm})^2}{(13.5\text{ mm})^2} = 233\text{ theoretical plates}$$

The height of a theoretical plate for each solute is

$$H_1 = \frac{L}{N_1} = \frac{0.500\text{ m}}{400\text{ plates}} \times \frac{1000\text{ mm}}{\text{m}} = 1.2\text{ mm/plate}$$

$$H_2 = \frac{L}{N_2} = \frac{0.500\text{ m}}{233\text{ plates}} \times \frac{1000\text{ mm}}{\text{m}} = 2.15\text{ mm/plate}$$

Your measurements for $t_{r,1}$, $t_{r,2}$, w_1, and w_2 will depend on the relative size of your monitor or printout; however, your values for N and for H should be similar to the answer above.

It is important to remember that a theoretical plate is an artificial construct and that a chromatographic column does not contain physical plates. In fact, the number of theoretical plates depends on both the properties of the column and the solute. As a result, the number of theoretical plates for a column may vary from solute to solute.

Peak Capacity

One advantage of improving column efficiency is that we can separate more solutes with baseline resolution. One estimate of the number of solutes that we can separate is

$$n_c = 1 + \frac{\sqrt{N}}{4}\ln\frac{V_{\text{max}}}{V_{\text{min}}} \tag{3.2.16}$$

where n_c is the column's ***peak capacity***, and V_{min} and V_{max} are the smallest and the largest volumes of mobile phase in which we can elute and detect a solute [Giddings, J. C. *Unified Separation Science*, Wiley-Interscience: New York, 1991]. A column with 10 000 theoretical plates, for example, can resolve no more than

$$n_c = 1 + \frac{\sqrt{10000}}{4}\ln\frac{30\text{mL}}{1\text{mL}} = 86\text{ solutes}$$

if V_{min} and V_{max} are 1 mL and 30 mL, respectively. This estimate provides an upper bound on the number of solutes and may help us exclude from consideration a column that does not have enough theoretical plates to separate a complex mixture. Just because a column's theoretical peak capacity is larger than the number of solutes, however, does not mean that a separation is feasible. In most situations the practical peak capacity is less than the theoretical peak capacity because the retention characteristics of some solutes are so similar that a separation is impossible. Nevertheless, columns with more theoretical plates, or with a greater range of possible elution volumes, are more likely to separate a complex mixture.

The smallest volume we can use is the column's void volume. The largest volume is determined either by our patience—the maximum analysis time we can tolerate—or by our inability to detect solutes because there is too much band broadening.

Asymmetric Peaks

Our treatment of chromatography in this section assumes that a solute elutes as a symmetrical Gaussian peak, such as that shown in Figure 12.2.4 . This ideal behavior occurs when the solute's partition coefficient, K_{D}

$$K_{\text{D}} = \frac{[S_{\text{s}}]}{[S_{\text{m}}]}$$

is the same for all concentrations of solute. If this is not the case, then the chromatographic peak has an asymmetric peak shape similar to those shown in Figure 12.2.9 . The chromatographic peak in Figure 12.2.9 a is an example of ***peak tailing***, which occurs when some sites on the stationary phase retain the solute more strongly than other sites. Figure 12.2.9 b, which is an example of ***peak fronting*** most often is the result of overloading the column with sample.

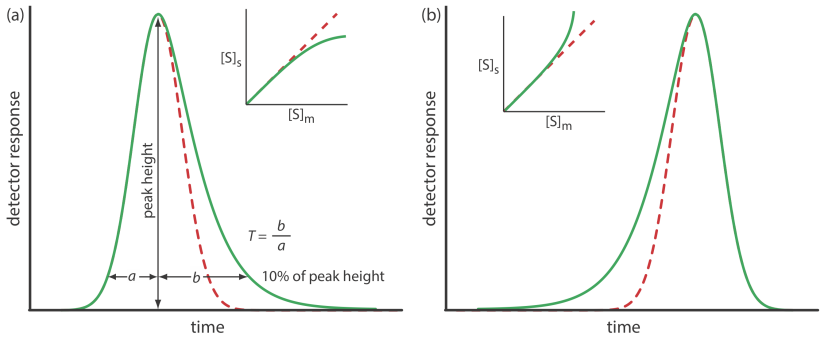

Figure 12.2.9 . Examples of asymmetric chromatographic peaks showing (a) peak tailing and (b) peak fronting. For both (a) and (b) the green chromatogram is the asymmetric peak and the red dashed chromatogram shows the ideal, Gaussian peak shape. The insets show the relationship between the concentration of solute in the stationary phase, $[S]_s$, and its concentration in the mobile phase, $[S]_m$. The dashed red lines show ideal behavior (K_D is constant for all conditions) and the green lines show nonideal behavior (K_D decreases or increases for higher total concentrations of solute). A quantitative measure of peak tailing, T, is shown in (a).

As shown in Figure 12.2.9 a, we can report a peak's asymmetry by drawing a horizontal line at 10% of the peak's maximum height and measuring the distance from each side of the peak to a line drawn vertically through the peak's maximum. The asymmetry factor, T, is defined as

$$T = \frac{b}{a}$$

The number of theoretical plates for an asymmetric peak shape is approximately

$$N \approx \frac{41.7 \times \frac{t_r^2}{(w_{0.1})^2}}{T + 1.25} = \frac{41.7 \times \frac{t_r^2}{(a+b)^2}}{T + 1.25}$$

where $w_{0.1}$ is the width at 10% of the peak's height [Foley, J. P.; Dorsey, J. G. *Anal. Chem.* **1983**, *55*, 730–737].

Asymmetric peaks have fewer theoretical plates, and the more asymmetric the peak the smaller the number of theoretical plates. For example, the following table gives values for N for a solute eluting with a retention time of 10.0 min and a peak width of 1.00 min.

b	a	T	N
0.5	0.5	1.00	1850
0.6	0.4	1.50	1520
0.7	0.3	2.33	1160
0.8	0.2	4.00	790

3.3: Optimizing Chromatographic Separations

Now that we have defined the solute retention factor, selectivity, and column efficiency we are able to consider how they affect the resolution of two closely eluting peaks. Because the two peaks have similar retention times, it is reasonable to assume that their peak widths are nearly identical. If the number of theoretical plates is the same for all solutes—not strictly true, but not a bad assumption—then from equation 12.2.15, the ratio t_r/w is a constant. If two solutes have similar retention times, then their peak widths must be similar. Equation 12.2.1, therefore, becomes

$$R_{AB} = \frac{t_{r,B} - t_{r,A}}{0.5\,(w_B + w_A)} \approx \frac{t_{r,B} - t_{r,A}}{0.5\,(2w_B)} = \frac{t_{r,B} - t_{r,A}}{w_B} \tag{3.3.1}$$

where *B* is the later eluting of the two solutes. Solving equation 12.2.15 for w_B and substituting into Equation 3.3.1 leaves us with the following result.

$$R_{AB} = \frac{\sqrt{N_B}}{4} \times \frac{t_{r,B} - t_{r,A}}{t_{r,B}} \tag{3.3.2}$$

Rearranging equation 12.2.8 provides us with the following equations for the retention times of solutes *A* and *B*.

$$t_{r,A} = k_A t_\mathrm{m} + t_\mathrm{m} \quad \text{and} \quad t_{\mathrm{r},B} = k_B t_\mathrm{m} + t_\mathrm{m}$$

After substituting these equations into Equation 3.3.2 and simplifying, we have

$$R_{AB} = \frac{\sqrt{N_B}}{4} \times \frac{k_B - k_A}{1 + k_B}$$

Finally, we can eliminate solute *A*'s retention factor by substituting in equation 12.2.9. After rearranging, we end up with the following equation for the resolution between the chromatographic peaks for solutes A and B.

$$R_{AB} = \frac{\sqrt{N_B}}{4} \times \frac{\alpha - 1}{\alpha} \times \frac{k_B}{1 + k_B} \tag{3.3.3}$$

In addition to resolution, another important factor in chromatography is the amount of time needed to elute a pair of solutes, which we can approximate using the retention time for solute *B*.

$$t_{r,s} = \frac{16 R_{AB}^2 H}{u} \times \left(\frac{\alpha}{\alpha - 1}\right)^2 \times \frac{(1 + k_B)^3}{k_B^2} \tag{3.3.4}$$

where *u* is the mobile phase's velocity.

> Although Equation 3.3.3 is useful for considering how a change in *N*, α, or *k* qualitatively affects resolution—which suits our purpose here—it is less useful for making accurate quantitative predictions of resolution, particularly for smaller values of *N* and for larger values of *R*. For more accurate predictions use the equation
>
> $$R_{AB} = \frac{\sqrt{N}}{4} \times (\alpha - 1) \times \frac{k_B}{1 + k_\mathrm{avg}}$$
>
> where k_avg is (k_A + k_B)/2. For a derivation of this equation and for a deeper discussion of resolution in column chromatography, see Foley, J. P. "Resolution Equations for Column Chromatography," *Analyst*, **1991**, *116*, 1275-1279.

Equation 3.3.3 and Equation 3.3.4 contain terms that correspond to column efficiency, selectivity, and the solute retention factor. We can vary these terms, more or less independently, to improve resolution and analysis time. The first term, which is a function of the number of theoretical plates (for Equation 3.3.3) or the height of a theoretical plate (for Equation 3.3.4), accounts for the effect of column efficiency. The second term is a function of α and accounts for the influence of column selectivity. Finally, the third term in both equations is a function of k_B and accounts for the effect of solute *B*'s retention factor. A discussion of how we can use these parameters to improve resolution is the subject of the remainder of this section.

Using the Retention Factor to Optimize Resolution

One of the simplest ways to improve resolution is to adjust the retention factor for solute *B*. If all other terms in Equation 3.3.3 remain constant, an increase in k_B will improve resolution. As shown by the green curve in Figure 12.3.1 , however, the improvement is greatest if the initial value of k_B is small. Once k_B exceeds a value of approximately 10, a further increase produces only a marginal improvement in resolution. For example, if the original value of k_B is 1, increasing its value to 10 gives an 82% improvement in resolution; a further increase to 15 provides a net improvement in resolution of only 87.5%.

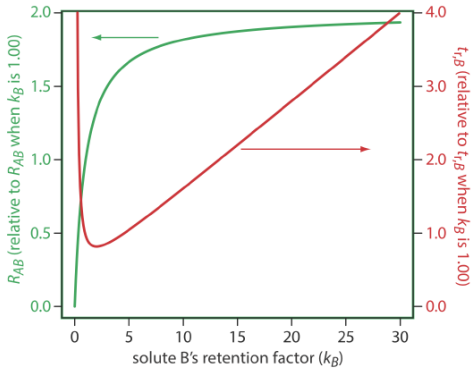

Figure 12.3.1 . Effect of k_B on the resolution for a pair of solutes, R_{AB}, and the retention time for the later eluting solute, $t_{r,B}$. The *y*-axes display the resolution and retention time relative to their respective values when k_B is 1.00.

Any improvement in resolution from increasing the value of k_B generally comes at the cost of a longer analysis time. The red curve in Figure 12.3.1 shows the relative change in the retention time for solute *B* as a function of its retention factor. Note that the minimum retention time is for $k_B = 2$. Increasing k_B from 2 to 10, for example, approximately doubles solute B's retention time.

> The relationship between retention factor and analysis time in Figure 12.3.1 works to our advantage if a separation produces an acceptable resolution with a large k_B. In this case we may be able to decrease k_B with little loss in resolution and with a significantly shorter analysis time.

To increase k_B without changing selectivity, α, any change to the chromatographic conditions must result in a general, nonselective increase in the retention factor for both solutes. In gas chromatography, we can accomplish this by decreasing the column's temperature. Because a solute's vapor pressure is smaller at lower temperatures, it spends more time in the stationary phase and takes longer to elute. In liquid chromatography, the easiest way to increase a solute's retention factor is to use a mobile phase that is a weaker solvent. When the mobile phase has a lower solvent strength, solutes spend proportionally more time in the stationary phase and take longer to elute.

Adjusting the retention factor to improve the resolution between one pair of solutes may lead to unacceptably long retention times for other solutes. For example, suppose we need to analyze a four-component mixture with baseline resolution and with a run-time of less than 20 min. Our initial choice of conditions gives the chromatogram in Figure 12.3.2 a. Although we successfully separate components 3 and 4 within 15 min, we fail to separate components 1 and 2. Adjusting conditions to improve the resolution for the first two components by increasing k_2 provides a good separation of all four components, but the run-time is too long (Figure 12.3.2 b). This problem of finding a single set of acceptable operating conditions is known as the ***general elution problem***.

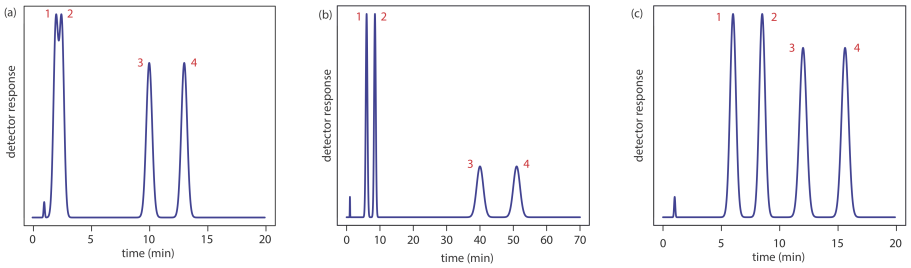

Figure 12.3.2 . Example showing the general elution problem in chromatography. See text for details.

One solution to the general elution problem is to make incremental adjustments to the retention factor as the separation takes place. At the beginning of the separation we set the initial chromatographic conditions to optimize the resolution for early eluting solutes. As the separation progresses, we adjust the chromatographic conditions to decrease the retention factor—and, therefore, to decrease the retention time—for each of the later eluting solutes (Figure 12.3.2 c). In gas chromatography this is accomplished by temperature programming. The column's initial temperature is selected such that the first solutes to elute are resolved fully. The temperature is then increased, either continuously or in steps, to bring off later eluting components with both an acceptable resolution and a reasonable analysis time. In liquid chromatography the same effect is obtained by increasing the solvent's eluting strength. This is known as a gradient elution. We will have more to say about each of these in later sections of this chapter.

Using Selectivity to Optimize Resolution

A second approach to improving resolution is to adjust the selectivity, α. In fact, for $\alpha \approx 1$ usually it is not possible to improve resolution by adjusting the solute retention factor, k_B, or the column efficiency, N. A change in α often has a more dramatic effect on resolution than a change in k_B. For example, changing α from 1.1 to 1.5, while holding constant all other terms, improves resolution by 267%. In gas chromatography, we adjust α by changing the stationary phase; in liquid chromatography, we change the composition of the mobile phase to adjust α.

To change α we need to selectively adjust individual solute retention factors. Figure 12.3.3 shows one possible approach for the liquid chromatographic separation of a mixture of substituted benzoic acids. Because the retention time of a compound's weak acid form and its weak base form are different, its retention time will vary with the pH of the mobile phase, as shown in Figure 12.3.3 a. The intersections of the curves in Figure 12.3.3 a show pH values where two solutes co-elute. For example, at a pH of 3.8 terephthalic acid and *p*-hydroxybenzoic acid elute as a single chromatographic peak.

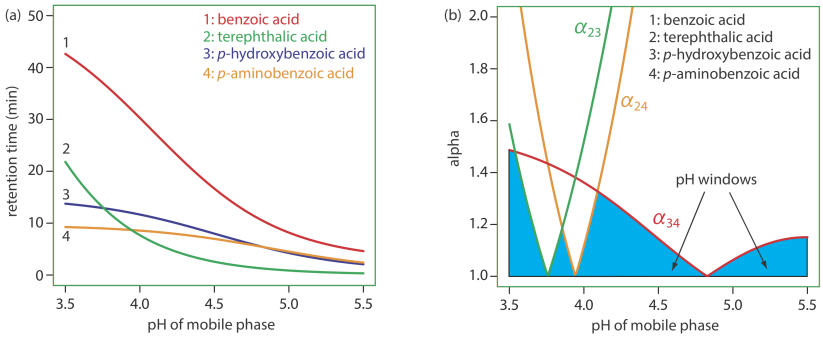

Figure 12.3.3 . Example showing how the mobile phase pH in liquid chromatography affects selectivity: (a) retention times for four substituted benzoic acids as a function of the mobile phase's pH; (b) alpha values for three pairs of solutes that are difficult to separate. See text for details. The mobile phase is an acetic acid/sodium acetate buffer and the stationary phase is a nonpolar hydrocarbon. Data from Harvey, D. T.; Byerly, S.; Bowman, A.; Tomlin, J. "Optimization of HPLC and GC Separations Using Response Surfaces," *J. Chem. Educ.* **1991**, *68*, 162–168.

Figure 12.3.3 a shows that there are many pH values where some separation is possible. To find the optimum separation, we plot a for each pair of solutes. The red, green, and orange curves in Figure 12.3.3 b show the variation in a with pH for the three pairs of solutes that are hardest to separate (for all other pairs of solutes, $\alpha > 2$ at all pH levels). The blue shading shows windows of pH values in which at least a partial separation is possible—this figure is sometimes called a window diagram—and the highest point in each window gives the optimum pH within that range. The best overall separation is the highest point in any window, which, for this example, is a pH of 3.5. Because the analysis time at this pH is more than 40 min (Figure 12.3.3 a), choosing a pH between 4.1–4.4 might produce an acceptable separation with a much shorter analysis time.

Let's use benzoic acid, C_6H_5COOH, to explain why pH can affect a solute's retention time. The separation uses an aqueous mobile phase and a nonpolar stationary phase. At lower pHs, benzoic acid predominately is in its weak acid form, C_6H_5COOH, and partitions easily into the nonpolar stationary phase. At more basic pHs, however, benzoic acid is in its weak base form, $C_6H_5COO^-$. Because it now carries a charge, its solubility in the mobile phase increases and its solubility in the nonpolar stationary phase decreases. As a result, it spends more time in the mobile phase and has a shorter retention time.

Although the usual way to adjust pH is to change the concentration of buffering agents, it also is possible to adjust pH by changing the column's temperature because a solute's pK_a value is pH-dependent; for a review, see Gagliardi, L. G.; Tascon,

M.; Castells, C. B. “Effect of Temperature on Acid–Base Equilibria in Separation Techniques: A Review,” *Anal. Chim. Acta*, **2015**, *889*, 35–57.

Using Column Efficiency to Optimize Resolution

A third approach to improving resolution is to adjust the column’s efficiency by increasing the number of theoretical plates, *N*. If we have values for k_B and α, then we can use Equation 3.3.3 to calculate the number of theoretical plates for any resolution. Table 12.3.1 provides some representative values. For example, if α = 1.05 and k_B = 2.0, a resolution of 1.25 requires approximately 24 800 theoretical plates. If our column provides only 12 400 plates, half of what is needed, then a separation is not possible. How can we double the number of theoretical plates? The easiest way is to double the length of the column, although this also doubles the analysis time. A better approach is to cut the height of a theoretical plate, *H*, in half, providing the desired resolution without changing the analysis time. Even better, if we can decrease *H* by more than 50%, it may be possible to achieve the desired resolution with an even shorter analysis time by also decreasing k_B or α.

Table 12.3.1 . Minimum Number of Theoretical Plates to Achieve Desired Resolution for Selected Values of k_B and α

	R_{AB} = 1.00		R_{AB} = 1.25		R_{AB} = 1.50	
k_B	$\alpha = 1.05$	$\alpha = 1.10$	$\alpha = 1.05$	$\alpha = 1.10$	$\alpha = 1.05$	$\alpha = 1.10$
0.5	63500	17400	99200	27200	143000	39200
1.0	28200	7740	44100	12100	63500	17400
1.5	19600	5380	30600	8400	44100	12100
2.0	15900	4360	24800	6810	35700	9800
3.0	12500	3440	19600	5380	28200	7740
5.0	10200	2790	15900	4360	22900	6270
10.0	8540	2340	13300	3660	19200	5270

To decrease the height of a theoretical plate we need to understand the experimental factors that affect band broadening. There are several theoretical treatments of band broadening. We will consider one approach that considers four contributions: variations in path lengths, longitudinal diffusion, mass transfer in the stationary phase, and mass transfer in the mobile phase.

Multiple Paths: Variations in Path Length

As solute molecules pass through the column they travel paths that differ in length. Because of this difference in path length, two solute molecules that enter the column at the same time will exit the column at different times. The result, as shown in Figure 12.3.4 , is a broadening of the solute’s profile on the column. The contribution of ***multiple paths*** to the height of a theoretical plate, H_p, is

$$H_p = 2\lambda d_p \tag{3.3.5}$$

where d_p is the average diameter of the particulate packing material and λ is a constant that accounts for the consistency of the packing. A smaller range of particle sizes and a more consistent packing produce a smaller value for λ. For a column without packing material, H_p is zero and there is no contribution to band broadening from multiple paths.

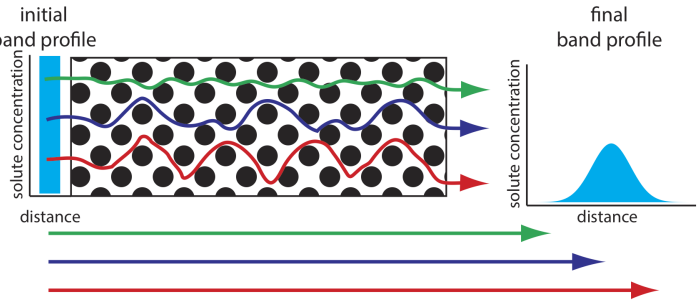

Figure 12.3.4 . The effect of multiple paths on a solute's band broadening. The solute's initial band profile is rectangular. As this band travels through the column, individual solute molecules travel different paths, three of which are shown by the meandering colored paths (the actual lengths of these paths are shown by the straight arrows at the bottom of the figure). Most solute molecules travel paths with lengths similar to that shown in blue, with a few traveling much shorter paths (green) or much longer paths (red). As a result, the solute's band profile at the end of the column is broader and Gaussian in shape.

An inconsistent packing creates channels that allow some solute molecules to travel quickly through the column. It also can creates pockets that temporarily trap some solute molecules, slowing their progress through the column. A more uniform packing minimizes these problems.

Longitudinal Diffusion

The second contribution to band broadening is the result of the solute's ***longitudinal diffusion*** in the mobile phase. Solute molecules are in constant motion, diffusing from regions of higher solute concentration to regions where the concentration of solute is smaller. The result is an increase in the solute's band width (Figure 12.3.5). The contribution of longitudinal diffusion to the height of a theoretical plate, H_d, is

$$H_d = \frac{2\gamma D_m}{u} \tag{3.3.6}$$

where D_m is the solute's diffusion coefficient in the mobile phase, u is the mobile phase's velocity, and γ is a constant related to the efficiency of column packing. Note that the effect of H_d on band broadening is inversely proportional to the mobile phase velocity: a higher velocity provides less time for longitudinal diffusion. Because a solute's diffusion coefficient is larger in the gas phase than in a liquid phase, longitudinal diffusion is a more serious problem in gas chromatography.

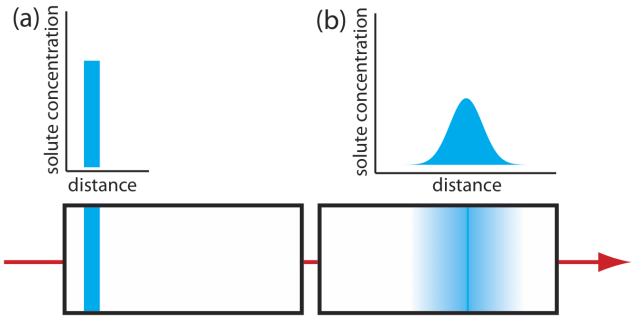

Figure 12.3.5 . The effect of longitudinal diffusion on a solute's band broadening. Two horizontal cross-sections through the column and the corresponding concentration versus distance profiles are shown, with (a) being earlier in time. The red arrow shows the direction in which the mobile phase is moving.

Mass Transfer

As the solute passes through the column it moves between the mobile phase and the stationary phase. We call this movement between phases ***mass transfer***. As shown in Figure 12.3.6 , band broadening occurs if the solute's movement within the mobile phase or within the stationary phase is not fast enough to maintain an equilibrium in its concentration between the two phases. On average, a solute molecule in the mobile phase moves down the column before it passes into the stationary phase. A solute molecule in the stationary phase, on the other hand, takes longer than expected to move back into the mobile phase. The contributions of mass transfer in the stationary phase, H_s, and mass transfer in the mobile phase, H_m, are given by the following equations

$$H_s = \frac{qkd_f^2}{(1+k)^2 D_s} u \tag{3.3.7}$$

$$H_m = \frac{fn\left(d_p^2, d_c^2\right)}{D_m} u \tag{3.3.8}$$

where d_f is the thickness of the stationary phase, d_c is the diameter of the column, D_s and D_m are the diffusion coefficients for the solute in the stationary phase and the mobile phase, k is the solute's retention factor, and q is a constant related to the column packing material. Although the exact form of H_m is not known, it is a function of particle size and column diameter. Note that the effect of H_s and H_m on band broadening is directly proportional to the mobile phase velocity because a smaller velocity provides more time for mass transfer.

> The abbreviation *fn* in Equation 3.3.7 means "is a function of."

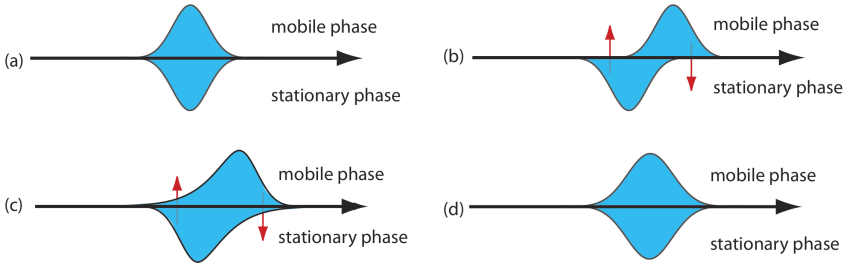

Figure 12.3.6 . Effect of mass transfer on band broadening: (a) Ideal equilibrium Gaussian profiles for the solute in the mobile phase and in the stationary phase. (b, c) If we allow the solute's band to move a small distance down the column, an equilibrium between the two phases no longer exits. The red arrows show the movement of solute—what we call the mass transfer of solute—from the stationary phase to the mobile phase, and from the mobile phase to the stationary phase. (d) Once equilibrium is reestablished, the solute's band is now broader.

Putting It All Together

The height of a theoretical plate is a summation of the contributions from each of the terms affecting band broadening.

$$H = H_p + H_d + H_s + H_m \tag{3.3.9}$$

An alternative form of this equation is the ***van Deemter equation***

$$H = A + \frac{B}{u} + Cu \tag{3.3.10}$$

which emphasizes the importance of the mobile phase's velocity. In the van Deemter equation, A accounts for the contribution of multiple paths (H_p), B/u accounts for the contribution of longitudinal diffusion (H_d), and Cu accounts for the combined contribution of mass transfer in the stationary phase and in the mobile phase (H_s and H_m).

There is some disagreement on the best equation for describing the relationship between plate height and mobile phase velocity [Hawkes, S. J. *J. Chem. Educ.* **1983**, *60*, 393–398]. In addition to the van Deemter equation, other equations include

$$H = \frac{B}{u} + (C_s + C_m)\, u$$

where C_s and C_m are the mass transfer terms for the stationary phase and the mobile phase and

$$H = Au^{1/3} + \frac{B}{u} + Cu$$

All three equations, and others, have been used to characterize chromatographic systems, with no single equation providing the best explanation in every case [Kennedy, R. T.; Jorgenson, J. W. *Anal. Chem.* **1989**, *61*, 1128–1135].

To increase the number of theoretical plates without increasing the length of the column, we need to decrease one or more of the terms in Equation 3.3.9. The easiest way to decrease H is to adjust the velocity of the mobile phase. For smaller mobile phase velocities, column efficiency is limited by longitudinal diffusion, and for higher mobile phase velocities efficiency is limited by the

two mass transfer terms. As shown in Figure 12.3.7 —which uses the van Deemter equation—the optimum mobile phase velocity is the minimum in a plot of H as a function of u.

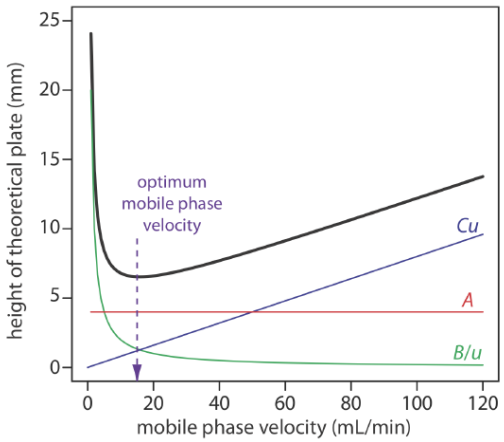

Figure 12.3.7 . Plot showing the relationship between the height of a theoretical plate, H, and the mobile phase's velocity, u, based on the van Deemter equation.

The remaining parameters that affect the terms in Equation 3.3.9 are functions of the column's properties and suggest other possible approaches to improving column efficiency. For example, both H_p and H_m are a function of the size of the particles used to pack the column. Decreasing particle size, therefore, is another useful method for improving efficiency.

> For a more detailed discussion of ways to assess the quality of a column, see Desmet, G.; Caooter, D.; Broeckhaven, K. "Graphical Data Represenation Methods to Assess the Quality of LC Columns," *Anal. Chem.* **2015**, *87*, 8593–8602.

Perhaps the most important advancement in chromatography columns is the development of open-tubular, or ***capillary columns***. These columns have very small diameters ($d_c \approx$ 50–500 μm) and contain no packing material ($d_p = 0$). Instead, the capillary column's interior wall is coated with a thin film of the stationary phase. Plate height is reduced because the contribution to H from H_p (Equation 3.3.5) disappears and the contribution from H_m (Equation 3.3.8) becomes smaller. Because the column does not contain any solid packing material, it takes less pressure to move the mobile phase through the column, which allows for longer columns. The combination of a longer column and a smaller height for a theoretical plate increases the number of theoretical plates by approximately $100\times$. Capillary columns are not without disadvantages. Because they are much narrower than packed columns, they require a significantly smaller amount of sample, which may be difficult to inject reproducibly. Another approach to improving resolution is to use thin films of stationary phase, which decreases the contribution to H from H_s (Equation 3.3.7).

> The smaller the particles, the more pressure is needed to push the mobile phase through the column. As a result, for any form of chromatography there is a practical limit to particle size.

3.4: Gas Chromatography

In ***gas chromatography*** (GC) we inject the sample, which may be a gas or a liquid, into an gaseous mobile phase (often called the carrier gas). The mobile phase carries the sample through a packed or a capillary column that separates the sample's components based on their ability to partition between the mobile phase and the stationary phase. Figure 12.4.1 shows an example of a typical gas chromatograph, which consists of several key components: a supply of compressed gas for the mobile phase; a heated injector, which rapidly volatilizes the components in a liquid sample; a column, which is placed within an oven whose temperature we can control during the separation; and a detector to monitor the eluent as it comes off the column. Let's consider each of these components.

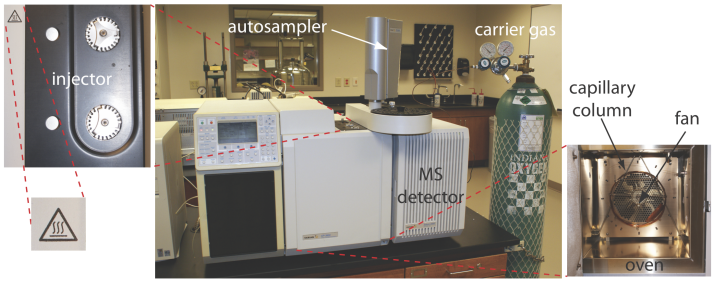

Figure 12.4.1 . Example of a typical gas chromatograph with insets showing the heated injection ports—note the symbol indicating that it is hot—and the oven that houses the column. This particular instrument is equipped with an autosampler for injecting samples, a capillary column, and a mass spectrometer (MS) as the detector. Note that the carrier gas is supplied by a tank of compressed gas.

Mobile Phase

The most common mobile phases for gas chromatography are He, Ar, and N_2, which have the advantage of being chemically inert toward both the sample and the stationary phase. The choice of carrier gas often is determined by the needs of instrument's detector. For a packed column the mobile phase velocity usually is 25–150 mL/min. The typical flow rate for a capillary column is 1–25 mL/min.

Chromatographic Columns

There are two broad classes of chromatographic columns: packed columns and capillary columns. In general, a packed column can handle larger samples and a capillary column can separate more complex mixtures.

Packed Columns

Packed columns are constructed from glass, stainless steel, copper, or aluminum, and typically are 2–6 m in length with internal diameters of 2–4 mm. The column is filled with a particulate solid support, with particle diameters ranging from 37–44 μm to 250–354 μm. Figure 12.4.2 shows a typical example of a packed column.

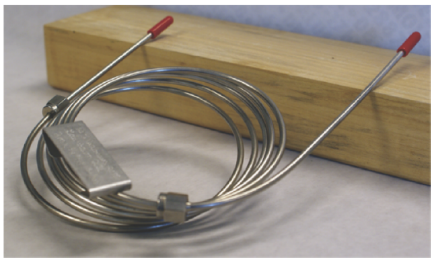

Figure 12.4.2 . Typical example of a packed column for gas chromatography. This column is made from stainless steel and is 2 m long with an internal diameter of 3.2 mm. The packing material in this column has a particle diameter of 149–177 μm. To put this in perspective, beach sand has a typical diameter of 700 μm and the diameter of fine grained sand is 250 μm.

The most widely used particulate support is diatomaceous earth, which is composed of the silica skeletons of diatoms. These particles are very porous, with surface areas ranging from 0.5–7.5 m^2/g, which provides ample contact between the mobile phase and the stationary phase. When hydrolyzed, the surface of a diatomaceous earth contains silanol groups (–SiOH), that serve as active sites for absorbing solute molecules in gas-solid chromatography (GSC).

In ***gas-liquid chromatography*** (GLC), we coat the packing material with a liquid mobile phase. To prevent uncoated packing material from adsorbing solutes, which degrades the quality of the separation, surface silanols are deactivated by reacting them with dimethyldichlorosilane and rinsing with an alcohol—typically methanol—before coating the particles with stationary phase.

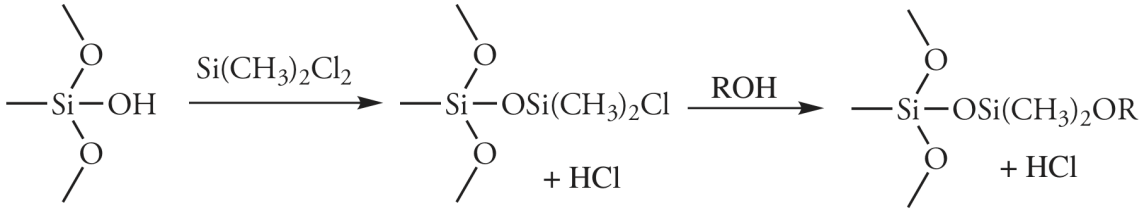

Figure 12.4.2 , for example, has approximately 1800 plates/m, or a total of approximately 3600 theoretical plates. If we assume a $V_{max}/V_{min} \approx 50$, then it has a peak capacity (equation 12.2.16) of

$$n_c = 1 + \frac{\sqrt{3600}}{4}\ln(50) \approx 60$$

Capillary Columns

A capillary, or ***open tubular column*** is constructed from fused silica and is coated with a protective polymer coating. Columns range from 15–100 m in length with an internal diameter of approximately 150–300 μm. Figure 12.4.3 shows an example of a typical capillary column.

Figure 12.4.3 . Typical example of a capillary column for gas chromatography. This column is 30 m long with an internal diameter of 247 μm. The interior surface of the capillary has a 0.25 μm coating of the liquid phase.

Capillary columns are of three principal types. In a ***wall-coated open tubular column*** (WCOT) a thin layer of stationary phase, typically 0.25 nm thick, is coated on the capillary's inner wall. In a ***porous-layer open tubular column*** (PLOT), a porous solid support—alumina, silica gel, and molecular sieves are typical examples—is attached to the capillary's inner wall. A ***support-coated open tubular column*** (SCOT) is a PLOT column that includes a liquid stationary phase. Figure 12.4.4 shows the differences between these types of capillary columns.

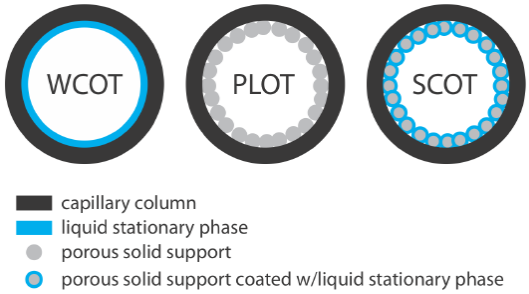

Figure 12.4.4 . Cross sections through the three types of capillary columns.

A capillary column provides a significant improvement in separation efficiency because it has more theoretical plates per meter and is longer than a packed column. For example, the capillary column in Figure 12.4.3 has almost 4300 plates/m, or a total of 129 000 theoretical plates. If we assume a $V_{max}/V_{min} \approx 50$, then it has a peak capacity of approximately 350. On the other hand, a packed column can handle a larger sample. Because of its smaller diameter, a capillary column requires a smaller sample, typically less than 10^{-2} μL.

Stationary Phases for Gas-Liquid Chromatography

Elution order in gas–liquid chromatography depends on two factors: the boiling point of the solutes, and the interaction between the solutes and the stationary phase. If a mixture's components have significantly different boiling points, then the choice of stationary phase is less critical. If two solutes have similar boiling points, then a separation is possible only if the stationary phase selectively interacts with one of the solutes. As a general rule, nonpolar solutes are separated more easily when using a nonpolar stationary phase, and polar solutes are easier to separate when using a polar stationary phase.

There are several important criteria for choosing a stationary phase: it must not react with the solutes, it must be thermally stable, it must have a low volatility, and it must have a polarity that is appropriate for the sample's components. Table 12.4.1 summarizes the properties of several popular stationary phases.

Table 12.4.1 . Selected Examples of Stationary Phases for Gas-Liquid Chromatography

stationary phase	polarity	trade name	temperature limit (°C)	representative applications
squalane	nonpolar	Squalane	150	low-boiling aliphatics hydrocarbons
Apezion L	nonpolar	Apezion L	300	amides, fatty acid methyl esters, terpenoids
polydimethyl siloxane	slightly polar	SE-30	300–350	alkaloids, amino acid derivatives, drugs, pesticides, phenols, steroids
phenylmethyl polysiloxane (50% phenyl, 50% methyl)	moderately polar	OV-17	375	alkaloids, drugs, pesticides, polyaromatic hydrocarbons, polychlorinated biphenyls
trifluoropropylmethyl polysiloxane (50% trifluoropropyl, 50% methyl)	moderately polar	OV-210	275	alkaloids, amino acid derivatives, drugs, halogenated compounds, ketones
cyanopropylphenylmethyl polysiloxane (50%cyanopropyl, 50% phenylmethyl)	polar	OV-225	275	nitriles, pesticides, steroids
polyethylene glycol	polar	Carbowax 20M	225	aldehydes, esters, ethers, phenols

Many stationary phases have the general structure shown in Figure 12.4.5 a. A stationary phase of polydimethyl siloxane, in which all the –R groups are methyl groups, $–CH_3$, is nonpolar and often makes a good first choice for a new separation. The order of elution when using polydimethyl siloxane usually follows the boiling points of the solutes, with lower boiling solutes eluting first. Replacing some of the methyl groups with other substituents increases the stationary phase's polarity and provides greater selectivity. For example, replacing 50% of the $–CH_3$ groups with phenyl groups, $–C_6H_5$, produces a slightly polar stationary phase. Increasing polarity is provided by substituting trifluoropropyl, $–C_3H_6CF$, and cyanopropyl, $–C_3H_6CN$, functional groups, or by using a stationary phase of polyethylene glycol (Figure 12.4.5 b).

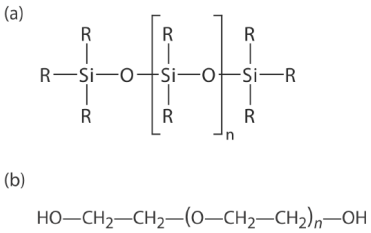

Figure 12.4.5 . General structures of common stationary phases: (a) substituted polysiloxane; (b) polyethylene glycol.

An important problem with all liquid stationary phases is their tendency to elute, or ***bleed*** from the column when it is heated. The temperature limits in Table 12.4.1 minimize this loss of stationary phase. Capillary columns with bonded or cross-linked stationary phases provide superior stability. A bonded stationary phase is attached chemically to the capillary's silica surface. Cross-linking, which is done after the stationary phase is in the capillary column, links together separate polymer chains to provide greater stability.

Another important consideration is the thickness of the stationary phase. From equation 12.3.7 we know that separation efficiency improves with thinner films of stationary phase. The most common thickness is 0.25 μm, although a thicker films is useful for highly volatile solutes, such as gases, because it has a greater capacity for retaining such solutes. Thinner films are used when separating low volatility solutes, such as steroids.

A few stationary phases take advantage of chemical selectivity. The most notable are stationary phases that contain chiral functional groups, which are used to separate enantiomers [Hinshaw, J. V. *LC* **.***GC* **1993**, *11*, 644–648].

Sample Introduction

Three factors determine how we introduce a sample to the gas chromatograph. First, all of the sample's constituents must be volatile. Second, the analytes must be present at an appropriate concentration. Finally, the physical process of injecting the sample must not degrade the separation. Each of these needs is considered in this section.

Preparing a Volatile Sample

Not every sample can be injected directly into a gas chromatograph. To move through the column, the sample's constituents must be sufficiently volatile. A solute of low volatility, for example, may be retained by the column and continue to elute during the analysis of subsequent samples. A nonvolatile solute will condense at the top of the column, degrading the column's performance.

We can separate a sample's volatile analytes from its nonvolatile components using any of the extraction techniques described in Chapter 7. A liquid–liquid extraction of analytes from an aqueous matrix into methylene chloride or another organic solvent is a common choice. Solid-phase extractions also are used to remove a sample's nonvolatile components.

An attractive approach to isolating analytes is a ***solid-phase microextraction*** (SPME). In one approach, which is illustrated in Figure 12.4.6 , a fused-silica fiber is placed inside a syringe needle. The fiber, which is coated with a thin film of an adsorbent material, such as polydimethyl siloxane, is lowered into the sample by depressing a plunger and is exposed to the sample for a predetermined time. After withdrawing the fiber into the needle, it is transferred to the gas chromatograph for analysis.

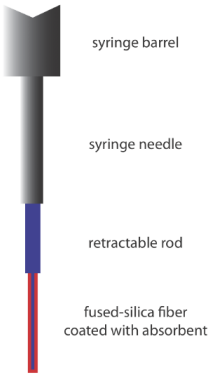

Figure 12.4.6 . Schematic diagram of a solid-phase microextraction device. The absorbent is shown in red.

Two additional methods for isolating volatile analytes are a purge-and-trap and headspace sampling. In a ***purge-and-trap***, we bubble an inert gas, such as He or N_2, through the sample, releasing—or purging—the volatile compounds. These compounds are carried by the purge gas through a trap that contains an absorbent material, such as Tenax, where they are retained. Heating the trap and back-flushing with carrier gas transfers the volatile compounds to the gas chromatograph. In ***headspace sampling*** we place the sample in a closed vial with an overlying air space. After allowing time for the volatile analytes to equilibrate between the sample and the overlying air, we use a syringe to extract a portion of the vapor phase and inject it into the gas chromatograph. Alternatively, we can sample the headspace with an SPME.

Thermal desorption is a useful method for releasing volatile analytes from solids. We place a portion of the solid in a glass-lined, stainless steel tube. After purging with carrier gas to remove any O_2 that might be present, we heat the sample. Volatile analytes are swept from the tube by an inert gas and carried to the GC. Because volatilization is not a rapid process, the volatile analytes often are concentrated at the top of the column by cooling the column inlet below room temperature, a process known as ***cryogenic focusing***. Once volatilization is complete, the column inlet is heated rapidly, releasing the analytes to travel through the column.

> The reason for removing O_2 is to prevent the sample from undergoing an oxidation reaction when it is heated.

To analyze a nonvolatile analyte we must convert it to a volatile form. For example, amino acids are not sufficiently volatile to analyze directly by gas chromatography. Reacting an amino acid, such as valine, with 1-butanol and acetyl chloride produces an esterified amino acid. Subsequent treatment with trifluoroacetic acid gives the amino acid's volatile N-trifluoroacetyl-*n*-butyl ester derivative.

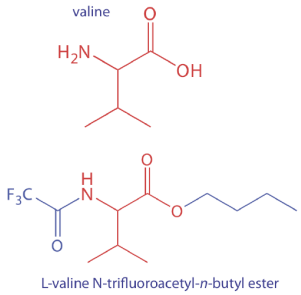

L-valine N-trifluoroacetyl-*n*-butyl ester

Adjusting the Analyte's Concentration

In an analyte's concentration is too small to give an adequate signal, then we must concentrate the analyte before we inject the sample into the gas chromatograph. A side benefit of many extraction methods is that they often concentrate the analytes. Volatile organic materials isolated from an aqueous sample by a purge-and-trap, for example, are concentrated by as much as $1000\times$.

If an analyte is too concentrated, it is easy to overload the column, resulting in peak fronting (see Figure 12.2.7) and a poor separation. In addition, the analyte's concentration may exceed the detector's linear response. Injecting less sample or diluting the sample with a volatile solvent, such as methylene chloride, are two possible solutions to this problem.

Injecting the Sample

In Chapter 12.3 we examined several explanations for why a solute's band increases in width as it passes through the column, a process we called band broadening. We also introduce an additional source of band broadening if we fail to inject the sample into the minimum possible volume of mobile phase. There are two principal sources of this precolumn band broadening: injecting the sample into a moving stream of mobile phase and injecting a liquid sample instead of a gaseous sample. The design of a gas chromatograph's injector helps minimize these problems.

An example of a simple injection port for a packed column is shown in Figure 12.4.7 . The top of the column fits within a heated injector block, with carrier gas entering from the bottom. The sample is injected through a rubber septum using a microliter syringe, such as the one shown in in Figure 12.4.8 . Injecting the sample directly into the column minimizes band broadening because it mixes the sample with the smallest possible amount of carrier gas. The injector block is heated to a temperature at least 50^oC above the boiling point of the least volatile solute, which ensures a rapid vaporization of the sample's components.

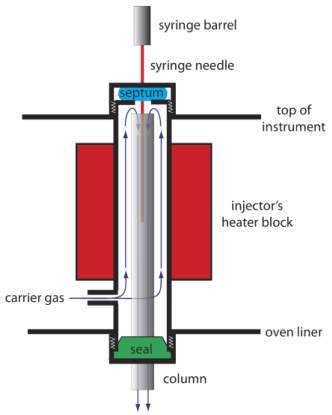

Figure 12.4.7 . Schematic diagram of a heated GC injector port for use with packed columns. The needle pierces a rubber septum and enters into the top of the column, which is located within a heater block.

Figure 12.4.8 . Example of a syringe for injecting samples into a gas chromatograph. This syringe has a maximum capacity of 10 µL with graduations every 0.1 µL.

Because a capillary column's volume is significantly smaller than that for a packed column, it requires a different style of injector to avoid overloading the column with sample. Figure 12.4.9 shows a schematic diagram of a typical split/splitless injector for use with a capillary column.

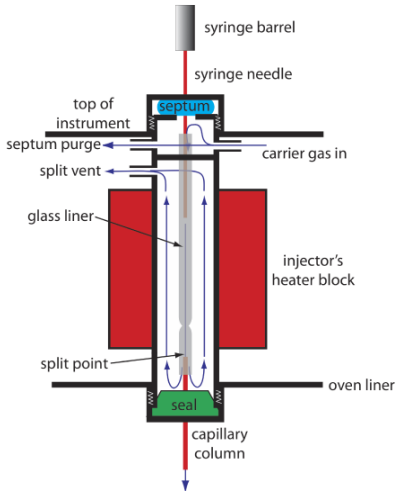

Figure 12.4.9 . Schematic diagram of a split/splitless injection port for use with capillary columns. The needle pierces a rubber septum and enters into a glass liner, which is located within a heater block. In a split injection the split vent is open; the split vent is closed for a splitless injection.

In a ***split injection*** we inject the sample through a rubber septum using a microliter syringe. Instead of injecting the sample directly into the column, it is injected into a glass liner where it mixes with the carrier gas. At the split point, a small fraction of the carrier gas and sample enters the capillary column with the remainder exiting through the split vent. By controlling the flow rate of the carrier gas as it enters the injector, and its flow rate through the septum purge and the split vent, we can control the fraction of sample that enters the capillary column, typically 0.1–10%.

> For example, if the carrier gas flow rate is 50 mL/min, and the flow rates for the septum purge and the split vent are 2 mL/min and 47 mL/min, respectively, then the flow rate through the column is 1 mL/min (= 50 – 2 – 47). The ratio of sample entering the column is 1/50, or 2%.

In a ***splitless injection***, which is useful for trace analysis, we close the split vent and allow all the carrier gas that passes through the glass liner to enter the column—this allows virtually all the sample to enters the column. Because the flow rate through the injector is low, significant precolumn band broadening is a problem. Holding the column's temperature approximately 20–25°C below the solvent's boiling point allows the solvent to condense at the entry to the capillary column, forming a barrier that traps the solutes. After allowing the solutes to concentrate, the column's temperature is increased and the separation begins.

For samples that decompose easily, an ***on-column injection*** may be necessary. In this method the sample is injected directly into the column without heating. The column temperature is then increased, volatilizing the sample with as low a temperature as is practical.

Temperature Control

Control of the column's temperature is critical to attaining a good separation when using gas chromatography. For this reason the column is placed inside a thermostated oven (see Figure 12.4.1). In an ***isothermal*** separation we maintain the column at a constant temperature. To increase the interaction between the solutes and the stationary phase, the temperature usually is set slightly below that of the lowest-boiling solute.

One difficulty with an isothermal separation is that a temperature that favors the separation of a low-boiling solute may lead to an unacceptably long retention time for a higher-boiling solute. ***Temperature programming*** provides a solution to this problem. At the beginning of the analysis we set the column's initial temperature below that for the lowest-boiling solute. As the separation progresses, we slowly increase the temperature at either a uniform rate or in a series of steps.

Detectors for Gas Chromatography

The final part of a gas chromatograph is the detector. The ideal detector has several desirable features: a low detection limit, a linear response over a wide range of solute concentrations (which makes quantitative work easier), sensitivity for all solutes or selectivity for a specific class of solutes, and an insensitivity to a change in flow rate or temperature.

Thermal Conductivity Detector (TCD)

One of the earliest gas chromatography detectors takes advantage of the mobile phase's thermal conductivity. As the mobile phase exits the column it passes over a tungsten-rhenium wire filament (see Figure 12.4.10 . The filament's electrical resistance depends on its temperature, which, in turn, depends on the thermal conductivity of the mobile phase. Because of its high thermal conductivity, helium is the mobile phase of choice when using a ***thermal conductivity detector*** (TCD).

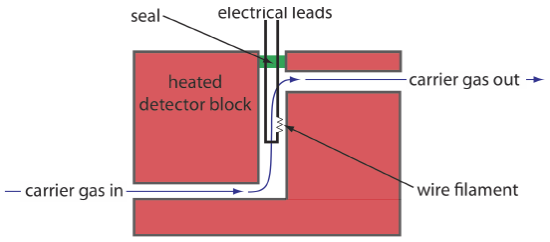

Figure 12.4.10 . Schematic diagram of a thermal conductivity detector showing one cell of a matched pair. The sample cell takes the carrier gas as it elutes from the column. A source of carrier gas that bypasses the column passes through a reference cell.

> Thermal conductivity, as the name suggests, is a measure of how easily a substance conducts heat. A gas with a high thermal conductivity moves heat away from the filament—and, thus, cools the filament—more quickly than does a gas with a low thermal conductivity.

When a solute elutes from the column, the thermal conductivity of the mobile phase in the TCD cell decreases and the temperature of the wire filament, and thus it resistance, increases. A reference cell, through which only the mobile phase passes, corrects for any time-dependent variations in flow rate, pressure, or electrical power, all of which affect the filament's resistance.

Because all solutes affect the mobile phase's thermal conductivity, the thermal conductivity detector is a universal detector. Another advantage is the TCD's linear response over a concentration range spanning 10^4–10^5 orders of magnitude. The detector also is non-destructive, which allows us to recover analytes using a postdetector cold trap. One significant disadvantage of the TCD detector is its poor detection limit for most analytes.

Flame Ionization Detector (FID)

The combustion of an organic compound in an H_2/air flame results in a flame that contains electrons and organic cations, presumably CHO^+. Applying a potential of approximately 300 volts across the flame creates a small current of roughly 10^{-9} to 10^{-12} amps. When amplified, this current provides a useful analytical signal. This is the basis of the popular ***flame ionization detector,*** a schematic diagram of which is shown in Figure 12.4.11 .

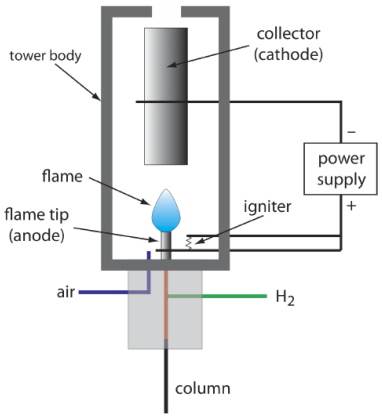

Figure 12.4.11 . Schematic diagram of a flame ionization detector. The eluent from the column mixes with H_2 and is burned in the presence of excess air. Combustion produces a flame that contains electrons and the cation $CHO^{+\cdot}$. Applying a potential between the flame's tip and the collector gives a current that is proportional to the concentration of cations in the flame.

Most carbon atoms—except those in carbonyl and carboxylic groups—generate a signal, which makes the FID an almost universal detector for organic compounds. Most inorganic compounds and many gases, such as H_2O and CO_2, are not detected, which makes the FID detector a useful detector for the analysis of organic analytes in atmospheric and aqueous environmental samples. Advantages of the FID include a detection limit that is approximately two to three orders of magnitude smaller than that for a thermal conductivity detector, and a linear response over 10^6–10^7 orders of magnitude in the amount of analyte injected. The sample, of course, is destroyed when using a flame ionization detector.

Electron Capture Detector (ECD)

The ***electron capture detector*** is an example of a selective detector. As shown in Figure 12.4.12 , the detector consists of a β-emitter, such as ^{63}Ni. The emitted electrons ionize the mobile phase, usually N_2, generating a standing current between a pair of electrodes. When a solute with a high affinity for capturing electrons elutes from the column, the current decreases, which serves as the signal. The ECD is highly selective toward solutes with electronegative functional groups, such as halogens and nitro groups, and is relatively insensitive to amines, alcohols, and hydrocarbons. Although its detection limit is excellent, its linear range extends over only about two orders of magnitude.

> A β-particle is an electron.

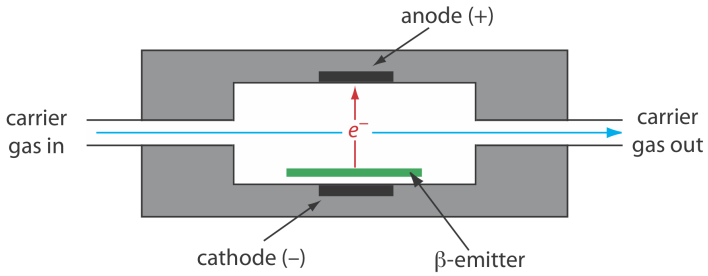

Figure 12.4.12 . Schematic diagram showing an electron capture detector.

Mass Spectrometer (MS)

A ***mass spectrometer*** is an instrument that ionizes a gaseous molecule using sufficient energy that the resulting ion breaks apart into smaller ions. Because these ions have different mass-to-charge ratios, it is possible to separate them using a magnetic field or

an electrical field. The resulting mass spectrum contains both quantitative and qualitative information about the analyte. Figure 12.4.13 shows a mass spectrum for toluene.

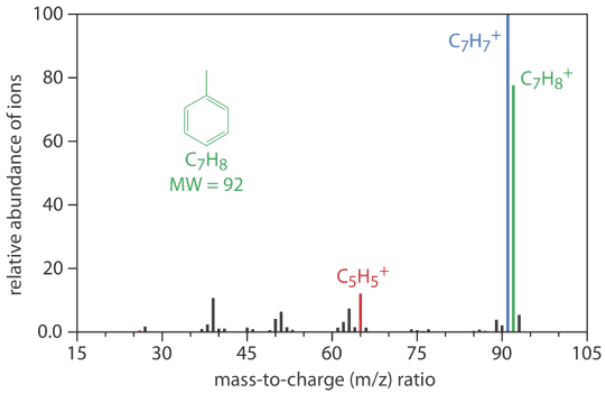

Figure 12.4.13 . Mass spectrum for toluene highlighting the molecular ion in green (m/z=92), and two fragment ions in blue (m/z=91) and in red (m/z= 65). A mass spectrum provides both quantitative and qualitative information: the height of any peak is proportional to the amount of toluene in the mass spectrometer and the fragmentation pattern is unique to toluene.

Figure 12.4.14 shows a block diagram of a typical gas chromatography-mass spectrometer (GC–MS) instrument. The effluent from the column enters the mass spectrometer's ion source in a manner that eliminates the majority of the carrier gas. In the ionization chamber the remaining molecules—a mixture of carrier gas, solvent, and solutes—undergo ionization and fragmentation. The mass spectrometer's mass analyzer separates the ions by their mass-to-charge ratio and a detector counts the ions and displays the mass spectrum.

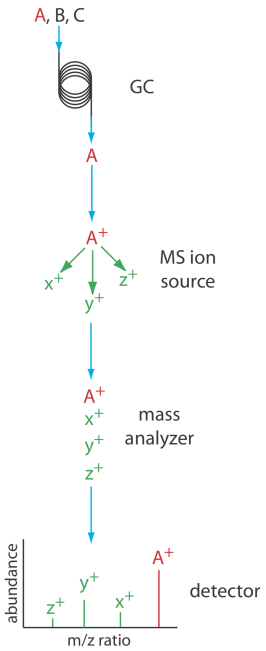

Figure 12.4.14 . Block diagram of GC– MS. A three component mixture enters the GC. When component A elutes from the column, it enters the MS ion source and ionizes to form the parent ion and several fragment ions. The ions enter the mass analyzer, which separates them by their mass-to-charge ratio, providing the mass spectrum shown at the detector.

There are several options for monitoring a chromatogram when using a mass spectrometer as the detector. The most common method is to continuously scan the entire mass spectrum and report the total signal for all ions that reach the detector during each scan. This total ion scan provides universal detection for all analytes. We can achieve some degree of selectivity by monitoring one or more specific mass-to-charge ratios, a process called selective-ion monitoring. A mass spectrometer provides excellent detection limits, typically 25 fg to 100 pg, with a linear range of 10^5 orders of magnitude. Because we continuously record the mass spectrum of the column's eluent, we can go back and examine the mass spectrum for any time increment. This is a distinct advantage for GC–MS because we can use the mass spectrum to help identify a mixture's components.

For more details on mass spectrometry see Introduction to Mass Spectrometry by Michael Samide and Olujide Akinbo, a resource that is part of the Analytical Sciences Digital Library.

Other Detectors

Two additional detectors are similar in design to a flame ionization detector. In the flame photometric detector, optical emission from phosphorous and sulfur provides a detector selective for compounds that contain these elements. The thermionic detector responds to compounds that contain nitrogen or phosphorous.

A Fourier transform infrared spectrophotometer (FT–IR) also can serve as a detector. In GC–FT–IR, effluent from the column flows through an optical cell constructed from a 10–40 cm Pyrex tube with an internal diameter of 1–3 mm. The cell's interior surface is coated with a reflecting layer of gold. Multiple reflections of the source radiation as it is transmit- ted through the cell increase the optical path length through the sample. As is the case with GC–MS, an FT–IR detector continuously records the column eluent's spectrum, which allows us to examine the IR spectrum for any time increment.

See Section 10.3 for a discussion of FT-IR spectroscopy and instrumentation.

Quantitative Applications

Gas chromatography is widely used for the analysis of a diverse array of samples in environmental, clinical, pharmaceutical, biochemical, forensic, food science and petrochemical laboratories. Table 12.4.2 provides some representative examples of applications.

Table 12.4.2 . Representative Applications of Gas Chromatography

area	applications
environmental analysis	green house gases (CO_2, CH_4, NO_x) in air pesticides in water, wastewater, and soil vehicle emissions trihalomethanes in drinking water
clinical analysis	drugs blood alcohols
forensic analysis	analysis of arson accelerants detection of explosives
consumer products	volatile organics in spices and fragrances trace organics in whiskey monomers in latex paint
petrochemical and chemical industry	purity of solvents refinery gas composition of gasoline

Quantitative Calculations

In a GC analysis the area under the peak is proportional to the amount of analyte injected onto the column. A peak's area is determined by integration, which usually is handled by the instrument's computer or by an electronic integrating recorder. If two peak are resolved fully, the determination of their respective areas is straightforward.

Before electronic integrating recorders and computers, two methods were used to find the area under a curve. One method used a manual planimeter; as you use the planimeter to trace an object's perimeter, it records the area. A second approach for finding a peak's area is the cut-and-weigh method. The chromatogram is recorded on a piece of paper and each peak of interest is cut out and weighed. Assuming the paper is uniform in thickness and density of fibers, the ratio of weights for two peaks is the same as the ratio of areas. Of course, this approach destroys your chromatogram.

Overlapping peaks, however, require a choice between one of several options for dividing up the area shared by the two peaks (Figure 12.4.15). Which method we use depends on the relative size of the two peaks and their resolution. In some cases, the use of peak heights provides more accurate results [(a) Bicking, M. K. L. Chromatography Online, April 2006; (b) Bicking, M. K. L. Chromatography Online, June 2006].

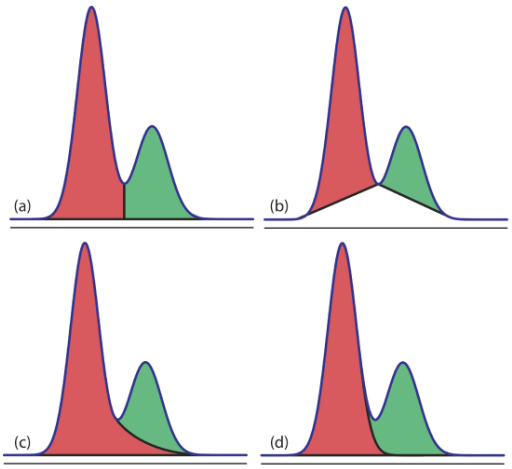

Figure 12.4.15 . Four methods for determining the areas under two overlapping chromatographic peaks: (a) the drop method; (b) the valley method; (c) the exponential skim method; and (d) the Gaussian skim method. Other methods for determining areas also are available.

For quantitative work we need to establish a calibration curve that relates the detector's response to the analyte's concentration. If the injection volume is identical for every standard and sample, then an external standardization provides both accurate and precise results. Unfortunately,even under the best conditions the relative precision for replicate injections may differ by 5%; often it is substantially worse. For quantitative work that requires high accuracy and precision, the use of internal standards is recommended.

> To review the method of internal standards, see Chapter 5.3.

Example 12.4.1

Marriott and Carpenter report the following data for five replicate injections of a mixture that contains 1% v/v methyl isobutyl ketone and 1% v/v *p*-xylene in dichloromethane [Marriott, P. J.; Carpenter, P. D. *J. Chem. Educ.* **1996**, *73*, 96–99].

injection	peak	peak area (arb. units)
I	1	48075
	2	78112
II	1	85829
	2	135404
III	1	84136
	2	132332
IV	1	71681
	2	112889
V	1	58054
	2	91287

Assume that *p*-xylene (peak 2) is the analyte, and that methyl isobutyl ketone (peak 1) is the internal standard. Determine the 95% confidence interval for a single-point standardization with and without using the internal standard.

Solution

For a single-point external standardization we ignore the internal standard and determine the relationship between the peak area for *p*-xylene, A_2, and the concentration, C_2, of *p*-xylene.

$$A_2 = kC_2$$

Substituting the known concentration for *p*-xylene (1% v/v) and the appropriate peak areas, gives the following values for the constant *k*.

$$78112 \quad 135404 \quad 132332 \quad 112889 \quad 91287$$

The average value for *k* is 110 000 with a standard deviation of 25 100 (a relative standard deviation of 22.8%). The 95% confidence interval is

$$\mu = \overline{X} \pm \frac{ts}{\sqrt{n}} = 111000 \pm \frac{(2.78)(25100)}{\sqrt{5}} = 111000 \pm 31200$$

For an internal standardization, the relationship between the analyte's peak area, A_2, the internal standard's peak area, A_1, and their respective concentrations, C_2 and C_1, is

$$\frac{A_2}{A_1} = k\frac{C_2}{C_1}$$

Substituting in the known concentrations and the appropriate peak areas gives the following values for the constant *k*.

$$1.5917 \quad 1.5776 \quad 1.5728 \quad 1.5749 \quad 1.5724$$

The average value for *k* is 1.5779 with a standard deviation of 0.0080 (a relative standard deviation of 0.507%). The 95% confidence interval is

$$\mu = \overline{X} \pm \frac{ts}{\sqrt{n}} = 1.5779 \pm \frac{(2.78)(0.0080)}{\sqrt{5}} = 1.5779 \pm 0.0099$$

Although there is a substantial variation in the individual peak areas for this set of replicate injections, the internal standard compensates for these variations, providing a more accurate and precise calibration.

Exercise 12.4.1

Figure 12.4.16 shows chromatograms for five standards and for one sample. Each standard and sample contains the same concentration of an internal standard, which is 2.50 mg/mL. For the five standards, the concentrations of analyte are 0.20 mg/mL, 0.40 mg/mL, 0.60 mg/mL, 0.80 mg/mL, and 1.00 mg/mL, respectively. Determine the concentration of analyte in the sample by (a) ignoring the internal standards and creating an external standards calibration curve, and by (b) creating an internal standard calibration curve. For each approach, report the analyte's concentration and the 95% confidence interval. Use peak heights instead of peak areas.

Answer

The following table summarizes my measurements of the peak heights for each standard and the sample, and their ratio (although your absolute values for peak heights will differ from mine, depending on the size of your monitor or printout, your relative peak height ratios should be similar to mine).

[standard] (mg/mL)	peak height of standard (mm)	peak height of analyte (mm)	peak height ratio
0.20	35	7	0.20
0.40	41	16	0.39
0.60	44	27	0.61
0.80	48	39	0.81

[standard] (mg/mL)	peak height of standard (mm)	peak height of analyte (mm)	peak height ratio
1.00	41	41	1.00
sample	39	21	0.54

Figure (a) shows the calibration curve and the calibration equation when we ignore the internal standard. Substituting the sample's peak height into the calibration equation gives the analyte's concentration in the sample as 0.49 mg/mL. The 95% confidence interval is ±0.24 mg/mL. The calibration curve shows quite a bit of scatter in the data because of uncertainty in the injection volumes.

Figure (b) shows the calibration curve and the calibration equation when we include the internal standard. Substituting the sample's peak height ratio into the calibration equation gives the analyte's concentration in the sample as 0.54 mg/mL. The 95% confidence interval is ±0.04 mg/mL.

To review the use of Excel or R for regression calculations and confidence intervals, see Chapter 5.5.

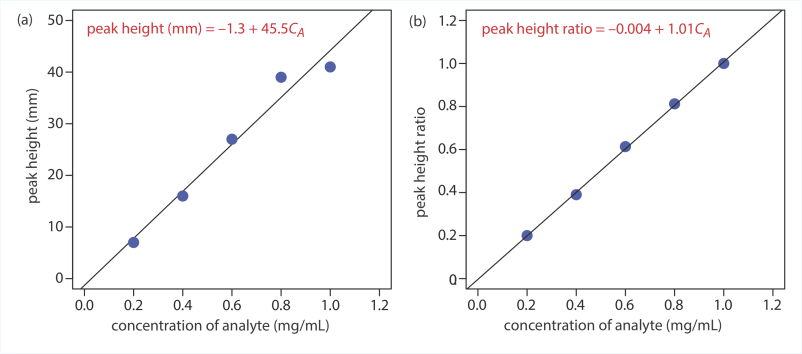

The data for this exercise were created so that the analyte's actual concentration is 0.55 mg/mL. Given the resolution of my ruler's scale, my answer is pretty reasonable. Your measurements may be slightly different, but your answers should be close to the actual values.

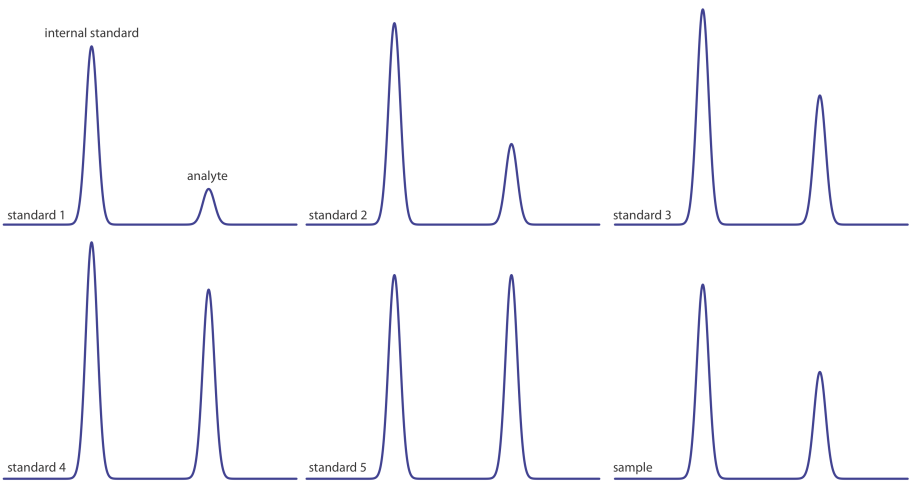

Figure 12.4.16 . Chromatograms for Practice Exercise 12.5.

Qualitative Applications

In addition to a quantitative analysis, we also can use chromatography to identify the components of a mixture. As noted earlier, when using an FT–IR or a mass spectrometer as the detector we have access to the eluent's full spectrum for any retention time. By interpreting the spectrum or by searching against a library of spectra, we can identify the analyte responsible for each chromatographic peak.

In addition to identifying the component responsible for a particular chromatographic peak, we also can use the saved spectra to evaluate peak purity. If only one component is responsible for a chromatographic peak, then the spectra should be identical throughout the peak's elution. If a spectrum at the beginning of the peak's elution is different from a spectrum taken near the end of the peak's elution, then at least two components are co-eluting.

When using a nonspectroscopic detector, such as a flame ionization detector, we must find another approach if we wish to identify the components of a mixture. One approach is to spike a sample with the suspected compound and look for an increase in peak height. We also can compare a peak's retention time to the retention time for a known compound if we use identical operating conditions.

Because a compound's retention times on two identical columns are not likely to be the same—differences in packing efficiency, for example, will affect a solute's retention time on a packed column—creating a table of standard retention times is not possible. ***Kovat's retention index*** provides one solution to the problem of matching retention times. Under isothermal conditions, the adjusted retention times for normal alkanes increase logarithmically. Kovat defined the retention index, *I*, for a normal alkane as 100 times the number of carbon atoms. For example, the retention index is 400 for butane, C_4H_{10}, and 500 for pentane, C_5H_{12}. To determine the a compound's retention index, I_{cpd}, we use the following formula

$$I_{cpd} = 100 \times \frac{\log t'_{r,cpd} - \log t'_{r,x}}{\log t'_{r,x+1} - \log t'_{r,x}} + I_x \tag{3.4.1}$$

where $t'_{r,cpd}$ is the compound's adjusted retention time, $t'_{r,x}$ and $t'_{r,x+1}$ are the adjusted retention times for the normal alkanes that elute immediately before the compound and immediately after the compound, respectively, and I_x is the retention index for the normal alkane that elutes immediately before the compound. A compound's retention index for a particular set of chromatographic conditions—stationary phase, mobile phase, column type, column length, temperature, etc.—is reasonably consistent from day- to-day and between different columns and instruments.

Tables of Kovat's retention indices are available; see, for example, the NIST Chemistry Webbook. A search for toluene returns 341 values of *I* for over 20 different stationary phases, and for both packed columns and capillary columns.

Example 12.4.2

In a separation of a mixture of hydrocarbons the following adjusted retention times are measured: 2.23 min for propane, 5.71 min for isobutane, and 6.67 min for butane. What is the Kovat's retention index for each of these hydrocarbons?

Solution

Kovat's retention index for a normal alkane is 100 times the number of carbons; thus, for propane, *I* = 300 and for butane, *I* = 400. To find Kovat's retention index for isobutane we use Equation 3.4.1.

$$I_{\text{isobutane}} = 100 \times \frac{\log(5.71) - \log(2.23)}{\log(6.67) - \log(2.23)} + 300 = 386$$

Exercise 12.4.2

When using a column with the same stationary phase as in Example 12.4.2 , you find that the retention times for propane and butane are 4.78 min and 6.86 min, respectively. What is the expected retention time for isobutane?

Answer

Because we are using the same column we can assume that isobutane's retention index of 386 remains unchanged. Using Equation 3.4.1, we have

$$386 = 100 \times \frac{\log x - \log(4.78)}{\log(6.86) - \log(4.78)} + 300$$

where *x* is the retention time for isobutane. Solving for *x*, we find that

$$0.86 = \frac{\log x - \log(4.78)}{\log(6.86) - \log(4.78)}$$

$$0.135 = \log x - 0.679$$

$$0.814 = \log x$$

$$x = 6.52$$

the retention time for isobutane is 6.5 min.

The best way to appreciate the theoretical and the practical details discussed in this section is to carefully examine a typical analytical method. Although each method is unique, the following description of the determination of trihalomethanes in drinking water provides an instructive example of a typical procedure. The description here is based on a Method 6232B in *Standard Methods for the Examination of Water and Wastewater*, 20th Ed., American Public Health Association: Washington, DC, 1998.

Representative Method 12.4.1: Determination of Trihalomethanes in Drinking Water

Description of Method

Trihalomethanes, such as chloroform, $CHCl_3$, and bromoform, $CHBr_3$, are found in most chlorinated waters. Because chloroform is a suspected carcinogen, the determination of trihalomethanes in public drinking water supplies is of considerable importance. In this method the trihalomethanes $CHCl_3$, $CHBrCl_2$, $CHBr_2Cl$, and $CHBr_3$ are isolated using a liquid–liquid extraction with pentane and determined using a gas chromatograph equipped with an electron capture detector.

Procedure

Collect the sample in a 40-mL glass vial equipped with a screw-cap lined with a TFE-faced septum. Fill the vial until it overflows, ensuring that there are no air bubbles. Add 25 mg of ascorbic acid as a reducing agent to quench the further production of trihalomethanes. Seal the vial and store the sample at 4°C for no longer than 14 days.

Prepare a standard stock solution for each trihalomethane by placing 9.8 mL of methanol in a 10-mL volumetric flask. Let the flask stand for 10 min, or until all surfaces wetted with methanol are dry. Weigh the flask to the nearest ±0.1 mg. Using a 100-µL syringe, add 2 or more drops of trihalomethane to the volumetric flask, allowing each drop to fall directly into the methanol. Reweigh the flask before diluting to volume and mixing. Transfer the solution to a 40-mL glass vial equipped with a TFE-lined screw-top and report the concentration in µg/mL. Store the stock solutions at –10 to –20°C and away from the light.

Prepare a multicomponent working standard from the stock standards by making appropriate dilutions of the stock solution with methanol in a volumetric flask. Choose concentrations so that calibration standards (see below) require no more than 20 µL of working standard per 100 mL of water.

Using the multicomponent working standard, prepare at least three, but preferably 5–7 calibration standards. At least one standard must be near the detection limit and the standards must bracket the expected concentration of trihalomethanes in the samples. Using an appropriate volumetric flask, prepare the standards by injecting at least 10 µL of the working standard below the surface of the water and dilute to volume. Gently mix each standard three times only. Discard the solution in the neck of the volumetric flask and then transfer the remaining solution to a 40-mL glass vial with a TFE-lined screw-top. If the standard has a headspace, it must be analyzed within 1 hr; standards without a headspace may be held for up to 24 hr.

Prepare an internal standard by dissolving 1,2-dibromopentane in hexane. Add a sufficient amount of this solution to pentane to give a final concentration of 30 µg 1,2-dibromopentane/L.

To prepare the calibration standards and samples for analysis, open the screw top vial and remove 5 mL of the solution. Recap the vial and weigh to the nearest ±0.1 mg. Add 2.00 mL of pentane (with the internal standard) to each vial and shake vigorously for 1 min. Allow the two phases to separate for 2 min and then use a glass pipet to transfer at least 1 mL of the pentane (the upper phase) to a 1.8-mL screw top sample vial equipped with a TFE septum, and store at 4°C until you are ready to inject them into the GC. After emptying, rinsing, and drying the sample's original vial, weigh it to the nearest ±0.1 mg and calculate the sample's weight to ±0.1 g. If the density is 1.0 g/mL, then the sample's weight is equivalent to its volume.

Inject a 1–5 μL aliquot of the pentane extracts into a GC equipped with a 2-mm ID, 2-m long glass column packed with a stationary phase of 10% squalane on a packing material of 80/100 mesh Chromosorb WAW. Operate the column at 67°C and a flow rate of 25 mL/min.

> A variety of other columns can be used. Another option, for example, is a 30-m fused silica column with an internal diameter of 0.32 mm and a 1 μm coating of the stationary phase DB-1. A linear flow rate of 20 cm/s is used with the following temperature program: hold for 5 min at 35°C; increase to 70°C at 10°C/min; increase to 200°C at 20°C/min.

Questions

1. A simple liquid–liquid extraction rarely extracts 100% of the analyte. How does this method account for incomplete extractions?

   Because we use the same extraction procedure for the samples and the standards, we reasonably expect that the extraction efficiency is the same for all samples and standards; thus, the relative amount of analyte in any two samples or standards is unaffected by an incomplete extraction.

2. Water samples are likely to contain trace amounts of other organic compounds, many of which will extract into pentane along with the trihalomethanes. A short, packed column, such as the one used in this method, generally does not do a particularly good job of resolving chromatographic peaks. Why do we not need to worry about these other compounds?

   An electron capture detector responds only to compounds, such as the trihalomethanes, that have electronegative functional groups. Because an electron capture detector will not respond to most of the potential interfering compounds, the chromatogram will have relatively few peaks other than those for the trihalomethanes and the internal standard.

3. Predict the order in which the four analytes elute from the GC column.

   Retention time should follow the compound's boiling points, eluting from the lowest boiling point to the highest boiling points. The expected elution order is $CHCl_3$ (61.2°C), $CHCl_2Br$ (90°C), $CHClBr_2$ (119°C), and $CHBr_3$ (149.1°C).

4. Although chloroform is an analyte, it also is an interferent because it is present at trace levels in the air. Any chloroform present in the laboratory air, for example, may enter the sample by diffusing through the sample vial's silicon septum. How can we determine whether samples are contaminated in this manner?

   A sample blank of trihalomethane-free water is kept with the samples at all times. If the sample blank shows no evidence for chloroform, then we can safely assume that the samples also are free from contamination.

5. Why is it necessary to collect samples without a headspace (a layer of air that overlays the liquid) in the sample vial?

   Because trihalomethanes are volatile, the presence of a headspace allows for the loss of analyte from the sample to the headspace, resulting in a negative determinate error.

6. In preparing the stock solution for each trihalomethane, the procedure specifies that we add two or more drops of the pure compound by dropping them into a volumetric flask that contains methanol. When preparing the calibration standards, however, the working standard must be injected below the surface of the methanol. Explain the reason for this difference.

   When preparing a stock solution, the potential loss of the volatile trihalomethane is unimportant because we determine its concentration by weight after adding it to the methanol and diluting to volume. When we prepare the calibration standard, however, we must ensure that the addition of trihalomethane is quantitative; thus, we inject it below the surface to avoid the potential loss of analyte.

Evaluation

Scale of Operation

Gas chromatography is used to analyze analytes present at levels ranging from major to ultratrace components. Depending on the detector, samples with major and minor analytes may need to be diluted before analysis. The thermal conductivity and flame ionization detectors can handle larger amounts of analyte; other detectors, such as an electron capture detector or a mass spectrometer, require substantially smaller amounts of analyte. Although the injection volume for gas chromatography is quite small—typically about a microliter—the amount of available sample must be sufficient that the injection is a representative subsample. For a trace analyte, the actual amount of injected analyte is often in the picogram range. Using Representative Method 12.4.1 as an example, a 3.0-μL injection of 1 μg/L $CHCl_3$ is equivalent to 15 pg of $CHCl_3$, assuming a 100% extraction efficiency.

Accuracy

The accuracy of a gas chromatographic method varies substantially from sample-to-sample. For routine samples, accuracies of 1–5% are common. For analytes present at very low concentration levels, for samples with complex matrices, or for samples that require significant processing before analysis, accuracy may be substantially poorer. In the analysis for trihalomethanes described in Representative Method 12.4.1, for example, determinate errors as large as ±25% are possible.

Precision

The precision of a gas chromatographic analysis includes contributions from sampling, sample preparation, and the instrument. The relative standard deviation due to the instrument typically is 1–5%, although it can be significantly higher. The principal limitations are detector noise, which affects the determination of peak area, and the reproducibility of injection volumes. In quantitative work, the use of an internal standard compensates for any variability in injection volumes.

Sensitivity

In a gas chromatographic analysis, sensitivity is determined by the detector's characteristics. Of particular importance for quantitative work is the detector's linear range; that is, the range of concentrations over which a calibration curve is linear. Detectors with a wide linear range, such as the thermal conductivity detector and the flame ionization detector, can be used to analyze samples over a wide range of concentrations without adjusting operating conditions. Other detectors, such as the electron capture detector, have a much narrower linear range.

Selectivity

Because it combines separation with analysis, chromatographic methods provide excellent selectivity. By adjusting conditions it usually is possible to design a separation so that the analytes elute by themselves, even when the mixture is complex. Additional selectivity is obtained by using a detector, such as the electron capture detector, that does not respond to all compounds.

Time, Cost, and Equipment

Analysis time can vary from several minutes for samples that contain only a few constituents, to more than an hour for more complex samples. Preliminary sample preparation may substantially increase the analysis time. Instrumentation for gas chromatography ranges in price from inexpensive (a few thousand dollars) to expensive (>$50,000). The more expensive models are designed for capillary columns, include a variety of injection options, and use more sophisticated detectors, such as a mass spectrometer, or include multiple detectors. Packed columns typically cost <$200, and the cost of a capillary column is typically $300–$1000.

3.5: High-Performance Liquid Chromatography

In ***high-performance liquid chromatography*** (HPLC) we inject the sample, which is in solution form, into a liquid mobile phase. The mobile phase carries the sample through a packed or capillary column that separates the sample's components based on their ability to partition between the mobile phase and the stationary phase. Figure 12.5.1 shows an example of a typical HPLC instrument, which has several key components: reservoirs that store the mobile phase; a pump for pushing the mobile phase through the system; an injector for introducing the sample; a column for separating the sample into its component parts; and a detector for monitoring the eluent as it comes off the column. Let's consider each of these components.

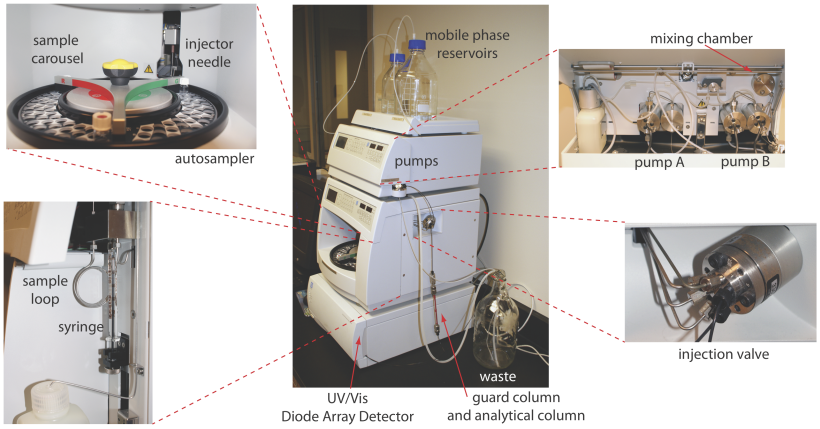

Figure 12.5.1 . Example of a typical high-performance liquid chromatograph with insets showing the pumps that move the mobile phase through the system and the plumbing used to inject the sample into the mobile phase. This particular instrument includes an autosampler. An instrument in which samples are injected manually does not include the features shown in the two left-most insets, and has a different style of loop injection valve.

A solute's retention time in HPLC is determined by its interaction with the stationary phase and the mobile phase. There are several different types of solute/stationary phase interactions, including liquid–solid adsorption, liquid–liquid partitioning, ion-exchange, and size-exclusion. This chapter deals exclusively with HPLC separations based on liquid–liquid partitioning. Other forms of liquid chromatography receive consideration in Chapter 12.6.

HPLC Columns

An HPLC typically includes two columns: an analytical column, which is responsible for the separation, and a guard column that is placed before the analytical column to protect it from contamination.

Analytical Columns

The most common type of HPLC column is a stainless steel tube with an internal diameter between 2.1 mm and 4.6 mm and a length between 30 mm and 300 mm (Figure 12.5.2). The column is packed with 3–10 μm porous silica particles with either an irregular or a spherical shape. Typical column efficiencies are 40000–60000 theoretical plates/m. Assuming a V_{max}/V_{min} of approximately 50, a 25-cm column with 50 000 plates/m has 12 500 theoretical plates and a peak capacity of 110.

Figure 12.5.2 . Typical packed column for HPLC. This particular column has an internal diameter of 4.6 mm and a length of 150 mm, and is packed with 5 μm particles coated with stationary phase.

Capillary columns use less solvent and, because the sample is diluted to a lesser extent, produce larger signals at the detector. These columns are made from fused silica capillaries with internal diameters from 44–200 μm and lengths of 50–250 mm. Capillary columns packed with 3–5 μm particles have been prepared with column efficiencies of up to 250 000 theoretical plates [Novotony, M. *Science*, **1989**, *246*, 51–57].

One limitation to a packed capillary column is the back pressure that develops when pumping the mobile phase through the small interstitial spaces between the particulate micron-sized packing material (Figure 12.5.3). Because the tubing and fittings that carry the mobile phase have pressure limits, a higher back pressure requires a lower flow rate and a longer analysis time. Monolithic columns, in which the solid support is a single, porous rod, offer column efficiencies equivalent to a packed capillary column while allowing for faster flow rates. A monolithic column—which usually is similar in size to a conventional packed column, although smaller, capillary columns also are available—is prepared by forming the mono- lithic rod in a mold and covering it with PTFE tubing or a polymer resin. Monolithic rods made of a silica-gel polymer typically have macropores with diameters of approximately 2 μm and mesopores—pores within the macropores—with diameters of approximately 13 nm [Cabrera, K. Chromatography Online, April 1, 2008].

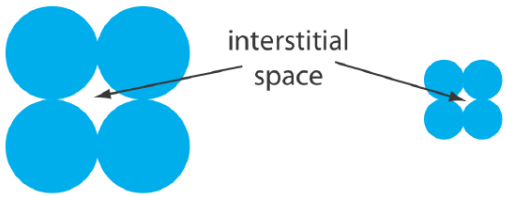

Figure 12.5.3 . The packing of smaller particles creates smaller interstitial spaces than the packing of larger particles. Although reducing particle size by 2× increases efficiency by a factor of 1.4, it also produces a 4-fold increase in back pressure.

Guard Columns

Two problems tend to shorten the lifetime of an analytical column. First, solutes that bind irreversibly to the stationary phase degrade the column's performance by decreasing the amount of stationary phase available for effecting a separation. Second, particulate material injected with the sample may clog the analytical column. To minimize these problems we place a guard column before the analytical column. A Guard column usually contains the same particulate packing material and stationary phase as the analytical column, but is significantly shorter and less expensive—a length of 7.5 mm and a cost one-tenth of that for the corresponding analytical column is typical. Because they are intended to be sacrificial, guard columns are replaced regularly.

> If you look closely at Figure 12.5.1 , you will see the small guard column just above the analytical column.

Stationary Phases for Liquid-Liquid Chromatography

In liquid–liquid chromatography the stationary phase is a liquid film coated on a packing material, typically 3–10 μm porous silica particles. Because the stationary phase may be partially soluble in the mobile phase, it may elute, or bleed from the column over time. To prevent the loss of stationary phase, which shortens the column's lifetime, it is bound covalently to the silica particles. ***Bonded stationary phases*** are created by reacting the silica particles with an organochlorosilane of the general form $Si(CH_3)_2RCl$, where R is an alkyl or substituted alkyl group.

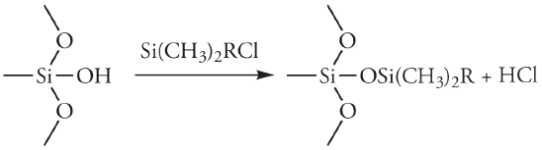

To prevent unwanted interactions between the solutes and any remaining –SiOH groups, $Si(CH_3)_3Cl$ is used to convert unreacted sites to $-\mathrm{SiOSi(CH_3)_3}$; such columns are designated as end-capped.

The properties of a stationary phase depend on the organosilane's alkyl group. If R is a polar functional group, then the stationary phase is polar. Examples of polar stationary phases include those where R contains a cyano ($–C_2H_4CN$), a diol ($–C_3H_6OCH_2CHOHCH_2OH$), or an amino ($–C_3H_6NH_2$) functional group. Because the stationary phase is polar, the mobile phase is a nonpolar or a moderately polar solvent. The combination of a polar stationary phase and a nonpolar mobile phase is called ***normal-phase chromatography***.

In ***reversed-phase chromatography***, which is the more common form of HPLC, the stationary phase is nonpolar and the mobile phase is polar. The most common nonpolar stationary phases use an organochlorosilane where the R group is an *n*-octyl (C_8) or *n*-octyldecyl (C_{18}) hydrocarbon chain. Most reversed-phase separations are carried out using a buffered aqueous solution as a polar

mobile phase, or using other polar solvents, such as methanol and acetonitrile. Because the silica substrate may undergo hydrolysis in basic solutions, the pH of the mobile phase must be less than 7.5.

> It seems odd that the more common form of liquid chromatography is identified as reverse-phase instead of normal phase. You might recall that one of the earliest examples of chromatography was Mikhail Tswett's separation of plant pigments using a polar column of calcium carbonate and a nonpolar mobile phase of petroleum ether. The assignment of normal and reversed, therefore, is all about precedence.

Mobile Phases

The elution order of solutes in HPLC is governed by polarity. For a normal-phase separation, a solute of lower polarity spends proportionally less time in the polar stationary phase and elutes before a solute that is more polar. Given a particular stationary phase, retention times in normal-phase HPLC are controlled by adjusting the mobile phase's properties. For example, if the resolution between two solutes is poor, switching to a less polar mobile phase keeps the solutes on the column for a longer time and provides more opportunity for their separation. In reversed-phase HPLC the order of elution is the opposite that in a normal-phase separation, with more polar solutes eluting first. Increasing the polarity of the mobile phase leads to longer retention times. Shorter retention times require a mobile phase of lower polarity.

Choosing a Mobile Phase: Using the Polarity Index

There are several indices that help in selecting a mobile phase, one of which is the polarity index [Snyder, L. R.; Glajch, J. L.; Kirkland, J. J. *Practical HPLC Method Development*, Wiley-Inter- science: New York, 1988]. Table 12.5.1 provides values of the polarity index, P', for several common mobile phases, where larger values of P' correspond to more polar solvents. Mixing together two or more mobile phases—assuming they are miscible—creates a mobile phase of intermediate polarity. For example, a binary mobile phase made by combining solvent *A* and solvent *B* has a polarity index, P'_{AB}, of

$$P'_{AB} = \Phi_A P'_A + \Phi_B P'_B \tag{3.5.1}$$

where P'_A and P'_B are the polarity indices for solvents *A* and *B*, and Φ_A and Φ_B are the volume fractions for the two solvents.

Table 12.5.1 . Properties of HPLC Mobile Phases

mobile phase	polarity index (P')	UV cutoff (nm)
cyclohexane	0.04	210
n-hexane	0.1	210
carbon tetrachloride	1.6	265
i-propyl ether	2.4	220
toluene	2.4	286
diethyl ether	2.8	218
tetrahydrofuran	4.0	220
ethanol	4.3	210
ethyl acetate	4.4	255
dioxane	4.8	215
methanol	5.1	210
acetonitrile	5.8	190
water	10.2	—

Example 12.5.1

A reversed-phase HPLC separation is carried out using a mobile phase of 60% v/v water and 40% v/v methanol. What is the mobile phase's polarity index?

Solution

Using Equation 3.5.1 and the values in Table 12.5.1 , the polarity index for a 60:40 water–methanol mixture is

$$P'_{AB} = \Phi_{\text{water}} P'_{\text{water}} + \Phi_{\text{methanol}} P'_{\text{methanol}}$$

$$P'_{AB} = 0.60 \times 10.2 + 0.40 \times 5.1 = 8.2$$

? Exercise 12.5.1

Suppose you need a mobile phase with a polarity index of 7.5. Explain how you can prepare this mobile phase using methanol and water.

Answer

If we let *x* be the fraction of water in the mobile phase, then 1 – *x* is the fraction of methanol. Substituting these values into Equation 3.5.1and solving for *x*

$$7.5 = 10.2x + 5.1(1 - x)$$

$$7.5 = 10.2x + 5.1 - 5.1x$$

$$2.4 = 5.1x$$

gives *x* as 0.47. The mobile phase is 47% v/v water and 53% v/v methanol.

As a general rule, a two unit change in the polarity index corresponds to an approximately 10-fold change in a solute's retention factor. Here is a simple example. If a solute's retention factor, *k*, is 22 when using water as a mobile phase (P' = 10.2), then switching to a mobile phase of 60:40 water–methanol (P' = 8.2) decreases *k* to approximately 2.2. Note that the retention factor becomes smaller because we are switching from a more polar mobile phase to a less polar mobile phase in a reversed-phase separation.

Choosing a Mobile Phase: Adjusting Selectivity

Changing the mobile phase's polarity index changes a solute's retention factor. As we learned in Chapter 12.3, however, a change in *k* is not an effective way to improve resolution when the initial value of *k* is greater than 10. To effect a better separation between two solutes we must improve the selectivity factor, α. There are two common methods for increasing α: adding a reagent to the mobile phase that reacts with the solutes in a secondary equilibrium reaction or switching to a different mobile phase.

Taking advantage of a secondary equilibrium reaction is a useful strategy for improving a separation [(a) Foley, J. P. *Chromatography*, **1987**, *7*, 118–128; (b) Foley, J. P.; May, W. E. Anal. Chem. 1987, 59, 102–109; (c) Foley, J. P.; May, W. E. Anal. Chem. 1987, 59, 110–115]. Figure 12.3.3, which we considered earlier in this chapter, shows the reversed-phase separation of four weak acids—benzoic acid, terephthalic acid, *p*-aminobenzoic acid, and *p*-hydroxybenzoic acid—on a nonpolar C_{18} column using an aqueous buffer of acetic acid and sodium acetate as the mobile phase. The retention times for these weak acids are shorter when using a less acidic mobile phase because each solute is present in an anionic, weak base form that is less soluble in the nonpolar stationary phase. If the mobile phase's pH is sufficiently acidic, the solutes are present as neutral weak acids that are more soluble in the stationary phase and take longer to elute. Because the weak acid solutes do not have identical pK_a values, the pH of the mobile phase has a different effect on each solute's retention time, allowing us to find the optimum pH for effecting a complete separation of the four solutes.

Acid–base chemistry is not the only example of a secondary equilibrium reaction. Other examples include ion-pairing, complexation, and the interaction of solutes with micelles. We will consider the last of these in Chapter 12.7 when we discuss micellar electrokinetic capillary chromatography.

In Example 12.5.1 we learned how to adjust the mobile phase's polarity by blending together two solvents. A polarity index, however, is just a guide, and binary mobile phase mixtures with identical polarity indices may not resolve equally a pair of solutes. Table 12.5.2 , for example, shows retention times for four weak acids in two mobile phases with nearly identical values for P'. Although the order of elution is the same for both mobile phases, each solute's retention time is affected differently by the choice of organic solvent. If we switch from using acetonitrile to tetrahydrofuran, for example, we find that benzoic acid elutes more quickly and that *p*-hydroxybenzoic acid elutes more slowly. Although we can resolve fully these two solutes using mobile phase that is 16% v/v acetonitrile, we cannot resolve them if the mobile phase is 10% tetrahydrofuran.

Table 12.5.2 . Retention Times for Four Weak Acids in Mobile Phases With Similar Polarity Indexes

retention time (min)	16% acetonitrile (CH_3CN) 84% pH 4.11 aqueous buffer (P' = 9.5)	10% tetrahydrofuran (THF) 90% pH 4.11 aqueous buffer (P' = 9.6)
$t_{r,\,BA}$	5.18	4.01
$t_{r,\,PH}$	1.67	2.91
$t_{r,\,PA}$	1.21	1.05
$t_{r,\,TP}$	0.23	0.54

Key: BA is benzoic acid; PH is *p*-hydroxybenzoic acid; PA is *p*-aminobenzoic acid; TP is terephthalic acid
Source: Harvey, D. T.; Byerly, S.; Bowman, A.; Tomlin, J. "Optimization of HPLC and GC Separations Using Re- sponse Surfaces," *J. Chem. Educ.* **1991**, *68*, 162–168.

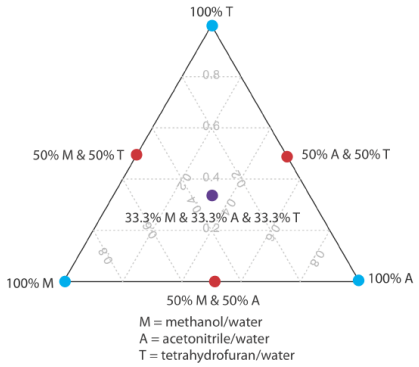

Figure 12.5.4 . Solvent triangle for optimizing a reversed-phase HPLC separation. The three blue circles show mobile phases consisting of an organic solvent and water. The three red circles are binary mobile phases created by combining equal volumes of the pure mobile phases. The ternary mobile phase shown by the purple circle contains all three of the pure mobile phases.

One strategy for finding the best mobile phase is to use the solvent triangle shown in Figure 12.5.4 , which allows us to explore a broad range of mobile phases with only seven experiments. We begin by adjusting the amount of acetonitrile in the mobile phase to produce the best possible separation within the desired analysis time. Next, we use Table 12.5.3 to estimate the composition of methanol/H_2O and tetrahydrofuran/H_2O mobile phases that will produce similar analysis times. Four additional mobile phases are prepared using the binary and ternary mobile phases shown in Figure 12.5.4 . When we examine the chromatograms from these seven mobile phases we may find that one or more provides an adequate separation, or we may identify a region within the solvent triangle where a separation is feasible. Figure 12.5.5 shows a resolution map for the reversed-phase separation of benzoic acid, terephthalic acid, *p*-aminobenzoic acid, and *p*-hydroxybenzoic acid on a nonpolar C_{18} column in which the maximum desired analysis time is set to 6 min [Harvey, D. T.; Byerly, S.; Bowman, A.; Tomlin, J. *J. Chem. Educ.* **1991**, *68*, 162–168]. The areas in blue, green, and red show mobile phase compositions that do not provide baseline resolution. The unshaded area represents mobile phase compositions where a separation is possible.

> The choice to start with acetonitrile is arbitrary—we can just as easily choose to begin with methanol or with tetrahydrofuran.

Table 12.5.3 . Composition of Mobile Phases With Approximately Equal Solvent Strengths

%v/v CH_3OH	% v/v CH_3CN	%v/v THF

%v/v CH_3OH	% v/v CH_3CN	%v/v THF
0	0	0
10	6	4
20	14	10
30	22	16
40	32	24
50	40	30
6	50	36
70	60	44
80	72	52
90	87	62
100	99	71

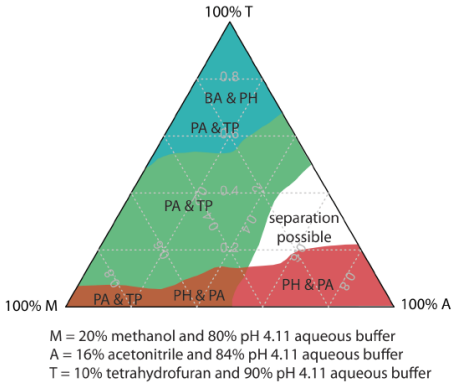

Figure 12.5.5 . Resolution map for the separation of benzoic acid (BA), terephthalic acid (TP), *p*-aminobenzoic acid (PA), and *p*-hydroxybenzoic acid (PH) on a nonpolar C_{18} column subject to a maximum analysis time of 6 min. The shaded areas represent regions where a separation is not possible, with the unresolved solutes identified. A separation is possible in the unshaded area. See Harvey, D. T.; Byerly, S.; Bowman, A.; Tomlin, J. "Optimization of HPLC and GC Separations Using Response Surfaces," *J. Chem. Educ.* **1991**, *68*, 162–168 for details on the mathematical model used to generate the resolution map.

Choosing a Mobile Phase: Isocratic and Gradient Elutions

A separation using a mobile phase that has a fixed composition is an ***isocratic elution***. One difficulty with an isocratic elution is that an appropriate mobile phase strength for resolving early-eluting solutes may lead to unacceptably long retention times for late-eluting solutes. Optimizing the mobile phase for late-eluting solutes, on the other hand, may provide an inadequate separation of early-eluting solutes. Changing the mobile phase's composition as the separation progresses is one solution to this problem. For a reversed-phase separation we use an initial mobile phase that is more polar. As the separation progresses, we adjust the composition of mobile phase so that it becomes less polar (see Figure 12.5.6). Such separations are called ***gradient elutions***.

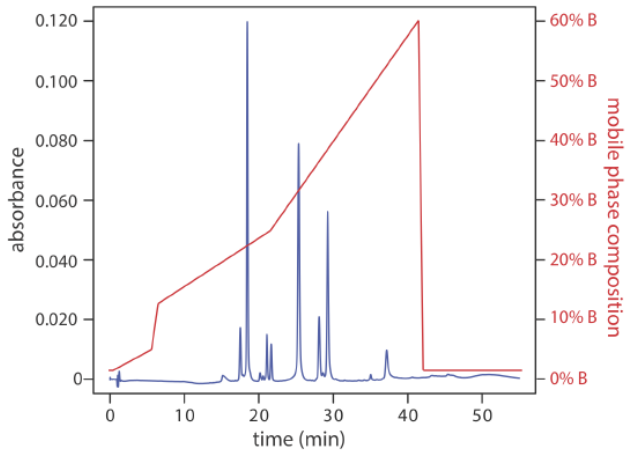

Figure 12.5.6 . Gradient elution separation of a mixture of flavonoids. Mobile phase A is an aqueous solution of 0.1% formic acid and mobile phase B is 0.1% formic acid in acetonitrile. The initial mobile phase is 98% A and 2% B. The percentage of mobile phase B increases in four steps: from 2% to 5% over 5 min, beginning at 0.5 min; from 5% to 12% over 1 min, beginning at 5.5 min; from 12% to 25% over 15 min, beginning at 6.5 min; and from 25% to 60% over 20 min, beginning at 21.5 min. Data provided by Christopher Schardon, Kyle Meinhardt, and Michelle Bushey, Department of Chemistry, Trinty University.

HPLC Plumbing

In a gas chromatograph the pressure from a compressed gas cylinder is sufficient to push the mobile phase through the column. Pushing a liquid mobile phase through a column, however, takes a great deal more effort, generating pressures in excess of several hundred atmospheres. In this section we consider the basic plumbing needed to move the mobile phase through the column and to inject the sample into the mobile phase.

Moving the Mobile Phase

A typical HPLC includes between 1–4 reservoirs for storing mobile phase solvents. The instrument in Figure 12.5.1 , for example, has two mobile phase reservoirs that are used for an isocratic elution or a gradient elution by drawing solvents from one or both reservoirs.

Before using a mobile phase solvent we must remove dissolved gases, such as N_2 and O_2, and small particulate matter, such as dust. Because there is a large drop in pressure across the column—the pressure at the column's entrance is as much as several hundred atmospheres, but it is atmospheric pressure at the column's exit—gases dissolved in the mobile phase are released as gas bubbles that may interfere with the detector's response. Degassing is accomplished in several ways, but the most common are the use of a vacuum pump or sparging with an inert gas, such as He, which has a low solubility in the mobile phase. Particulate materials, which may clog the HPLC tubing or column, are removed by filtering the solvents.

> Bubbling an inert gas through the mobile phase releases volatile dissolved gases. This process is called sparging.

The mobile phase solvents are pulled from their reservoirs by the action of one or more pumps. Figure 12.5.7 shows a close-up view of the pumps for the instrument in Figure 12.5.1 . The working pump and the equilibrating pump each have a piston whose back and forth movement maintains a constant flow rate of up to several mL/min and provides the high output pressure needed to push the mobile phase through the chromatographic column. In this particular instrument, each pump sends its mobile phase to a mixing chamber where they combine to form the final mobile phase. The relative speed of the two pumps determines the mobile phase's final composition.

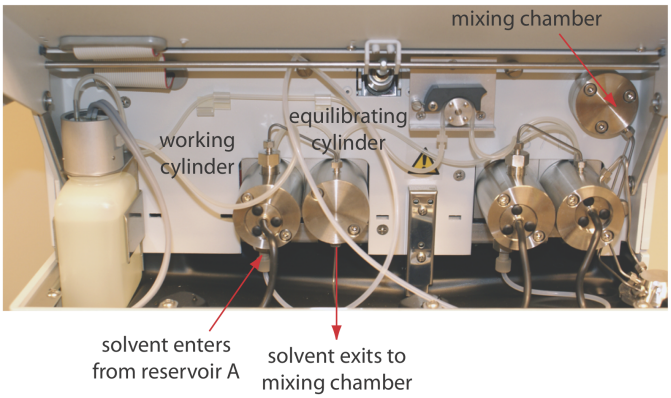

Figure 12.5.7 . Close-up view of the pumps for the instrument shown in Figure 12.5.1 . The working cylinder and the equilibrating cylinder for the pump on the left take solvent from reservoir A and send it to the mixing chamber. The pump on the right moves solvent from reservoir B to the mixing chamber. The mobile phase's flow rate is determined by the combined speeds of the two pumps. By changing the relative speeds of the two pumps, different binary mobile phases can be prepared.

The back and forth movement of a reciprocating pump creates a pulsed flow that contributes noise to the chromatogram. To minimize these pulses, each pump in Figure 12.5.7 has two cylinders. During the working cylinder's forward stoke it fills the equilibrating cylinder and establishes flow through the column. When the working cylinder is on its reverse stroke, the flow is maintained by the piston in the equilibrating cylinder. The result is a pulse-free flow.

There are other possible ways to control the mobile phase's composition and flow rate. For example, instead of the two pumps in Figure 12.5.7 , we can place a solvent proportioning valve before a single pump. The solvent proportioning value connects two or more solvent reservoirs to the pump and determines how much of each solvent is pulled during each of the pump's cycles. Another approach for eliminating a pulsed flow is to include a pulse damper between the pump and the column. A pulse damper is a chamber filled with an easily compressed fluid and a flexible diaphragm. During the piston's forward stroke the fluid in the pulse damper is compressed. When the piston withdraws to refill the pump, pressure from the expanding fluid in the pulse damper maintains the flow rate.

Injecting the Sample

The operating pressure within an HPLC is sufficiently high that we cannot inject the sample into the mobile phase by inserting a syringe through a septum, as is possible in gas chromatography. Instead, we inject the sample using a ***loop injector***, a diagram of which is shown in Figure 12.5.8 . In the load position a sample loop—which is available in a variety of sizes ranging from 0.5 µL to 5 mL—is isolated from the mobile phase and open to the atmosphere. The sample loop is filled using a syringe with a capacity several times that of the sample loop, with excess sample exiting through the waste line. After loading the sample, the injector is turned to the inject position, which redirects the mobile phase through the sample loop and onto the column.

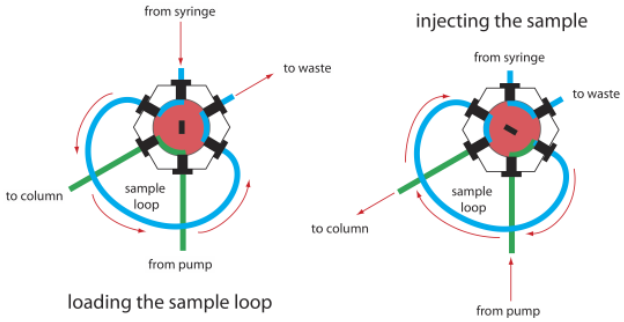

Figure 12.5.8 . Schematic diagram of a manual loop injector. In the load position the flow of mobile phase from the pump to the column (shown in green) is isolated from the sample loop, which is filled using a syringe (shown in blue). Rotating the inner valve (shown in red) to the inject position directs the mobile phase through the sample loop and onto the column.

The instrument in Figure 12.5.1 uses an autosampler to inject samples. Instead of using a syringe to push the sample into the sample loop, the syringe draws sample into the sample loop.

Detectors for HPLC

Many different types of detectors have been use to monitor HPLC separations, most of which use the spectroscopic techniques from Chapter 10 or the electrochemical techniques from Chapter 11.

Spectroscopic Detectors

The most popular HPLC detectors take advantage of an analyte's UV/Vis absorption spectrum. These detectors range from simple designs, in which the analytical wavelength is selected using appropriate filters, to a modified spectrophotometer in which the sample compartment includes a flow cell. Figure 12.5.9 shows the design of a typical flow cell when using a diode array spectrometer as the detector. The flow cell has a volume of 1–10 μL and a path length of 0.2–1 cm.

> To review the details of how we measure absorbance, see Chapter 10.2. More information about different types of instruments, including the diode array spectrometer, is in Chapter 10.3.

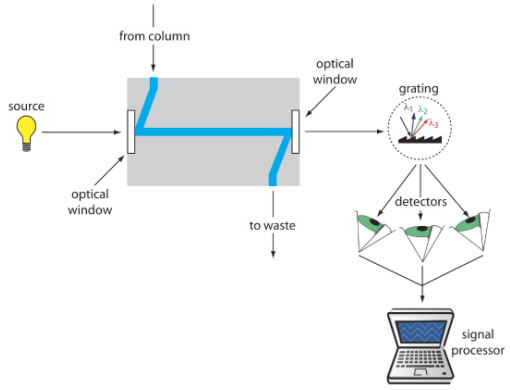

Figure 12.5.9 . Schematic diagram of a flow cell for a detector equipped with a diode array spectrometer.

When using a UV/Vis detector the resulting chromatogram is a plot of absorbance as a function of elution time (see Figure 12.5.10). If the detector is a diode array spectrometer, then we also can display the result as a three-dimensional chromatogram that shows absorbance as a function of wavelength and elution time. One limitation to using absorbance is that the mobile phase cannot absorb at the wavelengths we wish to monitor. Table 12.5.1 lists the minimum useful UV wavelength for several common HPLC solvents. Absorbance detectors provide detection limits of as little as 100 pg–1 ng of injected analyte.

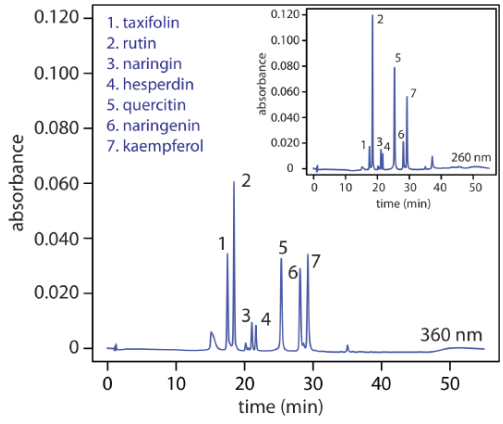

Figure 12.5.10 . HPLC separation of a mixture of flavonoids with UV/Vis detection at 360 nm and, in the inset, at 260 nm. The choice of wavelength affects each analyte's signal. By carefully choosing the wavelength, we can enhance the signal for the analytes of greatest interest. Data provided by Christopher Schardon, Kyle Meinhardt, and Michelle Bushey, Department of Chemistry, Trinty University.

If an analyte is fluorescent, we can place the flow cell in a spectrofluorimeter. As shown in Figure 12.5.11 , a fluorescence detector provides additional selectivity because only a few of a sample's components are fluorescent. Detection limits are as little as 1–10 pg of injected analyte.

See Chapter 10.6 for a review of fluorescence spectroscopy and spectrofluorimeters.

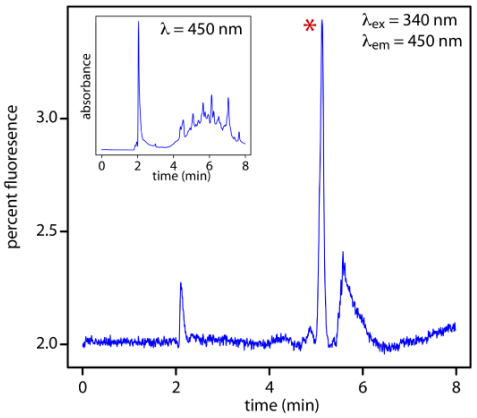

Figure 12.5.11 . HPLC chromatogram for the determination of riboflavin in urine using fluorescence detection with exci-tation at a wavelength of 340 nm and detection at 450 nm. The peak corresponding to riboflavin is marked with a red asterisk (*). The inset shows the same chromatogram when using a less-selective UV/Vis detector at a wavelength of 450 nm. Data provided by Jason Schultz, Jonna Berry, Kaelene Lundstrom, and Dwight Stoll, Department of Chemistry, Gustavus Adolphus College.

Electrochemical Detectors

Another common group of HPLC detectors are those based on electrochemical measurements such as amperometry, voltammetry, coulometry, and conductivity. Figure 12.5.12 , for example, shows an amperometric flow cell. Effluent from the column passes over the working electrode—held at a constant potential relative to a downstream reference electrode—that completely oxidizes or reduces the analytes. The current flowing between the working electrode and the auxiliary electrode serves as the analytical signal. Detection limits for amperometric electrochemical detection are from 10 pg–1 ng of injected analyte.

See Chapter 11.4 for a review of amperometry.

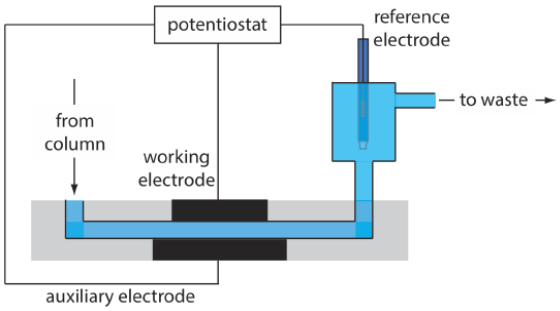

Figure 12.5.12 . Schematic diagram showing a flow cell for an amperometric electrochemical detector.

Other Detectors

Several other detectors have been used in HPLC. Measuring a change in the mobile phase's refractive index is analogous to monitoring the mobile phase's thermal conductivity in gas chromatography. A refractive index detector is nearly universal, responding to almost all compounds, but has a relatively poor detection limit of 0.1–1 μg of injected analyte. An additional limitation of a refractive index detector is that it cannot be used for a gradient elution unless the mobile phase components have identical refractive indexes.

Another useful detector is a mass spectrometer. Figure 12.5.13 shows a block diagram of a typical HPLC–MS instrument. The effluent from the column enters the mass spectrometer's ion source using an interface the removes most of the mobile phase, an essential need because of the incompatibility between the liquid mobile phase and the mass spectrometer's high vacuum environment. In the ionization chamber the remaining molecules—a mixture of the mobile phase components and solutes—undergo ionization and fragmentation. The mass spectrometer's mass analyzer separates the ions by their mass-to-charge ratio (m/z). A detector counts the ions and displays the mass spectrum.

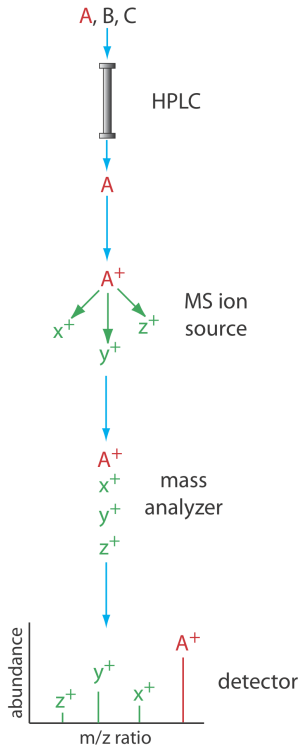

Figure 12.5.13 . Block diagram of an HPLC–MS. A three component mixture enters the HPLC. When component A elutes from the column, it enters the MS ion source and ionizes to form the parent ion and several fragment ions. The ions enter the mass analyzer, which separates them by their mass-to-charge ratio, providing the mass spectrum shown at the detector.

There are several options for monitoring the chromatogram when using a mass spectrometer as the detector. The most common method is to continuously scan the entire mass spectrum and report the total signal for all ions reaching the detector during each scan. This total ion scan provides universal detection for all analytes. As seen in Figure 12.5.14 , we can achieve some degree of selectivity by monitoring only specific mass-to-charge ratios, a process called selective-ion monitoring.

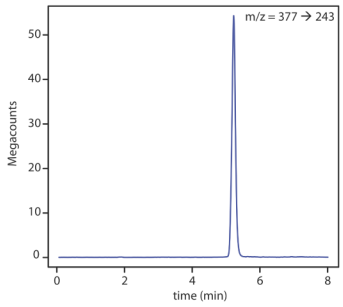

Figure 12.5.14 . HPLC–MS/MS chromatogram for the determination of riboflavin in urine. An initial parent ion with an m/z ratio of 377 enters a second mass spectrometer where it undergoes additional 20 ionization; the fragment ion with an m/z ratio of 243 provides the signal. The selectivity of this detector is evident when you compare this chromatogram to the one in Figure 12.5.11 , which uses fluoresence deterction. Data provided by Jason Schultz, Jonna Berry, Kaelene Lundstrom, and Dwight Stoll, Department of Chemistry, Gustavus Adolphus College.

The advantages of using a mass spectrometer in HPLC are the same as for gas chromatography. Detection limits are very good, typically 0.1–1 ng of injected analyte, with values as low as 1–10 pg for some samples. In addition, a mass spectrometer provides qualitative, structural information that can help to identify the analytes. The interface between the HPLC and the mass spectrometer is technically more difficult than that in a GC–MS because of the incompatibility of a liquid mobile phase with the mass spectrometer's high vacuum requirement.

> For more details on mass spectrometry see Introduction to Mass Spectrometry by Michael Samide and Olujide Akinbo, a resource that is part of the Analytical Sciences Digital Library.

Quantitative Applications

High-performance liquid chromatography is used routinely for both qualitative and quantitative analyses of environmental, pharmaceutical, industrial, forensic, clinical, and consumer product samples.

Preparing Samples for Analysis

Samples in liquid form are injected into the HPLC after a suitable clean-up to remove any particulate materials, or after a suitable extraction to remove matrix interferents. In determining polyaromatic hydrocarbons (PAH) in wastewater, for example, an extraction with CH_2Cl_2 serves the dual purpose of concentrating the analytes and isolating them from matrix interferents. Solid samples are first dissolved in a suitable solvent or the analytes of interest brought into solution by extraction. For example, an HPLC analysis for the active ingredients and the degradation products in a pharmaceutical tablet often begins by extracting the powdered tablet with a portion of mobile phase. Gas samples are collected by bubbling them through a trap that contains a suitable solvent. Organic isocyanates in industrial atmospheres are collected by bubbling the air through a solution of 1-(2-methoxyphenyl)piperazine in toluene. The reaction between the isocyanates and 1-(2-methoxyphenyl)piperazine both stabilizes them against degradation before the HPLC analysis and converts them to a chemical form that can be monitored by UV absorption.

Quantitative Calculations

A quantitative HPLC analysis is often easier than a quantitative GC analysis because a fixed volume sample loop provides a more precise and accurate injection. As a result, most quantitative HPLC methods do not need an internal standard and, instead, use external standards and a normal calibration curve.

> An internal standard is necessary when using HPLC–MS because the interface between the HPLC and the mass spectrometer does not allow for a reproducible transfer of the column's eluent into the MS's ionization chamber.

Example 12.5.2

The concentration of polynuclear aromatic hydrocarbons (PAH) in soil is determined by first extracting the PAHs with methylene chloride. The extract is diluted, if necessary, and the PAHs separated by HPLC using a UV/Vis or fluorescence detector. Calibration is achieved using one or more external standards. In a typical analysis a 2.013-g sample of dried soil is extracted with 20.00 mL of methylene chloride. After filtering to remove the soil, a 1.00-mL portion of the extract is removed and diluted to 10.00 mL with acetonitrile. Injecting 5 µL of the diluted extract into an HPLC gives a signal of 0.217 (arbitrary units) for the PAH fluoranthene. When 5 µL of a 20.0-ppm fluoranthene standard is analyzed using the same conditions, a signal of 0.258 is measured. Report the parts per million of fluoranthene in the soil.

Solution

For a single-point external standard, the relationship between the signal, *S*, and the concentration, *C*, of fluoranthene is

$$S = kC$$

Substituting in values for the standard's signal and concentration gives the value of *k* as

$$k = \frac{S}{C} = \frac{0.258}{20.0 \text{ ppm}} = 0.0129 \text{ ppm}^{-1}$$

Using this value for *k* and the sample's HPLC signal gives a fluoranthene concentration of

$$C = \frac{S}{k} = \frac{0.217}{0.0129 \text{ ppm}^{-1}} = 16.8 \text{ ppm}$$

for the extracted and diluted soil sample. The concentration of fluoranthene in the soil is

$$\frac{16.8 \text{ g/mL} \times \frac{10.00 \text{ mL}}{1.00 \text{ mL}} \times 20.00 \text{ mL}}{2.013 \text{ g sample}} = 1670 \text{ ppm fluoranthene}$$

Exercise 12.5.2

The concentration of caffeine in beverages is determined by a reversed-phase HPLC separation using a mobile phase of 20% acetonitrile and 80% water, and using a nonpolar C_8 column. Results for a series of 10-µL injections of caffeine standards are in the following table.

[caffeine] (mg/L)	peak area (arb. units)
50.0	226724
100.0	453762
125.0	559443
250.0	1093637

What is the concentration of caffeine in a sample if a 10-µL injection gives a peak area of 424195? The data in this problem comes from Kusch, P.; Knupp, G. "Simultaneous Determination of Caffeine in Cola Drinks and Other Beverages by Reversed-Phase HPTLC and Reversed-Phase HPLC," *Chem. Educator*, **2003**, *8*, 201–205.

Answer

The figure below shows the calibration curve and calibration equation for the set of external standards. Substituting the sample's peak area into the calibration equation gives the concentration of caffeine in the sample as 94.4 mg/L.

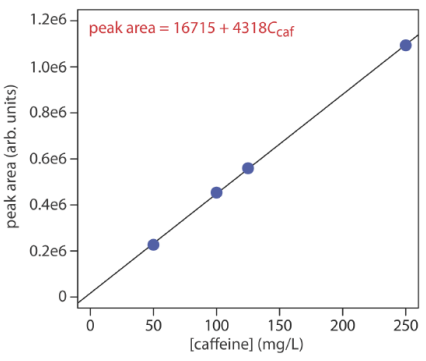

The best way to appreciate the theoretical and the practical details discussed in this section is to carefully examine a typical analytical method. Although each method is unique, the following description of the determination of fluoxetine in serum provides an instructive example of a typical procedure. The description here is based on Smyth, W. F. *Analytical Chemistry of Complex Matricies*, Wiley Teubner: Chichester, England, 1996, pp. 187–189.

Representative Method 12.5.1: Determination of Fluoxetine in Serum

Description of Method

Fluoxetine is another name for the antidepressant drug Prozac. The determination of fluoxetine in serum is an important part of monitoring its therapeutic use. The analysis is complicated by the complex matrix of serum samples. A solid-phase extraction followed by an HPLC analysis using a fluorescence detector provides the necessary selectivity and detection limits.

Procedure

Add a known amount of the antidepressant protriptyline, which serves as an internal standard, to each serum sample and to each external standard. To remove matrix interferents, pass a 0.5-mL aliquot of each serum sample or standard through a C_{18} solid-phase extraction cartridge. After washing the cartridge to remove the interferents, elute the remaining constituents, including the analyte and the internal standard, by washing the cartridge with 0.25 mL of a 25:75 v/v mixture of 0.1 M $HClO_4$ and acetonitrile. Inject a 20-µL aliquot onto a 15-cm × 4.6-mm column packed with a 5 µm C_8-bonded stationary phase. The isocratic mobile phase is 37.5:62.5 v/v acetonitrile and water (that contains 1.5 g of tetramethylammonium perchlorate and 0.1 mL of 70% v/v $HClO_4$).

Monitor the chromatogram using a fluorescence detector set to an excitation wave- length of 235 nm and an emission wavelength of 310 nm.

Questions

1. The solid-phase extraction is important because it removes constitutions in the serum that might interfere with the analysis. What types of interferences are possible?

> Blood serum, which is a complex mixture of compounds, is approximately 92% water, 6–8% soluble proteins, and less than 1% each of various salts, lipids, and glucose. A direct injection of serum is not advisable for three reasons. First, any particulate materials in the serum will clog the column and restrict the flow of mobile phase. Second, some of the compounds in the serum may absorb too strongly to the stationary phase, degrading the column's performance. Finally, although an HPLC can separate and analyze complex mixtures, an analysis is difficult if the number of constituents exceeds the column's peak capacity.

2. One advantage of an HPLC analysis is that a loop injector often eliminates the need for an internal standard. Why is an internal standard used in this analysis? What assumption(s) must we make when using the internal standard?

> An internal standard is necessary because of uncertainties introduced during the solid-phase extraction. For example, the volume of serum transferred to the solid-phase extraction cartridge, 0.5 mL, and the volume of solvent used to remove the analyte and internal standard, 0.25 mL, are very small. The precision and accuracy with which we can measure these volumes is not as good as when we use larger volumes. For example, if we extract the analyte into a volume of 0.24 mL instead of a volume of 0.25 mL, then the analyte's concentration increases by slightly more than 4%. In addition, the concentration of eluted analytes may vary from trial-to-trial due to variations in the amount of solution held up by the cartridge. Using an internal standard compensates for these variation. To be useful we must assume that the analyte and the internal standard are retained completely during the initial loading, that they are not lost when the cartridge is washed, and that they are extracted completely during the final elution.

3. Why does the procedure monitor fluorescence instead of monitoring UV absorption?

> Fluorescence is a more selective technique for detecting analytes. Many other commonly prescribed antidepressants (and their metabolites) elute with retention times similar to that of fluoxetine. These compounds, however, either do not fluoresce or are only weakly fluorescent.

4. If the peaks for fluoxetine and protriptyline are resolved insufficiently, how might you alter the mobile phase to improve their separation?

> Decreasing the amount of acetonitrile and increasing the amount of water in the mobile will increase retention times, providing more time to effect a separation.

Evaluation

With a few exceptions, the scale of operation, accuracy, precision, sensitivity, selectivity, analysis time, and cost for an HPLC method are similar to GC methods. Injection volumes for an HPLC method usually are larger than for a GC method because HPLC columns have a greater capacity. Because it uses a loop injection, the precision of an HPLC method often is better than a GC method. HPLC is not limited to volatile analytes, which means we can analyze a broader range of compounds. Capillary GC columns, on the other hand, have more theoretical plates, and can separate more complex mixtures.

3.6: Other Forms of Chromatography

At the beginning of Section 12.5, we noted that there are several different types of solute/stationary phase interactions in liquid chromatography, but limited our discussion to liquid–liquid chromatography. In this section we turn our attention to liquid chromatography techniques in which partitioning occurs by liquid–solid adsorption, ion-exchange, and size exclusion.

Liquid-Solid Chromatography

In ***liquid–solid adsorption chromatography*** (LSC) the column packing also serves as the stationary phase. In Tswett's original work the stationary phase was finely divided $CaCO_3$, but modern columns employ porous 3–10 μm particles of silica or alumina. Because the stationary phase is polar, the mobile phase usually is a nonpolar or a moderately polar solvent. Typical mobile phases include hexane, isooctane, and methylene chloride. The usual order of elution—from shorter to longer retention times—is

olefins < aromatic hydrocarbons < ethers < esters, aldehydes, ketones < alcohols, amines < amide < carboxylic acids

Nonpolar stationary phases, such as charcoal-based absorbents, also are used. For most samples, liquid–solid chromatography does not offer any special advantages over liquid–liquid chromatography. One exception is the analysis of isomers, where LSC excels.

Ion-Exchange Chromatography

In ***ion-exchange chromatography*** (IEC) the stationary phase is a cross-linked polymer resin, usually divinylbenzene cross-linked polystyrene, with covalently attached ionic functional groups (see Figure 12.6.1 and Table 12.6.1). The counterions to these fixed charges are mobile and are displaced by ions that compete more favorably for the exchange sites. Ion-exchange resins are divided into four categories: strong acid cation exchangers; weak acid cation exchangers; strong base anion exchangers; and weak base anion exchangers.

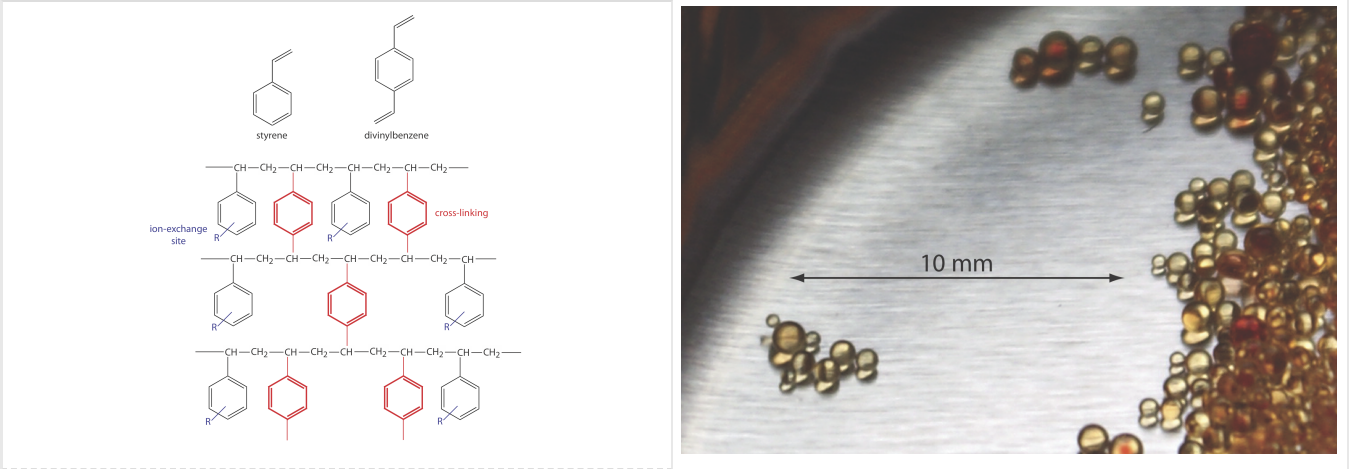

Figure 12.6.1 . Structures of styrene, divinylbenzene, and a styrene–divinylbenzene co-polymer modified for use as an ion-exchange resin are shown on the left. The ion-exchange sites, indicated by R and shown in blue, are mostly in the *para* position and are not necessarily bound to all styrene units. The cross-linking is shown in red. The photo on the right shows an example of the polymer beads. These beads are approximately 0.30–0.85 mm in diameter. Resins for use in ion-exchange chromatography typically are 5–11 μm in diameter.

Table 12.6.1 . Examples of Common Ion-Exchange Resins

type	functional group	examples
strong acid cation exchanger	sulfonic acid	$-SO_3^-$ $-CH_2CH_2SO_3^-$
weak acid cation exchanger	carboxylic acid	$-COO^-$ $-CH_2COO^-$
strong base anion exchanger	quaternary amine	$-CH_2N(CH_3)_3^+$ $-CH_2CH_2N(CH_2CH_3)_3^+$

type	functional group	examples
weak base anion exchanger	amine	$-\mathrm{NH}_4^+$ $-\mathrm{CH_2CH_2NH(CH_2CH_3)_3^+}$

Strong acid cation exchangers include a sulfonic acid functional group that retains it anionic form—and thus its capacity for ion-exchange—in strongly acidic solutions. The functional groups for a weak acid cation exchanger, on the other hand, are fully protonated at pH levels less then 4 and lose their exchange capacity. The strong base anion exchangers include a quaternary amine, which retains a positive charge even in strongly basic solutions. Weak base anion exchangers remain protonated only at pH levels that are moderately basic. Under more basic conditions a weak base anion exchanger loses a proton and its exchange capacity.

The ion-exchange reaction of a monovalent cation, M^+, exchange site is

$$-\mathrm{SO_3^-H^+}(s) + \mathrm{M^+}(aq) \rightleftharpoons -\mathrm{SO_3^-M^+}(s) + \mathrm{H^+}(aq)$$

The equilibrium constant for this ion-exchange reaction, which we call the selectivity coefficient, *K*, is

$$K = \frac{\left\{-\mathrm{SO_3^-M^+}\right\}\left[\mathrm{H^+}\right]}{\left\{-\mathrm{SO_3^-H^+}\right\}\left[\mathrm{M^+}\right]} \tag{3.6.1}$$

where we use curly brackets, { }, to indicate a surface concentration instead of a solution concentration.

> We don't usually think about a solid's concentration. There is a good reason for this. In most cases, a solid's concentration is a constant. If you break a piece of chalk into two parts, for example, the mass and the volume of each piece retains the same proportional relationship as in the original piece of chalk. When we consider an ion binding to a reactive site on the solid's surface, however, the fraction of sites that are bound, and thus the concentration of bound sites, can take on any value between 0 and some maximum value that is proportional to the density of reactive sites.

Rearranging Equation 3.6.1 shows us that the distribution ratio, *D*, for the exchange reaction

$$D = \frac{\text{amount of } \mathrm{M^+} \text{ in the stationary phase}}{\text{amount of } \mathrm{M^+} \text{ in the mobile phase}}$$

$$D = \frac{\left\{-\mathrm{SO_3^-M^+}\right\}}{\left[\mathrm{M^+}\right]} = K \times \frac{\left\{-\mathrm{SO_3^-H^+}\right\}}{\left[\mathrm{H^+}\right]} \tag{3.6.2}$$

is a function of the concentration of H^+ and, therefore, the pH of the mobile phase.

An ion-exchange resin's selectivity is somewhat dependent on whether it includes strong or weak exchange sites and on the extent of cross-linking. The latter is particularly important as it controls the resin's permeability, and, therefore, the accessibility of exchange sites. An approximate order of selectivity for a typical strong acid cation exchange resin, in order of decreasing *D*, is

$$\mathrm{Al^{3+} > Ba^{2+} > Pb^{2+} > Ca^{2+} > Ni^{2+} > Cd^{2+} > Cu^{2+} > Co^{2+} > Zn^{2+} > Mg^{2+} > Ag^+ > K^+ > NH_4^+ > Na^+ > H^+ > Li^+}$$

Note that highly charged cations bind more strongly than cations of lower charge, and that for cations of similar charge, those with a smaller hydrated radius (see Table 6.9.1 in Chapter 6), or that are more polarizable, bind more strongly. For a strong base anion exchanger the general elution order is

$$\mathrm{SO_4^{2-} > I^- > HSO_4^- > NO_3^- > Br^- > NO_2^- > Cl^- > HCO_3^- > CH3COO^- > OH^- > F^-}$$

Anions of higher charge and of smaller hydrated radius bind more strongly than anions with a lower charge and a larger hydrated radius.

The mobile phase in IEC usually is an aqueous buffer, the pH and ionic composition of which determines a solute's retention time. Gradient elutions are possible in which the mobile phase's ionic strength or pH is changed with time. For example, an IEC separation of cations might use a dilute solution of HCl as the mobile phase. Increasing the concentration of HCl speeds the elution rate for more strongly retained cations because the higher concentration of H^+ allows it to compete more successfully for the ion-exchange sites.

> From Equation 3.6.2, a cation's distribution ratio, *D*, becomes smaller when the concentration of H^+ in the mobile phase increases.

An ion-exchange resin is incorporated into an HPLC column either as 5–11 μm porous polymer beads or by coating the resin on porous silica particles. Columns typically are 250 mm in length with internal diameters ranging from 2–5 mm.

Measuring the conductivity of the mobile phase as it elutes from the column serves as a universal detector for cationic and anionic analytes. Because the mobile phase contains a high concentration of ions—a mobile phase of dilute HCl, for example, contains significant concentrations of H^+ and Cl^-—we need a method for detecting the analytes in the presence of a significant background conductivity.

To minimize the mobile phase's contribution to conductivity, an ***ion-suppressor column*** is placed between the analytical column and the detector. This column selectively removes mobile phase ions without removing solute ions. For example, in cation-exchange chromatography using a dilute solution of HCl as the mobile phase, the suppressor column contains a strong base anion-exchange resin. The exchange reaction

$$H^+(aq) + Cl^-(aq) + \text{Resin}^+ OH^-(s) \rightleftharpoons \text{Resin}^+ Cl^-(s) + H_2O(l)$$

replaces the mobile phase ions H^+ and Cl^- with H_2O. A similar process is used in anion-exchange chromatography where the suppressor column contains a cation-exchange resin. If the mobile phase is a solution of Na_2CO_3, the exchange reaction

$$2Na^+(aq) + CO_3^{2-}(aq) + 2\,\text{Resin}^- H^+(s) \rightleftharpoons 2\,\text{Resin}^- Na^+(s) + H_2CO_3(aq)$$

replaces a strong electrolyte, Na_2CO_3, with a weak electrolyte, H_2CO_3.

Ion-suppression is necessary when the mobile phase contains a high concentration of ions. ***Single-column ion chromatography***, in which an ion-suppressor column is not needed, is possible if the concentration of ions in the mobile phase is small. Typically the stationary phase is a resin with a low capacity for ion-exchange and the mobile phase is a very dilute solution of methane sulfonic acid for cationic analytes, or potassium benzoate or potassium hydrogen phthalate for anionic analytes. Because the background conductivity is sufficiently small, it is possible to monitor a change in conductivity as the analytes elute from the column.

A UV/Vis absorbance detector can be used if the analytes absorb ultraviolet or visible radiation. Alternatively, we can detect indirectly analytes that do not absorb in the UV/Vis if the mobile phase contains a UV/Vis absorbing species. In this case, when a solute band passes through the detector, a decrease in absorbance is measured at the detector.

Ion-exchange chromatography is an important technique for the analysis of anions and cations in water. For example, an ion-exchange chromatographic analysis for the anions F^-, Cl^-, Br^-, NO_2^-, NO_3^-, PO_4^{3-}, and SO_4^{2-} takes approximately 15 minutes (Figure 12.6.2). A complete analysis of the same set of anions by a combination of potentiometry and spectrophotometry requires 1–2 days. Ion-exchange chromatography also is used for the analysis of proteins, amino acids, sugars, nucleotides, pharmaceuticals, consumer products, and clinical samples.

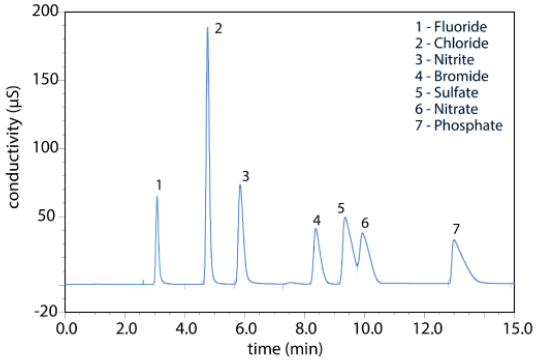

Figure 12.6.2 . Ion-exchange chromatographic analysis of water from Big Walnut Creek in Putnam County, Indiana. Data provided by Jeanette Pope, Department of Geosciences, DePauw University.

Size-Exclusion Chromatography

We have considered two classes of micron-sized stationary phases in this section: silica particles and cross-linked polymer resin beads. Both materials are porous, with pore sizes ranging from approximately 5–400 nm for silica particles, and from 5 nm to 100

μm for divinylbenzene cross-linked polystyrene resins. In ***size-exclusion chromatography***—which also is known by the terms molecular-exclusion or gel permeation chromatography—the separation of solutes depends upon their ability to enter into the pores of the stationary phase. Smaller solutes spend proportionally more time within the pores and take longer to elute from the column.

A stationary phase's size selectivity extends over a finite range. All solutes significantly smaller than the pores move through the column's entire volume and elute simultaneously, with a retention volume, V_r, of

$$V_r = V_i + V_o \tag{3.6.3}$$

where V_i is the volume of mobile phase occupying the stationary phase's pore space and V_o is volume of mobile phase in the remainder of the column. The largest solute for which Equation 3.6.3 holds is the column's inclusion limit, or permeation limit. Those solutes too large to enter the pores elute simultaneously with an retention volume of

$$V_r = V_o \tag{3.6.4}$$

Equation 3.6.4 defines the column's ***exclusion limit***.

For a solute whose size is between the inclusion limit and the exclusion limit, the amount of time it spends in the stationary phase's pores is proportional to its size. The retention volume for these solutes is

$$V_r = DV_i + V_o \tag{3.6.5}$$

where D is the solute's distribution ratio, which ranges from 0 at the exclusion limit to 1 at the inclusion limit. Equation 3.6.5 assumes that size-exclusion is the only interaction between the solute and the stationary phase that affects the separation. For this reason, stationary phases using silica particles are deactivated as described earlier, and polymer resins are synthesized without exchange sites.

Size-exclusion chromatography provides a rapid means for separating larger molecules, including polymers and biomolecules. A stationary phase for proteins that consists of particles with 30 nm pores has an inclusion limit of 7500 g/mol and an exclusion limit of 1.2×10^6 g/mol. Mixtures of proteins that span a wider range of molecular weights are separated by joining together in series several columns with different inclusion and exclusion limits.

Another important application of size-exclusion chromatography is the estimation of a solute's molecular weight (MW). Calibration curves are prepared using a series of standards of known molecular weight and measuring each standard's retention volume. As shown in Figure 12.6.3 , a plot of log(MW) versus V_r is roughly linear between the exclusion limit and the inclusion limit. Because a solute's retention volume is influenced by both its size and its shape, a reasonably accurate estimation of molecular weight is possible only if the standards are chosen carefully to minimize the effect of shape.

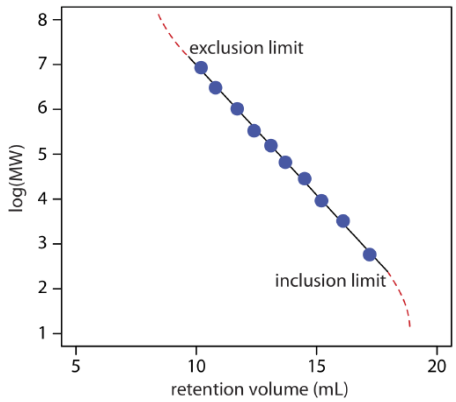

Figure 12.6.3 . Calibration curve for the determination of molecular weight by size-exclusion chromatography. The data shown here are adapted from Rouessac, F.; Rouessac, A. *Chemical Analysis: Modern Instrumentation Methods and Techniques*, Wiley: Chichester, England, 2004, p 141.

Size-exclusion chromatography is carried out using conventional HPLC instrumentation, replacing the HPLC column with an appropriate size-exclusion column. A UV/Vis detector is the most common means for obtaining the chromatogram.

Supercritical Fluid Chromatography

Although there are many analytical applications of gas chromatography and liquid chromatography, they can not separate and analyze all types of samples. Capillary column GC separates complex mixtures with excellent resolution and short analysis times. Its application is limited, however, to volatile analytes or to analytes made volatile by a suitable derivatization reaction. Liquid chromatography separates a wider range of solutes than GC, but the most common detectors—UV, fluorescence, and electrochemical— have poorer detection limits and smaller linear ranges than GC detectors, and are not as universal in their selectivity.

For some samples, ***supercritical fluid chromatography*** (SFC) provides a useful alternative to gas chromatography and liquid chromatography. The mobile phase in supercritical fluid chromatography is a gas held at a temperature and pressure that exceeds its critical point (Figure 12.6.4). Under these conditions the mobile phase is neither a gas nor a liquid. Instead, the mobile phase is a supercritical fluid.

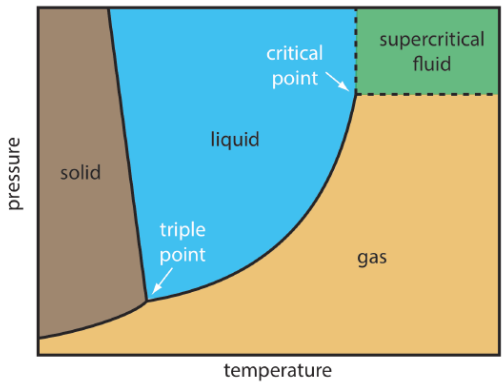

Figure 12.6.4 . Phase diagram showing the combinations of temperature and pres- sure for which a compound is in its solid state, its liquid state, and its gas state. For pressures and temperatures above the critical point, the compound is a supercritical fluid with properties intermediate between a gas and a liquid. Click here to see an interesting video demonstration of supercritical fluids from Nottingham Science City at the University of Nottingham.

Some properties of a supercritical fluid, as shown in Table 12.6.2 , are similar to a gas; other properties, however, are similar to a liquid. The viscosity of a supercritical fluid, for example, is similar to a gas, which means we can move a supercritical fluid through a capillary column or a packed column without the high pressures needed in HPLC. Analysis time and resolution, although not as good as in GC, usually are better than in conventional HPLC. The density of a supercritical fluid, on the other hand, is much closer to that of a liquid, which explains why supercritical fluids are good solvents. In terms of its separation power, a mobile phase in SFC behaves more like the liquid mobile phase in HPLC than the gaseous mobile phase in GC.

Table 12.6.2 . Typical Properties of Gases, Liquids, and Supercritical Fluids

phase	density (g/cm^3)	viscosity ($g\ cm^{-1}\ s^{-1}$)	diffusion coefficient ($cm^2\ s^{-1}$)
gas	$\approx 10^{-3}$	$\approx 10^{-4}$	≈ 0.1
supercritical fluid	$\approx 0.1 - 1$	$\approx 10^{-4} - 10^{-3}$	$\approx 10^{-4} - 10^{-3}$
liquid	≈ 1	$\approx 10^{-2}$	$\approx 10^{-3}$

The most common mobile phase for supercritical fluid chromatography is CO_2. Its low critical temperature of 31.1°C and its low critical pressure of 72.9 atm are relatively easy to achieve and maintain. Although supercritical CO_2 is a good solvent for nonpolar organics, it is less useful for polar solutes. The addition of an organic modifier, such as methanol, improves the mobile phase's elution strength. Other common mobile phases and their critical temperatures and pressures are listed in Table 12.6.3 .

Table 12.6.3 . Critical Points for Selected Supercritical Fluids

compound	critical temperature (°C)	critical pressure (atm)
carbon dioxide	31.3	72.9
ethane	32.4	48.3

compound	critical temperature (^{o}C)	critical pressure (atm)
nitrous oxide	36.5	71.4
ammonia	132.3	111.3
diethyl ether	193.6	36.3
isopropanol	235.3	47.0
methanol	240.5	78.9
ethanol	243.4	63.0
water	374.4	226.8

The instrumentation for supercritical fluid chromatography essentially is the same as that for a standard HPLC. The only important additions are a heated oven for the column and a pressure restrictor downstream from the column to maintain the critical pressure. Gradient elutions are accomplished by changing the applied pressure over time. The resulting change in the mobile phase's density affects its solvent strength. Detection is accomplished using standard GC detectors or HPLC detectors. Supercritical fluid chromatography has many applications in the analysis of polymers, fossil fuels, waxes, drugs, and food products.

3.7: Electrophoresis

Electrophoresis is a class of separation techniques in which we separate analytes by their ability to move through a conductive medium—usually an aqueous buffer—in response to an applied electric field. In the absence of other effects, cations migrate toward the electric field's negatively charged cathode. Cations with larger charge-to-size ratios—which favors ions of greater charge and of smaller size—migrate at a faster rate than larger cat- ions with smaller charges. Anions migrate toward the positively charged anode and neutral species do not experience the electrical field and remain stationary.

> As we will see shortly, under normal conditions even neutral species and anions migrate toward the cathode.

There are several forms of electrophoresis. In slab gel electrophoresis the conducting buffer is retained within a porous gel of agarose or polyacrylamide. Slabs are formed by pouring the gel between two glass plates separated by spacers. Typical thicknesses are 0.25–1 mm. Gel electrophoresis is an important technique in biochemistry where it frequently is used to separate DNA fragments and proteins. Although it is a powerful tool for the qualitative analysis of complex mixtures, it is less useful for quantitative work.

In ***capillary electrophoresis*** the conducting buffer is retained within a capillary tube with an inner diameter that typically is 25–75 μm. The sample is injected into one end of the capillary tube, and as it migrates through the capillary the sample's components separate and elute from the column at different times. The resulting ***electropherogram*** looks similar to a GC or an HPLC chromatogram, and provides both qualitative and quantitative information. Only capillary electrophoretic methods receive further consideration in this section.

Theory of Electrophoresis

In capillary electrophoresis we inject the sample into a buffered solution retained within a capillary tube. When an electric field is applied across the capillary tube, the sample's components migrate as the result of two types of actions: electrophoretic mobility and electroosmotic mobility. ***Electrophoretic mobility*** is the solute's response to the applied electrical field in which cations move toward the negatively charged cathode, anions move toward the positively charged anode, and neutral species remain stationary. The other contribution to a solute's migration is ***electroosmotic flow***, which occurs when the buffer moves through the capillary in response to the applied electrical field. Under normal conditions the buffer moves toward the cathode, sweeping most solutes, including the anions and neutral species, toward the negatively charged cathode.

Electrophoretic Mobility

The velocity with which a solute moves in response to the applied electric field is called its ***electrophoretic velocity***, ν_{ep}; it is defined as

$$\nu_{ep} = \mu_{ep} E \tag{3.7.1}$$

where μ_{ep} is the solute's electrophoretic mobility, and E is the magnitude of the applied electrical field. A solute's electrophoretic mobility is defined as

$$\mu_{ep} = \frac{q}{6\pi\eta r} \tag{3.7.2}$$

where q is the solute's charge, η is the buffer's viscosity, and r is the solute's radius. Using Equation 3.7.1 and Equation 3.7.2 we can make several important conclusions about a solute's electrophoretic velocity. Electrophoretic mobility and, therefore, electrophoretic velocity, increases for more highly charged solutes and for solutes of smaller size. Because q is positive for a cation and negative for an anion, these species migrate in opposite directions. A neutral species, for which q is zero, has an electrophoretic velocity of zero.

Electroosmotic Mobility

When an electric field is applied to a capillary filled with an aqueous buffer we expect the buffer's ions to migrate in response to their electrophoretic mobility. Because the solvent, H_2O, is neutral we might reasonably expect it to remain stationary. What we observe under normal conditions, however, is that the buffer moves toward the cathode. This phenomenon is called the electroosmotic flow.

Electroosmotic flow occurs because the walls of the capillary tubing carry a charge. The surface of a silica capillary contains large numbers of silanol groups (–SiOH). At a pH level greater than approximately 2 or 3, the silanol groups ionize to form negatively charged silanate ions ($–SiO^–$). Cations from the buffer are attracted to the silanate ions. As shown in Figure 12.7.1 , some of these cations bind tightly to the silanate ions, forming a fixed layer. Because the cations in the fixed layer only partially neutralize the negative charge on the capillary walls, the solution adjacent to the fixed layer—which is called the diffuse layer—contains more cations than anions. Together these two layers are known as the double layer. Cations in the diffuse layer migrate toward the cathode. Because these cations are solvated, the solution also is pulled along, producing the electroosmotic flow.

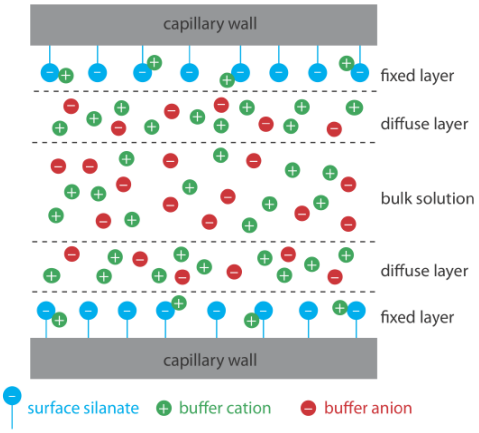

Figure 12.7.1 . Schematic diagram showing the origin of the double layer within a capillary tube. Although the net charge within the capillary is zero, the distribution of charge is not. The walls of the capillary have an excess of negative charge, which decreases across the fixed layer and the diffuse layer, reaching a value of zero in bulk solution.

> The anions in the diffuse layer, which also are solvated, try to move toward the anode. Because there are more cations than anions, however, the cations win out and the electroosmotic flow moves in the direction of the cathode.

The rate at which the buffer moves through the capillary, what we call its ***electroosmotic flow velocity***, ν_{eof}, is a function of the applied electric field, E, and the buffer's electroosmotic mobility, μ_{eof}.

$$\nu_{eof} = \mu_{eof} E \tag{3.7.3}$$

Electroosmotic mobility is defined as

$$\mu_{eof} = \frac{\varepsilon \zeta}{4 \pi \eta} \tag{3.7.4}$$

where ϵ is the buffer dielectric constant, ζ is the zeta potential, and η is the buffer's viscosity.

The ***zeta potential***—the potential of the diffuse layer at a finite distance from the capillary wall—plays an important role in determining the electroosmotic flow velocity. Two factors determine the zeta potential's value. First, the zeta potential is directly proportional to the charge on the capillary walls, with a greater density of silanate ions corresponding to a larger zeta potential. Below a pH of 2 there are few silanate ions and the zeta potential and the electroosmotic flow velocity approach zero. As the pH increases, both the zeta potential and the electroosmotic flow velocity increase. Second, the zeta potential is directly proportional to the thickness of the double layer. Increasing the buffer's ionic strength provides a higher concentration of cations, which decreases the thickness of the double layer and decreases the electroosmotic flow.

> The definition of zeta potential given here admittedly is a bit fuzzy. For a more detailed explanation see Delgado, A. V.; González-Caballero, F.; Hunter, R. J.; Koopal, L. K.; Lyklema, J. "Measurement and Interpretation of Electrokinetic Phenomena," *Pure. Appl. Chem.* **2005**, *77*, 1753–1805. Although this is a very technical report, Sections 1.3–1.5 provide a good introduction to the difficulty of defining the zeta potential and of measuring its value.

The electroosmotic flow profile is very different from that of a fluid moving under forced pressure. Figure 12.7.2 compares the electroosmotic flow profile with the hydrodynamic flow profile in gas chromatography and liquid chromatography. The uniform,

flat profile for electroosmosis helps minimize band broadening in capillary electrophoresis, improving separation efficiency.

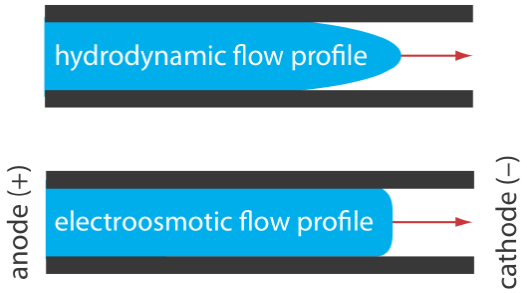

Figure 12.7.2 . Comparison of hydrodynamic flow and electroosmotic flow. The nearly uniform electroosmotic flow profile means that the electroosmotic flow velocity is nearly constant across the capillary.

Total Mobility

A solute's total velocity, ν_{tot}, as it moves through the capillary is the sum of its electrophoretic velocity and the electroosmotic flow velocity.

$$\nu_{tot} = \nu_{ep} + \nu_{eof}$$

As shown in Figure 12.7.3 , under normal conditions the following general relationships hold true.

$$(\nu_{tot})_{cations} > \nu_{eof}$$

$$(\nu_{tot})_{neutrals} = \nu_{eof}$$

$$(\nu_{tot})_{anions} < \nu_{eof}$$

Cations elute first in an order that corresponds to their electrophoretic mobilities, with small, highly charged cations eluting before larger cations of lower charge. Neutral species elute as a single band with an elution rate equal to the electroosmotic flow velocity. Finally, anions are the last components to elute, with smaller, highly charged anions having the longest elution time.

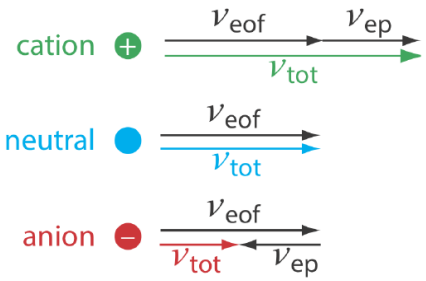

Figure 12.7.3 . Visual explanation for the general elution order in capillary electrophoresis. Each species has the same electroosmotic flow, ν_{eof}. Cations elute first because they have a positive electrophoretic velocity, ν_{ep}. Anions elute last because their negative electrophoretic velocity partially offsets the electroosmotic flow velocity. Neutrals elute with a velocity equal to the electroosmotic flow.

Migration Time

Another way to express a solute's velocity is to divide the distance it travels by the elapsed time

$$\nu_{tot} = \frac{l}{t_m} \tag{3.7.5}$$

where l is the distance between the point of injection and the detector, and t_{m} is the solute's migration time. To understand the experimental variables that affect migration time, we begin by noting that

$$\nu_{tot} = \mu_{tot} E = (\mu_{ep} + \mu_{eof}) E \tag{3.7.6}$$

Combining Equation 3.7.5 and Equation 3.7.6 and solving for t_{m} leaves us with

$$t_{\mathrm{m}} = \frac{l}{(\mu_{ep} + \mu_{eof})\, E} \tag{3.7.7}$$

The magnitude of the electrical field is

$$E = \frac{V}{L} \tag{3.7.8}$$

where V is the applied potential and L is the length of the capillary tube. Finally, substituting Equation 3.7.8 into Equation 3.7.7 leaves us with the following equation for a solute's migration time.

$$t_{\mathrm{m}} = \frac{lL}{(\mu_{ep} + \mu_{eof})\,V} \tag{3.7.9}$$

To decrease a solute's migration time—which shortens the analysis time—we can apply a higher voltage or use a shorter capillary tube. We can also shorten the migration time by increasing the electroosmotic flow, although this decreases resolution.

Efficiency

As we learned in Chapter 12.2, the efficiency of a separation is given by the number of theoretical plates, N. In capillary electrophoresis the number of theoretic plates is

$$N = \frac{l^2}{2Dt_m} = \frac{(\mu_{ep} + \mu_{eof})\,El}{2DL} \tag{3.7.10}$$

where D is the solute's diffusion coefficient. From Equation 3.7.10, the efficiency of a capillary electrophoretic separation increases with higher voltages. Increasing the electroosmotic flow velocity improves efficiency, but at the expense of resolution. Two additional observations deserve comment. First, solutes with larger electrophoretic mobilities—in the same direction as the electroosmotic flow—have greater efficiencies; thus, smaller, more highly charged cations are not only the first solutes to elute, but do so with greater efficiency. Second, efficiency in capillary electrophoresis is independent of the capillary's length. Theoretical plate counts of approximately 100 000–200 000 are not unusual.

> It is possible to design an electrophoretic experiment so that anions elute before cations—more about this later—in which smaller, more highly charged anions elute with greater efficiencies.

Selectivity

In chromatography we defined the selectivity between two solutes as the ratio of their retention factors. In capillary electrophoresis the analogous expression for selectivity is

$$\alpha = \frac{\mu_{ep,1}}{\mu_{ep,2}}$$

where $\mu_{ep,1}$ and $\mu_{ep,2}$ are the electrophoretic mobilities for the two solutes, chosen such that $\alpha \geq 1$. We can often improve selectivity by adjusting the pH of the buffer solution. For example, NH_4^+ is a weak acid with a pK_a of 9.75. At a pH of 9.75 the concentrations of NH_4^+ and NH_3 are equal. Decreasing the pH below 9.75 increases its electrophoretic mobility because a greater fraction of the solute is present as the cation NH_4^+. On the other hand, raising the pH above 9.75 increases the proportion of neutral NH_3, decreasing its electrophoretic mobility.

Resolution

The resolution between two solutes is

$$R = \frac{0.177(\mu_{ep,2} - \mu_{ep,1})\sqrt{V}}{\sqrt{D(\mu_{avg} + \mu_{eof}}} \tag{3.7.11}$$

where μ_{avg} is the average electrophoretic mobility for the two solutes. Increasing the applied voltage and decreasing the electroosmotic flow velocity improves resolution. The latter effect is particularly important. Although increasing electroosmotic flow improves analysis time and efficiency, it de- creases resolution.

Instrumentation

The basic instrumentation for capillary electrophoresis is shown in Figure 12.7.4 and includes a power supply for applying the electric field, anode and cathode compartments that contain reservoirs of the buffer solution, a sample vial that contains the sample, the capillary tube, and a detector. Each part of the instrument receives further consideration in this section.

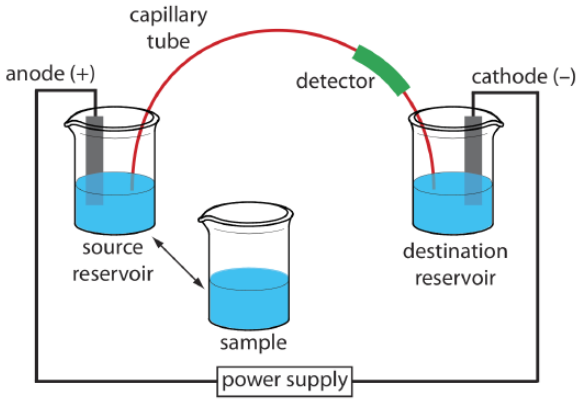

Figure 12.7.4 . Schematic diagram of the basic instrumentation for capillary electrophoresis. The sample and the source reservoir are switched when making injections.

Capillary Tubes

Figure 12.7.5 shows a cross-section of a typical capillary tube. Most capillary tubes are made from fused silica coated with a 15–35 μm layer of polyimide to give it mechanical strength. The inner diameter is typically 25–75 μm, which is smaller than the internal diameter of a capillary GC column, with an outer diameter of 200–375 μm.

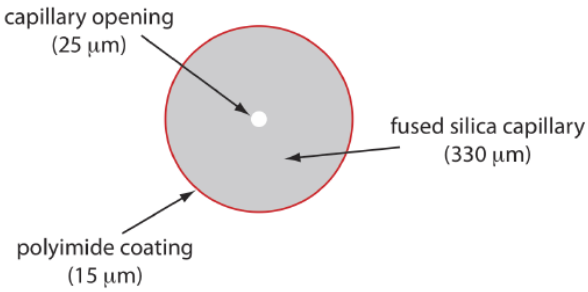

Figure 12.7.5 . Cross section of a capillary column for capillary electrophoresis. The dimensions shown here are typical and are scaled proportionally in this figure.

The capillary column's narrow opening and the thickness of its walls are important. When an electric field is applied to the buffer solution, current flows through the capillary. This current leads to the release of heat, which we call ***Joule heating***. The amount of heat released is proportional to the capillary's radius and to the magnitude of the electrical field. Joule heating is a problem because it changes the buffer's viscosity, with the solution at the center of the capillary being less viscous than that near the capillary walls. Because a solute's electrophoretic mobility depends on its viscosity (see Equation 3.7.2), solute species in the center of the capillary migrate at a faster rate than those near the capillary walls. The result is an additional source of band broadening that degrades the separation. Capillaries with smaller inner diameters generate less Joule heating, and capillaries with larger outer diameters are more effective at dissipating the heat. Placing the capillary tube inside a thermostated jacket is another method for minimizing the effect of Joule heating; in this case a smaller outer diameter allows for a more rapid dissipation of thermal energy.

Injecting the Sample

There are two common methods for injecting a sample into a capillary electrophoresis column: hydrodynamic injection and electrokinetic injection. In both methods the capillary tube is filled with the buffer solution. One end of the capillary tube is placed in the destination reservoir and the other end is placed in the sample vial.

Hydrodynamic injection uses pressure to force a small portion of sample into the capillary tubing. A difference in pressure is applied across the capillary either by pressurizing the sample vial or by applying a vacuum to the destination reservoir. The volume

of sample injected, in liters, is given by the following equation

$$V_{\text{inj}} = \frac{\Delta P d^4 \pi t}{128 \eta L} \times 10^3 \tag{3.7.12}$$

where ΔP is the difference in pressure across the capillary in pascals, d is the capillary's inner diameter in meters, t is the amount of time the pressure is applied in seconds, η is the buffer's viscosity in kg m^{-1} s^{-1}, and L is the length of the capillary tubing in meters. The factor of 10^3 changes the units from cubic meters to liters.

For a hydrodynamic injection we move the capillary from the source reservoir to the sample. The anode remains in the source reservoir. A hydrodynamic injection also is possible if we raise the sample vial above the destination reservoir and briefly insert the filled capillary.

Example 12.7.1

In a hydrodynamic injection we apply a pressure difference of 2.5×10^3 Pa (a $\Delta P \approx 0.02$ atm) for 2 s to a 75-cm long capillary tube with an internal diameter of 50 μm. Assuming the buffer's viscosity is 10^{-3} kg m^{-1} s^{-1}, what volume and length of sample did we inject?

Solution

Making appropriate substitutions into Equation 3.7.12 gives the sample's volume as

$$V_{inj} = \frac{\left(2.5 \times 10^3 \text{ kg m}^{-1} \text{ s}^{-2}\right) \left(50 \times 10^{-6} \text{ m}\right)^4 (3.14)(2 \text{ s})}{(128)\left(0.001 \text{ kg m}^{-1} \text{ s}^{-1}\right)(0.75 \text{ m})} \times 10^3 \text{L/m}^3$$

$$V_{inj} = 1 \times 10^{-9} \text{ L} = 1 \text{ nL}$$

Because the interior of the capillary is cylindrical, the length of the sample, l, is easy to calculate using the equation for the volume of a cylinder; thus

$$l = \frac{V_{\text{inj}}}{\pi r^2} = \frac{\left(1 \times 10^{-9} \text{ L}\right)\left(10^{-3} \text{ m}^3/\text{L}\right)}{(3.14)\left(25 \times 10^{-6} \text{ m}\right)^2} = 5 \times 10^{-4} \text{ m} = 0.5 \text{ mm}$$

Exercise 12.7.1

Suppose you need to limit your injection to less than 0.20% of the capillary's length. Using the information from Example 12.7.1 , what is the maximum injection time for a hydrodynamic injection?

Answer

The capillary is 75 cm long, which means that 0.20% of that sample's maximum length is 0.15 cm. To convert this to the maximum volume of sample we use the equation for the volume of a cylinder.

$$V_{inj} = l\pi r^2 = (0.15 \text{ cm})(3.14)\left(25 \times 10^{-4} \text{ cm}\right)^2 = 2.94 \times 10^{-6} \text{ cm}^3$$

Given that 1 cm^3 is equivalent to 1 mL, the maximum volume is 2.94×10^{-6} mL or 2.94×10^{-9} L. To find the maximum injection time, we first solve Equation 3.7.12 for t

$$t = \frac{128 V_{inj} \eta L}{P d^4 \pi} \times 10^{-3} \text{ m}^3/\text{L}$$

and then make appropriate substitutions.

$$t = \frac{(128)\left(2.94 \times 10^{-9} \text{ L}\right)\left(0.001 \text{ kg } \text{ m}^{-1} \text{ s}^{-1}\right)(0.75 \text{ m})}{\left(2.5 \times 10^3 \text{ kg m}^{-1} \text{ s}^{-2}\right)\left(50 \times 10^{-6} \text{ m}\right)^4 (3.14)} \times \frac{10^{-3} \text{ m}^3}{\text{L}} = 5.8 \text{ s}$$

The maximum injection time, therefore, is 5.8 s.

In an ***electrokinetic injection*** we place both the capillary and the anode into the sample and briefly apply an potential. The volume of injected sample is the product of the capillary's cross sectional area and the length of the capillary occupied by the sample. In turn, this length is the product of the solute's velocity (see Equation 3.7.6) and time; thus

$$V_{inj} = \pi r^2 L = \pi r^2 (\mu_{ep} + \mu_{eof}) E' t \tag{3.7.13}$$

where r is the capillary's radius, L is the capillary's length, and E' is the effective electric field in the sample. An important consequence of Equation 3.7.13 is that an electrokinetic injection is biased toward solutes with larger electrophoretic mobilities. If two solutes have equal concentrations in a sample, we inject a larger volume—and thus more moles—of the solute with the larger μ_{ep}.

> The electric field in the sample is different that the electric field in the rest of the capillary because the sample and the buffer have different ionic compositions. In general, the sample's ionic strength is smaller, which makes its conductivity smaller. The effective electric field is
>
> $$E' = E \times \frac{\chi_{\text{buffer}}}{\chi_{\text{sample}}}$$
>
> where χ_{buffer} and χ_{sample} are the conductivities of the buffer and the sample, respectively.

When an analyte's concentration is too small to detect reliably, it maybe possible to inject it in a manner that increases its concentration. This method of injection is called ***stacking***. Stacking is accomplished by placing the sample in a solution whose ionic strength is significantly less than that of the buffer in the capillary tube. Because the sample plug has a lower concentration of buffer ions, the effective field strength across the sample plug, E', is larger than that in the rest of the capillary.

We know from Equation 3.7.1 that electrophoretic velocity is directly proportional to the electrical field. As a result, the cations in the sample plug migrate toward the cathode with a greater velocity, and the anions migrate more slowly—neutral species are unaffected and move with the electroosmotic flow. When the ions reach their respective boundaries between the sample plug and the buffer, the electrical field decreases and the electrophoretic velocity of the cations decreases and that for the anions increases. As shown in Figure 12.7.6 , the result is a stacking of cations and anions into separate, smaller sampling zones. Over time, the buffer within the capillary becomes more homogeneous and the separation proceeds without additional stacking.

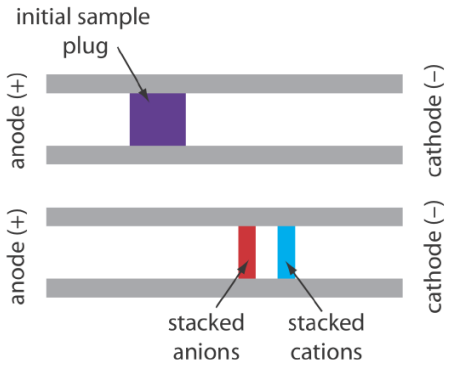

Figure 12.7.6 . The stacking of cations and anions. The top diagram shows the initial sample plug and the bottom diagram shows how the cations and anions are concentrated at opposite sides of the sample plug.

Applying the Electrical Field

Migration in electrophoresis occurs in response to an applied electric field. The ability to apply a large electric field is important because higher voltages lead to shorter analysis times (Equation 3.7.9), more efficient separations (Equation 3.7.10), and better resolution (Equation 3.7.11). Because narrow bored capillary tubes dissipate Joule heating so efficiently, voltages of up to 40 kV are possible.

> Because of the high voltages, be sure to follow your instrument's safety guidelines.

Detectors

Most of the detectors used in HPLC also find use in capillary electrophoresis. Among the more common detectors are those based on the absorption of UV/Vis radiation, fluorescence, conductivity, amperometry, and mass spectrometry. Whenever possible, detection is done “on-column” before the solutes elute from the capillary tube and additional band broadening occurs.

UV/Vis detectors are among the most popular. Because absorbance is directly proportional to path length, the capillary tubing’s small diameter leads to signals that are smaller than those obtained in HPLC. Several approaches have been used to increase the pathlength, including a Z-shaped sample cell and multiple reflections (see Figure 12.7.7). Detection limits are about 10^{-7} M.

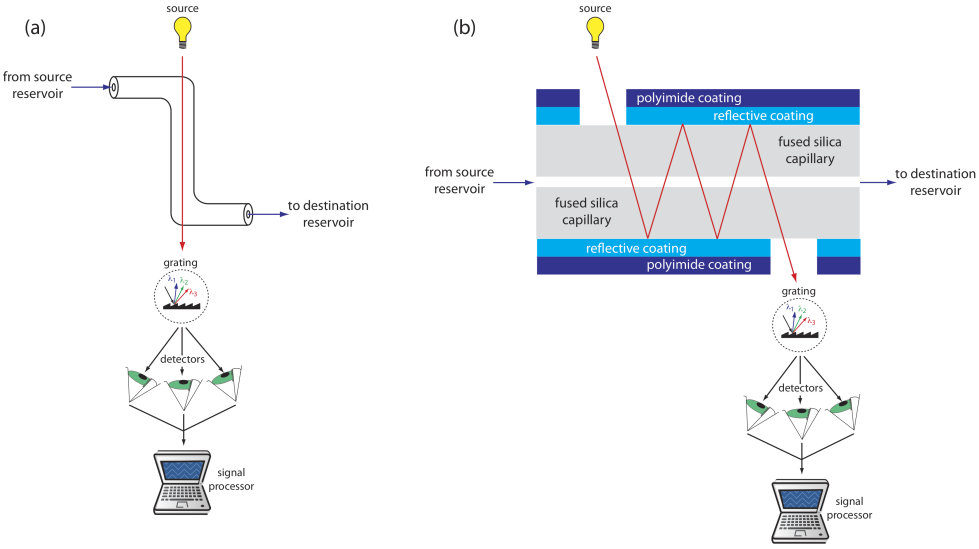

Figure 12.7.7 . Two approaches to on-column detection in capillary electrophoresis using a UV/Vis diode array spectrometer: (a) Z-shaped bend in capillary, and (b) multiple reflections.

Better detection limits are obtained using fluorescence, particularly when using a laser as an excitation source. When using fluorescence detection a small portion of the capillary’s protective coating is removed and the laser beam is focused on the inner portion of the capillary tubing. Emission is measured at an angle of 90º to the laser. Because the laser provides an intense source of radiation that can be focused to a narrow spot, detection limits are as low as 10^{-16} M.

Solutes that do not absorb UV/Vis radiation or that do not undergo fluorescence can be detected by other detectors. Table 12.7.1 provides a list of detectors for capillary electrophoresis along with some of their important characteristics.

Table 12.7.1 . Characteristics of Detectors for Capillary Electrophoresis

detector	selectivity (universal or analyte must ...)	detection limited (moles injected)	detection limit (molarity)	on-column detection?
UV/Vis absorbance	have a UV/Vis chromophore	$10^{-13} - 10^{-16}$	$10^{-5} - 10^{-7}$	yes
indirect absorbancd	universal	$10^{-12} - 10^{-15}$	$10^{-4} - 10^{-6}$	yes
fluoresence	have a favorable quantum yield	$10^{-13} - 10^{-17}$	$10^{-7} - 10^{-9}$	yes
laser fluorescence	have a favorable quantum yield	$10^{-18} - 10^{-20}$	$10^{-13} - 10^{-16}$	yes
mass spectrometer	universal (total ion) selective (single ion)	$10^{-16} - 10^{-17}$	$10^{-8} - 10^{-10}$	no
amperometry	undergo oxidation or reduction	$10^{-18} - 10^{-19}$	$10^{-7} - 10^{-10}$	no
conductivity	universal	$10^{-15} - 10^{-16}$	$10^{-7} - 10^{-9}$	no

detector	selectivity (universal or analyte must ...)	detection limited (moles injected)	detection limit (molarity)	on-column detection?
radiometric	be radioactive	$10^{-17} - 10^{-19}$	$10^{-10} - 10^{-12}$	yes

Capillary Electrophoresis Methods

There are several different forms of capillary electrophoresis, each of which has its particular advantages. Four of these methods are described briefly in this section.

Capillary Zone Electrophoresis (CZE)

The simplest form of capillary electrophoresis is ***capillary zone electrophoresis***. In CZE we fill the capillary tube with a buffer and, after loading the sample, place the ends of the capillary tube in reservoirs that contain additional buffer. Usually the end of the capillary containing the sample is the anode and solutes migrate toward the cathode at a velocity determined by their respective electrophoretic mobilities and the electroosmotic flow. Cations elute first, with smaller, more highly charged cations eluting before larger cations with smaller charges. Neutral species elute as a single band. Anions are the last species to elute, with smaller, more negatively charged anions being the last to elute.

We can reverse the direction of electroosmotic flow by adding an alkylammonium salt to the buffer solution. As shown in Figure 12.7.8 , the positively charged end of the alkyl ammonium ions bind to the negatively charged silanate ions on the capillary's walls. The tail of the alkyl ammonium ion is hydrophobic and associates with the tail of another alkyl ammonium ion. The result is a layer of positive charges that attract anions in the buffer. The migration of these solvated anions toward the anode reverses the electroosmotic flow's direction. The order of elution is exactly opposite that observed under normal conditions.

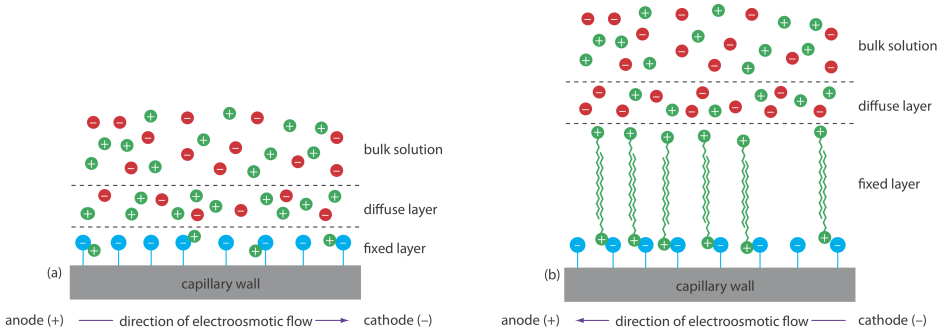

Figure 12.7.8 . Two modes of capillary zone electrophoresis showing (a) normal migration with electroosmotic flow toward the cathode and (b) reversed migration in which the electroosmotic flow is toward the anode.

Coating the capillary's walls with a nonionic reagent eliminates the electroosmotic flow. In this form of CZE the cations migrate from the anode to the cathode. Anions elute into the source reservoir and neutral species remain stationary.

Capillary zone electrophoresis provides effective separations of charged species, including inorganic anions and cations, organic acids and amines, and large biomolecules such as proteins. For example, CZE was used to separate a mixture of 36 inorganic and organic ions in less than three minutes [Jones, W. R.; Jandik, P. *J. Chromatog.* **1992**, *608*, 385–393]. A mixture of neutral species, of course, can not be resolved.

Micellar Electrokinetic Capillary Chromatography (MEKC)

One limitation to CZE is its inability to separate neutral species. ***Micellar electrokinetic capillary chromatography*** overcomes this limitation by adding a surfactant, such as sodium dodecylsulfate (Figure 12.7.9 a) to the buffer solution. Sodium dodecylsulfate, or SDS, consists of a long-chain hydrophobic tail and a negatively charged ionic functional group at its head. When the concentration of SDS is sufficiently large a micelle forms. A micelle consists of a spherical agglomeration of 40–100 surfactant molecules in which the hydrocarbon tails point inward and the negatively charged heads point outward (Figure 12.7.9 b).

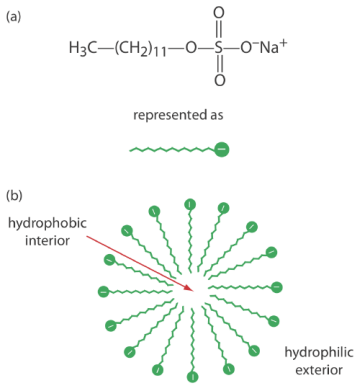

Figure 12.7.9 . (a) Structure of sodium dodecylsulfate and (b) cross section through a micelle showing its hydrophobic interior and its hydrophilic exterior.

Because micelles have a negative charge, they migrate toward the cathode with a velocity less than the electroosmotic flow velocity. Neutral species partition themselves between the micelles and the buffer solution in a manner similar to the partitioning of solutes between the two liquid phases in HPLC. Because there is a partitioning between two phases, we include the descriptive term chromatography in the techniques name. Note that in MEKC both phases are mobile.

The elution order for neutral species in MEKC depends on the extent to which each species partitions into the micelles. Hydrophilic neutrals are insoluble in the micelle's hydrophobic inner environment and elute as a single band, as they would in CZE. Neutral solutes that are extremely hy- drophobic are completely soluble in the micelle, eluting with the micelles as a single band. Those neutral species that exist in a partition equilibrium between the buffer and the micelles elute between the completely hydro- philic and completely hydrophobic neutral species. Those neutral species that favor the buffer elute before those favoring the micelles. Micellar electrokinetic chromatography is used to separate a wide variety of samples, including mixtures of pharmaceutical compounds, vitamins, and explosives.

Capillary Gel Electrophoresis (CGE)

In ***capillary gel electrophoresis*** the capillary tubing is filled with a polymeric gel. Because the gel is porous, a solute migrates through the gel with a velocity determined both by its electrophoretic mobility and by its size. The ability to effect a separation using size is helpful when the solutes have similar electrophoretic mobilities. For example, fragments of DNA of varying length have similar charge-to-size ratios, making their separation by CZE difficult. Because the DNA fragments are of different size, a CGE separation is possible.

The capillary used for CGE usually is treated to eliminate electroosmotic flow to prevent the gel from extruding from the capillary tubing. Samples are injected electrokinetically because the gel provides too much resistance for hydrodynamic sampling. The primary application of CGE is the separation of large biomolecules, including DNA fragments, proteins, and oligonucleotides.

Capillary Electrochromatography (CEC)

Another approach to separating neutral species is ***capillary electrochromatography***. In CEC the capillary tubing is packed with 1.5–3 μm particles coated with a bonded stationary phase. Neutral species separate based on their ability to partition between the stationary phase and the buffer, which is moving as a result of the electroosmotic flow; Figure 12.7.10 provides a representative example for the separation of a mixture of hydrocarbons. A CEC separation is similar to the analogous HPLC separation, but without the need for high pressure pumps. Efficiency in CEC is better than in HPLC, and analysis times are shorter.

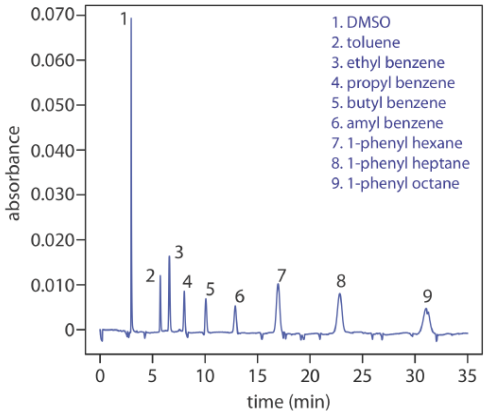

Figure 12.7.10 . Capillary electrochromatographic separation of a mixture of hydrocarbons in DMSO. The column contains a porous polymer of butyl methacrylate and lauryl acrylate (25%:75% mol:mol) with butane dioldacrylate as a crosslinker. Data provided by Zoe LaPier and Michelle Bushey, Department of Chemistry, Trinity University.

The best way to appreciate the theoretical and the practical details discussed in this section is to carefully examine a typical analytical method. Although each method is unique, the following description of the determination of a vitamin B complex by capillary zone electrophoresis or by micellar electrokinetic capillary chromatography provides an instructive example of a typical procedure. The description here is based on Smyth, W. F. *Analytical Chemistry of Complex Matrices*, Wiley Teubner: Chichester, England, 1996, pp. 154–156.

Representative Method 12.7.1: Determination of Vitamin B Complex by CZE or MEKC

Description of Method

The water soluble vitamins B_1 (thiamine hydrochloride), B_2 (riboflavin), B_3 (niacinamide), and B_6 (pyridoxine hydrochloride) are determined by CZE using a pH 9 sodium tetraborate-sodium dihydrogen phosphate buffer, or by MEKC using the same buffer with the addition of sodium dodecyl sulfate. Detection is by UV absorption at 200 nm. An internal standard of *o*-ethoxybenzamide is used to standardize the method.

Procedure

Crush a vitamin B complex tablet and place it in a beaker with 20.00 mL of a 50 % v/v methanol solution that is 20 mM in sodium tetraborate and 100.0 ppm in *o*-ethoxybenzamide. After mixing for 2 min to ensure that the B vitamins are dissolved, pass a 5.00-mL portion through a 0.45-μm filter to remove insoluble binders. Load an approximately 4 nL sample into a capillary column with an inner diameter of a 50 μm. For CZE the capillary column contains a 20 mM pH 9 sodium tetraborate-sodium dihydrogen phosphate buffer. For MEKC the buffer is also 150 mM in sodium dodecyl sulfate. Apply a 40 kV/m electrical field to effect both the CZE and MEKC separations.

Questions

1. Methanol, which elutes at 4.69 min, is included as a neutral species to indicate the electroosmotic flow. When using standard solutions of each vitamin, CZE peaks are found at 3.41 min, 4.69 min, 6.31 min, and 8.31 min. Examine the structures and pK_a information in Figure 12.7.11 and identify the order in which the four B vitamins elute.

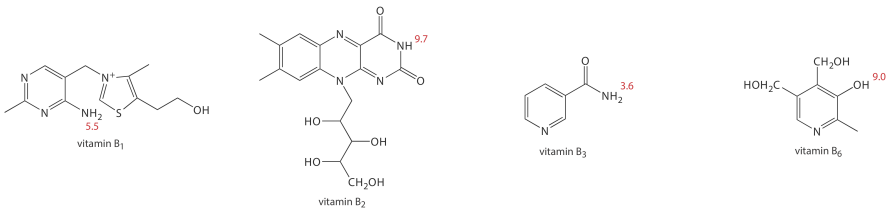

Figure 12.7.11 . Structures of the four water soluble B vitamins in their predominate forms at a pH of 9; pK_a values are shown in red.

At a pH of 9, vitamin B_1 is a cation and elutes before the neutral species methanol; thus it is the compound that elutes at 3.41 min. Vitamin B_3 is a neutral species at a pH of 9 and elutes with methanol at 4.69 min. The remaining two B vitamins are weak acids that partially ionize to weak base anions at a pH of 9. Of the two, vitamin B_6 is the stronger acid (a pK_a of 9.0 versus a pK_a of 9.7) and is present to a greater extent in its anionic form. Vitamin B_6, therefore, is the last of the vitamins to elute.

2. The order of elution when using MEKC is vitamin B_3 (5.58 min), vitamin B_6 (6.59 min), vitamin B_2 (8.81 min), and vitamin B_1 (11.21 min). What conclusions can you make about the solubility of the B vitamins in the sodium dodecylsulfate micelles? The micelles elute at 17.7 min.

The elution time for vitamin B_1 shows the greatest change, increasing from 3.41 min to 11.21 minutes. Clearly vitamin B_1 has the greatest solubility in the micelles. Vitamin B_2 and vitamin B3 have a more limited solubility in the micelles, and show only slightly longer elution times in the presence of the micelles. Interestingly, the elution time for vitamin B_6 decreases in the presence of the micelles.

3. For quantitative work an internal standard of *o*-ethoxybenzamide is added to all samples and standards. Why is an internal standard necessary?

Although the method of injection is not specified, neither a hydrodynamic injection nor an electrokinetic injection is particularly reproducible. The use of an internal standard compensates for this limitation.

Evaluation

When compared to GC and HPLC, capillary electrophoresis provides similar levels of accuracy, precision, and sensitivity, and it provides a comparable degree of selectivity. The amount of material injected into a capillary electrophoretic column is significantly smaller than that for GC and HPLC—typically 1 nL versus 0.1 µL for capillary GC and 1–100 µL for HPLC. Detection limits for capillary electrophoresis, however, are 100–1000 times poorer than that for GC and HPLC. The most significant advantages of capillary electrophoresis are improvements in separation efficiency, time, and cost. Capillary electrophoretic columns contain substantially more theoretical plates ($\approx 10^6$ plates/m) than that found in HPLC ($\approx 10^5$ plates/m) and capillary GC columns ($\approx 10^3$ plates/m), providing unparalleled resolution and peak capacity. Separations in capillary electrophoresis are fast and efficient. Furthermore, the capillary column's small volume means that a capillary electrophoresis separation requires only a few microliters of buffer, compared to 20–30 mL of mobile phase for a typical HPLC separation.

3.8: Problems

1. The following data were obtained for four compounds separated on a 20-m capillary column.

compound	t_r (min)	w (min)
A	8.04	0.15
B	8.26	0.15
C	8.43	0.16

(a) Calculate the number of theoretical plates for each compound and the average number of theoretical plates for the column, in mm.

(b) Calculate the average height of a theoretical plate.

(c) Explain why it is possible for each compound to have a different number of theoretical plates.

2. Using the data from Problem 1, calculate the resolution and the selectivity factors for each pair of adjacent compounds. For resolution, use both equation 12.2.1 and equation 12.3.3, and compare your results. Discuss how you might improve the resolution between compounds B and C. The retention time for an nonretained solute is 1.19 min.

3. Use the chromatogram in Figure 12.8.1 , obtained using a 2-m column, to determine values for t_r, w, t'_r, k, N, and H.

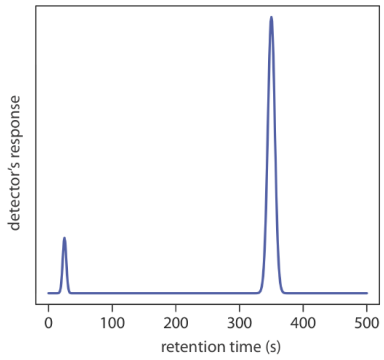

Figure 12.8.1 . Chromatogram for Problem 3.

4. Use the partial chromatogram in Figure 12.8.2 to determine the resolution between the two solute bands.

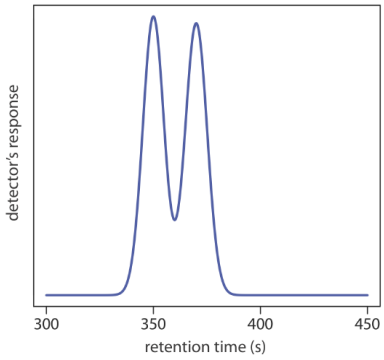

Figure 12.8.2 . Chromatogram for Problem 4.

5. The chromatogram in Problem 4 was obtained on a 2-m column with a column dead time of 50 s. Suppose you want to increase the resolution between the two components to 1.5. Without changing the height of a theoretical plate, what length column do you need? What height of a theoretical plate do you need to achieve a resolution of 1.5 without increasing the column's length?

6. Complete the following table.

N_B	α	k_B	R

N_B	α	k_B	R
100000	1.05	0.50	
10000	1.10		1.50
10000		4.0	1.00
	1.05	3.0	1.75

7. Moody studied the efficiency of a GC separation of 2-butanone on a dinonyl phthalate packed column [Moody, H. W. *J. Chem. Educ.* **1982**, *59*, 218–219]. Evaluating plate height as a function of flow rate gave a van Deemter equation for which A is 1.65 mm, B is 25.8 mm•mL min^{-1}, and C is 0.0236 mm•min mL^{-1}.

(a) Prepare a graph of H versus u for flow rates between 5 –120 mL/min.

(b) For what range of flow rates does each term in the Van Deemter equation have the greatest effect?

(c) What is the optimum flow rate and the corresponding height of a theoretical plate?

(d) For open-tubular columns the A term no longer is needed. If the B and C terms remain unchanged, what is the optimum flow rate and the corresponding height of a theoretical plate?

(e) Compared to the packed column, how many more theoretical plates are in the open-tubular column?

8. Hsieh and Jorgenson prepared 12–33 μm inner diameter HPLC columns packed with 5.44-μm spherical stationary phase particles [Hsieh, S.; Jorgenson, J. W. *Anal. Chem.* **1996**, *68*, 1212–1217]. To evaluate these columns they measured reduced plate height, h, as a function of reduced flow rate, v,

$$b = \frac{H}{d_p} \quad v = \frac{u d_p}{D_m}$$

where d_p is the particle diameter and D_m is the solute's diffusion coefficient in the mobile phase. The data were analyzed using van Deemter plots. The following table contains a portion of their results for norepinephrine.

internal diameter (μm)	A	B	C
33	0.63	1.32	0.10
33	0.67	1.30	0.08
23	0.40	1.34	0.09
23	0.58	1.11	0.09
17	0.31	1.47	0.11
17	0.40	1.41	0.11
12	0.22	1.53	0.11
12	0.19	1.27	0.12

(a) Construct separate van Deemter plots using the data in the first row and in the last row for reduced flow rates in the range 0.7–15. Determine the optimum flow rate and plate height for each case given d_p = 5.44 μm and $D_m = 6.23 \times 10^{-6}$ cm^2 s^{-1}.

(b) The A term in the van Deemter equation is strongly correlated with the column's inner diameter, with smaller diameter columns providing smaller values of A. Offer an explanation for this observation. *Hint: consider how many particles can fit across a capillary of each diameter.*

> When comparing columns, chromatographers often use dimensionless, reduced parameters. By including particle size and the solute's diffusion coefficient, the reduced plate height and reduced flow rate correct for differences between the packing material, the solute, and the mobile phase.

9. A mixture of *n*-heptane, tetrahydrofuran, 2-butanone, and *n*-propanol elutes in this order when using a polar stationary phase such as Carbowax. The elution order is exactly the opposite when using a nonpolar stationary phase such as polydimethyl siloxane. Explain the order of elution in each case.

10. The analysis of trihalomethanes in drinking water is described in Representative Method 12.4.1. A single standard that contains all four trihalomethanes gives the following results.

compound	concentration (ppb)	peak area
$CHCl_3$	1.30	1.35×10^4
$CHCl_2Br$	0.90	6.12×10^4
$CHClBr_2$	4.00	1.71×10^4
$CHBr_3$	1.20	1.52×10^4

Analysis of water collected from a drinking fountain gives areas of 1.56×10^4, 5.13×10^4, 1.49×10^4, and 1.76×10^4 for, respectively, $CHCl_3$, $CHCl_2Br$, $CHClBr_2$, and $CHBr_3$. All peak areas were corrected for variations in injection volumes using an internal standard of 1,2-dibromopentane. Determine the concentration of each of the trihalomethanes in the sample of water.

11. Zhou and colleagues determined the %w/w H_2O in methanol by capillary column GC using a polar stationary phase and a thermal conductivity detector [Zhou, X.; Hines, P. A.; White, K. C.; Borer, M. W. *Anal. Chem.* **1998**, *70*, 390–394]. A series of calibration standards gave the following results.

%w/w H_2O	peak height (arb. units)
0.00	1.15
0.0145	2.74
0.0472	6.33
0.0951	11.58
0.1757	20.43
0.2901	32.97

(a) What is the %w/w H_2O in a sample that has a peak height of 8.63?

(b) The %w/w H_2O in a freeze-dried antibiotic is determined in the following manner. A 0.175-g sample is placed in a vial along with 4.489 g of methanol. Water in the vial extracts into the methanol. Analysis of the sample gave a peak height of 13.66. What is the %w/w H_2O in the antibiotic?

12. Loconto and co-workers describe a method for determining trace levels of water in soil [Loconto, P. R.; Pan, Y. L.; Voice, T. C. *LC•GC* **1996**, *14*, 128–132]. The method takes advantage of the reaction of water with calcium carbide, CaC_2, to produce acetylene gas, C_2H_2. By carrying out the reaction in a sealed vial, the amount of acetylene produced is determined by sampling the headspace. In a typical analysis a sample of soil is placed in a sealed vial with CaC_2. Analysis of the headspace gives a blank corrected signal of 2.70×10^5. A second sample is prepared in the same manner except that a standard addition of 5.0 mg H_2O/g soil is added, giving a blank-corrected signal of 1.06×10^6. Determine the milligrams H_2O/g soil in the soil sample.

13. Van Atta and Van Atta used gas chromatography to determine the %v/v methyl salicylate in rubbing alcohol [Van Atta, R. E.; Van Atta, R. L. *J. Chem. Educ.* **1980**, *57*, 230–231]. A set of standard additions was prepared by transferring 20.00 mL of rubbing alcohol to separate 25-mL volumetric flasks and pipeting 0.00 mL, 0.20 mL, and 0.50 mL of methyl salicylate to the flasks. All three flasks were diluted to volume using isopropanol. Analysis of the three samples gave peak heights for methyl salicylate of 57.00 mm, 88.5 mm, and 132.5 mm, respectively. Determine the %v/v methyl salicylate in the rubbing alcohol.

14. The amount of camphor in an analgesic ointment is determined by GC using the method of internal standards [Pant, S. K.; Gupta, P. N.; Thomas, K. M.; Maitin, B. K.; Jain, C. L. *LC•GC* **1990**, *8*, 322–325]. A standard sample is prepared by placing 45.2 mg of camphor and 2.00 mL of a 6.00 mg/mL internal standard solution of terpene hydrate in a 25-mL volumetric flask and diluting to volume with CCl_4. When an approximately 2-µL sample of the standard is injected, the FID signals for the two

components are measured (in arbitrary units) as 67.3 for camphor and 19.8 for terpene hydrate. A 53.6-mg sample of an analgesic ointment is prepared for analysis by placing it in a 50-mL Erlenmeyer flask along with 10 mL of CCl_4. After heating to 50°C in a water bath, the sample is cooled to below room temperature and filtered. The residue is washed with two 5-mL portions of CCl_4 and the combined filtrates are collected in a 25-mL volumetric flask. After adding 2.00 mL of the internal standard solution, the contents of the flask are diluted to volume with CCl_4. Analysis of an approximately 2-µL sample gives FID signals of 13.5 for the terpene hydrate and 24.9 for the camphor. Report the %w/w camphor in the analgesic ointment.

15. The concentration of pesticide residues on agricultural products, such as oranges, is determined by GC-MS [Feigel, C. *Varian GC/MS Application Note*, Number 52]. Pesticide residues are extracted from the sample using methylene chloride and concentrated by evaporating the methylene chloride to a smaller volume. Calibration is accomplished using anthracene-d_{10} as an internal standard. In a study to determine the parts per billion heptachlor epoxide on oranges, a 50.0-g sample of orange rinds is chopped and extracted with 50.00 mL of methylene chloride. After removing any insoluble material by filtration, the methylene chloride is reduced in volume, spiked with a known amount of the internal standard and diluted to 10 mL in a volumetric flask. Analysis of the sample gives a peak–area ratio ($A_{analyte}/A_{intstd}$) of 0.108. A series of calibration standards, each containing the same amount of anthracene-d_{10} as the sample, gives the following results.

ppb heptachlor epoxide	$A_{analyte}/A_{intstd}$
20.0	0.065
60.0	0.153
200.0	0.637
500.0	1.554
1000.0	3.198

Report the nanograms per gram of heptachlor epoxide residue on the oranges.

16. The adjusted retention times for octane, toluene, and nonane on a particular GC column are 15.98 min, 17.73 min, and 20.42 min, respectively. What is the retention index for each compound?

17. The following data were collected for a series of normal alkanes using a stationary phase of Carbowax 20M.

alkane	t'_r (min)
pentane	0.79
hexane	1.99
heptane	4.47
octane	14.12
nonane	33.11

What is the retention index for a compound whose adjusted retention time is 9.36 min?

18. The following data were reported for the gas chromatographic analysis of *p*-xylene and methylisobutylketone (MIBK) on a capillary column [Marriott, P. J.; Carpenter, P. D. *J. Chem. Educ.* **1996**, *73*, 96–99].

injection mode	compound	t_r (min)	peak area (arb. units)	peak width (min)
split	MIBK	1.878	54285	0.028
	p-xylene	5.234	123483	0.044
splitless	MIBK	3.420	2493005	1.057
	p-xylene	5.795	3396656	1.051

Explain the difference in the retention times, the peak areas, and the peak widths when switching from a split injection to a splitless injection.

19. Otto and Wegscheider report the following retention factors for the reversed-phase separation of 2-aminobenzoic acid on a C_{18} column when using 10% v/v methanol as a mobile phase [Otto, M.; Wegscheider, W. *J. Chromatog.* **1983**, *258*, 11–22].

pH	k
2.0	10.5
3.0	16.7
4.0	15.8
5.0	8.0
6.0	2.2
7.0	1.8

Explain the effect of pH on the retention factor for 2-aminobenzene.

20. Haddad and associates report the following retention factors for the reversed-phase separation of salicylamide and caffeine [Haddad, P.; Hutchins, S.; Tuffy, M. *J. Chem. Educ.* **1983**, *60*, 166-168].

%v/v methanol	30%	35%	40%	45%	50%	55%
k_{sal}	2.4	1.6	1.6	1.0	0.7	0.7
k_{caff}	4.3	2.8	2.3	1.4	1.1	0.9

(a) Explain the trends in the retention factors for these compounds.

(b) What is the advantage of using a mobile phase with a smaller %v/v methanol? Are there any disadvantages?

21. Suppose you need to separate a mixture of benzoic acid, aspartame, and caffeine in a diet soda. The following information is available.

	t_r in aqueous mobile phase of pH			
compound	3.0	3.5	4.0	4.5
benzoic acid	7.4	7.0	6.9	4.4
aspartame	5.9	6.0	7.1	8.1
caffeine	3.6	3.7	4.1	4.4

(a) Explain the change in each compound's retention time.

(b) Prepare a single graph that shows retention time versus pH for each compound. Using your plot, identify a pH level that will yield an acceptable separation.

22. The composition of a multivitamin tablet is determined using an HPLC with a diode array UV/Vis detector. A 5-µL standard sample that contains 170 ppm vitamin C, 130 ppm niacin, 120 ppm niacinamide, 150 ppm pyridoxine, 60 ppm thiamine, 15 ppm folic acid, and 10 ppm riboflavin is injected into the HPLC, giving signals (in arbitrary units) of, respectively, 0.22, 1.35, 0.90, 1.37, 0.82, 0.36, and 0.29. The multivitamin tablet is prepared for analysis by grinding into a powder and transferring to a 125-mL Erlenmeyer flask that contains 10 mL of 1% v/v NH_3 in dimethyl sulfoxide. After sonicating in an ultrasonic bath for 2 min, 90 mL of 2% acetic acid is added and the mixture is stirred for 1 min and sonicated at 40°C for 5 min. The extract is then filtered through a 0.45-µm membrane filter. Injection of a 5-µL sample into the HPLC gives signals of 0.87 for vitamin C, 0.00 for niacin, 1.40 for niacinamide, 0.22 for pyridoxine, 0.19 for thiamine, 0.11 for folic acid, and 0.44 for riboflavin. Report the milligrams of each vitamin present in the tablet.

23. The amount of caffeine in an analgesic tablet was determined by HPLC using a normal calibration curve. Standard solutions of caffeine were prepared and analyzed using a 10-μL fixed-volume injection loop. Results for the standards are summarized in the following table.

concentration (ppm)	signal (arb. units)
50.0	8.354
100.0	16925
150.0	25218
200.0	33584
250.0	42002

The sample is prepared by placing a single analgesic tablet in a small beaker and adding 10 mL of methanol. After allowing the sample to dissolve, the contents of the beaker, including the insoluble binder, are quantitatively transferred to a 25-mL volumetric flask and diluted to volume with methanol. The sample is then filtered, and a 1.00-mL aliquot transferred to a 10-mL volumetric flask and diluted to volume with methanol. When analyzed by HPLC, the signal for caffeine is found to be 21 469. Report the milligrams of caffeine in the analgesic tablet.

24. Kagel and Farwell report a reversed-phase HPLC method for determining the concentration of acetylsalicylic acid (ASA) and caffeine (CAF) in analgesic tablets using salicylic acid (SA) as an internal standard [Kagel, R. A.; Farwell, S. O. *J. Chem. Educ.* **1983**, *60*, 163–166]. A series of standards was prepared by adding known amounts of ace- tylsalicylic acid and caffeine to 250-mL Erlenmeyer flasks and adding 100 mL of methanol. A 10.00-mL aliquot of a standard solution of salicylic acid was then added to each. The following results were obtained for a typical set of standard solutions.

	milligrams of		peak height ratios for	
standard	ASA	CAF	ASA/SA	CAF/SA
1	200.0	20.0	20.5	10.6
2	250.0	40.0	25.1	23.0
3	300.0	60.0	30.9	36.8

A sample of an analgesic tablet was placed in a 250-mL Erlenmeyer flask and dissolved in 100 mL of methanol. After adding a 10.00-mL portion of the internal standard, the solution was filtered. Analysis of the sample gave a peak height ratio of 23.2 for ASA and of 17.9 for CAF.

(a) Determine the milligrams of ASA and CAF in the tablet.

(b) Why is it necessary to filter the sample?

(c) The directions indicate that approximately 100 mL of methanol is used to dissolve the standards and samples. Why is it not necessary to measure this volume more precisely?

(d) In the presence of moisture, ASA decomposes to SA and acetic acid. What complication might this present for this analysis? How might you evaluate whether this is a problem?

25. Bohman and colleagues described a reversed-phase HPLC method for the quantitative analysis of vitamin A in food using the method of standard additions Bohman, O.; Engdahl, K. A.; Johnsson, H. *J. Chem. Educ.* **1982**, *59*, 251–252]. In a typical example, a 10.067-g sample of cereal is placed in a 250-mL Erlenmeyer flask along with 1 g of sodium ascorbate, 40 mL of ethanol, and 10 mL of 50% w/v KOH. After refluxing for 30 min, 60 mL of ethanol is added and the solution cooled to room temperature. Vitamin A is extracted using three 100-mL portions of hexane. The combined portions of hexane are evaporated and the residue containing vitamin A transferred to a 5-mL volumetric flask and diluted to volume with methanol. A standard addition is prepared in a similar manner using a 10.093-g sample of the cereal and spiking with 0.0200 mg of vitamin A. Injecting the sample and standard addition into the HPLC gives peak areas of, respectively, 6.77×10^3 and 1.32×10^4. Report the vitamin A content of the sample in milligrams/100 g cereal.

26. Ohta and Tanaka reported on an ion-exchange chromatographic method for the simultaneous analysis of several inorganic anions and the cations Mg^{2+} and Ca^{2+} in water [Ohta, K.; Tanaka, K. *Anal. Chim. Acta* **1998**, *373*, 189–195]. The mobile phase includes the ligand 1,2,4-benzenetricarboxylate, which absorbs strongly at 270 nm. Indirect detection of the analytes is possible because its absorbance decreases when complexed with an anion.

(a) The procedure also calls for adding the ligand EDTA to the mobile phase. What role does the EDTA play in this analysis?

(b) A standard solution of 1.0 mM $NaHCO_3$, 0.20 mM $NaNO_2$, 0.20 mM $MgSO_4$, 0.10 mM $CaCl_2$, and 0.10 mM $Ca(NO_3)_2$ gives the following peak areas (arbitrary units).

ion	HCO_3^-	Cl^-	NO_2^-	NO_3^-
peak area	373.5	322.5	264.8	262.7
ion	Ca^{2+}	Mg^{2+}	SO_4^{2-}	
peak area	458.9	352.0	341.3	

Analysis of a river water sample (pH of 7.49) gives the following results.

ion	HCO_3^-	Cl^-	NO_2^-	NO_3^-
peak area	310.0	403.1	3.97	157.6
ion	Ca^{2+}	Mg^{2+}	SO_4^{2-}	
peak area	734.3	193.6	324.3	

Determine the concentration of each ion in the sample.

(c) The detection of HCO_3^- actually gives the total concentration of carbonate in solution ($[CO_3^{2-}]+[HCO_3^-]+[H_2CO_3]$). Given that the pH of the water is 7.49, what is the actual concentration of HCO_3^-?

(d) An independent analysis gives the following additional concentrations for ions in the sample: $[Na^+]$ = 0.60 mM; $[NH_4^+]$ = 0.014 mM; and $[K^+]$ = 0.046 mM. A solution's ion balance is defined as the ratio of the total cation charge to the total anion charge. Determine the charge balance for this sample of water and comment on whether the result is reasonable.

27. The concentrations of Cl^-, NO_2^-, and SO_4^{2-} are determined by ion chromatography. A 50-µL standard sample of 10.0 ppm Cl^-, 2.00 ppm NO_2^-, and 5.00 ppm SO_4^{2-} gave signals (in arbitrary units) of 59.3, 16.1, and 6.08 respectively. A sample of effluent from a wastewater treatment plant is diluted tenfold and a 50-µL portion gives signals of 44.2 for Cl^-, 2.73 for NO_2^-, and 5.04 for SO_4^{2-}. Report the parts per million for each anion in the effluent sample.

28. A series of polyvinylpyridine standards of different molecular weight was analyzed by size-exclusion chromatography, yielding the following results.

formula weight	retention volume (mL)
600000	6.42
100000	7.98
30000	9.30
3000	10.94

When a preparation of polyvinylpyridine of unknown formula weight is analyzed, the retention volume is 8.45 mL. Report the average formula weight for the preparation.

29. Diet soft drinks contain appreciable quantities of aspartame, benzoic acid, and caffeine. What is the expected order of elution for these compounds in a capillary zone electrophoresis separation using a pH 9.4 buffer given that aspartame has pK_a values of 2.964 and 7.37, benzoic acid has a pK_a of 4.2, and the pK_a for caffeine is less than 0. Figure 12.8.3 provides the structures of these compounds.

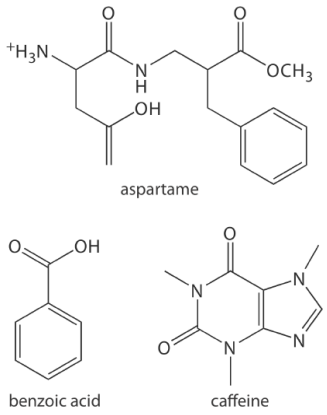

Figure 12.8.3

. Structures for the compounds in Problem 29.

30. Janusa and coworkers describe the determination of chloride by CZE [Janusa, M. A.; Andermann, L. J.; Kliebert, N. M.; Nannie, M. H. *J. Chem. Educ.* **1998**, *75*, 1463–1465]. Analysis of a series of external standards gives the following calibration curve.

$$\text{area} = -883 + 5590 \times \text{ppm } Cl^-$$

A standard sample of 57.22% w/w Cl^- is analyzed by placing 0.1011-g portions in separate 100-mL volumetric flasks and diluting to volume. Three unknowns are prepared by pipeting 0.250 mL, 0.500 mL, an 0.750 mL of the bulk unknown in separate 50-mL volumetric flasks and diluting to volume. Analysis of the three unknowns gives areas of 15 310, 31 546, and 47 582, respectively. Evaluate the accuracy of this analysis.

31. The analysis of NO_3^- in aquarium water is carried out by CZE using IO_4^- as an internal standard. A standard solution of 15.0 ppm NO_3^- and 10.0 ppm IO_4^- gives peak heights (arbitrary units) of 95.0 and 100.1, respectively. A sample of water from an aquarium is diluted 1:100 and sufficient internal standard added to make its concentration 10.0 ppm in IO_4^-. Analysis gives signals of 29.2 and 105.8 for NO_3^- and IO_4^-, respectively. Report the ppm NO_3^- in the sample of aquarium water.

32. Suggest conditions to separate a mixture of 2-aminobenzoic acid (pK_{a1} = 2.08, pK_{a2} = 4.96), benzylamine (pK_a = 9.35), and 4-methylphenol (pK_{a2} = 10.26) by capillary zone electrophoresis. Figure $PageIndex4$ provides the structures of these compounds.

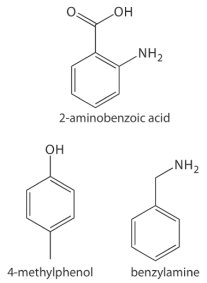

Figure 12.8.4 . Structures for the compounds in Problem 32.

33. McKillop and associates examined the electrophoretic separation of some alkylpyridines by CZE [McKillop, A. G.; Smith, R. M.; Rowe, R. C.; Wren, S. A. C. *Anal. Chem.* **1999**, *71*, 497–503]. Separations were carried out using either 50-µm or 75-µm inner diameter capillaries, with a total length of 57 cm and a length of 50 cm from the point of injection to the detector. The run buffer was a pH 2.5 lithium phosphate buffer. Separations were achieved using an applied voltage of 15 kV. The electroosmotic mobility, μ_{eof}, as measured using a neutral marker, was found to be 6.398×10^{-5} cm^2 V^{-1} s^{-1}. The diffusion coefficient for alkylpyridines is 1.0×10^{-5} cm^2 s^{-1}.

(a) Calculate the electrophoretic mobility for 2-ethylpyridine given that its elution time is 8.20 min.

(b) How many theoretical plates are there for 2-ethylpyridine?

(c) The electrophoretic mobilities for 3-ethylpyridine and 4-ethylpyridine are 3.366×10^{-4} cm^2 V^{-1} s^{-1} and 3.397×10^{-4} cm^2 V^{-1} s^{-1}, respectively. What is the expected resolution between these two alkylpyridines?

(d) Explain the trends in electrophoretic mobility shown in the following table.

alkylpyridine	μ_{ep} ($cm^2\ V^{-1}\ s^{-1}$)
2-methylpyridine	3.581×10^{-4}
2-ethylpyridine	3.222×10^{-4}
2-propylpyridine	2.923×10^{-4}
2-pentylpyridine	2.534×10^{-4}
2-hexylpyridine	2.391×10^{-4}

(e) Explain the trends in electrophoretic mobility shown in the following table.

alkylpyridine	μ_{ep} ($cm^2\ V^{-1}\ s^{-1}$)
2-ethylpyridine	3.222×10^{-4}
3-ethylpyridine	3.366×10^{-4}
4-ethylpyridine	3.397×10^{-4}

(f) The pK_a for pyridine is 5.229. At a pH of 2.5 the electrophoretic mobility of pyridine is 4.176×10^{-4} $cm^2\ V^{-1}\ s^{-1}$. What is the expected electrophoretic mobility if the run buffer's pH is 7.5?

3.9: Additional Resources

The following set of experiments introduce students to the applications of chromatography and electrophoresis. Experiments are grouped into five categories: gas chromatography, high-performance liquid chromatography, ion-exchange chromatography, size-exclusion chromatography, and electrophoresis.

Gas Chromatography

- Bishop, R. D., Jr. "Using GC–MS to Determine Relative Reactivity Ratios," *J. Chem. Educ.* **1995**, *72*, 743–745.
- Elderd, D. M.; Kildahl, N. K.; Berka, L. H. "Experiments for Modern Introductory Chemistry: Identification of Arson Accelerants by Gas Chromatography," *J. Chem. Educ.* **1996**, *73*, 675–677.
- Fleurat-Lessard, P.; Pointet, K.; Renou-Gonnord, M.-F. "Quantitative Determination of PAHs in Diesel Engine Exhausts by GC–MS," *J. Chem. Educ.* **1999**, *76*, 962–965.
- Galipo, R. C.; Canhoto, A. J.; Walla, M. D.; Morgan, S. L. "Analysis of Volatile Fragrance and Flavor Compounds by Headspace Solid Phase Microextraction and GC–MS," *J. Chem. Educ.* **1999**, *76*, 245–248.
- Graham, R. C.; Robertson, J. K. "Analysis of Trihalomethanes in Soft Drinks," *J. Chem. Educ.* **1988**, *65*, 735–737.
- Heinzen, H.; Moyan, P.; Grompone, A. "Gas Chromatographic Determination of Fatty Acid Compositions," *J. Chem. Educ.* **1985**, *62*, 449–450.
- Kegley, S. E.; Hansen, K. J.; Cunningham, K. L. "Determination of Polychlorinated Biphenyls (PCBs) in River and Bay Sediments," *J. Chem. Educ.* **1996**, *73*, 558–562.
- Kostecka, K. S.; Rabah, A.; Palmer, C. F., Jr. "GC/MS Analysis of the Aromatic Composition of Gasoline," *J. Chem. Educ.* **1995**, *72*, 853–854.
- Quach, D. T.; Ciszkowski, N. A.; Finlayson-Pitts, B. J. "A New GC-MS Experiment for the Undergraduate Instrumental Analysis Laboratory in Environmental Chemistry: Methyl-t-butyl Ether and Benzene in Gasoline," *J. Chem. Educ.* **1998**, *75*, 1595–1598.
- Ramachandran, B. R.; Allen, J. M.; Halpern, A. M. "Air–Water Partitioning of Environmentally Important Organic Compounds," *J. Chem. Educ.* **1996**, *73*, 1058–1061.
- Rice, G. W. "Determination of Impurities in Whiskey Using Internal Standard Techniques," *J. Chem. Educ.* **1987**, *64*, 1055–1056.
- Rubinson, J. F.; Neyer-Hilvert, J. "Integration of GC-MS Instrumentation into the Undergraduate Laboratory: Separation and Identification of Fatty Acids in Commercial Fats and Oils," *J. Chem. Educ.* **1997**, *74*, 1106–1108.
- Rudzinski, W. E.; Beu, S. "Gas Chromatographic Determination of Environmentally Significant Pesticides," *J. Chem. Educ.* **1982**, *59*, 614–615.
- Sobel, R. M.; Ballantine, D. S.; Ryzhov, V. "Quantitation of Phenol Levels in Oil of Wintergreen Using Gas Chromatography–Mass Spectrometry with Selected Ion Monitoring," *J. Chem. Educ.* **2005**, *82*, 601–603.
- Welch, W. C.; Greco, T. G. "An Experiment in Manual Multiple Headspace Extraction for Gas Chromatography," *J. Chem. Educ.* **1993**, *70*, 333–335.
- Williams, K. R.; Pierce, R. E. "The Analysis of Orange Oil and the Aqueous Solubility of d-Limone," *J. Chem. Educ.* **1998**, *75*, 223–226.
- Wong, J. W.; Ngim, K. K.; Shibamoto, T.; Mabury, S. A.; Eiserich, J. P.; Yeo, H. C. H. "Determination of Formaldehyde in Cigarette Smoke," *J. Chem. Educ.* **1997**, *74*, 1100–1103.
- Yang, M. J.; Orton, M. L., Pawliszyn, J. "Quantitative Determination of Caffeine in Beverages Using a Combined SPME-GC/MS Method," *J. Chem. Educ.* **1997**, *74*, 1130–1132.

High-Performance Liquid Chromatography

- Batchelor, J. D.; Jones, B. T. "Determination of the Scoville Heat Value for Hot Sauces and Chilies: An HPLC Experiment," *J. Chem. Educ.* **2000**, *77*, 266–267.
- Beckers, J. L. "The Determination of Caffeine in Coffee: Sense or Nonsense?" *J. Chem. Educ.* **2004**, *81*, 90–93.
- Betts, T. A. "Pungency Quantitation of Hot Pepper Sauces Using HPLC," *J. Chem. Educ.* **1999**, *76*, 240–244.
- Bidlingmeyer, B. A.; Schmitz, S. "The Analysis of Artificial Sweeteners and Additives in Beverages by HPLC," *J. Chem. Educ.* **1991**, *68*, A195–A200.
- Bohman, O.; Engdahl, K.-A.; Johnsson, H. "High Performance Liquid Chromatography of Vitamin A: A Quantitative Determination," *J. Chem. Educ.* **1982**, *59*, 251–252.

- Brenneman, C. A.; Ebeler, S. E. “Chromatographic Separations Using Solid-Phase Extraction Cartridges: Separation of Wine Phenolics,” *J. Chem. Educ.* **1999**, *76*, 1710–1711.
- Cantwell, F. F.; Brown, D. W. “Liquid Chromatographic Determination of Nitroanilines,” *J. Chem. Educ.* **1981**, *58*, 820–823.
- DiNunzio, J. E. “Determination of Caffeine in Beverages by High Performance Liquid Chromatography,” *J. Chem. Educ.* **1985**, *62*, 446–447.
- Ferguson, G. K. “Quantitative HPLC Analysis of an Analgesic/Caffeine Formulation: Determination of Caffeine,” *J. Chem. Educ.* **1998**, *75*, 467–469.
- Ferguson, G. K. “Quantitative HPLC Analysis of a Psychotherapeutic Medication: Simultaneous Determination of Amitriptyline Hydrochloride and Perphenazine,” *J. Chem. Educ.* **1998**, *75*, 1615–1618.
- Goodney, D. E. “Analysis of Vitamin C by High-Pressure Liquid Chromatography,” *J. Chem. Educ.* **1987**, *64*, 187–188.
- Guevremont, R.; Quigley, M. N. “Determination of Paralytic Shellfish Poisons Using Liquid Chromatography,” *J. Chem. Educ.* **1994**, *71*, 80–81.
- Haddad, P.; Hutchins, S.; Tuffy, M. “High Performance Liquid Chromatography of Some Analgesic Compounds,” *J. Chem. Educ.* **1983**, *60*, 166–168.
- Huang, J.; Mabury, S. A.; Sagebiel, J. C. “Hot Chili Peppers: Extraction, Cleanup, and Measurement of Capscaicin,” *J. Chem. Educ.* **2000**, *77*, 1630–1631.
- Joeseph, S. M.; Palasota, J. A. “The Combined Effect of pH and Percent Methanol on the HPLC Separation of Benzoic Acid and Phenol,” *J. Chem. Educ.* **2001**, *78*, 1381–1383.
- Lehame, S. “The Separation of Copper, Iron, and Cobalt Tetramethylene Dithiocarbamates by HPLC,” *J. Chem. Educ.* **1986**, *63*, 727–728.
- Luo, P.; Luo, M. Z.; Baldwin, R. P. “Determination of Sugars in Food Products,” *J. Chem. Educ.* **1993**, *70*, 679–681.
- Mueller, B. L.; Potts, L. W. “HPLC Analysis of an Asthma Medication,” *J. Chem. Educ.* **1988**, *65*, 905–906.
- Munari, M.; Miurin, M.; Goi, G. “Didactic Application to Riboflavin HPLC Analysis,” *J. Chem. Educ.* **1991**, *68*, 78–79.
- Orth, D. L. “HPLC Determination of Taurine in Sports Drinks,” *J. Chem. Educ.* **2001**, *78*, 791– 792.
- Remcho, V. T.; McNair, H. M.; Rasmussen, H. T. “HPLC Method Development with the Photodiode Array Detector,” *J. Chem. Educ.* **1992**, *69*, A117–A119.
- Richardson, W. W., III; Burns, L. “HPLC of the Polypeptides in a Hydrolyzate of Egg-White Lysozyme,” *J. Chem. Educ.* **1988**, *65*, 162–163.
- Silveira, A., Jr.; Koehler, J. A.; Beadel, E. F., Jr.; Monore, P. A. “HPLC Analysis of Chlorophyll a, Chlorophyll b, and β-Carotene in Collard Greens,” *J. Chem. Educ.* **1984**, *61*, 264–265.
- Siturmorang, M.; Lee, M. T. B.; Witzeman, L. K.; Heineman, W. R. “Liquid Chromatography with Electrochemical Detection (LC-EC): An Experiment Using 4-Aminophenol,” *J. Chem. Educ.* **1998**, *75*, 1035–1038.
- Sottofattori, E.; Raggio, R.; Bruno, O. “Milk as a Drug Analysis Medium: HPLC Determination of Isoniazid,” *J. Chem. Educ.* **2003**, *80*, 547–549.
- Strohl, A. N. “A Study of Colas: An HPLC Experiment,” *J. Chem. Educ.* **1985**, *62*, 447–448.
- Tran, C. D.; Dotlich, M. “Enantiomeric Separation of Beta-Blockers by High Performance Liquid Chromatography,” *J. Chem. Educ.* **1995**, *72*, 71–73.
- Van Arman, S. A.; Thomsen, M. W. “HPLC for Undergraduate Introductory Laboratories,” *J. Chem. Educ.* **1997**, *74*, 49–50.
- Wingen, L. M.; Low, J. C.; Finlayson-Pitts, B. J. “Chromatography, Absorption, and Fluorescence: A New Instrumental Analysis Experiment on the Measurement of Polycyclic Aromatic Hydrocarbons in Cigarette Smoke,” *J. Chem. Educ.* **1998**, *75*, 1599–1603.

Ion-Exchange Chromatography

- Bello, M. A.; Gustavo González, A. “Determination of Phosphate in Cola Beverages Using Nonsuppressed Ion Chromatography,” *J. Chem. Educ.* **1996**, *73*, 1174–1176.
- Kieber, R. J.; Jones, S. B. “An Undergraduate Laboratory for the Determination of Sodium, Potassium, and Chloride,” *J. Chem. Educ.* **1994**, *71*, A218–A222.
- Koubek, E.; Stewart, A. E. “The Analysis of Sulfur in Coal,” *J. Chem. Educ.* **1992**, *69*, A146–A148.
- Sinniah, K.; Piers, K. “Ion Chromatography: Analysis of Ions in Pond Water,” *J. Chem. Educ.* **2001**, *78*, 358–362.
- Xia, K.; Pierzynski, G. “Competitive Sorption between Oxalate and Phosphate in Soil: An Environmental Chemistry Laboratory Using Ion Chromatography,” *J. Chem. Educ.* **2003**, *80*, 71–75.

Size-Exchange Chromatography

- Brunauer, L. S.; Davis, K. K. “Size Exclusion Chromatography: An Experiment for High School and Community College Chemistry and Biotechnology Laboratory Programs,” *J. Chem. Educ.* **2008**, *85*, 683–685.
- Saiz, E.; Tarazona, M. P. “Size-Exclusion Chromatography Using Dual Detection,” *Chem. Educator* **2000**, *5*, 324–328.

Electrophoresis

- Almarez, R. T.; Kochis, M. “Microscale Capillary Electrophoresis: A Complete Instrumentation Experiment for Chemistry Students at the Undergraduate Junior or Senior Level,” *J. Chem. Educ.* **2003**, *80*, 316–319.
- Beckers, J. L. “The Determination of Caffeine in Coffee: Sense or Nonsense?” *J. Chem. Educ.* **2004**, *81*, 90–93.
- Beckers, J. L. “The Determination of Vanillin in a Vanilla Extract,” *J. Chem. Educ.* **2005**, *82*, 604– 606.
- Boyce, M. “Separation and Quantification of Simple Ions by Capillary Zone Electrophoresis,” *J. Chem. Educ.* **1999**, *76*, 815–819.
- Conradi, S.; Vogt, C.; Rohde, E. “Separation of Enatiomeric Barbiturates by Capillary Electrophoresis Using a Cyclodextrin-Containing Run Buffer,” *J. Chem. Educ.* **1997**, *74*, 1122–1125.
- Conte, E. D.; Barry, E. F.; Rubinstein, H. “Determination of Caffeine in Beverages by Capillary Zone Electrophoresis,” *J. Chem. Educ.* **1996**, *73*, 1169–1170.
- Demay, S.; Martin-Girardeau, A.; Gonnord, M.-F. “Capillary Electrophoretic Quantitative Analysis of Anions in Drinking Water,” *J. Chem. Educ.* **1999**, *76*, 812–815.
- Emry, R.; Cutright, R. D.; Wright, J.; Markwell, J. “Candies to Dye for: Cooperative, Open-Ended Student Activities to Promote Understanding of Electrophoretic Fractionation,” *J. Chem. Educ.* **2000**, *77*, 1323–1324.
- Gardner, W. P.; Girard, J. E. “Analysis of Common Household Cleaner-Disinfectants by Capillary Electrophoresis,” *J. Chem. Educ.* **2000**, *77*, 1335–1338.
- Gruenhagen, J. A.; Delaware, D.; Ma, Y. “Quantitative Analysis of Non-UV-Absorbing Cations in Soil Samples by High-Performance Capillary Electrophoresis,” *J. Chem. Educ.* **2000**, *77*, 1613–1616.
- Hage, D. S.; Chattopadhyay, A.; Wolfe, C. A. C.; Grundman, J.; Kelter, P. B. “Determination of Nitrate and Nitrite in Water by Capillary Electrophoresis,” *J. Chem. Educ.* **1998**, *75*, 1588–1590.
- Herman, H. B.; Jezorek, J. R.; Tang, Z. “Analysis of Diet Tonic Water Using Capillary Electrophoresis,” *J. Chem. Educ.* **2000**, *77*, 743–744.
- Janusa, M. A.; Andermann, L. J.; Kliebert, N. M.; Nannie, M. H. “Determination of Chloride Concentration Using Capillary Electrophoresis,” *J. Chem. Educ.* **1998**, *75*, 1463–1465.
- McDevitt, V. L.; Rodríguez, A.; Williams, K. R. “Analysis of Soft Drinks: UV Spectrophotometry, Liquid Chromatography, and Capillary Electrophoresis,” *J. Chem. Educ.* **1998**, *75*, 625–629.
- Palmer, C. P. “Demonstrating Chemical and Analytical Concepts in the Undergraduate Laboratory Using Capillary Electrophoresis and Micellar Electrokinetic Chromatography,” *J. Chem. Educ.* **1999**, *76*, 1542–1543.
- Pursell, C. J.; Chandler, B.; Bushey, M. M. “Capillary Electrophoresis Analysis of Cations in Water Samples,” *J. Chem. Educ.* **2004**, *81*, 1783–1786.
- Solow, M. “Weak Acid p*K*a Determination Using Capillary Zone Electrophoresis,” *J. Chem. Educ.* **2006**, *83*, 1194–1195.
- Thompson, L.; Veening, H.; Strain, T. G. “Capillary Electrophoresis in the Undergraduate Instrumental Analysis Laboratory: Determination of Common Analgesic Formulations,” *J. Chem. Educ.* **1997**, *74*, 1117–1121.
- Vogt, C.; Conradi, S.; Rhode, E. “Determination of Caffeine and Other Purine Compounds in Food and Pharmaceuticals by Micellar Electrokinetic Chromatography” *J. Chem. Educ.* **1997**, *74*, 1126– 1130.
- Weber, P. L.; Buck, D. R. “Capillary Electrophoresis: A Fast and Simple Method for the Determination of the Amino Acid Composition of Proteins,” *J. Chem. Educ.* **1994**, *71*, 609–612.
- Welder, F.; Colyer, C. L. “Using Capillary Electrophoresis to Determine the Purity of Acetylsalicylic Acid Synthesized in the Undergraduate Laboratory,” *J. Chem. Educ.* **2001**, *78*, 1525–1527.
- Williams, K. R.; Adhyaru, B.; German, I.; Russell, T. “Determination of a Diffusion Coefficient by Capillary Electrophoresis,” *J. Chem. Educ.* **2002**, *79*, 1475–1476.

The following texts provide a good introduction to the broad field of separations, including chromatography and electrophoresis.

- Giddings, J. C. *Unified Separation Science*, Wiley-Interscience: New York 1991.
- Karger, B. L.; Snyder, L. R.; Harvath, C. *An Introduction to Separation Science*, Wiley-Interscience: New York, 1973
- Miller, J. M. *Separation Methods in Chemical Analysis*, Wiley-Interscience: New York, 1975.
- Poole, C. F. *The Essence of Chromatography*, Elsevier: Amsterdam, 2003.

A more recent discussion of peak capacity is presented in the following papers.

- Chester, T. L. “Further Considerations of Exact Equations for Peak Capacity in Isocratic Liquid Chromatography,” *Anal. Chem.* **2014**, *86*, 7239–7241.
- Davis, J. M.; Stoll, D. R.; Carr, P. W. “Dependence of Effective Peak Capacity in Comprehensive Two-Dimensional Separations on the Distribution of Peak Capacity between the Two Dimensions,” *Anal. Chem.* **2008**, *80*, 8122–8134.
- Li, X.; Stoll, D. R.; Carr, P. W. “Equation for Peak Capacity Estimation in Two-Dimensional Liquid Chromatography,” *Anal. Chem.* **2009**, *81*, 845–850.
- Shen, Y.; Lee, M. “General Equation for Peak Capacity in Column Chromatography,” *Anal. Chem*. **1998**, *70*, 3853–3856.

The following references may be consulted for more information on gas chromatography.

- Grob, R. L., ed, *Modern Practice of Gas Chromatography*, Wiley-Interscience: New York, 1972.
- Hinshaw, J. V. “A Compendium of GC Terms and Techniques,” *LC•GC* **1992**, *10*, 516–522.
- Ioffe, B. V.; Vitenberg, A. G. *Head-Space Analysis and Related Methods in Gas Chromatography*, Wiley-Interscience: New York, 1982.
- Kitson, F. G.; Larsen, B. S.; McEwen, C. N. *Gas Chromatography and Mass Spectrometry: A Practical Guide*, Academic Press: San Diego, 1996.
- McMaster, M. C. *GC/MS: A Practical User’s Guide*, Wiley-Interscience: Hoboken, NJ, 2008.

The following references provide more information on high-performance liquid chromatography.

- Dorschel, C. A.; Ekmanis, J. L.; Oberholtzer, J. E.; Warren, Jr. F. V.; Bidlingmeyer, B. A. “LC Detectors,” *Anal. Chem.* **1989**, *61*, 951A–968A.
- Ehlert, S.; Tallarek, U. “High-pressure liquid chromatography in lab-on-a-chip devices,” *Anal. Bioanal. Chem.* **2007**, *388*, 517–520.
- Francois, I.; Sandra, K.; Sandra, P. “Comprehensive liquid chromatography: Fundamental aspects and practical considerations—A review,” *Anal. Chim. Acta* **2009**, *641*, 14–31.
- Harris, C. M. “Shrinking the LC Landscape,” *Anal. Chem.* **2003**, *75*, 64A–69A.
- Meyer, V. R. *Pitfalls and Errors of HPLC in Pictures*, Wiley-VCH: Weinheim, Germany, 2006.
- Pozo, O. J.; Van Eenoo, P.; Deventer, K.; Delbeke, F. T. “Detection and characterization of anabolic steroids in doping analysis by LC–MS,” *Trends Anal. Chem.* **2008**, *27*, 657–671.
- Scott, R. P. W. “Modern Liquid Chromatography,” *Chem. Soc. Rev.* **1992**, *21*, 137–145.
- Simpson, C. F., ed. *Techniques in Liquid Chromatography*, Wiley-Hayden: Chichester, England; 1982.
- Snyder, L. R.; Glajch, J. L.; Kirkland, J. J. *Practical HPLC Method Development*, Wiley-Interscience: New York,1988.
- van de Merbel, N. C. “Quantitative determination of endogenous compounds in biological samples using chromatographic techniques,” *Trends Anal. Chem.* **2008**, *27*, 924–933.
- Yeung, E. S. “Chromatographic Detectors: Current Status and Future Prospects,” *LC•GC* **1989**, *7*, 118–128.

The following references may be consulted for more information on ion chromatography.

- Shpigun, O. A.; Zolotov, Y. A. *Ion Chromatography in Water Analysis*, Ellis Horwood: Chichester, England, 1988.
- Smith, F. C. Jr.; Chang, R. C. *The Practice of Ion Chromatography*, Wiley-Interscience: New York, 1983.

The following references may be consulted for more information on supercritical fluid chromatography.

- Palmieri, M. D. “An Introduction to Supercritical Fluid Chromatography. Part I: Principles and Applications,” *J. Chem. Educ.* **1988**, *65*, A254–A259.
- Palmieri, M. D. “An Introduction to Supercritical Fluid Chromatography. Part II: Applications and Future Trends,” *J. Chem. Educ*. **1989**, *66*, A141–A147.

The following references may be consulted for more information on capillary electrophoresis.

- Baker, D. R. *Capillary Electrophoresis*, Wiley-Interscience: New York, 1995.
- Copper, C. L. “Capillary Electrophoresis: Part I. Theoretical and Experimental Background,” *J. Chem. Educ*. **1998**, *75*, 343–347.
- Copper, C. L.; Whitaker, K. W. “Capillary Electrophoresis: Part II. Applications,” *J. Chem. Educ*. **1998**, *75*, 347–351.
- DeFrancesco, L. “Capillary Electrophoresis: Finding a Niche,” *Today’s Chemist at Work*, February 2002, 59–64.

- Ekins, R. P. “Immunoassay, DNA Analysis, and Other Ligand Binding Assay Techniques: From Electropherograms to Multiplexed, Ultrasensative Microarrays on a Chip,” *J. Chem. Educ.* **1999**, *76*, 769– 780.
- Revermann, T.; Götz, S.; Künnemeyer, J.; Karst, U. “Quantitative analysis by microchip capillary electrophoresis—current limitations and problem-solving strategies,” *Analyst* **2008**, *133*, 167–174.
- Timerbaev, A. R. “Capillary electrophoresis coupled to mass spectrometry for biospeciation analysis: critical evaluation,” *Trends Anal. Chem.* **2009**, *28*, 416–425.
- Unger, K. K.; Huber, M.; Hennessy, T. P.; Hearn, M. T. W.; Walhagen, K. “A Critical Appraisal of Capillary Electrochromatography,” *Anal. Chem.* **2002**, *74*, 200A–207A.
- Varenne, A.; Descroix, S. “Recent strategies to improve resolution in capillary electrophoresis—A review,” *Anal. Chim. Acta* **2008**, *628*, 9–23.
- Vetter, A. J.; McGowan, G. J. “The Escalator—An Analogy for Explaining Electroosmotic Flow,” J. Chem. Educ. 2001, 78, 209–211.
- Xu, Y. “Tutorial: Capillary Electrophoresis,” *Chem. Educator*, **1996**, *1(2)*, 1–14.

The application of spreadsheets and computer programs for modeling chromatography is described in the following papers.

- Abbay, G. N.; Barry, E. F.; Leepipatpiboon, S.; Ramstad, T.; Roman, M. C.; Siergiej, R. W.; Snyder, L. R.; Winniford, W. L. “Practical Applications of Computer Simulation for Gas Chromatography Method Development,” *LC•GC* **1991**, *9*, 100–114.
- Drouen, A.; Dolan, J. W.; Snyder, L. R.; Poile, A.; Schoenmakers, P. J. “Software for Chromatographic Method Development,” *LC•GC* **1991**, *9*, 714–724.
- Kevra, S. A.; Bergman, D. L.; Maloy, J. T. “A Computational Introduction to Chromatographic Bandshape Analysis,” *J. Chem. Educ.* **1994**, *71*, 1023–1028.
- Rittenhouse, R. C. “HPLC for Windows: A Computer Simulation of High-Performance Liquid Chromatography,” *J. Chem. Educ.* **1995**, *72*, 1086–1087.
- Shalliker, R. A.; Kayillo, S.; Dennis, G. R. “Optimizing Chromatographic Separations: An Experiment Using an HPLC Simulator,” *J. Chem. Educ.* **2008**, *85*, 1265–1268.
- Sundheim, B. R. “Column Operations: A Spreadsheet Model,” *J. Chem. Educ.* **1992**, *69*, 1003– 1005.

The following papers discuss column efficiency, peak shapes, and overlapping chromatographic peaks.

- Bildingmeyer, B. A.; Warren, F. V., Jr. “Column Efficiency Measurement,” *Anal. Chem.* **1984**, *56*, 1583A–1596A.
- Hawkes, S. J. “Distorted Chromatographic Peaks,” *J. Chem. Educ.* **1994**, *71*, 1032–1033.
- Hinshaw, J. “Pinning Down Tailing Peaks,” *LC•GC* **1992**, *10*, 516–522.
- Meyer, V. K. “Chromatographic Integration Errors: A Closer Look at a Small Peak,” *LC•GC North America* **2009**, *27*, 232–244.
- Reid, V. R.; Synovec, R. E. “High-speed gas chromatography: The importance of instrumentation optimization and the elimination of extra-column band broadening,” *Talanta* **2008**, *76*, 703–717.

3.10: Chapter Summary and Key Terms

Chapter Summary

Chromatography and electrophoresis are powerful analytical techniques that both separate a sample into its components and provide a means for determining each component's concentration. Chromatographic separations utilize the selective partitioning of the sample's components between a stationary phase that is immobilized within a column and a mobile phase that passes through the column.

The effectiveness of a chromatographic separation is described by the resolution between two chromatographic bands and is a function of each component's retention factor, the column's efficiency, and the column's selectivity. A solute's retention factor is a measure of its partitioning into the stationary phase, with larger retention factors corresponding to more strongly retained solutes. The column's selectivity for two solutes is the ratio of their retention factors, providing a relative measure of the column's ability to retain the two solutes. Column efficiency accounts for those factors that cause a solute's chromatographic band to increase in width during the separation. Column efficiency is defined in terms of the number of theoretical plates and the height of a theoretical plate, the later of which is a function of a number of parameters, most notably the mobile phase's flow rate. Chromatographic separations are optimized by increasing the number of theoretical plates, by increasing the column's selectivity, or by increasing the solute retention factor.

In gas chromatography the mobile phase is an inert gas and the stationary phase is a nonpolar or polar organic liquid that either is coated on a particulate material and packed into a wide-bore column, or coated on the walls of a narrow-bore capillary column. Gas chromatography is useful for the analysis of volatile components.

In high-performance liquid chromatography the mobile phase is either a nonpolar solvent (normal phase) or a polar solvent (reversed-phase). A stationary phase of opposite polarity, which is bonded to a particulate material, is packed into a wide-bore column. HPLC is applied to a wider range of samples than GC; however, the separation efficiency for HPLC is not as good as that for capillary GC.

Together, GC and HPLC account for the largest number of chromatographic separations. Other separation techniques, however, find special- ized applications: of particular importance are ion-exchange chromatography for separating anions and cations; size-exclusion chromatography for separating large molecules; and supercritical fluid chromatography for the analysis of samples that are not easily analyzed by GC or HPLC.

In capillary zone electrophoresis a sample's components are separated based on their ability to move through a conductive medium under the influence of an applied electric field. Positively charged solutes elute first, with smaller, more highly charged cations eluting before larger cations of lower charge. Neutral species elute without undergoing further separation. Finally, anions elute last, with smaller, more negatively charged anions being the last to elute. By adding a surfactant, neutral species can be separated by micellar electrokinetic capillary chromatography. Electrophoretic separations also can take advantage of the ability of polymeric gels to separate solutes by size (capillary gel electrophoresis), and the ability of solutes to partition into a stationary phase (capillary electrochromatography). In comparison to GC and HPLC, capillary electrophoresis provides faster and more efficient separations.

Key Terms

adjusted retention time	adsorption chromatography	band broadening
baseline width	bleed	bonded stationary phase
capillary column	capillary electrochromatography	capillary electrophoresis
capillary gel electrophoresis	capillary zone electrophoresis	chromatogram
chromatography	column chromatography	counter-current extraction
cryogenic focusing	electrokinetic injection	electroosmotic flow
electroosmotic flow velocity	electron capture detector	electropherogram
electrophoresis	electrophoretic mobility	electrophoretic velocity
exclusion limit	flame ionization detector	fronting
gas chromatography	gas–liquid chromatography	gas–solid chromatography
general elution problem	guard column	gradient elution
headspace sampling	high-performance liquid chromatography	hydrodynamic injection
inclusion limit	ion-exchange chromatography	ion suppressor column
isocratic elution	isothermal	Joule heating
Kovat's retention index	liquid–solid adsorption chromatography	longitudinal diffusion
loop injector	mass spectrometer	mass spectrum
mass transfer	micelle	micellar electrokinetic capillary chromatography
mobile phase	monolithic column	multiple paths
nonretained solutes	normal-phase chromatography	on-column injection
open tubular column	packed columns	partition chromatography
peak capacity	planar chromatography	polarity index
porous-layer open tubular column	purge-and-trap	resolution
retention factor	retention time	reversed-phase chromatography
selectivity factor	single-column ion chromatography	solid-phase microextraction
split injection	splitless injection	stacking
stationary phase	supercritical fluid chromatography	support-coated open tubular column
tailing	temperature programming	theoretical plate
thermal conductivity detector	van Deemter equation	void time
wall-coated open-tubular column	zeta potential	

CHAPTER OVERVIEW

4: Kinetic Methods

There are many ways to categorize analytical techniques, several of which we introduced in earlier chapters. In Chapter 3 we classified techniques by whether the signal is proportional to the absolute amount of analyte or the relative amount of analyte. For example, precipitation gravimetry is a total analysis technique because the precipitate's mass is proportional to the absolute amount, or moles, of analyte. UV/Vis absorption spectroscopy, on the other hand, is a concentration technique because absorbance is proportional to the relative amount, or concentration, of analyte.

A second way to classify analytical techniques is to consider the source of the analytical signal. For example, gravimetry encompasses all techniques in which the analytical signal is a measurement of mass or a change in mass. Spectroscopy, on the other hand, includes those techniques in which we probe a sample with an energetic particle, such as the absorption of a photon. This is the classification scheme used in organizing Chapters 8–11.

An additional way to classify analytical techniques is by whether the analyte's concentration is determined under a state of equilibrium or by the kinetics of a chemical reaction or a physical process. The analytical methods described in Chapter 8–11 mostly involve measurements made on systems in which the analyte is at equilibrium. In this chapter we turn our attention to measurements made under nonequilibrium conditions.

Thumbnail: Determination of a reaction's intermediate rate from the slope of a line tangent to a curve showing the change in the analyte's concentration as a function of time.

4.1: Kinetic Techniques versus Equilibrium Techniques

In an equilibrium method the analytical signal is determined by an equilibrium reaction that involves the analyte or by a steady-state process that maintains the analyte's concentration. When we determine the concentration of iron in water by measuring the absorbance of the orange-red $\mathrm{Fe(phen)_3^{2+}}$ complex, the signal depends upon the concentration of $\mathrm{Fe(phen)_3^{2+}}$, which, in turn, is determined by the complex's formation constant. In the flame atomic absorption determination of Cu and Zn in tissue samples, the concentration of each metal in the flame remains constant because each step in the process of atomizing the sample is in a steady-state. In a ***kinetic method*** the analytical signal is determined by the rate of a reaction that involves the analyte or by a nonsteady-state process. As a result, the analyte's concentration changes during the time in which we monitor the signal.

In many cases we can choose to complete an analysis using either an equilibrium method or a kinetic method by changing when we measure the analytical signal. For example, one method for determining the concentration of nitrite, $\mathrm{NO_2^-}$, in groundwater utilizes the two-step diazotization re-action shown in Figure 13.1.1 [Method 4500-$\mathrm{NO_2^-}$ B in *Standard Methods for the Analysis of Waters and Wastewaters*, American Public Health Association: Washington, DC, 20th Ed., 1998]. The final product, which is a reddish-purple azo dye, absorbs visible light at a wavelength of 543 nm. Because neither reaction in Figure 13.1.1 is rapid, the absorbance —which is directly proportional to the concentration of nitrite—is measured 10 min after we add the last reagent, a lapse of time that ensures that the concentration of the azo dyes reaches the steady-state value required of an equilibrium method.

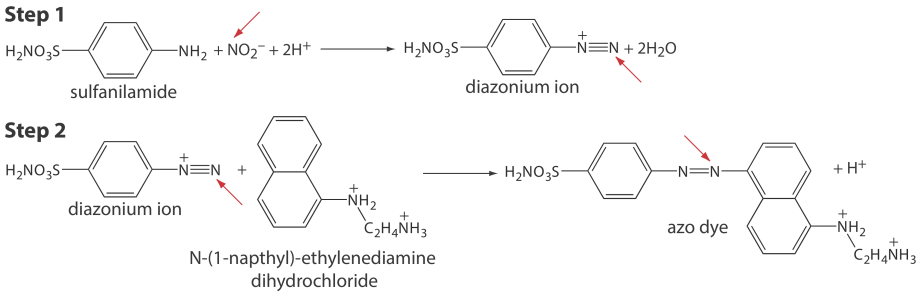

Figure 13.1.1 . Analytical scheme for the analysis of NO-2 in groundwater. The red arrows highlights the nitrogen in $\mathrm{NO_2^-}$ that becomes part of the azo dye.

We can use the same set of reactions as the basis for a kinetic method if we measure the solution's absorbance during this 10-min development period, obtaining information about the reaction's rate. If the measured rate is a function of the concentration of $\mathrm{NO_2^-}$, then we can use the rate to determine its concentration in the sample [Karayannis, M. I.; Piperaki, E. A.; Maniadaki, M. M. *Anal. Lett.* **1986**, *19*, 13–23].

There are many potential advantages to a kinetic method of analysis, perhaps the most important of which is the ability to use chemical reactions and systems that are slow to reach equilibrium. In this chapter we examine three techniques that rely on measurements made while the analytical system is under kinetic control: chemical kinetic techniques, in which we measure the rate of a chemical reaction; radiochemical techniques, in which we measure the decay of a radioactive element; and flow injection analysis, in which we inject the analyte into a continuously flowing carrier stream, where its mixes with and reacts with reagents in the stream under conditions controlled by the kinetic processes of convection and diffusion.

4.2: Chemical Kinetics

The earliest analytical methods based on chemical kinetics—which first appear in the late nineteenth century—took advantage of the catalytic activity of enzymes. In a typical method of that era, an enzyme was added to a solution that contained a suitable substrate and their reaction was monitored for a fixed time. The enzyme's activity was determined by the change in the substrate's concentration. Enzymes also were used for the quantitative analysis of hydrogen peroxide and carbohydrates. The development of chemical kinetic methods continued in the first half of the twentieth century with the introduction of nonenzymatic catalysts and noncatalytic reactions.

Despite the diversity of chemical kinetic methods, by 1960 they no longer were in common use. The principal limitation to their broader acceptance was a susceptibility to significant errors from uncontrolled or poorly controlled variables—temperature and pH are two such examples—and the presence of interferents that activate or inhibit catalytic reactions. By the 1980s, improvements in instrumentation and data analysis methods compensated for these limitations, ensuring the further development of chemical kinetic methods of analysis [Pardue, H. L. *Anal. Chim. Acta* **1989**, *216*, 69–107].

Theory and Practice

Every chemical reaction occurs at a finite rate, which makes it a potential candidate for a chemical kinetic method of analysis. To be effective, however, the chemical reaction must meet three necessary conditions: (1) the reaction must not occur too quickly or too slowly; (2) we must know the reaction's rate law; and (3) we must be able to monitor the change in concentration for at least one species. Let's take a closer look at each of these requirements.

> The material in this section assumes some familiarity with chemical kinetics, which is part of most courses in general chemistry. For a review of reaction rates, rate laws, and integrated rate laws, see the material in Appendix 17.

Reaction Rate

The ***rate*** of the chemical reaction—how quickly the concentrations of reactants and products change during the reaction—must be fast enough that we can complete the analysis in a reasonable time, but also slow enough that the reaction does not reach equilibrium while the reagents are mixing. As a practical limit, it is not easy to study a reaction that reaches equilibrium within several seconds without the aid of special equipment for rapidly mixing the reactants.

> We will consider two examples of instrumentation for studying reactions with fast kinetics later in this chapter.

Rate Law

The second requirement is that we must know the reaction's ***rate law***—the mathematical equation that describes how the concentrations of reagents affect the rate—for the period in which we are making measurements. For example, the rate law for a reaction that is first order in the concentration of an analyte, *A*, is

$$\text{rate} = -\frac{d[A]}{dt} = k[A] \tag{4.2.1}$$

where *k* is the reaction's ***rate constant***.

> Because the concentration of *A* decreases during the reactions, *d*[*A*] is negative. The minus sign in Equation 4.2.1 makes the rate positive. If we choose to follow a product, *P*, then *d*[*P*] is positive because the product's concentration increases throughout the reaction. In this case we omit the minus sign.

An ***integrated rate law*** often is a more useful form of the rate law because it is a function of the analyte's initial concentration. For example, the integrated rate law for Equation 4.2.1 is

$$\ln [A]_t = \ln [A]_0 - kt \tag{4.2.2}$$

or

$$[A]_t = [A]_0 e^{-kt} \tag{4.2.3}$$

where $[A]_0$ is the analyte's initial concentration and $[A]_t$ is the analyte's concentration at time t.

Unfortunately, most reactions of analytical interest do not follow a simple rate law. Consider, for example, the following reaction between an analyte, A, and a reagent, R, to form a single product, P

$$A + R \rightleftharpoons P$$

where k_f is the rate constant for the forward reaction, and k_r is the rate constant for the reverse reaction. If the forward and the reverse reactions occur as single steps, then the rate law is

$$\text{rate } = -\frac{d[A]}{dt} = k_f[A][R] - k_r[P] \tag{4.2.4}$$

> The first term, $k_f[A][R]$ accounts for the loss of A as it reacts with R to make P, and the second term, $k_r[P]$ accounts for the formation of A as P converts back to A and to R.

Although we know the reaction's rate law, there is no simple integrated form that we can use to determine the analyte's initial concentration. We can simplify Equation 4.2.4 by restricting our measurements to the beginning of the reaction when the concentration of product is negligible.

Under these conditions we can ignore the second term in Equation 4.2.4, which simplifies to

$$\text{rate } = -\frac{d[A]}{dt} = k_f[A][R] \tag{4.2.5}$$

The integrated rate law for Equation 4.2.5, however, is still too complicated to be analytically useful. We can further simplify the kinetics by making further adjustments to the reaction conditions [Mottola, H. A. *Anal. Chim. Acta* **1993**, *280*, 279–287]. For example, we can ensure pseudo-first-order kinetics by using a large excess of R so that its concentration remains essentially constant during the time we monitor the reaction. Under these conditions Equation 4.2.5 simplifies to

$$\text{rate } = -\frac{d[A]}{dt} = k_f[A][R]_0 = k'[A] \tag{4.2.6}$$

where $k' = k_f[R]_0$. The integrated rate law for Equation 4.2.6 then is

$$\ln [A]_t = \ln [A]_0 - k't \tag{4.2.7}$$

or

$$[A]_t = [A]_0 e^{-k't} \tag{4.2.8}$$

It may even be possible to adjust the conditions so that we use the reaction under pseudo-zero-order conditions.

$$\text{rate } = -\frac{d[A]}{dt} = k_f[A]_0[R]_0 = k''t \tag{4.2.9}$$

$$[A]_t = [A]_0 - k''t \tag{4.2.10}$$

where $k'' = k_f[A]_0[R]_0$.

> To say that the reaction is pseudo-first-order in A means the reaction behaves as if it is first order in A and zero order in R even though the underlying kinetics are more complicated. We call k' a pseudo-first-order rate constant. To say that a reaction is pseudo-zero-order means the reaction behaves as if it is zero order in A and zero order in R even though the underlying kinetics are more complicated. We call k'' the pseudo-zero-order rate constant.

Monitoring the Reaction

The final requirement is that we must be able to monitor the reaction's progress by following the change in concentration for at least one of its species. Which species we choose to monitor is not important: it can be the analyte, a reagent that reacts with the

analyte, or a product. For example, we can determine the concentration of phosphate by first reacting it with Mo(VI) to form 12-molybdophosphoric acid (12-MPA).

$$H_3PO_4(aq) + 6Mo(VI)(aq) \longrightarrow 12-MPA(aq) + 9H^+(aq) \quad (4.2.11)$$

Next, we reduce 12-MPA to heteropolyphosphomolybdenum blue, PMB. The rate of formation of PMB is measured spectrophotometrically, and is proportional to the concentration of 12-MPA. The concentration of 12-MPA, in turn, is proportional to the concentration of phosphate [see, for example, (a) Crouch, S. R.; Malmstadt, H. V. *Anal. Chem.* **1967**, *39*, 1084–1089; (b) Crouch, S. R.; Malmstadt, H. V. *Anal. Chem.* **1967**, *39*, 1090–1093; (c) Malmstadt, H. V.; Cordos, E. A.; Delaney, C. J. *Anal. Chem.* **1972**, *44(12)*, 26A–41A]. We also can follow reaction 13.11 spectrophotometrically by monitoring the formation of the yellow-colored 12-MPA [Javier, A. C.; Crouch, S. R.; Malmstadt, H. V. *Anal. Chem.* **1969**, *41*, 239–243].

> Reaction 4.2.11 is, of course, unbalanced; the additional hydrogens on the reaction's right side come from the six Mo(VI) that appear on the reaction's left side where Mo(VI) is thought to be present as the molybdate dimer $HMo_2O_6^+$.

Classifying Chemical Kinetic Methods

Figure 13.2.1 provides one useful scheme for classifying chemical kinetic methods of analysis. Methods are divided into two broad categories: direct- computation methods and curve-fitting methods. In a direct-computation method we calculate the analyte's initial concentration, $[A]_0$, using the appropriate rate law. For example, if the reaction is first-order in analyte, we can use Equation 4.2.2 to determine $[A]_0$ given values for k, t, and $[A]_t$. With a curve-fitting method, we use regression to find the best fit between the data—for example, $[A]_t$ as a function of time—and the known mathematical model for the rate law. If the reaction is first-order in analyte, then we fit Equation 4.2.2 to the data using k and $[A]_0$ as adjustable parameters.

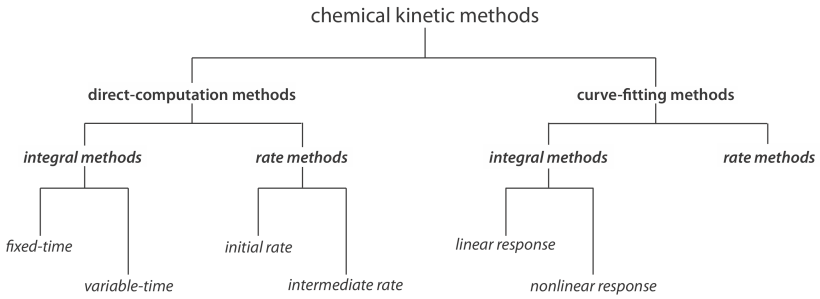

Figure 13.2.1 . Classification of chemical kinetic methods of analysis adapted from Pardue, H. L. "Kinetic Aspects of Analytical Chemistry," *Anal. Chim. Acta* **1989**, *216*, 69–107.

Direct-Computation Fixed-Time Integral Methods

A direct-computation integral method uses the integrated form of the rate law. In a ***one-point fixed-time integral method***, for example, we determine the analyte's concentration at a single time and calculate the analyte's initial concentration, $[A]_0$, using the appropriate integrated rate law. To determine the reaction's rate constant, k, we run a separate experiment using a standard solution of analyte. Alternatively, we can determine the analyte's initial concentration by measuring $[A]_t$ for several standards that contain known concentrations of analyte and construct a calibration curve.

Example 13.2.1

The concentration of nitromethane, CH_3NO_2, is determined from the kinetics of its decomposition reaction. In the presence of excess base the reaction is pseudo-first-order in nitromethane. For a standard solution of 0.0100 M nitromethane, the concentration of nitromethane after 2.00 s is 4.24×10^{-4} M. When a sample that contains an unknown amount of nitromethane is analyzed, the concentration of nitromethane remaining after 2.00 s is 5.35×10^{-4} M. What is the initial concentration of nitromethane in the sample?

Solution

First, we determine the value for the pseudo-first-order rate constant, k'. Using Equation 4.2.7 and the result for the standard, we find its value is

$$k' = \frac{\ln [A]_0 - \ln [A]_t}{t} = \frac{\ln (0.0100) - \ln (4.24 \times 10^{-4})}{2.00 \text{ s}} = 1.58 \text{ s}^{-1}$$

Next we use Equation 4.2.8 to calculate the initial concentration of nitromethane in the sample.

$$[A]_0 = \frac{[A]_t}{e^{-k't}} = \frac{5.35 \times 10^{-4} \text{ M}}{e^{-(1.58 \text{ s}^{-1})(2.00 \text{ s})}} = 0.0126 \text{ M}$$

Equation 4.2.7 and Equation 4.2.8 are equally appropriate integrated rate laws for a pseudo-first-order reaction. The decision to use Equation 4.2.7 to calculate k' and Equation 4.2.8 to calculate $[A]_0$ is a matter of convenience.

Exercise 13.2.1

In a separate determination for nitromethane, a series of external standards gives the following concentrations of nitromethane after a 2.00 s decomposition under pseudo-first-order conditions.

$[CH_3NO_2]_0$ (M)	$[CH_3NO_2]_{t = 2.00 \text{ s}}$ (M)
0.0100	3.82×10^{-4}
0.0200	8.19×10^{-3}
0.0300	1.15×10^{-3}
0.0400	1.65×10^{-3}
0.0500	2.14×10^{-3}
0.0600	2.53×10^{-3}
0.0700	3.21×10^{-3}
0.0800	3.35×10^{-3}
0.0900	3.99×10^{-3}
0.100	4.13×10^{-3}

Analysis of a sample under the same conditions gives a nitromethane concentration of 2.21×10^{-3} M after 2 s. What is the initial concentration of nitromethane in the sample?

Answer

The calibration curve and the calibration equation for the external standards are shown below. Substituting 2.21×10^{-3} M for $[CH_3NO_2]_{t = 2s}$ gives $[CH_3NO_2]_0$ as 5.21×10^{-2} M.

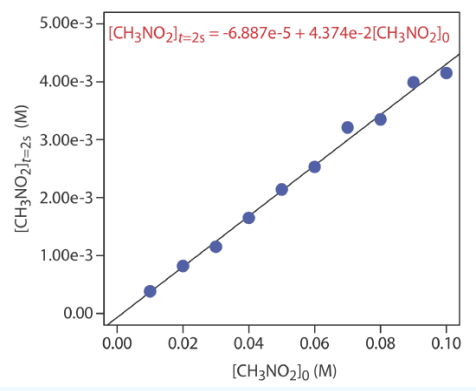

In Example 13.2.1 we determine the analyte's initial concentration by measuring the amount of analyte that has not reacted. Sometimes it is more convenient to measure the concentration of a reagent that reacts with the analyte, or to measure the

concentration of one of the reaction's products. We can use a one-point fixed-time integral method if we know the reaction's stoichiometry. For example, if we measure the concentration of the product, *P*, in the reaction

$$A + R \rightarrow P$$

then the concentration of the analyte at time *t* is

$$[A]_t = [A]_0 - [P]_t \tag{4.2.12}$$

because the stoichiometry between the analyte and product is 1:1. If the reaction is pseudo-first-order in *A*, then substituting Equation 4.2.12 into Equation 4.2.7 gives

$$\ln([A]_0 - [P]_t) = \ln [A]_0 - k't \tag{4.2.13}$$

which we simplify by writing in exponential form.

$$[A]_0 - [P]_t = [A]_0 e^{-k't} \tag{4.2.14}$$

Finally, solving Equation 4.2.14 for $[A]_0$ gives the following equation.

$$[A]_0 = \frac{[P]_t}{1 - e^{-k't}} \tag{4.2.15}$$

Example 13.2.2

The concentration of thiocyanate, SCN^-, is determined from the pseudo-first-order kinetics of its reaction with excess Fe^{3+} to form a reddish-colored complex of $Fe(SCN)^{2+}$. The reaction's progress is monitored by measuring the absorbance of $Fe(SCN)^{2+}$ at a wavelength of 480 nm. When using a standard solution of 0.100 M SCN^-, the concentration of $Fe(SCN)^{2+}$ after 10 s is 0.0516 M. The concentration of $Fe(SCN)^{2+}$ in a sample that contains an unknown amount of SCN^- is 0.0420 M after 10 s. What is the initial concentration of SCN^- in the sample?

Solution

First, we must determine a value for the pseudo-first-order rate constant, k'. Using Equation 4.2.13, we find that its value is

$$k' = \frac{\ln [A]_0 - \ln([A]_0 - [P]_1)}{t} = \frac{\ln(0.100) - \ln(0.100 - 0.0516)}{10.0\ \text{s}} = 0.0726\ \text{s}^{-1}$$

Next, we use Equation 4.2.15 to determine the initial concentration of SCN^- in the sample.

$$[A]_0 = \frac{[P]_t}{1 - e^{-k't}} = \frac{0.0420\text{M}}{1 - e^{-(0.0726\ \text{s}^{-1})(10.0\ \text{s})}} = 0.0868\text{M}$$

Exercise 13.2.2

In a separate determination for SCN^-, a series of external standards gives the following concentrations of $Fe(SCN)^{2+}$ after a 10.0 s reaction with excess Fe^{3+} under pseudo-first-order conditions.

$[SCN^-]$ (M)	$[Fe(SCN)^{2+}]_{t = 10.0\ s}$ (M)
5.00×10^{-3}	1.79×10^{-3}
1.50×10^{-2}	8.24×10^{-3}
2.50×10^{-2}	1.28×10^{-2}
3.50×10^{-2}	1.85×10^{-2}
4.50×10^{-2}	2.21×10^{-2}
5.50×10^{-2}	2.81×10^{-2}
6.50×10^{-2}	3.27×10^{-2}

$[SCN^-]$ (M)	$[Fe(SCN)^{2+}]_{t = 10.0\ s}$ (M)
7.50×10^{-2}	3.91×10^{-2}
8.50×10^{-2}	4.23×10^{-2}
9.50×10^{-2}	4.89×10^{-2}

Analysis of a sample under the same conditions gives an $Fe(SCN)^{2+}$ concentration of 3.52×10^{-2} M after 10 s. What is the initial concentration of SCN^- in the sample?

Answer

The calibration curve and the calibration equation for the external standards are shown below. Substituting 3.52×10^{-2} M for $[Fe(SCN)^{2+}]_{t = 10\ s}$ gives $[SCN^-]_0$ as 6.87×10^{-2} M.

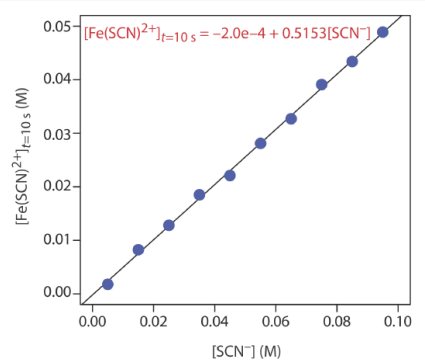

A one-point fixed-time integral method has the advantage of simplicity because we need only a single measurement to determine the analyte's initial concentration. As with any method that relies on a single determination, a one-point fixed-time integral method can not compensate for a constant determinate error. In a ***two-point fixed-time integral method*** we correct for constant determinate errors by making measurements at two points in time and use the difference between the measurements to determine the analyte's initial concentration. Because it affects both measurements equally, the difference between the measurements is independent of a constant de- terminate error. For a pseudo-first-order reaction in which we measure the analyte's concentration at times t_1 and t_2, we can write the following two equations.

$$[A]_{t_1} = [A]_0 e^{-k' t_1} \tag{4.2.16}$$

$$[A]_{t_2} = [A]_0 e^{-k' t_2} \tag{4.2.17}$$

Subtracting Equation 4.2.17 from Equation 4.2.16 and solving for $[A]_0$ leaves us with

$$[A]_0 = \frac{[A]_{t_1} - [A]_{t_2}}{e^{-k' t_1} - e^{-k' t_2}} \tag{4.2.18}$$

To determine the rate constant, k', we measure $[A]_{t_1}$ and $[A]_{t_2}$ for a standard solution of analyte. Having obtained a value for k', we can determine $[A]_0$ by measuring the analyte's concentration at t_1 and t_2. We also can determine the analyte's initial concentration using a calibration curve consisting of a plot of ($[A]_{t_1} - [A]_{t_2}$) versus $[A]_0$.

A fixed-time integral method is particularly useful when the signal is a linear function of concentration because we can replace the reactant's concentration with the corresponding signal. For example, if we follow a reaction spectrophotometrically under conditions where the analyte's concentration obeys Beer's law

$$(Abs)_t = \varepsilon b [A]_t$$

then we can rewrite Equation 4.2.8 and Equation 4.2.18 as

$$(Abs)_t = [A]_0 e^{-k'} \varepsilon b = c [A]_0$$

$$[A]_t = \frac{(Abs)_{t_1} - (Abs)_{t_2}}{e^{-k't_1} - e^{-k't_2}} \times (\epsilon b)^{-1} = c'[(Abs)_{t_1} - (Abs)_{t_2}]$$

where $(Abs)_t$ is the absorbance at time t, and c and c' are constants.

Direct-Computation Variable-Time Integral Methods

In a ***variable-time integral method*** we measure the total time, Δ_t, needed to effect a specific change in concentration for one species in the chemical reaction. One important application is the quantitative analysis of catalysts, which takes advantage of the catalyst's ability to increase the rate of reaction. As the concentration of catalyst increased, Δ_t decreases. For many catalytic systems the relationship between Δ_t and the catalyst's concentration is

$$\frac{1}{\Delta t} = F_{cat}[A]_0 + F_{uncat} \tag{4.2.19}$$

where $[A]_0$ is the catalyst's concentration, and F_{cat} and F_{uncat} are constants that account for the rate of the catalyzed and uncatalyzed reactions [Mark, H. B.; Rechnitz, G. A. *Kinetics in Analytical Chemistry*, Interscience: New York, 1968].

Example 13.2.3

Sandell and Kolthoff developed a quantitative method for iodide based on its ability to catalyze the following redox reaction [Sandell, E. B.; Kolthoff, I. M. *J. Am. Chem. Soc.* **1934**, *56*, 1426].

$$As^{3+}(aq) + 2Ce^{4+}(aq) \longrightarrow As^{5+}(aq) + 2Ce^{3+}(aq)$$

An external standards calibration curve was prepared by adding 1 mL of a KI standard to a mixture of 2 mL of 0.05 M As^{3+}, 1 mL of 0.1 M Ce^{4+}, and 1 mL of 3 M H_2SO_4, and measuring the time for the yellow color of Ce^{4+} to disappear. The following table summarizes the results for one analysis.

$[I^-]$ (µg/mL)	Δ_t (min)
5.0	0.9
2.5	1.8
1.0	4.5

What is the concentration of I^- in a sample if Δ_t is 3.2 min?

Solution

Figure 13.2.2 shows the calibration curve and the calibration equation for the external standards based on Equation 4.2.19. Substituting 3.2 min for Δ_t gives the concentration of I^- in the sample as 1.4 µg/mL.

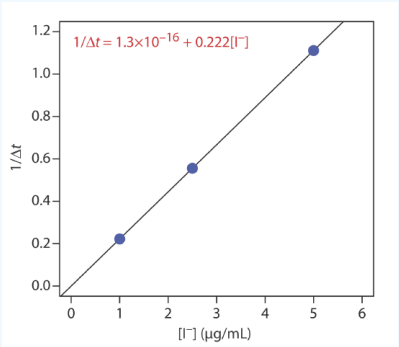

Figure 13.2.2 . Calibration curve and calibration equation for Example 13.2.3.

Direct-Computation Rate Methods

In a ***rate method*** we use the differential form of the rate law—Equation 4.2.1 is one example of a differential rate law—to determine the analyte's concentration. As shown in Figure 13.2.3 , the rate of a reaction at time t, $(rate)_t$, is the slope of a line

tangent to a curve that shows the change in concentration as a function of time. For a reaction that is first-order in analyte, the rate at time *t* is

$$(rate)_t = k[A]_t$$

Substituting in Equation 4.2.3 leaves us with the following equation relating the rate at time *t* to the analyte's initial concentration.

$$(\text{rate})_t = k[A]_0 e^{-kt}$$

If we measure the rate at a fixed time, then both *k* and e^{-kt} are constant and we can use a calibration curve of $(rate)_t$ versus $[A]_0$ for the quantitative analysis of the analyte.

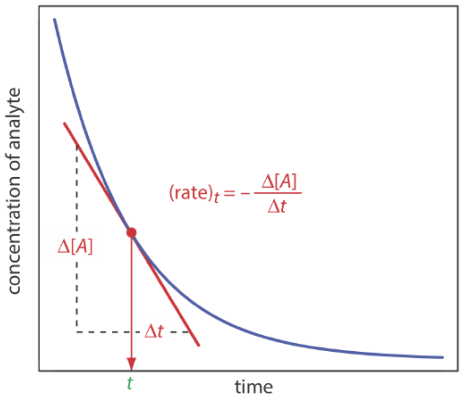

Figure 13.2.3 . Determination of a reaction's instantaneous rate at time *t* from the slope of a line tangent to a curve that shows the change in the analyte's concentration as a function of time.

There are several advantages to using the reaction's ***initial rate*** ($t = 0$). First, because the reaction's rate decreases over time, the initial rate provides the greatest sensitivity. Second, because the initial rate is measured under nearly pseudo-zero-order conditions, in which the change in concentration with time effectively is linear, it is easier to determine the slope. Finally, as the reaction of interest progresses competing reactions may develop, which complicating the kinetics: using the initial rate eliminates these complications. One disadvantage of the initial rate method is that there may be insufficient time to completely mix the reactants. This problem is avoided by using an intermediate rate measured at a later time ($t > 0$).

As a general rule (see Mottola, H. A. "Kinetic Determinations of Reactants Utilizing Uncatalyzed Reactions," *Anal. Chim. Acta* **1993**, *280*, 279–287), the time for measuring a reaction's initial rate should result in the consumption of no more than 2% of the reactants. The smaller this percentage, the more linear the change in concentration as a function of time.

Example 13.2.4

The concentration of norfloxacin, a commonly prescribed antibacterial agent, is determined using the initial rate method. Norfloxacin is converted to an N-vinylpiperazine derivative and reacted with 2,3,5,6-tetra-chloro-1,4-benzoquinone to form an N-vinylpiperazino-substituted ben-zoquinone derivative that absorbs strongly at 625 nm [Darwish, I. A.; Sultan, M. A.; Al-Arfaj, H. A. *Talanta* **2009**, *78*, 1383–1388]. The initial rate of the reaction—as measured by the change in absorbance as a function of time (AU/min)—is pseudo-first order in norfloxacin. The following data were obtained for a series of external norfloxacin standards.

[norfloxacin] (μg/mL)	initial rate (AU/min)
63	0.0139
125	0.0355
188	0.0491
251	0.0656
313	0.0859

To analyze a sample of prescription eye drops, a 10.00-mL portion is extracted with dichloromethane. The extract is dried and the norfloxacin reconstituted in methanol and diluted to 10 mL in a volumetric flask. A 5.00-mL portion of this solution is diluted to volume in a 100-mL volumetric flask. Analysis of this sample gives an initial rate of 0.0394 AU/min.

What is the concentration of norfloxacin in the eye drops in mg/mL?

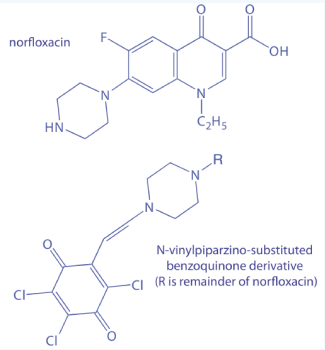

Solution

Figure 13.2.4 shows the calibration curve and the calibration equation for the external standards. Substituting 0.0394 AU/min for the initial rate and solving for the concentration of norfloxacin gives a result of 152 μg/mL. This is the concentration in a diluted sample of the extract. The concentration in the extract before dilution is

$$\frac{152\ \mu g}{\text{mL}} \times \frac{100.0\ \text{mL}}{5.00\ \text{mL}} \times \frac{1\ \text{mg}}{1000\ \mu g} = 3.04\ \text{mg/mL}$$

Because the dried extract was reconstituted using a volume identical to that of the original sample, the concentration of norfloxacin in the eye drops is 3.04 mg/mL.

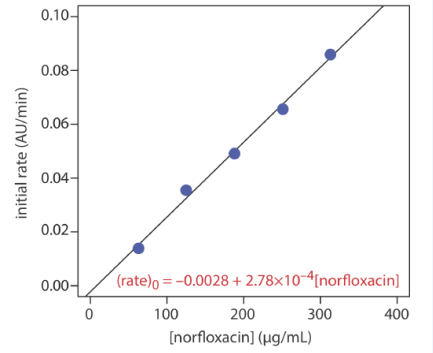

Figure 13.2.4 . Calibration curve and calibration equation for Example 13.2.4 .

Curve-Fitting Methods

In a direct-computation method we determine the analyte's concentration by solving the appropriate rate equation at one or two discrete times. The relationship between the analyte's concentration and the measured response is a function of the rate constant, which we determine in a separate experiment using a single external standard (see Example 13.2.1 or Example 13.2.2), or a calibration curve (see Example 13.2.3 or Example 13.2.4).

In a ***curve-fitting method*** we continuously monitor the concentration of a reactant or a product as a function of time and use a regression analysis to fit the data to an appropriate differential rate law or integrated rate law. For example, if we are monitoring the concentration of a product for a reaction that is pseudo-first-order in the analyte, then we can fit the data to the following rearranged form of Equation 4.2.15

$$[P]_t = [A]_0 \left(1 - e^{-k't}\right)$$

using $[A]_0$ and k' as adjustable parameters. Because we use data from more than one or two discrete times, a curve-fitting method is capable of producing more reliable results.

Example 13.2.5

The data shown in the following table were collected for a reaction that is known to be pseudo-zero-order in analyte. What is the initial concentration of analyte in the sample and the rate constant for the reaction?

time (s)	$[A]_t$ (mM)	time (s)	$[A]_t$ (mM)
3	0.0731	8	0.0448
4	0.0728	9	0.0404
5	0.0681	10	0.0339
6	0.0582	11	0.0217
7	0.0511	12	0.0143

Solution

From Equation 4.2.10 we know that for a pseudo-zero-order reaction a plot of $[A]_t$ versus time is linear with a slope of $-k''$ and a y-intercept of $[A]_0$. Figure 13.2.5 shows a plot of the kinetic data and the result of a linear regression analysis. The initial concentration of analyte is 0.0986 mM and the rate constant is 0.00677 M^{-1} s^{-1}.

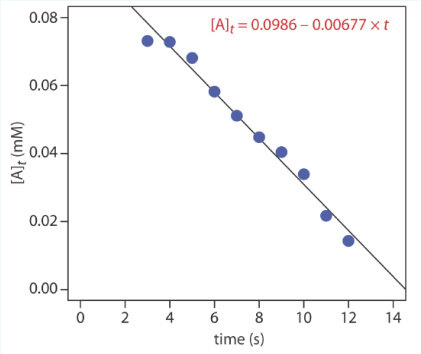

Figure 13.2.5 . Result of fitting Equation 4.2.10 to the data in Example 13.2.5 .

The best way to appreciate the theoretical and the practical details discussed in this section is to carefully examine a typical analytical method. Although each method is unique, the following description of the determination of creatinine in urine provides an instructive example of a typical procedure. The description here is based on Diamandis, E. P.; Koupparis, M. A.; Hadjiioannou, T. P. "Kinetic Studies with Ion Selective Electrodes: Determination of Creatinine in Urine with a Picrate Ion Selective Electrode," *J. Chem. Educ.* **1983**, *60*, 74–76.

Representative Method 13.2.1: Determination of Creatinine in Urine

Description of Method

Creatine is an organic acid in muscle tissue that supplies energy for muscle contractions. One of its metabolic products is creatinine, which is excreted in urine. Because the concentration of creatinine in urine and serum is an important indication of renal function, a rapid method for its analysis is clinically important. In this method the rate of reaction between creatinine and picrate in an alkaline medium is used to determine the concentration of creatinine in urine. Under the conditions of the analysis the reaction is first order in picrate, creatinine, and hydroxide.

$$\text{rate} = k[\text{picrate}][\text{creatinine}]\left[OH^-\right]$$

The reaction is monitored using a picrate ion selective electrode.

Procedure

Prepare a set of external standards that contain 0.5–3.0 g/L creatinine using a stock solution of 10.00 g/L creatinine in 5 mM H_2SO_4, diluting each standard to volume using 5 mM H_2SO_4. Prepare a solution of 1.00×10^{-2} M sodium picrate. Pipet 25.00 mL

of 0.20 M NaOH, adjusted to an ionic strength of 1.00 M using Na_2SO_4, into a thermostated reaction cell at 25°C. Add 0.500 mL of the 1.00×10^{-2} M picrate solution to the reaction cell. Suspend a picrate ion selective in the solution and monitor the potential until it stabilizes. When the potential is stable, add 2.00 mL of a creatinine external standard and record the potential as a function of time. Repeat this procedure using the remaining external standards. Construct a calibration curve of $\Delta E/\Delta t$ versus the initial concentration of creatinine. Use the same procedure to analyze samples, using 2.00 mL of urine in place of the external standard. Determine the concentration of creatinine in the sample using the calibration curve.

Questions

1. The analysis is carried out under conditions that are pseudo-first order in picrate. Show that under these conditions the change in potential as a function of time is linear.

The potential, *E*, of the picrate ion selective electrode is given by the Nernst equation

$$E = K - \frac{RT}{F}\ln[\text{ picrate }]$$

where *K* is a constant that accounts for the reference electrodes, the junction potentials, and the ion selective electrode's asymmetry potential, *R* is the gas constant, *T* is the temperature, and *F* is Faraday's constant. We know from Equation 4.2.7 that for a pseudo-first-order reaction, the concentration of picrate at time *t* is

$$\ln[\text{picrate}]_t = \ln[\text{picrate}]_0 - k't$$

where k' is the pseudo-first-order rate constant. Substituting this integrated rate law into the ion selective electrode's Nernst equation leaves us with the following result.

$$E_t = K - \frac{RT}{F}(\ln[\text{picrate}]_0 - k't)$$

$$E_t = K - \frac{RT}{F}\ln[\text{picrate}]_0 + \frac{RT}{F}k't$$

Because *K* and (*RT*/*F*)ln[picrate]$_0$ are constants, a plot of E_t versus *t* is a straight line with a slope of $\frac{RT}{F}k'$.

2. Under the conditions of the analysis, the rate of the reaction is pseudo-first-order in picrate and pseudo-zero-order in creatinine and OH^-. Explain why it is possible to prepare a calibration curve of $\Delta E/\Delta t$ versus the concentration of creatinine.

The slope of a plot of E_t versus *t* is $\Delta E/\Delta t = RTk'/F$ = *RTk*′/*F* (see the previous question). Because the reaction is carried out under conditions where it is pseudo-zero-order in creatinine and OH^-, the rate law is

$$\text{rate} = k[\text{picrate}][\text{creatinine}]_0[OH^-]_0 = k'[\text{picrate}]$$

The pseudo-first-order rate constant, k', is

$$k' = k[\text{ creatinine }]_0\left[OH^-\right]_0 = c[\text{creatinine}]_0$$

where *c* is a constant equivalent to *k*[OH^-]$_0$. The slope of a plot of E_t versus *t*, therefore, is linear function of creatinine's initial concentration

$$\frac{\Delta E}{\Delta t} = \frac{RTk'}{F} = \frac{RTc}{F}[\text{creatinine}]_0$$

and a plot of $\Delta E/\Delta t$ versus the concentration of creatinine can serve as a calibration curve.

3. Why is it necessary to thermostat the reaction cell?

The rate of a reaction is temperature-dependent. The reaction cell is thermostated to maintain a constant temperature to prevent a determinate error from a systematic change in temperature, and to minimize indeterminate errors from random fluctuations in temperature.

4. Why is it necessary to prepare the NaOH solution so that it has an ionic strength of 1.00 M?

The potential of the picrate ion selective electrode actually responds to the activity of the picrate anion in solution. By adjusting the NaOH solution to a high ionic strength we maintain a constant ionic strength in all standards and samples.

Because the relationship between activity and concentration is a function of ionic strength, the use of a constant ionic strength allows us to write the Nernst equation in terms of picrate's concentration instead of its activity.

Making Kinetic Measurements

When using Representative Method 13.2.1 to determine the concentration of creatinine in urine, we follow the reactions kinetics using an ion selective electrode. In principle, we can use any of the analytical techniques in Chapters 8–12 to follow a reaction's kinetics provided that the reaction does not proceed to an appreciable extent during the time it takes to make a measurement. As you might expect, this requirement places a serious limitation on kinetic methods of analysis. If the reaction's kinetics are slow relative to the analysis time, then we can make a measurement without the analyte undergoing a significant change in concentration. If the reaction's rate is too fast—which often is the case—then we introduce a significant error if our analysis time is too long.

One solution to this problem is to stop, or quench the reaction by adjusting experimental conditions. For example, many reactions show a strong dependence on pH and are quenched by adding a strong acid or a strong base. Figure 13.2.6 shows a typical example for the enzymatic analysis of *p*-nitrophenylphosphate, which uses the enzyme wheat germ acid phosphatase to hydrolyze the analyte to *p*-nitrophenol. The reaction has a maximum rate at a pH of 5. Increasing the pH by adding NaOH quenches the reaction and converts the colorless *p*-nitrophenol to the yellow-colored *p*-nitrophenolate, which absorbs at 405 nm.

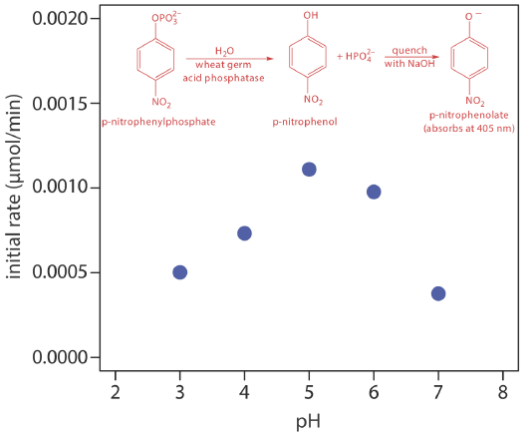

Figure 13.2.6 . Initial rate for the enzymatic hydrolysis of *p*-nitrophenylphosphate using wheat germ acid phosphatase. Increasing the pH quenches the reaction and coverts colorless *p*-nitrophenol to the yellow-colored *p*-nitrophenolate, which absorbs at 405 nm.

An additional problem when the reaction's kinetics are fast is ensuring that we rapidly and reproducibly mix the sample and the reagents. For a fast reaction, we need to make our measurements within a few seconds—or even a few milliseconds—of combining the sample and reagents. This presents us with a problem and an advantage. The problem is that rapidly and reproducibly mixing the sample and the reagent requires a dedicated instrument, which adds an additional expense to the analysis. The advantage is that a rapid, automated analysis allows for a high throughput of samples. Instruments for the automated kinetic analysis of phosphate using reaction 4.2.11, for example, have sampling rates of approximately 3000 determinations per hour.

A variety of instruments have been developed to automate the kinetic analysis of fast reactions. One example, which is shown in Figure 13.2.7 , is the ***stopped-flow analyzer***. The sample and the reagents are loaded into separate syringes and precisely measured volumes are dispensed into a mixing chamber by the action of a syringe drive. The continued action of the syringe drive pushes the mixture through an observation cell and into a stopping syringe. The back pressure generated when the stopping syringe hits the stopping block completes the mixing, after which the reaction's progress is monitored spectrophotometrically. With a stopped-flow analyzer it is possible to complete the mixing of sample and reagent, and initiate the kinetic measurements in approximately 0.5 ms. By attaching an autosampler to the sample syringe it is possible to analyze up to several hundred samples per hour.

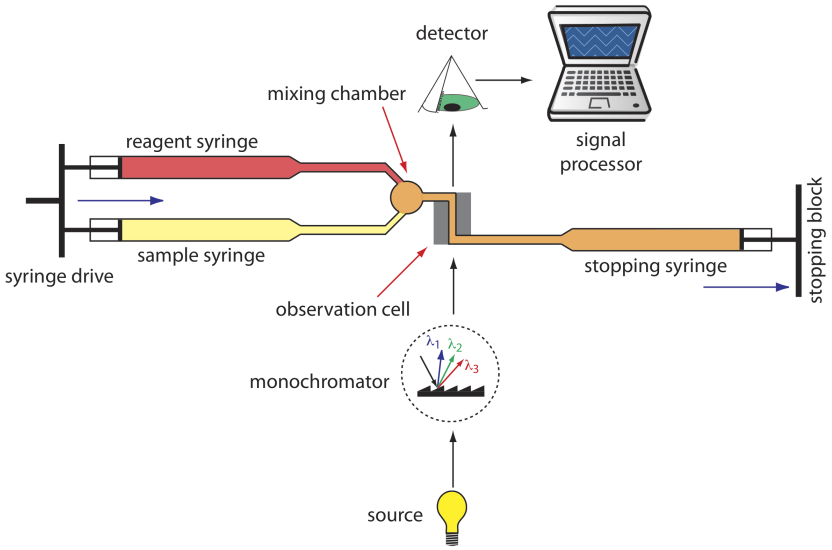

Figure 13.2.7 . Schematic diagram of a stopped-flow analyzer. The blue arrows show the direction in which the syringes are moving.

Another instrument for kinetic measurements is the ***centrifugal analyzer***, a partial cross section of which is shown in Figure 13.2.8 . The sample and the reagents are placed in separate wells, which are oriented radially around a circular transfer disk. As the centrifuge spins, the centrifugal force pulls the sample and the reagents into the cuvette where mixing occurs. A single optical source and detector, located below and above the transfer disk's outer edge, measures the absorbance each time the cuvette passes through the optical beam. When using a transfer disk with 30 cuvettes and rotating at 600 rpm, we can collect 10 data points per second for each sample.

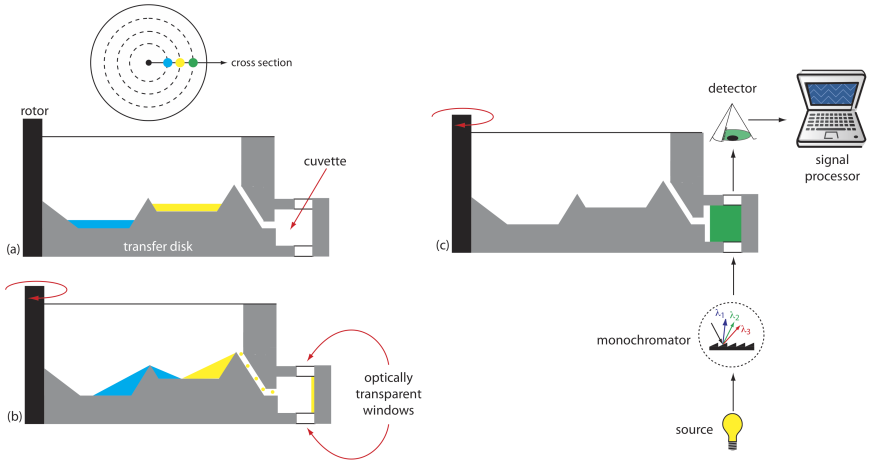

Figure 13.2.8 . Cross sections through a centrifugal analyzer showing (a) the wells that hold the sample and the reagents, (b) the mixing of the sample and the reagents, and (c) the configuration of the spectrophotometric detector.

The ability to collect lots of data and to collect it quickly requires appropriate hardware and software. Not surprisingly, automated kinetic analyzers developed in parallel with advances in analog and digital circuitry—the hardware—and computer software for smoothing, integrating, and differentiating the analytical signal. For an early discussion of the importance of hardware and software, see Malmstadt, H. V.; Delaney, C. J.; Cordos, E. A. "Instruments for Rate Determinations," *Anal. Chem.* **1972**, *44(12)*, 79A–89A.

Quantitative Applications

Chemical kinetic methods of analysis continue to find use for the analysis of a variety of analytes, most notably in clinical laboratories where automated methods aid in handling the large volume of samples. In this section we consider several general quantitative applications.

Enzyme-Catalyzed Reactions

Enzymes are highly specific catalysts for biochemical reactions, with each enzyme showing a selectivity for a single reactant, or ***substrate***. For example, the enzyme acetylcholinesterase catalyzes the decomposition of the neurotransmitter acetylcholine to choline and acetic acid. Many enzyme–substrate reactions follow a simple mechanism that consists of the initial formation of an enzyme–substrate complex, *ES*, which subsequently decomposes to form product, releasing the enzyme to react again.

$$E + S \underset{k_{-1}}{\overset{k_1}{\rightleftharpoons}} ES \underset{k_{-2}}{\overset{k_2}{\rightleftharpoons}} E + P \tag{4.2.20}$$

where k_1, k_{-1}, k_2, and k_{-2} are rate constants. If we make measurement early in the reaction, the concentration of products is negligible and we can ignore the step described by the rate constant k_{-2}. Under these conditions the reaction's rate is

$$\text{rate } = \frac{d[P]}{dt} = k_2[ES] \tag{4.2.21}$$

To be analytically useful we need to write Equation 4.2.21 in terms of the concentrations of the enzyme, *E*, and the substrate, *S*. To do this we use the steady-state approximation, in which we assume the concentration of *ES* remains essentially constant. Following an initial period, during which the enzyme–substrate complex first forms, the rate at which *ES* forms

$$\frac{d[ES]}{dt} = k_1[E][S] = k_1\left([E]_0 - [ES]\right)[S] \tag{4.2.22}$$

is equal to the rate at which it disappears

$$-\frac{d[ES]}{dt} = k_{-1}[ES] + k_2[ES] \tag{4.2.23}$$

where $[E]_0$ is the enzyme's original concentration. Combining Equation 4.2.22 and Equation 4.2.23 gives

$$k_1\left([E]_0 - [ES]\right)[S] = k_{-1}[ES] + k_2[ES]$$

which we solve for the concentration of the enzyme–substrate complex

$$[ES] = \frac{[E]_0[S]}{\frac{k_{-1}+k_2}{k_1} + [S]} = \frac{[E]_0[S]}{K_m + [S]} \tag{4.2.24}$$

where K_m is the ***Michaelis constant***. Substituting Equation 4.2.24 into Equation 4.2.21 leaves us with our final rate equation.

$$\frac{d[P]}{dt} = \frac{k_2[E]_0[S]}{K_m + [S]} \tag{4.2.25}$$

A plot of Equation 4.2.25, as shown in Figure 13.2.9 , helps us define conditions where we can use the rate of an enzymatic reaction for the quantitative analysis of an enzyme or a substrate. For high substrate concentrations, where $[S] >> K_m$, Equation 4.2.25 simplifies to

$$\frac{d[P]}{dt} = \frac{k_2[E]_0[S]}{K_m + [S]} \approx \frac{k_2[E]_0[S]}{[S]} = k_2[E]_0 = V_{\text{max}} \tag{4.2.26}$$

where V_{max} is the maximum rate for the catalyzed reaction. Under these conditions the reaction is pseudo-zero-order in substrate, and we can use V_{max} to calculate the enzyme's concentration, typically using a variable-time method. At lower substrate concentrations, where $[S] << K_m$, Equation 4.2.25 becomes

$$\frac{d[P]}{dt} = \frac{k_2[E]_0[S]}{K_m + [S]} \approx \frac{k_2[E]_0[S]}{K_m} = \frac{V_{\text{max}}[S]}{K_m} \tag{4.2.27}$$

Because the reaction is first-order in substrate we can use the reaction's rate to determine the substrate's concentration using a fixed-time method.

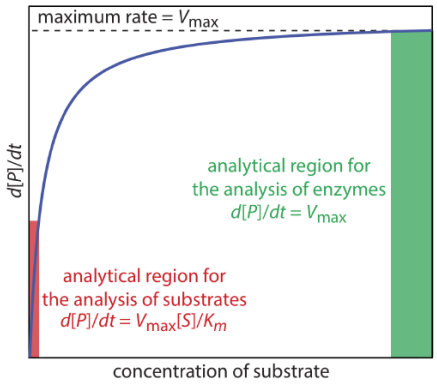

Figure 13.2.9 . Plot of Equation 4.2.25 showing limits for the analysis of substrates and enzymes in an enzyme-catalyzed chemical kinetic method of analysis. The curve in the region highlighted in red obeys Equation 4.2.27 and the curve in the area highlighted in green follows Equation 4.2.26.

Chemical kinetic methods have been applied to the quantitative analysis of a number of enzymes and substrates [Guilbault, G. G. Handbook of Enzymatic Methods of Analysis, Marcel Dekker: New York, 1976]. One example, is the determination of glucose based on its oxidation by the enzyme glucose oxidase

$$\text{glucose}(aq) + \text{H}_2\text{O}(g) \xrightarrow{\text{glucose oxidase}} \text{gluconolactone}(aq) + \text{H}_2\text{O}_2(aq)$$

under conditions where Equation 4.2.20 is valid. The reaction is monitored by following the rate of change in the concentration of dissolved O_2 using an appropriate voltammetric technique.

> One method for measuring the concentration of dissolved O_2 is the Clark amperometric sensor described in Chapter 11.

Nonenzyme-Catalyzed Reactions

The variable-time method also is used to determine the concentration of nonenzymatic catalysts. One example uses the reduction of H_2O_2 by thiosulfate, iodide, or hydroquinone, a reaction catalyzed by trace amounts of selected metal ions. For example the reduction of H_2O_2 by I^-

$$2\text{I}^-(aq) + \text{H}_2\text{O}_2(aq) + 2\text{H}_3\text{O}^+(aq) \longrightarrow 4\text{H}_2\text{O}(l) + \text{I}_2(aq)$$

is catalyzed by Mo(VI), W(VI), and Zr(IV). A variable-time analysis is conducted by adding a small, fixed amount of ascorbic acid to each solution. As I_2 is produced it rapidly oxidizes the ascorbic acid and is reduced back to I^-. Once all the ascorbic acid is consumed, the presence of excess I_2 provides a visual endpoint.

Noncatalytic Reactions

Chemical kinetic methods are not as common for the quantitative analysis of analytes in noncatalytic reactions. Because they lack the enhancement of reaction rate that a catalyst affords, a noncatalytic method generally is not useful for determining small concentrations of analyte. Noncatalytic methods for inorganic analytes usually are based on a complexation reaction. One example is the determination of aluminum in serum by measuring the initial rate for the formation of its complex with 2-hydroxy-1-napthaldehyde *p*-methoxybenzoyl-hydrazone [Ioannou. P. C.; Piperaki, E. A. *Clin. Chem.* **1986**, *32*, 1481–1483]. The greatest number of noncatalytic methods, however, are for the quantitative analysis of organic analytes. For example, the insecticide methyl parathion has been determined by measuring its rate of hydrolysis in alkaline solutions [Cruces Blanco, C.; Garcia Sanchez, F. *Int. J. Environ. Anal. Chem.* **1990**, *38*, 513–523].

Characterization Applications

Chemical kinetic methods also find use in determining rate constants and in elucidating reaction mechanisms. Two examples from the kinetic analysis of enzymes illustrate these applications.

Determining V_{max} and K_m for Enzyme-Catalyzed Reactions

The value of V_{max} and K_m for an enzymatic reaction are of significant interest in the study of cellular chemistry. For an enzyme that follows the mechanism in reaction 4.2.20, V_{max} is equivalent to $k2 \times [E]_0$, where $[E]_0$ is the enzyme's concentration and k_2 is the

enzyme's turnover number. An enzyme's turnover number is the maximum number of substrate molecules converted to product by a single active site on the enzyme, per unit time. A turnover number, therefore, provides a direct indication of the active site's catalytic efficiency. The Michaelis constant, K_m, is significant because it provides an estimate of the substrate's intracellular concentration [(a) Northup, D. B. *J. Chem. Educ.* **1998**, *75*, 1153–1157; (b) Zubay, G. *Biochemistry*, Macmillan Publishing Co.: New York, 2nd Ed., p 269].

An enzyme's turnover number also is know as k_{cat} and is equal to $V_{max}/[E]_0$. For the mechanism in reaction 4.2.20, k_{cat} is equivalent to k_2. For more complicated mechanisms, k_{cat} is a function of additional rate constants.

As shown in Figure 13.2.9 , we can find values for V_{max} and K_m by measuring the reaction's rate for small and for large concentrations of the substrate. Unfortunately, this is not always practical as the substrate's limited solubility may prevent us from using the large substrate concentrations needed to determine V_{max}. Another approach is to rewrite Equation 4.2.25 by taking its reciprocal

\[\frac{1}{d[P] / d t}=\frac{1}{v}=\frac{K_{m}}{V_{\max }} \times \frac{1}{[S]}+\frac{1}{V_{\max }} \label{13.28}\]

where v is the reaction's rate. As shown in Figure 13.2.10 , a plot of $1/v$ versus 1/[S], which is called a double reciprocal or Lineweaver–Burk plot, is a straight line with a slope of K_m/V_{max}, a y-intercept of $1/V_{max}$, and an x-intercept of $-1/K_m$.

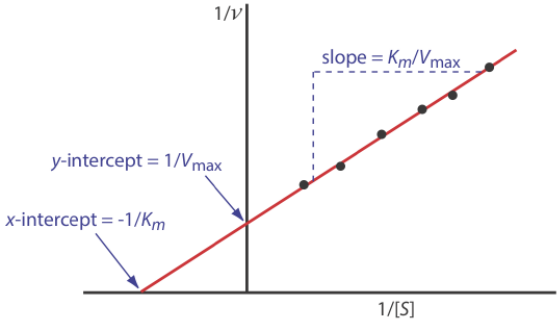

Figure 13.2.10 . Lineweaver–Burk plot of Equation 4.2.25 using Equation ???.

In Chapter 5 we noted that when faced with a nonlinear model—and Equation 4.2.25 is one example of a nonlinear model—it may be possible to rewrite the equation in a linear form. This is the strategy used here. Linearizing a nonlinear model is not without limitations, two of which deserve a brief mention. First, because we are unlikely to have data for large substrate concentrations, we will not have many data points for small values of 1/[S]. As a result, our determination of the y-intercept's value relies on a significant extrapolation. Second, taking the reciprocal of the rate distorts the experimental error in a way that may invalidate the assumptions of a linear regression. Nonlinear regression provides a more rigorous method for fitting Equation 4.2.25 to experimental data. The details are beyond the level of this textbook, but you may consult Massart, D. L.; Vandeginste, B. G. M.; Buydens, L. M. C. De Jong, S.; Lewi, P. J.; Smeyers-Verbeke, J. "Nonlinear Regression," which is Chapter 11 in *Handbook of Chemometrics and Qualimetrics: Part A*, Elsevier: Amsterdam, 1997, for additional details. The simplex algorithm described in Chapter 14 of this text also can be used to fit a nonlinear equation to experimental data.

Example 13.2.6

The reaction between nicotineamide mononucleotide and ATP to form nicotineamide–adenine dinucleotide and pyrophosphate is catalyzed by the enzyme nicotinamide mononucleotide adenylyltransferase [(a) Atkinson, M. R.; Jackson, J. F.; Morton, R. K. *Biochem. J.* **1961**, *80*, 318–323; (b) Wilkinson, G. N. *Biochem. J.* **1961**, *80*, 324–332]. The following table provides typical data obtained at a pH of 4.95. The substrate, S, is nicotinamide mononucleotide and the initial rate, v, is the μmol of nicotinamide–adenine dinucleotide formed in a 3-min reaction period.

[S] (mM)	v (μmol)	[S] (mM)	v (μmol)
0.138	0.148	0.560	0.324
0.220	0.171	0.766	0.390

[S] (mM)	v (µmol)	[S] (mM)	v (µmol)
0.291	0.234	1.460	0.493

Determine values for V_{max} and K_m.

Solution

Figure 13.2.11 shows the Lineweaver–Burk plot for this data and the result-ng regression equation. Using the *y*-intercept, we calculate V_{max} as

$$V_{max} = \frac{1}{y\text{-intercept}} = \frac{1}{1.708\ \mu\text{mol}^{-1}} = 0.585\ \mu\text{mol}$$

and using the slope we find that K_m is

$$K_m = \text{slope} \times V_{max} = 0.7528\ \mu\text{mol}^{-1}\text{mM} \times 0.585\ \mu\text{mol} = 0.440\text{mM}$$

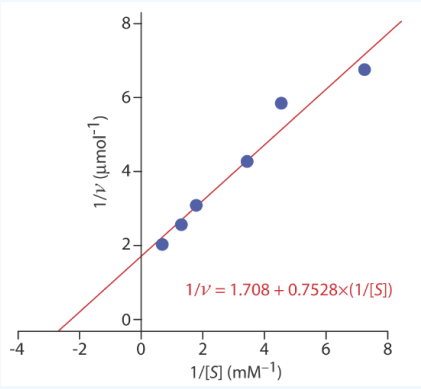

Figure 13.2.11 . Lineweaver–Burk plot and regression equation for the data in Example 13.2.6 .

Exercise 13.2.3

The following data were collected during the oxidation of catechol (the substrate) to *o*-quinone by the enzyme *o*-diphenyl oxidase. The reaction was followed by monitoring the change in absorbance at 540 nm. The data in this exercise is adapted from jkimball.

[catechol] (mM):	0.3	0.6	1.2	4.8
rate (Δ AU/min):	0.020	0.035	0.048	0.081

Answer

The figure below shows the Lineweaver–Burk plot and the equation for the data. The *y*-intercept of 9.974 min/(ΔAU is equivalent to $1/V_{max}$; thus, V_{max} is 0.10 Δ AU/min. The slope of 11.89 min/(\Delta\)AU•mM is equivalent to K_m/V_{max}; thus, K_m is 1.2 mM.

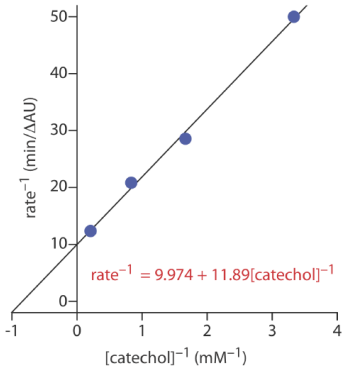

Elucidating Mechanisms for the Inhibition of Enzyme Catalysis

When an ***inhibitor*** interacts with an enzyme it decreases the enzyme's catalytic efficiency. An irreversible inhibitor binds covalently to the enzyme's active site, producing a permanent loss in catalytic efficiency even if we decrease the inhibitor's concentration. A reversible inhibitor forms a noncovalent complex with the enzyme, resulting in a temporary decrease in catalytic efficiency. If we remove the inhibitor, the enzyme's catalytic efficiency returns to its normal level.

There are several pathways for the reversible binding of an inhibitor and an enzyme, as shown in Figure 13.2.12 . In ***competitive inhibition*** the substrate and the inhibitor compete for the same active site on the enzyme. Because the substrate cannot bind to an enzyme–inhibitor complex, *EI*, the enzyme's catalytic efficiency for the substrate decreases. With ***noncompetitive inhibition*** the substrate and the inhibitor bind to different active sites on the enzyme, forming an enzyme–substrate–inhibitor, or *ESI* complex. The formation of an *ESI* complex decreases catalytic efficiency because only the enzyme–substrate complex reacts to form the product. Finally, in ***uncompetitive inhibition*** the inhibitor binds to the enzyme–substrate complex, forming an inactive *ESI* complex.

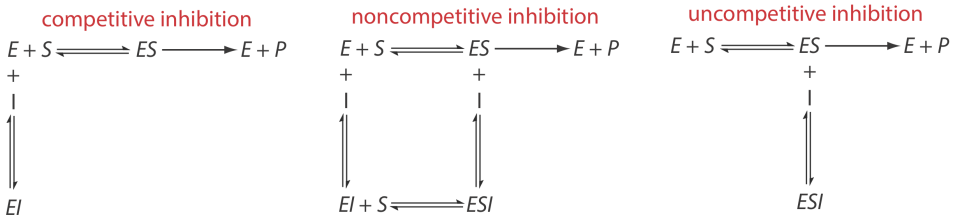

Figure 13.2.12 . Mechanisms for the reversible inhibition of enzyme catalysis. *E*: enzyme, *S*: substrate, *P*: product, *I*: inhibitor, *ES*: enzyme–substrate complex, *EI*: enzyme–inhibitor com- plex, *ESI*: enzyme–substrate–inhibitor complex.

We can identify the type of reversible inhibition by observing how a change in the inhibitor's concentration affects the relationship between the rate of reaction and the substrate's concentration. As shown in Figure 13.2.13 , when we display kinetic data using as a Lineweaver-Burk plot it is easy to determine which mechanism is in effect. For example, an increase in slope, a decrease in the *x*-intercept, and no change in the *y*-intercept indicates competitive inhibition. Because the inhibitor's binding is reversible, we can still obtain the same maximum velocity—thus the constant value for the *y*-intercept—by adding enough substrate to completely displace the inhibitor. Because it takes more substrate, the value of K_m increases, which explains the increase in the slope and the decrease in the *x*-intercept's value.

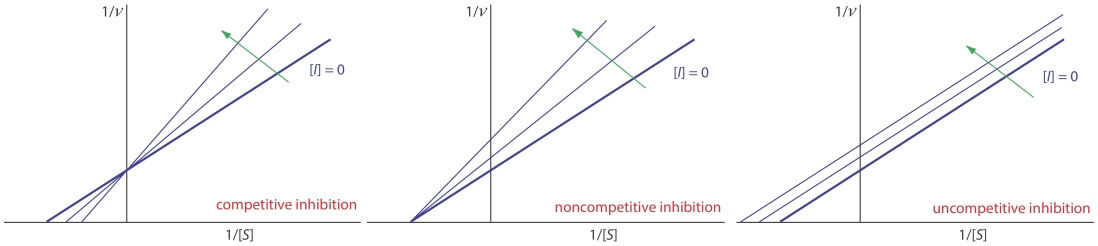

Figure 13.2.13 . Lineweaver–Burk plots for competitive inhibition, noncompetitive inhibition, and uncompetitive inhibition. The thick blue line in each plot shows the kinetic behavior in the absence of inhibitor, and the thin blue lines in each plot show the change in behavior for increasing concentrations of the inhibitor. In each plot, the inhibitor's concentration increases in the direction of the green arrow.

Example 13.2.7

Exercise 13.2.3 provides kinetic data for the oxidation of catechol (the substrate) to *o*-quinone by the enzyme *o*-diphenyl oxidase in the absence of an inhibitor. The following additional data are available when the reaction is run in the presence of *p*-hydroxybenzoic acid, PBHA. Is PBHA an inhibitor for this reaction and, if so, what type of inhibitor is it? The data in this exercise are adapted from jkimball.

[catechol] (mM):	0.3	0.6	1.2	4.8
rate (Δ AU/min):	0.011	0.019	0.022	0.060

Solution

Figure 13.2.14 shows the resulting Lineweaver–Burk plot for the data in Exercise 13.2.3 and Example 13.2.7 . Although the two *y*-intercepts are not identical in value—the result of uncertainty in measuring the rates—the plot suggests that PBHA is a competitive inhibitor for the enzyme's reaction with catechol.

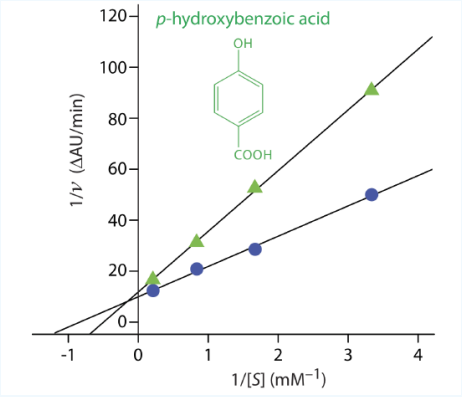

Figure 13.2.14 . Lineweaver–Burk plots for the data in Exercise 13.2.3 and Example 13.2.7 .

Exercise 13.2.4

Exercise 13.2.3 provides kinetic data for the oxidation of catechol (the substrate) to *o*-quinone by the enzyme *o*-diphenyl oxidase in the absence of an inhibitor. The following additional data are available when the reaction is run in the presence of phenylthiourea. Is phenylthiourea an inhibitor for this reaction and, if so, what type of inhibitor is it? The data in this exercise are adapted from jkimball.

[catechol] (mM):	0.3	0.6	1.2	4.8
rate (Δ AU/min):	0.010	0.016	0.024	0.040

Answer

The figure below shows the Lineweaver–Burk plots for the two sets of data. The nearly identical *x*-intercepts suggests that phenylthiourea is a noncompetitive inhibitor.

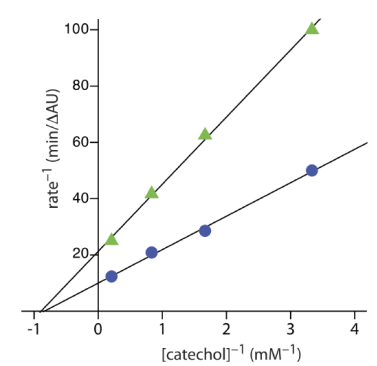

Evaluation of Chemical Kinetic Methods

Scale of Operation

The detection limit for a chemical kinetic method ranges from minor components to ultratrace components, and is determined by two factors: the rate of the reaction and the instrumental technique used to monitor the rate. Because the signal is directly proportional to the reaction's rate, a faster reaction generally results in a lower detection limit. All other factors being equal, detection limits are smaller for catalytic reactions than for noncatalytic reactions. Not surprisingly, some of the earliest chemical kinetic methods took advantage of catalytic reactions. For example, ultratrace levels of Cu (<1 ppb) are determined by measuring its catalytic effect on the redox reaction between hydroquinone and H_2O_2.

In the absence of a catalyst, most chemical kinetic methods for organic compounds use reactions with relatively slow rates, which limits the analysis to minor and to higher concentration trace analytes. Noncatalytic chemical kinetic methods for inorganic compounds that use metal–ligand complexation reactions may be fast or slow, with detection limits ranging from trace to minor analyte.

The second factor that influences a method's detection limit is the instrumentation used to monitor the reaction's progress. Most reactions are monitored spectrophotometrically or electrochemically. The scale of operation for these techniques are discussed in Chapter 10 and Chapter 11.

Accuracy

As noted earlier, a chemical kinetic method potentially is subject to larger errors than an equilibrium method due to the effect of uncontrolled or poorly controlled variables, such as temperature or pH. Although a direct-computation chemical kinetic method can achieve moderately accurate results (a relative error of 1–5%), the accuracy often is much worse. Curve-fitting methods provide significant improvements in accuracy because they use more data. In one study, for example, accuracy was improved by two orders of magnitude—from errors of 500% to 5%—by replacing a direct-computation analysis with a curve-fitting analysis [Pauch, J. B.; Margerum, D. W. *Anal. Chem.* **1969**, *41*, 226–232]. Although not discussed in this chapter, data analysis methods that include the ability to compensate for experimental errors can lead to a significant improvement in accuracy [(a) Holler, F. J.; Calhoun, R. K.; MClanahan, S. F. *Anal. Chem.* **1982**, *54*, 755–761; (b) Wentzel, P. D.; Crouch, S. R. *Anal. Chem.* **1986**, *58*, 2851–2855; (c) Wentzel, P. D.; Crouch, S. R. *Anal. Chem.* **1986**, *58*, 2855–2858].

Precision

The precision of a chemical kinetic method is limited by the signal-to-noise ratio of the instrumentation used to monitor the reaction's progress. When using an integral method, a precision of 1–2% is routinely possible. The precision for a differential method may be somewhat poorer, particularly if the signal is noisy.

Sensitivity

We can improve the sensitivity of a one-point fixed-time integral method by making measurements under conditions where the concentration of the monitored species is as large as possible. When monitoring the analyte's concentration—or the concentration of any other reactant—we want to take measurements early in the reaction before its concentration decreases. On the other hand, if

we choose to monitor one of the reaction's products, then it is better to take measurements at longer times. For a two-point fixed-time integral method, we can improve sensitivity by increasing the difference between times t_1 and t_2. As discussed earlier, the sensitivity of a rate method improves when we choose to measure the initial rate.

Selectivity

The analysis of closely related compounds, as discussed in earlier chapters, often is complicated by their tendency to interfere with each other. To overcome this problem we usually need to separate the analyte and the interferent before completing the analysis. One advantage of a chemical kinetic method is that it often is possible adjust the reaction conditions so that the analyte and the interferent have different reaction rates. If the difference in their respective rates is large enough, then one species will react completely before the other species has a chance to react.

> The need to analyze multiple analytes in complex mixtures is, of course, one of the advantages of the separation techniques covered in Chapter 12. Kinetic techniques provide an alternative approach for simple mixtures.

We can use the appropriate integrated rate laws to find the conditions necessary to separate a faster reacting species from a more slowly reacting species. Let's consider a system that consists of an analyte, *A*, and an interferent, *B*, both of which show first-order kinetics with a common reagent. To avoid an interference, the relative magnitudes of their rate constants must be sufficiently different. The fractions, *f*, of *A* and *B* that remain at any point in time, *t*, are defined by the following equations

$$(f_A)_t = \frac{[A]_t}{[A]_0} \tag{4.2.28}$$

$$(f_B)_t = \frac{[B]_t}{[B]_0} \tag{4.2.29}$$

where $[A]_0$ and $[B]_0$ are the initial concentrations of *A* and *B*, respectively. Rearranging Equation 4.2.2 and substituting in Equation 4.2.28 or Equation 4.2.29 leaves use with the following two equations.

$$\ln \frac{[A]_t}{[A]_0} = \ln (f_A)_t = -k_A t \tag{4.2.30}$$

$$\ln \frac{[B]_t}{[B]_0} = \ln (f_B)_t = -k_B t \tag{4.2.31}$$

where k_A and k_B are the rate constants for *A* and for *B*. Dividing Equation 4.2.30 by Equation 4.2.31 leave us with

$$\frac{k_A}{k_B} = \frac{\ln (f_A)_t}{\ln (f_B)_t}$$

Suppose we want 99% of *A* to react before 1% of *B* reacts. The fraction of *A* that remains is 0.01 and the fraction of *B* that remains is 0.99, which requires that

$$\frac{k_A}{k_B} = \frac{\ln (f_A)_t}{\ln (f_B)_t} = \frac{\ln(0.01)}{\ln(0.99)} = 460$$

the rate constant for *A* must be at least 460 times larger than that for *B*. When this condition is met we can determine the analyte's concentration before the interferent begins to react. If the analyte has the slower reaction, then we can determine its concentration after we allow the interferent to react to completion.

This method of adjusting reaction rates is useful if we need to analyze an analyte in the presence of an interferent, but is impractical if both *A* and *B* are analytes because the condition that favors the analysis of *A* will not favor the analysis of *B*. For example, if we adjust conditions so that 99% of *A* reacts in 5 s, then 99% of *B* must react within 0.01 s if it has the faster kinetics, or in 2300 s if it has the slower kinetics. The reaction of *B* is too fast or too slow to make this a useful analytical method.

What do we do if the difference in the rate constants for *A* and *B* are not significantly different? We still can complete an analysis if we can simultaneously monitor both species. Because both *A* and *B* react at the same time, the integrated form of the first-order rate law becomes

$$C_t = [A]_t + [B]_t = [A]_0 e^{-k_A t} + [B]_0 e^{-k_B t} \tag{4.2.32}$$

where C_t is the total concentration of A and B at time, t. If we measure C_t at times t_1 and t_2, we can solve the resulting pair of simultaneous equations to determine values $[A]_0$ and $[B]_0$. The rate constants k_A and k_B are determined in separate experiments using standard solutions of A and B.

Equation 4.2.32 can also serve as the basis for a curve-fitting method. As shown in Figure 13.2.15 , a plot of $\ln(C_t)$ as a function of time consists of two regions. At shorter times the plot is curved because A and B react simultaneously. At later times, however, the concentration of the faster reacting component, A, decreases to zero, and Equation 4.2.32 simplifies to

$$C_t \approx [B]_t = [B]_0 e^{-k_B t}$$

Under these conditions, a plot of $\ln(C_t)$ versus time is linear. Extrapolating the linear portion to t = 0 gives $[B]_0$, with $[A]_0$ determined by difference.

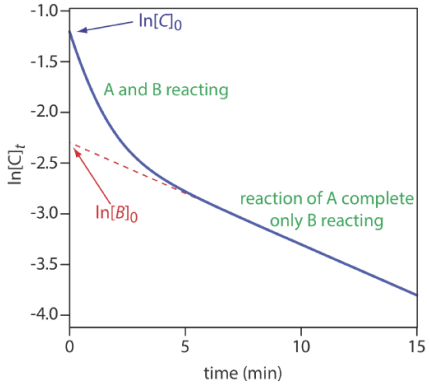

Figure 13.2.15 . Kinetic determination of a slower reacting analyte, B, in the presence of a faster reacting analyte, A. The rate constants for the two analytes are: k_A = 1 min^{-1} and k_B = 0.1 min^{-1}.

Example 13.2.8

Use the data in Figure 13.2.15 to determine the concentrations of A and B in the original sample.

Solution

Extrapolating the linear part of the curve back to t = 0 gives $\ln[B]_0$ as –2.3, or a $[B]_0$ of 0.10 M. At t = 0, $\ln[C]_0$ is –1.2, which corresponds to a $[C]_0$ of 0.30 M. Because $[C]_0 = [A]_0 + [B]_0$, the concentration of A in the original sample is 0.20 M.

Time, Cost, and Equipment

An automated chemical kinetic method of analysis provides a rapid means for analyzing samples, with throughputs ranging from several hundred to several thousand determinations per hour. The initial start-up costs may be fairly high because an automated analysis requires a dedicated instrument designed to meet the specific needs of the analysis. When measurements are handled manually, a chemical kinetic method requires routinely available equipment and instrumentation, although the sample throughput is much lower than with an automated method.

4.3: Radiochemistry

Atoms that have the same number of protons but a different number of neutrons are ***isotopes***. To identify an isotope we use the notation ${}^{A}_{Z}E$, where E is the element's atomic symbol, Z is the element's atomic number, and A is the element's atomic mass number. Although an element's different isotopes have the same chemical properties, their nuclear properties are not identical. The most important difference between isotopes is their stability. The nuclear configuration of a stable isotope remains constant with time. Unstable isotopes, however, disintegrate spontaneously, emitting radioactive particles as they transform into a more stable form.

> An element's atomic number, Z, is equal to the number of protons and its atomic mass, A, is equal to the sum of the number of protons and neutrons. We represent an isotope of carbon-13 as ${}^{13}_{6}\text{C}$ because carbon has six protons and seven neutrons. Sometimes we omit Z from this notation—identifying the element and the atomic number is repetitive because all isotopes of carbon have six protons and any atom that has six protons is an isotope of carbon. Thus, ${}^{13}\text{C}$ and C–13 are alternative notations for this isotope of carbon.

The most important types of radioactive particles are alpha particles, beta particles, gamma rays, and X-rays. An ***alpha particle***, α, is equivalent to a helium nucleus, ${}^{4}_{2}\text{He}$. When an atom emits an alpha particle, the product in a new atom whose atomic number and atomic mass number are, respectively, 2 and 4 less than its unstable parent. The decay of uranium to thorium is one example of alpha emission.

$$ {}^{238}_{92}\text{U} \longrightarrow {}^{234}_{90}\text{Th} + \alpha $$

A beta particle, β, comes in one of two forms. A ***negatron***, ${}^{0}_{-1}\beta$, is produced when a neutron changes into a proton, increasing the atomic number by one, as shown here for lead.

$$ {}^{214}_{82}\text{Pb} \longrightarrow {}^{214}_{83}\text{Bi} + {}^{0}_{-1}\beta $$

The conversion of a proton to a neutron results in the emission of a ***positron***, ${}^{0}_{1}\beta$.

$$ {}^{30}_{15}\text{P} \longrightarrow {}^{30}_{14}\text{Si} + {}^{0}_{1}\beta $$

> A negatron, which is the more common type of beta particle, is equivalent to an electron.

The emission of an alpha or a beta particle often produces an isotope in an unstable, high energy state. This excess energy is released as a ***gamma ray***, γ, or as an X-ray. Gamma ray and X-ray emission may also occur without the release of an alpha particle or a beta particle.

Theory and Practice

A radioactive isotope's rate of decay, or activity, follows first-order kinetics

$$ A = -\frac{dN}{dt} = \lambda N \tag{4.3.1} $$

where A is the isotope's activity, N is the number of radioactive atoms present in the sample at time t, and λ is the isotope's decay constant. Activity is expressed as the number of disintegrations per unit time.

As with any first-order process, we can rewrite Equation 4.3.1 in an integrated form.

$$ N_t = N_0 e^{-\lambda t} \tag{4.3.2} $$

Substituting Equation 4.3.2 into Equation 4.3.2 gives

$$ A = \lambda N_0 e^{-\lambda t} = A_0 e^{-\lambda t} \tag{4.3.3} $$

If we measure a sample's activity at time t we can determine the sample's initial activity, A_0, or the number of radioactive atoms originally present in the sample, N_0.

An important characteristic property of a radioactive isotope is its ***half-life***, $t_{1/2}$, which is the amount of time required for half of the radioactive atoms to disintegrate. For first-order kinetics the half-life is

$$t_{1/2} = \frac{0.693}{\lambda} \tag{4.3.4}$$

Because the half-life is independent of the number of radioactive atoms, it remains constant throughout the decay process. For example, if 50% of the radioactive atoms remain after one half-life, then 25% remain after two half-lives, and 12.5% remain after three half-lives.

> Suppose we begin with an N_0 of 1200 atoms During the first half-life, 600 atoms disintegrate and 600 remain. During the second half-life, 300 of the 600 remaining atoms disintegrate, leaving 300 atoms or 25% of the original 1200 atoms. Of the 300 remaining atoms, only 150 remain after the third half-life, or 12.5% of the original 1200 atoms.

Kinetic information about a radioactive isotope usually is given in terms of its half-life because it provides a more intuitive sense of the isotope's stability. Knowing, for example, that the decay constant for $^{90}_{38}\text{Sr}$ is 0.0247 yr^{-1} does not give an immediate sense of how fast it disintegrates. On the other hand, knowing that its half-life is 28.1 yr makes it clear that the concentration of $^{90}_{38}\text{Sr}$ in a sample remains essentially constant over a short period of time.

Instrumentation

Alpha particles, beta particles, gamma rays, and X-rays are measured by using the particle's energy to produce an amplified pulse of electrical current in a detector. These pulses are counted to give the rate of disintegration. There are three common types of detectors: gas-filled detectors, scintillation counters, and semiconductor detectors. A gas-filled detector consists of a tube that contains an inert gas, such as Ar. When a radioactive particle enters the tube it ionizes the inert gas, producing an Ar^+/e^- ion-pair. Movement of the electron toward the anode and of the Ar^+ toward the cathode generates a measurable electrical current. A ***Geiger counter*** is one example of a gas-filled detector. A ***scintillation counter*** uses a fluorescent material to convert radioactive particles into easy to measure photons. For example, one solid-state scintillation counter consists of a NaI crystal that contains 0.2% TlI, which produces several thousand photons for each radioactive particle. Finally, in a semiconductor detector, adsorption of a single radioactive particle promotes thousands of electrons to the semiconductor's conduction band, increasing conductivity.

Quantitative Applications

In this section we consider three common quantitative radiochemical methods of analysis: the direct analysis of a radioactive isotope by measuring its rate of disintegration, neutron activation, and isotope dilution.

Direct Analysis of Radioactive Analytes

The concentration of a long-lived radioactive isotope remains essentially constant during the period of analysis. As shown in Example 13.3.1 , we can use the sample's activity to calculate the number of radioactive particles in the sample.

Example 13.3.1

The activity in a 10.00-mL sample of wastewater that contains $^{90}_{38}\text{Sr}$ is 9.07×10^6 disintegrations/s. What is the molar concentration of $^{90}_{38}\text{Sr}$ in the sample? The half-life for $^{90}_{38}\text{Sr}$ is 28.1 yr.

Solution

Solving Equation 4.3.4 for λ, substituting into Equation 4.3.1, and solving for N gives

$$N = \frac{A \times t_{1/2}}{0.693}$$

Before we can determine the number of atoms of $^{90}_{38}\text{Sr}$ in the sample we must express its activity and its half-life using the same units. Converting the half-life to seconds gives $t_{1/2}$ as 8.86×10^8 s; thus, there are

$$\frac{\left(9.07 \times 10^6 \text{ disintegrations/s}\right)\left(8.86 \times 10^8 \text{ s}\right)}{0.693} = 1.16 \times 10^{16} \text{ atoms} ^{90}_{38}\text{Sr}$$

The concentration of $^{90}_{38}\text{Sr}$ in the sample is

$$\frac{1.16 \times 10^{16} \text{ atoms } {}^{90}_{38}\text{Sr}}{\left(6.022 \times 10^{23} \text{ atoms/mol}\right)(0.01000\text{L})} = 1.93 \times 10^{-6} \text{ M } {}^{90}_{38}\text{Sr}$$

The direct analysis of a short-lived radioactive isotope using the method outlined in Example 13.3.1 is less useful because it provides only a transient measure of the isotope's concentration. Instead, we can measure its activity after an elapsed time, *t*, and use Equation 4.3.3 to calculate N_0.

Neutron Activation Analysis

Few analytes are naturally radioactive. For many analytes, however, we can induce radioactivity by irradiating the sample with neutrons in a process called ***neutron activation analysis*** (NAA). The radioactive element formed by neutron activation decays to a stable isotope by emitting a gamma ray, and, possibly, other nuclear particles. The rate of gamma-ray emission is proportional to the analyte's initial concentration in the sample. For example, if we place a sample containing non-radioactive ${}^{27}_{13}\text{Al}$ in a nuclear reactor and irradiate it with neutrons, the following nuclear reaction takes place.

$${}^{27}_{13}\text{Al} + {}^{1}_{0}\text{n} \longrightarrow {}^{28}_{13}\text{Al}$$

The radioactive isotope of ${}^{13}\text{Al}$ has a characteristic decay process that includes the release of a beta particle and a gamma ray.

$${}^{28}_{13}\text{Al} \longrightarrow {}^{28}_{14}\text{Al} + {}^{0}_{-1}\beta + \gamma$$

When irradiation is complete, we remove the sample from the nuclear reactor, allow any short-lived radioactive interferences to decay into the background, and measure the rate of gamma-ray emission.

The initial activity at the end of irradiation depends on the number of atoms that are present. This, in turn, is a equal to the difference between the rate of formation for ${}^{28}_{13}\text{Al}$ and its rate of disintegration

$$\frac{dN_{{}^{28}_{13}\text{Al}}}{dt} = \Phi\sigma N_{{}^{27}_{13}\text{Al}} - \lambda N_{{}^{28}_{13}\text{Al}} \tag{4.3.5}$$

where Φ is the neutron flux and σ is the reaction cross-section, or probability that a ${}^{27}_{13}\text{Al}$ nucleus captures a neutron. Integrating Equation 4.3.5 over the time of irradiation, t_i, and multiplying by λ gives the initial activity, A_0, at the end of irradiation as

$$A_0 = \lambda N_{{}^{28}_{13}\text{Al}} = \Phi\sigma N_{{}^{27}_{13}\text{Al}}(1 - e^{-kt})$$

If we know the values for A_0, Φ, σ, λ, and t_i, then we can calculate the number of atoms of ${}^{27}_{13}\text{Al}$ initially present in the sample.

A simpler approach is to use one or more external standards. Letting $(A_0)_x$ and $(A_0)_s$ represent the analyte's initial activity in an unknown and in an external standard, and letting w_x and w_s represent the analyte's weight in the unknown and in the external standard, we obtain the following pair of equations

$$(A_0)_x = kw_x \tag{4.3.6}$$

$$(A_0)_s = kw_s \tag{4.3.7}$$

that we can solve to determine the analyte's mass in the sample.

As noted earlier, gamma ray emission is measured following a period during which we allow short-lived interferents to decay into the background. As shown in Figure 13.3.1 , we determine the sample's or the standard's initial activity by extrapolating a curve of activity versus time back to *t* = 0. Alternatively, if we irradiate the sample and the standard at the same time, and if we measure their activities at the same time, then we can substitute these activities for $(A_0)_x$ and $(A_0)_s$. This is the strategy used in the following example.

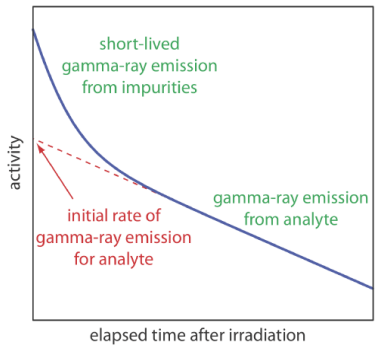

Figure 13.3.1 . Plot of gamma-ray emission as a function of time showing how the analyte's initial activity is determined.

Example 13.3.2

The concentration of Mn in steel is determined by a neutron activation analysis using the method of external standards. A 1.000-g sample of an unknown steel sample and a 0.950-g sample of a standard steel known to contain 0.463% w/w Mn are irradiated with neutrons for 10 h in a nuclear reactor. After a 40-min delay the gamma ray emission is 2542 cpm (counts per minute) for the unknown and 1984 cpm for the external standard. What is the %w/w Mn in the unknown steel sample?

Solution

Combining equations 4.3.6 and 4.3.7 gives

$$w_x = \frac{A_x}{A_s} \times w_s$$

The weight of Mn in the external standard is

$$w_s = \frac{0.00463 \text{ g Mn}}{\text{g steel}} \times 0.950 \text{ g steel} = 0.00440 \text{ g Mn}$$

Substituting into the above equation gives

$$w_x = \frac{2542 \text{ cpm}}{1984 \text{ cpm}} \times 0.00440 \text{ g Mn} = 0.00564 \text{ g Mn}$$

Because the original mass of steel is 1.000 g, the %w/w Mn is 0.564%.

Among the advantages of neutron activation are its applicability to almost all elements in the periodic table and that it is nondestructive to the sample. Consequently, NAA is an important technique for analyzing archeological and forensic samples, as well as works of art.

Isotope Dilution

Another important radiochemical method for the analysis of nonradioactive analytes is ***isotope dilution***. An external source of analyte is prepared in a radioactive form with a known activity, A_T, for its radioactive decay—we call this form of the analyte a ***tracer***. To prepare a sample for analysis we add a known mass of the tracer, w_T, to a portion of sample that contains an unknown mass, w_x , of analyte. After homogenizing the sample and tracer, we isolate w_A grams of analyte by using a series of appropriate chemical and physical treatments. Because these chemical and physical treatments cannot distinguish between radioactive and nonradioactive forms of the analyte, the isolated material contains both. Finally, we measure the activity of the isolated sample, A_A. If we recover all the analyte—both the radioactive tracer and the nonradioactive analyte—then A_A and A_T are equal and $w_x = w_A - w_T$. Normally, we fail to recover all the analyte. In this case A_A is less than A_T, and

$$A_A = A_T \times \frac{w_A}{w_x + w_T} \tag{4.3.8}$$

The ratio of weights in Equation 4.3.8 accounts for any loss of activity that results from our failure to recover all the analyte. Solving Equation 4.3.8 for w_x gives

$$w_x = \frac{A_T}{A_A} w_A - w_T \tag{4.3.9}$$

How we process the sample depends on the analyte and the sample's matrix. We might, for example, digest the sample to bring the analyte into solution. After filtering the sample to remove the residual solids, we might precipitate the analyte, isolate it by filtration, dry it in an oven, and obtain its weight.

Given that the goal of an analysis is to determine the amount of nonradioactive analyte in our sample, the realization that we might not recover all the analyte might strike you as unsettling. Recall from Chapter 7.7, that a single liquid–liquid extraction rarely has an extraction efficiency of 100%. One advantage of isotope dilution is that the extraction efficiency for the nonradioactive analyte and for the tracer are the same. If we recover 50% of the tracer, then we also recover 50% of the nonradioactive analyte. Because we know how much tracer we added to the sample, we can determine how much of the nonradioactive analyte is in the sample.

Example 13.3.3

The concentration of insulin in a production vat is determined by isotope dilution. A 1.00-mg sample of insulin labeled with ^{14}C having an activity of 549 cpm is added to a 10.0-mL sample taken from the production vat. After homogenizing the sample, a portion of the insulin is separated and purified, yielding 18.3 mg of pure insulin. The activity for the isolated insulin is measured at 148 cpm. How many mg of insulin are in the original sample?

Solution

Substituting known values into Equation 4.3.8 gives

$$w_x = \frac{549 \text{ cpm}}{148 \text{ cpm}} \times 18.3 \text{ mg} - 1.00 \text{ mg} = 66.9 \text{ mg insulin}$$

Equation 4.3.8 and Equation 4.3.9 are valid only if the tracer's half-life is considerably longer than the time it takes to conduct the analysis. If this is not the case, then the decrease in activity is due both to the incomplete recovery and the natural decrease in the tracer's activity. Table 13.3.1 provides a list of several common tracers for isotope dilution.

Table 13.3.1 . Common Tracers for Isotope Dilution

isotope	half-life
^{3}H	12.5 years
^{14}C	5730 years
^{32}P	14.3 days
^{35}S	87.1 days
^{45}Ca	152 days
^{55}Fe	2.91 years
^{60}Co	5.3 years
^{131}I	8 days

An important feature of isotope dilution is that it is not necessary to recover all the analyte to determine the amount of analyte present in the original sample. Isotope dilution, therefore, is useful for the analysis of samples with complex matrices, where a complete recovery of the analyte is difficult.

Characterization Applications

One example of a characterization application is the determination of a sample's age based on the decay of a radioactive isotope naturally present in the sample. The most common example is carbon-14 dating, which is used to determine the age of natural organic materials.

As cosmic rays pass through the upper atmosphere, some $^{14}_{7}\text{N}$ atoms in the atmosphere capture high energy neutrons, converting them into $^{14}_{6}\text{C}$. The $^{14}_{6}\text{C}$ then migrates into the lower atmosphere where it oxidizes to form C-14 labeled CO_2. Animals and plants subsequently incorporate this labeled CO_2 into their tissues. Because this is a steady-state process, all plants and animals have the same ratio of $^{14}_{6}\text{C}$ to $^{12}_{6}\text{C}$ in their tissues. When an organism dies, the radioactive decay of $^{14}_{6}\text{C}$ to $^{14}_{7}\text{N}$ by $^{0}_{-1}\beta$ emission (t = 5730 years) leads to predictable reduction in the $^{14}_{6}\text{C}$ to $^{12}_{6}\text{C}$ ratio. We can use the change in this ratio to date samples that are as much as 30000 years old, although the precision of the analysis is best when the sample's age is less than 7000 years. The accuracy of carbon-14 dating depends upon our assumption that the natural $^{14}_{6}\text{C}$ to $^{12}_{6}\text{C}$ ratio in the atmosphere is constant over time. Some variation in the ratio has occurred as the result of the increased consumption of fossil fuels and the production of $^{14}_{6}\text{C}$ during the testing of nuclear weapons. A calibration curve prepared using samples of known age—examples of samples include tree rings, deep ocean sediments, coral samples, and cave deposits—limits this source of uncertainty.

There is no need to prepare a calibration curve for each analysis. Instead, there is a universal calibration curve known as IntCal. The most recent such curve, IntCal13 is described in the following paper: Reimer, P. J., et. al. "IntCal13 and Marine 13 Radiocarbon Age Calibration Curve 0–50,000 Years Cal BP," *Radiocarbon* **2013**, *55*, 1869–1887. This calibration spans 50 000 years before the present (BP).

Example 13.3.4

To determine the age of a fabric sample, the relative ratio of $^{14}_{6}\text{C}$ to $^{12}_{6}\text{C}$ was measured yielding a result of 80.9% of that found in modern fibers. How old is the fabric?

Solution

Equation 4.3.3 and Equation 4.3.4 provide us with a method to convert a change in the ratio of $^{14}_{6}\text{C}$ to $^{12}_{6}\text{C}$ to the fabric's age. Letting A_0 be the ratio of $^{14}_{6}\text{C}$ to $^{12}_{6}\text{C}$ in modern fibers, we assign it a value of 1.00. The ratio of $^{14}_{6}\text{C}$ to $^{12}_{6}\text{C}$ in the sample, A, is 0.809. Solving gives

$$t = \ln\frac{A_0}{A} \times \frac{t_{1/2}}{0.693} = \ln\frac{1.00}{0.809} \times \frac{5730\text{ yr}}{0.693} = 1750\text{ yr}$$

Other isotopes can be used to determine a sample's age. The age of rocks, for example, has been determined from the ratio of the number of $^{238}_{92}\text{U}$ to the number of stable $^{206}_{82}\text{Pb}$ atoms produced by radioactive decay. For rocks that do not contain uranium, dating is accomplished by comparing the ratio of radioactive $^{40}_{19}\text{K}$ to the stable $^{40}_{18}\text{Ar}$. Another example is the dating of sediments collected from lakes by measuring the amount of $^{210}_{82}\text{Pb}$ that is present.

Evaluation

Radiochemical methods routinely are used for the analysis of trace analytes in macro and meso samples. The accuracy and precision of radiochemical methods generally are within the range of 1–5%. We can improve the precision—which is limited by the random nature of radioactive decay—by counting the emission of radioactive particles for as long a time as is practical. If the number of counts, M, is reasonably large ($M \geq 100$), and the counting period is significantly less than the isotope's half-life, then the percent relative standard deviation for the activity, $(\sigma_A)_{rel}$, is approximately

$$(\sigma_A)_{\text{rel}} = \frac{1}{\sqrt{M}} \times 100$$

For example, if we determine the activity by counting 10 000 radioactive particles, then the relative standard deviation is 1%. A radiochemical method's sensitivity is inversely proportional to $(\sigma_A)_{rel}$, which means we can improve the sensitivity by counting more particles.

Selectivity rarely is of concern when using a radiochemical method because most samples have only a single radioactive isotope. When several radioactive isotopes are present, we can determine each isotope's activity by taking advantage of differences in the energies of their respective radioactive particles or differences in their respective decay rates.

In comparison to most other analytical techniques, radiochemical methods usually are more expensive and require more time to complete an analysis. Radiochemical methods also are subject to significant safety concerns due to the analyst's potential exposure to high energy radiation and the need to safely dispose of radioactive waste.

4.4: Flow Injection Analysis

The focus of this chapter is on methods in which we measure a time-dependent signal. Chemical kinetic methods and radiochemical methods are two examples. In this section we consider the technique of flow injection analysis in which we inject the sample into a flowing carrier stream that gives rise to a transient signal at the detector. Because the shape of this transient signal depends on the physical and chemical kinetic processes that take place in the carrier stream during the time between injection and detection, we include flow injection analysis in this chapter.

Theory and Practice

Flow injection analysis (FIA) was developed in the mid-1970s as a highly efficient technique for the automated analyses of samples [see, for example, (a) Ruzicka, J.; Hansen, E. H. *Anal. Chim. Acta* **1975**, *78*, 145–157; (b) Stewart, K. K.; Beecher, G. R.; Hare, P. E. *Anal. Biochem.* **1976**, *70*, 167–173; (c) Valcárcel, M.; Luque de Castro, M. D. *Flow Injection Analysis: Principles and Applications*, Ellis Horwood: Chichester, England, 1987]. Unlike the centrifugal analyzer described earlier in this chapter (see Figure 13.2.8), in which the number of samples is limited by the transfer disk's size, FIA allows for the rapid, sequential analysis of an unlimited number of samples. FIA is one example of a continuous-flow analyzer, in which we sequentially introduce samples at regular intervals into a liquid carrier stream that transports them to the detector.

A schematic diagram detailing the basic components of a flow injection analyzer is shown in Figure 13.4.1 . The reagent that serves as the carrier is stored in a reservoir, and a propelling unit maintains a constant flow of the carrier through a system of tubing that comprises the transport system. We inject the sample directly into the flowing carrier stream, where it travels through one or more mixing and reaction zones before it reaches the detector's flow-cell. Figure 13.4.1 is the simplest design for a flow injection analyzer, which consists of a single channel and a single reagent reservoir. Multiple channel instruments that merge together separate channels, each of which introduces a new reagent into the carrier stream, also are possible. A more detailed discussion of FIA instrumentation is found in the next section.

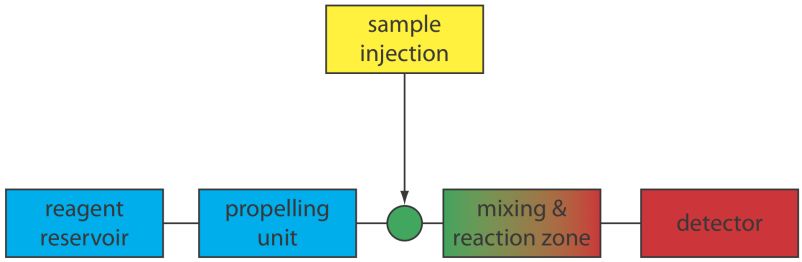

Figure 13.4.1 . Schematic diagram of a simple flow injection analyzer showing its basic components. After its injection into the carrier stream the samples mixes and reacts with the carrier stream's reagents before reaching the detector.

When we first inject a sample into the carrier stream it has the rectangular flow profile of width *w* shown in Figure 13.4.2 a. As the sample moves through the mixing zone and the reaction zone, the width of its flow profile increases as the sample disperses into the carrier stream. Dispersion results from two processes: convection due to the flow of the carrier stream and diffusion due to the concentration gradient between the sample and the carrier stream. Convection occurs by laminar flow. The linear velocity of the sample at the tube's walls is zero, but the sample at the center of the tube moves with a linear velocity twice that of the carrier stream. The result is the parabolic flow profile shown in Figure 13.4.2 b. Convection is the primary means of dispersion in the first 100 ms following the sample's injection.

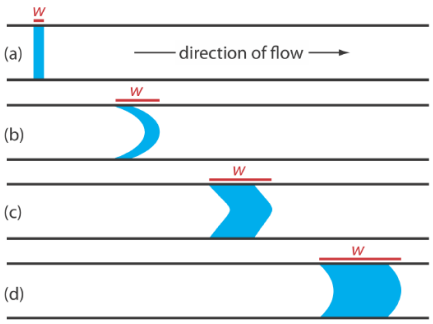

Figure 13.4.2 . Effect of dispersion on the shape of a sample's flow profile, shown in blue, at different times during a flow injection analysis: (a) at injection; (b) when convection dominates dispersion; (c) when convection and diffusion contribute to dispersion; and (d) when diffusion dominates dispersion. The red line shows the width, *w*, of the samples flow profile.

The second contribution to the sample's dispersion is diffusion due to the concentration gradient that exists between the sample and the carrier stream. As shown in Figure 13.20, diffusion occurs parallel (axially) and perpendicular (radially) to the direction in which the carrier stream is moving. Only radial diffusion is important in a flow injection analysis. Radial diffusion decreases the sample's linear velocity at the center of the tubing, while the sample at the edge of the tubing experiences an increase in its linear velocity. Diffusion helps to maintain the integrity of the sample's flow profile (Figure 13.4.2 c) and prevents adjacent samples in the carrier stream from dispersing into one another. Both convection and diffusion make significant contributions to dispersion from approximately 3–20 s after the sample's injection. This is the normal time scale for a flow injection analysis. After approximately 25 s, diffusion is the only significant contributor to dispersion, resulting in a flow profile similar to that shown in Figure 13.4.2 d.

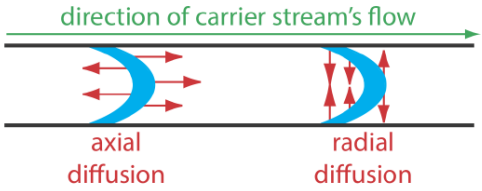

Figure 13.4.3 . Illustration showing axial and radial diffusion. The blue band is the sample's flow profile and the red arrows indicate the direction of diffusion.

An FIA curve, or ***fiagram***, is a plot of the detector's signal as a function of time. Figure 13.4.4 shows a typical fiagram for conditions in which both convection and diffusion contribute to the sample's dispersion. Also shown on the figure are several parameters that characterize a sample's fiagram. Two parameters define the time for a sample to move from the injector to the detector. Travel time, t_a, is the time between the sample's injection and the arrival of its leading edge at the detector. Residence time, T, on the other hand, is the time required to obtain the maximum signal. The difference between the residence time and the travel time is t', which approaches zero when convection is the primary means of dispersion, and increases in value as the contribution from diffusion becomes more important.

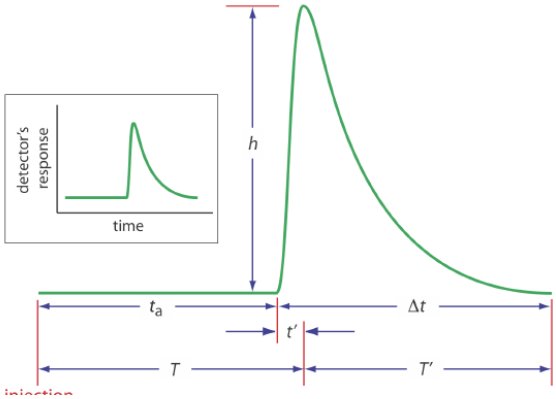

Figure 13.4.4 . Typical fiagram for flow injection analysis showing the detector's response as a function of time. See the text for an explanation of the parameters, t_a, t', Δt, T', and h.

The time required for the sample to pass through the detector's flow cell—and for the signal to return to the baseline—is also described by two parameters. The baseline-to-baseline time, Δt, is the time between the arrival of the sample's leading edge to the departure of its trailing edge. The elapsed time between the maximum signal and its return to the baseline is the return time, T'. The final characteristic parameter of a fiagram is the sample's peak height, *h*.

Of the six parameters shown in Figure 13.4.4 , the most important are peak height and the return time. Peak height is important because it is directly or indirectly related to the analyte's concentration. The sensitivity of an FIA method, therefore, is determined by the peak height. The return time is important because it determines the frequency with which we may inject samples. Figure 13.4.5 shows that if we inject a second sample at a time T' after we inject the first sample, there is little overlap of the two FIA curves. By injecting samples at intervals of T', we obtain the maximum possible sampling rate.

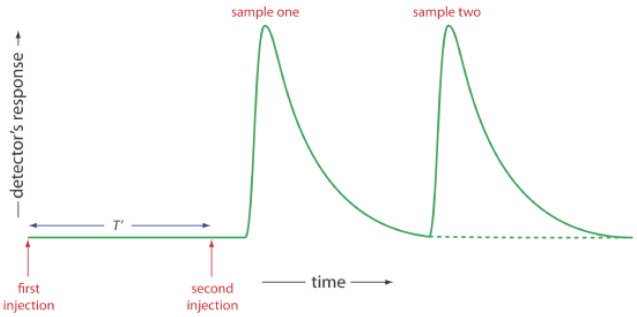

Figure 13.4.5 . Effect of return time, T', on sampling frequency.

Peak heights and return times are influenced by the dispersion of the sample's flow profile and by the physical and chemical properties of the flow injection system. Physical parameters that affect *h* and T' include the volume of sample we inject, the flow rate, the length, diameter and geometry of the mixing zone and the reaction zone, and the presence of junctions where separate channels merge together. The kinetics of any chemical reactions between the sample and the reagents in the carrier stream also influ-ence the peak height and return time.

Unfortunately, there is no good theory that we can use to consistently predict the peak height and the return time for a given set of physical and chemical parameters. The design of a flow injection analyzer for a particular analytical problem still occurs largely by a process of experimentation. Nevertheless, we can make some general observations about the effects of physical and chemical parameters. In the absence of chemical effects, we can improve sensitivity—that is, obtain larger peak heights—by injecting larger samples, by increasing the flow rate, by decreasing the length and diameter of the tubing in the mixing zone and the reaction zone, and by merging separate channels before the point where the sample is injected. With the exception of sample volume, we can increase the sampling rate—that is, decrease the return time—by using the same combination of physical parameters. Larger sample volumes, however, lead to longer return times and a decrease in sample throughput. The effect of chemical reactivity depends on whether the species we are monitoring is a reactant or a product. For example, if we are monitoring a reactant, we can improve sensitivity by choosing conditions that decrease the residence time, *T*, or by adjusting the carrier stream's composition so that the reaction occurs more slowly.

Instrumentation

The basic components of a flow injection analyzer are shown in Figure 13.4.6 and include a pump to propel the carrier stream and the reagent streams, a means to inject the sample into the carrier stream, and a detector to monitor the composition of the carrier stream. Connecting these units is a transport system that brings together separate channels and provides time for the sample to mix with the carrier stream and to react with the reagent streams. We also can incorporate separation modules into the transport system. Each of these components is considered in greater detail in this section.

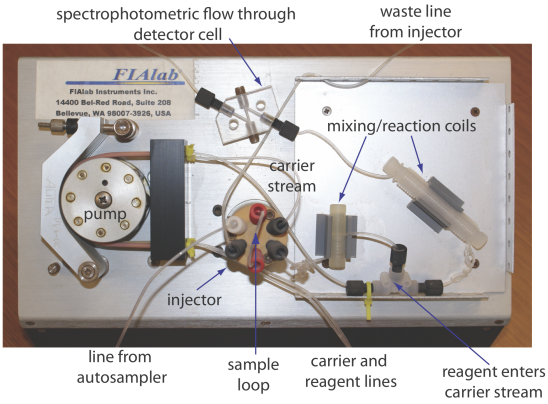

Figure 13.4.6 . Example of a typical flow injection analyzer that shows the pump, the injector, the transport system, which consists of mixing/reaction coils and junctions, and the detector (minus the spectrophotometer). This particular configuration has two channels: the carrier stream and a reagent line.

Propelling Unit

The propelling unit moves the carrier stream through the flow injection analyzer. Although several different propelling units have been used, the most common is a ***peristaltic pump***, which, as shown in Figure 13.4.7 , consists of a set of rollers attached to the outside of a rotating drum. Tubing from the reagent reservoirs fits between the rollers and a fixed plate. As the drum rotates the rollers squeeze the tubing, forcing the contents of the tubing to move in the direction of the rotation. Peristaltic pumps provide a constant flow rate, which is controlled by the drum's speed of rotation and the inner diameter of the tubing. Flow rates from 0.0005–40 mL/min are possible, which is more than adequate to meet the needs of FIA where flow rates of 0.5–2.5 mL/min are common. One limitation to a peristaltic pump is that it produces a pulsed flow—particularly at higher flow rates—that may lead to oscillations in the signal.

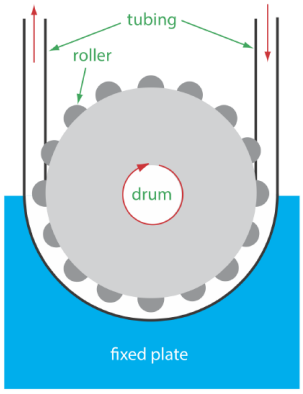

Figure 13.4.7 . Schematic diagram of a peristaltic pump.

Injector

The sample, typically 5–200 μL, is injected into the carrier stream. Although syringe injections through a rubber septum are possible, the more common method—as seen in Figure 13.4.6 —is to use a rotary, or loop injector similar to that used in an HPLC. This type of injector provides for a reproducible sample volume and is easily adaptable to automation, an important feature when high sampling rates are needed.

Detector

The most common detectors for flow injection analysis are the electrochemical and optical detectors used in HPLC. These detectors are discussed in Chapter 12 and are not considered further in this section. FIA detectors also have been designed around the use of ion selective electrodes and atomic absorption spectroscopy.

Transport System

The heart of a flow injection analyzer is the transport system that brings together the carrier stream, the sample, and any reagents that react with the sample. Each reagent stream is considered a separate channel, and all channels must merge before the carrier stream reaches the detector. The complete transport system is called a ***manifold***.

The simplest manifold has a single channel, the basic outline of which is shown in Figure 13.4.8 . This type of manifold is used for direct analysis of analyte that does not require a chemical reaction. In this case the carrier stream serves only as a means for rapidly and reproducibly transporting the sample to the detector. For example, this manifold design has been used for sample introduction in atomic absorption spectroscopy, achieving sampling rates as high as 700 samples/h. A single-channel manifold also is used for determining a sample's pH or determining the concentration of metal ions using an ion selective electrode.

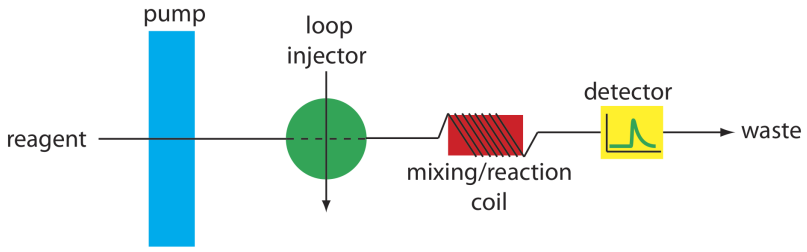

Figure 13.4.8 . Example of a single-channel manifold in which the reagent serves as the carrier stream and as a species that reacts with the sample. The mixing/reaction coil is wrapped around a plastic cylinder.

We can also use the single-channel manifold in Figure 13.4.8 for an analysis in which we monitor the product of a chemical reaction between the sample and a reactant. In this case the carrier stream both transports the sample to the detector and reacts with the sample. Because the sample must mix with the carrier stream, a lower flow rate is used. One example is the determination of chloride in water, which is based on the following sequence of reactions.

$$\mathrm{Hg(SCN)_2}(aq) + 2\mathrm{Cl^-}(aq) \rightleftharpoons \mathrm{HgCl_2}(aq) + 2\mathrm{SCN^-}(aq)$$

$$\mathrm{Fe^{3+}}(aq) + \mathrm{SCN^-}(aq) \rightleftharpoons \mathrm{Fe(SCN)^{2+}}(aq)$$

The carrier stream consists of an acidic solution of $Hg(SCN)_2$ and Fe^{3+}. Injecting a sample that contains chloride into the carrier stream displaces thiocyanate from $Hg(SCN)_2$. The displaced thiocyanate then reacts with Fe^{3+} to form the red-colored $Fe(SCN)^{2+}$ complex, the absorbance of which is monitored at a wavelength of 480 nm. Sampling rates of approximately 120 samples per hour have been achieved with this system [Hansen, E. H.; Ruzicka, J. *J. Chem. Educ.* **1979**, *56*, 677–680].

Most flow injection analyses that include a chemical reaction use a manifold with two or more channels. Including additional channels provides more control over the mixing of reagents and the interaction between the reagents and the sample. Two configurations are possible for a dual-channel system. A dual-channel manifold, such as the one shown in Figure 13.4.9 a, is used when the reagents cannot be premixed because of their reactivity. For example, in acidic solutions phosphate reacts with molybdate to form the heteropoly acid $H_3P(Mo_{12}O_{40})$. In the presence of ascorbic acid the molybdenum in the heteropoly acid is reduced from Mo(VI) to Mo(V), forming a blue-colored complex that is monitored spectrophotometrically at 660 nm [Hansen, E. H.; Ruzicka, J. *J. Chem. Educ.* **1979**, *56*, 677–680]. Because ascorbic acid reduces molybdate, the two reagents are placed in separate channels that merge just before the loop injector.

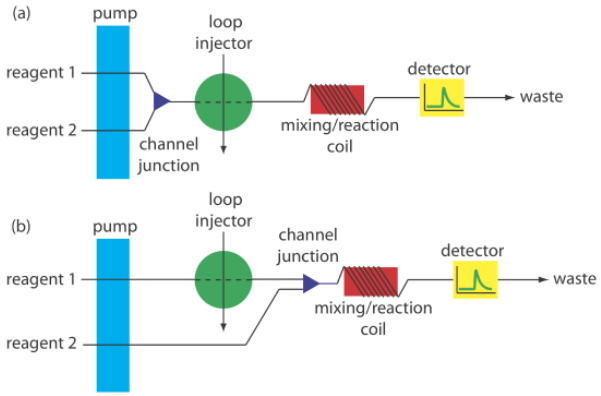

Figure 13.4.9 . Two examples of a dual-channel manifold for flow injection analysis. In (a) the two channels merge before the loop injector, and in (b) the two channels merge after the loop injector.

A dual-channel manifold also is used to add a second reagent after injecting the sample into a carrier stream, as shown in Figure 13.4.9 b. This style of manifold is used for the quantitative analysis of many analytes, including the determination of a wastewater's chemical oxygen demand (COD) [Korenaga, T.; Ikatsu, H. *Anal. Chim. Acta* **1982**, *141*, 301–309]. Chemical oxygen

demand is a measure of the amount organic matter in the wastewater sample. In the conventional method of analysis, COD is determined by refluxing the sample for 2 h in the presence of acid and a strong oxidizing agent, such as $K_2Cr_2O_7$ or $KMnO_4$. When refluxing is complete, the amount of oxidant consumed in the reaction is determined by a redox titration. In the flow injection version of this analysis, the sample is injected into a carrier stream of aqueous H_2SO_4, which merges with a solution of the oxidant from a secondary channel. The oxidation reaction is kinetically slow and, as a result, the mixing coil and the reaction coil are very long—typically 40 m—and submerged in a thermostated bath. The sampling rate is lower than that for most flow injection analyses, but at 10–30 samples/h it is substantially greater than the redox titrimetric method.

More complex manifolds involving three or more channels are common, but the possible combination of designs is too numerous to discuss. One example of a four-channel manifold is shown in Figure 13.4.10 .

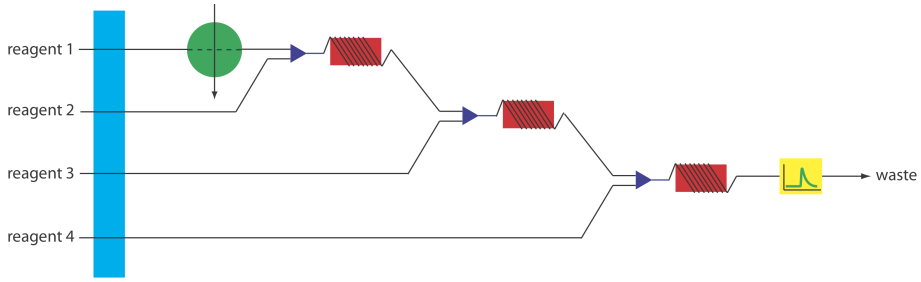

Figure 13.4.10 . Example of a four-channel manifold for a flow injection analysis.

Separation Modules

By incorporating a separation module into the flow injection manifold we can include a separation—dialysis, gaseous diffusion and liquid-liquid extractions are examples—in a flow injection analysis. Although these separations are never complete, they are reproducible if we carefully control the experimental conditions.

Dialysis and gaseous diffusion are accomplished by placing a semipermeable membrane between the carrier stream containing the sample and an acceptor stream, as shown in Figure 13.4.11 . As the sample stream passes through the separation module, a portion of those species that can cross the semipermeable membrane do so, entering the acceptor stream. This type of separation module is common for the analysis of clinical samples, such as serum and urine, where a dialysis membrane separates the analyte from its complex matrix. Semipermeable gaseous diffusion membranes are used for the determination of ammonia and carbon dioxide in blood. For example, ammonia is determined by injecting the sample into a carrier stream of aqueous NaOH. Ammonia diffuses across the semipermeable membrane into an acceptor stream that contains an acid–base indicator. The resulting acid–base reaction between ammonia and the indicator is monitored spectrophotometrically.

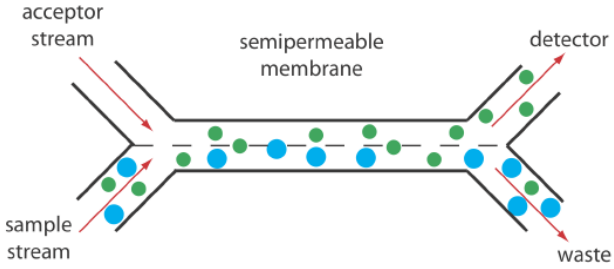

Figure 13.4.11 . Separation module for a flow injection analysis using a semipermeable membrane. The smaller green solutes can pass through the semipermeable membrane and enter the acceptor stream, but the larger blue solutes cannot. Although the separation is not complete—note that some of the green solute remains in the sample stream and exits as waste—it is reproducible if we do not change the experimental conditions.

Liquid–liquid extractions are accomplished by merging together two immiscible fluids, each carried in a separate channel. The result is a segmented flow through the separation module, consisting of alternating portions of the two phases. At the outlet of the separation module the two fluids are separated by taking advantage of the difference in their densities. Figure 13.4.12 shows a typical configuration for a separation module in which the sample is injected into an aqueous phase and extracted into a less dense organic phase that passes through the detector.

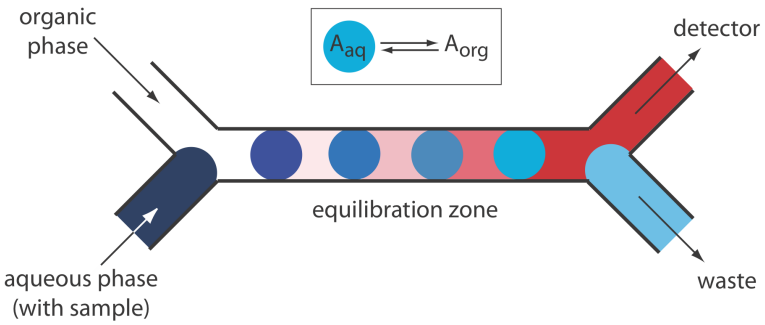

Figure 13.4.12 . Separation module for flow injection analysis using a liquid–liquid extraction. The inset shows the equilibrium reaction. As the sample moves through the equilibration zone, the analyte extracts into the organic phase.

Quantitative Applications

In a quantitative flow injection method a calibration curve is determined by injecting a series of external standards that contain known concentrations of analyte. The calibration curve's format—examples include plots of absorbance versus concentration and of potential versus concentration—depends on the method of detection. Calibration curves for standard spectroscopic and electrochemical methods are discussed in Chapter 10 and in Chapter 11, respectively and are not considered further in this chapter.

Flow injection analysis has been used to analyze a wide variety of samples, including environmental, clinical, agricultural, industrial, and pharmaceutical samples. The majority of analyses involve environmental and clinical samples, which is the focus of this section.

Quantitative flow injection methods have been developed for cationic, anionic, and molecular pollutants in wastewater, freshwaters, groundwaters, and marine waters, three examples of which were described in the previous section. Table 13.4.1 provides a partial listing of other analytes that have been determined using FIA, many of which are modifications of standard spectrophotometric and potentiometric methods. An additional advantage of FIA for environmental analysis is the ability to provide for the continuous, in situ monitoring of pollutants in the field [Andrew, K. N.; Blundell, N. J.; Price, D.; Worsfold, P. J. *Anal. Chem.* **1994**, *66*, 916A–922A].

Table 13.4.1 . Selected Flow Injection Analysis Methods for Environmental Samples

analyte	sample	sample volume (µL)	concentration range	sampling frequency (h^{-1})
Ca^{2+}	freshwater	20	0.8–7.2 ppm	80
Cu^{2+}	groundwater	70–700	100–400 ppb	20
Pb^{2+}	groundwater	70–700	0–40 ppb	20
Zn^{2+}	seawater	1000	1–100 ppb	30–60
NH_4^+	seawater	60	0.18–18.1 ppb	288
NO_3^-	rainwater	1000	1–10 ppb	40
SO_4^{2-}	freshwater	400	4–140 ppb	180
CN^-	industrial	10	0.3–100 ppm	40

Source: Adapted from Valcárcel, M.; Luque de Castro, M. D. *Flow-Injection Analysis: Principles and Practice*, Ellis Horwood: Chichester, England, 1987.

As noted in Chapter 9, several standard methods for the analysis of water involve an acid–base, complexation, or redox titration. It is easy to adapt these titrations to FIA using a single-channel manifold similar to that shown in Figure 13.4.8 [Ramsing, A. U.; Ruzicka, J.; Hansen, E. H. *Anal. Chim. Acta* **1981**, *129*, 1–17]. The titrant—whose concentration must be stoichiometrically less than that of the analyte—and a visual indicator are placed in the reagent reservoir and pumped continuously through the manifold. When we inject the sample it mixes thoroughly with the titrant in the carrier stream. The reaction between the analyte, which is in excess, and the titrant produces a relatively broad rectangular flow profile for the sample. As the sample moves toward the detector, additional mixing oc- curs and the width of the sample's flow profile decreases. When the sample passes through the detector, we

determine the width of its flow profile, ΔT, by monitoring the indicator's absorbance. A calibration curve of ΔT versus log[analyte] is prepared using standard solutions of analyte.

Flow injection analysis has also found numerous applications in the analysis of clinical samples, using both enzymatic and nonenzymatic methods. Table 13.4.2 summarizes several examples.

Table 13.4.2 . Selected Flow Injection Analysis Methods for Clinical Samples

analyte	sample	sample volume (µL)	concentration range	sampling frequency (h^{-1})
nonenzymatic methods				
Cu^{2+}	serum	20	0.7–1.5 ppm	70
Cl^-	serum	60	50–150 meq/L	125
PO_4^{3-}	serum	200	10–60 ppm	130
total CO_2	serum	50	10–50 mM	70
chlorpromazine	blood plasma	200	1.5–9 μM	24
enzymatic methods				
glucose	blood serum	26.5	0.5–15 mM	60
urea	blood serum	30	4–20 mM	60
ethanol	blood	30	5–30 ppm	50

Source: Adapted from Valcárcel, M.; Luque de Castro, M. D. *Flow-Injection Analysis: Principles and Practice*, Ellis Horwood: Chichester, England, 1987.

The best way to appreciate the theoretical and the practical details discussed in this section is to carefully examine a typical analytical method. Although each method is unique, the following description of the determination of phosphate provides an instructive example of a typical procedure. The description here is based on Guy, R. D.; Ramaley, L.; Wentzell, P. D. "An Experiment in the Sampling of Solids for Chemical Analysis," *J. Chem. Educ.* **1998**, *75*, 1028–1033. As the title suggests, the primary focus of this chapter is on sampling. A flow injection analysis, however, is used to analyze samples.

Representative Method 13.4.1: Determination of Phosphate by FIA

Description of Method

The FIA determination of phosphate is an adaptation of a standard spectrophotometric analysis for phosphate. In the presence of acid, phosphate reacts with ammonium molybdate to form a yellow-colored complex in which molybdenum is present as Mo(VI).

$$H_3PO_4(aq) + 12H_2MoO_4(aq) \rightleftharpoons H_3P(Mo_{12}O_{40})(aq) + 12H_2O(l)$$

In the presence of a reducing agent, such as ascorbic acid, the yellow-colored complex is reduced to a blue-colored complex of Mo(V).

Procedure

Prepare the following three solutions: (a) 5.0 mM ammonium molybdate in 0.40 M HNO_3; (b) 0.7% w/v ascorbic acid in 1% v/v glycerin; and a (c) 100.0 ppm phosphate standard using KH_2PO_4. Using the phosphate standard, prepare a set of external standards with phosphate concentrations of 10, 20, 30, 40, 50 and 60 ppm. Use a manifold similar to that shown in Figure 13.4.9 a, placing a 50-cm mixing coil between the pump and the loop injector and a 50-cm reaction coil between the loop injector and the detector. For both coils, use PTFE tubing with an internal diameter of 0.8 mm. Set the flow rate to 0.5 mL/min. Prepare a calibration curve by injecting 50 µL of each standard, measuring the absorbance at 650 nm. Samples are analyzed in the same manner.

Questions

1. How long does it take a sample to move from the loop injector to the detector?

The reaction coil is 50-cm long with an internal diameter of 0.8 mm. The volume of this tubing is

$$V = l\pi r^2 = 50\text{cm} \times 3.14 \times \left(\frac{0.08\text{cm}}{2}\right)^2 = 0.25\text{cm}^3 = 0.25\text{mL}$$

With a flow rate of 0.5 mL/min, it takes about 30 s for a sample to pass through the system.

2. The instructions for the standard spectrophotometric method indicate that the absorbance is measured 5–10 min after adding the ascorbic acid. Why is this waiting period necessary in the spectrophotometric method, but not necessary in the FIA method?

The reduction of the yellow-colored Mo(VI) complex to the blue-colored Mo(V) complex is a slow reaction. In the standard spectro-photometric method it is difficult to control reproducibly the time between adding the reagents to the sample and measuring the sample's absorbance. To achieve good precision we allow the reaction to proceed to completion before we measure the absorbance. As seen by the answer to the previous question, in the FIA method the flow rate and the dimensions of the reaction coil determine the reaction time. Because this time is controlled precisely, the reaction occurs to the same extent for all standards and samples. A shorter reaction time has the advantage of allowing for a higher throughput of samples.

3. The spectrophotometric method recommends using phosphate standards of 2–10 ppm. Explain why the FIA method uses a different range of standards.

In the FIA method we measure the absorbance before the formation of the blue-colored Mo(V) complex is complete. Because the absorbance for any standard solution of phosphate is always smaller when using the FIA method, the FIA method is less sensitive and higher concentrations of phosphate are necessary.

4. How would you incorporate a reagent blank into the FIA analysis?

A reagent blank is obtained by injecting a sample of distilled water in place of the external standard or the sample. The reagent blank's absorbance is subtracted from the absorbances obtained for the standards and samples.

Example 13.4.1

The following data were obtained for a set of external standards when using Representative Method 13.4.1 to analyze phosphate in a wastewater sample.

$[PO_4^{3-}]$ (ppm)	absorbance
10.00	0.079
20.00	0.160
30.00	0.233
40.00	0.316
60.00	0.482

What is the concentration of phosphate in a sample if it gives an absorbance of 0.287?

Solution

Figure 13.4.13 shows the external standards calibration curve and the calibration equation. Substituting in the sample's absorbance gives the con- centration of phosphate in the sample as 36.1 ppm.

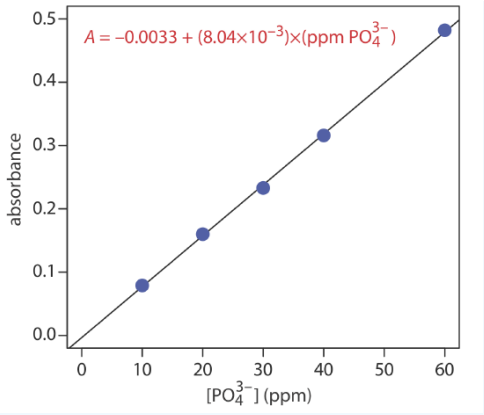

Figure 13.4.13 . Calibration curve and equation for the data in Example 13.4.1 .

Evaluation

The majority of flow injection analysis applications are modifications of conventional titrimetric, spectrophotometric, and electrochemical methods of analysis; thus, it is appropriate to compare FIA methods to these conventional methods. The scale of operations for FIA allows for the routine analysis of minor and trace analytes, and for macro, meso, and micro samples. The ability to work with microliter injection volumes is useful when the sample is scarce. Conventional methods of analysis usually have smaller detection limits.

The accuracy and precision of FIA methods are comparable to conven- tional methods of analysis; however, the precision of FIA is influenced by several variables that do not affect conventional methods, including the stability of the flow rate and the reproducibility of the sample's injection. In addition, results from FIA are more susceptible to temperature variations.

In general, the sensitivity of FIA is less than that for conventional methods of analysis for at least two reasons. First, as with chemical kinetic methods, measurements in FIA are made under nonequilibrium conditions when the signal has yet to reach its maximum value. Second, dispersion dilutes the sample as it moves through the manifold. Because the variables that affect sensitivity are known, we can design the FIA manifold to optimize the method's sensitivity.

Selectivity for an FIA method often is better than that for the corresponding conventional method of analysis. In many cases this is due to the kinetic nature of the measurement process, in which potential interferents may react more slowly than the analyte. Contamination from external sources also is less of a problem because reagents are stored in closed reservoirs and are pumped through a system of transport tubing that is closed to the environment.

Finally, FIA is an attractive technique when considering time, cost, and equipment. When using an autosampler, a flow injection method can achieve very high sampling rates. A sampling rate of 20–120 samples/h is not unusual and sampling rates as high as 1700 samples/h are possible. Because the volume of the flow injection manifold is small, typically less than 2 mL, the consumption of reagents is substantially smaller than that for a conventional method. This can lead to a significant decrease in the cost per analysis. Flow injection analysis does require the need for additional equipment—a pump, a loop injector, and a manifold—which adds to the cost of an analysis.

For a review of the importance of flow injection analysis, see Hansen, E. H.; Miró, M. "How Flow-Injection Analysis (FIA) Over the Past 25 Years has Changed Our Way of Performing Chemical Analyses," *TRAC, Trends Anal. Chem.* **2007**, *26*, 18–26.

4.5: Problems

1. Equation 13.2.18 shows how $[A]_0$ is determined using a two-point fixed-time integral method in which the concentration of *A* for the pseudo-first-order reaction

$$A + R \longrightarrow P$$

is measured at times t_1 and t_2. Derive a similar equation for the case where the product is monitored under pseudo-first order conditions.

2. The concentration of phenylacetate is determined from the kinetics of its pseudo-first order hydrolysis reaction in an ethylamine buffer. When a standard solution of 0.55 mM phenylacetate is analyzed, the concentration of phenylacetate after 60 s is 0.17 mM. When a sample is analyzed the concentration of phenylacetate that remains after 60 s is 0.23 mM. What is the concentration of phenylacetate in the sample?

3. In the presence of acid, iodide is oxidized by hydrogen peroxide

$$2\mathrm{I}^-(aq) + \mathrm{H_2O_2}(aq) + 2\mathrm{H_3O}^+(aq) \longrightarrow 4\mathrm{H_2O}(l) + \mathrm{I_2}(aq)$$

When I^- and H_3O^+ are present in excess, we can use the reaction's kinetics of the reaction, which is pseudo-first order in H_2O_2, to determine the concentration of H_2O_2 by following the production of I_2 with time. In one analysis the solution's absorbance at 348 nm was measured after 240 s. Analysis of a set of standard gives the results shown below.

$[H_2O_2]$ (μM)	absorbance
100.0	0.236
200.0	0.471
400.0	0.933
800.0	1.872

What is the concentration of H_2O_2 in a sample if its absorbance is 0.669 after 240 s?

4. The concentration of chromic acid is determined by reducing it under conditions that are pseudo-first order in analyte. One approach is to monitor the reaction absorbance at a wavelength of 355 nm. A standard of 5.1×10^{-4} M chromic acid yields absorbances of 0.855 and 0.709 at 100 s and 300 s after the reaction's initiation. When a sample is analyzed under identical conditions, the absorbances are 0.883 and 0.706. What is the concentration of chromic acid in the sample?

5. Malmstadt and Pardue developed a variable time method for the determination of glucose based on its oxidation by the enzyme glucose oxidase [Malmstadt, H. V.; Pardue, H. L. *Anal. Chem.* **1961** *33*, 1040–1047]. To monitor the reaction's progress, iodide is added to the samples and standards. The H_2O_2 produced by the oxidation of glucose reacts with I^-, forming I_2 as a product. The time required to produce a fixed amount of I_2 is determined spectrophotometrically. The following data was reported for a set of calibration standards

[glucose] (ppm)	time (s)		
5.0	146.5	150.0	149.6
10.0	69.2	67.1	66.0
20.0	34.8	35.0	34.0
30.0	22.3	22.7	22.6
40.0	16.7	16.5	17.0
50.0	13.3	13.3	13.8

To verify the method a standard solution of 20.0 ppm glucose was analyzed in the same way as the standards, requiring 34.6 s to produce the same extent of reaction. Determine the concentration of glucose in the standard and the percent error for the analysis.

6. Deming and Pardue studied the kinetics for the hydrolysis of *p*-nitrophenyl phosphate by the enzyme alkaline phosphatase [Deming, S. N.; Pardue, H. L. *Anal. Chem.* **1971**, *43*, 192–200]. The reaction's progress was monitored by measuring the absorbance of *p*-nitrophenol, which is one of the reaction's products. A plot of the reaction's rate (with units of μmol mL–1 sec–1) versus the volume, *V*, in milliliters of a serum calibration standard that contained the enzyme, yielded a straight line with the following equation.

$$\text{rate } = 2.7 \times 10^{-7} \mu\text{mol mL}^{-1}\ \text{s}^{-1} + \left(3.485 \times 10^{-5} \mu\text{mol mL}^{-2}\ \text{s}^{-1}\right) V$$

A 10.00-mL sample of serum is analyzed, yielding a rate of 6.84×10^{-5} μmol mL^{-1} sec^{-1}. How much more dilute is the enzyme in the serum sample than in the serum calibration standard?

7. The following data were collected for a reaction known to be pseudo-first order in analyte, *A*, during the time in which the reaction is monitored.

time (s)	$[A]_t$ (mM)
2	1.36
4	1.24
6	1.12
8	1.02
10	0.924
12	0.838
14	0.760
16	0.690
18	0.626
20	0.568

What is the rate constant and the initial concentration of analyte in the sample?

8. The enzyme acetylcholinesterase catalyzes the decomposition of acetylcholine to choline and acetic acid. Under a given set of conditions the enzyme has a K_m of 9×10^{-5} M and a k_2 of 1.4×10^4 s^{-1}. What is the concentration of acetylcholine in a sample if the reaction's rate is 12.33 μM s^{-1} in the presence of 6.61×10^{-7} M enzyme? You may assume the concentration of acetylcholine is significantly smaller than K_m.

9. The enzyme fumarase catalyzes the stereospecific addition of water to fumarate to form l-malate. A standard 0.150 μM solution of fumarase has a rate of reaction of 2.00 μM min^{-1} under conditions in which the substrate's concentration is significantly greater than K_m. The rate of reaction for a sample under identical condition is 1.15 mM min^{-1}. What is the concentration of fumarase in the sample?

10. The enzyme urease catalyzes the hydrolysis of urea. The rate of this reaction is determined for a series of solutions in which the concentration of urea is changed while maintaining a fixed urease concentration of 5.0 mM. The following data are obtained.

[urea] (μM)	rate (μM s^{-1})
0.100	6.25
0.200	12.5
0.300	18.8
0.400	25.0
0.500	31.2
0.600	37.5

[urea] (μM)	rate (μM s^{-1})
0.700	43.7
0.800	50.0
0.900	56.2
1.00	62.5

Determine the values of V_{max}, k_2, and K_m for urease.

11. To study the effect of an enzyme inhibitor V_{max} and K_m are measured for several concentrations of inhibitor. As the concentration of the inhibitor increases V_{max} remains essentially constant, but the value of K_m increases. Which mechanism for enzyme inhibition is in effect?

12. In the case of competitive inhibition, the equilibrium between the enzyme, *E*, the inhibitor, *I*, and the enzyme–inhibitor complex, *EI*, is described by the equilibrium constant K_{EI}. Show that for competitive inhibition the equation for the rate of reaction is

$$\frac{d[P]}{dt} = \frac{V_{max}[S]}{K_m\{1+([I]/K_{El})\}+[S]}$$

where K_I is the formation constant for the *EI* complex

$$E + I \rightleftharpoons EI$$

You may assume that $k_2 << k_{-1}$.

13. Analytes *A* and *B* react with a common reagent *R* with first-order kinetics. If 99.9% of *A* must react before 0.1% of *B* has reacted, what is the minimum acceptable ratio for their respective rate constants?

14. A mixture of two analytes, *A* and *B*, is analyzed simultaneously by monitoring their combined concentration, $C = [A] + [B]$, as a function of time when they react with a common reagent. Both *A* and *B* are known to follow first-order kinetics with the reagent, and *A* is known to react faster than *B*. Given the data in the following table, determine the initial concentrations of *A* and *B*, and the first-order rate constants, k_A and k_B.

time (min)	[*C*] (mM)
1	0.313
6	0.200
11	0.136
16	0.098
21	0.074
26	0.058
31	0.047
36	0.038
41	0.032
46	0.027
51	0.023
56	0.019
61	0.016
66	0.014

time (min)	[*C*] (mM)
71	0.012

15. Table 13.3.1 provides a list of several isotopes used as tracers. The half-lives for these isotopes also are listed. What is the rate constant for the radioactive decay of each isotope?

16. ^{60}Co is a long-lived isotope ($t_{1/2}$ = 5.3 yr) frequently used as a radiotracer. The activity in a 5.00-mL sample of a solution of ^{60}Co is 2.1×10^{7} disintegrations/sec. What is the molar concentration of ^{60}Co in the sample?

17. The concentration of Ni in a new alloy is determined by a neutron activation analysis. A 0.500-g sample of the alloy and a 1.000-g sample of a standard alloy that is 5.93% w/w Ni are irradiated with neutrons in a nuclear reactor. When irradiation is complete, the sample and the standard are allowed to cool and their gamma ray activities measured. Given that the activity is 1020 cpm for the sample and 3540 cpm for the standard, determine the %w/w Ni in the alloy.

18. The vitamin B_{12} content of a multivitamin tablet is determined by the following procedure. A sample of 10 tablets is dissolved in water and diluted to volume in a 100-mL volumetric flask. A 50.00-mL portion is removed and 0.500 mg of radioactive vitamin B_{12} having an activity of 572 cpm is added as a tracer. The sample and tracer are homogenized and the vitamin B_{12} isolated and purified, producing 18.6 mg with an activity of 361 cpm. Calculate the milligrams of vitamin B_{12} in a multivitamin tablet.

19. The oldest sample that can be dated by ^{14}C is approximately 30 000 yr. What percentage of the ^{14}C remains after this time span?

20. Potassium–argon dating is based on the nuclear decay of ^{40}K to ^{40}Ar ($t_{1/2} = 1.3 \times 10^{9}$ yr). If no ^{40}Ar is originally present in the rock, and if ^{40}Ar cannot escape to the atmosphere, then the relative amounts of ^{40}K and ^{40}Ar can be used to determine the age of the rock. When a 100.0-mg rock sample is analyzed it is found to contain 4.63×10^{-6} mol of ^{40}K and 2.09×10^{-6} mol ^{40}Ar. How old is the rock sample?

21. The steady state activity for ^{14}C in a sample is 13 cpm per gram of carbon. If counting is limited to 1 hr, what mass of carbon is needed to give a percent relative standard deviation of 1% for the sample's activity? How long must we monitor the radioactive decay from a 0.50-g sample of carbon to give a percent relative standard deviation of 1.0% for the activity?

22. To improve the sensitivity of a FIA analysis you might do any of the following: inject a larger volume of sample, increase the flow rate, decrease the length and the diameter of the manifold's tubing, or merge separate channels before injecting the sample. For each action, explain why it leads to an improvement in sensitivity.

23. The figure below shows a fiagram for a solution of 50.0-ppm PO_4^{3-} using the method in Representative Method 13.4.1. Determine values for *h*, t_a, *T*, *t* ′, Δt, and *T* ′. What is the sensitivity of this FIA method, assuming a linear relationship between absorbance and concentration? How many samples can be analyzed per hour?

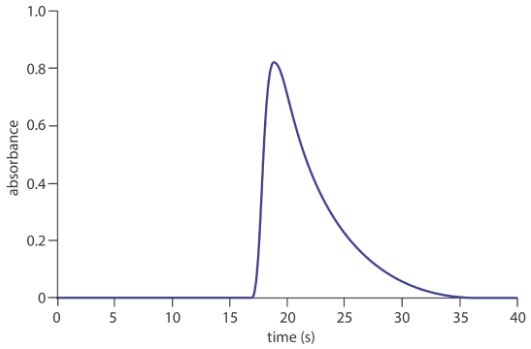

24. A sensitive method for the flow injection analysis of Cu^{2+} is based on its ability to catalyze the oxidation of di-2-pyridyl ketone hydrazone (DPKH) [Lazaro, F.; Luque de Castro, M. D.; Valcárcel, M. Analyst, 1984, 109, 333–337]. The product of the reaction is fluorescent and is used to generate a signal when using a fluorimeter as a detector. The yield of the reaction is at a maximum when the solution is made basic with NaOH. The fluorescence, however, is greatest in the presence of HCl. Sketch an appropriate FIA manifold for this analysis.

25. The concentration of chloride in seawater is determined by a flow injection analysis. The analysis of a set of calibration standards gives the following results.

[Cl^-] (ppm)	absorbance	[Cl^-] (ppm)	absorbance
5.00	0.057	40.00	0.478
10.00	0.099	50.00	0.594
20.00	0.230	75.00	0.840
30.00	0.354		

A 1.00-mL sample of seawater is placed in a 500-mL volumetric flask and diluted to volume with distilled water. When injected into the flow injection analyzer an absorbance of 0.317 is measured. What is the concentration of Cl^- in the sample?

26. Ramsing and co-workers developed an FIA method for acid–base titrations using a carrier stream that is 2.0×10^{-3} M NaOH and that contains the acid–base indicator bromothymol blue [Ramsing, A. U.; Ruzicka, J.; Hansen, E. H. *Anal. Chim. Acta* **1981**, *129*, 1–17]. Standard solutions of HCl were injected, and the following values of Δt were measured from the resulting fiagrams.

[HCl] (M)	Δt (s)	[HCl] (M)	Δt (s)
0.008	3.13	0.080	7.71
0.010	3.59	0.100	8.13
0.020	5.11	0.200	9.27
0.040	6.39	0.400	10.45
0.060	7.06	0.600	11.40

A sample with an unknown concentration of HCl is analyzed five times, giving values of 7.43, 7.28, 7.41, 7.37, and 7.33 s for Δt. Determine the concentration of HCl in the sample.

27. Milardovíc and colleagues used a flow injection analysis method with an amperometric biosensor to determine the concentration of glucose in blood [MilardoviĆ, S.; Kruhak, I.; Ivekovic, D.; Rumenjak, V.; Tkalčec, M.; Grabaric, B. S. *Anal. Chim. Acta* **1997**, *350*, 91–96]. Given that a blood sample that is 6.93 mM in glucose has a signal of 7.13 nA, what is the concentration of glucose in a sample of blood if its signal is 11.50 nA?

28. Fernández-Abedul and Costa-García developed an FIA method to determine cocaine in samples using an amperometric detector [Fernández-Abedul, M; Costa-García, A. *Anal. Chim. Acta* **1996**, *328*, 67–71]. The following signals (arbitrary units) were collected for 12 replicate injections of a 6.2×10^{-6} M sample of cocaine, $C_{17}H_{21}NO_4$.

24.5	24.1	24.1
23.8	23.9	25.1
23.9	24.8	23.7
23.3	23.2	23.2

(a) What is the relative standard deviation for this sample?

(b) The following calibration data are available

[cocaine] (μM)	signal (arb. units)
0.18	0.8
0.36	2.1
0.60	2.4
0.81	3.2
1.0	4.5

[cocaine] (μM)	signal (arb. units)
2.0	8.1
4.0	14.4
6.0	21.6
8.0	27.1
10.0	32.9

In a typical analysis a 10.0-mg sample is dissolved in water and diluted to volume in a 25-mL volumetric flask. A 125-mL aliquot is transferred to a 25-mL volumetric flask and diluted to volume with a pH 9 buffer. When injected into the flow injection apparatus a signal of 21.4 (arb. units) is obtained. What is the %w/w cocaine in the sample?

29. Holman, Christian, and Ruzicka described an FIA method to determine the concentration of H_2SO_4 in nonaqueous solvents [Holman, D. A.; Christian, G. D.; Ruzicka, J. *Anal. Chem.* **1997**, *69*, 1763–1765]. Agarose beads (22–45 mm diameter) with a bonded acid–base indicator are soaked in NaOH and immobilized in the detector's flow cell. Samples of H_2SO_4 in *n*-butanol are injected into the carrier stream. As a sample passes through the flow cell, an acid–base reaction takes place between H_2SO_4 and NaOH. The endpoint of the neutralization reaction is signaled by a change in the bound indicator's color and is detected spectrophotometrically. The elution volume needed to reach the titration's endpoint is inversely proportional to the concentration of H_2SO_4; thus, a plot of endpoint volume versus $[H_2SO_4]^{-1}$ is linear. The following data is typical of that obtained using a set of external standards.

$[H_2SO_4]$ (mM)	end point volume (mL)
0.358	0.266
0.436	0.227
0.560	0.176
0.752	0.136
1.38	0.075
2.98	0.037
5.62	0.017

What is the concentration of H_2SO_4 in a sample if its endpoint volume is 0.157 mL?

4.6: Additional Resources

The following set of experiments introduce students to the applications of chemical kinetic methods, including enzyme kinetic methods, and flow injection analysis.

Chemical Kinetic Methods

- Abramovitch, D. A.; Cunningham, L. K.; Litwer, M. R. "Decomposition Kinetics of Hydrogen Peroxide: Novel Lab Experiments Employing Computer Technology," *J. Chem. Educ.* **2003**, *80*, 790–792.
- Antuch, M.; Ramos, Y.; Álvarez, R. "Simulated Analysis of Linear Reversible Enzyme Inhibition with SCILAB," *J. Chem. Educ.* **2014**, *91*, 1203–1206.
- Bateman, Jr. R. C.; Evans, J. A. "Using the Glucose Oxidase/Peroxidase Systems in Enzyme Kinetics," *J. Chem. Educ.* **1995**, *72*, A240–A241.
- Bendinskas, K.; DiJacomo, C.; Krill, A.; Vitz, E. "Kinetics of Alcohol Dehydrogenase-Catalyzed Oxidation of Ethanol Followed by Visible Spectroscopy," *J. Chem. Educ.* **1068**, *82*, 1068–1070.
- Clark, C. R. "A Stopped-Flow Kinetics Experiment for Advanced Undergraduate Laboratories: Formation of Iron(III) Thiocyanate," *J. Chem. Educ.* **1997**, *74*, 1214–1217.
- Diamandis, E. P.; Koupparis, M. A.; Hadjiionnou, T. P. "Kinetic Studies with Ion-Selective Electrodes: Determination of Creatinine in Urine with a Picrate Ion-Selective Electrode," *J. Chem. Educ.* **1983**, *60*, 74–76.
- Dias, A. A.; Pinto, P. A.; Fraga, I.; Bezerra, R. M. F. "Diagnosis of Enzyme Inhibition Using Excel Solver: A Combined Dry and Wet Laboratory Exercise," *J. Chem. Educ.* **2014**, *91*, 1017–1021.
- El Seoud, O. A.; Galgano, P. D.; Arêas, E. P. G.; Moraes, J. M. "Learning Chemistry from Good and (Why Not?) Problematic Results: Kinetics of the pH-Independent Hydrolysis of 4-Nitrophenyl Chloroformate," *J. Chem. Educ.* **2015**, *92*, 752–756.
- Frey, M. W.; Frey, S. T.; Soltau, S. R. "Exploring the pH Dependence of L-leucine-*p*-nitroanilide Cleavage by Aminopeptidase Aeromonas Proteolytica: A Combined Buffer-Enzyme Kinetics Experiment for the General Chemistry Laboratory," *Chem. Educator* **2010**, *15*, 117–120.
- Gooding, J. J.; Yang, W.; Situmorang, M. "Bioanalytical Experiments for the Undergraduate Laboratory: Monitoring Glucose in Sport Drinks," *J. Chem. Educ.* **2001**, *78*, 788–790.
- Hamilton, T. M.; Dobie-Galuska, A. A.; Wietstock, S. M. "The *o*-Phenylenediamine-Horseradish Peroxidase System: Enzyme Kinetics in the General Chemistry Lab," *J. Chem. Educ.* **1999**, *76*, 642– 644.
- Johnson, K. A. "Factors Affecting Reaction Kinetics of Glucose Oxidase," *J. Chem. Educ.* **2002**, *79*, 74–76.
- Mowry, S.; Ogren, P. J. "Kinetics of Methylene Blue Reduction by Ascorbic Acid," *J. Chem. Educ.* **1999**, *76*, 970–974.
- Nyasulu, F. W.; Barlag, R. "Gas Pressure Sensor Monitored Iodide-Catalyzed Decomposition Kinetics of Hydrogen Peroxide: An Initial Rate Approach," *Chem. Educator* **2008**, *13*, 227–230.
- Nyasulu, F. W.; Barlag, R. "Thermokinetics: Iodide-Catalyzed Decomposition Kinetics of Hydrogen Peroxide; An Integrated Rate Approach," *Chem. Educator* **2010**, *15*, 168–170.
- Pandey, S.; McHale, M. E. R.; Horton, A. M.; Padilla, S. A.; Trufant, A. L.; De La Sancha, N. U.; Vela, E.; Acree, Jr., W. E. "Kinetics-Based Indirect Spectrophotometric Method for the Simultaneous Determination of MnO_4^- and $Cr_2O_7^{2-}$," *J. Chem. Educ.* **1998**, *75*, 450–452.
- Stock, E.; Morgan, M. "A Spectroscopic Analysis of the Kinetics of the Iodine Clock Reaction without Starch," *Chem. Educator* **2010**, *15*, 158–161.
- Vasilarou, A.-M. G.; Georgiou, C. A. "Enzymatic Spectrophotometric Reaction Rate Determination of Glucose in Fruit Drinks and Carbonated Beverages," *J. Chem. Educ.* **2000**, *77*, 1327–1329.
- Williams, K. R.; Adhyaru, B.; Timofeev, J.; Blankenship, M. K. "Decomposition of Aspartame. A Kinetics Experiment for Upper-Level Chemistry Laboratories," *J. Chem. Educ.* **2005**, *82*, 924–925.

Flow Injection Methods

- Carroll, M. K.; Tyson, J. F. "An Experiment Using Time-Based Detection in Flow Injection Analysis," *J. Chem. Educ.* **1993**, *70*, A210–A216.
- ConceiÇão, A. C. L.; Minas da Piedade, M. E. "Determination of Acidity Constants by Gradient Flow-Injection Titration," *J. Chem. Educ.* **2006**, *83*, 1853–1856.
- Hansen, E. H.; Ruzicka, J. "The Principles of Flow Injection Analysis as Demonstrated by Three Lab Exercises," *J. Chem. Educ.* **1979**, *56*, 677–680.

- McKelvie, I. D.; Cardwell, T. J.; Cattrall, R. W. “A Microconduit Flow Injection Analysis Demonstration using a 35-mm Slide Projector,” *J. Chem. Educ.* **1990**, *67*, 262–263.
- Meyerhoff, M. E.; Kovach, P. M. “An Ion-Selective Electrode/Flow Injection Analysis Experiment: Determination of Potassium in Serum,” *J. Chem. Educ.* **1983**, *60*, 766–768.
- Nóbrega, J. A.; Rocha, F. R. P. “Ionic Strength Effect on the Rate of Reduction of Hexacyanoferrate(II) by Ascorbic Acid,” *J. Chem. Educ.* **1997**, *74*, 560–562.
- Ríos, A.; Luque de Castro, M.; Valcárcel, M. “Determination of Reaction Stoichiometries by Flow Injection Analysis,” *J. Chem. Educ.* **1986**, *63*, 552–553.
- Stults, C. L. M.; Wade, A. P.; Crouch, S. R. “Investigation of Temperature Effects on Dispersion in a Flow Injection Analyzer,” *J. Chem. Educ.* **1988**, *65*, 645–647.
- Wolfe, C. A. C.; Oates, M. R.; Hage, D. S. “Automated Protein Assay Using Flow Injection Analysis,” *J. Chem. Educ.* **1998**, *75*, 1025–1028.

The following sources provides a general review of the importance of chemical kinetics in analytical chemistry.

- Bergmyer, H. U.; Grassl, M. *Methods of Enzymatic Analysis*, Verlag Chemie: Deerfield Beach, FL, 3rd Ed., 1983.
- Doménech-Carbó, A. “Dating: An Analytical Task,” *ChemTexts* **2015**, *1:5*.
- Laitinen, H. A.; Ewing, G. W., eds., *A History of Analytical Chemistry*, The Division of Analytical Chemistry of the American Chemical Society: Washington, D. C., 1977, pp. 97–102.
- Malmstadt, H. V.; Delaney, C. J.; Cordos, E. A. “Reaction-Rate Methods of Chemical Analysis,” *Crit. Rev. Anal. Chem.* **1972**, *2*, 559–619.
- Mark, H. B.; Rechnitz, G. A. *Kinetics in Analytical Chemistry*, Wiley: New York, 1968.
- Mottola, H. A. “Catalytic and Differential Reaction-Rate Methods of Chemical Analysis,” *Crit. Rev. Anal. Chem.* **1974**, *4*, 229–280.
- Mottola, H. A. “Some Kinetic Aspects Relevant to Contemporary Analytical Chemistry,” *J. Chem. Educ.* **1981**, *58*, 399–403.
- Mottola, H. A. *Kinetic Aspects of Analytical Chemistry*, Wiley: New York, 1988.
- Pardue, H. L. “A Comprehensive Classification of Kinetic Methods of Analysis Used in Clinical Chemistry,” Clin. Chem. 1977, 23, 2189–2201.
- Pardue, H. L. “Kinetic Aspects of Analytical Chemistry,” *Anal. Chim. Acta*, **1989**, *216*, 69–107.
- Perez-Bendito, D.; Silva, M. *Kinetic Methods in Analytical Chemistry*, Ellis Horwood: Chichester, 1988.
- Pisakiewicz, D. *Kinetics of Chemical and Enzyme-Catalyzed Reactions*, Oxford University Press: New York, 1977.

The following instrumental analysis textbooks may be consulted for further information on the detectors and signal analyzers used in radiochemical methods of analysis.

- Skoog, D. A.; Holler, F. J.; Nieman, T. A. *Principles of Instrumental Analysis*, 5th Ed., Saunders College Publishing/Harcourt Brace and Co.: Philadelphia., 1998, Chapter 32.
- Strobel, H. A.; Heineman, W. R. *Chemical Instrumentation: A Systematic Approach*, 3rd Ed., Wiley-Interscience: New York, 1989.

The following resources provide additional information on the theory and application of flow injection analysis.

- Andrew, K. N.; Blundell, N. J.; Price, D.; Worsfold, P. J. “Flow Injection Techniques for Water Monitoring,” *Anal. Chem.* **1994**, *66*, 916A–922A.
- Betteridge, D. “Flow Injection Analysis,” *Anal. Chem.* **1978**, *50*, 832A–846A.
- Kowalski, B. R.; Ruzicka, J. Christian, G. D. “Flow Chemography - The Future of Chemical Education,” *Trends Anal. Chem.* **1990**, *9*, 8–13.
- Mottola, H. A. “Continuous Flow Analysis Revisited,” *Anal. Chem.* **1981**, *53*, 1312A–1316A.
- Ruzicka, J. “Flow Injection Analysis: From Test Tube to Integrated Microconduits,” *Anal. Chem.* **1983**, *55*, 1040A–1053A.
- Ruzicka, J.; Hansen, E. H. *Flow-Injection Analysis*, Wiley-Interscience: New York, 1989.
- Ruzicka, J.; Hansen, E. H. “Retro-Review of Flow-Injection Analysis,” *Trends Anal. Chem.* **2008**, *27*, 390–393.
- Silvestre, C. I. C.; Santos, J. L. M.; Lima, J. L. F. C.; Zagatto, E. A. G. “Liquid-Liquid Extraction in Flow Analysis: A Critical Review,” *Anal. Chim. Acta* **2009**, *652*, 54–65.
- Stewart, K. K. “Flow Injection Analysis: New Tools for Old Assays, New Approaches to Analytical Measurements,” *Anal. Chem.* **1983**, *55*, 931A–940A.

- Tyson, J. F. “Atomic Spectrometry and Flow Injection Analysis: A Synergic Combination,” *Anal. Chim. Acta*, **1988**, *214*, 57–75.
- Valcarcel, M.; Luque de Castro, M. D. *Flow-Injection Analysis: Principles and Applications*, Ellis Horwood: Chichester, England, 1987.

4.7: Chapter Summary and Key Terms

Chapter Summary

Kinetic methods of analysis use the rate of a chemical or s physical process to determine an analyte's concentration. Three types of kinetic methods are discussed in this chapter: chemical kinetic methods, radiochemical methods, and flow injection methods.

Chemical kinetic methods use the rate of a chemical reaction and either its integrated or its differential rate law. For an integral method, we determine the concentration of analyte—or the concentration of a reactant or product that is related stoichiometrically to the analyte—at one or more points in time following the reaction's initiation. The initial concentration of analyte is then determined using the integrated form of the reaction's rate law. Alternatively, we can measure the time required to effect a given change in concentration. In a differential kinetic method we measure the rate of the reaction at a time *t*, and use the differential form of the rate law to determine the analyte's concentration.

Chemical kinetic methods are particularly useful for reactions that are too slow for other analytical methods. For reactions with fast kinetics, automation allows for sampling rates of more than 100 samples/h. Another important application of chemical kinetic methods is the quantitative analysis of enzymes and their substrates, and the characterization of enzyme catalysis.

Radiochemical methods of analysis take advantage of the decay of radioactive isotopes. A direct measurement of the rate at which a radioactive isotope decays is used to determine its concentration. For an analyte that is not naturally radioactive, neutron activation can be used to induce radio- activity. Isotope dilution, in which we spike a radioactively-labeled form of analyte into the sample, is used as an internal standard for quantitative work.

In flow injection analysis we inject the sample into a flowing carrier stream that usually merges with additional streams of reagents. As the sample moves with the carrier stream it both reacts with the contents of the carrier stream and with any additional reagent streams, and undergoes dispersion. The resulting fiagram of signal versus time bears some resemblance to a chromatogram. Unlike chromatography, however, flow injection analysis is not a separation technique. Because all components in a sample move with the carrier stream's flow rate, it is possible to introduce a second sample before the first sample reaches the detector. As a result, flow injection analysis is ideally suited for the rapid throughput of samples.

Key Terms

alpha particle	beta particle	centrifugal analyzer
competitive inhibitor	curve-fitting method	enzyme
equilibrium method	fiagram	flow injection analysis
gamma ray	Geiger counter	half-life
inhibitor	initial rate	integrated rate law
intermediate rate	isotope	isotope dilution
kinetic method	Lineweaver-Burk plot	manifold
Michaelis constant	negatron	neutron activation
noncompetitive inhibitor	one-point fixed-time integral method	peristaltic pump
positron	quench	rate
rate constant	rate law	rate method
scintillation counter	steady-state approximation	stopped-flow analyzer
substrate	tracer	two-point fixed-time integral method
uncompetitive inhibitor	variable time integral method	

CHAPTER OVERVIEW

5: Developing a Standard Method

In Chapter 1 we made a distinction between analytical chemistry and chemical analysis. Among the goals of analytical chemistry are improving established methods of analysis, extending existing methods of analysis to new types of samples, and developing new analytical methods. Once we develop a new method, its routine application is best described as chemical analysis. We recognize the status of these established methods by calling them standard methods.

Numerous examples of standard methods are presented and discussed in Chapters 8–13. What we have yet to consider is what constitutes a standard method. In this chapter we discuss how we develop a standard method, including optimizing the experimental procedure, verifying that the method produces acceptable precision and accuracy in the hands of a single analyst, and validating the method for general use.

5.1: Optimizing the Experimental Procedure

In the presence of H_2O_2 and H_2SO_4, a solution of vanadium forms a reddish brown color that is believed to be a compound with the general formula $(VO)_2(SO_4)_3$. The intensity of the solution's color depends on the concentration of vanadium, which means we can use its absorbance at a wavelength of 450 nm to develop a quantitative method for vanadium.

The intensity of the solution's color also depends on the amounts of H_2O_2 and H_2SO_4 that we add to the sample—in particular, a large excess of H_2O_2 decreases the solution's absorbance as it changes from a reddish brown color to a yellowish color [*Vogel's Textbook of Quantitative Inorganic Analysis*, Longman: London, 1978, p. 752.]. Developing a ***standard method*** for vanadium based on this reaction requires that we optimize the amount of H_2O_2 and H_2SO_4 added to maximize the absorbance at 450 nm. Using the terminology of statisticians, we call the solution's absorbance the system's ***response***. Hydrogen peroxide and sulfuric acid are ***factors*** whose concentrations, or ***factor levels***, determine the system's response. To optimize the method we need to find the best combination of factor levels. Usually we seek a maximum response, as is the case for the quantitative analysis of vanadium as $(VO)_2(SO_4)_3$. In other situations, such as minimizing an analysis's percent error, we seek a minimum response.

> We will return to this analytical method for vanadium in Example 14.1.4 and Problem 11 from the end-of-chapter problems.

Response Surfaces

One of the most effective ways to think about an optimization is to visualize how a system's response changes when we increase or decrease the levels of one or more of its factors. We call a plot of the system's response as a function of the factor levels a ***response surface***. The simplest response surface has one factor and is drawn in two dimensions by placing the responses on the *y*-axis and the factor's levels on the *x*-axis. The calibration curve in Figure 14.1.1 is an example of a one-factor response surface. We also can define the response surface mathematically. The response surface in Figure 14.1.1 , for example, is

$$A = 0.008 + 0.0896C_A$$

where A is the absorbance and C_A is the analyte's concentration in ppm.

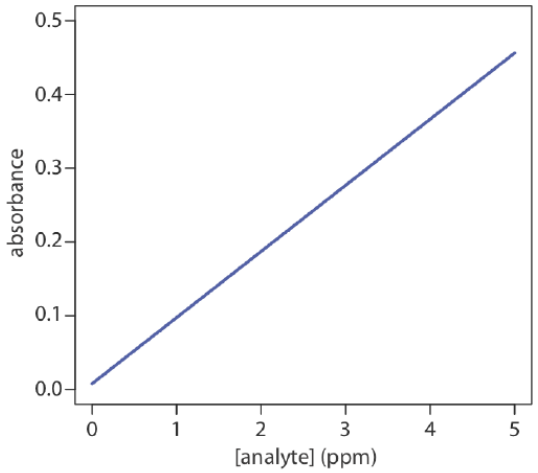

Figure 14.1.1 . A calibration curve is an example of a one-factor response surface. The responses (absorbance) are plotted on the *y*-axis and the factor levels (concentration of analyte) are plotted on the *x*-axis.

For a two-factor system, such as the quantitative analysis for vanadium described earlier, the response surface is a flat or curved plane in three dimensions. As shown in Figure 14.1.2 a, we place the response on the *z*-axis and the factor levels on the *x*-axis and the *y*-axis. Figure 14.1.2 a shows a pseudo-three dimensional wireframe plot for a system that obeys the equation

$$R = 3.0 - 0.30A + 0.020AB$$

where R is the response, and A and B are the factors. We also can represent a two-factor response surface using the two-dimensional level plot in Figure 14.1.2 b, which uses a color gradient to show the response on a two-dimensional grid, or using the two-dimensional contour plot in Figure 14.1.2 c, which uses contour lines to display the response surface.

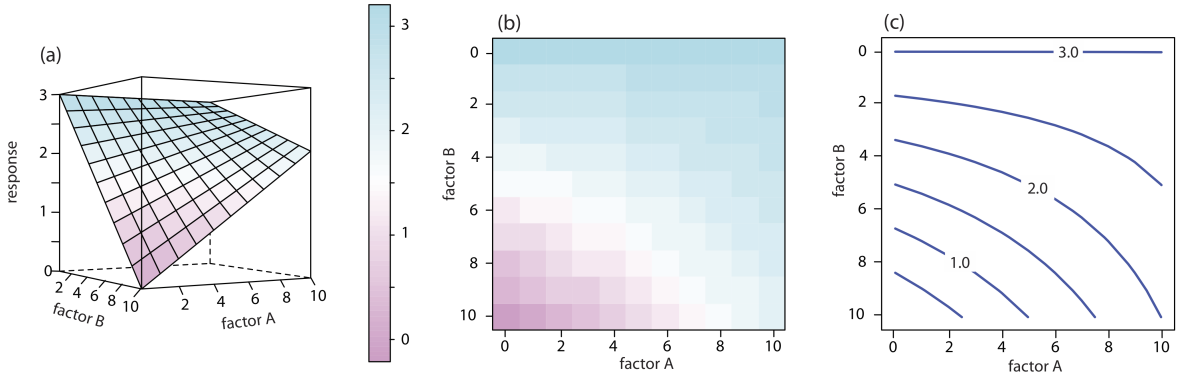

Figure 14.1.2 . Three examples of a two-factor response surface displayed as (a) a pseudo-three-dimensional wireframe plot, (b) a two-dimensional level plot, and (c) a two-dimensional contour plot. We call the display in (a) a pseudo-three dimensional response surface because we show the presence of three dimensions on the page's flat, two-dimensional surface.

We also can overlay a level plot and a contour plot. See Figure 14.1.7 b for a typical example.

The response surfaces in Figure 14.1.2 cover a limited range of factor levels ($0 \le A \le 10$, $0 \le B \le 10$), but we can extend each to more positive or to more negative values because there are no constraints on the factors. Most response surfaces of interest to an analytical chemist have natural constraints imposed by the factors, or have practical limits set by the analyst. The response surface in Figure 14.1.1 , for example, has a natural constraint on its factor because the analyte's concentration cannot be less than zero.

We express this constraint as $C_A \ge 0$.

If we have an equation for the response surface, then it is relatively easy to find the optimum response. Unfortunately, when developing a new analytical method, we rarely know any useful details about the response surface. Instead, we must determine the response surface's shape and locate its optimum response by running appropriate experiments. The focus of this section is on useful experimental methods for characterizing a response surface. These experimental methods are divided into two broad categories: searching methods, in which an algorithm guides a systematic search for the optimum response, and modeling methods, in which we use a theoretical model or an empirical model of the response surface to predict the optimum response.

Searching Algorithms for Response Surfaces

Figure 14.1.3 shows a portion of the South Dakota Badlands, a barren landscape that includes many narrow ridges formed through erosion. Suppose you wish to climb to the highest point on this ridge. Because the shortest path to the summit is not obvious, you might adopt the following simple rule: look around you and take one step in the direction that has the greatest change in elevation, and then repeat until no further step is possible. The route you follow is the result of a systematic search that uses a ***searching algorithm***. Of course there are as many possible routes as there are starting points, three examples of which are shown in Figure 14.1.3 . Note that some routes do not reach the highest point—what we call the ***global optimum***. Instead, many routes reach a ***local optimum*** from which further movement is impossible.

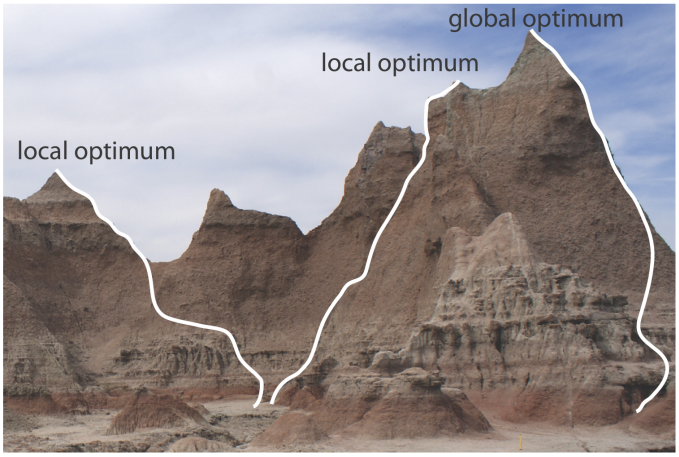

Figure 14.1.3 . Finding the highest point on a ridge using a searching algorithm is one useful method for finding the optimum on a response surface. The path on the far right reaches the highest point, or the global optimum. The other two paths reach local optima. This ridge is part of the South Dakota Badlands National Park. Searching algorithms have names: the one described here is the method of steepest ascent.

We can use a systematic searching algorithm to locate the optimum response for an analytical method. We begin by selecting an initial set of factor levels and measure the response. Next, we apply the rules of our searching algorithm to determine a new set of factor levels and measure its response, continuing this process until we reach an optimum response. Before we consider two common searching algorithms, let's consider how we evaluate a searching algorithm.

Effectiveness and Efficiency

A searching algorithm is characterized by its effectiveness and its efficiency. To be ***effective***, a searching algorithm must find the response surface's global optimum, or at least reach a point near the global optimum. A searching algorithm may fail to find the global optimum for several reasons, including a poorly designed algorithm, uncertainty in measuring the response, and the presence of local optima. Let's consider each of these potential problems.

A poorly designed algorithm may prematurely end the search before it reaches the response surface's global optimum. As shown in Figure 14.1.4 , when climbing a ridge that slopes up to the northeast, an algorithm is likely to fail it if limits your steps only to the north, south, east, or west. An algorithm that cannot responds to a change in the direction of steepest ascent is not an effective algorithm.

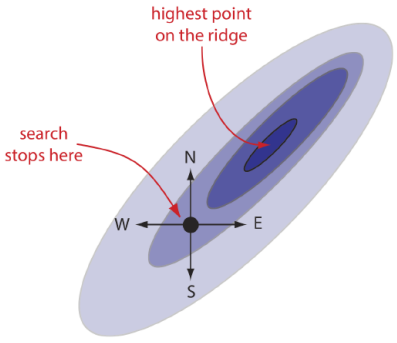

Figure 14.1.4 . Example showing how a poorly designed searching algorithm—limited to moving only north, south, east, or west—can fail to find a response surface's global optimum.

All measurements contain uncertainty, or noise, that affects our ability to characterize the underlying signal. When the noise is greater than the local change in the signal, then a searching algorithm is likely to end before it reaches the global optimum. Figure 14.1.5 provides a different view of Figure 14.1.3 , which shows us that the relatively flat terrain leading up to the ridge is heavily weathered and very uneven. Because the variation in local height (the noise) exceeds the slope (the signal), our searching algorithm ends the first time we step up onto a less weathered local surface.

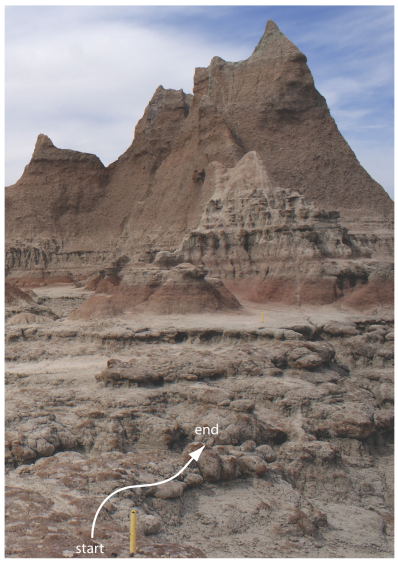

Figure 14.1.5 . Another view of the ridge in Figure 14.1.3 that shows the weathered terrain leading up to the ridge. The yellow rod at the bottom of the figure, which marks the trail, is about 18 in high.

Finally, a response surface may contain several local optima, only one of which is the global optimum. If we begin the search near a local optimum, our searching algorithm may never reach the global optimum. The ridge in Figure 14.1.3 , for example, has many peaks. Only those searches that begin at the far right will reach the highest point on the ridge. Ideally, a searching algorithm should reach the global optimum regardless of where it starts.

A searching algorithm always reaches an optimum. Our problem, of course, is that we do not know if it is the global optimum. One method for evaluating a searching algorithm's effectiveness is to use several sets of initial factor levels, find the optimum response for each, and compare the results. If we arrive at or near the same optimum response after starting from very different locations on the response surface, then we are more confident that is it the global optimum.

Efficiency is a searching algorithm's second desirable characteristic. An efficient algorithm moves from the initial set of factor levels to the optimum response in as few steps as possible. In seeking the highest point on the ridge in Figure 14.1.5 , we can increase the rate at which we approach the optimum by taking larger steps. If the step size is too large, however, the difference between the experimental optimum and the true optimum may be unacceptably large. One solution is to adjust the step size during the search, using larger steps at the beginning and smaller steps as we approach the global optimum.

One-Factor-at-a-Time Optimization

A simple algorithm for optimizing the quantitative method for vanadium described earlier is to select initial concentrations for H_2O_2 and H_2SO_4 and measure the absorbance. Next, we optimize one reagent by increasing or decreasing its concentration—holding constant the second reagent's concentration—until the absorbance decreases. We then vary the concentration of the second reagent—maintaining the first reagent's optimum concentration—until we no longer see an increase in the absorbance. We can stop this process, which we call a ***one-factor-at-a-time optimization***, after one cycle or repeat the steps until the absorbance reaches a maximum value or it exceeds an acceptable threshold value.

A one-factor-at-a-time optimization is consistent with a notion that to determine the influence of one factor we must hold constant all other factors. This is an effective, although not necessarily an efficient experimental design when the factors are independent [Sharaf, M. A.; Illman, D. L.; Kowalski, B. R. *Chemometrics*, Wiley-Interscience: New York, 1986]. Two factors are independent when a change in the level of one factor does not influence the effect of a change in the other factor's level. Table 14.1.1 provides an example of two independent factors.

Table 14.1.1 . Example of Two Independent Factors

factor A	factor B	response
A_1	B_1	40
A_2	B_1	80

factor A	factor B	response
A_1	B_2	60
A_2	B_2	100

If we hold factor B at level B_1, changing factor A from level A_1 to level A_2 increases the response from 40 to 80, or a change in response, ΔR of

$$R = 80 - 40 = 40$$

If we hold factor B at level B_2, we find that we have the same change in response when the level of factor A changes from A_1 to A_2.

$$R = 100 - 60 = 40$$

We can see this independence visually if we plot the response as a function of factor A's level, as shown in Figure 14.1.6 . The parallel lines show that the level of factor B does not influence factor A's effect on the response.

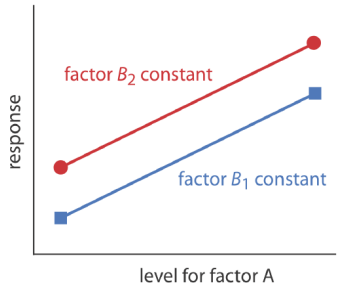

Figure 14.1.6 . Factor effect plot for two independent factors. Note that the two lines are parallel, indicating that the level for factor B does not influence how factor A's level affects the response.

Exercise 14.1.1

Using the data in Table 14.1.1 , show that the effect of factor B on the response is independent of factor A.

Answer

If we hold factor A at level A_1, changing factor B from level B_1 to level B_2 increases the response from 40 to 60, or a change, ΔR, of

$$\Delta R = 60 - 40 = 20$$

If we hold factor A at level A_2, we find that we have the same change in response when the level of factor B changes from B_1 to B_2.

$$\Delta R = 100 - 80 = 20$$

Mathematically, two factors are independent if they do not appear in the same term in the equation that describes the response surface. Equation 14.1.1 , for example, describes a response surface with independent factors because no term in the equation includes both factor A and factor B.

$$R = 2.0 + 0.12A + 0.48B - 0.03A^2 - 0.03B^2 \tag{5.1.1}$$

Figure 14.1.7 shows the resulting pseudo-three-dimensional surface and a contour map for Equation 5.1.1.

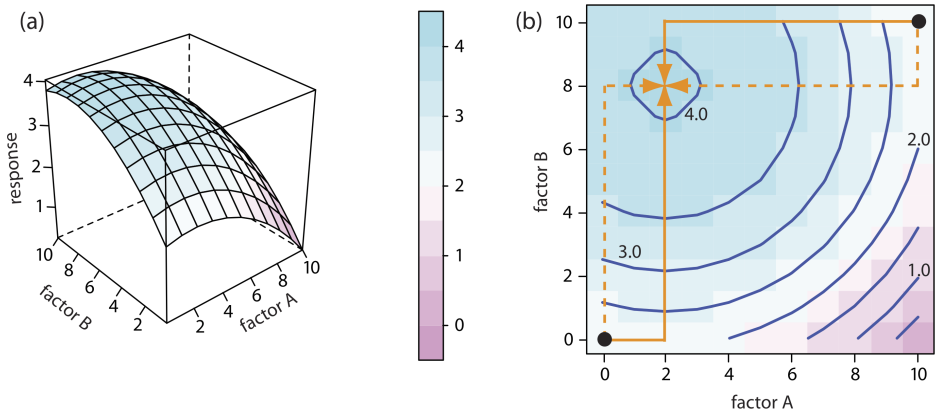

Figure 14.1.7 . The response surface for two independent factors based on Equation 5.1.1, displayed as (a) a wireframe, and as (b) an overlaid contour plot and level plot. The orange lines in (b) show the progress of one-factor-at-a-time optimizations beginning from two starting points (•) and optimizing factor *A* first (solid line) or factor *B* first (dashed line). All four trials reach the optimum response of (2,8) in a single cycle.

The easiest way to follow the progress of a searching algorithm is to map its path on a contour plot of the response surface. Positions on the response surface are identified as (*a*, *b*) where *a* and *b* are the levels for factor *A* and for factor *B*. The contour plot in Figure 14.1.7 b, for example, shows four one-factor-at-a-time optimizations of the response surface for Equation 5.1.1. The effectiveness and efficiency of this algorithm when optimizing independent factors is clear—each trial reaches the optimum response at (2, 8) in a single cycle.

Unfortunately, factors often are not independent. Consider, for example, the data in Table 14.1.2

Table 14.1.2 . Example of Two Dependent Factors

factor A	factor B	response
A_1	B_1	20
A_2	B_1	80
A_1	B_2	60
A_2	B_2	80

where a change in the level of factor *B* from level B_1 to level B_2 has a significant effect on the response when factor *A* is at level A_1

$$R = 60 - 20 = 40$$

but no effect when factor *A* is at level A_2.

$$R = 80 - 80 = 0$$

Figure 14.1.8 shows this ***dependent*** relationship between the two factors. Factors that are dependent are said to interact and the equation for the response surface' includes an interaction term that contains both factor *A* and factor *B*. The final term in equation 14.1.2 , for example, accounts for the interaction between factor *A* and factor *B*.

$$R = 5.5 + 1.5A + 0.6B - 0.15A^2 - 0.245B^2 - 0.0857AB \tag{5.1.2}$$

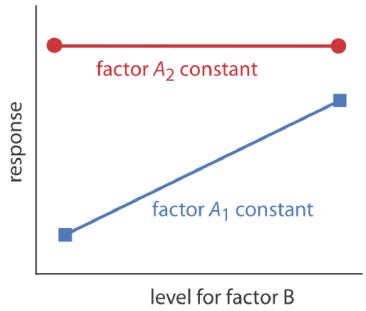

Figure 14.1.8 . Factor effect plot for two dependent factors. Note that the two lines are not parallel, indicating that the level for factor *A* influences how factor *B*'s level affects the response.

Figure 14.1.9 shows the resulting pseudo-three-dimensional surface and a contour map for Equation 5.1.2.

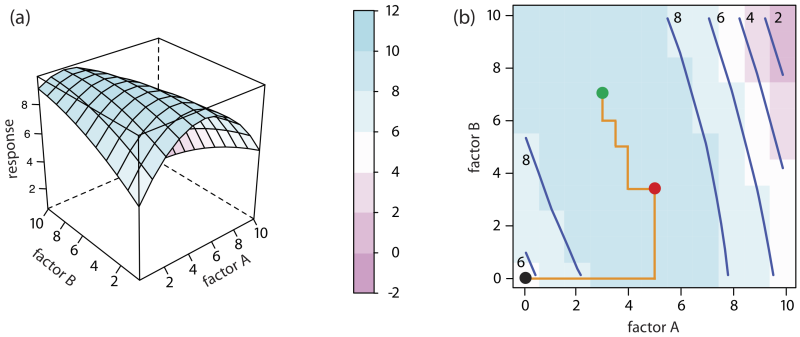

Figure 14.1.9 . The response surface for two dependent factors based on Equation 5.1.2, displayed as (a) a wireframe, and as (b) an overlaid contour plot and level plot. The orange lines in (b) show the progress of one-factor-at-a-time optimization beginning from the starting point (•) and optimizing factor *A* first. The red dot (•) marks the end of the first cycle. It takes four cycles to reach the optimum response of (3, 7) as shown by the green dot (•).

? Exercise 14.1.2

Using the data in Table 14.1.2 , show that the effect of factor *A* on the response is dependent on factor *B*.

Answer

If we hold factor *B* at level B_1, changing factor *A* from level A_1 to level A_2 increases the response from 20 to 80, or a change, ΔR, of

$$\Delta R = 80 - 20 = 60$$

If we hold factor *B* at level B_2, we find that the change in response when the level of factor *A* changes from A_1 to A_2 is now 20.

$$\Delta R = 80 - 60 = 20$$

The progress of a one-factor-at-a-time optimization for Equation 5.1.2 is shown in Figure 14.1.9 b. Although the optimization for dependent factors is effective, it is less efficient than that for independent factors. In this case it takes four cycles to reach the optimum response of (3, 7) if we begin at (0, 0).

Simplex Optimization

One strategy for improving the efficiency of a searching algorithm is to change more than one factor at a time. A convenient way to accomplish this when there are two factors is to begin with three sets of initial factor levels as the vertices of a triangle. After measuring the response for each set of factor levels, we identify the combination that gives the worst response and replace it with a new set of factor levels using a set of rules (Figure 14.1.10). This process continues until we reach the global optimum or until no further optimization is possible. The set of factor levels is called a ***simplex***. In general, for *k* factors a simplex is a $k+1$ dimensional geometric figure [(a) Spendley, W.; Hext, G. R.; Himsworth, F. R. *Technometrics* **1962**, *4*, 441–461; (b) Deming, S. N.; Parker, L. R. *CRC Crit. Rev. Anal. Chem.* **1978** *7(3)*, 187–202].

Thus, for two factors the simplex is a triangle. For three factors the simplex is a tetrahedron.

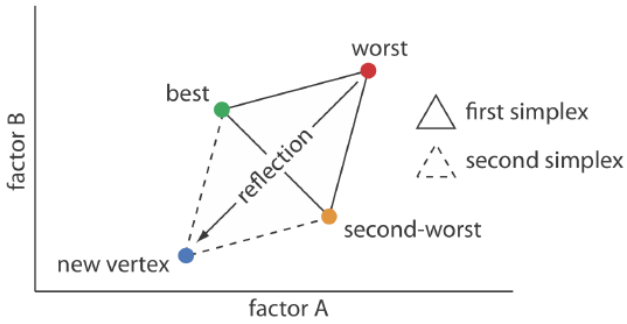

Figure 14.1.10 . Example of a two-factor simplex. The original simplex is formed by the green, orange, and red vertices. Replacing the worst vertex with a new vertex moves the simplex to a new position on the response surface.

To place the initial two-factor simplex on the response surface, we choose a starting point (a, b) for the first vertex and place the remaining two vertices at ($a + s_a$, b) and ($a + 0.5s_a$, $b + 0.87s_b$) where s_a and s_b are step sizes for factor A and for factor B [Long, D. E. *Anal. Chim. Acta* **1969**, *46*, 193–206]. The following set of rules moves the simplex across the response surface in search of the optimum response:

Rule 1. Rank the vertices from best (v_b) to worst (v_w).

Rule 2. Reject the worst vertex (v_w) and replace it with a new vertex (v_n) by reflecting the worst vertex through the midpoint of the remaining vertices. The new vertex's factor levels are twice the average factor levels for the retained vertices minus the factor levels for the worst vertex. For a two-factor optimization, the equations are shown here where v_s is the third vertex.

$$a_{v_n} = 2\left(\frac{a_{v_b} + a_{v_s}}{2}\right) - a_{v_w} \tag{5.1.3}$$

$$b_{v_n} = 2\left(\frac{b_{v_b} + b_{v_s}}{2}\right) - b_{v_w} \tag{5.1.4}$$

Rule 3. If the new vertex has the worst response, then return to the previous vertex and reject the vertex with the second worst response, (v_s) calculating the new vertex's factor levels using rule 2. This rule ensures that the simplex does not return to the previous simplex.

Rule 4. Boundary conditions are a useful way to limit the range of possible factor levels. For example, it may be necessary to limit a factor's concentration for solubility reasons, or to limit the temperature because a reagent is thermally unstable. If the new vertex exceeds a boundary condition, then assign it the worst response and follow rule 3.

The variables a and b in Equation 5.1.3 and Equation 5.1.4 are the factor levels for factor A and for factor B, respectively. Problem 3 in the end-of-chapter problems asks you to derive these equations.

Because the size of the simplex remains constant during the search, this algorithm is called a ***fixed-sized simplex optimization***. Example 14.1.1 illustrates the application of these rules.

Example 14.1.1

Find the optimum for the response surface in Figure 14.1.9 using the fixed-sized simplex searching algorithm. Use (0, 0) for the initial factor levels and set each factor's step size to 1.00.

Solution

Letting a = 0, b =0, s_a = 1.00, and s_b = 1.00 gives the vertices for the initial simplex as

$$\text{vertex } 1{:}(a, b) = (0, 0)$$

$$\text{vertex } 2{:}(a + s_a, b) = (1.00, 0)$$

$$\text{vertex } 3\text{:}(a+0.5s_a, b+0.87s_b) = (0.50, 0.87)$$

The responses, from Equation 5.1.2, for the three vertices are shown in the following table

vertex	*a*	*b*	response
v_1	0	0	5.50
v_2	1.00	0	6.85
v_3	0.50	0.87	6.68

with v_1 giving the worst response and v_3 the best response. Following Rule 1, we reject v_1 and replace it with a new vertex using Equation 5.1.3 and Equation 5.1.4; thus

$$a_{v_4} = 2\left(\frac{1.00+0.50}{2}\right) - 0 = 1.50$$

$$b_{v_4} = 2\left(\frac{0+0.87}{2}\right) - 0 = 0.87$$

The following table gives the vertices of the second simplex.

vertex	*a*	*b*	response
v_2	1.50	0	6.85
v_3	0.50	0.87	6.68
v_4	1.50	0.87	7.80

with v_3 giving the worst response and v_4 the best response. Following Rule 1, we reject v_3 and replace it with a new vertex using Equation 5.1.3 and Equation 5.1.4; thus

$$a_{v_5} = 2\left(\frac{1.00+1.50}{2}\right) - 0.50 = 2.00$$

$$b_{v_5} = 2\left(\frac{0+0.87}{2}\right) - 0.87 = 0$$

The following table gives the vertices of the third simplex.

vertex	*a*	*b*	response
v_2	1.50	0	6.85
v_4	1.50	0.87	780
v_5	2.00	0	7.90

The calculation of the remaining vertices is left as an exercise. Figure 14.1.11 shows the progress of the complete optimization. After 29 steps the simplex begins to repeat itself, circling around the optimum response of (3, 7).

The size of the initial simplex ultimately limits the effectiveness and the efficiency of a fixed-size simplex searching algorithm. We can increase its efficiency by allowing the size of the simplex to expand or to contract in response to the rate at which we approach the optimum. For example, if we find that a new vertex is better than any of the vertices in the preceding simplex, then we expand the simplex further in this direction on the assumption that we are moving directly toward the optimum. Other conditions might cause us to contract the simplex—to make it smaller—to encourage the optimization to move in a different direction. We call this a ***variable-sized simplex optimization***. Consult this chapter's additional resources for further details of the variable-sized simplex optimization.

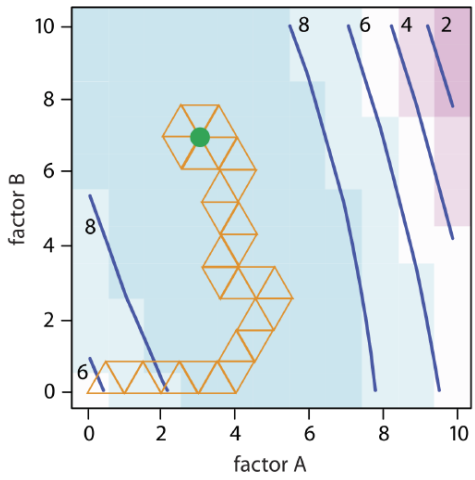

Figure 14.1.11 . Progress of the fixed-size simplex optimization in Example 14.1.1 . The green dot (•) marks the optimum response of (3,7). Optimization ends when the simplexes begin to circle around a single vertex.

Mathematical Models of Response Surfaces

A response surface is described mathematically by an equation that relates the response to its factors. Equation 5.1.1 and Equation 5.1.2 provide two examples of such mathematical models. If we measure the response for several combinations of factor levels, then we can model the response surface by using a regression analysis to fit an appropriate equation to the data. There are two broad categories of models that we can use for a regression analysis: theoretical models and empirical models.

Theoretical Models of the Response Surface

A theoretical model is derived from the known chemical and physical relationships between the response and its factors. In spectrophotometry, for example, Beer's law is a theoretical model that relates an analyte's absorbance, A, to its concentration, C_A

$$A = \epsilon b C_A$$

where ϵ is the molar absorptivity and b is the pathlength of the electromagnetic radiation passing through the sample. A Beer's law calibration curve, therefore, is a theoretical model of a response surface.

> For a review of Beer's law, see Chapter 10.2. Figure 14.1.1 in this chapter is an example of a Beer's law calibration curve.

Empirical Models of the Response Surface

In many cases the underlying theoretical relationship between the response and its factors is unknown. We still can develop a model of the response surface if we make some reasonable assumptions about the underlying relationship between the factors and the response. For example, if we believe that the factors A and B are independent and that each has only a first-order effect on the response, then the following equation is a suitable model.

$$R = \beta_0 + \beta_a A + \beta_b B$$

where R is the response, A and B are the factor levels, and β_0, β_a, and β_b are adjustable parameters whose values are determined by a linear regression analysis. Other examples of equations include those for dependent factors

$$R = \beta_0 + \beta_a A + \beta_b B + \beta_{ab} AB$$

and those with higher-order terms.

$$R = \beta_0 + \beta_a A + \beta_b B + \beta_{aa} A^2 + \beta_{bb} B^2$$

Each of these equations provides an ***empirical model*** of the response surface because it has no basis in a theoretical understanding of the relationship between the response and its factors. Although an empirical model may provide an excellent description of the

response surface over a limited range of factor levels, it has no basis in theory and we cannot reliably extend it to unexplored parts of the response surface.

> The calculations for a linear regression when the model is first-order in one factor (a straight line) are described in Chapter 5.4. A complete mathematical treatment of linear regression for models that are second-order in one factor or which contain more than one factor is beyond the scope of this text. The computations for a few special cases, however, are straightforward and are considered in this section. A more comprehensive treatment of linear regression is available in several of this chapter's additional resources.

Factorial Designs

To build an empirical model we measure the response for at least two levels for each factor. For convenience we label these levels as high, H_f, and low, L_f, where f is the factor; thus H_A is the high level for factor A and L_B is the low level for factor B. If our empirical model contains more than one factor, then each factor's high level is paired with both the high level and the low level for all other factors. In the same way, the low level for each factor is paired with the high level and the low level for all other factors. As shown in Figure 14.1.12 , this requires 2^k experiments where k is the number of factors. This experimental design is known as a ***2^k factorial design***.

> Another system of notation is to use a plus sign (+) to indicate a factor's high level and a minus sign (–) to indicate its low level. We will use H or L when writing an equation and a plus sign or a minus sign in tables.

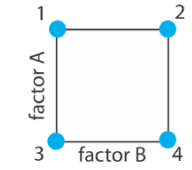

factor levels

trial	A	B
1	+	–
2	+	+
3	–	–
4	–	+

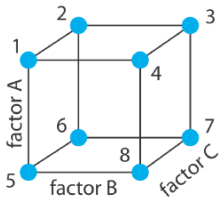

factor levels

trial	A	B	C
1	+	–	–
2	+	–	+
3	+	+	+
4	+	+	–
5	–	–	–
6	–	–	+
7	–	+	+
8	–	+	–

Figure 14.1.12 . 2^k factorial designs for (top) $k = 2$, and for (bottom) $k = 3$. A 2^2 factorial design requires four experiments and a 2^3 factorial design requires eight experiments.

Coded Factor Levels

The calculations for a 2^k factorial design are straightforward and easy to complete with a calculator or a spreadsheet. To simplify the calculations, we code the factor levels using $+1$ for a high level and -1 for a low level. Coding has two additional advantages: scaling the factors to the same magnitude makes it easier to evaluate each factor's relative importance, and it places the model's intercept, β_0, at the center of the experimental design. As shown in Example 14.1.2 , it is easy to convert between coded and uncoded factor levels.

Example 14.1.2

To explore the effect of temperature on a reaction, we assign 30ºC to a coded factor level of -1 and assign a coded level $+1$ to a temperature of 50ºC. What temperature corresponds to a coded level of -0.5 and what is the coded level for a temperature of 60ºC?

Solution

The difference between -1 and $+1$ is 2, and the difference between 30°C and 50°C is 20°C; thus, each unit in coded form is equivalent to 10°C in uncoded form. With this information, it is easy to create a simple scale between the coded and the uncoded values, as shown in Figure 14.1.13 . A temperature of 35°C corresponds to a coded level of -0.5 and a coded level of $+2$ corresponds to a temperature of 60°C.

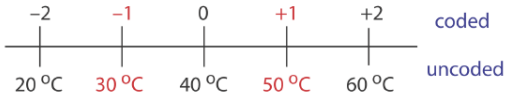

Figure 14.1.13 . The relationship between the coded factor levels and the uncoded factor levels for Example 14.1.2 . The numbers in red are the values defined in the 2^2 factorial design.

Determining the Empirical Model

Let's begin by considering a simple example that involves two factors, *A* and *B*, and the following empirical model.

$$R = \beta_0 + \beta_a A + \beta_b B + \beta_{ab} AB \tag{5.1.5}$$

A 2^k factorial design with two factors requires four runs. Table 14.1.3 provides the uncoded levels (*A* and *B*), the coded levels (*A** and *B**), and the responses (*R*) for these experiments. The terms β_0, β_a, β_b, and β_{ab} in Equation 5.1.5 account for, respectively, the mean effect (which is the average response), the first-order effects due to factor *A* and to factor *B*, and the interaction between the two factors.

Table 14.1.3 . Example of Uncoded and Coded Factor Levels and Responses for a 2^k Factorial Design

run	*A*	*B*	*A**	*B**	*R*
1	15	30	+1	+1	22.5
2	15	10	+1	−1	11.5
3	5	30	−1	+1	17.5
4	5	10	−1	−1	8.5

Equation 5.1.5 has four unknowns—the four beta terms—and Table 14.1.3 describes the four experiments. We have just enough information to calculate values for β_0, β_a, β_b, and β_{ab}. When working with the coded factor levels, the values of these parameters are easy to calculate using the following equations, where *n* is the number of runs.

$$\beta_0 \approx b_0 = \frac{1}{n}\sum_{i=1}^{n} R_i \tag{5.1.6}$$

$$\beta_a \approx b_a = \frac{1}{n}\sum_{i=1}^{n} A_i^* R_i \tag{5.1.7}$$

$$\beta_b \approx b_b = \frac{1}{n}\sum_{i=1}^{n} B_i^* R_i \tag{5.1.8}$$

$$\beta_{ab} \approx b_{ab} = \frac{1}{n}\sum_{i=1}^{n} A_i^* B_i^* R_i \tag{5.1.9}$$

Solving for the estimated parameters using the data in Table 14.1.3

$$b_0 = \frac{22.5 + 11.5 + 17.5 + 8.5}{4} = 15.0$$

$$b_a = \frac{22.5 + 11.5 - 17.5 - 8.5}{4} = 2.0$$

$$b_b = \frac{22.5 - 11.5 + 17.5 - 8.5}{4} = 5.0$$

$$b_{ab} = \frac{22.5 - 11.5 - 17.5 + 8.5}{4} = 0.5$$

leaves us with the coded empirical model for the response surface.

$$R = 15.0 + 2.0A^* + 5.0B^* + 0.05A^*B^* \tag{5.1.10}$$

Recall that we introduced coded factor levels with the promise that they simplify calculations. Although we can convert this coded model into its uncoded form, there is no need to do so. If we need to know the response for a new set of factor levels, we just convert them into coded form and calculate the response. For example, if *A* is 10 and *B* is 15, then *A** is 0 and *B** is –0.5. Substituting these values into Equation 5.1.10 gives a response of 12.5.

We can extend this approach to any number of factors. For a system with three factors—*A*, *B*, and *C*—we can use a 2^3 factorial design to determine the parameters in the following empirical model

$$R = \beta_0 + \beta_a A + \beta_b B + \beta_c C + \beta_{ab} AB + \beta_{ac} AC + \beta_{bc} BC + \beta_{abc} ABC \tag{5.1.11}$$

where *A*, *B*, and *C* are the factor levels. The terms β_0, β_a, β_b, and β_{ab} are estimated using Equation 5.1.6, Equation 5.1.7, Equation 5.1.8, and Equation 5.1.9, respectively. To find estimates for the remaining parameters we use the following equations.

$$\beta_c \approx b_c = \frac{1}{n}\sum_{i=1}^{n} C_i^* R \tag{5.1.12}$$

$$\beta_{ac} \approx b_{ac} = \frac{1}{n}\sum_{i=1}^{n} A_i^* C_i^* R \tag{5.1.13}$$

$$\beta_{bc} \approx b_{bc} = \frac{1}{n}\sum_{i=1}^{n} B_i^* C_i^* R \tag{5.1.14}$$

$$\beta_{abc} \approx b_{abc} = \frac{1}{n}\sum_{i=1}^{n} A_i^* B_i^* C_i^* R \tag{5.1.15}$$

Example 14.1.3

Table 14.1.4 lists the uncoded factor levels, the coded factor levels, and the responses for a 2^3 factorial design. Determine the coded empirical model for the response surface based on Equation 5.1.11. What is the expected response when *A* is 10, *B* is 15, and *C* is 50?

Solution

Equation 5.1.11 has eight unknowns—the eight beta terms—and Table 14.1.4 describes eight experiments. We have just enough information to calculate values for β_0, β_a, β_b, β_{ab}, β_{ac}, β_{bc}, and β_{abc}; these values are

$$b_0 = \frac{1}{8} \times (137.25 + 54.75 + 73.75 + 30.25 + 61.75 + 30.25 + 41.25 + 18.75) = 56.0$$

$$b_a = \frac{1}{8} \times (137.25 + 54.75 + 73.75 + 30.25 - 61.75 - 30.25 - 41.25 - 18.75) = 18.0$$

$$b_b = \frac{1}{8} \times (137.25 + 54.75 - 73.75 - 30.25 + 61.75 + 30.25 - 41.25 - 18.75) = 15.0$$

$$b_c = \frac{1}{8} \times (137.25 - 54.75 + 73.75 - 30.25 + 61.75 - 30.25 + 41.25 - 18.75) = 22.5$$

$$b_{ab} = \frac{1}{8} \times (137.25 + 54.75 - 73.75 - 30.25 - 61.75 - 30.25 + 41.25 + 18.75) = 7.0$$

$$b_{ac} = \frac{1}{8} \times (137.25 - 54.75 + 73.75 - 30.25 - 61.75 + 30.25 - 41.25 + 18.75) = 9.0$$

$$b_{bc} = \frac{1}{8} \times (137.25 - 54.75 - 73.75 + 30.25 + 61.75 - 30.25 - 41.25 + 18.75) = 6.0$$

$$b_{abc} = \frac{1}{8} \times (137.25 - 54.75 - 73.75 + 30.25 - 61.75 + 30.25 + 41.25 - 18.75) = 3.75$$

The coded empirical model, therefore, is

$$R = 56.0 + 18.0A^* + 15.0B^* + 22.5C^* + 7.0A^*B^* + 9.0A^*C^* + 6.0B^*C^* + 3.75A^*B^*C^*$$

To find the response when A is 10, B is 15, and C is 50, we first convert these values into their coded form. Figure 14.1.14 helps us make the appropriate conversions; thus, A^* is 0, B^* is -0.5, and C^* is $+1.33$. Substituting back into the empirical model gives a response of

$$R = 56.0 + 18.0(0) + 15.0(-0.5) + 22.5(+1.33) + 7.0(0)(-0.5) + 9.0(0)(+1.33) + 6.0(-0.5)(+1.33) + 3.75(0)(-0.5)(+1.33) = 74.435 \approx 74.4$$

Table 14.1.4 . Example of Uncoded and Coded Factor Levels and Responses for the 2^3 Factorial Design in Example 14.1.3 .

run	A	B	C	A^*	B^*	C^*	R
1	15	30	45	+1	+1	+1	137.5
2	15	30	15	+1	+1	−1	54.75
3	15	10	45	+1	−1	+1	73.75
4	15	10	15	+1	−1	−1	30.25
5	5	30	45	−1	+1	+1	61.75
6	5	30	15	−1	+1	−1	30.25
7	5	10	45	−1	−1	+1	41.25
8	5	10	15	−1	−1	−1	18.75

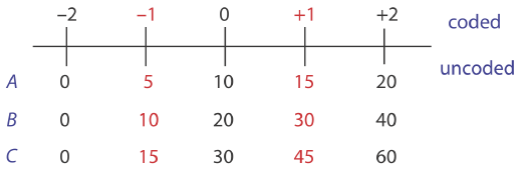

Figure 14.1.14 . The relationship between the coded factor levels and the uncoded factor levels for Example 14.1.3 . The numbers in red are the values defined in the 2^3 factorial design.

A 2^k factorial design can model only a factor's first-order effect, including first-order interactions, on the response. A 2^2 factorial design, for example, includes each factor's first-order effect (β_a and β_b) and a first-order interaction between the factors (β_{ab}). A 2^k factorial design cannot model higher-order effects because there is insufficient information. Here is simple example that illustrates the problem. Suppose we need to model a system in which the response is a function of a single factor, A. Figure 14.1.15 a shows the result of an experiment using a 2^1 factorial design. The only empirical model we can fit to the data is a straight line.

$$R = \beta_0 + \beta_a A$$

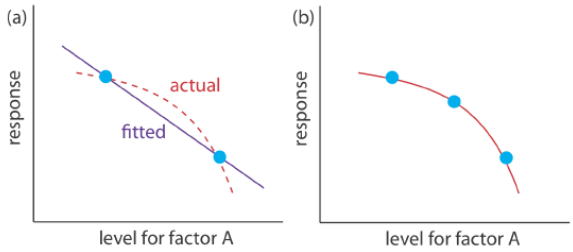

Figure 14.1.15 . A curved one-factor response surface, in red, showing (a) the limitation of using a 2^1 factorial design, which can fit only a straight-line to the data, and (b) the application of a 3^1 factorial design that takes into account second-order effects.

If the actual response is a curve instead of a straight-line, then the empirical model is in error. To see evidence of curvature we must measure the response for at least three levels for each factor. We can fit the 3^1 factorial design in Figure 14.1.15 b to an empirical model that includes second-order factor effects.

$$R = \beta_0 + \beta_a A + \beta_{aa} A^2$$

In general, an *n*-level factorial design can model single-factor and interaction terms up to the $(n - 1)$th order.

We can judge the effectiveness of a first-order empirical model by measuring the response at the center of the factorial design. If there are no higher-order effects, then the average response of the trials in a 2^k factorial design should equal the measured response at the center of the factorial design. To account for influence of random errors we make several determinations of the response at the center of the factorial design and establish a suitable confidence interval. If the difference between the two responses is significant, then a first-order empirical model probably is inappropriate.

One of the advantages of working with a coded empirical model is that b_0 is the average response of the $2 \times k$ trials in a 2^k factorial design.

Example 14.1.4

One method for the quantitative analysis of vanadium is to acidify the solution by adding H_2SO_4 and oxidizing the vanadium with H_2O_2 to form a red-brown soluble compound with the general formula $(VO)_2(SO_4)_3$. Palasota and Deming studied the effect of the relative amounts of H_2SO_4 and H_2O_2 on the solution's absorbance, reporting the following results for a 2^2 factorial design [Palasota, J. A.; Deming, S. N. *J. Chem. Educ.* **1992**, *62*, 560–563].

H_2SO_4	H_2O_2	absorbance
$+1$	$+1$	0.330
$+1$	-1	0.359
-1	$+1$	0.293
-1	-1	0.420

Four replicate measurements at the center of the factorial design give absorbances of 0.334, 0.336, 0.346, and 0.323. Determine if a first-order empirical model is appropriate for this system. Use a 90% confidence interval when accounting for the effect of random error.

Solution

We begin by determining the confidence interval for the response at the center of the factorial design. The mean response is 0.335 with a standard deviation of 0.0094, which gives a 90% confidence interval of

$$\mu = \overline{X} \pm \frac{ts}{\sqrt{n}} = 0.335 \pm \frac{(2.35)(0.0094)}{\sqrt{4}} = 0.335 \pm 0.011$$

The average response, $\overline{R}$, from the factorial design is

$$\overline{R} = \frac{0.330 + 0.359 + 0.293 + 0.420}{4} = 0.350$$

Because $\overline{R}$ exceeds the confidence interval's upper limit of 0.346, we can reasonably assume that a 2^2 factorial design and a first-order empirical model are inappropriate for this system at the 95% confidence level.

Central Composite Designs

One limitation to a 3^k factorial design is the number of trials we need to run. As shown in Figure 14.1.16 , a 3^2 factorial design requires 9 trials. This number increases to 27 for three factors and to 81 for 4 factors.

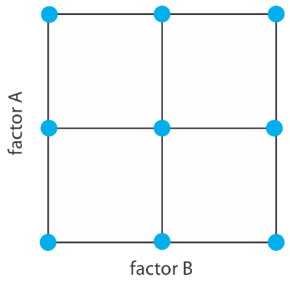

Figure 14.1.16 . A 3^k factorial design for k = 2.

A more efficient experimental design for a system that contains more than two factors is a central composite design, two examples of which are shown in Figure 14.1.17 . The central composite design consists of a 2^k factorial design, which provides data to estimate each factor's first-order effect and interactions between the factors, and a star design that has $2^k + 1$ points, which provides data to estimate second-order effects. Although a central composite design for two factors requires the same number of trials, nine, as a 3^2 factorial design, it requires only 15 trials and 25 trials when using three factors or four factors. See this chapter's additional resources for details about the central composite designs.

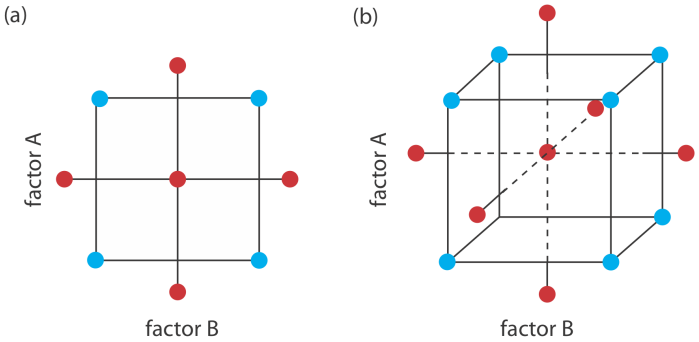

Figure 14.1.17 . Two examples of a central composite design for (a) k = 2 and (b) k = 3. The points in blue are a 2^k factorial design, and the points in red are a star design.

5.2: Verifying the Method

After developing and optimizing a method, the next step is to determine how well it works in the hands of a single analyst. Three steps make up this process: determining single-operator characteristics, completing a blind analysis of standards, and determining the method's ruggedness. If another standard method is available, then we can analyze the same sample using both the standard method and the new method, and compare the results. If the result for any single test is unacceptable, then the method is not a suitable standard method.

Single Operator Characteristics

The first step in verifying a method is to determine the precision, accuracy, and detection limit when a single analyst uses the method to analyze a standard sample. The detection limit is determined by analyzing an appropriate reagent blank. Precision is determined by analyzing replicate portions of the sample, preferably more than ten. Accuracy is evaluated using a *t*-test to compare the experimental results to the known amount of analyte in the standard. Precision and accuracy are evaluated for several different concentrations of analyte, including at least one concentration near the detection limit, and for each different sample matrix. Including different concentrations of analyte helps to identify constant sources of determinate error and to establish the range of concentrations for which the method is applicable.

Blind Analysis of Standard Samples

Single-operator characteristics are determined by analyzing a standard sample that has a concentration of analyte known to the analyst. The second step in verifying a method is a ***blind analysis*** of standard samples. Although the concentration of analyte in the standard is known to a supervisor, the information is withheld from the analyst. After analyzing the standard sample several times, the analyte's average concentration is reported to the test's supervisor. To be accepted, the experimental mean must be within three standard deviations—as determined from the single-operator characteristics—of the analyte's known concentration.

> An even more stringent requirement is to require that the experimental mean be within two standard deviations of the analyte's known concentration.

Ruggedness Testing

An optimized method may produce excellent results in the laboratory that develops a method, but poor results in other laboratories. This is not particularly surprising because a method typically is optimized by a single analyst using the same reagents, equipment, and instrumentation for each trial. Any variability introduced by different analysts, reagents, equipment, and instrumentation is not included in the single-operator characteristics. Other less obvious factors may affect an analysis, including environmental factors, such as the temperature or relative humidity in the laboratory; if the procedure does not require control of these conditions, then they may contribute to variability. Finally, the analyst who optimizes the method usually takes particular care to perform the analysis in exactly the same way during every trial, which may minimize the run-to-run variability.

An important step in developing a standard method is to determine which factors have a pronounced effect on the quality of the results. Once we identify these factors, we can write specific instructions that specify how these factors must be controlled. A procedure that, when carefully followed, produces results of high quality in different laboratories is considered rugged. The method by which the critical factors are discovered is called ***ruggedness testing*** [Youden, W. J. *Anal. Chem.* **1960**, *32(13)*, 23A–37A].

> For example, if temperature is a concern, we might specify that it be held at 25 ± 2^{o}C.

Ruggedness testing usually is performed by the laboratory that develops the standard method. After identifying potential factors, their effects on the response are evaluated by performing the analysis at two levels for each factor. Normally one level is that specified in the procedure, and the other is a level likely encountered when the procedure is used by other laboratories.

This approach to ruggedness testing can be time consuming. If there are seven potential factors, for example, a 2^7 factorial design can evaluate each factor's first-order effect. Unfortunately, this requires a total of 128 trials—too many trials to be a practical solution. A simpler experimental design is shown in Table 14.2.1 , in which the two factor levels are identified by upper case and lower case letters. This design, which is similar to a 2^3 factorial design, is called a fractional factorial design. Because it includes

only eight runs, the design provides information only the average response and the seven first-order factor effects. It does not provide sufficient information to evaluate higher-order effects or interactions between factors, both of which are probably less important than the first-order effects.

Table 14.2.1 . Experimental Design for a Ruggedness Test Involving Seven Factors

run	A	B	C	D	E	F	G	response
1	*A*	*B*	*C*	*D*	*E*	*F*	*G*	R_1
2	*A*	*B*	*c*	*D*	*e*	*f*	*g*	R_2
3	*A*	*b*	*C*	*d*	*E*	*f*	*g*	R_3
4	*A*	*b*	*c*	*d*	*e*	*F*	*G*	R_4
5	*a*	*B*	*C*	*d*	*e*	*F*	*g*	R_5
6	*a*	*B*	*c*	*d*	*E*	*f*	*G*	R_6
7	*a*	*b*	*C*	*D*	*e*	*f*	*G*	R_7
8	*a*	*b*	*c*	*D*	*E*	*F*	*g*	*R*

The experimental design in Table 14.2.1 is balanced in that each of a factor's two levels is paired an equal number of times with the upper case and lower case levels for every other factor. To determine the effect, *E*, of changing a factor's level, we subtract the average response when the factor is at its upper case level from the average value when it is at its lower case level.

$$E = \frac{(\sum R_i)_{\text{upper case}}}{4} - \frac{(\sum R_i)_{\text{lower case}}}{4} \tag{5.2.1}$$

Because the design is balanced, the levels for the remaining factors appear an equal number of times in both summation terms, canceling their effect on *E*. For example, to determine the effect of factor *A*, E_A, we subtract the average response for runs 5–8 from the average response for runs 1–4. Factor *B* does not affect *E* because its upper case levels in runs 1 and 2 are canceled by the upper case levels in runs 5 and 6, and its lower case levels in runs 3 and 4 are canceled by the lower case levels in runs 7 and 8. After we calculate each of the factor effects we rank them from largest to smallest without regard to sign, identifying those factors whose effects are substantially larger than the other factors.

> To see that this is design is balanced, look closely at the last four runs. Factor *A* is present at its level *a* for all four of these runs. For each of the remaining factors, two levels are upper case and two levels are lower case. Runs 5–8 provide information about the effect of *a* on the response, but do not provide information about the effect of any other factor. Runs 1, 2, 5, and 6 provide information about the effect of *B*, but not of the remaining factors. Try a few other examples to convince yourself that this relationship is general.

We also can use this experimental design to estimate the method's expected standard deviation due to the effects of small changes in uncontrolled or poorly controlled factors [Youden, W. J. "Statistical Techniques for Collaborative Tests," in *Statistical Manual of the Association of Official Analytical Chemists*, Association of Official Analytical Chemists: Washington, D. C., 1975, p. 35].

$$s = \sqrt{\frac{2}{7}\sum_{i=1}^{n} E_i^2} \tag{5.2.2}$$

If this standard deviation is too large, then the procedure is modified to bring under control the factors that have the greatest effect on the response.

> Why does this model estimate the seven first-order factor effects, *E*, and not seven of the 20 possible first-order interactions? With eight experiments, we can only choose to calculate seven parameters (plus the average response). The calculation of E_D, for example, also gives the value for E_{AB}. You can convince yourself of this by replacing each upper case letter with a $+1$ and

each lower case letter with a -1 and noting that $A \times B = D$. We choose to report the first-order factor effects because they likely are more important than interactions between factors.

Example 14.2.1

The concentration of trace metals in sediment samples collected from rivers and lakes are determined by extracting with acid and analyzing the extract by atomic absorption spectrophotometry. One procedure calls for an overnight extraction using dilute HCl or HNO_3. The samples are placed in plastic bottles with 25 mL of acid and then placed on a shaker operated at a moderate speed and at ambient temperature. To determine the method's ruggedness, the effect of the following factors was studied using the experimental design in Table 14.2.1 .

Factor A: extraction time	*A* = 24 h	*a* = 12 h
Factor B: shaking speed	*B* = medium	*b* = high
Factor C: acid type	*C* = HCl	c = HNO_3
Factor D: acid concentration	*D* = 0.1 M	*d* = 0.05 M
Factor E: volume of acid	*E* = 25 mL	*e* = 35 mL
Factor F: type of container	*F* = plastic	*f* = glass
Factor G: temperature	*G* = ambient	*g* = 25ºC

Eight replicates of a standard sample that contains a known amount of analyte are carried through the procedure. The percentage of analyte recovered in the eight samples are as follows: R_1 = 98.9, R_2 = 99.0, R_3 = 97.5, R_4 = 97.7, R_5 = 97.4, R_6 = 97.3, R_7 = 98.6, and R_8 = 98.6. Identify the factors that have a significant effect on the response and estimate the method's expected standard deviation.

Solution

To calculate the effect of changing each factor's level we use Equation 5.2.1 and substitute in appropriate values. For example, E_A is

$$E_A = \frac{98.9 + 99.0 + 97.5 + 97.7}{4} - \frac{97.4 + 97.3 + 98.6 + 98.6}{4} = 0.30$$

Completing the remaining calculations and ordering the factors by the absolute values of their effects

Factor *D* = 1.30, Factor *A* = 0.35, Factor *E* = –0.10, Factor *B* = 0.05, Factor *C* = –0.05, Factor *F* = 0.05, Factor *G* = 0.00

shows us that the concentration of acid (Factor *D*) has a substantial effect on the response, with a concentration of 0.05 M providing a much lower percent recovery. The extraction time (Factor *A*) also appears significant, but its effect is not as important as the acid's concentration. All other factors appear insignificant. The method's estimated standard deviation is

$$s = \sqrt{\frac{2}{7} \times \left[(1.30)^2 + (0.35)^2 + (-0.10)^2 + (0.05)^2 + (-0.05)^2 + (0.05)^2 + (0.00)^2\right]} = 0.72$$

which, for an average recovery of 98.1% gives a relative standard deviation of approximately 0.7%. If we control the acid's concentration so that its effect approaches that for factors *B*, *C*, and *F*, then the relative standard deviation becomes 0.18, or approximately 0.2%.

Equivalency Testing

If an approved standard method is available, then a new method should be evaluated by comparing results to those obtained when using the standard method. Normally this comparison is made at a minimum of three concentrations of analyte to evaluate the new method over a wide dynamic range. Alternatively, we can plot the results obtained using the new method against results obtained using the approved standard method. A slope of 1.00 and a *y*-intercept of 0.0 provides evidence that the two methods are equivalent.

5.3: Validating the Method as a Standard Method

For an analytical method to be useful, an analyst must be able to achieve results of acceptable accuracy and precision. Verifying a method, as described in the previous section, establishes this goal for a single analyst. Another requirement for a useful analytical method is that an analyst should obtain the same result from day-to-day, and different labs should obtain the same result when analyzing the same sample. The process by which we approve a method for general use is known as ***validation*** and it involves a collaborative test of the method by analysts in several laboratories. Collaborative testing is used routinely by regulatory agencies and professional organizations, such as the U. S. Environmental Protection Agency, the American Society for Testing and Materials, the Association of Official Analytical Chemists, and the American Public Health Association. Many of the representative methods in earlier chapters are identified by these agencies as validated methods.

When an analyst performs a single analysis on a single sample the difference between the experimentally determined value and the expected value is influenced by three sources of error: random errors, systematic errors inherent to the method, and systematic errors unique to the analyst. If the analyst performs enough replicate analyses, then we can plot a distribution of results, as shown in Figure 14.3.1 a. The width of this distribution is described by a standard deviation that provides an estimate of the random errors affecting the analysis. The position of the distribution's mean, $\overline{X}$, relative to the sample's true value, μ, is determined both by systematic errors inherent to the method and those systematic errors unique to the analyst. For a single analyst there is no way to separate the total systematic error into its component parts.

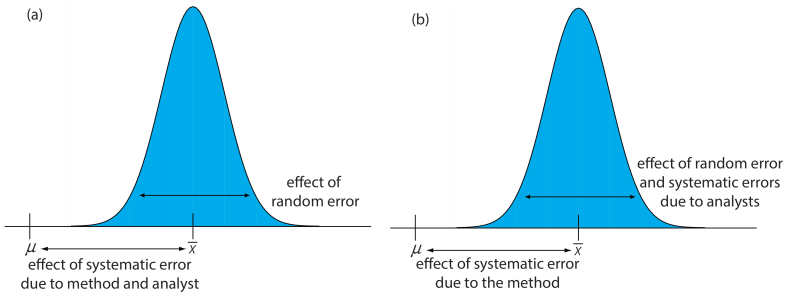

Figure 14.3.1 . Partitioning of random errors, systematic errors due to the analyst, and systematic errors due to the method for (a) replicate analyses performed by a single analyst and (b) single determinations performed by several analysts.

The goal of a collaborative test is to determine the magnitude of all three sources of error. If several analysts each analyze the same sample one time, the variation in their collective results (see Figure 14.3.1 b) includes contributions from random errors and systematic errors (biases) unique to the analysts. Without additional information, we cannot separate the standard deviation for this pooled data into the precision of the analysis and the systematic errors introduced by the analysts. We can use the position of the distribution, to detect the presence of a systematic error in the method.

Two-Sample Collaborative Testing

The design of a collaborative test must provide the additional information needed to separate random errors from the systematic errors introduced by the analysts. One simple approach—accepted by the Association of Official Analytical Chemists—is to have each analyst analyze two samples that are similar in both their matrix and in their concentration of analyte. To analyze the results we represent each analyst as a single point on a two-sample scatterplot, using the result for one sample as the *x*-coordinate and the result for the other sample as the *y*-coordinate [Youden, W. J. "Statistical Techniques for Collaborative Tests," in *Statistical Manual of the Association of Official Analytical Chemists*, Association of Official Analytical Chemists: Washington, D. C., 1975, pp 10–11].

As shown in Figure 14.3.2 , a two-sample chart places each analyst into one of four quadrants, which we identify as (+, +), (–, +), (–, –) and (+, –). A plus sign indicates the analyst's result for a sample is greater than the mean for all analysts and a minus sign indicates the analyst's result is less than the mean for all analysts. The quadrant (+, –), for example, contains those analysts that exceeded the mean for sample *X* and that undershot the mean for sample *Y*. If the variation in results is dominated by random errors, then we expect the points to be distributed randomly in all four quadrants, with an equal number of points in each quadrant. Furthermore, as shown in Figure 14.3.2 a, the points will cluster in a circular pattern whose center is the mean values for the two samples. When systematic errors are significantly larger than random errors, then the points fall primarily in the (+, +) and the (–, –) quadrants, forming an elliptical pattern around a line that bisects these quadrants at a 45º angle, as seen in Figure 14.3.2 b.

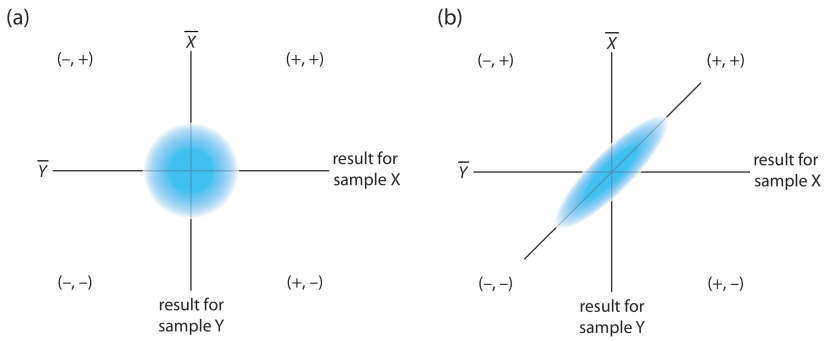

Figure 14.3.2 . Typical two-sample plots when (a) random errors are significantly larger than systematic errors due to the analysts, and (b) when systematic errors due to the analysts are significantly larger than the random errors.

A visual inspection of a two-sample chart is an effective method for qualitatively evaluating the capabilities of a proposed standard method, as shown in Figure 14.3.3 . The length of a perpendicular line from any point to the 45° line is proportional to the effect of random error on that analyst's results. The distance from the intersection of the axes—which corresponds to the mean values for samples *X* and *Y*—to the perpendicular projection of a point on the 45° line is proportional to the analyst's systematic error. An ideal standard method has small random errors and small systematic errors due to the analysts, and has a compact clustering of points that is more circular than elliptical.

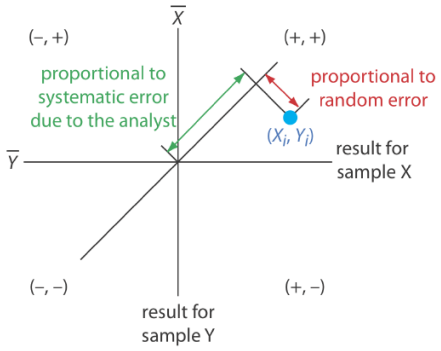

Figure 14.3.3 . Relationship between the result for a single analyst (in blue) and the contribution of random error (red arrow) and the contribution from the analyst's systematic error (green arrow).

We also can use the data in a two-sample chart to separate the total variation in the data, σ_{tot}, into contributions from random error, σ_{rand}, and from systematic errors due to the analysts, σ_{syst} [Youden, W. J. "Statistical Techniques for Collaborative Tests," in *Statistical Manual of the Association of Official Analytical Chemists*, Association of Official Analytical Chemists: Washington, D. C., 1975, pp 22–24]. Because an analyst's systematic errors are present in his or her analysis of both samples, the difference, *D*, between the results estimates the contribution of random error.

$$D = X_i - Y_i$$

To estimate the total contribution from random error we use the standard deviation of these differences, s_D, for all analysts

$$s_D = \sqrt{\frac{\sum_{i=1}^{n}(D_i - \overline{D})^2}{2(n-1)}} = s_{\text{rand}} \approx \sigma_{\text{rand}} \tag{5.3.1}$$

where *n* is the number of analysts. The factor of 2 in the denominator of Equation 5.3.1 is the result of using two values to determine D_i. The total, *T*, of each analyst's results

$$T_i = X_i + Y_i$$

contains contributions from both random error and twice the analyst's systematic error.

$$\sigma_{\text{tot}}^2 = \sigma_{\text{rand}}^2 + 2\sigma_{\text{syst}}^2 \tag{5.3.2}$$

The standard deviation of the totals, s_T, provides an estimate for σ_{tot}.

$$s_T = \sqrt{\frac{\sum_{i=1}^{n}\left(T_i - \overline{T}\right)^2}{2(n-1)}} = s_{tot} \approx \sigma_{tot} \tag{5.3.3}$$

Again, the factor of 2 in the denominator is the result of using two values to determine T_i.

If the systematic errors are significantly larger than the random errors, then s_T is larger than s_D, a hypothesis we can evaluate using a one-tailed *F*-test

$$F = \frac{s_T^2}{s_D^2}$$

where the degrees of freedom for both the numerator and the denominator are $n - 1$. As shown in the following example, if s_T is significantly larger than s_D we can use Equation 5.3.2 to separate σ_{tot}^2 into components that represent the random error and the systematic error.

Example 14.3.1

As part of a collaborative study of a new method for determining the amount of total cholesterol in blood, you send two samples to 10 analysts with instructions that they analyze each sample one time. The following results, in mg total cholesterol per 100 mL of serum, are returned to you.

analyst	sample 1	sample 2
1	245.0	229.4
2	247.4	249.7
3	246.0	240.4
4	244.9	235.5
5	255.7	261.7
6	248.0	239.4
7	249.2	255.5
8	255.1	224.3
9	255.0	246.3
10	243.1	253.1

Use this data estimate σ_{rand} and σ_{syst} for the method.

Solution

Figure 14.3.4 provides a two-sample plot of the results. The clustering of points suggests that the systematic errors of the analysts are significant. The vertical line at 245.9 mg/100 mL is the average value for sample 1 and the average value for sample 2 is indicated by the horizontal line at 243.5 mg/100 mL. To estimate σ_{rand} and σ_{syst} we first calculate values for D_i and T_i.

analyst	D_i	T_i
1	15.6	474.4
2	–2.3	497.1
3	5.6	486.4
4	9.4	480.4
5	–6.0	517.4

analyst	D_i	T_i
6	8.6	487.4
7	–6.3	504.7
8	0.8	449.4
9	8.7	501.3
10	–10.0	496.2

Next, we calculate the standard deviations for the differences, s_D, and the totals, s_T, using Equation 5.3.1 and Equation 5.3.2, obtaining s_D = 5.95 and s_T = 13.3. To determine if the systematic errors between the analysts are significant, we use an *F*-test to compare s_T and s_D.

$$F = \frac{s_T^2}{s_D^2} = \frac{(13.3)^2}{(5.95)^2} = 5.00$$

Because the *F*-ratio is larger than *F*(0.05,9,9), which is 3.179, we conclude that the systematic errors between the analysts are significant at the 95% confidence level. The estimated precision for a single analyst is

$$\sigma_{\text{rand}} \approx s_{\text{rand}} = s_D = 5.95$$

The estimated standard deviation due to systematic errors between analysts is calculated from Equation 5.3.2.

$$\sigma_{\text{syst}} = \sqrt{\frac{\sigma_{\text{tot}}^2 - \sigma_{\text{rand}}^2}{2}} \approx \sqrt{\frac{s_t^2 - s_D^2}{2}} = \sqrt{\frac{(13.3)^2 - (5.95)^2}{2}} = 8.41$$

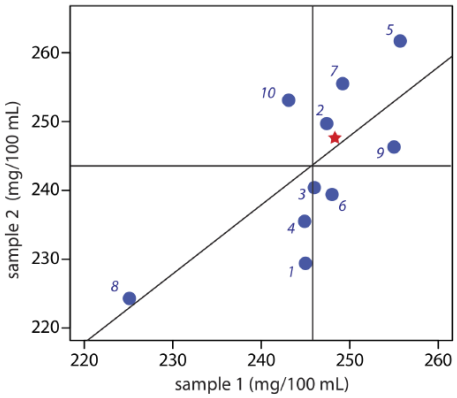

Figure 14.3.4 . Two-sample plot for the data in Example 14.3.1 . The number by each blue point indicates the analyst. The true values for each sample (see Example 14.3.2) are indicated by the red star.

If the true values for the two samples are known, we also can test for the presence of a systematic error in the method. If there are no systematic method errors, then the sum of the true values, μ_{tot}, for samples *X* and *Y*

$$\mu_{\text{tot}} = \mu_X + \mu_Y$$

should fall within the confidence interval around T . We can use a two-tailed *t*-test of the following null and alternate hypotheses

$$H_0 : \overline{T} = \mu_{\text{tot}} \quad H_{\text{A}} : \overline{T} \neq \mu_{\text{tot}}$$

to determine if there is evidence for a systematic error in the method. The test statistic, t_{exp}, is

$$t_{\text{exp}} = \frac{|\overline{T} - \mu_{\text{tot}}|\sqrt{n}}{s_T\sqrt{2}} \tag{5.3.4}$$

with n – 1 degrees of freedom. We include the 2 in the denominator because s_T (see Equation 5.3.3 underestimates the standard deviation when comparing $\overline{T}$ to μ_{tot}.

Example 14.3.2

The two samples analyzed in Example 14.3.1 are known to contain the following concentrations of cholesterol: $\mu_{samp\,1}$ = 248.3 mg/100 mL and $\mu_{samp\,2}$ = 247.6 mg/100 mL. Determine if there is any evidence for a systematic error in the method at the 95% confidence level.

Solution

Using the data from Example 14.3.1 and the true values for the samples, we know that s_T is 13.3, and that

$$\overline{T} = \overline{X}_{samp\,1} + \overline{X}_{samp\,2} = 245.9 + 243.5 = 489.4 \text{ mg/100 mL}$$

$$\mu_{tot} = \mu_{samp\,1} + mu_{samp\,2} = 248.3 + 247.6 = 495.9 \text{ mg/100 mL}$$

Substituting these values into Equation 5.3.4 gives

$$t_{exp} = \frac{|489.4 - 495.9|\sqrt{10}}{13.3\sqrt{2}} = 1.09$$

Because this value for t_{exp} is smaller than the critical value of 2.26 for t(0.05, 9), there is no evidence for a systematic error in the method at the 95% confidence level.

Example 14.3.1 and Example 14.3.2 illustrate how we can use a pair of similar samples in a collaborative test of a new method. Ideally, a collaborative test involves several pairs of samples that span the range of analyte concentrations for which we plan to use the method. In doing so, we evaluate the method for constant sources of error and establish the expected relative standard deviation and bias for different levels of analyte.

Collaborative Testing and Analysis of Variance

In a two-sample collaborative test we ask each analyst to perform a single determination on each of two separate samples. After reducing the data to a set of differences, *D*, and a set of totals, *T*, each characterized by a mean and a standard deviation, we extract values for the random errors that affect precision and the systematic differences between then analysts. The calculations are relatively simple and straightforward.

An alternative approach to a collaborative test is to have each analyst perform several replicate determinations on a single, common sample. This approach generates a separate data set for each analyst and requires a different statistical treatment to provide estimates for σ_{rand} and for σ_{syst}.

There are several statistical methods for comparing three or more sets of data. The approach we consider in this section is an ***analysis of variance*** (ANOVA). In its simplest form, a one-way ANOVA allows us to explore the importance of a single variable—the identity of the analyst is one example—on the total variance. To evaluate the importance of this variable, we compare its variance to the variance explained by indeterminate sources of error.

We first introduced variance in Chapter 4 as one measure of a data set's spread around its central tendency. In the context of an analysis of variance, it is useful for us to understand that variance is simply a ratio of two terms: a sum of squares for the differences between individual values and their mean, and the degrees of freedom. For example, the variance, s^2, of a data set consisting of n measurements is

$$s^2 = \frac{\sum_{i=1}^{n}\left(X_i - \overline{X}\right)^2}{n-1}$$

where X_i is the value of a single measurement and $\overline{X}$ is the mean. The ability to partition the variance into a sum of squares and the degrees of freedom greatly simplifies the calculations in a one-way ANOVA.

Let's use a simple example to develop the rationale behind a one-way ANOVA calculation. The data in Table 14.3.1 are from four analysts, each asked to determine the purity of a single pharmaceutical preparation of sulfanilamide. Each column in Table 14.3.1

provides the results for an individual analyst. To help us keep track of this data, we will represent each result as X_{ij}, where *i* identifies the analyst and *j* indicates the replicate. For example, $X_{3,5}$ is the fifth replicate for the third analyst, or 94.24%.

Table 14.3.1 . Determination of the %Purity of a Sulfanilamide Preparation by Four Analysts

replicate	analyst A	analyst B	analyst C	analyst D
1	94.09	99.55	95.14	93.88
2	94.64	98.24	94.62	94.23
3	95.08	101.1	95.28	96.05
4	94.54	100.4	94.59	93.89
5	95.38	100.1	94.24	94.95
6	93.62	—	—	95.49
$\overline{X}$	94.56	99.88	94.77	94.75
s	0.641	1.073	0.428	0.899

The data in Table 14.3.1 show variability in the results obtained by each analyst and in the difference in the results between the analysts. There are two sources for this variability: indeterminate errors associated with the analytical procedure that are experienced equally by each analyst, and systematic or determinate errors introduced by the individual analysts.

One way to view the data in Table 14.3.1 is to treat it as a single large sample, characterized by a global mean and a global variance

$$\overline{\overline{X}} = \frac{\sum_{i=1}^{h} \sum_{i=1}^{n} X_{ij}}{N} \tag{5.3.5}$$

$$\overline{\overline{s}}^2 = \frac{\sum_{i=1}^{h} \sum_{j=1}^{n_i} \left(X_{ij} - \overline{\overline{X}} \right)^2}{N-1} \tag{5.3.6}$$

where *h* is the number of samples (in this case the number of analysts), n_i is the number of replicates for the *i*th sample (in this case the *i*th analyst), and *N* is the total number of data points (in this case 22). The global variance—which includes all sources of variability that affect the data—provides an estimate of the combined influence of indeterminate errors and systematic errors.

A second way to work with the data in Table 14.3.1 is to treat the results for each analyst separately. If we assume that each analyst experiences the same indeterminate errors, then the variance, s^2, for each analyst provides a separate estimate of σ^2_{rand}. To pool these individual variances, which we call the ***within-sample variance***, s^2_w, we square the difference between each replicate and its corresponding mean, add them up, and divide by the degrees of freedom.

$$\sigma^2_{\text{rnd}} \approx s^2_w = \frac{\sum_{i=1}^{h} \sum_{j=1}^{n_i} \left(X_{ij} - \overline{X}_i \right)^2}{N-h} \tag{5.3.7}$$

> Carefully compare our description of Equation 5.3.7 to the equation itself. It is important that you understand why Equation 5.3.7 provides our best estimate of the indeterminate errors that affect the data in Table 14.3.1 . Note that we lose one degree of freedom for each of the *h* means included in the calculation.

To estimate the systematic errors, σ^2_{syst}, that affect the results in Table 14.3.1 we need to consider the differences between the analysts. The variance of the individual mean values about the global mean, which we call the ***between-sample variance***, s^2_b, is

$$s^2_b = \frac{\sum_{i=1}^{h} n_i \left(\overline{X}_i - \overline{\overline{X}} \right)^2}{h-1} \tag{5.3.8}$$

where we lose one degree of freedom for the global mean. The between-sample variance includes contributions from both indeterminate errors and systematic errrors; thus

$$s_b^2 = \sigma_{\text{rand}}^2 + \bar{n}\sigma_{\text{syst}}^2 \tag{5.3.9}$$

where $\bar{n}$ is the average number of replicates per analyst.

$$\bar{n} = \frac{\sum_{i=1}^{h} n_i}{h}$$

Note the similarity between Equation 5.3.9 and Equation 5.3.2. The analysis of the data in a two-sample plot is the same as a one-way analysis of variance with h = 2.

In a one-way ANOVA of the data in Table 14.3.1 we make the null hypothesis that there are no significant differences between the mean values for the analysts. The alternative hypothesis is that at least one of the mean values is significantly different. If the null hypothesis is true, then σ_{syst}^2 must be zero and s_w^2 and s_b^2 should have similar values. If s_b^2 is significantly greater than s_w^2 , then σ_{syst}^2 is greater than zero. In this case we must accept the alternative hypothesis that there is a significant difference between the means for the analysts. The test statistic is the F-ratio

$$F_{\text{exp}} = \frac{s_b^2}{s_w^2}$$

which is compared to the critical value F(a, h – 1, N – h). This is a one-tailed significance test because we are interested only in whether s_b^2 is significantly greater than s_w^2.

Both s_b^2 and s_w^2 are easy to calculate for small data sets. For larger data sets, calculating s_w^2 is tedious. We can simplify the calculations by taking advantage of the relationship between the sum-of-squares terms for the global variance (Equation 5.3.6), the within-sample variance (equation ref{14.7}), and the between-sample variance (Equation 5.3.8). We can split the numerator of Equation 5.3.6, which is the total sum-of-squares, SS_t, into two terms

$$SS_t = SS_w + SS_b$$

where SS_w is the sum-of-squares for the within-sample variance and SS_b is the sum-of-squares for the between-sample variance. Calculating SS_t and SS_b gives SS_w by difference. Finally, dividing SS_w and SS_b by their respective degrees of freedom gives s_w^2 and s_b^2. Table 14.3.2 summarizes the equations for a one-way ANOVA calculation. Example 14.3.3 walks you through the calculations, using the data in Table 14.3.1 .

Table 14.3.2 . Summary of Calculations for a One-Way Analysis of Variance

source	sum-of-squares	degrees of freedom	variance	expected variance	F-ratio
between samples	$SS_b = \sum_{i=1}^{h} n_i(\bar{X}_i - \bar{\bar{X}})^2$	$h-1$	$s_b^2 = \frac{SS_b}{h-1}$	$s_b^2 = \sigma_{\text{rand}}^2 + \bar{n}\sigma_{\text{syst}}^2$	$F_{\text{exp}} = \frac{s_b^2}{s_w^2}$
within samples	$SS_t = SS_w + SS_b$	$N-h$	$s_w^2 = \frac{SS_w}{N-h}$	$s_w^2 = \sigma_{\text{rand}}^2$	
total	$SS_t = \sum_{i=1}^{h}\sum_{j=1}^{n_i}(X_{ij} - \bar{\bar{X}})^2$ $SS_t = \bar{\bar{s^2}}(N-1)$	$N-1$			

Example 14.3.3

The data in Table 14.3.1 are from four analysts, each asked to determine the purity of a single pharmaceutical preparation of sulfanilamide. Determine if the difference in their results is significant at $\alpha = 0.05$. If such a difference exists, estimate values for σ_{rand}^2 and σ_{syst}.

Solution

To begin we calculate the global mean (Equation 5.3.5) and the global variance (Equation 5.3.6) for the pooled data, and the means for each analyst; these values are summarized here.

$$\overline{\overline{X}} = 95.87 \qquad \overline{\overline{s^2}} = 5.506$$

$$\overline{X}_A = 94.56 \quad \overline{X}_B = 99.88 \quad \overline{X}_C = 94.77 \quad \overline{X}_D = 94.75$$

Using these values we calculate the total sum of squares

$$SS_t = \overline{\overline{s^2}}(N-1) = (5.506)(22-1) = 115.63$$

the between sample sum of squares

$$SS_b = \sum_{i=1}^{h} n_i \left(\overline{X}_i - \overline{\overline{X}} \right)^2 = 6(94.56-95.87)^2 + 5(99.88-95.87)^2 + 5(94.77-95.87)^2 + 6(94.75-95.87)^2$$

$$= 104.27$$

and the within sample sum of squares

$$SS_w = SS_t - SS_b = 115.63 - 104.27 = 11.36$$

The remainder of the necessary calculations are summarized in the following table.

source	sum of squares	degrees of freedom	variance
between samples	104.27	$h-1=4-1=3$	34.76
within samples	11.36	$N-h=22-4=18$	0.631

Comparing the variances we find that

$$F_{\text{exp}} = \frac{s_b^2}{s_w^2} = \frac{34.76}{0.631} = 55.09$$

Because F_{exp} is greater than $F(0.05, 3, 18)$, which is 3.16, we reject the null hypothesis and accept the alternative hypothesis that the work of at least one analyst is significantly different from the remaining analysts. Our best estimate of the within sample variance is

$$\sigma_{\text{rand}}^2 \approx s_w^2 = 0.631$$

and our best estimate of the between sample variance is

$$\sigma_{\text{syst}}^2 = \frac{s_b^2 - s_w^2}{\overline{n}} = \frac{35.76 - 0.631}{22/4} = 6.205$$

In this example the variance due to systematic differences between the analysts is almost an order of magnitude greater than the variance due to the method's precision.

Having demonstrated that there is significant difference between the analysts, we can use a modified version of the *t*-test—known as ***Fisher's least significant difference***—to determine the source of the difference. The test statistic for comparing two mean values is the *t*-test from Chapter 4, except we replace the pooled standard deviation, s_{pool}, by the square root of the within-sample variance from the analysis of variance.

$$t_{\text{exp}} = \frac{\left| \overline{X}_1 - \overline{X}_2 \right|}{\sqrt{s_w^2}} \times \sqrt{\frac{n_1 n_2}{n_1 + n_2}} \tag{5.3.10}$$

We compare t_{exp} to its critical value $t(\alpha, \nu)$ using the same significance level as the ANOVA calculation. The degrees of freedom are the same as that for the within sample variance. Since we are interested in whether the larger of the two means is significantly greater than the other mean, the value of $t(\alpha, \nu)$ is that for a one-tailed significance test.

You might ask why we bother with the analysis of variance if we are planning to use a *t*-test to compare pairs of analysts. Each *t*-test carries a probability, α, of claiming that a difference is significant even though it is not (a type 1 error). If we set α to 0.05 and complete six *t*-tests, the probability of a type 1 error increases to 0.265. Knowing that there is a significant difference within a data set—what we gain from the analysis of variance—protects the *t*-test.

Example 14.3.4

In Example 14.3.3 we showed that there is a significant difference between the work of the four analysts in Table 14.3.1 . Determine the source of this significant difference.

Solution

Individual comparisons using Fisher's least significant difference test are based on the following null hypothesis and the appropriate one-tailed alternative hypothesis.

$$H_0 : \overline{X}_1 = \overline{X}_2 \qquad H_A : \overline{X}_1 > \overline{X}_2 \quad \text{or} \quad H_A : \overline{X}_1 < \overline{X}_2$$

Using Equation 5.3.10 we calculate values of t_{exp} for each possible comparison and compare them to the one-tailed critical value of 1.73 for $t(0.05, 18)$. For example, t_{exp} for analysts A and B is

$$(t_{exp})_{AB} = \frac{|94.56 - 99.88|}{\sqrt{0.631}} \times \sqrt{\frac{6 \times 5}{6 + 5}} = 11.06$$

Because $(t_{exp})_{AB}$ is greater than $t(0.05,18)$ we reject the null hypothesis and accept the alternative hypothesis that the results for analyst *B* are significantly greater than those for analyst *A*. Continuing with the other pairs it is easy to show that $(t_{exp})_{AC}$ is 0.437, $(t_{exp})_{AD}$ is 0.414, $(t_{exp})_{BC}$ is 10.17, $(t_{exp})_{BD}$ is 10.67, and $(t_{exp})_{CD}$ is 0.04.. Collectively, these results suggest that there is a significant systematic difference between the work of analyst *B* and the work of the other analysts. There is, of course no way to decide whether any of the four analysts has done accurate work.

We have evidence that analyst *B*'s result is significantly different than the results for analysts *A*, *C*, and *D*, and we have no evidence that there is any significant difference between the results of analysts *A*, *C*, and *D*. We do not know if analyst *B*'s results are accurate, or if the results of analysts *A*, *C*, and *D* are accurate. In fact, it is possible that none of the results in Table 14.3.1 are accurate.

We can extend an analysis of variance to systems that involve more than a single variable. For example, we can use a two-way ANOVA to determine the effect on an analytical method of both the analyst and the instrumentation. The treatment of multivariate ANOVA is beyond the scope of this text, but is covered in several of the texts listed in this chapter's additional resources.

What is a Reasonable Result for a Collaborative Study?

Collaborative testing provides us with a method for estimating the variability (or reproducibility) between analysts in different labs. If the variability is significant, we can determine what portion is due to indeterminate method errors, σ^2_{rand}, and what portion is due to systematic differences between the analysts, σ^2_{syst}. What is left unanswered is the following important question: What is a reasonable value for a method's reproducibility?

An analysis of nearly 10 000 collaborative studies suggests that a reasonable estimate for a method's reproducibility is

$$R = 2^{(1-0.5 \log C)} \tag{5.3.11}$$

where *R* is the percent relative standard deviation for the results included in the collaborative study and *C* is the fractional amount of analyte in the sample on a weight-to-weight basis. Equation 5.3.1 is thought to be independent of the type of analyte, the type of matrix, and the method of analysis. For example, when a sample in a collaborative study contains 1 microgram of analyte per gram of sample, *C* is 10^{-6} the estimated relative standard deviation is

$$R = 2^{(1-0.5 \log 10^{-6})} = 16\%$$

Example 14.3.5

What is the estimated relative standard deviation for the results of a collaborative study when the sample is pure analyte (100% w/w analyte)? Repeat for the case where the analyte's concentration is 0.1% w/w.

Solution

When the sample is 100% w/w analyte (C = 1) the estimated relative standard deviation is

$$R = 2^{(1-0.5 \log 1)} = 2\%$$

We expect that approximately two-thirds of the participants in the collaborative study ($\pm 1\sigma$) will report the analyte's concentration within the range of 98% w/w to 102% w/w. If the analyte's concentration is 0.1% w/w (C = 0.001), the estimated relative standard deviation is

$$R = 2^{(1-0.5 \log 0.01)} = 5.7\%$$

and we expect that approximately two-thirds of the analysts will report the analyte's concentration within the range of 0.094% w/w to 0.106% w/w.

Of course, Equation 5.3.11 only estimates the expected relative standard. If the method's relative standard deviation falls with a range of one-half to twice the estimated value, then it is acceptable for use by analysts in different laboratories. The percent relative standard deviation for a single analyst should be one-half to two-thirds of that for the variability between analysts.

For details on Equation 5.3.11, see (a) Horwitz, W. *Anal. Chem.* **1982**, **54**, 67A–76A; (b) Hall, P.; Selinger, B. *Anal. Chem.* **1989**, *61*, 1465–1466; (c) Albert, R.; Horwitz, W. *Anal. Chem.* **1997**, *69*, 789–790, (d) "The Amazing Horwitz Function," AMC Technical Brief 17, July 2004; (e) Lingser, T. P. J. Trends Anal. Chem. 2006, 25, 1125. For a discussion of the equation's limitations, see Linsinger, T. P. J.; Josephs, R. D. "Limitations of the Application of the Horwitz Equation," *Trends Anal. Chem.* **2006**, *25*, 1125–1130, as well as a rebuttal (Thompson, M. "Limitations of the Application of the Horwitz Equation: A Rebuttal," *Trends Anal. Chem.* **2007**, *26*, 659–661) and response to the rebuttal (Linsinger, T. P. J.; Josephs, R. D. "Reply to Professor Michael Thompson's Rebuttal," *Trends Anal. Chem.* **2007**, *26*, 662–663.

5.4: Using Excel and R for an Analysis of Variance

Although the calculations for an analysis of variance are relatively straight-forward, they become tedious when working with large data sets. Both Excel and R include functions for completing an analysis of variance. In addition, R provides a function for identifying the source(s) of significant differences within the data set.

Excel

Excel's Analysis ToolPak includes a tool to help you complete an analysis of variance. Let's use the ToolPak to complete an analysis of variance on the data in Table 14.3.1. Enter the data from Table 14.3.1 into a spreadsheet as shown in Figure 14.4.1 .

	A	B	C	D	E
1	replicate	analyst A	analyst B	analyst C	analyst D
2	1	94.09	99.55	95.14	93.88
3	2	94.64	98.24	94.62	94.23
4	3	95.08	101.1	95.28	96.05
5	4	94.54	100.4	94.59	93.89
6	5	95.38	100.1	94.24	94.59
7	6	93.62			95.49

Figure 14.4.1 . Portion of a spreadsheet containing the data from Table 14.3.1.

To complete the analysis of variance select **Data Analysis...** from the **Tools** menu, which opens a window entitled "*Data Analysis*." Scroll through the window, select **Analysis: Single Factor** from the available options and click **OK**. Place the cursor in the box for the "*Input range*" and then click and drag over the cells B1:E7. Select the radio button for "*Grouped by: columns*" and check the box for "*Labels in the first row*." In the box for "*Alpha*" enter 0.05 for α. Select the radio button for "*Output range*," place the cursor in the box and click on an empty cell; this is where Excel will place the results. Clicking **OK** generates the information shown in Figure 14.4.2 . The small value of 3.05×10^{-9} for falsely rejecting the null hypothesis indicates that there is a significant source of variation between the analysts.

Anova: Single Factor

SUMMARY

Groups	*Count*	*Sum*	*Average*	*Variance*
analyst A	6	567.35	94.5583333	0.41081667
analyst B	5	499.39	99.878	1.15142
analyst C	5	473.87	94.774	0.18318
analyst D	6	568.49	94.7483333	0.80889667

ANOVA

Source of Variation	*SS*	*df*	*MS*	*F*	*P-value*	*F crit*
Between Groups	104.197961	3	34.7326535	54.6637742	3.0463E-09	3.1599076
Within Groups	11.4369667	18	0.63538704			
Total	115.634927	21				

Figure 14.4.2 . Output from Excel's one-way analysis of variance of the data in Table 14.3.1. The summary table provides the mean and variance for each analyst. The ANOVA table summarizes the sum-of-squares terms (*SS*), the degrees of freedom (*df*), the variances (*MS* for mean square), the value of F_{exp} and the critical value of *F*, and the probability of incorrectly rejecting the null hypothesis that there is no significant difference between the analysts.

R

To complete an analysis of variance for the data in Table 14.3.1 using R, we first need to create several objects. The first object contains each result from Table 14.3.1.

```
> results = c(94.090, 94.640, 95.008, 94.540, 95.380, 93.620, 99.550, 98.240, 101.100,
100.400, 100.100, 95.140, 94.620, 95.280, 94.590, 94.240, 93.880, 94.230, 96.050,
93.890, 94.950, 95.490)
```

The second object contains labels that identify the source of each entry in the first object. The following code creates this object.

```
> analyst = c(rep("a",6), rep("b",5), rep("c",5), rep("d",6))
```

Next, we combine the two objects into a table with two columns, one that contains the data (*results*) and one that contains the labels (*analyst*).

```
> df= data.frame(results, labels= factor(analyst))
```

The command **factor** indicates that the object *analyst* contains the categorical factors for the analysis of variance. The command for an analysis of variance takes the following form

```
anova(lm(data ~ factors), data = data.frame)
```

where *data* and *factors* are the columns that contain the data and the categorical factors, and *data.frame* is the name we assigned to the data table. Figure 14.4.3 shows the resulting output. The small value of 3.05×10^{-9} for falsely rejecting the null hypothesis indicates that there is a significant source of variation between the analysts.

anova(lm(results~labels, data=df); Analysis of Variance Table; Response: results; Df, Sum Sq, Mean Sq, F value, Pr(>F); labels: 3 104.198 34.733 54.664 3.04e-09; Residuals 18 11.366 0.631; ---; Signif. codes: 0 '***' 0.001 '**' 0.01 '*' 0.05 '.' 0.` " 1" style="width: 411px; height: 183px;" width="411px" height="183px" src="/@api/deki/files/186753/Figure14.24.png">

Figure 14.4.3 . Output of an R session for an analysis of variance for the data in Table 14.3.1. In the table, "labels" is the between-sample variance and "residuals" is the within-sample variance. The *p*-value of 3.04e-09 is the probability of incorrectly rejecting the null hypothesis that the within-sample and between-sample variances are the same.

Having found a significant difference between the analysts, we want to identify the source of this difference. R does not include Fisher's least significant difference test, but it does include a function for a related method called Tukey's honest significant difference test. The command for this test takes the following form

```
> TukeyHSD(aov(lm(data ~ factors), data = data.frame), conf. level = 0.5)
```

where *data* and *factors* are the columns that contain the data and the categorical factors, and *data.frame* is the name we assigned to the data table. Figure 14.4.4 shows the output of this command and its interpretation. The small probability values when comparing analyst B to each of the other analysts indicates that this is the source of the significant difference identified in the analysis of variance.

TukeyHSD(aoc(results~labels, data=df)); Tukey multiple comparisons of means; 95% family-wise confidence level; Fit: aov(formula=results~labels, data=df); $labels; diff, lwr, upr, p adj; b-a 5.31966667, 3.928277, 6.711057, 0.0000000; c-a 0.21566667 -1.175723 1.607057 0.9710635; d-a 0.280000000 -1.046638 1.606638 0.9318110; c-b -5.10400000 -6.557260 -3.650740 0.0000001; d-b -5.03966667 -6.431057 -3.648277 0.0000000; d-c 0.06433333 -1.327057 1.455723 0.9991718" style="width: 306px; height: 228px;" width="306px" height="228px" src="/@api/deki/files/186754/Figure4.25.png">

Figure 14.4.4 . Output of an R session for a Tukey honest significance difference test using the data in Table 14.3.1. For each possible comparison of analysts, the table gives the actual difference between the analysts, "diff," and the smallest, "lwr," and the largest, "upr," differences for a 95% confidence interval. The "p adj" is the probability that a difference of zero falls within this confidence interval. The smaller the *p*-value, the greater the probability that the difference between the analysts is significant.

5.5: Problems

1. For each of the following equations determine the optimum response using a one-factor-at-a-time searching algorithm. Begin the search at (0,0) by first changing factor *A*, using a step-size of 1 for both factors. The boundary conditions for each response surface are $0 \le A \le 10$ and $0 \le B \le 10$. Continue the search through as many cycles as necessary until you find the optimum response. Compare your optimum response for each equation to the true optimum. Note: These equations are from Deming, S. N.; Morgan, S. L. *Experimental Design: A Chemometric Approach*, Elsevier: Amsterdam, 1987, and pseudo-three dimensional plots of the response surfaces can be found in their Figures 11.4, 11.5 and 11.14.

(a) $R = 1.68 + 0.24A + 0.56B - 0.04A^2 - 0.04B^2$ $\mu_{opt} = (3, 7)$

(b) $R = 4.0 - 0.4A + 0.08AB$ $\mu_{opt} = (10, 10)$

(c) $R = 3.264 + 1.537A + 0.5664B - 0.1505A^2 - 0.02734B^2 - 0.05785AB$ $\mu_{opt} = (3.91, 6.22)$

2. Use a fixed-sized simplex searching algorithm to find the optimum response for the equation in Problem 1c. For the first simplex, set one vertex at (0,0) with step sizes of one. Compare your optimum response to the true optimum.

3. Show that equation 14.1.3 and equation 14.1.4 are correct.

4. A 2^k factorial design was used to determine the equation for the response surface in Problem 1b. The uncoded levels, coded levels, and the responses are shown in the following table. Determine the uncoded equation for the response surface.

A	*B*	*A**	*B**	response
8	8	+1	+1	5.92
8	2	+1	–1	2.08
2	8	–1	+1	4.48
2	2	–1	–1	3.52

5. Koscielniak and Parczewski investigated the influence of Al on the determination of Ca by atomic absorption spectrophotometry using the 2*k* factorial design shown in the following table [Koscielniak, P.; Parczewski, A. *Anal. Chim. Acta* **1983**, *153*, 111–119].

$[Ca^{2+}]$ (ppm)	$[Al^{3+}]$ (ppm)	*Ca**	*Al**	response
10	160	+1	+1	54.92
10	0	+1	–1	98.44
4	16	–1	+1	19.18
4	0	–1	–1	38.52

(a) Determine the uncoded equation for the response surface.

(b) If you wish to analyze a sample that is 6.0 ppm Ca^{2+}, what is the maximum concentration of Al^{3+} that can be present if the error in the response must be less than 5.0%?

6. Strange studied a chemical reaction using a 23 factorial design [Strange, R. S. *J. Chem. Educ.* **1990**, *67*, 113–115].

factor	high (+1) level	low (–1) level
X: temperature	140°C	120°C
Y: catalyst	type B	type A
Z: [reactant]	0.50 M	0.25 M

run	*X**	*Y**	*Z**	% yield

run	*X**	*Y**	*Z**	% yield
1	–1	–1	–1	28
2	+1	–1	–1	17
3	–1	+1	–1	41
4	+1	+1	–1	34
5	–1	–1	+1	56
6	+1	–1	+1	51
7	–1	+1	+1	42
8	+1	+1	+1	36

(a) Determine the coded equation for this data.

(b) If β terms of less than ± 1 are insignificant, what main effects and what interaction terms in the coded equation are important? Write down this simpler form for the coded equation.

(c) Explain why the coded equation for this data can not be transformed into an uncoded form.

(d) Which is the better catalyst, A or B?

(e) What is the yield if the temperature is set to 125ºC, the concentration of the reactant is 0.45 M, and we use the appropriate catalyst?

7. Pharmaceutical tablets coated with lactose often develop a brown discoloration. The primary factors that affect the discoloration are temperature, relative humidity, and the presence of a base acting as a catalyst. The following data have been reported for a 2^3 factorial design [Armstrong, N. A.; James, K. C. *Pharmaceutical Experimental Design and Interpretation*, Taylor and Francis: London, 1996 as cited in Gonzalez, A. G. *Anal. Chim. Acta* **1998**, *360*, 227–241].

factor	high (+1) level	low (–1) level
X: benzocaine	present	absent
Y: temperature	40ºC	25ºC
Z: relative humidity	75%	50%

run	*X**	*Y**	*Z**	color (arb. unit)
1	–1	–1	–1	1.55
2	+1	–1	–1	5.40
3	–1	+1	–1	3.50
4	+1	+1	–1	6.75
5	–1	–1	+1	2.45
6	+1	–1	+1	3.60
7	–1	+1	+1	3.05
8	+1	+1	+1	7.10

(a) Determine the coded equation for this data.

(b) If β terms of less than 0.5 are insignificant, what main effects and what interaction terms in the coded equation are important? Write down this simpler form for the coded equation.

8. The following data for a 2^3 factorial design were collected during a study of the effect of temperature, pressure, and residence time on the % yield of a reaction [Akhnazarova, S.; Kafarov, V. *Experimental Optimization in Chemistry and Chemical Engineering*, MIR Publishers: Moscow, 1982 as cited in Gonzalez, A. G. *Anal. Chim. Acta* **1998**, *360*, 227–241].

factor	high (+1) level	low (–1) level
X: temperature	200ºC	100ºC
Y: pressure	0.6 MPa	0.2 MPa
Z: residence time	20 min	10 min

run	*X**	*Y**	*Z**	% yield
1	–1	–1	–1	2
2	+1	–1	–1	6
3	–1	+1	–1	4
4	+1	+1	–1	8
5	–1	–1	+1	10
6	+1	–1	+1	18
7	–1	+1	+1	8
8	+1	+1	+1	12

(a) Determine the coded equation for this data.

(b) If β terms of less than 0.5 are insignificant, what main effects and what interaction terms in the coded equation are important? Write down this simpler form for the coded equation.

(c) Three runs at the center of the factorial design—a temperature of 150ºC, a pressure of 0.4 MPa, and a residence time of 15 min—give percent yields of 8%, 9%, and 8.8%. Determine if a first-order empirical model is appropriate for this system at $\alpha = 0.05$.

9. Duarte and colleagues used a factorial design to optimize a flow-injection analysis method for determining penicillin [Duarte, M. M. M. B.; de O. Netro, G.; Kubota, L. T.; Filho, J. L. L.; Pimentel, M. F.; Lima, F.; Lins, V. *Anal. Chim. Acta* **1997**, *350*, 353–357]. Three factors were studied: reactor length, carrier flow rate, and sample volume, with the high and low values summarized in the following table.

factor	high (+1) level	low (–1) level
X: reactor length	1.3 cm	2.0 cm
Y: carrier flow rate	1.6 mL/min	2.2 mL/min
Z: sample volume	100 μL	150 μL

The authors determined the optimum response using two criteria: the greatest sensitivity, as determined by the change in potential for the potentiometric detector, and the largest sampling rate. The following table summarizes their optimization results.

run	*X**	*Y**	*Z**	ΔE (mV)	sample/h
1	–1	–1	–1	37.45	21.5
2	+1	–1	–1	31.70	26.0
3	–1	+1	–1	32.10	30.0
4	+1	+1	–1	27.30	33.0

5	–1	–1	+1	39.85	21.0
6	+1	–1	+1	32.85	19.5
7	–1	+1	+1	35.00	30.0
8	+1	+1	+1	32.15	34.0

(a) Determine the coded equation for the response surface where ΔE is the response.

(b) Determine the coded equation for the response surface where sample/h is the response.

(c) Based on the coded equations in (a) and in (b), do conditions that favor sensitivity also improve the sampling rate?

(d) What conditions would you choose if your goal is to optimize both sensitivity and sampling rate?

10. Here is a challenge! McMinn, Eatherton, and Hill investigated the effect of five factors for optimizing an H_2-atmosphere flame ionization detector using a 2^5 factorial design [McMinn, D. G.; Eatherton, R. L.; Hill, H. H. *Anal. Chem.* **1984**, *56*, 1293–1298]. The factors and their levels were

factor	high (+1) level	low (–1) level
A: H_2 flow rate	1460 mL/min	1382 mL/min
B: SiH_4	20.0 ppm	12.2 ppm
C: $O_2 + N_2$ flow rate	255 mL/min	210 mL/min
D: O_2/N_2 ratio	1.36	1.19
E: electrode height	75 (arb. unit)	55 (arb. unit)

The coded ("+" = +1, "–" = –1) factor levels and responses, *R*, for the 32 experiments are shown in the following table

run	*A**	*B**	*C**	*D**	*E**	*R*	run	*A**	*B**	*C**	*D**	*E**	*R*
1	–	–	–	–	–	0.36	17	–	–	–	–	+	0.39
2	+	–	–	–	–	0.51	18	+	–	–	–	+	0.45
3	–	+	–	–	–	0.15	19	–	+	–	–	+	0.32
4	+	+	–	–	–	0.39	20	+	+	–	–	+	0.25
5	–	–	+	–	–	0.79	21	–	–	+	–	+	0.18
6	+	–	+	–	–	0.83	22	+	–	+	–	+	0.29
7	–	+	+	–	–	0.74	23	–	+	+	–	+	0.07
8	+	+	+	–	–	0.69	24	+	+	+	–	+	0.19
9	–	–	–	+	–	0.60	25	–	–	–	+	+	0.53
10	+	–	–	+	–	0.82	26	+	–	–	+	+	0.60
11	–	+	–	+	–	0.42	27	–	+	–	+	+	0.36
12	+	+	–	+	–	0.59	28	+	+	–	+	+	0.43
13	–	–	+	+	–	0.96	29	–	–	+	+	+	0.23
14	+	–	+	+	–	0.87	30	+	–	+	+	+	0.51
15	–	+	+	+	–	0.76	31	–	+	+	+	+	0.13
16	+	+	+	+	–	0.74	32	+	+	+	+	+	0.43

(a) Determine the coded equation for this response surface, ignoring β terms less than ± 0.03.

(b) A simplex optimization of this system finds optimal values for the factors of A = 2278 mL/min, B = 9.90 ppm, C = 260.6 mL/min, and D = 1.71. The value of E was maintained at its high level. Are these values consistent with your analysis of the factorial design.

11. A good empirical model provides an accurate picture of the response surface over the range of factor levels within the experimental design. The same model, however, may yield an inaccurate prediction for the response at other factor levels. For this reason, an empirical model, is tested before it is extrapolated to conditions other than those used in determining the model. For example, Palasota and Deming studied the effect of the relative amounts of H_2SO_4 and H_2O_2 on the absorbance of solutions of vanadium using the following central composite design [Palasota, J. A.; Deming, S. N. *J. Chem. Educ.* **1992**, *62*, 560–563].

run	drops of 1% H_2SO_4	drops of 20% H_2O_2
1	15	22
2	10	20
3	20	20
4	8	15
5	15	15
6	15	15
7	15	15
8	15	15
9	22	15
10	10	10
11	20	10
12	15	8

The reaction of H_2SO_4 and H_2O_2 generates a red-brown solution whose absorbance is measured at a wavelength of 450 nm. A regression analysis on their data yields the following uncoded equation for the response (absorbance $\times$ 1000).

$$R = 835.90 - 36.82X_1 - 21.34X_2 + 0.52X_1^2 + 0.15X_2^2 + 0.98X_1X_2$$

where X_1 is the drops of H_2O_2, and X_2 is the drops of H_2SO_4. Calculate the predicted absorbances for 10 drops of H_2O_2 and 0 drops of H_2SO_4, 0 drops of H_2O_2 and 10 drops of H_2SO_4, and for 0 drops of each reagent. Are these results reasonable? Explain. What does your answer tell you about this empirical model?

12. A newly proposed method is tested for its single-operator characteristics. To be competitive with the standard method, the new method must have a relative standard deviation of less than 10%, with a bias of less than 10%. To test the method, an analyst performs 10 replicate analyses on a standard sample known to contain 1.30 ppm of analyte. The results for the 10 trials are 1.25 ppm, 1.26 ppm, 1.29 ppm, 1.56 ppm, 1.46 ppm, 1.23 ppm, 1.49 ppm, 1.27 ppm, 1.31 ppm, and 1.43 ppm. Are the single operator characteristics for this method acceptable?

13. A proposed gravimetric method was evaluated for its ruggedness by varying the following factors.

Factor A: sample size	A = 1 g	a = 1.1 g
Factor B: pH	B = 6.5	b = 6.0
Factor C: digestion time	C = 3 h	c = 1 h
Factor D: number of rinses	D = 3	d = 5
Factor E: precipitant	E = reagent 1	e = reagent 2

Factor F: digestion temperature	F = 50ºC	f = 60ºC
Factor G: drying temperature	G = 100ºC	g = 140ºC

A standard sample that contains a known amount of analyte is carried through the procedure using the experimental design in Table 14.3.1. The percentage of analyte actually found in the eight trials are as follows: R_1 = 98.9, R_2 = 98.5, R_3 = 97.7, R_4 = 97.0, R_5 = 98.8, R_6 = 98.5, R_7 = 97.7, and R_8 = 97.3. Determine which factors, if any, appear to have a significant affect on the response, and estimate the expected standard deviation for the method.

14. The two-sample plot for the data in Example 14.3.1 is shown in Figure 14.3.4. Identify the analyst whose work is (a) the most accurate, (b) the most precise, (c) the least accurate, and (d) the least precise.

15. Chichilo reports the following data for the determination of the %w/w Al in two samples of limestone [Chichilo, P. J. *J. Assoc. Offc. Agr. Chemists* **1964**, *47*, 1019 as reported in Youden, W. J. "Statistical Techniques for Collaborative Tests," in *Statistical Manual of the Association of Official Analytical Chemists*, Association of Official Analytical Chemists: Washington, D. C., 1975].

analyst	sample 1	sample 2
1	1.35	1.57
2	1.35	1.33
3	1.34	1.47
4	1.50	1.60
5	1.52	1.62
6	1.39	1.52
7	1.30	1.36
8	1.32	1.33

Construct a two-sample plot for this data and estimate values for σ_{rand} and for σ_{syst}.

16. The importance of between-laboratory variability on the results of an analytical method are determined by having several laboratories analyze the same sample. In one such study, seven laboratories analyzed a sample of homogenized milk for a selected aflatoxin [Massart, D. L.; Vandeginste, B. G. M; Deming, S. N.; Michotte, Y.; Kaufman, L. *Chemometrics: A Textbook*, Elsevier: Amsterdam, 1988]. The results, in ppb, are summarized below.

lab A	lab B	lab C	lab D	lab E	lab F	lab G
1.6	4.6	1.2	1.5	6.0	6.2	3.3
2.9	2.8	1.9	2.7	3.9	3.8	3.8
3.5	3.0	2.9	3.4	4.3	5.5	5.5
4.5	4.5	1.1	2.0	5.8	4.2	4.9
2.2	3.1	2.9	3.4	4.0	5.3	4.5

(a) Determine if the between-laboratory variability is significantly greater than the within-laboratory variability at $\alpha = 0.05$. If the between-laboratory variability is significant, then determine the source(s) of that variability.

(b) Estimate values for σ^2_{rand} and for σ^2_{syst}.

17. Show that the total sum-of-squares (SS_t) is the sum of the within-sample sum-of-squares (SS_w) and the between-sample sum-of-squares (SS_b). See Table 14.3.2 for the relevant equations.

18. Eighteen analytical students are asked to determine the %w/w Mn in a sample of steel, with the results shown here.

0.26%	0.28%	0.27%	0.24%	0.26%	0.25%
0.26%	0.28%	0.25%	0.24%	0.26%	0.25%
0.29%	0.24%	0.27%	0.23%	0.26%	0.24%

(a) Given that the steel sample is 0.26% w/w Mn, estimate the expected relative standard deviation for the class' results.

(b) Are the actual results consistent with the estimated relative standard deviation?

5.6: Additional Resources

The following set of experiments provide practical examples of the optimization of experimental conditions. Examples include simplex optimization, factorial designs for developing empirical models of response surfaces, and fitting experimental data to theoretical models of the response surface.

- Amenta, D. S.; Lamb, C. E.; Leary, J. J. “Simplex Optimization of Yield of *sec*-Butylbenzene in a Friedel-Crafts Alkylation,” *J. Chem. Educ.* **1979**, *56*, 557–558.
- Gozálvez, J. M.; García-Diaz, J. C. “Mixture Design Experiments Applied to the Formulation of Colo- rant Solutions,” *J. Chem. Educ.* **2006**, *83*, 647–650.
- Harvey, D. T.; Byerly, S.; Bowman, A.; Tomlin, J. “Optimization of HPLC and GC Separations Using Response Surfaces,” *J. Chem. Educ.* **1991**, *68*, 162–168.
- Krawcyzk, T.; Shupska, R.; Baj, S. “Applications of Chemiluminescence in the Teaching of Experimental Design,” *J. Chem. Educ.* **2015**, *92*, 317–321.
- Leggett, D. L. “Instrumental Simplex Optimization,” *J. Chem. Educ.* **1983**, *60*, 707–710.
- Oles, P. J. “Fractional Factorial Experimental Design as a Teaching Tool for Quantitative Analysis,” *J. Chem. Educ.* **1998**, *75*, 357–359.
- Palasota, J. A.; Deming, S.N. “Central Composite Experimental Design,” *J. Chem. Educ.* **1992**, *69*, 560–561.
- Sangsila, S.; Labinaz, G.; Poland, J. S.; vanLoon, G. W. “An Experiment on Sequential Simplex Optimization of an Atomic Absorption Analysis Procedure,” *J. Chem. Educ.* **1989**, *66*, 351–353.
- Santos-Delgado, M. J.; Larrea-Tarruella, L. “A Didactic Experience of Statistical Analysis for the De- termination of Glycine in a Nonaqueous Medium using ANOVA and a Computer Program,” *J. Chem. Educ.* **2004**, *81*, 97–99.
- Shavers, C. L.; Parsons, M. L.; Deming, S. N. “Simplex Optimization of Chemical Systems,” *J. Chem Educ.* **1979**, *56*, 307–309.
- Stieg, S. “A Low-Noise Simplex Optimization Experiment,” *J. Chem. Educ.* **1986**, *63*, 547–548.
- Stolzberg, R. J. “Screening and Sequential Experimentation: Simulations and Flame Atomic Absorption Spectrometry Experiments,” *J. Chem. Educ.* **1997**, *74*, 216–220.
- Van Ryswyk, H.; Van Hecke, G. R. “Attaining Optimal Conditions,” *J. Chem. Educ.* **1991**, *66*, 878– 882.

The following texts and articles provide an excellent discussion of optimization methods based on searching algorithms and mathematical modeling use factorial designs, including a discussion of the relevant calculations. A few of these sources discuss other types of experimental designs.

- Analytical Methods Committee “Experimental design and optimization (1): an introduction to some basic concepts,” AMCTB 24, 2006.
- Analytical Methods Committee “Experimental design and optimization (2): handling uncontrolled factors,” AMCTB 26, 2006.
- Analytical Methods Committee “Experimental design and optimization (3): some fractional factorial designs,” AMCTB 36, 2009.
- Analytical Methods Committee “Experimental design and optimisation (4): Plackett–Burman de- signs,” AMCTB 55, 2013.
- Bayne, C. K.; Rubin, I. B. *Practical Experimental Designs and Optimization Methods for Chemists*, VCH Publishers: Deerfield Beach, FL; 1986.
- Bezerra, M. A.; Santelli, R. E.; Oliveira, E. P.; Villar, L. S.; Escaleira, L. A. “Response surface methodology (RSM) as a tool for optimization in analytical chemistry,” *Talanta* **2008**, *76*, 965–977.
- Box, G. E. P. “Statistical Design in the Study of Analytical Methods,” *Analyst* **1952**, *77*, 879–891.
- Deming, S. N.; Morgan, S. L. *Experimental Design: A Chemometric Approach*, Elsevier: Amsterdam, 1987.
- Ferreira, S. L. C.; dos Santos, W. N. L.; Quintella, C. M.; Neto, B. B.; Bosque-Sendra, J. M. “Doehlert Matrix: A Chemometric Tool for Analytical Chemistry—Review,” *Talanta* **2004**, *63*, 1061–1067.
- Ferreira, S. L. C.; Bruns, R. E.; Ferreira, H. S.; Matos, G. D.; David, J. M.; Brandão, G. C.; da Silva, E. G. P.; Portugal, L. A.; dos Reis, P. S.; Souza, A. S.; dos Santos, W. N. L. “Box-Behnken Design: An Alternative for the Optimization of Analytical Methods,” *Anal. Chim. Acta* **2007**, *597*, 179–186.
- Gonzalez, A. G. “Two Level Factorial Experimental Designs Based on Multiple Linear Regression Models: A Tutorial Digest Illustrated by Case Studies,” *Anal. Chim. Acta* **1998**, *360*, 227–241.
- Goupy, J. “What Kind of Experimental Design for Finding and Checking Robustness of Analytical Methods?” *Anal. Chim. Acta* **2005**, *544*, 184–190.

- Hendrix, C. D. “What Every Technologist Should Know About Experimental Design,” *Chemtech* **1979**, *9*, 167–174.
- Hendrix, C. D. “Through the Response Surface with Test Tube and Pipe Wrench,” *Chemtech* **1980**, *10*, 488–497.
- Leardi, R. “Experimental Design: A Tutorial,” *Anal. Chim. Acta* **2009**, *652*, 161–172.
- Liang, Y. “Comparison of Optimization Methods,” *Chromatography Review* **1985**, *12(2)*, 6–9.
- Morgan, E. *Chemometrics: Experimental Design*, John Wiley and Sons: Chichester, 1991.
- Walters, F. H.; Morgan, S. L.; Parker, L. P., Jr.; Deming, S. N. *Sequential Simplex Optimization*, CRC Press: Boca Raton, FL, 1991.

The following texts provide additional information about ANOVA calculations, including discussions of two-way analysis of variance.

- Graham, R. C. *Data Analysis for the Chemical Sciences*, VCH Publishers: New York, 1993.
- Miller, J. C.; Miller, J. N. *Statistics for Analytical Chemistry*, Ellis Horwood Limited: Chichester, 1988.

The following resources provide additional information on the validation of analytical methods.

- Gonzalez, A. G.; Herrador, M. A. “A Practical Guide to Analytical Method Validation, Including Measurement Uncertainty and Accuracy Profiles,” *Trends Anal. Chem.* **2007**, *26*, 227–238.
- Thompson, M.; Ellison, S. L. R.; Wood, R. “Harmonized Guidelines for Single-Laboratory Validation of Analytical Methods,” *Pure Appl. Chem.* **2002**, *74*, 835–855.

5.7: Chapter Summary and Key Terms

Chapter Summary

One of the goals of analytical chemistry is to develop new analytical methods that are accepted as standard methods. In this chapter we have considered how a standard method is developed, including finding the optimum experimental conditions, verifying that the method produces acceptable precision and accuracy, and validating the method for general use.

To optimize a method we try to find the combination of experimental parameters that produces the best result or response. We can visualize this process as being similar to finding the highest point on a mountain. In this analogy, the mountain's topography corresponds to a response surface, which is a plot of the system's response as a function of the factors under our control.

One method for finding the optimum response is to use a searching algorithm. In a one-factor-at-a-time optimization, we change one factor while holding constant all other factors until there is no further improvement in the response. The process continues with the next factor, cycling through the factors until there is no further improvement in the response.

This approach to finding the optimum response often is effective, but usually is not efficient. A searching algorithm that is both effective and efficient is a simplex optimization, the rules of which allow us to change the levels of all factors simultaneously.

Another approach to optimizing a method is to develop a mathematical model of the response surface. Such models can be theoretical, in that they are derived from a known chemical and physical relationship between the response and its factors. Alternatively, we can develop an empirical model, which does not have a firm theoretical basis, by fitting an empirical equation to our experimental data. One approach is to use a 2^k factorial design in which each factor is tested at both a high level and a low level, and paired with the high level and the low level for all other factors.

After optimizing a method it is necessary to demonstrate that it can produce acceptable results. Verifying a method usually includes establishing single-operator characteristics, the blind analysis of standard samples, and determining the method's ruggedness. Single-operator characteristics include the method's precision, accuracy, and detection limit when used by a single analyst. To test against possible bias on the part of the analyst, he or she analyzes a set of blind samples in which the analyst does not know the concentration of analyte. Finally, we use ruggedness testing to determine which experimental factors must be carefully controlled to avoid unexpectedly large determinate or indeterminate sources of error.

The last step in establishing a standard method is to validate its transferability to other laboratories. An important step in the process of validating a method is collaborative testing, in which a common set of samples is analyzed by different laboratories. In a well-designed collaborative test it is possible to establish limits for the method's precision and accuracy.

Key Terms

2^k factorial design	analysis of variance	between-sample variance
blind analysis	central composite design	collaborative testing
dependent	effective	efficiency
empirical model	factor	factor level
Fisher's least significant difference	fixed-size simplex optimization	global optimum
independent	local optimum	one-factor-at-a-time optimization
response	response surface	ruggedness testing
searching algorithm	simplex	standard method
theoretical model	validation	variable-sized simplex optimization
within-sample variance		

CHAPTER OVERVIEW

6: Quality Assurance

In Chapter 14 we discussed the process of developing a standard method, including optimizing the experimental procedure, verifying that the method produces acceptable precision and accuracy in the hands of a signal analyst, and validating the method for general use by the broader analytical community. Knowing that a method meets suitable standards is important if we are to have confidence in our results. Even so, using a standard method does not guarantee that the result of an analysis is acceptable. In this chapter we introduce the quality assurance procedures used in industry and government labs for the real-time monitoring of routine chemical analyses.

Thumbnail: Examples of property control charts that show a sequence of results.

6.1: The Analytical Perspective Revisited

As we noted in Chapter 1, each area of chemistry brings a unique perspective to the broader discipline of chemistry. For analytical chemistry this perspective is as an approach to solving problems, one representation of which is shown in Figure 15.1.1 .

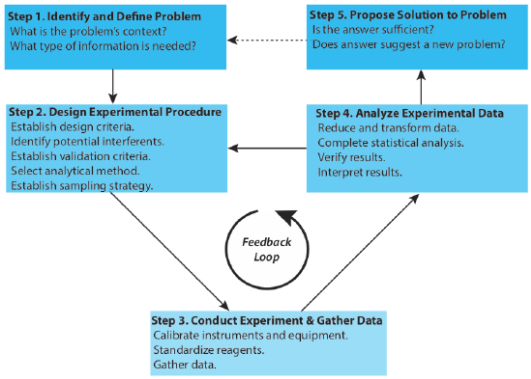

Figure 15.1.1 . Flow diagram showing one view of the analytical approach to solving problems. This diagram is modified after Atkinson, G. F. *J. Chem. Educ.* **1982**, *59*, 201–202.

> Figure 15.1.1 is the same as Figure 1.2.1. You may wish to review our earlier discussion of this figure and of the analytical approach to solving problem.

If you examine an analytical method it often seems that its development was a straightforward process of moving from a problem to its solution. Unfortunately—or, perhaps, fortunately for those who consider themselves analytical chemists!—developing an analytical method seldom is routine. Even a well-established standard analytical method, carefully followed, can yield poor data.

An important feature of the analytical approach in Figure 15.1.1 is the feedback loop that includes steps 2, 3, and 4, in which the outcome of one step may lead us to reevaluate the other steps. For example, after standardizing a spectrophotometric method for the analysis of iron (step 3), we may find that its sensitivity does not meet our original design criteria (step 2). In response, we might choose a different method, change the original design criteria, or work to improve the sensitivity.

The feedback loop in Figure 15.1.1 is maintained by a quality assurance program, whose objective is to control systematic and random sources of error [see, for example (a) Taylor, J. K. *Anal. Chem.* **1981**, *53*, 1588A–1596A; (b) Taylor, J. K. *Anal. Chem.* **1983**, *55*, 600A–608A; (c) Taylor, J. K. *Am. Lab* October 1985, *53*, 67–75; (d) Nadkarni, R. A. *Anal. Chem.* **1991**, *63*, 675A–682A; (e) Valcárcel, M.; Ríos, A. *Trends Anal. Chem.* **1994**, *13*, 17–23.] The underlying assumption of a quality assurance program is that results obtained when an analysis is under ***statistical control*** are free of bias and are characterized by well-defined confidence intervals. When used properly, a quality assurance program identifies the practices necessary to bring a system into statistical control, allows us to determine if the system remains in statistical control, and suggests a course of corrective action if the system falls out of statistical control.

> An analysis is in a state of statistical control when it is reproducible and free from bias.

The focus of this chapter is on the two principal components of a ***quality assurance program***: quality control and quality assessment. In addition, we will give considerable attention to the use of control charts for monitoring the quality of analytical data.

6.2: Quality Control

Quality control encompasses all activities that bring an analysis into statistical control. The most important facet of quality control is a set of written directives that describe relevant laboratory-specific, technique-specific, sample-specific, method-specific, and protocol-specific operations. ***Good laboratory practices*** (GLPs) describe the general laboratory operations that we must follow in any analysis. These practices include properly recording data and maintaining records, using chain-of-custody forms for samples, specifying and purifying chemical reagents, preparing commonly used reagents, cleaning and calibrating glassware, training laboratory personnel, and maintaining the laboratory facilities and general laboratory equipment.

> For one example of quality control, see Keith, L. H.; Crummett, W.; Deegan, J., Jr.; Libby, R. A.; Taylor, J. K.; Wentler, G. "Principles of Environmental Analysis," *Anal. Chem.* **1983**, *55*, 2210–2218. This article describes guidelines developed by the Subcommittee on Environmental Analytical Chemistry, a subcommittee of the American Chemical Society's Committee on Environmental Improvement.

Good measurement practices (GMPs) describe those operations specific to a technique. In general, GMPs provide instructions for maintaining, calibrating, and using equipment and instrumentation. For example, a GMP for a titration describes how to calibrate the buret (if required), how to fill the buret with titrant, the correct way to read the volume of titrant in the buret, and the correct way to dispense the titrant.

The directions for analyzing a specific analyte in a specific matrix are described by a ***standard operations procedure*** (SOP). The SOP indicates how we process the sample in the laboratory, how we separate the analyte from potential interferents, how we standardize the method, how we measure the analytical signal, how we transform the data into the desired result, and how we use quality assessment tools to maintain quality control. If the laboratory is responsible for sampling, then the SOP also states how we must collect, process, and preserve the sample in the field. An SOP may be developed and used by a single laboratory, or it may be a standard procedure approved by an organization such as the American Society for Testing Materials or the Federal Food and Drug Administration. A typical SOP is provided in the following example.

Example 15.2.1

Provide an SOP for the determination of cadmium in lake sediments using atomic absorption spectroscopy and a normal calibration curve.

Solution

Collect sediment samples using a bottom grab sampler and store them at 4°C in acid-washed polyethylene bottles during transportation to the laboratory. Dry the samples to constant weight at 105°C and grind them to a uniform particle size. Extract the cadmium in a 1-g sample of sediment by adding the sediment and 25 mL of 0.5 M HCl to an acid-washed 100-mL polyethylene bottle and shaking for 24 h. After filtering, analyze the sample by atomic absorption spectroscopy using an air–acetylene flame, a wavelength of 228.8 nm, and a slit width of 0.5 nm. Prepare a normal calibration curve using five standards with nominal concentrations of 0.20, 0.50, 1.00, 2.00, and 3.00 ppm. Periodically check the accuracy of the calibration curve by analyzing the 1.00-ppm standard. An accuracy of $\pm$ 10% is considered acceptable.

Although an SOP provides a written procedure, it is not necessary to follow the procedure exactly as long as we are careful to identify any modifications. On the other hand, we must follow all instructions in a ***protocol for a specific purpose*** (PSP)—the most detailed of the written quality control directives—before an agency or a client will accept our results. In many cases the required elements of a PSP are established by the agency that sponsors the analysis. For example, a lab working under contract with the Environmental Protection Agency must develop a PSP that addresses such items as sampling and sample custody, frequency of calibration, schedules for the preventive maintenance of equipment and instrumentation, and management of the quality assurance program.

Two additional aspects of a quality control program deserve mention. The first is that the individuals responsible for collecting and analyzing the samples can critically examine and reject individual samples, measurements, and results. For example, when analyzing sediments for cadmium (see the SOP in Example 15.2.1) we might choose to screen sediment samples, discarding a sample that contains foreign objects—such as rocks, twigs, or trash—replacing it with an additional sample. If we observe a sudden change in the performance of the atomic absorption spectrometer, we may choose to reanalyze the affected samples. We may also

decide to reanalyze a sample if the result of its analysis clearly is unreasonable. By identifying those samples, measurements, and results subject to gross systematic errors, inspection helps control the quality of an analysis.

The second additional consideration is the certification of an analyst's competence to perform the analysis for which he or she is responsible. Before an analyst is allowed to perform a new analytical method, he or she may be required to analyze successfully an independent check sample with acceptable accuracy and precision. The check sample is similar in composition to samples that the analyst will analyze later, with a concentration that is 5 to 50 times that of the method's detection limit.

6.3: Quality Assessment

The written directives of a quality control program are a necessary, but not a sufficient condition for obtaining and maintaining a state of statistical control. Although quality control directives explain how to conduct an analysis, they do not indicate whether the system is under statistical control. This is the role of ***quality assessment***, the second component of a quality assurance program.

The goals of quality assessment are to determine when an analysis has reached a state of statistical control, to detect when an analysis falls out of statistical control, and to suggest possible reasons for this loss of statistical control. For convenience, we divide quality assessment into two categories: internal methods coordinated within the laboratory, and external methods organized and maintained by an outside agency.

Internal Methods of Quality Assessment

The most useful methods for quality assessment are those coordinated by the laboratory, which provide immediate feedback about the analytical method's state of statistical control. Internal methods of quality assessment include the analysis of duplicate samples, the analysis of blanks, the analysis of standard samples, and spike recoveries.

Analysis of Duplicate Samples

An effective method for determining the precision of an analysis is to analyze ***duplicate samples***. Duplicate samples are obtained by dividing a single gross sample into two parts, although in some cases the duplicate samples are independently collected gross samples. We report the results for the duplicate samples, X_1 and X_2, by determining the difference, d, or the relative difference, $(d)_r$, between the two samples

$$d = X_1 - X_2$$

$$(d)_r = \frac{d}{(X_1 + X_2)/2} \times 100$$

and comparing to an accepted value, such as those in Table 15.3.1 for the analysis of waters and wastewaters. Alternatively, we can estimate the standard deviation using the results for a set of n duplicates

$$s = \sqrt{\frac{\sum_{i=1}^{n} d_i^2}{2n}}$$

where d_i is the difference between the i^{th} pair of duplicates. The degrees of freedom for the standard deviation is the same as the number of duplicate samples. If we combine duplicate samples from several sources, then the precision of the measurement process must be approximately the same for each.

Table 15.3.1 : Quality Assessment Limits for the Analysis of Waters and Wastewaters

analyte	$(d)_r$: [analyte] < 20 × MDL (±%)	$(d)_r$: [analyte] > 20 × MDL (±%)	spike recovery limit (%)
acids	40	20 × MDL (±%)">20	60–140
anions	25	20 × MDL (±%)">10	80–120
bases or neutrals	40	20 × MDL (±%)">20	70–130
carbamate pesticides	40	20 × MDL (±%)">20	50–150
herbicides	40	20 × MDL (±%)">20	40–160
metals	25	20 × MDL (±%)">10	80–120
other inorganics	25	20 × MDL (±%)">10	80–120
volatile organics	40	20 × MDL (±%)">20	70–130

Abbreviation: MDL = method's detection limit

Source: Table 1020.1 in *Standard Methods for the Analysis of Water and Wastewater*, American Public Health Association: Washington, D. C., 18th Ed. 1992.

Example 15.3.1

To evaluate the precision for the determination of potassium in blood serum, duplicate analyses were performed on six samples, yielding the following results in mg K/L.

Table of potassium tests in blood serum

duplicate	X_1	X_2
1	160	147
2	196	202
3	207	196
4	185	193
5	172	188
6	133	119

Estimate the standard deviation for the analysis.

Solution

To estimate the standard deviation we first calculate the difference, d, and the squared difference, d^2, for each duplicate. The results of these calculations are summarized in the following table.

Table of potassium tests in blood serum

duplicate	$d = X_1 - X_2$	d^2
1	13	169
2	–6	36
3	11	121
4	–8	64
5	–16	256
6	14	196

Finally, we calculate the standard deviation

$$s = \sqrt{\frac{169 + 36 + 121 + 64 + 256 + 196}{2 \times 6}} = 8.4$$

Exercise 15.3.1

To evaluate the precision of a glucometer—a device a patient uses at home to monitor his or her blood glucose level—duplicate analyses are performed on samples drawn from five individuals, yielding the following results in mg glucose/100 mL.

duplicate	X_1	X_2
1	148.5	149.1
2	96.5	98.8
3	174.9	174.5
4	118.1	118.9

duplicate	X_1	X_2
5	72.7	70.4

Estimate the standard deviation for the analysis.

Answer

To estimate the standard deviation we first calculate the difference, d, and the squared difference, d^2, for each duplicate. The results of these calculations are summarized in the following table.

duplicate	$d = X_1 - X_2$	d^2
1	–0.6	0.36
2	–2.3	5.29
3	0.4	0.16
4	–0.8	0.64
5	2.3	5.29

Finally, we calculate the standard deviation.

$$s = \sqrt{\frac{0.36 + 5.29 + 0.16 + 0.64 + 5.29}{2 \times 5}} = 1.08$$

Analysis of Blanks

We introduced the use of a blank in Chapter 3 as a way to correct the signal for contributions from sources other than the analyte. The most common blank is a ***method blank*** in which we take an analyte free sample through the analysis using the same reagents, glassware, and instrumentation. A method blank allows us to identify and to correct systematic errors due to impurities in the reagents, contaminated glassware, and poorly calibrated instrumentation. At a minimum, a new method blank is analyzed whenever we prepare a new reagent, or after we analyze a sample with a high concentration of analyte as residual carryover of analyte may produce a positive determinate error.

When we collect samples in the field, additional blanks are needed to correct for potential sampling errors [Keith, L. H. *Environmental Sampling and Analysis: A Practical Guide*, Lewis Publishers: Chelsea, MI, 1991]. A ***field blank*** is an analyte-free sample carried from the laboratory to the sampling site. At the sampling site the blank is transferred to a clean sample container, which exposes it to the local environment. The field blank is then preserved and transported back to the laboratory for analysis. A field blank helps identify systematic errors due to sampling, transport, and analysis. A trip blank is an analyte-free sample carried from the laboratory to the sampling site and back to the laboratory without being opened. A trip blank helps to identify systematic errors due to cross-contamination of volatile organic compounds during transport, handling, storage, and analysis.

A method blank also is called a reagent blank. The contamination of reagents over time is a significant concern. The regular use of a method blank compensates for this contamination.

Analysis of Standards

Another tool for monitoring an analytical method's state of statistical control is to analyze a standard that contains a known concentration of analyte. A standard reference material (SRM) is the ideal choice, provided that the SRM's matrix is similar to that of our samples. A variety of SRMs are available from the National Institute of Standards and Technology (NIST). If a suitable SRM is not available, then we can use an independently prepared synthetic sample if it is prepared from reagents of known purity. In all cases, the analyte's experimentally determined concentration in the standard must fall within predetermined limits before the analysis is considered under statistical control.

Table 4.2.6 in Chapter 4 provides a summary of SRM 2346, a standard sample of Gingko biloba leaves with certified values for the concentrations of flavonoids, terpene ketones, and toxic elements, such as mercury and lead.

Spike Recoveries

One of the most important quality assessment tools is the recovery of a known addition, or spike, of analyte to a method blank, a field blank, or a sample. To determine a ***spike recovery***, the blank or sample is split into two portions and a known amount of a standard solution of analyte is added to one portion. The analyte's concentration is determined for both the spiked, *F*, and unspiked portions, *I*, and the percent recovery, %*R*, is calculated as

$$\%R = \frac{F - I}{A} \times 100$$

where *A* is the concentration of analyte added to the spiked portion.

Example 15.3.2

A spike recovery for the analysis of chloride in well water was performed by adding 5.00 mL of a 250.0 ppm solution of Cl^- to a 50-mL volumetric flask and diluting to volume with the sample. An unspiked sample was prepared by adding 5.00 mL of distilled water to a separate 50-mL volumetric flask and diluting to volume with the sample. Analysis of the sample and the spiked sample return chloride concentrations of 18.3 ppm and 40.9 ppm, respectively. Determine the spike recovery.

Solution

To calculate the concentration of the analyte added in the spike, we take into account the effect of dilution.

$$A = 250.0\text{ppm} \times \frac{5.00\text{mL}}{50.0\text{mL}} = 25.0\text{ppm}$$

Thus, the spike recovery is

$$\%R = \frac{40.9 - 18.3}{25.0} \times 100 = 90.4\%$$

Exercise 15.3.2

To test a glucometer, a spike recovery is carried out by measuring the amount of glucose in a sample of a patient's blood before and after spiking it with a standard solution of glucose. Before spiking the sample the glucose level is 86.7 mg/100 mL and after spiking the sample it is 110.3 mg/100 mL. The spike is prepared by adding 10.0 µL of a 25 000 mg/100mL standard to a 10.0-mL portion of the blood. What is the spike recovery for this sample.

Answer

Adding a 10.0-µL spike to a 10.0-mL sample is a 1000-fold dilution; thus, the concentration of added glucose is 25.0 mg/100 mL and the spike recovery is

$$\%R = \frac{110.3 - 86.7}{25.0} \times 100 = 94.4\%$$

We can use a spike recovery on a method blank and a field blank to evaluate the general performance of an analytical procedure. A known concentration of analyte is added to each blank at a concentration that is 5 to 50 times the method's detection limit. A systematic error during sampling and transport will result in an unacceptable recovery for the field blank, but not for the method blank. A systematic error in the laboratory, however, affects the recoveries for both the field blank and the method blank.

Spike recoveries on a sample are used to detect systematic errors due to the sample's matrix, or to evaluate the stability of a sample after its collection. Ideally, samples are spiked in the field at a concentration that is 1 to 10 times the analyte's expected concentration or 5 to 50 times the method's detection limit, whichever is larger. If the recovery for a field spike is unacceptable, then a duplicate sample is spiked in the laboratory and analyzed immediately. If the laboratory spike's recovery is acceptable, then the poor recovery for the field spike likely is the result of the sample's deterioration during storage. If the recovery for the laboratory spike also is unacceptable, the most probable cause is a matrix-dependent relationship between the analytical signal and

the analyte's concentration. In this case the sample is analyzed by the method of standard additions. Typical limits for spike recoveries for the analysis of waters and wastewaters are shown in Table 15.3.1 .

> Figure 15.4.1, which we will discuss in the next section, illustrates the use of spike recoveries as part of a quality assessment program.

External Methods of Quality Assessment

Internal methods of quality assessment always carry some level of suspicion because there is a potential for bias in their execution and interpretation. For this reason, external methods of quality assessment also play an important role in a quality assurance program. One external method of quality assessment is the certification of a laboratory by a sponsoring agency. Certification of a lab is based on its successful analysis of a set of ***proficiency standards*** prepared by the sponsoring agency. For example, laboratories involved in environmental analyses may be required to analyze standard samples prepared by the Environmental Protection Agency. A second example of an external method of quality assessment is a laboratory's voluntary participation in a collaborative test sponsored by a professional organization, such as the Association of Official Analytical Chemists. Finally, an individual contracting with a laboratory can perform his or her own external quality assessment by submitting blind duplicate samples and blind standards to the laboratory for analysis. If the results for the quality assessment samples are unacceptable, then there is good reason to question the laboratory's results for other samples.

> See Chapter 14 for a more detailed description of collaborative testing.

6.4: Evaluating Quality Assurance Data

In the previous section we described several internal methods of quality assessment that provide quantitative estimates of the systematic errors and the random errors in an analytical method. Now we turn our attention to how we incorporate this quality assessment data into a complete quality assurance program. There are two general approaches to developing a quality assurance program: a prescriptive approach, in which we prescribe an exact method of quality assessment, and a performance-based approach in which we can use any form of quality assessment, provided that we can demonstrate an acceptable level of statistical control [Poppiti, J. *Environ. Sci. Technol.* **1994**, *28*, 151A–152A].

Prescriptive Approach

With a prescriptive approach to quality assessment, duplicate samples, blanks, standards, and spike recoveries are measured using a specific protocol. We compare the result of each analysis to a single predetermined limit, taking an appropriate corrective action if the limit is exceeded. Prescriptive approaches to quality assurance are common for programs and laboratories subject to federal regulation. For example, the Food and Drug Administration (FDA) specifies quality assurance practices that must be followed by laboratories that analyze products regulated by the FDA.

Figure 15.4.1 provides a typical example of a prescriptive approach to quality assessment. Two samples, *A* and *B*, are collected at the sample site. Sample *A* is split into two equal-volume samples, A_1 and A_2. Sample *B* is also split into two equal-volume samples, one of which, B_{SF}, is spiked in the field with a known amount of analyte. A field blank, D_F, also is spiked with the same amount of analyte. All five samples (A_1, A_2, *B*, B_{SF}, and *DF*) are preserved if necessary and transported to the laboratory for analysis.

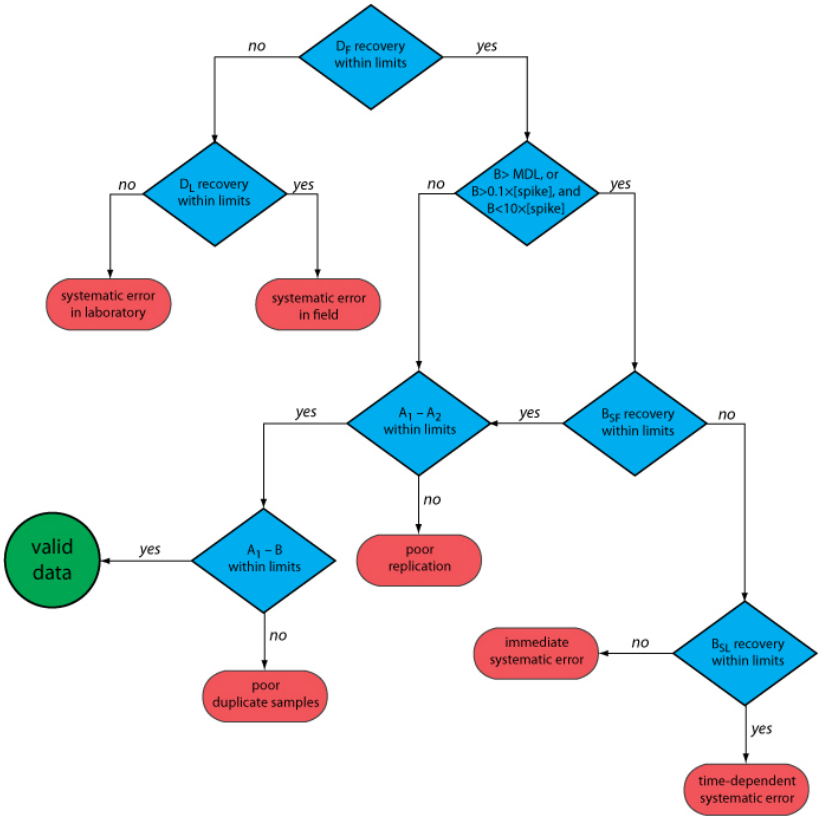

Figure 15.4.1 . Example of a prescriptive approach to quality assurance for laboratories monitoring waters and wastewaters. Adapted from Environmental Monitoring and Support Laboratory, U. S. Environmental Protection Agency, "Handbook for Analytical Quality Control in Water and Wastewater Laboratories," March 1979.

After returning to the lab, the first sample that is analyzed is the field blank. If its spike recovery is unacceptable—an indication of a systematic error in the field or in the lab—then a laboratory method blank, D_L, is prepared and analyzed. If the spike recovery for the method blank is unsatisfactory, then the systematic error originated in the laboratory; this is error the analyst can find and correct before proceeding with the analysis. An acceptable spike recovery for the method blank, however, indicates that the

systematic error occurred in the field or during transport to the laboratory, casting uncertainty on the quality of the samples. The only recourse is to discard the samples and return to the field to collect new samples.

If the field blank is satisfactory, then sample B is analyzed. If the result for sample B is above the method's detection limit, or if it is within the range of 0.1 to 10 times the amount of analyte spiked into B_{SF}, then a spike recovery for B_{SF} is determined. An unacceptable spike recovery for B_{SF} indicates the presence of a systematic error that involves the sample. To determine the source of the systematic error, a laboratory spike, B_{SL}, is prepared using sample B and analyzed. If the spike recovery for B_{SL} is acceptable, then the systematic error requires a long time to have a noticeable effect on the spike recovery. One possible explanation is that the analyte has not been preserved properly or it has been held beyond the acceptable holding time. An unacceptable spike recovery for B_{SL} suggests an immediate systematic error, such as that due to the influence of the sample's matrix. In either case the systematic errors are fatal and must be corrected before the sample is reanalyzed.

If the spike recovery for B_{SF} is acceptable, or if the result for sample B is below the method's detection limit, or outside the range of 0.1 to 10 times the amount of analyte spiked in B_{SF}, then the duplicate samples A_1 and A_2 are analyzed. The results for A_1 and A_2 are discarded if the difference between their values is excessive. If the difference between the results for A_1 and A_2 is within the accepted limits, then the results for samples A_1 and B are compared. Because samples collected from the same sampling site at the same time should be identical in composition, the results are discarded if the difference between their values is unsatisfactory and the results accepted if the difference is satisfactory.

The protocol in Figure 15.4.1 requires four to five evaluations of quality assessment data before the result for a single sample is accepted, a process that we must repeat for each analyte and for each sample. Other prescriptive protocols are equally demanding. For example, Figure 3.6.1 in Chapter 3 shows a portion of a quality assurance protocol for the graphite furnace atomic absorption analysis of trace metals in aqueous solutions. This protocol involves the analysis of an initial calibration verification standard and an initial calibration blank, followed by the analysis of samples in groups of ten. Each group of samples is preceded and followed by continuing calibration verification (CCV) and continuing calibration blank (CCB) quality assessment samples. Results for each group of ten samples are accepted only if both sets of CCV and CCB quality assessment samples are acceptable.

The advantage of a prescriptive approach to quality assurance is that all laboratories use a single consistent set of guideline. A significant disadvantage is that it does not take into account a laboratory's ability to produce quality results when determining the frequency of collecting and analyzing quality assessment data. A laboratory with a record of producing high quality results is forced to spend more time and money on quality assessment than perhaps is necessary. At the same time, the frequency of quality assessment may be insufficient for a laboratory with a history of producing results of poor quality.

Performance-Based Approach

In a performance-based approach to quality assurance, a laboratory is free to use its experience to determine the best way to gather and monitor quality assessment data. The tools of quality assessment remain the same— duplicate samples, blanks, standards, and spike recoveries—because they provide the necessary information about precision and bias. What a laboratory can control is the frequency with which it analyzes quality assessment samples and the conditions it chooses to signal when an analysis no longer is in a state of statistical control.

The principal tool for performance-based quality assessment is a ***control chart***, which provides a continuous record of quality assessment data. The fundamental assumption is that if an analysis is under statistical control, individual quality assessment results are distributed randomly around a known mean with a known standard deviation. When an analysis moves out of statistical control, the quality assessment data is influenced by additional sources of error, which increases the standard deviation or changes the mean value.

Control charts were developed in the 1920s as a quality assurance tool for the control of manufactured products [Shewhart, W. A. *Economic Control of the Quality of Manufactured Products*, Macmillan: London, 1931]. Although there are many types of control charts, two are common in quality assessment programs: a property control chart, in which we record single measurements or the means for several replicate measurements, and a precision control chart, in which we record ranges or standard deviations. In either case, the control chart consists of a line that represents the experimental result and two or more boundary lines whose positions are determined by the precision of the measurement process. The position of the data points about the boundary lines determines whether the analysis is in statistical control.

Constructing a Property Control Chart

The simplest property control chart is a sequence of points, each of which represents a single determination of the property we are monitoring. To construct the control chart, we analyze a minimum of 7–15 samples while the system is under statistical control. The center line (*CL*) of the control chart is the average of these *n* samples.

$$CL = \overline{X} = \frac{\sum_{i=1}^{n} X_i}{n}$$

> The more samples in the original control chart, the easier it is to detect when an analysis is beginning to drift out of statistical control. Building a control chart with an initial run of 30 or more samples is not an unusual choice.

Boundary lines around the center line are determined by the standard deviation, *S*, of the *n* points

$$S = \sqrt{\frac{\sum_{i=1}^{n} \left(X_i - \overline{X}\right)^2}{n-1}}$$

The upper and lower warning limits (*UWL* and *LWL*) and the upper and lower control limits (*UCL* and *LCL*) are given by the following equations.

$$\begin{aligned} UWL &= CL + 2S \\ LWL &= CL - 2S \\ UCL &= CL + 3S \\ LCL &= CL - 3S \end{aligned}$$

> Why these limits? Examine Table 4.4.2 in Chapter 4 and consider your answer to this question. We will return to this point later in this chapter when we consider how to use a control chart.

Example 15.4.1

Construct a property control chart using the following spike recovery data (all values are for percentage of spike recovered).

sample:	1	2	3	4	5
result:	97.3	98.1	100.3	99.5	100.9
sample:	6	7	8	9	10
result:	98.6	96.9	99.6	101.1	100.4
sample:	11	12	13	14	15
result:	100.0	95.9	98.3	99.2	102.1
sample:	16	17	18	19	20
result:	98.5	101.7	100.4	99.1	100.3

Solution

The mean and the standard deviation for the 20 data points are 99.4% and 1.6%, respectively. Using these values, we find that the *UCL* is 104.2%, the *UWL* is 102.6%, the *LWL* is 96.2%, and the *LCL* is 94.6%. To construct the control chart, we plot the data points sequentially and draw horizontal lines for the center line and the four boundary lines. The resulting property control chart is shown in Figure 15.4.2 .

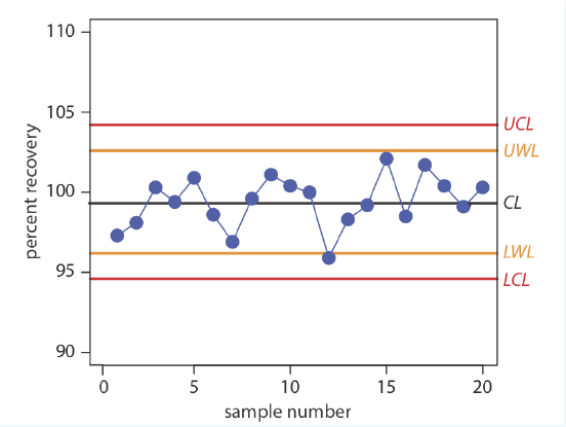

Figure 15.4.2 . Property control chart for Example 15.4.1 . The warning limits are shown in **orange** and the control limits in **red**.

Exercise 15.4.1

A control chart is a useful method for monitoring a glucometer's performance over time. One approach is to use the glucometer to measure the glucose level of a standard solution. An initial analysis of the standard yields a mean value of 249.4 mg/100 mL and a standard deviation of 2.5 mg/100 mL. An analysis of the standard over 20 consecutive days gives the following results.

day:	1	2	3	4	5	6	7	8	9	10
result:	248.1	246.0	247.9	249.4	250.9	249.7	250.2	250.3	247.3	245.6
day:	11	12	13	14	15	16	17	18	19	20
result:	246.2	250.8	249.0	254.3	246.1	250.8	248.1	246.7	253.5	251.0

Construct a control chart of the glucometer's performance.

Answer

The *UCL* is 256.9, the *UWL* is 254.4, the *CL* is 249.4, the *LWL* is 244.4, and the *LCL* is 241.9 mg glucose/100 mL. Figure 15.4.3 shows the resulting property control plot.

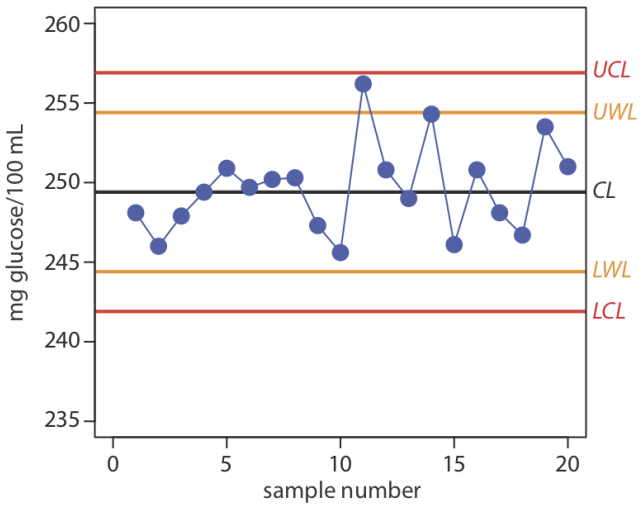

Figure 15.4.3 . Property control chart for Exercise 15.4.1 .

We also can construct a control chart using the mean for a set of replicate determinations on each sample. The mean for the *i*th sample is

$$\overline{X}_i = \frac{\sum_{j=1}^{n_{rep}} X_{ij}}{n_{rep}}$$

where X_{ij} is the *j*th replicate and n_{rep} is the number of replicate determinations for each sample. The control chart's center line is

$$CL = \frac{\sum_{i=1}^{n} \overline{X}_i}{n}$$

where *n* is the number of samples used to construct the control chart. To determine the standard deviation for the warning limits and the control limits, we first calculate the variance for each sample.

$$s_i^2 = \frac{\sum_{j=1}^{n_{rep}} \left(X_{ij} - \overline{X}_i \right)^2}{n_{rep} - 1}$$

The overall standard deviation, *S*, is the square root of the average variance for the samples used to construct the control plot.

$$S = \sqrt{\frac{\sum_{i=1}^{n} s_i^2}{n}}$$

The resulting warning and control limits are given by the following four equations.

$$UWL = CL + \frac{2S}{\sqrt{n_{rep}}}$$
$$LWL = CL - \frac{2S}{\sqrt{n_{rep}}}$$
$$UCL = CL + \frac{3S}{\sqrt{n_{rep}}}$$
$$LCL = CL - \frac{3S}{\sqrt{n_{rep}}}$$

> When using means to construct a property control chart, all samples must have the same number of replicates.

Constructing a Precision Control Chart

A precision control chart shows how the precision of an analysis changes over time. The most common measure of precision is the range, *R*, between the largest and the smallest results for n_{rep} analyses on a sample.

$$R = X_{\text{largest}} - X_{\text{smallest}}$$

To construct the control chart, we analyze a minimum of 15–20 samples while the system is under statistical control. The center line (*CL*) of the control chart is the average range of these *n* samples.

$$\overline{R} = \frac{\sum_{i=1}^{n} R_i}{n}$$

The upper warning line and the upper control line are given by the following equations

$$UWL = f_{UWL} \times \overline{R}$$
$$UCL = f_{UCL} \times \overline{R}$$

where f_{UWL} and f_{UCL} are statistical factors determined by the number of replicates used to determine the range. Table 15.4.1 provides representative values for f_{UWL} and f_{UCL}. Because the range is greater than or equal to zero, there is no lower control limit and no lower warning limit.

Table 15.4.1 . Statistical Factors for the Upper Warning Limit and the Upper Control Limit of a Precision Control Chart

replicates	f_{UWL}	f_{UCL}
2	2.512	3.267
3	2.050	2.575
4	1.855	2.282
5	1.743	2.115
6	1.669	2.004

Example 15.4.2

Construct a precision control chart using the following ranges, each determined from a duplicate analysis of a 10.0-ppm calibration standard.

sample:	1	2	3	4	5
result:	0.36	0.09	0.11	0.06	0.25
sample:	6	7	8	9	10
result:	0.15	0.28	0.27	0.03	0.28
sample:	11	12	13	14	15
result:	0.21	0.19	0.06	0.13	0.37
sample:	16	17	18	19	20
result:	0.01	0.19	0.39	0.05	0.05

Solution

The average range for the duplicate samples is 0.176. Because two replicates were used for each point the *UWL* and *UCL* are

$$UWL = 2.512 \times 0.176 = 0.44$$
$$UCL = 3.267 \times 0.176 = 0.57$$

The resulting property control chart is shown in Figure 15.4.4 .

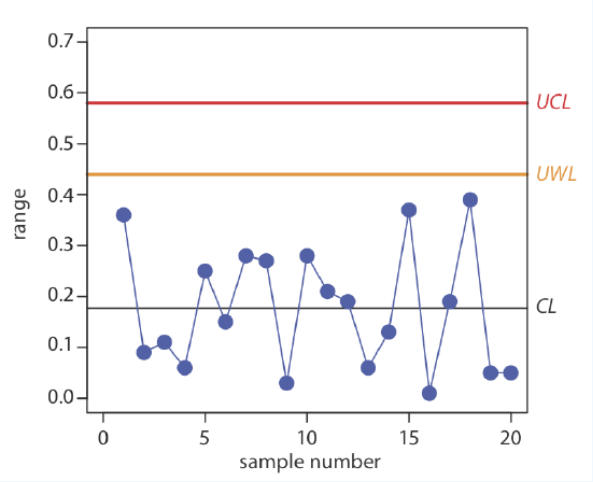

Figure 15.4.4 . Precision control chart for Example 15.4.2 . The warning limits are shown in **orange** and the control limits in **red**.

The precision control chart in Figure 15.4.4 is strictly valid only for the replicate analysis of identical samples, such as a calibration standard or a standard reference material. Its use for the analysis of nonidentical samples—as often is the case in clinical analyses

and environmental analyses—is complicated by the fact that the range usually is not independent of the magnitude of the measurements. For example, Table 15.4.2 shows the relationship between the average range and the concentration of chromium in 91 water samples. The significant difference in the average range for different concentrations of chromium makes impossible a single precision control chart. As shown in Figure 15.4.5 , one solution is to prepare separate precision control charts, each of which covers a range of concentrations for which $\overline{R}$ is approximately constant.

Table 15.4.2 . Average Range for the Concentration of Chromium in Duplicate Water Samples

[Cr] (ppb)	number of duplicate samples	$\overline{R}$
5 to $<$ 10	32	0.32
10 to $<$ 25	15	0.57
25 to $<$ 50	16	1.12
50 to $<$ 150	15	3.80
150 to \(< 500)	8	5.25
$>$ 500	5	76.0

Source: Environmental Monitoring and Support Laboratory, U. S. Environmental Protection Agency, “Handbook for Analytical Quality Control in Water and Wastewater Laboratories,” March 1979.

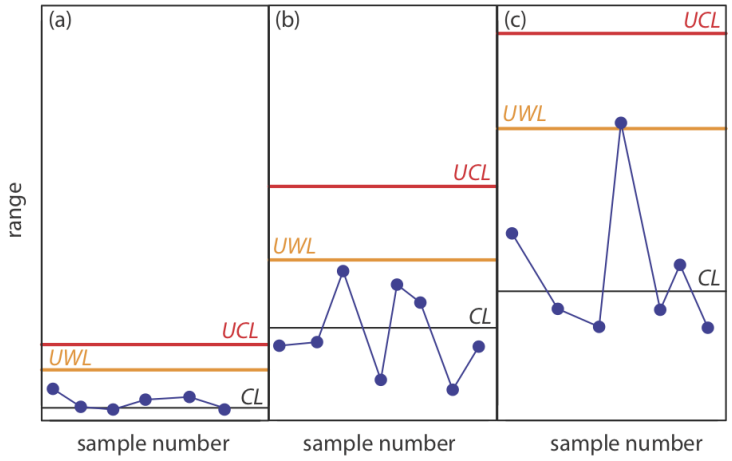

Figure 15.4.5 . Example showing the use of a precision control chart for samples that span a range of analyte concentrations. The precision control charts are for (a) low concentrations of analyte; (b) intermediate concentrations of analyte; and (c) high concentrations of analyte.

Interpreting Control Charts

The purpose of a control chart is to determine if an analysis is in a state of statistical control. We make this determination by examining the location of individual results relative to the warning limits and the control limits, and by examining the distribution of results around the central line. If we assume that the individual results are normally distributed, then the probability of finding a point at any distance from the control limit is determined by the properties of a normal distribution [Mullins, E. *Analyst*, **1994**, *119*, 369–375.]. We set the upper and the lower control limits for a property control chart to $CL \pm 3S$ because 99.74% of a normally distributed population falls within three standard deviations of the population’s mean. This means that there is only a 0.26% probability of obtaining a result larger than the *UCL* or smaller than the *LCL*. When a result exceeds a control limit, the most likely explanation is a systematic error in the analysis or a loss of precision. In either case, we assume that the analysis no longer is in a state of statistical control.

Rule 1. An analysis is no longer under statistical control if any single point exceeds either the *UCL* or the *LCL*.

By setting the upper and lower warning limits to $CL \pm 2S$, we expect that no more than 5% of the results will exceed one of these limits; thus

Rule 2. An analysis is no longer under statistical control if two out of three consecutive points are between the *UWL* and the *UCL* or between the *LWL* and the *LCL*.

If an analysis is under statistical control, then we expect a random distribution of results around the center line. The presence of an unlikely pattern in the data is another indication that the analysis is no longer under statistical control.

Rule 3. An analysis is no longer under statistical control if seven consecutive results are completely above or completely below the center line.

Rule 4. An analysis is no longer under statistical control if six consecutive results increase (or decrease) in value.

Rule 5. An analysis is no longer under statistical control if 14 consecutive results alternate up and down in value.

Rule 6. An analysis is no longer under statistical control if there is any obvious nonrandom pattern to the results.

Figure 15.4.6 shows three examples of control charts in which the results indicate that an analysis no longer is under statistical control. The same rules apply to precision control charts with the exception that there are no lower warning limits and lower control limits.

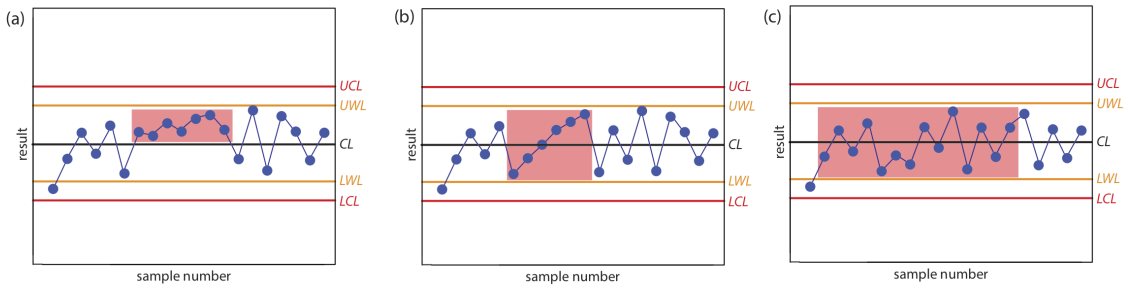

Figure 15.4.6 . Examples of property control charts that show a sequence of results—indicated by the highlighting—that violate (a) rule 3; (b) rule 4; and (c) rule 5.

? Exercise 15.4.2

In Exercise 15.4.1 you created a property control chart for a glucometer. Examine your property control chart and evaluate the glucometer's performance. Does your conclusion change if the next three results are 255.6, 253.9, and 255.8 mg/100 mL?

Answer

Although the variation in the results appears to be greater for the second 10 samples, the results do not violate any of the six rules. There is no evidence in Figure 15.4.3 that the analysis is out of statistical control. The next three results, in which two of the three results are between the *UWL* and the *UCL*, violates the second rule. Because the analysis is no longer under statistical control, we must stop using the glucometer until we determine the source of the problem.

Using Control Charts for Quality Assurance

Control charts play an important role in a performance-based program of quality assurance because they provide an easy to interpret picture of the statistical state of an analysis. Quality assessment samples such as blanks, standards, and spike recoveries are monitored with property control charts. A precision control chart is used to monitor duplicate samples.

The first step in using a control chart is to determine the mean value and the standard deviation (or range) for the property being measured while the analysis is under statistical control. These values are established using the same conditions that will be present during subsequent analyses. Preliminary data is collected both throughout the day and over several days to account for short-term and for long-term variability. An initial control chart is prepared using this preliminary data and discrepant points identified using the rules discussed in the previous section. After eliminating questionable points, the control chart is replotted. Once the control chart is in use, the original limits are adjusted if the number of new data points is at least equivalent to the amount of data used to construct the original control chart. For example, if the original control chart includes 15 points, new limits are calculated after collecting 15 additional points. The 30 points are pooled together to calculate the new limits. A second modification is made after

collecting an additional 30 points. Another indication that a control chart needs to be modified is when points rarely exceed the warning limits. In this case the new limits are recalculated using the last 20 points.

Once a control chart is in use, new quality assessment data is added at a rate sufficient to ensure that the analysis remains in statistical control. As with prescriptive approaches to quality assurance, when the analysis falls out of statistical control, all samples analyzed since the last successful verification of statistical control are reanalyzed. The advantage of a performance-based approach to quality assurance is that a laboratory may use its experience, guided by control charts, to determine the frequency for collecting quality assessment samples. When the system is stable, quality assessment samples can be acquired less frequently.

6.5: Problems

1. Make a list of good laboratory practices for the lab that accompanies this course, or another lab if this course does not have an associated laboratory. Explain the rationale for each item on your list.

2. Write directives outlining good measurement practices for (a) a buret, for (b) a pH meter, and for (c) a spectrophotometer.

3. A atomic absorption method for the analysis of lead in an industrial wastewater has a method detection limit of 10 ppb. The relationship between the absorbance and the concentration of lead, as determined from a calibration curve, is

$$A = 0.349 \times (\text{ppm Pb})$$

Analysis of a sample in duplicate gives absorbance values of 0.554 and 0.516. Is the precision between these two duplicates acceptable based on the limits in Table 15.3.1?

4. The following data were obtained for the duplicate analysis of a 5.00 ppm NO_3^- standard.

sample	X_1 (ppm)	X_2 (ppm)
1	5.02	4.90
2	5.10	5.18
3	5.07	4.95
4	4.96	5.01
5	4.88	4.98
6	5.04	4.97

Calculate the standard deviation for these duplicate samples. If the maximum limit for the relative standard deviation is 1.5%, are these results acceptable?

5. Gonzalez and colleagues developed a voltammetric method for the determination of *tert*-butylhydroxyanisole (BHA) in chewing gum [Gonzalez, A.; Ruiz, M. A.; Yanez-Sedeno, P.; Pingarron, J. M. *Anal. Chim. Acta* **1994**, *285*, 63–71.]. Analysis of a commercial chewing gum gave a result of 0.20 mg/g. To evaluate the accuracy of this results, the authors performed five spike recoveries, adding an amount of BHA equivalent to 0.135 mg/g to each sample. The experimentally determined concentrations of BHA in these samples were reported as 0.342, 0.340, 0.340, 0.324, and 0.322 mg/g. Determine the percent recovery for each sample and the mean percent recovery.

6. A sample is analyzed following the protocol shown in Figure 15.4.1 using a method with a detection limit of 0.05 ppm. The relationship between the analytical signal, S_{meas}, and the concentration of the analyte in parts per million, C_A, as determined from a calibration curve, is

$$S_{meas} = 0.273 \times C_A$$

Answer the following questions if the limit for a successful spike recovery is ±10%:

(a) A field blank is spiked with the analyte to a concentration of 2.00 ppm and returned to the lab. Analysis of the spiked field blank gives a signal of 0.573. Is the spike recovery for the field blank acceptable?

(b) The analysis of a spiked field blank is unacceptable. To determine the source of the problem, a spiked method blank is prepared by spiking distilled water with the analyte to a concentration of 2.00 ppm. Analysis of the spiked method blank gives a signal of 0.464. Is the source of the problem in the laboratory or in the field?

(c) The analysis for a spiked field sample, $B_{SF,}$ is unacceptable. To determine the source of the problem, the sample is spiked in the laboratory by adding sufficient analyte to increase the concentration by 2.00 ppm. Analysis of the sample before and after the spike gives signals of 0.456 for B and a signal of 1.03 for B_{SL}. Considering this data, what is the most likely source of the systematic error?

7. The following data were obtained for the repetitive analysis of a stable standard [*Standard Methods for the Analysis of Waters and Wastewaters*, American Public Health Association: Washington, D. C., 18th Ed., 1992. The data is from Table 1030:I].

sample	X_i (ppm)	sample	X_i (ppm)	sample	X_i (ppm)
1	35.1	10	35.0	18	36.4
2	33.2	11	31.4	19	32.1
3	33.7	12	35.6	20	38.2
4	35.9	13	30.2	21	33.1
5	33.5	14	32.7	22	34.9
6	34.5	15	31.1	23	36.2
7	34.4	16	34.8	24	34.0
8	34.3	17	34.3	25	33.8
9	31.8				

Construct a property control chart for these data and evaluate the state of statistical control.

8. The following data were obtained for the repetitive spike recoveries of field samples [*Standard Methods for the Analysis of Waters and Wastewaters*, American Public Health Association: Washington, D. C., 18th Ed., 1992. The data is from Table 1030:II].

sample	% recovery	sample	% recovery	sample	% recovery
1	94.6	10	104.6	18	104.6
2	93.1	11	123.8	19	91.5
3	100.0	12	93.8	20	83.1
4	122.3	13	80.0	21	100.8
5	120.8	14	99.2	22	123.1
6	93.1	15	101.5	23	96.2
7	117.7	16	74.6	24	96.9
8	96.2	17	108.5	25	102.3
9	73.8				

Construct a property control chart for these data and evaluate the state of statistical control.

9. The following data were obtained for the duplicate analysis of a stable standard [*Standard Methods for the Analysis of Waters and Wastewaters*, American Public Health Association: Washington, D. C., 18th Ed., 1992. The data is from Table 1030:I].

sample	X_1 (ppm)	X_2 (ppm)	sample	X_1 (ppm)	X_2 (ppm)
1	50	46	14	36	36
2	37	36	15	47	45
3	22	19	16	16	20
4	17	20	17	18	21
5	32	34	18	26	22
6	46	46	19	35	36
7	26	28	20	36	25
8	26	30	21	49	51

sample	X_1 (ppm)	X_2 (ppm)	sample	X_1 (ppm)	X_2 (ppm)
9	61	58	22	33	32
10	44	45	23	40	38
11	40	44	24	16	13
12	36	35	25	39	42
13	29	31			

6.6: Additional Resources

The following experiments introduce aspects of quality assurance and quality control.

- Bell, S. C.; Moore, J. “Integration of Quality Assurance/Quality Control into Quantitative Analysis,” *J. Chem. Educ.* **1998**, *75*, 874–877.
- Cancilla, D. A. “Integration of Environmental Analytical Chemistry with Environmental Law: The Development of a Problem-Based Laboratory,” *J. Chem. Educ.* **2001**, *78*, 1652–1660.
- Claycomb, G. D.; Venable, F. A. “Selection, Evaluation, and Modification of a Standard Operating Procedure as a Mechanism for Introducing an Undergraduate Student to Chemical Research: A Case Study,” *J. Chem. Educ.* **2015**, *92*, 256–262.
- Laquer, F. C. “Quality Control Charts in the Quantitative Analysis Laboratory Using Conductance Measurement,” *J. Chem. Educ.* **1990**, *67*, 900–902.
- Marcos, J.; Ríos, A.; Valcárcel, M. “Practicing Quality Control in a Bioanalytical Experiment,” *J. Chem. Educ.* **1995**, *72*, 947–949.

The following texts and articles may be consulted for an additional discussion of quality assurance and quality control.

- Amore, F. “Good Analytical Practices,” *Anal. Chem.* **1979**, *51*, 1105A–1110A.
- Anderson, J. E. T. “On the development of quality assurance,” *TRAC-Trend. Anal. Chem.* **2014**, *60*, 16–24.
- Barnard, Jr. A. J.; Mitchell, R. M.; Wolf, G. E. “Good Analytical Practices in Quality Control,” *Anal. Chem.* **1978**, *50*, 1079A–1086A.
- Cairns, T.; Rogers, W. M. “Acceptable Analytical Data for Trace Analysis,” *Anal. Chem.* **1993**, *55*, 54A–57A.
- Taylor, J. K. *Quality Assurance of Chemical Measurements*, Lewis Publishers: Chelsa, MI, 1987.
- Wedlich, R. C.; Libera, A. E.; Pires, A.; Therrien, M. T. “Good Laboratory Practice. Part 1. An Introduction,” *J. Chem. Educ.* **2013**, *90*, 854–857.
- Wedlich, R. C.; Libera, A. E.; Pires, A.; Tellarini, C. “Good Laboratory Practice. Part 1. Recording and Retaining Raw Data,” *J. Chem. Educ.* **2013**, *90*, 858–861.
- Wedlich, R. C.; Libera, A. E.; Fazzino, L.; Fransen, J. M. “Good Laboratory Practice. Part 1. Imple- menting Good Laboratory Practice in the Analytical Lab,” *J. Chem. Educ.* **2013**, *90*, 862–865.

Additional information about the construction and use of control charts may be found in the following sources.

- Miller, J. C.; Miller, J. N. Statistics for Analytical Chemistry, 2nd Ed., Ellis Horwood Limited: Chich-ester, 1988.
- Ouchi, G. I. “Creating Control Charts with a Spreadsheet Program,” *LC•GC* **1993**, *11*, 416–423.
- Ouchi, G. I. “Creating Control Charts with a Spreadsheet Program,” *LC•GC* **1997**, *15*, 336–344.
- Simpson, J. M. “Spreadsheet Statistics,” *J. Chem. Educ.* **1994**, *71*, A88–A89.

6.7: Chapter Summary and Key Terms

Summary

Few analyses are so straightforward that high quality results are obtained with ease. Good analytical work requires careful planning and an attention to detail. Creating and maintaining a quality assurance program is one way to help ensure the quality of analytical results. Quality assurance programs usually include elements of quality control and quality assessment.

Quality control encompasses all activities used to bring a system into statistical control. The most important facet of quality control is written documentation, including statements of good laboratory practices, good measurement practices, standard operating procedures, and protocols for a specific purpose.

Quality assessment includes the statistical tools used to determine whether an analysis is in a state of statistical control, and, if possible, to suggest why an analysis has drifted out of statistical control. Among the tools included in quality assessment are the analysis of duplicate samples, the analysis of blanks, the analysis of standards, and the analysis of spike recoveries.

Another important quality assessment tool, which provides an ongoing evaluation of an analysis, is a control chart. A control chart plots a property, such as a spike recovery, as a function of time. Results that exceed warning and control limits, or unusual patterns of results indicate that an analysis is no longer under statistical control.

Key Terms

control chart	duplicate samples	field blank
good laboratory practices	good measurement practices	method blank
proficiency standard	protocol for a specific purpose	quality assessment
quality assurance program	quality control	reagent blank
spike recovery	standard operations procedure	statistical control
trip blank		

CHAPTER OVERVIEW

7: Appendix

7.1: Normality

Normality expresses concentration in terms of the equivalents of one chemical species that react stoichiometrically with another chemical species. Note that this definition makes an equivalent, and thus normality, a function of the chemical reaction. Although a solution of H_2SO_4 has a single molarity, its normality depends on its reaction.

We define the number of equivalents, *n*, using a reaction unit, which is the part of a chemical species that participates in the chemical reaction. In a precipitation reaction, for example, the reaction unit is the charge of the cation or the anion that participates in the reaction; thus, for the reaction

$$\mathrm{Pb}^{2+}(aq) + 2\mathrm{I}^{-}(aq) \rightleftharpoons \mathrm{PbI}_2(s)$$

n = 2 for Pb^{2+} and *n* = 1 for I^-. In an acid–base reaction, the reaction unit is the number of H^+ ions that an acid donates or that a base accepts. For the reaction between sulfuric acid and ammonia

$$\mathrm{H_2SO_4}(aq) + 2\mathrm{NH_3}(aq) \rightleftharpoons 2\mathrm{NH_4^+}(aq) + \mathrm{SO_4^{2-}}$$

n = 2 for H_2SO_4 because sulfuric acid donates two protons, and *n* = 1 for NH_3 because each ammonia accepts one proton. For a complexation reaction, the reaction unit is the number of electron pairs that the metal accepts or that the ligand donates. In the reaction between Ag^+ and NH_3

$$\mathrm{Ag^+}(aq) + 2\mathrm{NH_3}(aq) \rightleftharpoons \mathrm{Ag(NH_3)_2^+}(aq)$$

n = 2 for Ag^+ because the silver ion accepts two pairs of electrons, and *n* = 1 for NH_3 because each ammonia has one pair of electrons to donate. Finally, in an oxidation–reduction reaction the reaction unit is the number of electrons released by the reducing agent or accepted by the oxidizing agent; thus, for the reaction

$$2\mathrm{Fe}^{3+}(aq) + \mathrm{Sn}^{2+}(aq) \rightleftharpoons \mathrm{Sn}^{4+}(aq) + 2\mathrm{Fe}^{2+}(aq)$$

n = 1 for Fe^{3+} and *n* = 2 for Sn^{2+}. Clearly, determining the number of equivalents for a chemical species requires an understanding of how it reacts.

Normality is the number of equivalent weights, *EW*, per unit volume. An equivalent weight is the ratio of a chemical species' formula weight, *FW*, to the number of its equivalents, *n*.

$$EW = \frac{FW}{n}$$

The following simple relationship exists between normality, *N*, and molarity, M,

$$N = n \times M$$

7.2: Propagation of Uncertainty

In Chapter 4 we considered the basic mathematical details of a propagation of uncertainty, limiting our treatment to the propagation of measurement error. This treatment is incomplete because it omits other sources of uncertainty that contribute to the overall uncertainty in our results. Consider, for example, Exercise 4.3.1, in which we determined the uncertainty in a standard solution of Cu^{2+} prepared by dissolving a known mass of Cu wire with HNO_3, diluting to volume in a 500-mL volumetric flask, and then diluting a 1-mL portion of this stock solution to volume in a 250-mL volumetric flask. To calculate the overall uncertainty we included the uncertainty in weighing the sample and the uncertainty in using the volumetric glassware. We did not consider other sources of uncertainty, including the purity of the Cu wire, the effect of temperature on the volumetric glassware, and the repeatability of our measurements. In this appendix we take a more detailed look at the propagation of uncertainty, using the standardization of NaOH as an example.

Standardizing a Solution of NaOH

Because solid NaOH is an impure material, we cannot directly prepare a stock solution by weighing a sample of NaOH and diluting to volume. Instead, we determine the solution's concentration through a process called a standardization. A fairly typical procedure is to use the NaOH solution to titrate a carefully weighed sample of previously dried potassium hydrogen phthalate, $C_8H_5O_4K$, which we will write here, in shorthand notation, as KHP. For example, after preparing a nominally 0.1 M solution of NaOH, we place an accurately weighed 0.4-g sample of dried KHP in the reaction vessel of an automated titrator and dissolve it in approximately 50 mL of water (the exact amount of water is not important). The automated titrator adds the NaOH to the KHP solution and records the pH as a function of the volume of NaOH. The resulting titration curve provides us with the volume of NaOH needed to reach the titration's endpoint.

> The example below is adapted from Ellison, S. L. R.; Rosslein, M.; Williams, A. EURACHEM/CITAC Guide: Quantifying Uncertainty in Analytical Measurement, 3nd Edition, 2012. See Chapter 5 for further details about standardizations and see Chapter 9 for further details about titrations

The end point of the titration is the volume of NaOH that corresponds to the stoichiometric reaction between NaOH and KHP.

$$\mathrm{NaOH}(aq) + \mathrm{C_8H_5O_4K}(aq) \longrightarrow \mathrm{C_8H_4O_4^{2-}}(aq) + \mathrm{K^+}(aq) + \mathrm{Na^+}(aq) + \mathrm{H_2O}(l)$$

Knowing the mass of KHP and the volume of NaOH needed to reach the endpoint, we use the following equation to calculate the molarity of the NaOH solution.

$$C_{\text{NaOH}} = \frac{1000 \times m_{\text{KHP}} \times P_{\text{KHP}}}{FW_{\text{KHP}} \times V_{\text{NaOH}}}$$

where C_{NaOH} is the concentration of NaOH (in mol KHP/L), m_{KHP} is the mass of KHP taken (in g), P_{KHP} is the purity of the KHP (where P_{KHP} = 1 means the KHP is pure and has no impurities), FW_{KHP} is the molar mass of KHP (in g KHP/mol KHP), and V_{NaOH} is the volume of NaOH (in mL). The factor of 1000 simply converts the volume in mL to L.

Identifying and Analyzing Sources of Uncertainty

Although it seems straightforward, identifying sources of uncertainty requires care as it easy to overlook important sources of uncertainty. One approach is to use a cause-and-effect diagram, also known as an Ishikawa diagram—named for its inventor, Kaoru Ishikawa—or a fish bone diagram. To construct a cause-and-effect diagram, we first draw an arrow that points to the desired result; this is the diagram's trunk. We then add five main branch lines to the trunk, one for each of the four parameters that determine the concentration of NaOH (m_{KHP}, P_{KHP}, FW_{KHP}, and V_{NaOH}) and one for the method's repeatability, R. Next we add additional branches to the main branch for each of these five factors, continuing until we account for all potential sources of uncertainty. Figure 16.2.1 shows the complete cause-and-effect diagram for this analysis.

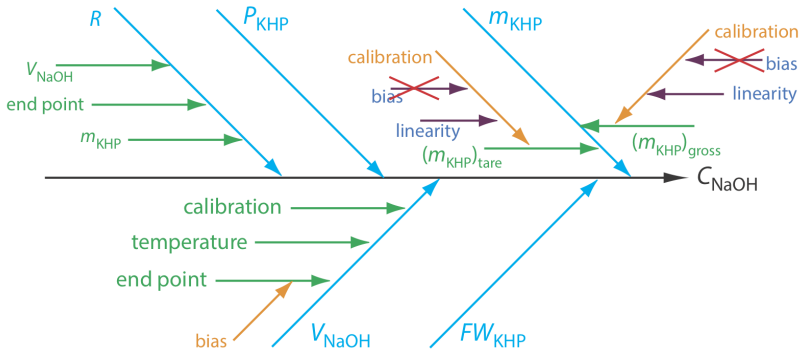

Figure 16.2.1 : Cause-and-effect diagram for the standardization of NaOH by titration against KHP. The trunk, shown in black, represents the concentration of NaOH. The remaining arrows represent the sources of uncertainty that affect C_{NaOH}. The blue arrows, for example, represent the primary sources of uncertainty that affect C_{NaOH}, and the green arrows represent secondary sources of uncertainty that affect the primary sources of uncertainty. See the text for additional details.

Before we continue, let's take a closer look at Figure 16.2.1 to make sure that we understand each branch of the diagram. To determine the mass of KHP, m_{KHP}, we make two measurements: taring the balance and weighing the gross sample. Each of these measurements is subject to a calibration uncertainty. When we calibrate a balance, we essentially are creating a calibration curve of the balance's signal as a function of mass. Any calibration curve is subject to an uncertainty in the *y*-intercept (bias) and an uncertainty in the slope (linearity). We can ignore the calibration bias because it contributes equally to both $(m_{KHP})_{gross}$ and $(m_{KHP})_{tare}$, and because we determine the mass of KHP by difference.

$$m_{KHP} = (m_{KHP})_{gross} - (m_{KHP})_{tare}$$

The volume of NaOH, V_{NaOH}, at the end point has three sources of uncertainty. First, an automated titrator uses a piston to deliver NaOH to the reaction vessel, which means the volume of NaOH is subject to an uncertainty in the piston's calibration. Second, because a solution's volume varies with temperature, there is an additional source of uncertainty due to any fluctuation in the ambient temperature during the analysis. Finally, there is a bias in the titration's end point if the NaOH reacts with any species other than the KHP.

Repeatability, *R*, is a measure of how consistently we can repeat the analysis. Each instrument we use—the balance and the automated titrator—contributes to this uncertainty. In addition, our ability to consistently detect the end point also contributes to repeatability. Finally, there are no secondary factors that affect the uncertainty of the KHP's purity, P_{KHP}, or its molar mass, FW_{KHP}.

Estimating the Standard Deviation for Measurements

To complete a propagation of uncertainty we must express each measurement's uncertainty in the same way, usually as a standard deviation. Measuring the standard deviation for each measurement requires time and is not always practical. Fortunately, most manufacture provides a tolerance range for glassware and instruments. A 100-mL volumetric glassware, for example, has a tolerance of ± 0.1 mL at a temperature of 20 °C. We can convert a tolerance range to a standard deviation using one of the following three approaches.

Assume a Uniform Distribution

Figure 16.2.2 a shows a uniform distribution between the limits of $\pm x$, in which each result between the limits is equally likely. A uniform distribution is the choice when the manufacturer provides a tolerance range without specifying a level of confidence and when there is no reason to believe that results near the center of the range are more likely than results at the ends of the range. For a uniform distribution the estimated standard deviation, *s*, is

$$s = \frac{x}{\sqrt{3}}$$

This is the most conservative estimate of uncertainty as it gives the largest estimate for the standard deviation.

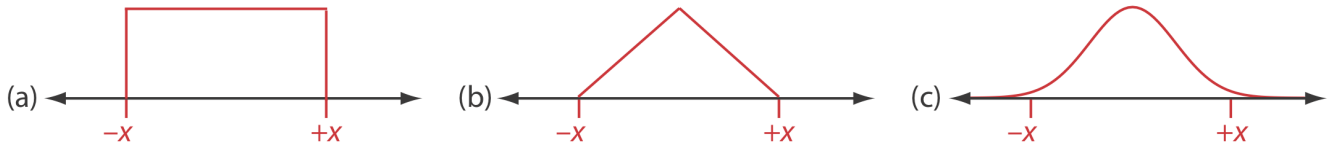

Figure 16.2.2 : Three possible distributions for estimating the standard deviation from a range: (a) a uniform distribution; (b) a triangular distribution; and (c) a normal distribution.

Assume a Triangular Distribution

Figure 16.2.2 b shows a triangular distribution between the limits of $\pm x$, in which the most likely result is at the center of the distribution, decreasing linearly toward each limit. A triangular distribution is the choice when the manufacturer provides a tolerance range without specifying a level of confidence and when there is a good reason to believe that results near the center of the range are more likely than results at the ends of the range. For a triangular distribution the estimated standard deviation, *s*, is

$$s = \frac{x}{\sqrt{6}}$$

This is a less conservative estimate of uncertainty as, for any value of *x*, the standard deviation is smaller than that for a uniform distribution.

Assume a Normal Distribution

Figure 16.2.2 c shows a normal distribution that extends, as it must, beyond the limits of $\pm x$, and which is centered at the mid-point between –*x* and +*x*. A normal distribution is the choice when we know the confidence interval for the range. For a normal distribution the estimated standard deviation, *s*, is

$$s = \frac{x}{z}$$

where *z* is 1.96 for a 95% confidence interval and 3.00 for a 99.7% confidence interval.

Completing the Propagation of Uncertainty

Now we are ready to return to our example and determine the uncertainty for the standardization of NaOH. First we establish the uncertainty for each of the five primary sources—the mass of KHP, the volume of NaOH at the end point, the purity of the KHP, the molar mass for KHP, and the titration's repeatability. Having established these, we can combine them to arrive at the final uncertainty.

Uncertainty in the Mass of KHP

After drying the KHP, we store it in a sealed container to prevent it from readsorbing moisture. To find the mass of KHP we first weigh the container, obtaining a value of 60.5450 g, and then weigh the container after removing a portion of KHP, obtaining a value of 60.1562 g. The mass of KHP, therefore, is 60.5450 – 60.1562 = 0.3888 g, or 388.8 mg.

To find the uncertainty in this mass we examine the balance's calibration certificate, which indicates that its tolerance for linearity is ± 0.15 mg. We will assume a uniform distribution because there is no reason to believe that any result within this range is more likely than any other result. Our estimate of the uncertainty for any single measurement of mass, *u*(*m*), is

$$u(m) = \frac{0.15 \text{ mg}}{\sqrt{3}} = \pm 0.087 \text{ mg}$$

Because we determine the mass of KHP by subtracting the container's final mass from its initial mass, the uncertainty in the mass of KHP $u(m_{\text{KHP}})$, is given by the following propagation of uncertainty.

$$u(m_{\text{KHP}}) = \sqrt{(0.087 \text{ mg})^2 + (0.087 \text{ mg})^2} = \pm 0.12 \text{ mg}$$

Uncertainty in the Volume of NaOH

After we place the sample of KHP in the automated titrator's reaction vessel and dissolve the KHP with water, we complete the titration and find that it takes 18.64 mL of NaOH to reach the end point. To find the uncertainty in this volume we need to consider,

as shown in Figure 16.2.1 , three sources of uncertainty: the automated titrator's calibration, the ambient temperature, and any bias in determining the end point.

To find the uncertainty from the automated titrator's calibration we examine the instrument's certificate, which indicates a range of ± 0.03 mL for a 20-mL piston. Because we expect that an effective manufacturing process is more likely to produce a piston that operates near the center of this range than at the extremes, we will assume a triangular distribution. Our estimate of the uncertainty due to the calibration, $u(V_{\text{cal}})$ is

$$u(V_{\text{cal}}) = \frac{0.03 \text{ mL}}{\sqrt{6}} = \pm 0.012 \text{ mL}$$

To determine the uncertainty due to the lack of temperature control, we draw on our prior work in the lab, which has established a temperature variation of $\pm 3\,^{\circ}\text{C}$ with a confidence level of 95%. To find the uncertainty, we convert the temperature range to a range of volumes using water's coefficient of expansion

$$(2.1 \times 10^{-4\,\circ}\text{C}) \times (\pm 3\,^{\circ}\text{C}) \times 18.64 \text{ mL} = \pm 0.012 \text{ mL}$$

and then estimate the uncertainty due to temperature, $u(V_{\text{temp}})$ as

$$u(V_{\text{temp}}) = \frac{\pm 0.012 \text{ mL}}{1.96} = \pm 0.006 \text{ mL}$$

Titrations using NaOH are subject to a bias due to the adsorption of CO_2, which can react with OH^-, as shown here.

$$CO_2(aq) + 2\,OH^-(aq) \longrightarrow CO_3^{2-}(aq) + H_2O(l)$$

If CO_2 is present, the volume of NaOH at the end point includes both the NaOH that reacts with the KHP and the NaOH that reacts with CO_2. Rather than trying to estimate this bias, it is easier to bathe the reaction vessel in a stream of argon, which excludes CO_2 from the automated titrator's reaction vessel.

Adding together the uncertainties for the piston's calibration and the lab's temperature gives the uncertainty in the uncertainty in the volume of NaOH, $u(V_{\text{NaOH}})$ as

$$u(V_{\text{NaOH}}) = \sqrt{(0.012 \text{ mL})^2 + (0.006 \text{ mL})^2} = \pm 0.013 \text{ mL}$$

Uncertainty in the Purity of KHP

According to the manufacturer, the purity of KHP is $100\% \pm 0.05\%$, or 1.0 ± 0.0005. Assuming a rectangular distribution, we report the uncertainty, $u(P_{\text{KHP}})$ as

$$u(P_{\text{KHP}}) = \frac{\pm 0.0005}{\sqrt{3}} = \pm 0.00029$$

Uncertainty in the Molar Mass of KHP

The molar mass of $C_8H_5O_4K$ is 204.2212 g/mol, based on the following atomic weights: 12.0107 for carbon, 1.00794 for hydrogen, 15.9994 for oxygen, and 39.0983 for potassium. Each of these atomic weights has an quoted uncertainty that we can convert to a standard uncertainty assuming a rectangular distribution, as shown here (the details of the calculations are left to you).

element	quoted uncertainty (per atom)	standard uncertainty (per atom)	number of atoms	total uncertainty
carbon	± 0.008	± 0.00046	8	± 0.00368
hydrogen	± 0.00007	0.000040	5	± 0.00020
oxygen	± 0.0003	± 0.00017	4	± 0.00068
potassium	± 0.0001	± 0.000058	1	± 0.000058

Adding together these uncertainties gives the uncertainty in the molar mass, $u(M_{\text{KHP}})$, as

$$u(FW_{\text{KHP}}) = \sqrt{(0.00368)^2 + (0.00020)^2 + (0.00068)^2 + (0.0.000058)^2} = \pm 0.0037 \text{ g/mL}$$

Uncertainty in the Titration's Repeatability

To estimate the uncertainty due to repeatability we complete five titrations, obtaining the following results for the concentration of NaOH: 0.1021 M, 0.1022 M, 0.1022 M, 0.1021 M, and 0.1021 M. The relative standard deviation, s_{rel}, for these titrations is

$$s_{rel} = \frac{s}{\overline{X}} = \frac{5.48 \times 10^{-5}}{0.1021} = \pm 0.0005$$

If we treat the ideal repeatability as 1.0, then the uncertainty due to repeatability, $u(R)$, is the relative standard deviation, or, in this case, 0.0005.

Combining the Uncertainties

The table below summarizes the five primary sources of uncertainty.

term	source	value, x	uncertainty, u(x)
m_{KHP}	mass of KHP	0.3888 g	± 0.00012 g
V_{naOH}	volume of NaOH at endpoint	18.64 mL	± 0.013 mL
P_{KHP}	purity of KHP	1.0	± 0.00029
M_{KHP}	molar mass of KHP	204.2212 g/mol	± 0.0037 g/mol
R	repeatability	1.0	± 0.0005

As described earlier, we calculate the concentration of NaOH we use the following equation, which is slightly modified to include a term for the titration's repeatability, which, as described above, has a value of 1.0.

$$C_{\text{NaOH}} = \frac{1000 \times m_{\text{KHP}} \times P_{\text{KHP}}}{FW_{\text{KHP}} \times V_{\text{NaOH}}} \times R$$

Using the values from our table, we find that the concentration of NaOH is

$$C_{\text{NaOH}} = \frac{1000 \times 0.3888 \times 1.0}{204.2212 \times 18.64} \times 1.0 = 0.1021 \text{ M}$$

Because the calculation of C_{NaOH} includes only multiplication and division, the uncertainty in the concentration, $u(C_{\text{NaOH}})$ is given by the following propagation of uncertainty.

$$\frac{u(C_{\text{NaOH}})}{C_{\text{NaOH}}} = \frac{u(C_{\text{NaOH}})}{0.1021} = \sqrt{\frac{(0.00012)^2}{(0.3888)^2} + \frac{(0.00029)^2}{(1.0)^2} + \frac{(0.0037)^2}{(204.2212)^2} + \frac{(0.013)^2}{(18.64)^2} + \frac{(0.0005)^2}{(1.0)^2}}$$

Solving for $u(C_{\text{NaOH}})$ gives its value as ± 0.00010 M, which is the final uncertainty for the analysis.

Evaluating the Sources of Uncertainty

Figure 16.2.3 shows the relative uncertainty in the concentration of NaOH and the relative uncertainties for each of the five contributions to the total uncertainty. Of the contributions, the most important is the volume of NaOH, and it is here to which we should focus our attention if we wish to improve the overall uncertainty for the standardization.

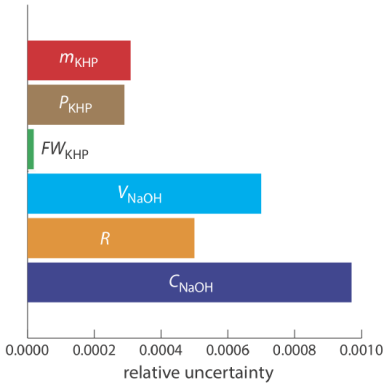

Figure 16.2.3 : Bar graph showing the relative uncertainty in C_{NaOH}, and the relative uncertainty in each of the main factors affecting the overall uncertainty.

7.3: Single-Sided Normal Distribution

Table 16.3.1 , at the bottom of this appendix, gives the proportion, *P*, of the area under a normal distribution curve that lies to the right of a deviation, *z*

$$z = \frac{X - \mu}{\sigma}$$

where *X* is the value for which the deviation is defined, μ is the distribution's mean value and σ is the distribution's standard deviation. For example, the proportion of the area under a normal distribution to the right of a deviation of 0.04 is 0.4840 (see entry in red in the table), or 48.40% of the total area (see the area shaded blue in Figure 16.3.1). The proportion of the area to the left of the deviation is 1 – *P*. For a deviation of 0.04, this is 1 – 0.4840, or 51.60%.

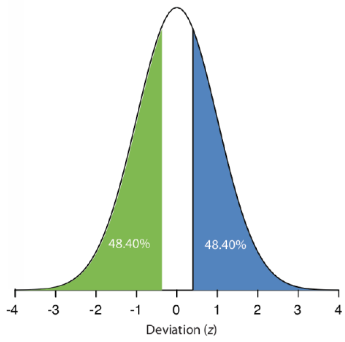

Figure 16.3.1 . Normal distribution curve showing the area under a curve greater than a deviation of +0.04 (blue) and with a deviation less than –0.04 (green).

When the deviation is negative—that is, when *X* is smaller than μ—the value of *z* is negative. In this case, the values in the table give the area to the left of *z*. For example, if *z* is –0.04, then 48.40% of the area lies to the left of the deviation (see area shaded green in Figure 16.3.1 .

To use the single-sided normal distribution table, sketch the normal distribution curve for your problem and shade the area that corresponds to your answer (for example, see Figure 16.3.2 , which is for Example 4.4.2).

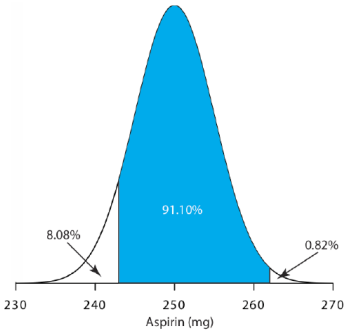

Figure 16.3.2 . Normal distribution for the population of aspirin tablets in Example 4.4.2. The population's mean and standard deviation are 250 mg and 5 mg, respectively. The shaded area shows the percentage of tablets containing between 243 mg and 262 mg of aspirin.

This divides the normal distribution curve into three regions: the area that corresponds to our answer (shown in blue), the area to the right of this, and the area to the left of this. Calculate the values of *z* for the limits of the area that corresponds to your answer. Use the table to find the areas to the right and to the left of these deviations. Subtract these values from 100% and, voilà, you have your answer.

Table 16.3.1 : Values for a Single-Sided Normal Distribution

z	0.00	0.01	0.02	0.03	0.04	0.05	0.06	0.07	0.08	0.09
0.0	0.5000	0.4960	0.4920	0.4880	0.4840	0.4801	0.4761	0.4721	0.4681	0.4641
0.1	0.4602	0.4562	0.4522	0.4483	0.4443	0.4404	0.4365	0.4325	0.4286	0.4247
0.2	0.4207	0.4168	0.4129	0.4090	0.4502	0.4013	0.3974	0.3396	0.3897	0.3859

0.3	0.3821	0.3783	0.3745	0.3707	0.3669	0.3632	0.3594	0.3557	0.3520	0.3483
0.4	0.3446	0.3409	0.3372	0.3336	0.3300	0.3264	0.3228	0.3192	0.3156	0.3121
0.5	0.3085	0.3050	0.3015	0.2981	0.2946	0.2912	0.2877	0.2843	0.2810	0.2776
0.6	0.2743	0.2709	0.2676	0.2643	0.2611	0.2578	0.2546	0.2514	0.2483	0.2451
0.7	0.2420	0.2389	0.2358	0.2327	0.2296	0.2266	0.2236	0.2206	0.2177	0.2148
0.8	0.2119	0.2090	0.2061	0.2033	0.2005	0.1977	0.1949	0.1922	0.1894	0.1867
0.9	0.1841	0.1814	0.1788	0.1762	0.1736	0.1711	0.1685	0.1660	0.1635	0.1611
1.0	0.1587	0.1562	0.1539	0.1515	0.1492	0.1469	0.1446	0.1423	0.1401	0.1379
1.1	0.1357	0.1335	0.1314	0.1292	0.1271	0.1251	0.1230	0.1210	0.1190	0.1170
1.2	0.1151	0.1131	0.1112	0.1093	0.1075	0.1056	0.1038	0.1020	0.1003	0.0985
1.3	0.0968	0.0951	0.0934	0.0918	0.0901	0.0885	0.0869	0.0853	0.0838	0.0823
1.4	0.0808	0.0793	0.0778	0.0764	0.0749	0.0735	0.0721	0.0708	0.0694	0.0681
1.5	0.0668	0.0655	0.0643	0.0630	0.0618	0.0606	0.0594	0.0582	0.0571	0.0559
1.6	0.0548	0.0537	0.0526	0.0516	0.0505	0.0495	0.0485	0.0475	0.0465	0.0455
1.7	0.0466	0.0436	0.0427	0.0418	0.0409	0.0401	0.0392	0.0384	0.0375	0.0367
1.8	0.0359	0.0351	0.0344	0.0336	0.0329	0.0322	0.0314	0.0307	0.0301	0.0294
1.9	0.0287	0.0281	0.0274	0.0268	0.0262	0.0256	0.0250	0.0244	0.0239	0.0233
2.0	0.0228	0.0222	0.0217	0.0212	0.0207	0.0202	0.0197	0.0192	0.0188	0.0183
2.1	0.0179	0.0174	0.0170	0.0166	0.0162	0.0158	0.0154	0.0150	0.0146	0.0143
2.2	0.0139	0.0136	0.0132	0.0129	0.0125	0.0122	0.0119	0.0116	0.0113	0.0110
2.3	0.0107	0.0104	0.0102		0.00964		0.00914		0.00866	
2.4	0.00820		0.00776		0.00734		0.00695		0.00657	
2.5	0.00621		0.00587		0.00554		0.00523		0.00494	
2.6	0.00466		0.00440		0.00415		0.00391		0.00368	
2.7	0.00347		0.00326		0.00307		0.00289		0.00272	
2.8	0.00256		0.00240		0.00226		0.00212		0.00199	
2.9	0.00187		0.00175		0.00164		0.00154		0.00144	
3.0	0.00135									
3.1	0.000968									
3.2	0.000687									
3.3	0.000483									
3.4	0.000337									
3.5	0.000233									
3.6	0.000159									
3.7	0.000108									
3.8	0.0000723									
3.9	0.0000481									

4.0	0.0000317									

7.4: Critical Values for t-Test

Assuming we have calculated t_{exp}, there are two approaches to interpreting a *t*-test. In the first approach we choose a value of α for rejecting the null hypothesis and read the value of $t(\alpha, \nu)$ from the table below. If $t_{exp} > t(\alpha, \nu)$, we reject the null hypothesis and accept the alternative hypothesis. In the second approach, we find the row in the table below that corresponds to the available degrees of freedom and move across the row to find (or estimate) the a that corresponds to $t_{exp} = t(\alpha, \nu)$; this establishes largest value of α for which we can retain the null hypothesis. Finding, for example, that α is 0.10 means that we retain the null hypothesis at the 90% confidence level, but reject it at the 89% confidence level. The examples in this textbook use the first approach.

Table 16.4.1 : Critical Values of t for the t-Test

Values of t for…				
…a confidence interval of:	90%	95%	98%	99%
…an α value of:	0.10	0.05	0.02	0.01
Degrees of Freedom				
1	6.314	12.706	31.821	63.657
2	2.920	4.303	6.965	9.925
3	2.353	3.182	4.541	5.841
4	2.132	2.776	3.747	4.604
5	2.015	2.571	3.365	4.032
6	1.943	2.447	3.143	3.707
7	1.895	2.365	2.998	3.499
8	1.860	2.306	2.896	3.255
9	1.833	2.262	2.821	3.250
10	1.812	2.228	2.764	3.169
12	1.782	2.179	2.681	3.055
14	1.761	2.145	2.624	2.977
16	1.746	2.120	2.583	2.921
18	1.734	2.101	2.552	2.878
20	1.725	2.086	2.528	2.845
30	1.697	2.042	2.457	2.750
50	1.676	2.009	2.311	2.678
∞	1.645	1.960	2.326	2.576

The values in this table are for a two-tailed *t*-test. For a one-tailed test, divide the α values by 2. For example, the last column has an α value of 0.005 and a confidence interval of 99.5% when conducting a one-tailed *t*-test.

7.5: Critical Values for F-Test

The following tables provide values for $F(0.05, \nu_{\text{num}}, \nu_{\text{denom}})$ for one-tailed and for two-tailed *F*-tests. To use these tables, we first decide whether the situation calls for a one-tailed or a two-tailed analysis and calculate F_{exp}

$$F_{\text{exp}} = \frac{s_A^2}{s_B^2}$$

where S_A^2 is greater than s_B^2. Next, we compare *F*exp to $F(0.05, \nu_{\text{num}}, \nu_{\text{denom}})$ and reject the null hypothesis if $F_{\text{exp}} > F(0.05, \nu_{\text{num}}, \nu_{\text{denom}})$. You may replace *s* with σ if you know the population's standard deviation.

Table 16.5.1 : Critical Values of F for a One-Tailed F-Test

$\frac{\nu_{\text{num}} \longrightarrow}{\nu_{denom} \downarrow}$	1	2	3	4	5	6	7	8	9	10	15	20	∞
1	161.4	199.5	215.7	224.6	230.2	234.0	236.8	238.9	240.5	241.9	245.9	248.0	254.3
2	18.51	19.00	19.16	19.25	19.30	19.33	19.35	19.37	19.38	19.40	19.43	19.45	19.50
3	10.13	9.552	9.277	9.117	9.013	8.941	8.887	8.845	8.812	8.786	8.703	8.660	8.526
4	7.709	6.994	6.591	6.388	6.256	6.163	6.094	6.041	5.999	5.964	5.858	5.803	5.628
5	6.608	5.786	5.409	5.192	5.050	4.950	4.876	4.818	4.722	4.753	4.619	4.558	4.365
6	5.987	5.143	4.757	4.534	4.387	4.284	4.207	4.147	4.099	4.060	3.938	3.874	3.669
7	5.591	4.737	4.347	4.120	3.972	3.866	3.787	3.726	3.677	3.637	3.511	3.445	3.230
8	5.318	4.459	4.066	3.838	3.687	3.581	3.500	3.438	3.388	3.347	3.218	3.150	2.928
9	5.117	4.256	3.863	3.633	3.482	3.374	3.293	3.230	3.179	3.137	3.006	2.936	2.707
10	4.965	4.103	3.708	3.478	3.326	3.217	3.135	3.072	3.020	2.978	2.845	2.774	2.538
11	4.844	3.982	3.587	3.257	3.204	3.095	3.012	2.948	2.896	2.854	2.719	2.646	2.404
12	4.747	3.885	3.490	3.259	3.106	2.996	2.913	2.849	2.796	2.753	2.617	2.544	2.296
13	4.667	3.806	3.411	3.179	3.025	2.915	2.832	2.767	2.714	2.671	2.533	2.459	2.206
14	4.600	3.739	3.344	3.112	2.958	2.848	2.764	2.699	2.646	2.602	2.463	2.388	2.131
15	4.534	3.682	3.287	3.056	2.901	2.790	2.707	2.641	2.588	2.544	2.403	2.328	2.066
16	4.494	3.634	3.239	3.007	2.852	2.741	2.657	2.591	2.538	2.494	2.352	2.276	2.010
17	4.451	3.592	3.197	2.965	2.810	2.699	2.614	2.548	2.494	2.450	2.308	2.230	1.960
18	4.414	3.555	3.160	2.928	2.773	2.661	2.577	2.510	2.456	2.412	2.269	2.191	1.917
19	4.381	3.552	3.127	2.895	2.740	2.628	2.544	2.477	2.423	2.378	2.234	2.155	1.878
20	4,351	3.493	3.098	2.866	2.711	2.599	2.514	2.447	2.393	2.348	2.203	2.124	1.843
∞	3.842	2.996	2.605	2.372	2.214	2.099	2.010	1.938	1.880	1.831	1.666	1.570	1.000

Table 16.5.2 : Critical Values of F for a Two-Tailed F-Test

$\frac{\nu_{\text{num}} \longrightarrow}{\nu_{denom} \downarrow}$	1	2	3	4	5	6	7	8	9	10	15	20	∞
1	647.8	799.5	864.2	899.6	921.8	937.1	948.2	956.7	963.3	968.6	984.9	993.1	1018
2	38.51	39.00	39.17	39.25	39.30	39.33	39.36	39.37	39.39	39.40	39.43	39.45	39.50
3	17.44	16.04	15.44	15.10	14.88	14.73	14.62	14.54	14.47	14.42	14.25	14.17	13.90
4	12.22	10.65	9.979	9.605	9.364	9.197	9.074	8.980	8.905	8.444	8.657	8.560	8.257
5	10.01	8.434	7.764	7.388	7.146	6.978	6.853	6.757	6.681	6.619	6.428	6.329	6.015
6	8.813	7.260	6.599	6.227	5.988	5.820	5.695	5.600	5.523	5.461	5.269	5.168	4.894
7	8.073	6.542	5.890	5.523	5.285	5.119	4.995	4.899	4.823	4.761	4.568	4.467	4.142
8	7.571	6.059	5.416	5.053	4.817	4.652	4.529	4.433	4.357	4.259	4.101	3.999	3.670
9	7.209	5.715	5.078	4.718	4.484	4.320	4.197	4.102	4.026	3.964	3.769	3.667	3.333
10	6.937	5.456	4.826	4.468	4.236	4.072	3.950	3.855	3.779	3.717	3.522	3.419	3.080
11	6.724	5.256	4.630	4.275	4.044	3.881	3.759	3.644	3.588	3.526	3.330	3.226	2.883
12	6.544	5.096	4.474	4.121	3.891	3.728	3.607	3.512	3.436	3.374	3.177	3.073	2.725
13	6.414	4.965	4.347	3.996	3.767	3.604	3.483	3.388	3.312	3.250	3.053	2.948	2.596
14	6.298	4.857	4.242	3.892	3.663	3.501	3.380	3.285	3.209	3.147	2.949	2.844	2.487
15	6.200	4.765	4.153	3.804	3.576	3.415	3.293	3.199	3.123	3.060	2.862	2.756	2.395

16	6.115	4.687	4.077	3.729	3.502	3.341	3.219	3.125	3.049	2.986	2.788	2.681	2.316
17	6.042	4.619	4.011	3.665	3.438	3.277	3.156	3.061	2.985	2.922	2.723	2.616	2.247
18	5.978	4.560	3.954	3.608	3.382	3.221	3.100	3.005	2.929	2.866	2.667	2.559	2.187
19	5.922	4.508	3.903	3.559	3.333	3.172	3.051	2.956	2.880	2.817	2.617	2.509	2.133
20	5.871	4.461	3.859	3.515	3.289	3.128	3.007	2.913	2.837	2.774	2.573	2.464	2.085
∞	5.024	3.689	3.116	2.786	2.567	2.408	2.288	2.192	2.114	2.048	1.833	1.708	1.000

7.6: Critical Values for Dixon's Q-Test

The following table provides critical values for $Q(\alpha, n)$, where α is the probability of incorrectly rejecting the suspected outlier and n is the number of samples in the data set. There are several versions of Dixon's *Q*-Test, each of which calculates a value for Q_{ij} where *i* is the number of suspected outliers on one end of the data set and *j* is the number of suspected outliers on the opposite end of the data set. The critical values for *Q* here are for a single outlier, Q_{10}, where

$$Q_{\text{exp}} = Q_{10} = \frac{|\text{outlier's value} - \text{nearest value}|}{\text{largest value} - \text{smallest value}}$$

The suspected outlier is rejected if Q_{exp} is greater than $Q(\alpha, n)$. For additional information consult Rorabacher, D. B. "Statistical Treatment for Rejection of Deviant Values: Critical Values of Dixon's '*Q*' Parameter and Related Subrange Ratios at the 95% confidence Level," *Anal. Chem.* **1991**, *63*, 139–146.

Table 16.6.1 : Critical Values for Dixon's Q-Test

$\frac{\alpha \longrightarrow}{n \downarrow}$	**0.1**	**0.05**	**0.04**	**0.02**	**0.01**
3	0.941	0.970	0.976	0.988	0.994
4	0.765	0.829	0.846	0.889	0.926
5	0.642	0.710	0.729	0.780	0.821
6	0.560	0.625	0.644	0.698	0.740
7	0.507	0.568	0.586	0.637	0.680
8	0.468	0.526	0.543	0.590	0.634
9	0.437	0.493	0.510	0.555	0.598
10	0.412	0.466	0.483	0.527	0.568

7.7: Critical Values for Grubb's Test

The following table provides critical values for $G(\alpha, n)$, where α is the probability of incorrectly rejecting the suspected outlier and *n* is the number of samples in the data set. There are several versions of Grubb's Test, each of which calculates a value for G_{ij} where *i* is the number of suspected outliers on one end of the data set and *j* is the number of suspected outliers on the opposite end of the data set. The critical values for *G* given here are for a single outlier, G_{10}, where

$$G_{\text{exp}} = G_{10} = \frac{|X_{out} - \overline{X}|}{s}$$

The suspected outlier is rejected if G_{exp} is greater than $G(\alpha, n)$.

Table 16.7.1 : Critical Values for the Grubb's Test

$\frac{\alpha \longrightarrow}{n \downarrow}$	**0.05**	**0.01**
3	1.155	1.155
4	1.481	1.496
5	1.715	1.764
6	1.887	1.973
7	2.020	2.139
8	2.126	2.274
9	2.215	2.387
10	2.290	2.482
11	2.355	2.564
12	2.412	2.636
13	2.462	2.699
14	2.507	2.755
15	2.549	2.755

7.8: Recommended Primary Standards

All compounds are of the highest available purity. Metals are cleaned with dilute acid to remove any surface impurities and rinsed with distilled water. Unless otherwise indicated, compounds are dried to a constant weight at 110 °C. Most of these compounds are soluble in dilute acid (1:1 HCl or 1:1 HNO_3), with gentle heating if necessary; some of the compounds are water soluble.

Element	Compound	FW (g/mol)	Comments
aluminum	Al metal	26.982	
antimony	Sb metal	121.760	
	$KSbOC_4H_4O_6$	324.92	prepared by drying $KSbC_4H_4O_6 \cdot \frac{1}{2}H_2O$ at 100 °C and storing in a desicator
arsenic	As metal	74.922	
	As_2O_3	197.84	toxic
barium	$BaCO_3$	197.84	dry at 200 °C for 4 h
bismuth	Bi metal	208.98	
boron	H_3BO_3	61.83	do not dry
bromine	KBr	119.01	
cadmium	Cd metal	112.411	
	CdO	128.40	
calcium	$CaCO_3$	100.09	
cerium	Ce metal	140.116	
	$(NH_4)_2Ce(NO_3)_4$	548.23	
cesium	Cs_2CO_3	325.82	
	Cs_2SO_4	361.87	
chlorine	NaCl	58.44	
chromium	Cr metal	51.996	
	$K_2Cr_2O_7$	294.19	
cobalt	Co metal	58.933	
copper	Cu metal	63.546	
	CuO	79.54	
fluorine	NaF	41.99	do not store solutions in glass containers
iodine	KI	166.00	
	KIO_3	214.00	
iron	Fe metal	55.845	
lead	Pb metal	207.2	
lithium	Li_2CO_3	73.89	
magnesium	Mg metal	24.305	
manganese	Mn metal	54.938	

Element	Compound	FW (g/mol)	Comments
mercury	Hg metal	200.59	
molybdenum	Mo metal	95.94	
nickel	Ni metal	58.693	
phosphorous	KH_2PO_4	136.09	
	P_2O_5	141.94	
potassium	KCl	74.56	
	K_2CO_3	138.21	
	$K_2Cr_2O_7$	294.19	
	$KHC_8H_4O_2$	204.23	
silicon	Si metal	28.085	
	SiO_2	60.08	
silver	Ag metal	107.868	
	$AgNO_3$	169.87	
sodium	NaCl	58.44	
	Na_2CO_3	106.00	
	$Na_2C_2O_4$	134.00	
strontium	$SrCO_3$	147.63	
sulfur	elemental S	32.066	
	K_2SO_4	174.27	
	Na_2SO_4	142.04	
tin	Sn metal	118.710	
titanium	Ti metal	47.867	
tungsten	W metal	183.84	
uranium	U metal	238.029	
	U_3O_8	842.09	
vanadium	V metal	50.942	
zinc	Zn metal	81.37	

Sources:

- Smith, B. W.; Parsons, M. L. *J. Chem. Educ.* **1973**, *50*, 679–681
- Moody, J. R.; Greenburg, P. R.; Pratt, K. W.; Rains, T. C. *Anal. Chem.* **1988**, *60*, 1203A–1218A.

7.9: Correcting Mass for the Buoyancy of Air

Calibrating a balance does not eliminate all sources of determinate error that might affect the signal. Because of the buoyancy of air, an object always weighs less in air than it does in a vacuum. If there is a difference between the object's density and the density of the weights used to calibrate the balance, then we can make a correction for buoyancy [Battino, R.; Williamson, A. G. *J. Chem. Educ.* **1984**, *61*, 51–52]. An object's true weight in vacuo, W_v, is related to its weight in air, W_a, by the equation

$$W_v = W_a \times \left[1 + \left(\frac{1}{D_o} - \frac{1}{D_w}\right) \times 0.0012\right] \tag{7.9.1}$$

where D_o is the object's density, D_w is the density of the calibration weight, and 0.0012 is the density of air under normal laboratory conditions (all densities are in units of g/cm^3). The greater the difference between D_o and D_w the more serious the error in the object's measured weight.

The buoyancy correction for a solid is small and frequently ignored. The correction may be significant, however, for low density liquids and gases. This is particularly important when calibrating glassware. For example, we can calibrate a volumetric pipet by carefully filling the pipet with water to its calibration mark, dispensing the water into a tared beaker, and determining the water's mass. After correcting for the buoyancy of air, we use the water's density to calculate the volume dispensed by the pipet.

Example 16.9.1

A 10-mL volumetric pipet is calibrated following the procedure outlined above, using a balance calibrated with brass weights with a density of 8.40 g/cm^3. At 25°C the pipet dispenses 9.9736 g of water. What is the actual volume dispensed by the pipet and what is the determinate error in this volume if we ignore the buoyancy correction? At 25°C the density of water is 0.997 05 g/cm^3.

Solution

Using Equation 7.9.1 the water's true weight is

$$W_v = 9.9736 \text{ g} \times \left[1 + \left(\frac{1}{0.99705} - \frac{1}{8.40}\right) \times 0.0012\right] = 9.9842 \text{ g}$$

and the actual volume of water dispensed by the pipet is

$$\frac{9.9842 \text{ g}}{0.99705 \text{ g/cm}^3} = 10.014 \text{ cm}^3$$

If we ignore the buoyancy correction, then we report the pipet's volume as

$$\frac{9.9736 \text{ g}}{0.99705 \text{ g/cm}^3} = 10.003 \text{ cm}^3$$

introducing a negative determinate error of –0.11%.

Exercise 16.9.1

To calibrate a 10-mL pipet a measured volume of water is transferred to a tared flask and weighed, yielding a mass of 9.9814 grams. (a) Calculate, with and without correcting for buoyancy, the volume of water delivered by the pipet. Assume the density of water is 0.99707 g/cm^3 and that the density of the weights is 8.40 g/cm^3. (b) What is the absolute error and the relative error introduced if we fail to account for the effect of buoyancy? Is this a significant source of determinate error for the calibration of a pipet? Explain.

Answer

For (a), without accounting for buoyancy, the volume of water is

$$\frac{9.9814 \text{ g}}{0.99707 \text{ g/cm}^3} = 10.011 \text{ cm}^3 = 10.011 \text{ mL}$$

When we correct for buoyancy, however, the volume is

$$W_v = 9.9814 \text{ g} \times \left[1 + \left(\frac{1}{0.99707 \text{ g/cm}^3} - \frac{1}{8.40 \text{ g/cm}^3}\right) \times 0.0012 \text{ g/cm}^3\right] = 9.920 \text{ g}$$

For (b), the absolute and relative errors in the mass are

$$10.011 \text{ mL} - 10.021 \text{ mL} = -0.010 \text{ mL}$$

$$\frac{-0.010 \text{ mL}}{10.021 \text{ mL}} \times 100 = -0.10\%$$

Table 4.2.8 shows us that the standard deviation for the calibration of a 10-mL pipet is on the order of ±0.006 mL. Failing to correct for the effect of buoyancy gives a determinate error of –0.010 mL that is slightly larger than ±0.006 mL, suggesting that it introduces a small, but significant determinate error.

Exercise 16.9.2

Repeat the questions in Exercise 16.9.1 for the case where a mass of 0.2500 g is measured for a solid that has a density of 2.50 g/cm^3.

Answer

The sample's true weight is

$$W_v = 0.2500 \text{ g} \times \left[1 + \left(\frac{1}{2.50 \text{ g/cm}^3} - \frac{1}{8.40 \text{ g/cm}^3}\right) \times 0.0012 \text{ g/cm}^3\right] = 0.2501 \text{ g}$$

In this case the absolute and relative errors in mass are –0.0001 g and –0.040%.

Exercise 16.9.3

Is the failure to correct for buoyancy a constant or proportional source of determinate error?

Answer

The true weight is the product of the weight measured in air and the buoyancy correction factor, which makes this a proportional error. The percentage error introduced when we ignore the buoyancy correction is independent of mass and a function only of the difference between the density of the object being weighed and the density of the calibration weights.

Exercise 16.9.4

What is the minimum density of a substance necessary to keep the buoyancy correction to less than 0.01% when using brass calibration weights with a density of 8.40 g/cm^3?

Answer

To determine the minimum density, we note that the buoyancy correction factor equals 1.00 if the density of the calibration weights and the density of the sample are the same. The correction factor is greater than 1.00 if D_o is smaller than D_w; thus, the following inequality applies

$$\left(\frac{1}{D_o} - \frac{1}{8.40}\right) \times 0.0012 \leq (1.00)(0.0001)$$

Solving for D_o shows that the sample's density must be greater than 4.94 g/cm^3 to ensure an error of less than 0.01%.

7.10: Solubility Products

The following table provides pK_{sp} and K_{sp} values for selected compounds, organized by the anion. All values are from Martell, A. E.; Smith, R. M. *Critical Stability Constants*, Vol. 4. Plenum Press: New York, 1976. Unless otherwise stated, values are for 25 °C and zero ionic strength.

Bromide (Br^-)	pK_{sp}	K_{sp}
$CuBr$	8.3	$5. \times 10^{-9}$
$AgBr$	12.3	5.0×10^{-13}
Hg_2Br_2	22.25	5.6×10^{-23}
$HgBr_2$ ($\mu = 0.5$ M)	18.9	1.3×10^{-19}
$PbBr_2$ ($\mu = 0.5$ M)	5.68	2.1×10^{-6}

Carbonate (CO_3^{2-})	pK_{sp}	K_{sp}
$MgCO_3$	7.46	3.5×10^{-8}
$CaCO_3$ (calcite)	8.35	4.5×10^{-9}
$CaCO_3$ (aragonite)	8.22	6.0×10^{-9}
$SrCO_3$	9.03	9.3×10^{-10}
$BaCO_3$	8.3	5.0×10^{-9}
$MnCO_3$	9.3	5.0×10^{-10}
$FeCO_3$	10.68	2.1×10^{-11}
$CoCO_3$	9.98	1.0×10^{-10}
$NiCO_3$	6.87	1.3×10^{-7}
Ag_2CO_3	11.09	8.1×10^{-12}
Hg_2CO_3	16.05	8.9×10^{-17}
$ZnCO_3$	10	1.0×10^{-10}
$CdCO_3$	13.74	1.8×10^{-14}
$PbCO_3$	13.13	7.4×10^{-14}

Chloride (Cl^-)	pK_{sp}	K_{sp}
$CuCl$	6.73	1.9×10^{-7}
$AgCl$	9.74	1.8×10^{-10}
Hg_2Cl_2	17.91	1.2×10^{-18}
$PbCl_2$	4.78	2.0×10^{-19}

Chromate (CrO_4^{2-})	pK_{sp}	K_{sp}
$BaCrO_4$	9.67	2.1×10^{-10}
$CuCrO_4$	5.44	3.6×10^{-6}

Chromate (CrO_4^{2-})	pK_{sp}	K_{sp}
Ag_2CrO_4	11.92	1.2×10^{-12}
Hg_2CrO_4	8.7	2.0×10^{-9}

Cyanide (CN^-)	pK_{sp}	K_{sp}
$AgCN$	15.66	2.2×10^{-16}
$Zn(CN)_2$ ($\mu = 3.0$ M)	15.5	$3. \times 10^{-16}$
$Hg_2(CN)_2$	39.3	$5. \times 10^{-40}$

Ferrocyanide ($Fe(CN)_6^{4-}$)	pK_{sp}	K_{sp}
$Zn_2[Fe(CN)_6]$	15.68	2.1×10^{-16}
$Cd_2[Fe(CN)_6]$	17.38	4.2×10^{-18}
$Pb_2[Fe(CN)_6]$	18.02	9.5×10^{-19}

Fluoride (F^-)	pK_{sp}	K_{sp}
MgF_2	8.18	6.6×10^{-9}
CaF_2	10.41	3.9×10^{-11}
SrF_2	8.54	2.9×10^{-9}
BaF_2	5.76	1.7×10^{-6}
PbF_2	7.44	3.6×10^{-8}

Hydroxide (OH^-)	pK_{sp}	K_{sp}
$Mg(OH)_2$	11.15	7.1×10^{-12}
$Ca(OH)_2$	5.19	6.5×10^{-6}
$Ba(OH)_2 \cdot 8\,H_2O$	3.6	$3. \times 10^{-4}$
$La(OH)_3$	20.7	$2. \times 10^{-21}$
$Mn(OH)_2$	12.8	1.6×10^{-13}
$Fe(OH)_2$	15.1	$8. \times 10^{-16}$
$Co(OH)_2$	14.9	1.3×10^{-15}
$Ni(OH)_2$	15.2	$6. \times 10^{-16}$
$Cu(OH)_2$	19.32	4.8×10^{-20}
$Fe(OH)_3$	38.8	1.6×10^{-39}
$Co(OH)_3$ ($T = 19^\circ C$)	44.5	$3. \times 10^{-45}$
Ag_2O ($+ H_2O \rightleftharpoons 2\,Ag^+ + 2\,OH^-$)	15.42	3.8×10^{-16}
Cu_2O ($+ H_2O \rightleftharpoons 2\,Cu^+ + 2\,OH^-$)	29.4	$4.u \times 10^{-30}$
$Zn(OH)_2$ (amorphous)	15.52	3.0×10^{-16}
$Cd(OH)_2(\beta)$	14.35	4.5×10^{-15}

Hydroxide (OH^-)	pK_{sp}	K_{sp}
$HgO\ (red)\ (+\ H_2O \rightleftharpoons Hg^{2+} + 2\,OH^-)$	25.44	3.6×10^{-26}
$SnO\ (+\ H_2O \rightleftharpoons Hg^{2+} + 2\,OH^-)$	26.2	$6. \times 10^{-27}$
$PbO\ (yellow)\ (+\ H_2O \rightleftharpoons +Pb^{2+} + 2\,OH^-$	15.1	$8. \times 10^{-16}$
$Al(OH)_3\ (\alpha)$	33.5	$3. \times 10^{-34}$

Iodate (IO_3^-)	pK_{sp}	K_{sp}
$Ca(IO_3)_2$	6.15	7.1×10^{-7}
$Ba(IO_3)_2$	8.81	1.5×10^{-9}
$AgIO_3$	7.51	3.1×10^{-8}
$Hg_2(IO_3)_2$	17.89	1.3×10^{-18}
$Zn(IO_3)_2$	5.41	3.9×10^{-6}
$Cd(IO_3)_2$	7.64	2.3×10^{-8}
$Pb(IO_3)_2$	12.61	2.5×10^{-13}

Iodide (I^-)	pK_{sp}	K_{sp}
AgI	16.08	8.3×10^{-17}
Hg_2I_2	28.33	4.7×10^{-29}
$HgI_2\ (\mu = 0.5\ M)$	27.95	1.1×10^{-28}
PbI_2	8.1	7.9×10^{-9}

Oxalate ($C_2O_4^{2-}$)	pK_{sp}	K_{sp}
$CaC_2O_4\ (\mu = 0.1\ M,\ T = 20^\circ C)$	7.9	1.3×10^{-8}
$BaC_2O_4\ (\mu = 0.1\ M,\ T = 20^\circ C)$	6	$1. \times 10^{-6}$
$SrC_2O_4\ (\mu = 0.1\ M,\ T = 20^\circ C)$	6.4	$4. \times 10^{-7}$

Phosphate (PO_4^{3-})	pK_{sp}	K_{sp}
$Fe_3(PO_4)_2 \cdot 8\,H_2O$	36	$1. \times 10^{-36}$
$Zn_3(PO_4)_2 \cdot 4\,H_2O$	35.3	$5. \times 10^{-36}$
Ag_3PO_4	17.55	2.8×10^{-18}
$Pb_3(PO_4)_2\ (T = 38\ ^\circ C)$	43.55	3.0×10^{-44}

Sulfate (SO_4^{2-})	pK_{sp}	K_{sp}
$CaSO_4$	4.62	2.4×10^{-5}
$SrSO_4$	6.5	3.2×10^{-7}
$BaSO_4$	9.96	1.1×10^{-10}
Ag_2SO_4	4.83	1.5×10^{-5}

Sulfate (SO_4^{2-})	pK_{sp}	K_{sp}
Hg_2SO_4	6.13	7.4×10^{-7}
$PbSO_4$	7.79	1.6×10^{-8}

Sulfide (S^{2-})	pK_{sp}	K_{sp}
MnS (green)	13.5	$3. \times 10^{-14}$
FeS	18.1	$8. \times 10^{-19}$
CoS (β)	25.6	$3. \times 10^{-26}$
NiS (γ)	26.6	$3. \times 10^{-27}$
CuS	36.1	$8. \times 10^{-37}$
Cu_2S	48.5	$3. \times 10^{-49}$
Ag_2S	50.1	$8. \times 10^{-51}$
ZnS (α)	24.7	$2. \times 10^{-25}$
CdS	27	$1. \times 10^{-27}$
Hg_2S (red)	53.3	$5. \times 10^{-54}$
PbS	27.5	$3. \times 10^{-28}$

Thiocyanate (SCN^-)	pK_{sp}	K_{sp}
CuSCN ($\mu = 5.0$ M)	13.4	4.0×10^{-14}
AgSCN	11.97	1.1×10^{-12}
$Hg_2(SCN)_2$	19.52	3.0×10^{-20}
$Hg_2(SCN)_2$ ($\mu = 1.0$ M)	19.56	2.8×10^{-20}

7.11: Acid Dissociation Constants

The following table provides pK_a and K_a values for selected weak acids. All values are from Martell, A. E.; Smith, R. M. *Critical Stability Constants*, Vols. 1–4. Plenum Press: New York, 1976. Unless otherwise stated, values are for 25 °C and for zero ionic strength. Those values in brackets are considered less reliable.

Weak acids are arranged alphabetically by the names of the neutral compounds from which they are derived. In some cases—such as acetic acid—the compound is the weak acid. In other cases—such as for the ammonium ion—the neutral compound is the conjugate base. Chemical formulas or structural formulas are shown for the fully protonated weak acid. Successive acid dissociation constants are provided for polyprotic weak acids; where there is ambiguity, the specific acidic proton is identified.

To find the K_b value for a conjugate weak base, recall that

$$K_a \times K_b = K_w$$

for a conjugate weak acid, HA, and its conjugate weak base, A^-.

compound	conjugate acid	pK_a	K_a
acetic acid	CH_3COOH	4.757	1.75×10^{-5}
adipic acid	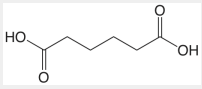	4.42 5.42	3.8×10^{-5} 3.8×10^{-6}
alanine	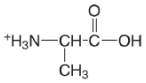	2.348 (COOH) 9.867 (NH_3)	4.49×10^{-3} 1.36×10^{-10}
aminobenzene	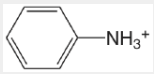	4.601	2.51×10^{-5}
4-aminobenzene sulfonic acid		3.232	5.86×10^{-4}
2-aminobenzoic acid	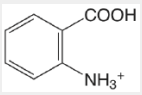	2.08 (COOH) 4.96 (NH_3)	8.3×10^{-3} 1.1×10^{-5}
2-aminophenol ($T = 20^\circ C$)	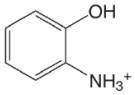	4.78 (NH_3) 9.97 (OH)	1.7×10^{-5} 1.05×10^{-10}
ammonia	NH_4^+	9.244	5.70×10^{-10}
arginine	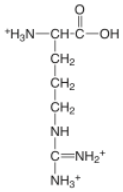	1.823 (COOH) 8.991 (NH_3) [12.48] (NH_2)	1.50×10^{-2} 1.02×10^{-9} $[3.3 \times 10^{-13}]$
arsenic acid	H_3AsO_4	2.24 6.96 11.50	5.8×10^{-3} 1.1×10^{-7} 3.2×10^{-12}

compound	conjugate acid	pK_a	K_a
asparagine ($\mu = 0.1$ M)	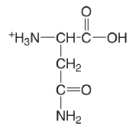	2.14 (COOH) 8.72 (NH_3)	7.2×10^{-3} 1.9×10^{-9}
aspartic acid	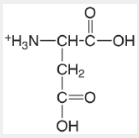	1.990 (α-COOH) 3.900 (β-COOH) 10.002 (NH_3)	1.02×10^{-2} 1.26×10^{-4} 9.95×10^{-11}
benzoic acid	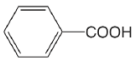	4.202	6.28×10^{-5}
benzylamine	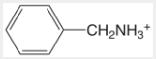	9.35	4.5×10^{-10}
boric acid (pK_{a2}, pK_{a3}: $T = 20^\circ$C)	H_3BO_3	9.236 [12.74] [13.80]	5.81×10^{-10} [1.82×10^{-13}] [1.58×10^{-14}]
carbonic acid	H_2CO_3	6.352 10.329	4.45×10^{-7} 4.69×10^{-11}
catechol	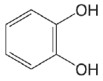	9.40 12.8	4.0×10^{-10} 1.6×10^{-13}
chloracetic acid	$ClCH_2COOH$	2.865	1.36×10^{-3}
chromic acid (pK_{a1}: $T = 20^\circ$C)	H_2CrO_4	–0.2 6.51	1.6 3.1×10^{-7}
citric acid	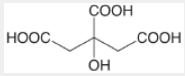	3.128 (COOH) 4.761 (COOH) 6.396 (COOH)	7.45×10^{-4} 1.73×10^{-5} 4.02×10^{-7}
cupferron ($\mu = 0.1$ M)	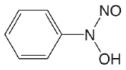	4.16	6.9×10^{-5}
cysteine	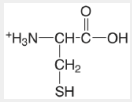	[1.71] (COOH) 8.36 (SH) 10.77 (NH_3)	[1.9×10^{-2}] 4.4×10^{-9} 1.7×10^{-11}
dichloracetic acid	$Cl_2CHCOOH$	1.30	5.0×10^{-2}
diethylamine	$(CH_3CH_2)_2NH_2^+$	10.933	1.17×10^{-11}
dimethylamine	$(CH_3)_2NH_2^+$	10.774	1.68×10^{-11}
dimethylglyoxime	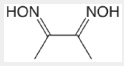	10.66 12.0	2.2×10^{-11} $1. \times 10^{-12}$
ethylamine	$CH_3CH_2NH_3^+$	10.636	2.31×10^{-11}
ethylenediamine	$+H_3NCH_2CH_2NH_3^+$	6.848 9.928	1.42×10^{-7} 1.18×10^{-10}

compound	conjugate acid	pK_a	K_a
ethylenediaminetetracetic acid (EDTA) ($\mu = 0.1$ M)	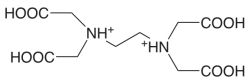	0.0 (COOH) 1.5 (COOH) 2.0 (COOH) 2.66 (COOH) 6.16 (NH) 10.24 (NH)	1.0 3.2×10^{-2} 1.0×10^{-2} 2.2×10^{-3} 6.9×10^{-7} 5.8×10^{-11}
formic acid	$HCOOH$	3.745	1.80×10^{-4}
fumaric acid	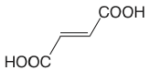	3.053 4.494	8.85×10^{-4} 3.21×10^{-5}
glutamic acid	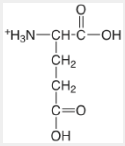	2.33 (α-COOH) 4.42 (λ-COOH) 9.95 (NH_3)	5.9×10^{-3} 3.8×10^{-5} 1.12×10^{-10}
glutamine	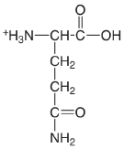	2.17 (COOH) 9.01 (NH_3)	6.8×10^{-3} 9.8×10^{-10}
glycine	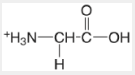	2.350 (COOH) 9.778 (NH_3)	4.47×10^{-3} 1.67×10^{-10}
glycolic acid	$HOOCH_2COOH$	3.881 (COOH)	1.48×10^{-4}
histidine ($\mu = 0.1$ M)	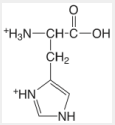	1.7 (COOH) 6.02 (NH) 9.08 (NH_3)	$2. \times 10^{-2}$ 9.5×10^{-7} 8.3×10^{-10}
hydrogen cyanide	HCN	9.21	6.2×10^{-10}
hydrogen fluroride	HF	3.17	6.8×10^{-4}
hydrogen peroxide	H_2O_2	11.65	2.2×10^{-12}
hydrogen sulfide	H_2S	7.02 13.9	9.5×10^{-8} 1.3×10^{-14}
hydrogen thiocyanate	$HSCN$	0.9	1.3×10^{-1}
8-hydroxyquinoline	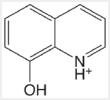	4.9 (NH) 9.81 (OH)	1.2×10^{-5} 1.6×10^{-10}
hydroxylamine	$HONH_3^+$	5.96	1.1×10^{-6}
hypobromous acid	$HOBr$	8.63	2.3×10^{-9}
hypochlorous acid	$HOCl$	7.53	3.0×10^{-8}
hypoiodous acid	HOI	10.64	2.3×10^{-11}
iodic acid	HIO_3	0.77	1.7×10^{-1}

compound	conjugate acid	pK_a	K_a
isoleucine	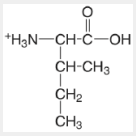	2.319 (COOH) 9.754 (NH_3)	4.8×10^{-3} 1.76×10^{-10}
leucine	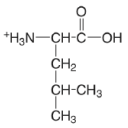	2.329 (COOH) 9.747 (NH_3)	4.69×10^{-3} 1.79×10^{-10}
lysine ($\mu = 0.1$ M)	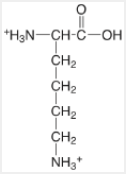	2.04 (COOH) 9.08 (α-NH_3) 10.69 (ϵ-NH_3)	9.1×10^{-3} 8.3×10^{-10} 2.0×10^{-11}
maleic acid		1.910 6.332	1.23×10^{-2} 4.66×10^{-7}
malic acid	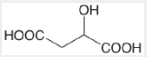	3.459 (COOH) 5.097 (COOH)	3.48×10^{-4} 8.00×10^{-6}
malonic acid	$HOOCCH_2COOH$	2.847 5.696	1.42×10^{-3} 2.01×10^{-6}
methionine ($\mu = 0.1$ M)	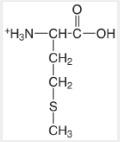	2.20 (COOH) 9.05 (NH_3)	6.3×10^{-3} 8.9×10^{-10}
methylamine	$CH_3NH_3^+$	10.64	2.3×10^{-11}
2-methylanaline	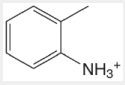	4.447	3.57×10^{-5}
4-methylanaline	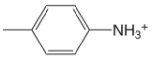	5.084	8.24×10^{-6}
2-methylphenol	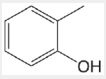	10.28	5.2×10^{-11}
4-methylphenol	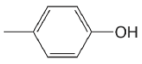	10.26	5.5×10^{-11}
nitrilotriacetic acid ($T = 20^\circ C), pK_{a1:}$ $\mu = 0.1$ M)	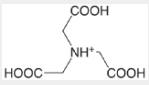	1.1 (COOH) 1.650 (COOH) 2.940 (COOH) 10.334 (NH_3)	$8. \times 10^{-2}$ 2.24×10^{-2} 1.15×10^{-3} 4.63×10^{-11}
2-nitrobenzoic acid	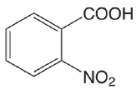	2.179	6.62×10^{-3}

compound	conjugate acid	pK_a	K_a
3-nitrobenzoic acid	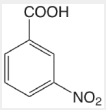	3.449	3.56×10^{-4}
4-nitrobenzoic acid	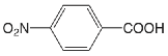	3.442	3.61×10^{-4}
2-nitrophenol	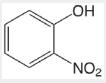	7.21	6.2×10^{-8}
3-nitrophenol	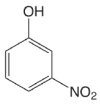	8.39	4.1×10^{-9}
4-nitrophenol	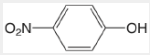	7.15	7.1×10^{-8}
nitrous acid	HNO_2	3.15	7.1×10^{-4}
oxalic acid	$H_2C_2O_4$	1.252 4.266	5.60×10^{-2} 5.42×10^{-5}
1,10-phenanthroline	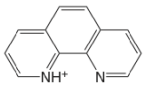	4.86	1.38×10^{-5}
phenol	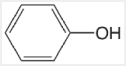	9.98	1.05×10^{-10}
phenylalanine	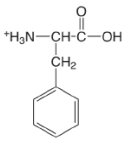	2.20 (COOH) 9.31 (NH_3)	6.3×10^{-3} 4.9×10^{-10}
phosphoric acid	H_3PO_4	2.148 7.199 12.35	7.11×10^{-3} 6.32×10^{-8} 4.5×10^{-13}
phthalic acid	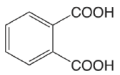	2.950 5.408	1.12×10^{-3} 3.91×10^{-6}
piperdine	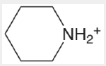	11.123	7.53×10^{-12}
proline	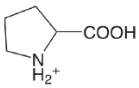	1.952 (COOH) 10.650 (NH)	1.12×10^{-2} 2.29×10^{-11}
propanoic acid	CH_3CH_2COOH	4.874	1.34×10^{-5}
propylamine	$CH_3CH_2CH_2NH_3^+$	10.566	2.72×10^{-11}
pyridine	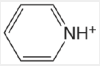	5.229	5.90×10^{-6}

compound	conjugate acid	pK_a	K_a
resorcinol	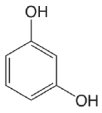	9.30 11.06	5.0×10^{-10} 8.7×10^{-12}
salicylic acid	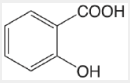	2.97 (COOH) 13.74 (OH)	1.1×10^{-3} 1.8×10^{-14}
serine	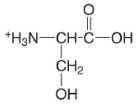	2.187 (COOH) 9.209 (NH_3)	6.50×10^{-3} 6.18×10^{-10}
succinic acid		4.207 5.636	6.21×10^{-5} 2.31×10^{-6}
sulfuric acid	H_2SO_4	strong 1.99	— 1.0×10^{-2}
sulfurous acid	H_2SO_3	1.91 7.18	1.2×10^{-2} 6.6×10^{-8}
D-tartaric acid	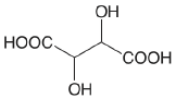	3.036 (COOH) 4.366 (COOH)	9.20×10^{-4} 4.31×10^{-5}
threonine	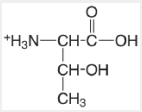	2.088 (COOH) 9.100 (NH_3)	8.17×10^{-3} 7.94×10^{-10}
thiosulfuric acid	$H_2S_2O_3$	0.6 1.6	$3. \times 10^{-1}$ $3. \times 10^{-2}$
trichloracetic acid ($\mu = 0.1$ M)	Cl_3CCOOH	0.66	2.2×10^{-1}
triethanolamine	$(HOCH_2CH_2)_3NH^+$	7.762	1.73×10^{-8}
triethylamine	$(CH_3CH_2)_3NH^+$	10.715	1.93×10^{-11}
trimethylamine	$(CH_3)_3NH^+$	9.800	1.58×10^{-10}
tris(hydroxymethyl)amino methane (TRIS or THAM)	$(HOCH_2)_3CNH_3^+$	8.075	8.41×10^{-9}
tryptophan ($\mu = 0.1$ M)	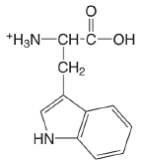	2.35 (COOH) 9.33 (NH_3)	4.5×10^{-3} 4.7×10^{-10}
tyrosine (pK_{a1}: $\mu = 0.1$ M)	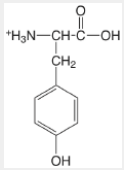	2.17 (COOH) 9.19 (NH_3) 10.47 (OH)	6.8×10^{-3} 6.5×10^{-10} 3.4×10^{-11}

compound	conjugate acid	pK_a	K_a
valine	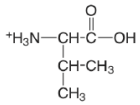	2.286 (COOH) 9.718 (NH_3)	5.18×10^{-3} 1.91×10^{-10}

7.12: Formation Constants

The following table provides K_i and β_i values for selected metal–ligand complexes, arranged by the ligand. All values are from Martell, A. E.; Smith, R. M. *Critical Stability Constants*, Vols. 1–4. Plenum Press: New York, 1976. Unless otherwise stated, values are for 25 °C and zero ionic strength. Those values in brackets are considered less reliable.

Acetate CH_3COO^-	log K_1	log K_2	log K_3	log K_4	log K_5	log K_6
Mg^{2+}	1.27					
Ca^{2+}	1.18					
Ba^{2+}	1.07					
Mn^{2+}	1.40					
Fe^{2+}	1.40					
Co^{2+}	1.46					
Ni^{2+}	1.43					
Cu^{2+}	2.22	1.41				
Ag^{+}	0.73	–0.09				
Zn^{2+}	1.57					
Cd^{2+}	1.93	1.22	–0.89			
Pb^{2+}	2.68	1.40				

Ammonia NH_3	log K_1	log K_2	log K_3	log K_4	log K_5	log K_6
Ag^{+}	3.31	3.91				
Co^{2+} (T = 20 °C)	1.99	1.51	0.93	0.64	0.06	–0.73
Ni^{2+}	2.72	2.17	1.66	1.12	0.67	–0.03
Cu^{2+}	4.04	3.43	2.80	1.48		
Zn^{2+}	2.21	2.29	2.36	2.03		
Cd^{2+}	2.55	2.01	1.34	0.84		

Chloride Cl^-	log K_1	log K_2	log K_3	log K_4	log K_5	log K_6
Cu^{2+}	0.40					
Fe^{3+}	1.48	0.65				
Ag^{+} ($\mu = 5.0$ M)	3.70	1.92	0.78	–0.3		
Zn^{2+}	0.43	0.18	–0.11	–0.3		
Cd^{2+}	1.98	1.62	–0.2	–0.7		
Pb^{2+}	1.59	0.21	–0.1	–0.3		

Cyanide CN^-	log K_1	log K_2	log K_3	log K_4	log K_5	log K_6
Fe^{2+}						35.4 (β_6)
Fe^{3+}						43.6 (β_6)
Ag^+		20.48 (β_2)	0.92			
Zn^{2+}		11.07 (β_2)	4.98	3.57		
Cd^{2+}	6.01	5.11	4.53	2.27		
Hg^{2+}	17.00	15.75	3.56	2.66		
Ni^{2+}				30.22 (β_4)		

Ethylenediamine $H_2NCH_2CH_2NH_2$	log K_1	log K_2	log K_3	log K_4	log K_5	log K_6
Ni^{2+}	7.38	6.18	4.11			
Cu^{2+}	10.48	9.07				
Ag^+ (T = 20 °C, $\mu = 0.1$ M)	4.700	3.00				
Zn^{2+}	5.66	4.98	3.25			
Cd^{2+}	5.41	4.50	2.78			

EDTA 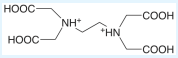	log K_1	log K_2	log K_3	log K_4	log K_5	log K_6
Mg^{2+} (T = 20 °C, $\mu = 0.1$ M)	8.79					
Ca^{2+} (T = 20 °C, $\mu = 0.1$ M)	10.69					
Ba^{2+} (T = 20 °C, $\mu = 0.1$ M)	7.86					
Bi^{3+} (T = 20 °C, $\mu = 0.1$ M)	27.8					
Co^{2+} (T = 20 °C, $\mu = 0.1$ M)	16.31					
Ni^{2+} (T = 20 °C, $\mu = 0.1$ M)	18.62					
Cu^{2+} (T = 20 °C, $\mu = 0.1$ M)	18.80					
Cr^{3+} (T = 20 °C, $\mu = 0.1$ M)	[23.4]					
Fe^{3+} (T = 20 °C, $\mu = 0.1$ M)	25.1					

EDTA 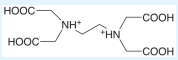	log K_1	log K_2	log K_3	log K_4	log K_5	log K_6
Ag^+ (T = 20 °C, $\mu = 0.1$ M)	7.32					
Zn^{2+} (T = 20 °C, $\mu = 0.1$ M)	16.50					
Cd^{2+} (T = 20 °C, $\mu = 0.1$ M)	16.46					
Hg^{2+} (T = 20 °C, $\mu = 0.1$ M)	21.7					
Pb^{2+} (T = 20 °C, $\mu = 0.1$ M)	18.04					
Al^{3+} (T = 20 °C, $\mu = 0.1$ M)	16.3					

Fluoride F^-	log K_1	log K_2	log K_3	log K_4	log K_5	log K_6
Al^{3+}	6.11	5.01	3.88	3.0	1.4	0.4

Hydroxide OH^-	log K_1	log K_2	log K_3	log K_4	log K_5	log K_6
Al^{3+}	9.01	[9.69]	[8.3]	6.0		
Co^{2+}	4.3	4.1	1.3	0.5		
Fe^{2+}	4.5	]2.9]	2,6	–0.4		
Fe^{3+}	11.81	10.5	12.1			
Ni^{2+}	4.1	3.9	3.			
Pb^{2+}	6.3	4.6	3.0			
Zn^{2+}	5.0	[6.1]	2.5	[1.2]		

Iodide I^-	log K_1	log K_2	log K_3	log K_4	log K_5	log K_6
Ag^+	6.58	[5.12]	[1.4]			
Cd^{2+} (T = 18 °C)	2.28	1.64	1.08	1.0		
Pb^{2+}	1.92	1.28	0.7	0.6		

Nitriloacetate 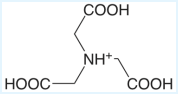	log K_1	log K_2	log K_3	log K_4	log K_5	log K_6
Mg^{2+} (T = 20 °C, $\mu = 0.1$ M)	5.41					

Nitriloacetate 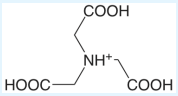	$\log K_1$	$\log K_2$	$\log K_3$	$\log K_4$	$\log K_5$	$\log K_6$
Ca^{2+} (T = 20 °C, $\mu = 0.1$ M)	6.41					
Ba^{2+} (T = 20 °C, $\mu = 0.1$ M)	4.82					
Mn^{2+} (T = 20 °C, $\mu = 0.1$ M)	7.44					
Fe^{2+} (T = 20 °C, $\mu = 0.1$ M)	8.33					
Co^{2+} (T = 20 °C, $\mu = 0.1$ M)	10.38					
Ni^{2+} (T = 20 °C, $\mu = 0.1$ M)	11.53					
Cu^{2+} (T = 20 °C, $\mu = 0.1$ M)	12.96					
Fe^{3+} (T = 20 °C, $\mu = 0.1$ M)	15.9					
Zn^{2+} (T = 20 °C, $\mu = 0.1$ M)	10.67					
Cd^{2+} (T = 20 °C, $\mu = 0.1$ M)	9.83					
Pb^{2+} (T = 20 °C, $\mu = 0.1$ M)	11.39					

Oxalate $C_2O_4^{2-}$	$\log K_1$	$\log K_2$	$\log K_3$	$\log K_4$	$\log K_5$	$\log K_6$
Ca^{2+} ($\mu = 1$ M)	1.66	1.03				
Fe^{2+} ($\mu = 1$ M)	3.05	2.10				
Co^{2+}	4.72	2.28				
Ni^{2+}	5.16					
Cu^{2+}	6.23	4.04				
Fe^{3+} ($\mu = 0.5$ M)	7.53	6.11	4.83			
Zn^{2+}	4.87	2.78				

1,10-phenanthroline 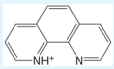	$\log K_1$	$\log K_2$	$\log K_3$	$\log K_4$	$\log K_5$	$\log K_6$

1,10-phenanthroline 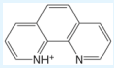	$\log K_1$	$\log K_2$	$\log K_3$	$\log K_4$	$\log K_5$	$\log K_6$
Fe^{2+}			20.7 (β_3)			
Mn^{2+} ($\mu = 0.1$ M)	4.0	3.3	3.0			
Cu^{2+} ($\mu = 0.1$ M)	7.08	6.64	6.08			
Ni^{2+}	8.6	8.1	7.6			
Fe^{3+}			13.8 (β_3)			
Ag^{+} ($\mu = 0.1$ M)	5.02	7.04				
Zn^{2+}	6.2	[5.9]	[5.2]			

Thiosulfate $S_2O_3^{2-}$	$\log K_1$	$\log K_2$	$\log K_3$	$\log K_4$	$\log K_5$	$\log K_6$
Ag^{+} (T = 20 °C)	8.82	4.85	0.53			

Thiocyanate SCN^{-}	$\log K_1$	$\log K_2$	$\log K_3$	$\log K_4$	$\log K_5$	$\log K_6$
Mn^{2+}	1.23					
Fe^{2+}	1.31					
Co^{2+}	1.71					
Ni^{2+}	1.76					
Cu^{2+}	2.33					
Fe^{3+}	3.02					
Ag^{+}	4.8	3.43	1.27	0.2		
Zn^{2+}	1.33	0.58	0.09	–0.4		
Cd^{2+}	1.89	0.89	0.02	–0.5		
Hg^{2+}		17.26 (β_2)	2.71	1.83		

7.13: Standard Reduction Potentials

The following table provides E^o and $E^{o'}$ values for selected reduction reactions. Values are from the following sources (primarily the first two):

- Bard, A. J.; Parsons, B.; Jordon, J., eds. *Standard Potentials in Aqueous Solutions*, Dekker: New York, 1985
- Milazzo, G.; Caroli, S.; Sharma, V. K. *Tables of Standard Electrode Potentials*, Wiley: London, 1978;
- Swift, E. H.; Butler, E. A. *Quantitative Measurements and Chemical Equilibria*, Freeman: New York, 1972.
- Bratsch, S. G. "Standard Electrode Potentials and Temperature Coefficients in Water at 298.15K, *J. Phys. Chem. Ref. Data*, **1989**, *18*, 1–21.
- Latimer, W. M. *Oxidation Potentials*, 2nd. Ed., Prentice-Hall: Englewood Cliffs, NJ, 1952

Solids, gases, and liquids are identified; all other species are aqueous. Reduction reactions in acidic solution are written using H^+ in place of H_3O^+. You may rewrite a reaction by replacing H^+ with H_3O^+ and adding to the opposite side of the reaction one molecule of H_2O per H^+; thus

$$H_3AsO_4 + 2H^+ + 2e^- \rightleftharpoons HAsO_2 + 2H_2O$$

becomes

$$H_3AsO_4 + 2H_3O^+ + 2e^- \rightleftharpoons HAsO_2 + 4H_2O$$

Conditions for formal potentials ($E^{o'}$) are listed next to the potential.

For most of the reduction half-reactions gathered here, there are minor differences in values provided by the references above. In most cases, these differences are small and will not affect calculations. In a few cases the differences are not insignificant and the user may find discrepancies in calculations. For example, Bard, Parsons, and Jordon report an E^o value of –1.285 V for

$$Zn(OH)_4^{2-} + 2e^- \rightleftharpoons Zn(s) + 4OH^-$$

while Milazzo, Caroli, and Sharma report the value as –1.214 V, Swift reports the value as –1.22, Bratsch reports the value as –1.199 V, and Latimer reports the value as –1.216 V.

Aluminum	E (V)	$E^{o'}$ (V)
$Al^{3+} + 3e^- \rightleftharpoons Al(s)$	–1.676	
$Al(OH)_4^- + 3e^- \rightleftharpoons Al(s) + 4OH^-$	–2.310	
$AlF_6^{3-} + 3e^- \rightleftharpoons Al(s) + 6F^-$	–2.07	

Antimony	E (V)	$E^{o'}$ (V)
$Sb + 3H^+ + 3e^- \rightleftharpoons SbH_3(g)$	–0.510	
$Sb_2O_5 + 6H^+ + 4e^- \rightleftharpoons 2SbO^+ + 3H_2O(l)$	0.605	
$SbO^+ + 2H^+ + 3e^- \rightleftharpoons Sb(s) + H_2O(l)$	0.212	

Arsenic	E (V)	$E^{o'}$ (V)
$As(s) + 3H^+ + 3e^- \rightleftharpoons AsH_3(g)$	–0.225	
$H_3AsO_4 + 2H^+ + 2e^- \rightleftharpoons HAsO_2 + 2H_2O(l)$	0.560	
$HAsO_2 + 3H^+ + 3e^- \rightleftharpoons As(s) + 2H_2O(l)$	0.240	

Barium	E (V)	$E^{o'}$ (V)
$Ba^{2+} + 2e^- \rightleftharpoons Ba(s)$	–2.92	
$BaO(s) + 2H^+ + 2e^- \rightleftharpoons Ba(s) + H_2O(l)$	–2.166	

Beryllium	E (V)	$E^{o'}$ (V)
$Be^{2+} + 2e^- \rightleftharpoons Be(s)$	–1.99	

Bismuth	E (V)	$E^{o'}$ (V)
$Bi^{3+} + 3e^- \rightleftharpoons Bi(s)$	0.317	
$BiCl_4^- + 3e^- \rightleftharpoons Bi(s) + 4Cl^-$	0.199	

Boron	E (V)	$E^{o'}$ (V)
$B(OH)_3 + 3H^+ + 3e^- \rightleftharpoons B(s) + 3H_2O(l)$	–0.890	
$B(OH)_4^- + 3e^- \rightleftharpoons B(s) + 4OH^-$	–1.811	

Bromine	E (V)	$E^{o'}$ (V)
$Br_2(l) + 2e^- \rightleftharpoons 2Br^-$	1.087	
$HOBr + H^+ + 2e^- \rightleftharpoons Br^- + H_2O(l)$	1.341	
$HOBr + H^+ + e^- \rightleftharpoons \frac{1}{2}Br_2 + H_2O(l)$	1.604	
$BrO^- + H_2O(l) + 2e^- \rightleftharpoons Br^- + 2OH^-$		0.76 in 1 M NaOH
$BrO_3^- + 6H^+ + 5e^- \rightleftharpoons \frac{1}{2}Br_2(l) + 3H_2O(l)$	1.5	
$BrO_3^- + 6H^+ + 6e^- \rightleftharpoons Br^- + 3H_2O(l)$	1.478	

Cadmium	E (V)	$E^{o'}$ (V)
$Cd^{2+} + 2e^- \rightleftharpoons Cd(s)$	–0.4030	
$Cd(CN)_4^{2-} + 2e^- \rightleftharpoons Cd(s) + 4CN^-$	–0.943	
$Cd(NH_3)_4^{2+} + 2e^- \rightleftharpoons Cd(s) + 4NH_3$	–0.622	

Calcium	E (V)	$E^{o'}$ (V)
$Ca^{2+} + 2e^- \rightleftharpoons Ca(s)$	–2.84	

Carbon	E (V)	$E^{o'}$ (V)
$CO_2(g) + 2H^+ + 2e^- \rightleftharpoons CO(g) + H_2O(l)$	–0.106	
$CO_2(g) + 2H^+ + 2e^- \rightleftharpoons HCO_2H$	–0.20	
$2CO_2(g) + 2H^+ + 2e^- \rightleftharpoons H_2C_2O_4$	–0.481	
$HCHO + 2H^+ + 2e^- \rightleftharpoons CH_3OH$	0.2323	

Cerium	E (V)	$E^{o'}$ (V)
$Ce^{3+} + 3e^- \rightleftharpoons Ce(s)$	–2.336	

Cerium	E (V)	$E^{o'}$ (V)
$Ce^{4+} + 3e^- \rightleftharpoons Ce^{3+}(s)$	–1.336	1.70 in 1 M $HClO_4$ 1.44 in 1 M H_2SO_4 1.61 in 1 M HNO_3 1.28 in 1 M HCl

Chlorine	E (V)	$E^{o'}$ (V)
$Cl_2(g) + 2e^- \rightleftharpoons 2Cl^-$	1.396	1.70 in 1 M $HClO_4$ 1.44 in 1 M H_2SO_4 1.61 in 1 M HNO_3 1.28 in 1 M HCl
$ClO^- + H_2O(l) + e^- \rightleftharpoons \frac{1}{2}Cl_2(g) + 2OH^-$		0.421 in 1 M NaOH
$ClO^- + H_2O(l) + 2e^- \rightleftharpoons Cl^- + 2OH^-$		0.890 in 1 M NaOH
$HClO_2 + 2H^+ + 2e^- \rightleftharpoons HOCl + H_2O(l)$	1.64	

Chlorine	E (V)	$E^{o'}$ (V)
$ClO_3^- + 2H^+ + e^- \rightleftharpoons ClO_2(g) + H_2O(l)$	1.175	
$ClO_3^- + 3H^+ + 2e^- \rightleftharpoons HClO_2 + H_2O(l)$	1.181	
$ClO_4^- + 2H^+ + 2e^- \rightleftharpoons ClO_3^- + H_2O(l)$	1.201	

Chromium	E (V)	$E^{o'}$ (V)
$Cr^{3+} + 3e^- \rightleftharpoons Cr(s)$	–0.424	
$Cr^{2+} + 2e^- \rightleftharpoons Cr(s)$	–0.90	
$Cr_2O_7^{2-} + 14H^+ + 6e^- \rightleftharpoons 2Cr^{3+} + 7H_2O(l)$	1.36	
$CrO_4^{2-} + 4H_2O(l) + 3e^- \rightleftharpoons Cr(OH)_4^- + 4OH^-$		–0.13 in 1 M NaOH

Cobalt	E (V)	$E^{o'}$ (V)
$Co^{2+} + 2e^- \rightleftharpoons Co(s)$	–0.277	
$Co^{3+} + 3e^- \rightleftharpoons Co(s)$	1.92	
$Co(NH_3)_6^{3+} + e^- \rightleftharpoons Co(NH_3)_6^{2+}$	0.1	
$Co(OH)_3(s) + e^- \rightleftharpoons Co(OH)_2(s) + OH^-$	0.17	
$Co(OH)_2(s) + 2e^- \rightleftharpoons Co(s) + 2OH^-$	–0.746	

Copper	E (V)	$E^{o'}$ (V)
$Cu^+ + e^- \rightleftharpoons Cu(s)$	0.520	
$Cu^{2+} + e^- \rightleftharpoons Cu^+$	0.159	
$Cu^{2+} + 2e^- \rightleftharpoons Cu(s)$	0.3419	
$Cu^{2+} + I^- + e^- \rightleftharpoons CuI(s)$	0.86	
$Cu^{2+} + Cl^- + e^- \rightleftharpoons CuCl(s)$	0.559	

Fluorine	E (V)	$E^{o'}$ (V)
$F_2(g) + 2H^+ + 2e^- \rightleftharpoons 2HF(g)$	3.053	

Fluorine	E (V)	$E^{o'}$ (V)
$F_2(g) + 2e^- \rightleftharpoons 2F^-$	2.87	
$F_2(g) + 2H^+ + 2e^- \rightleftharpoons 2HF(g)$	3.053	

Gallium	E (V)	$E^{o'}$ (V)
$Ga^{3+} + 3e^- \rightleftharpoons Ga(s)$	–0.529	

Gold	E (V)	$E^{o'}$ (V)
$Au^+ + e^- \rightleftharpoons Au(s)$	1.83	
$Au^{3+} + 2e^- \rightleftharpoons Au^+$	1.36	
$Au^{3+} + 3e^- \rightleftharpoons Au(s)$	1.52	
$AuCl_4^- + 3e^- \rightleftharpoons Au(s) + 4Cl^-$	1.002	

Hydrogen	E (V)	$E^{o'}$ (V)
$2H^+ + 2e^- \rightleftharpoons H_2(g)$	0.00000	
$H_2O(l) + e^- \rightleftharpoons \frac{1}{2}H_2(g) + OH^-$	–0.828	

Iodine	E (V)	$E^{o'}$ (V)
$I_2(s) + 2e^- \rightleftharpoons 2I^-$	0.5355	

Iodine	E (V)	$E^{o'}$ (V)
$I_3^- + 2e^- \rightleftharpoons 3I^-$	0.536	
$HIO + H^+ + 2e^- \rightleftharpoons I^- + H_2O(l)$	0.985	
$IO_3^- + 6H^+ + 5e^- \rightleftharpoons \frac{1}{2}I_2(s) + 3H_2O(l)$	1.195	
$IO_3^- + 3H_2O(l) + 6e^- \rightleftharpoons I^- + 6OH^-$	0.257	

Iron	E (V)	$E^{o'}$ (V)
$Fe^{2+} + 2e^- \rightleftharpoons Fe(s)$	–0.44	
$Fe^{3+} + 3e^- \rightleftharpoons Fe(s)$	–0.037	
$Fe^{3+} + e^- \rightleftharpoons Fe^{2+}$	0.771	0.70 in 1 M HCl 0.767 in 1 M $HClO_4$ 0.746 in 1 M HNO_3 0.68 in 1 M H_2SO_4 0.44 in 0.3 M H_3PO_4
$Fe(CN)_6^{3-} + e^- \rightleftharpoons Fe(CN)_6^{4-}$	0.356	
$Fe(phen)_3^{3+} + e^- \rightleftharpoons Fe(phen)_3^{2+}$	1.147	

Lanthanum	E (V)	$E^{o'}$ (V)
$La^{3+} + 3e^- \rightleftharpoons La(s)$	–2.38	

Lead	E (V)	$E^{o'}$ (V)

Lead	E (V)	$E^{o'}$ (V)
$Pb^{2+} + 2e^- \rightleftharpoons Pb(s)$	–0.126	
$PbO_2(s) + 4H^+ + 2e^- \rightleftharpoons Pb^{2+} + 2H_2O(l)$	1.46	
$PbO_2(s) + SO_4^{2-} + 4H^+ + 2e^- \rightleftharpoons PbSO_4(s) + 2H_2O(l)$	1.690	
$PbO_2(s) + 4H^+ + 2e^- \rightleftharpoons Pb^{2+} + 2H_2O(l)$	1.46	
$PbSO_4(s) + 2e^- \rightleftharpoons Pb(s) + SO_4^{2-}$	–0.356	
$PbO_2(s) + SO_4^{2-} + 4H^+ + 2e^- \rightleftharpoons PbSO_4(s) + 2H_2O(l)$	1.690	
$PbSO_4(s) + 2e^- \rightleftharpoons Pb(s) + SO_4^{2-}$	–0.356	

Lithium	E (V)	$E^{o'}$ (V)
$Li^+ + e^- \rightleftharpoons Li(s)$	–3.040	

Magnesium	E (V)	$E^{o'}$ (V)
$Mg^{2+} + 2e^- \rightleftharpoons Mg(s)$	–2.356	
$Mg(OH)_2(s) + 2e^- \rightleftharpoons Mg(s) + 2OH^-$	–2.687	

Manganese	E (V)	$E^{o'}$ (V)
$Mn^{2+} + 2e^- \rightleftharpoons Mn(s)$	–1.17	
$Mn^{3+} + e^- \rightleftharpoons Mn^{2+}$	1.5	
$MnO_2(s) + 4H^+ + 2e^- \rightleftharpoons Mn^{2+} + 2H_2O(l)$	1.23	
$MnO_4^- + 4H^+ + 3e^- \rightleftharpoons MnO_2(s) + 2H_2O(l)$	1.70	
$MnO_4^- + 8H^+ + 5e^- \rightleftharpoons Mn^{2+} + 4H_2O(l)$	1.51	
$MnO_4^- + 2H_2O(l) + 3e^- \rightleftharpoons MnO_2(s) + 4OH^-$	0.60	

Mercury	E (V)	$E^{o'}$ (V)
$Hg^{2+} + 2e^- \rightleftharpoons Hg(l)$	0.8535	
$2Hg^{2+} + 2e^- \rightleftharpoons Hg_2^{2+}$	0.911	

Mercury	E (V)	$E^{o'}$ (V)
$Hg_2^{2+} + 2e^- \rightleftharpoons 2Hg(l)$	0.7960	
$Hg_2Cl_2(s) + 2e^- \rightleftharpoons 2Hg(l) + 2Cl^-$	0.2682	
$HgO(s) + 2H^+ + 2e^- \rightleftharpoons Hg(l) + H_2O(l)$	0.926	
$Hg_2Br_2(s) + 2e^- \rightleftharpoons 2Hg(l) + 2Br^-$	1.392	
$Hg_2I_2(s) + 2e^- \rightleftharpoons 2Hg(l) + 2I^-$	–0.0405	

Molybdenum	E (V)	$E^{o'}$ (V)
$Mo^{3+} + 3e^- \rightleftharpoons Mo(s)$	–0.2	
$MoO_2(s) + 4H^+ + 4e^- \rightleftharpoons Mo(s) + 2H_2O(l)$	–0.152	
$MoO_4^{2-} + 4H_2O(l) + 6e^- \rightleftharpoons Mo(s) + 8OH^-$	–0.913	

Nickel	E (V)	$E^{o'}$ (V)

Nickel	E (V)	$E^{o'}$ (V)
$Ni^{2+} + 2e^- \rightleftharpoons Ni(s)$	–0.257	
$Ni(OH)_2(s) + 2e^- \rightleftharpoons Ni(s) + 2OH^-$	–0.72	
$Ni(NH_3)_6^{2+} + 2e^- \rightleftharpoons Ni(s) + 6NH_3$	–0.49	

Nickel	E (V)	$E^{o'}$ (V)
$Ni^{2+} + 2e^- \rightleftharpoons Ni(s)$	–0.257	
$Ni(OH)_2(s) + 2e^- \rightleftharpoons Ni(s) + 2OH^-$	–0.72	
$Ni(NH_3)_6^{2+} + 2e^- \rightleftharpoons Ni(s) + 6NH_3$	–0.49	

Nitrogen	E (V)	$E^{o'}$ (V)
$N_2(g) + 5H^+ + 4e^- \rightleftharpoons N_2H_5^+$	–0.23	
$N_2O(g) + 2H^+ + 2e^- \rightleftharpoons N_2(g) + H_2O(l)$	1.77	
$2NO(g) + 2H^+ + 2e^- \rightleftharpoons N_2O(g) + H_2O(l)$	1.59	
$HNO_2 + H^+ + e^- \rightleftharpoons NO(g) + H_2O(l)$	0.996	
$2HNO_2 + 4H^+ + 4e^- \rightleftharpoons N_2O(g) + 3H_2O(l)$	1.297	
$NO_3^- + 3H^+ + 2e^- \rightleftharpoons HNO_2 + H_2O(l)$	0.94	

Oxygen	E (V)	$E^{o'}$ (V)
$O_2(g) + 2H^+ + 2e^- \rightleftharpoons H_2O_2$	0.695	
$O_2(g) + 4H^+ + 4e^- \rightleftharpoons 2H_2O(l)$	1.229	
$H_2O_2 + 2H^+ + 2e^- \rightleftharpoons 2H_2O(l)$	1.763	
$O_2(g) + 2H_2O(l) + 4e^- \rightleftharpoons 4OH^-$	0.401	
$O_3(g) + 2H^+ + 2e^- \rightleftharpoons O_2(g) + H_2O(l)$	2.07	

Phosphorous	E (V)	$E^{o'}$ (V)
$P(s, white) + 3H^+ + 3e^- \rightleftharpoons PH_3(g)$	–0.063	
$H_3PO_3 + 2H^+ + 2e^- \rightleftharpoons H_3PO_2 + H_2O(l)$	–0.499	
$H_3PO_4 + 2H^+ + 2e^- \rightleftharpoons H_3PO_3 + H_2O(l)$	–0.276	

Platinum	E (V)	$E^{o'}$ (V)
$Pt^{2+} + 2e^- \rightleftharpoons Pt(s)$	1.188	
$PtCl_4^{2-} + 2e^- \rightleftharpoons Pt(s) + 4Cl^-$	0.758	

Potasium	E (V)	$E^{o'}$ (V)
$K^+ + e^- \rightleftharpoons K(s)$	–2.924	

Ruthenium	E (V)	$E^{o'}$ (V)
$Ru^{3+} + 3e^- \rightleftharpoons Ru(s)$	0.249	
$RuO_2(s) + 4H^+ + 4e^- \rightleftharpoons Ru(s) + 2H_2O(l)$	0.68	
$Ru(NH_3)_6^{3+} + e^- \rightleftharpoons Ru(NH_3)_6^{2+}$	0.10	
$Ru(CN)_6^{3-} + e^- \rightleftharpoons Ru(CN)_6^{4-}$	0.86	

Selenium	E (V)	$E^{o'}$ (V)
$\mathrm{Se}(s) + 2e^- \rightleftharpoons \mathrm{Se}^{2-}$		–0.67 in 1 M NaOH
$\mathrm{Se}(s) + 2\mathrm{H}^+ + 2e^- \rightleftharpoons \mathrm{H_2Se}(g)$	–0.115	
$\mathrm{H_2SeO_3} + 4\mathrm{H}^+ + 4e^- \rightleftharpoons \mathrm{Se}(s) + 3\mathrm{H_2O}(l)$	0.74	
$\mathrm{SeO_4^{3-}} + 4\mathrm{H}^+ + e^- \rightleftharpoons \mathrm{H_2SeO_3} + \mathrm{H_2O}(l)$	1.151	

Silicon	E (V)	$E^{o'}$ (V)
$\mathrm{SiF_6^{2-}} + 4e^- \rightleftharpoons \mathrm{Si}(s) + 6\mathrm{F}^-$	–1.37	
$\mathrm{SiO_2}(s) + 4\mathrm{H}^+ + 4e^- \rightleftharpoons \mathrm{Si}(s) + 2\mathrm{H_2O}(l)$	–0.909	
$\mathrm{SiO_2}(s) + 8\mathrm{H}^+ + 8e^- \rightleftharpoons \mathrm{SiH_4}(g) + 2\mathrm{H_2O}(l)$	–0.516	

Silver	E (V)	$E^{o'}$ (V)
$\mathrm{Ag}^+ + e^- \rightleftharpoons \mathrm{Ag}(s)$	0.7996	
$\mathrm{AgBr}(s) + e^- \rightleftharpoons \mathrm{Ag}(s) + \mathrm{Br}^-$	0.071	
$\mathrm{Ag_2C_2O_4}(s) + 2e^- \rightleftharpoons 2\mathrm{Ag}(s) + \mathrm{C_2O_4^{2-}}$	0.47	
$\mathrm{AgCl}(s) + e^- \rightleftharpoons \mathrm{Ag}(s) + \mathrm{Cl}^-$	0.2223	
$\mathrm{AgI}(s) + e^- \rightleftharpoons \mathrm{Ag}(s) + \mathrm{I}^-$	–0.152	
$\mathrm{Ag_2S}(s) + 2e^- \rightleftharpoons 2\mathrm{Ag}(s) + \mathrm{S}^{2-}$	–0.71	
$\mathrm{Ag(NH_3)_2^+} + e^- \rightleftharpoons \mathrm{Ag}(s) + 2\mathrm{NH_3}$	–0.373	

Sodium	E (V)	$E^{o'}$ (V)
$\mathrm{Na}^+ + e^- \rightleftharpoons \mathrm{Na}(s)$	–2.713	

Strontium	E (V)	$E^{o'}$ (V)
$\mathrm{Sr}^{2+} + 2e^- \rightleftharpoons \mathrm{Sr}(s)$	–2.89	

Sulfur	E (V)	$E^{o'}$ (V)
$\mathrm{S}(s) + 2e^- \rightleftharpoons \mathrm{S}^{2-}$	–0.407	
$\mathrm{S}(s) + 2\mathrm{H}^+ + 2e^- \rightleftharpoons \mathrm{H_2S}(g)$	0.144	
$\mathrm{S_2O_6^{2-}} + 4\mathrm{H}^+ + 2e^- \rightleftharpoons 2\mathrm{H_2SO_3}$	0.569	
$\mathrm{S_2O_8^{2-}} + 2e^- \rightleftharpoons 2\mathrm{SO_4^{2-}}$	1.96	
$\mathrm{S_4O_6^{2-}} + 2e^- \rightleftharpoons 2\mathrm{S_2O_3^{2-}}$	0.080	
$2\mathrm{SO_3^{2-}} + 2\mathrm{H_2O}(l) + 2e^- \rightleftharpoons \mathrm{S_2O_4^{2-}} + 4\mathrm{OH}^-$	–1.13	
$2\mathrm{SO_3^{2-}} + 3\mathrm{H_2O}(l) + 4e^- \rightleftharpoons \mathrm{S_2O_3^{2-}} + 6\mathrm{OH}^-$		–0.576 in 1 M NaOH
$2\mathrm{SO_4^{2-}} + 4\mathrm{H}^+ + 2e^- \rightleftharpoons \mathrm{S_2O_6^{2-}} + 2\mathrm{H_2O}(l)$	–0.25	
$\mathrm{SO_4^{2-}} + \mathrm{H_2O}(l) + 2e^- \rightleftharpoons \mathrm{SO_3^{2-}} + 2\mathrm{OH}^-$	–0.936	
$\mathrm{SO_4^{2-}} + 4\mathrm{H}^+ + 2e^- \rightleftharpoons \mathrm{H_2SO_3} + \mathrm{H_2O}(l)$	0.172	

Thallium	E (V)	$E^{o\prime}$ (V)
$Tl^{3+} + 2e^- \rightleftharpoons Tl^+$		1.25 in 1 M $HClO_4$ 0.77 in 1 M HCl
$Tl^{3+} + 3e^- \rightleftharpoons Tl(s)$	0.742	

Tin	E (V)	$E^{o\prime}$ (V)
$Sn^{2+} + 2e^- \rightleftharpoons Sn(s)$		–0.19 in 1 M HCl
$Sn^{4+} + 2e^- \rightleftharpoons Sn^{2+}$	0.154	0.139 in 1 M HCl

Titanium	E (V)	$E^{o\prime}$ (V)
$Ti^{2+} + 2e^- \rightleftharpoons Ti(s)$	–0.163	
$Ti^{3+} + e^- \rightleftharpoons Ti^{2+}$	–0.37	

Tungsten	E (V)	$E^{o\prime}$ (V)
$WO_2(s) + 4H^+ + 4e^- \rightleftharpoons W(s) + 2H_2O(l)$	–0.119	
$WO_3(s) + 6H^+ + 6e^- \rightleftharpoons W(s) + 3H_2O(l)$	–0.090	

Uranium	E (V)	$E^{o\prime}$ (V)
$U^{3+} + 3e^- \rightleftharpoons U(s)$	–1.66	
$U^{4+} + e^- \rightleftharpoons U^{3+}$	–0.52	
$UO_2^+ + 4H^+ + e^- \rightleftharpoons U^{4+} + 2H_2O(l)$	0.27	
$UO_2^{2+} + e^- \rightleftharpoons UO_2^+$	0.16	
$UO_2^{2+} + 4H^+ + 2e^- \rightleftharpoons U^{4+} + 2H_2O(l)$	0.327	

Vanadium	E (V)	$E^{o\prime}$ (V)
$V^{2+} + 2e^- \rightleftharpoons V(s)$	–1.13	
$V^{3+} + e^- \rightleftharpoons V^{2+}$	–0.255	
$VO^{2+} + 2H^+ + e^- \rightleftharpoons V^{3+} + H_2O(l)$	0.337	
$VO_2^+ + 2H^+ + e^- \rightleftharpoons VO^{2+} + H_2O(l)$	1.000	

Zinc	E (V)	$E^{o\prime}$ (V)
$Zn^{2+} + 2e^- \rightleftharpoons Zn(s)$	–0.7618	
$Zn(OH)_4^{2-} + 2e^- \rightleftharpoons Zn(s) + 4OH^-$	–1.285	
$Zn(NH_3)_4^{2+} + 2e^- \rightleftharpoons Zn(s) + 4NH_3$	–1.04	
$Zn(CN)_4^{2-} + 2e^- \rightleftharpoons Zn(s) + 4CN^-$	–1.34	

7.14: Random Number Table

The following table provides a list of random numbers in which the digits 0 through 9 appear with approximately equal frequency. Numbers are arranged in groups of five to make the table easier to view. This arrangement is arbitrary, and you can treat the table as a sequence of random individual digits (1, 2, 1, 3, 7, 4...going down the first column of digits on the left side of the table), as a sequence of three digit numbers (111, 212, 104, 367, 739... using the first three columns of digits on the left side of the table), or in any other similar manner.

Let's use the table to pick 10 random numbers between 1 and 50. To do so, we choose a random starting point, perhaps by dropping a pencil onto the table. For this exercise, we will assume that the starting point is the fifth row of the third column, or 12032 (highlighted in **red** below). Because the numbers must be between 1 and 50, we will use the last two digits, ignoring all two-digit numbers less than 01 or greater than 50. Proceeding down the third column, and moving to the top of the fourth column if necessary, gives the following 10 random numbers: 32, 01, 05, 16, 15, 38, 24, 10, 26, 14.

These random numbers (1000 total digits) are a small subset of values from the publication *Million Random Digits* (Rand Corporation, 2001) and used with permission. Information about the publication, and a link to a text file containing the million random digits is available at http://www.rand.org/pubs/monograph_reports/MR1418/.

11164	36318	75061	37674	26320	75100	10431	20418	19228	91792
21215	91791	76831	58678	87054	31687	93205	43685	19732	08468
10438	44482	66558	37649	08882	90870	12462	41810	01806	02977
36792	26236	33266	66583	60881	97395	20461	36742	02852	50564
73944	04773	12032	51414	82384	38370	00249	80709	72605	67497
49563	12872	14063	93104	78483	72717	68714	18048	25005	04151
64208	48237	41701	73117	33242	42314	83049	21933	92813	04763
51486	72875	38605	29341	80749	80151	33835	52602	79147	08868
99756	26360	64516	17971	48478	09610	04638	17141	09227	10606
71325	55217	13015	72907	00431	45117	33827	92873	02953	85474
65285	97198	12138	53010	95601	15838	16805	61004	43516	17020
17264	57327	38224	29301	31381	38109	34976	65692	98566	29550
95639	99754	31199	92558	68368	04985	51092	37780	40261	14479
61555	76404	86210	11808	12841	45147	97438	60022	12645	62000
78137	98768	04689	87130	79225	08153	84967	64539	79493	74917
62490	99215	84987	28759	19177	14733	24550	28067	68894	38490
24216	63444	21283	07044	92729	37284	13211	37485	10415	36457
16975	95428	33226	55903	31605	43817	22250	03918	46999	98501
59138	39542	71168	57609	91510	77904	74244	50940	31553	62562
29478	59652	50414	31966	87912	87514	12944	49862	96566	48825

7.15: Polarographic Half-Wave Potentials

The following table provides $E_{1/2}$ values for selected reduction reactions. Values are from Dean, J. A. *Analytical Chemistry Handbook*, McGraw-Hill: New York, 1995.

Element	$E_{1/2}$ (volts vs. SCE)	Matrix
$Al^{3+}(aq) + 3\,e^- \rightleftharpoons Al(s)$	–0.5	0.2 M acetate (pH 4.5–4.7)
$Cd^{2+}(aq) + 2\,e^- \rightleftharpoons Cd(s)$	–0.6	0.1 M KCl 0.050 M H_2SO_4 1 M HNO_3
$Cr^{3+}(aq) + 3\,e^- \rightleftharpoons Cr(s)$	–0.35 $(+3 \longrightarrow +2)$ –1.70 $(+2 \longrightarrow 0)$	1 M NH_4Cl plus 1 M NH_3 1 M NH_4^{+}/NH_3 buffer (pH 8–9)
$Co^{3+}(aq) + 3\,e^- \rightleftharpoons Co(s)$	–0.5 $(+3 \longrightarrow +2)$ –1.3 $(+2 \longrightarrow 0)$	1 M NH_4Cl plus 1 M NH_3
$Co^{2+}(aq) + 2\,e^- \rightleftharpoons Co(s)$	–1.03	1 M KSCN
$Cu^{2+}(aq) + 2\,e^- \rightleftharpoons Cu(s)$	0.04 –0.22	0.1 M KSCN 0.1 M NH_4ClO_4 1 M Na_2SO_4 0.5 M potassium citrate (pH 7.5)
$Fe^{3+}(aq) + 3\,e^- \rightleftharpoons Fe(s)$	–0.17 $(+3 \longrightarrow +2)$ –1.52 $(+2 \longrightarrow 0)$	0.5 M sodium tartrate (pH 5.8)
$Fe^{3+}(aq) + e^- \rightleftharpoons Fe^{2+}(aq)$	–0.27	0.2 M $Na_2C_2O_4$ (pH < 7.9)
$Pb^{2+}(aq) + 2\,e^- \rightleftharpoons Pb(s)$	–0.405 –0.435	1 M HNO_3 1 M KCl
$Mn^{2+}(aq) + 2\,e^- \rightleftharpoons Mn(s)$	–1.65	1 M NH_4Cl plus 1 M NH_3
$Ni^{2+}(aq) + 2\,e^- \rightleftharpoons Ni(s)$	–0.70 –1.09	1 M KSCN 1 M NH_4Cl plus 1 M NH_3
$Zn^{2+}(aq) + 2\,e^- \rightleftharpoons Zn(s)$	–0.995 –1.33	0.1 M KCl 1 M NH_4Cl plus 1 M NH_3

7.16: Countercurrent Separations

In 1949, Lyman Craig introduced an improved method for separating analytes with similar distribution ratios [Craig, L. C. *J. Biol. Chem.* **1944**, *155*, 519–534]. The technique, which is known as a countercurrent liquid–liquid extraction, is outlined in Figure 16.16.1 and discussed in detail below. In contrast to a sequential liquid–liquid extraction, in which we repeatedly extract the sample containing the analyte, a countercurrent extraction uses a serial extraction of both the sample and the extracting phases. Although countercurrent separations are no longer common—chromatographic separations are far more efficient in terms of resolution, time, and ease of use—the theory behind a countercurrent extraction remains useful as an introduction to the theory of chromatographic separations.

To track the progress of a countercurrent liquid-liquid extraction we need to adopt a labeling convention. As shown in Figure 16.16.1 , in each step of a countercurrent extraction we first complete the extraction and then transfer the upper phase to a new tube that contains a portion of the fresh lower phase. Steps are labeled sequentially beginning with zero. Extractions take place in a series of tubes that also are labeled sequentially, starting with zero. The upper and lower phases in each tube are identified by a letter and number, with the letters U and L representing, respectively, the upper phase and the lower phase, and the number indicating the step in the countercurrent extraction in which the phase was first introduced. For example, U_0 is the upper phase introduced at step 0 (during the first extraction), and L_2 is the lower phase introduced at step 2 (during the third extraction). Finally, the partitioning of analyte in any extraction tube results in a fraction *p* remaining in the upper phase, and a fraction *q* remaining in the lower phase. Values of *q* are calculated using Equation 7.16.1, which is identical to Equation 7.7.6 in Chapter 7.

$$(q_{\text{aq}})_1 = \frac{(\text{mol aq})_1}{(\text{mol aq})_0} = \frac{V_{\text{aq}}}{DV_{\text{org}} + V_{\text{aq}}} \tag{7.16.1}$$

The fraction *p*, of course is equal to 1 – *q*. Typically V_{aq} and V_{org} are equal in a countercurrent extraction, although this is not a requirement.

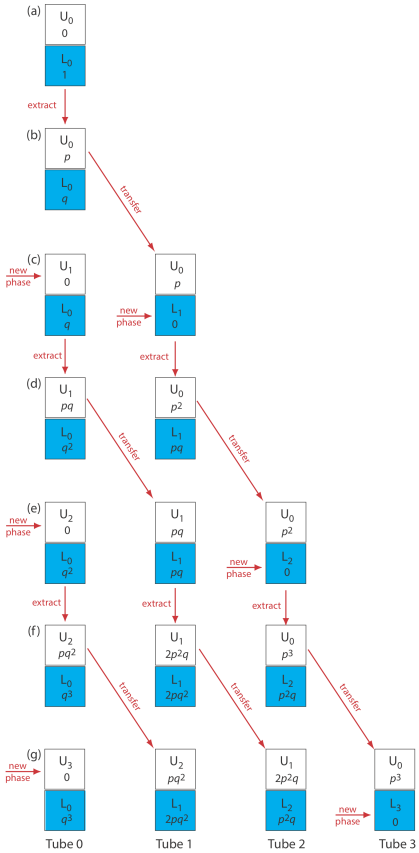

Figure 16.16.1 . Scheme for a countercurrent extraction: (a) The sample containing the analyte begins in L_0 and is extracted with a fresh portion of the upper, or mobile phase; (b) The extraction takes place, transferring a fraction p of analyte to the upper phase and leaving a fraction q of analyte in the lower, or stationary phase; (c) When the extraction is complete, the upper phase is transferred to the next tube, which contains a fresh portion of the sample's solvent, and a fresh portion of the upper phase is added to tube 0. In (d) through (g), the process continues, with the addition of two more tubes.

Let's assume that the analyte we wish to isolate is present in an aqueous phase of 1 M HCl, and that the organic phase is benzene. Because benzene has the smaller density, it is the upper phase, and 1 M HCl is the lower phase. To begin the countercurrent extraction we place the aqueous sample that contains the analyte in tube 0 along with an equal volume of benzene. As shown in Figure 7.16.1a, before the extraction all the analyte is present in phase L_0. When the extraction is complete, as shown in Figure 7.16.1b, a fraction p of the analyte is present in phase U_0, and a fraction q is in phase L_0. This completes step 0 of the countercurrent extraction. If we stop here, there is no difference between a simple liquid–liquid extraction and a countercurrent extraction.

After completing step 0, we remove phase U_0 and add a fresh portion of benzene, U_1, to tube 0 (see Figure 7.16.1c). This, too, is identical to a simple liquid-liquid extraction. Here is where the power of the countercurrent extraction begins—instead of setting aside the phase U_0, we place it in tube 1 along with a portion of analyte-free aqueous 1 M HCl as phase L_1 (see Figure 7.16.1c). Tube 0 now contains a fraction q of the analyte, and tube 1 contains a fraction p of the analyte. Completing the extraction in tube 0 results in a fraction p of its contents remaining in the upper phase, and a fraction q remaining in the lower phase. Thus, phases U_1 and L_0 now contain, respectively, fractions pq and q^2 of the original amount of analyte. Following the same logic, it is easy to show that the phases U_0 and L_1 in tube 1 contain, respectively, fractions p^2 and pq of analyte. This completes step 1 of the extraction (see Figure 7.16.1d). As shown in the remainder of Figure 16.16.1 , the countercurrent extraction continues with this cycle of phase transfers and extractions.

In a countercurrent liquid–liquid extraction, the lower phase in each tube remains in place, and the upper phase moves from tube 0 to successively higher numbered tubes. We recognize this difference in the movement of the two phases by referring to the lower phase as a stationary phase and the upper phase as a mobile phase. With each transfer some of the analyte in tube r moves to tube $r+1$, while a portion of the analyte in tube $r-1$ moves to tube r. Analyte introduced at tube 0 moves with the mobile phase, but at a rate that is slower than the mobile phase because, at each step, a portion of the analyte transfers into the stationary phase. An

analyte that preferentially extracts into the stationary phase spends proportionally less time in the mobile phase and moves at a slower rate. As the number of steps increases, analytes with different values of q eventually separate into completely different sets of extraction tubes.

We can judge the effectiveness of a countercurrent extraction using a histogram that shows the fraction of analyte present in each tube. To determine the total amount of analyte in an extraction tube we add together the fraction of analyte present in the tube's upper and lower phases following each transfer. For example, at the beginning of step 3 (see Figure 7.16.1g) the upper and lower phases of tube 1 contain fractions pq^2 and $2pq^2$ of the analyte, respectively; thus, the total fraction of analyte in the tube is $3pq^2$. Table 16.16.1 summarizes this for the steps outlined in Figure 16.16.1 . A typical histogram, calculated assuming distribution ratios of 5.0 for analyte A and 0.5 for analyte B, is shown in Figure 16.16.2 . Although four steps is not enough to separate the analytes in this instance, it is clear that if we extend the countercurrent extraction to additional tubes, we will eventually separate the analytes.

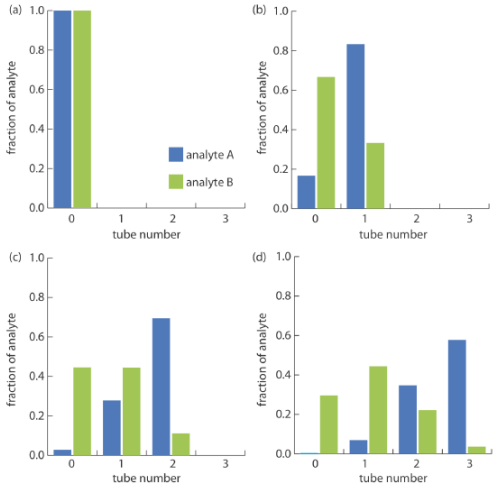

Figure 16.16.2 . Progress of a countercurrent extraction for the separation of analytes A and B showing the fraction of analyte in each tube after (a) step 0, (b) step 1, (c) step 2, and (d) step 3. The distribution ratio, D, is 5.0 for analyte A and 0.5 for analyte B. The volumes of the two phases are identical.

Table 16.16.1 . Fraction of Analyte Remaining in Tube r After Extraction Step n for a Countercurrent Extraction

n↓r ⟶	0	1	2	3
} \)">0	1	—	—	—
} \)">1	q	p	—	—
} \)">2	q^2	$2pq$	p^2	—
} \)">3	q^3	$3pq$	$3p^2q$	p^3

Figure 16.16.1 and Table 16.16.1 show how an analyte's distribution changes during the first four steps of a countercurrent extraction. Now we consider how we can generalize these results to calculate the amount of analyte in any tube, at any step during the extraction. You may recognize the pattern of entries in Table 16.16.1 as following the binomial distribution

$$f(r,n) = \frac{n!}{(n-r)!r!}p^r q^{n-r} \tag{7.16.2}$$

where $f(r, n)$ is the fraction of analyte present in tube r at step n of the countercurrent extraction, with the upper phase containing a fraction $p \times f(r,n)$ of analyte and the lower phase containing a fraction $q \times f(r,n)$ of the analyte.

Example 16.16.1

The countercurrent extraction shown in Figure 16.16.2 is carried out through step 30. Calculate the fraction of analytes A and B in tubes 5, 10, 15, 20, 25, and 30.

Solution

To calculate the fraction, q, for each analyte in the lower phase we use Equation 7.16.1. Because the volumes of the lower and upper phases are equal, we get

$$q_A = \frac{1}{D_A + 1} = \frac{1}{5+1} = 0.167 \qquad q_B = \frac{1}{D_B + 1} = \frac{1}{0.5+1} = 0.667$$

Because we know that $p + q = 1$, we also know that p_A is 0.833 and that p_B is 0.333. For analyte A, the fraction in tubes 5, 10, 15, 20, 25, and 30 after the 30th step are

$$f(5,30) = \frac{30!}{(30-5)!5!}(0.833)^5(0.167)^{30-5} = 2.1 \times 10^{-15} \approx 0$$

$$f(10,30) = \frac{30!}{(30-10)!10!}(0.833)^{10}(0.167)^{30-10} = 1.4 \times 10^{-9} \approx 0$$

$$f(15,30) = \frac{30!}{(30-15)!5!}(0.833)^{15}(0.167)^{30-15} = 2.2 \times 10^{-5} \approx 0$$

$$f(20,30) = \frac{30!}{(30-20)!20!}(0.833)^{20}(0.167)^{30-20} = 0.013$$

$$f(25,30) = \frac{30!}{(30-25)!25!}(0.833)^{25}(0.167)^{30-25} = 0.192$$

$$f(30,30) = \frac{30!}{(30-30)!30!}(0.833)^{30}(0.167)^{30-30} = 0.004$$

The fraction of analyte B in tubes 5, 10, 15, 20, 25, and 30 is calculated in the same way, yielding respective values of 0.023, 0.153, 0.025, 0, 0, and 0. Figure 16.16.3 , which provides the complete histogram for the distribution of analytes A and B, shows that 30 steps is sufficient to separate the two analytes.

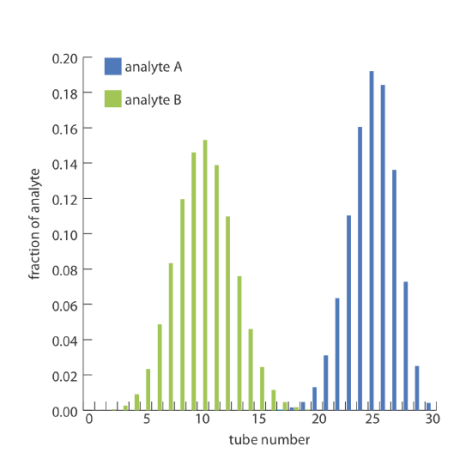

Figure 16.16.3 . Progress of a countercurrent extraction for the separation of analyte A and B showing the fraction of analyte in each tube after 30 steps. The distribution ratio, *D*, is 5.0 for analyte A and 0.5 for analyte B. The volumes of the two phases are identical.

Constructing a histogram using Equation 7.16.2 is tedious, particularly when the number of steps is large. Because the fraction of analyte in most tubes is approximately zero, we can simplify the histogram's construction by solving Equation 7.16.2 only for those tubes containing an amount of analyte that exceeds a threshold value. For a binomial distribution, we can use the mean and standard deviation to determine which tubes contain a significant fraction of analyte. The properties of a binomial distribution were covered in Chapter 4, with the mean, μ, and the standard deviation, σ, given as

$$\mu = np$$

$$\sigma = \sqrt{np(1-p)} = \sqrt{npq}$$

Furthermore, if both *np* and *nq* are greater than 5, then a binomial distribution closely approximates a normal distribution and we can use the properties of a normal distribution to determine the location of the analyte and its recovery [see Mark, H.; Workman, J. *Spectroscopy* **1990**, *5(3)*, 55–56].

Example 16.16.2

Two analytes, A and B, with distribution ratios of 9 and 4, respectively, are separated using a countercurrent extraction in which the volumes of the upper and lower phases are equal. After 100 steps determine the 99% confidence interval for the location of each analyte.

Solution

The fraction, *q*, of each analyte that remains in the lower phase is calculated using Equation 7.16.1. Because the volumes of the lower and upper phases are equal, we find that

$$q_A = \frac{1}{D_A + 1} = \frac{1}{9+1} = 0.10 \qquad q_B = \frac{1}{D_B + 1} = \frac{1}{4+1} = 0.20$$

Because we know that $p + q = 1$, we also know that p_A is 0.90 and p_B is 0.80. After 100 steps, the mean and the standard deviation for the distribution of analytes A and B are

$$\mu_A = np_A = (100)(0.90) = 90 \text{ and } \sigma_A = \sqrt{np_A q_A} = \sqrt{(100)(0.90)(0.10)} = 3$$

$$\mu_B = np_B = (100)(0.80) = 80 \text{ and } \sigma_A = \sqrt{np_A q_A} = \sqrt{(100)(0.80)(0.20)} = 4$$

Given that np_A, np_B, nq_A, and nq_B are all greater than 5, we can assume that the distribution of analytes follows a normal distribution and that the confidence interval for the tubes containing each analyte is

$$r = \mu \pm z\sigma$$

where *r* is the tube's number and the value of *z* is determined by the desired significance level. For a 99% confidence interval the value of *z* is 2.58 (see Appendix 4); thus,

$$r_A = 90 \pm (2.58)(3) = 90 \pm 8$$

$$r_B = 80 \pm (2.58)(4) = 80 \pm 10$$

Because the two confidence intervals overlap, a complete separation of the two analytes is not possible using a 100 step countercurrent extraction. The complete distribution of the analytes is shown in Figure 16.16.4 .

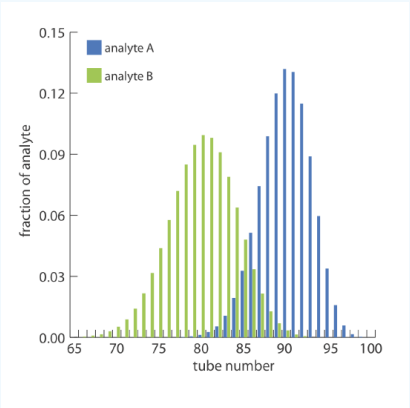

Figure 16.16.4 . Progress of the countercurrent extraction after 100 steps. Although analyte A moves more quickly than analyte B, the similarity of their distribution ratios, and thus the similarity in their values of *q*, means the separation of analytes A and B is not yet complete.

Example 16.16.3

For the countercurrent extraction in Example 16.16.2 , calculate the recovery and the separation factor for analyte A if the contents of tubes 85–99 are pooled together.

Solution

From Example 16.16.2 we know that after 100 steps of the countercurrent extraction, analyte A is normally distributed about tube 90 with a standard deviation of 3. To determine the fraction of analyte A in tubes 85–99, we use the single-sided normal distribution in Appendix 3 to determine the fraction of analyte in tubes 0–84, and in tube 100. The fraction of analyte A in tube 100 is determined by calculating the deviation *z*

$$z = \frac{r - \mu}{\sigma} = \frac{99 - 90}{3} = 3$$

and using the table in Appendix 3 to determine the corresponding fraction. For *z* = 3 this corresponds to 0.135% of analyte A. To determine the fraction of analyte A in tubes 0–84 we again calculate the deviation

$$z = \frac{r - \mu}{\sigma} = \frac{84 - 90}{3} = -1.67$$

From Appendix 3 we find that 4.75% of analyte A is present in tubes 0–84. Analyte A's recovery, therefore, is

$$100\% - 4.75\% - 0.135\% \approx 95\%$$

To calculate the separation factor we determine the recovery of analyte B in tubes 85–99 using the same general approach as for analyte A, finding that approximately 89.4% of analyte B remains in tubes 0–84 and that essentially no analyte B is in tube 100. The recovery for B, therefore, is

$$100\% - 89.4\% - 0\% \approx 10.6\%$$

and the separation factor is

$$S_{\mathrm{B/A}} = \frac{R_{\mathrm{A}}}{R_{\mathrm{B}}} = \frac{10.6}{95} = 0.112$$

7.17: Review of Chemical Kinetics

A reaction's equilibrium position defines the extent to which the reaction can occur. For example, we expect a reaction with a large equilibrium constant, such as the dissociation of HCl in water

$$\mathrm{HCl}(aq) + \mathrm{H_2O}(l) \longrightarrow \mathrm{H_3O^+}(aq) + \mathrm{Cl^-}(aq)$$

to proceed nearly to completion. A large equilibrium constant, however, does not guarantee that a reaction will reach its equilibrium position. Many reactions with large equilibrium constants, such as the reduction of $\mathrm{MnO_4^-}$ by $\mathrm{H_2O}$

$$4\,\mathrm{MnO_4^-}(aq) + 2\,\mathrm{H_2O}(l) \longrightarrow 4\,\mathrm{MnO_2}(s) + 3\,\mathrm{O_2}(g) + 4\,\mathrm{OH^-}(aq)$$

do not occur to an appreciable extent. The study of the rate at which a chemical reaction approaches its equilibrium position is called kinetics.

Chemical Reaction Rates

A study of a reaction's kinetics begins with the measurement of its reaction rate. Consider, for example, the general reaction shown below, involving the aqueous solutes A, B, C, and D, with stoichiometries of *a*, *b*, *c*, and *d*.

$$a\mathrm{A} + b\mathrm{B} \rightleftharpoons c\mathrm{C} + d\mathrm{D} \tag{7.17.1}$$

The rate, or velocity, at which this reaction approaches its equilibrium position is determined by following the change in concentration of one reactant or one product as a function of time. For example, if we monitor the concentration of reactant A, we express the rate as

$$R = -\frac{d[\mathrm{A}]}{dt} \tag{7.17.2}$$

where *R* is the measured rate expressed as a change in concentration of A as a function of time. Because a reactant's concentration decreases with time, we include a negative sign so that the rate has a positive value.

We also can determine the rate by following the change in concentration of a product as a function of time, which we express as

$$R' = +\frac{d[\mathrm{C}]}{dt} \tag{7.17.3}$$

Rates determined by monitoring different species do not necessarily have the same value. The rate *R* in Equation 7.17.2 and the rate R' in Equation 7.17.3 have the same value only if the stoichiometric coefficients of A and C in reaction 7.17.1 are identical. In general, the relationship between the rates *R* and R' is

$$R = \frac{a}{c} \times R'$$

The Rate Law

A rate law describes how a reaction's rate is affected by the concentration of each species in the reaction mixture. The rate law for Reaction 7.17.1 takes the general form of

$$R = k[\mathrm{A}]^{\alpha}[\mathrm{B}]^{\beta}[\mathrm{C}]^{\gamma}[\mathrm{D}]^{\delta}[\mathrm{E}]^{\epsilon}\ldots \tag{7.17.4}$$

where *k* is the rate constant, and α, β, γ, δ, and ϵ are the reaction orders of the reaction for each species present in the reaction.

There are several important points about the rate law in Equation 7.17.4. First, a reaction's rate may depend on the concentrations of both reactants and products, as well as the concentration of a species that does not appear in the reaction's overall stoichiometry. Species E in Equation 7.17.4, for example, may be a catalyst that does not appear in the reaction's overall stoichiometry, but which increases the reaction's rate. Second, the reaction order for a given species is not necessarily the same as its stoichiometry in the chemical reaction. Reaction orders may be positive, negative, or zero, and may take integer or non-integer values. Finally, the reaction's overall reaction order is the sum of the individual reaction orders for each species. Thus, the overall reaction order for Equation 7.17.4 is $\alpha + \beta + \gamma + \delta + \epsilon$.

Kinetic Analysis of Selected Reactions

In this section we review the application of kinetics to several simple chemical reactions, focusing on how we can use the integrated form of the rate law to determine reaction orders. In addition, we consider how we can determine the rate law for a more complex system.

First-Order Reactions

The simplest case we can treat is a first-order reaction in which the reaction's rate depends on the concentration of only one species. The simplest example of a first-order reaction is an irreversible thermal decomposition of a single reactant, which we represent as

$$\mathrm{A} \longrightarrow \text{products} \tag{7.17.5}$$

with a rate law of

$$R = -\frac{d[\mathrm{A}]}{dt} = k[\mathrm{A}] \tag{7.17.6}$$

The simplest way to demonstrate that a reaction is first-order in A, is to double the concentration of A and note the effect on the reaction's rate. If the observed rate doubles, then the reaction is first-order in A. Alternatively, we can derive a relationship between the concentration of A and time by rearranging Equation 7.17.6 and integrating.

$$\frac{d[\mathrm{A}]}{[\mathrm{A}]} = -k dt$$

$$\int_{[A]_0}^{[A]_t} \frac{1}{[A]} d[A] = -k \int_o^t dt \tag{7.17.7}$$

Evaluating the integrals in Equation 7.17.7 and rearranging

$$\ln \frac{[\mathrm{A}]_t}{[\mathrm{A}]_0} = -kt \tag{7.17.8}$$

$$\ln[\mathrm{A}]_t = \ln[\mathrm{A}]_0 - kt \tag{7.17.9}$$

shows that for a first-order reaction, a plot of $\ln[\mathrm{A}]_t$ versus time is linear with a slope of –*k* and a *y*-intercept of $\ln[\mathrm{A}]_0$. Equation 7.17.8 and Equation 7.17.9 are known as integrated forms of the rate law. Reaction 7.17.5 is not the only possible form of a first-order reaction. For example, the reaction

$$\mathrm{A} + \mathrm{B} \longrightarrow \text{products} \tag{7.17.10}$$

will follow first-order kinetics if the reaction is first-order in A and if the concentration of B does not affect the reaction's rate, which may happen if the reaction's mechanism involves at least two steps. Imagine that in the first step, A slowly converts to an intermediate species, C, which reacts rapidly with the remaining reactant, B, in one or more steps, to form the products.

$$\mathrm{A} \longrightarrow \mathrm{B}(\text{slow})$$

$$\mathrm{B} + \mathrm{C} \longrightarrow \text{products}$$

Because a reaction's rate depends only on those species in the slowest step—usually called the rate-determining step—and any preceding steps, species B will not appear in the rate law.

Second-Order Reactions

The simplest reaction demonstrating second-order behavior is

$$2\,\mathrm{A} \longrightarrow \text{products}$$

for which the rate law is

$$R = -\frac{d[\mathrm{A}]}{dt} = k[\mathrm{A}]^2$$

Proceeding as we did earlier for a first-order reaction, we can easily derive the integrated form of the rate law.

$$\frac{d[\mathrm{A}]}{[\mathrm{A}]^2} = -k dt$$

$$\int_{[\mathrm{A}]_0}^{[\mathrm{A}]_t} = -k \int_0^t dt$$

$$\frac{1}{[\mathrm{A}]_t} = kt + \frac{1}{[\mathrm{A}]_0}$$

For a second-order reaction, therefore, a plot of $([\mathrm{A}]_t)^{-1}$ versus t is linear with a slope of k and a y-intercept of $([\mathrm{A}]_0)^{-1}$. Alternatively, we can show that a reaction is second-order in A by observing the effect on the rate when we change the concentration of A. In this case, doubling the concentration of A produces a four-fold increase in the reaction's rate.

Example 16.17.1

The following data were obtained during a kinetic study of the hydration of *p*-methoxyphenylacetylene by measuring the relative amounts of reactants and products by NMR [data from Kaufman, D,; Sterner, C.; Masek, B.; Svenningsen, R.; Samuelson, G. *J. Chem. Educ.* **1982**, *59*, 885–886].

time (min)	% p-methoxyphenylacetylene
67	85.9
161	70.0
241	57.6
381	40.7
479	32.4
545	27.7
604	24

Solution

To determine the reaction's order we plot ln(%p-methoxyphenylacetylene) versus time for a first-order reaction, and (%p-methoxyphenylacetylene)$^{-1}$ versus time for a second-order reaction (see below). Because a straight-line for the first-order plot fits the data nicely, we conclude that the reaction is first-order in *p*-meth- oxyphenylacetylene. Note that when we plot the data using the equation for a second-order reaction, the data show curvature that does not fit the straight-line model.

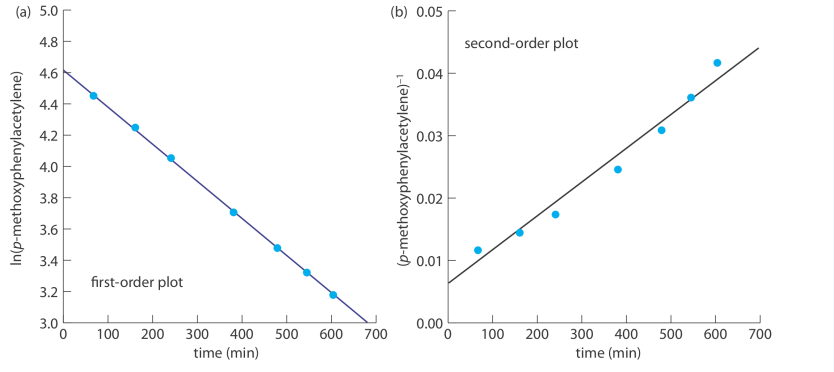

Pseudo-Order Reactions and the Method of Initial Rates

Unfortunately, most reactions of importance in analytical chemistry do not follow the simple first-order or second-order rate laws discussed above. We are more likely to encounter the second-order rate law given in Equation 7.17.11 than that in Equation

$$R = k[\mathrm{A}][\mathrm{B}] \tag{7.17.11}$$

Demonstrating that a reaction obeys the rate law in Equation 7.17.11 is complicated by the lack of a simple integrated form of the rate law. Often we can simplify the kinetics by carrying out the analysis under conditions where the concentrations of all species but one are so large that their concentrations effectively remain constant during the reaction. For example, if the concentration of B is selected such that $[\mathrm{B}] >> [\mathrm{A}]$, then Equation 7.17.11 simplifies to

$$R = k'[\mathrm{A}]$$

where the rate constant k' is equal to $k[\mathrm{B}]$. Under these conditions, the reaction appears to follow first-order kinetics in A; for this reason we identify the reaction as pseudo-first-order in A. We can verify the reaction order for A using either the integrated rate law or by observing the effect on the reaction's rate of changing the concentration of A. To find the reaction order for B, we repeat the process under conditions where $[\mathrm{A}] >> [\mathrm{B}]$.

A variation on the use of pseudo-ordered reactions is the initial rate method. In this approach we run a series of experiments in which we change one-at-a-time the concentration of each species that might affect the reaction's rate and measure the resulting initial rate. Comparing the reaction's initial rate for two experiments in which only the concentration of one species is different allows us to determine the reaction order for that species. The application of this method is outlined in the following example.

Example 16.17.2

The following data was collected during a kinetic study of the iodation of acetone by measuring the concentration of unreacted I_2 in solution [data from Birk, J. P.; Walters, D. L. *J. Chem. Educ.* **1992**, *69*, 585–587].

experiment number	$[C_3H_6O]$ (M)	$[H_3O^+]$ (M)	$[I_2]$ (M)	Rate (M s^{-1})
1	1.33	0.0404	6.65×10^{-3}	1.78×10^{-6}
2	1.33	0.0809	6.65×10^{-3}	3.89×10^{-6}
3	1.33	0.162	6.65×10^{-3}	8.11×10^{-6}
4	1.33	0.323	6.65×10^{-3}	1.66×10^{-5}
5	0.167	0.323	6.65×10^{-3}	1.64×10^{-6}
6	0.333	0.323	6.65×10^{-3}	3.76×10^{-6}
7	0.667	0.323	6.65×10^{-3}	7.55×10^{-6}
8	0.333	0.323	3.32×10^{-3}	3.57×10^{-6}

Solution

The order of the rate law with respect to the three reactants is determined by comparing the rates of two experiments in which there is a change in concentration for only one of the reactants. For example, in Experiments 1 and 2, only the $[H_3O^+]$ changes; as doubling the $[H_3O^+]$ doubles the rate, we know that the reaction is first-order in H_3O^+. Working in the same manner, Experiments 6 and 7 show that the reaction is also first order with respect to $[C_3H_6O]$, and Experiments 6 and 8 show that the rate of the reaction is independentof the $[I_2]$. Thus, the rate law is

$$R = k[C_3H_6O][H_3O^+]$$

To determine the value of the rate constant, we substitute the rate, the $[H_3O^+]$, and the $[H_3O^+]$ for each experiment into the rate law and solve for k. Using the data from Experiment 1, for example, gives a rate constant of $3.31 \times 10^{-5}\ M^{-1}\ s^{-1}$. The average rate constant for the eight experiments is $3.49 \times 10^{-5}\ M^{-1}\ s^{-1}$.

7.18: Atomic Weights of the Elements

The atomic weight of any isotope of an element is referenced to ^{12}C, which is assigned an exact atomic weight of 12. The atomic weight of an element, therefore, is calculated using the atomic weights of its isotopes and the known abundance of those isotopes. For some elements the isotopic abundance varies slightly from material- to-material such that the element's atomic weight in any specific material falls within a range of possible value; this is the case for carbon, for which the range of atomic masses is reported as [12.0096, 12.0116]. For such elements, a conventional, or representative atomic weight often is reported, chosen such that it falls within the range with an uncertainty of ±1 in the last reported digit; in the case of carbon, for example, the representative atomic weight is 12.011. The atomic weights reported here—most to five significant figures, but a few to just three or four significant figures—are taken from the IUPAC technical report ("Atomic Weights of the Elements 2011," *Pure Appl.Chem.* **2013**, *85*, 1047–1078). Values in ( ) are uncertainties in the last significant figure quoted and values in [ ] are the mass number for the longest lived isotope for elements that have no stable isotopes. The atomic weights for the elements B, Br, C, Cl, H, Li, Mg, N, O, Si, S, Tl are representative values.

At. No.	Symbol	Name	At. Wt.	At. No.	Symbol	Name	At. Wt.
1	H	hydrogen	1.008	60	Nd	neodymium	144.24
2	He	helium	4.0026	61	Pm	promethium	[145]
3	Li	lithium	6.94	62	Sm	samarium	150.36(2)
4	Be	beryllium	9.0122	63	Eu	europium	151.96
5	B	boron	10.81	64	Gd	gadolinium	157.25(3)
6	C	carbon	12.011	65	Tb	terbium	158.93
7	N	nitrogen	14.007	66	Dy	dysprosium	162.50
8	O	oxygen	15.999	67	Ho	holmium	164.93
9	F	fluorine	18.998	68	Er	erbium	167.26
10	Ne	neon	20.180	69	Tm	thulium	168.93
11	Na	sodium	22.990	70	Yb	ytterbium	173.05
12	Mg	magnesium	24.305	71	Lu	lutetium	174.97
13	Al	aluminum	26.982	72	Hf	halfnium	178.49(2)
14	Si	silicon	28.085	73	Ta	tantalum	180.95
15	P	phosphorous	30.974	74	W	tungsten	183.84
16	S	sulfur	32.06	75	Re	rhenium	186.21
17	Cl	chlorine	35.45	76	Os	osmium	190.23(3)
18	Ar	argon	39.948	77	Ir	iridium	192.22
19	K	potassium	39.098	78	Pt	platinum	195.08
20	Ca	calcium	40.078(4)	79	Au	gold	196.97
21	Sc	scandium	44.956	80	Hg	mercury	200.59
22	Ti	titanium	47.867	81	Tl	thallium	204.38
23	V	vanadium	50.942	82	Pb	lead	207.2
24	Cr	chromium	51.996	83	Bi	bismuth	208.98
25	Mn	manganese	54.938	84	Po	polonium	[209]

At. No.	Symbol	Name	At. Wt.	At. No.	Symbol	Name	At. Wt.
26	Fe	iron	55.845(2)	85	At	astatine	[210]
27	Co	cobalt	58.933	86	Rn	radon	[222]
28	Ni	nickel	58.693	87	Fr	francium	[223]
29	Cu	copper	63.546(3)	88	Ra	radium	[226]
30	Zn	zinc	65.38(2)	89	Ac	actinium	[227]
31	Ga	gallium	69.723	90	T	thoriium	232.04
32	Ge	germanium	72.630	91	Pa	protactinium	231.04
33	As	arsenic	74.922	92	U	uranium	238.03
34	Se	selenium	78.96(3)	93	Np	neptunium	[237]
35	Br	bromine	79.904	94	Pu	plutonium	[244]
36	Kr	krypton	83.798(2)	95	Am	americium	[243]
37	Rb	rubidium	85.468	96	Cm	curium	[247]
38	Sr	strontium	87.62	97	Bk	berkelium	[247]
39	Y	yttrium	88.906	98	Cf	californium	[251]
40	Zr	zirconium	91.224(2)	99	Es	einsteinium	[252]
41	Nb	niobium	92.906(2)	100	Fm	fermium	[257]
42	Mo	molybdenum	95.96(2)	101	Md	mendelevium	[258]
43	Tc	technetium	[97]	102	No	nobelium	[259]
44	Ru	ruthenium	101.07(2)	103	Lr	lawrencium	[262]
45	Rh	rhodium	102.91	104	Rf	futherfordium	[267]
46	Pa	palladium	106.42	105	Db	dubnium	[270]
47	Ag	silver	107.87	106	Sg	seaborgiuim	[271]
48	Cd	cadmium	112.41	107	Bh	bohrium	[270]
49	In	indium	114.82	108	Hs	hassium	[277]
50	Sn	tin	118.71	109	Mt	meitnerium	[276]
51	Sb	antimony	121.76	110	Ds	darmstadium	[281]
52	Te	tellurium	127.60(3)	111	Rg	roentgenium	[282]
53	I	iodine	126.90	112	Cn	copernicium	[285]
54	Xe	xenon	131.29	113	Uut	ununtrium	[285]
55	Cs	cesium	132.91	114	Fl	flerovium	[289]
56	Ba	barium	137.33	115	Uup	ununpentium	[289]
57	La	lanthanum	138.91	116	Lv	livermorium	[293]
58	Ce	cerium	140.12	117	Uus	ununseptium	[294]
59	Pr	praseodymium	140.91	118	Uno	ununoctium	[294]

Index

Glossary

Sample Word 1 | Sample Definition 1

Detailed Licensing

Overview

Title: Analytical Chemistry Volume II (Harvey)

Webpages: 85

Applicable Restrictions: Noncommercial

All licenses found:

- CC BY-NC-SA 4.0: 97.6% (83 pages)
- Undeclared: 2.4% (2 pages)

By Page

Detailed Licensing

Overview

Title: Analytical Chemistry Volume II (Harvey)

Webpages: 85

Applicable Restrictions: Noncommercial

All licenses found:

- CC BY-NC-SA 4.0: 97.6% (83 pages)
- Undeclared: 2.4% (2 pages)

By Page